Genome Wide Analysis of DNA Repair by Expression Profiling

A thesis submitted in partial fulfilment of the requirements
for the degree of Doctor of Philosophy by:

Andrew James Ridley

Department of Pathology and Cancer Studies
School of Medicine, Cardiff University
December 2006

ProQuest LLC
789 East Eisenhower Parkway
P.O. Box 1346
Ann Arbor, MI 48106-1346

DECLARATION

This work has not previously been accepted in substance for any degree and is not concurrently submitted in candidature for any degree.

Signed ...A. T. Hall.....(candidate) Date...15/05/07.....

STATEMENT 1

This thesis is being submitted in partial fulfilment of the requirements for the degree of .....PhD.....(insert MCh, MD, MPhil, PhD etc, as appropriate)

Signed ...A. T. Hall.....(candidate) Date....15/05/07.....

STATEMENT 2

This thesis is the result of my own independent work/investigation, except where otherwise stated.
Other sources are acknowledged by explicit references.

Signed ...A. T. Hall.....(candidate) Date....15/05/07.....

STATEMENT 3

I hereby give consent for my thesis, if accepted, to be available for photocopying and for inter-library loan, and for the title and summary to be made available to outside organisations.

Signed ...A. T. Hall.....(candidate) Date ....15/05/07.....

STATEMENT 4 - BAR ON ACCESS APPROVED

I hereby give consent for my thesis, if accepted, to be available for photocopying and for inter-library loans **after expiry of a bar on access** approved by the Graduate Development Committee.

Signed .....(candidate) Date .....

ACKNOWLEDGEMENTS

Firstly, I would like to take this opportunity to thank my supervisor's Dr. Chris Jones and Prof. David Wynford-Thomas, for giving me the opportunity to undertake my research in such a fascinating field.

I would like to express my deepest gratitude to Profs. David Kipling and Ray Walters who have provided continuous support and advice throughout the preparation of this manuscript. I would also like to thank Dr. Zaruhi Poghosyan (technical expert) for her advice on the materials and methods section of this manuscript.

I would also like to thank the other members of the DNA repair group including; Rebecca Capper (for the preparation of the pBABE-neo-hTERT supernatant and the construction of the MRC-5 pBABE-neo-hTERT cell line), Dr. Matthew Peake (for expert advise on microarray experimentation and analysis and generating the MRC-5 microarray dataset), Dr. Simon Reed (for general advice) and Dr. Shirong Yu (for undertaking the immuno-slot-blot assays).

I would like to give a warm thanks to all the technical staff in the Pathology Dept. who have contributed to the repertoire of laboratory techniques that I have become proficient in during the course of my PhD. In particular, I would like to thank Dr. Peter Giles for developing MADRAS, as without MADRAS the analysis of microarry data would have been incredibly time consuming. I would also like to thank Megan Musson for performing the microarray hybridisations. From other laboratories, I would also like to thank James Colley (for providing technical assistance on the characterisation of the *XPC* and *CSA* gene variants) and Matthew Caley (for technical assistance on the XP-C TRAP assay).

Finally, I would like to dedicate this thesis to my Mother who has been a continued support and inspiration throughout my life, particularly during times of adversity. She has given me the inner-strength and encouragement to continue when times have been hard. THANK YOU.

SUMMARY

Xeroderma pigmentosum (XP) and Cockayne syndrome (CS) are syndromes characterised by defects in nucleotide excision repair (NER), they can be distinguished by contrasting clinical manifestations. Although the genes responsible for XP and CS have been identified, the precise molecular roles of the normal proteins remains poorly understood. In the present study, primary dermal fibroblasts derived from patients assigned to XP complementation group C (XP-C; XP8CA) and CS type A (CS-A; CS3BE) were characterised. Patient XP8CA was homozygous for a 2 bp TG deletion in the *XPC* gene at codon 547 resulting in a premature termination at position 572, while patient CS3BE was a compound heterozygote for a 37G>T (E13X) and a novel 479C>T (A160V) mutation in *CKN1*, the gene that encodes the CSA protein. Permanent XP-C and CS-A cell lines were established by transducing primary XP8CA and CS3BE fibroblasts with a retroviral vector, expressing the catalytic subunit of telomerase, hTERT. The reconstitution of telomerase activity resulted in: (1) the preservation of the primary NER capabilities; (2) an extension of proliferative lifespan; (3) maintenance of the p53/p21$^{WAF1/CIP1}$ and pRb/p16^{INK4A} tumour suppressor pathways. Using microarrays, the UV-induced global transcriptional response of telomerised XP-C and CS-A fibroblasts was characterised. The data indicate that UV-irradiation resulted in the differential regulation of a diverse range of cellular responses such as transcription, cell cycle arrest, DNA repair and apoptosis. Additionally, cell-type-specific signatures were observed in telomerised XP-C and CS-A fibroblasts. The utility of RNAi was also demonstrated by transiently ablating XPC or CSA function in telomerised repair competent (MRC-5) fibroblasts, and a stable, permanent mutant was constructed by retrovirally transducing the telomerised CS-A cell line with an *XPC*-specific shRNA construct. Thus, permanent and stable telomerase-immortalised XP-C and CS-A cell lines have been established and partially characterised at both the genetic and molecular level, so providing *in vitro* models for investigating NER.

CONTENTS

LIST OF FIGURES

TABLES

ABBREVIATIONS

6-4PP	6-4 pyrimidine-pyrimidone photoproduct
A	Adenosine
A	Alanine
aa	Amino acid
AAR	Access, repair, restore
ABC	Avidin biotinylated complex
ACF	ATP-utilising chromatin assembly and re-modelling factor
ACGM	Advisory Committee on Genetic Modification
ADP	Adenosine diphosphate
AK	Actinic ketatosis
Ala	Alanine
AMP	Ampicillin
ANOVA	Analysis of variance
Apaf1	Apoptotic protease activating factor
APS	Ammonium persulphate
ARF	Alternative reading frame
Arg	Arginine
ARR	Acess, repair, restore
AT	Ataxia telangiectasia
ATF-3	Activating transcription factor 3
ATM	Ataxia telangiectasia-mutated
ATP	Adenosine triphosphate
ATR	Ataxia telangiectasia-related
Bax	BCL2-associated X protein
BCC	Basal cell carcinoma
Bcl2	B-cell CLL/lymphoma 2
BER	Base excision repair
BLM	Bloom syndrome
BSA	Bovine serum albumin
C	Cytosine
C	CS-A
C. elegans	*Caenorhabditis elegans*
CAF-1	Chromatin assembly factor 1
CAK	cdk-activating kinase complex
CBS	Central Biotechnology Service
Ccng2	Cyclin G2
CDK	Cyclin dependent kinase
CDKN1A	Cyclin dependent kinase inhibitor 1A
cDNA	Complementary DNA
CEL	Cell file
ChIP	Chromatin immunoprecipitation

CHO	Chinese hamster ovary
CIP1	CDK interacting protein
CNS	Central nervous system
CO_2	Carbon dioxide
COFS	Cerebro-oculo-facio-skeletal syndrome
CPD	Cyclobutane pyrimidine dimer
cRNA	Complementary RNA
CRUK	Cancer Research United Kingdom
CS	Cockayne syndrome
CSA	Cockayne syndrome type A
CSB	Cockayne syndrome type B
CSN	COP9 signalosome
CT	Threshold cycle
CTD	C-terminal domain
C-terminal	Carboxy-terminal
CUL4A	Cullin4A
DAB	Diaminobenzidine
DAT	Data file
DDB	Damage-specific DNA binding protein
del	Deletion
DEPC	Diethylprocarbonate
DHFR	Dihydrofolate reductase
DMEM	Dulbecco's Modified Eagle's Medium
DMSO	Dimethyl sulphoxide
DNA	Deoxyribonucleic acid
DNase	Deoxyribonuclease
dNTP	Deoxynucleotide 5-tri-phosphate
DSB	Double-strand break
DSC	DeSanctis-Cacchione syndrome
dsRNA	Double-stranded RNA
DTR	Heparin-binding EGF-like growth factor
DTT	Dithiothreitol
DUB	Deubiquitylating enzyme
E	Glutamic acid
E.coli	*Escherichia coli*
E2F	E-box factor 2
E3	Ubiquitin ligase
EASE	Expression Analysis Systematic Explorer
ECACC	European Collection of Cell Culture
ECF	Enhanced chemifluorescence
ECL	Enhanched chemiluminescence
ECM	Extracellular matrix
EDTA	Ethylenediamine tetracetate
EGF	Epidermal growth factor

EGTA	Ethyleneglycol tetraacetic acid
EMEM	Eagle's minimum essential medium
ERCC	Excision repair cross-complementing
EtOH	Ethanol
EXOSAP	Exonuclease I Shrimp alkaline phosphatase
Fas (APO1)	TNF receptor superfamily member 6
FCS	Foetal calf serum
FDR	False discovery rate
FDXR	Ferredoxin reductase
FEN-1	Flap endonuclease 1
FRET	Fluorescence resonance energy transfer
G	Guanine
G_0	Quiescence
G_1	Gap phase 1
G_2	Gap phase 2
GADD45	Growth arrest and DNA-damage-inducible, alpha
GAPDH	Glyceraldehyde-3-phosphate dehydrogenase
GAR	Goat anti-rabbit
GDF15	Growth differentiation factor 15
GGR	Global genome repair
GH	Glycine-histidine
Gln	Glutamine
Glu	Glutamic acid
GSEA	Gene Set Enrichment Analysis
H	Histidine
HAT	Histone acetyltransferase
HBSS	Hepes buffered saline solution
HDACs	Histone deacetylases
HDF	Human diploid fibroblast
HEK	Human embryonic kidney
HG	Human genome
HGPS	Hutchinson-Gilford progeria syndrome
His	Histidine
HIV-1	Human immunodeficiency virus-1
HPV E6	Human papillomavirus type 16 E6 protein
HPV E7	Human papillomavirus type 16 E7 protein
HR	Homologous recombination
hr	Hour
HRP	Horse radish peroxidase
hTERC	Human RNA telomerase component
hTERT	Human telomerase reverse transcriptase
IC	Infection control
ICC	Immunocytochemistry

Id1	Inhibitor of DNA binding 1
IFN	Interferon
iGA	Iterative Group Analysis
IGF	Insulin-like growth factor
IGF-BP3	Insulin-like growth factor-binding protein 3
INK4	Inhibitor of CDK4
IPA	Ingenuity Pathway Analysis
IR	Ionising radiation
ITAS	Internal telomerase amplification standard
IVT	*in vitro* transcription
K	Lysine
KD	Knockdown
kDa	Kilo dalton
KILLER (DR5)	TNF receptor superfamily member 10a
LB	Luria Bertani
LFS	Li-Fraumeni syndrome
LMPCR	Ligation-mediated PCR
LTAg	Large T antigen
Lys	Lysine
M	Molar
M	MRC-5
M0	Mortality stage 0
M1	Mortality stage 1
MADRAS	Microarray data review and annotation system
MAS 5.0	Microarray Suite 5.0
MCM-7	Mini-chromosome maintenance-7
MDC1	Mediator of DNA damage checkpoint 1
MDFs	Mouse dermal fibroblasts
MDM2	Murine double minute 2
Mdm2	Transformed 3T3 cell double minute 2, p53 binding protein
MIG5	Ras-related C3 botulinum toxin substrate 1
MM	Mismatch
MMP	Matrix metalloproteinase
MMR	Mismatch repair
MoMuLV	Moloney murine leukaemia virus
mRNA	Messenger RNA
MSCV	Murine stem cell virus
NADPH	Nicotinamide adenine dinucleotide
NBS	Nijmegen breakage syndrome
NBS1	Nibrin
NC	Negative control
NCBI	National Centre for Biotechnology Information
NEAA	Non-essential amino acids
NEDD8	Neuronal precursor-cell-expressed developmentally downregulated protein-8

neo	Neomycin phosphotransferase gene (G418) resistant
NER	Nucleotide excision repair
NF-B	Nuclear factor of kappa light polypeptide gene enhancer in B-cells
NHEJ	Non-homologous end joining
NIGMS	National Institute of General Medical Sciences
nm	Nano meter
NMD	Nonsense-mediated decay
NP40	Nonident P40 (octyphenoxy polytoxy ethanol)
nt	Nucleotide
N-terminal	Amino-terminal
OD	Optical density
OH	Hydroxyl
ORF	Open reading frame
P	Passage
p33ING1b	Inhibitor of growth family 1
p53AIP1	p53-upregulated apoptosis-inducing protein 1
PAGE	Polyacrylamide gel electrophoresis
PARP	Poly(ADP-ribose) polymerase
PBS	Phosphate buffered saline
PCA	Principle component analysis
PCNA	Proliferating cell nuclear antigen
PCR	Polymerase chain reaction
PDs	Population doublings
PG	Prostaglandins
PGK	Phosphoglycerate kinase
PIDD	Leucine-rich repeats and death domain containing
PIGa	Galectin-7
PKR	dsRNA-dependent protein kinase
PLG	Phase lock gel
PM	Perfect match
PMAIP1 (NOXA)	Phorbol-12-myristate-13-acetate-induced protein 1
pMSCV	Murine embryonic stem cell virus
PMSF	Phenylmethylsulphonyl fluoride
PNS	Peripheral nervous system
Pol	Polymerase eta
POLH	DNA polymerase
PP	Polyclonal population
PPM1D (wip1)	Protein 1D magnesium-dependent
ppRb	Hyperphosphorylated retinoblastoma protein
pRb	Retinoblastoma susceptibility gene product
pRb	Hypophosphorylated retinoblastoma protein
Pro	Proline
pRS	pRetroSuper
PTC	Premature termination codon

Pu	Purine
PUMA	p53-upregulated modulator of apoptosis
puro	Puromycin resistance gene
PVDF	Polyvinylidene difluoride
Py	Pyrimidine
Q	Glutamine
QC	Quality control
qRT-PCR	Quantitative reverse transcriptase PCR
R	Arginine
RAG	Rabbit anti-goat
RAM	Rabbit anti-mouse
RBS	Robert's syndrome
RFC	Replication factor C
RNA	Ribonucleic acid
RNA Pol II	RNA polymerase II
RNAi	RNA interference
RNase	Ribonuclease
ROS	Reactive oxygen species
RPA	Replication protein A
rpm	Revolutions per minute
S phase	DNA synthesis phase
SA-G	Senescence associated--galactosidase
SAM	Significance analysis of microarrays
SAPE	Streptavidin phycoerythrin
SAT	Spermidine/spermine N1-acetyl transferase 1
SCC	Squamous cell carcinoma
SDS	Sodium dodecyl sulphate
Ser	Serine
shRNA	Short hairpin RNA
SIPS	Stress-induced premature senescence
siRNA	Short interfering RNA
SNP	Single nucleotide polymorphism
SOC	Super optimal catabolite
ssDNA	Single-stranded DNA
STAGA	SPT3, TAFII31-GCN51 acetylase
SUMO-1	Ubiquitin-related modifier-1
SV40	Simian virus 40
T	Thymine
TAD	Transactivation domain
Taq	*Thermus aquaticus*
TBE	Tris-base, boric acid, EDTA
TBP	TATA-binding protein
TBST	Tris-base sodium chloride Tween 20
TCR	Transcription-coupled repair

TEMED	N,N,N',N'-tetramethylethylenediamine
TFBS	Transcription factor binding site
TFIIB	Transcription factor II B
TFIIH	Transcription factor II H
TFTC	TBP-free TAFII complex
TGT	Target signal
TIMP	Tissue inhibitor of metalloproteinase
TLS	Translesion synthesis
TP53	Tumour protein 53
TP53BP1	Tumor protein p53 binding protein 1
TRAP	Telomeric repeat amplification protocol
TRF	Terminal restriction fragment
TRF2	Telomeric repeat binding factor 2
Tris	Tris (hydroxymethyl)aminoethane
Trp	Tryptophan
TTD	Trichothiodystrophy
Tween 20	Polyoxyethylenesorban monolaurate
U	Uridine
UBA	Ubiquitin-associated
ubL	Ubiquitin-like
UDS	Unscheduled DNA synthesis
UTR	Untranslated region
UV	Ultraviolet
UV^{s}S	UV-sensitive syndrome
V	Volts
V	Valine
Val	Valine
W	Tryptophan
WAF1	Wild-type p53-activated fragment 1
WCE	Whole cell extract
WD	Tryptophan-aspartic acid
WS	Werner syndrome
X	XP-C
XAB	XPA binding protein
X-Gal	5-bromo-4-chloro-3-indoly--D-galactopyranoside
XP	Xeroderma pigmentosum
XPA	Xeroderma pigmentosum complementation group A
XPB	Xeroderma pigmentosum complementation group B
XPC	Xeroderma pigmentosum complementation group C
XPD	Xeroderma pigmentosum complementation group D
XPE	Xeroderma pigmentosum complementation group E
XPF	Xeroderma pigmentosum complementation group F
XPG	Xeroderma pigmentosum complementation group G
XP-V	XP variant

Chapter 1

General Introduction

1.1 DNA damage

The human genome is composed of three billion base pairs and comprises approximately 20-30,000 genes (Lander *et al.*, 2001; Venter *et al.*, 2001). The preservation of cellular deoxyribonucleic acid (DNA) is fundamental for the accurate transmission of genetic information from parental to daughter cells. However, the chemical structure and integrity of DNA is under perpetual attack from spontaneous modifications induced by replication errors, and a plethora of exogenous and endogenous sources of DNA damage. It has been estimated that the various sources of spontaneous base damage elicit modifications in approximately 25,000 bases per human genome per cell per day, out of the estimated $3x10^9$ bases present within the genome (Friedberg, 2001). The continued presence of DNA damage in the human genome has potential deleterious implications. At the cellular level, genome damage impedes fundamental DNA metabolic processes, such as transcription, replication and recombination, resulting in cell cycle arrest, senescence, apoptosis and genome instability. Moreover, at the organismal level, DNA damage has been implicated in a multiplicity of genetically inherited disorders, carcinogenesis and ageing (de Boer *et al.*, 2000).

The most prevalent sources of DNA damage are derived from exogenous physical and chemical agents, such as ultraviolet (UV) light, ionising radiation (IR) and toxiuos chemicals, including those found in cigarette smoke. Moreover, normal cellular metabolism can damage DNA because the generation of adenosine triphosphate (ATP) by the mitochondria, via the electron transport chain, results in the production of various reactive oxygen species (ROS), such as superoxide anion, singlet oxygen and hydrogen peroxide. Further sources of ROS include enzymes and processes required for normal cellular functionality, such as

nicotinamide adenine dinucleotide (NADPH)- oxidases, cyclooxygenases and lipid peroxidation. It is noteworthy that even in the absence of environmental genotoxins (such as UV light and cigarette smoke) human cells are subjected to >10,000 base modifications per day, resulting from endogenous sources of genotoxins (Lindahl, 1993; Setlow, 2001). Modifications in DNA structure and integrity can also occur spontaneously through the instability of chemical bonds, resulting in deamination and depurination (reviewed by Lindahl, 1993).

1.1.1 Consequences of UV-induced damage

UV light is a major source of DNA damage, and provides the principle etiological agent causing cutaneous neoplasia. Both epidemiological and molecular investigations have implicated that non-melanoma skin malignancies (such as basal cell carcinoma (BCC) and squamous cell carcinoma (SCC)) are associated with extreme exposure to the UV constituent of sunlight (reviewed by Ananthaswamy & Pierceall, 1990). The UV spectrum is categorised into three distinct wavelength ranges: UVA (320-400 nm), UVB (290-320 nm) and UVC (<290 nm). Although UVC possesses the highest energy, and is the most biologically damaging constituent of the UV spectrum, UVC is filtered by the stratospheric ozone layer and absorbed by atmospheric oxygen.

UVA has been implicated as the principal source of UV exposure, constituting 90% of the terrestrial UV (Afaq *et al.*, 2005). It is thought that UVA accounts for approximately 10-20% of the carcinogenic dose of the sun (de Laat *et al.*, 1997). Conversely, only 1-10% of UV radiation that penetrates the Earth's atmosphere is UVB (de Gruijl, 1999; Woodhead *et al.*, 1999).

UV can inflict damage on DNA both directly (type I), and indirectly (type II) through the excitation of a photosensitizer molecule with oxygen, resulting in the generation of ROS. Although both UVA and UVB cause oxidative damage, UVA is thought to cause its detrimental effects predominantly via this indirect mechanism, whilst UVB causes damage directly (Danpure & Tyrrell, 1976). At the organismal level, UVA radiation contributes to the carcinogenicity of the sun

(reviewed by Pfeifer *et al.*, 2005), photoaging of the skin (Krutmann, 2000) and the development of cataracts in the eye lens (Balasubramanian, 2000). Additionally, UVA has deleterious consequences at the cellular and molecular level, causing growth inhibition, cytotoxicity, cell membrane and cytoskeletal abnormalities and the abolition of enzymatic activity (Matsui & DeLeo, 1991; Krutmann, 2000; de Gruijl, 2000). Moreover, detrimental effects on the immune system have been correlated with UV-A exposure (Ullrich *et al.*, 1989).

In addition, cells possess photosensitive biomolecules known as chromophores, such as porphyrins, heme, ferritin, flavins and melanin precursors/polymers, which accept photons from UV radiation (Tyrrell & Keyse, 1990; Vile *et al.*, 1994; Kvam *et al.*, 2000). This results in the subsequent transfer of electrons to a higher energy state. The displacement of excited energy from one chromophore to another can initiate a chain reaction, which is dependent upon the structural nature of the chromophore, wavelength of radiation and the intricacy and quantity of different biomolecules present. The principal endogenous chromophores for UV radiation include DNA and reactive oxygen-generating species. DNA constitutes the principal cellular chromophore for UVC; the aromatic ring structure of the constituent bases in DNA facilitates the efficient absorption of short wavelength UV (<300 nm). Unlike UVB, UVA is not significantly absorbed by DNA *per se*. UVA induces modifications to DNA structure and chemistry indirectly, through the photoexcitation of these endogenous photosensitising biomolecules. These chromophores transfer their energy to molecular oxygen, resulting in the generation of ROS, such as superoxide and hydrogen peroxide, which promotes oxidative DNA damage and initiates mutagenesis.

The epidermis contains antioxidant defence mechanisms, including enzymes such a superoxide dismutase, glutathione peroxidase and catalase, which removes ROS from the skin (Moysan *et al.*, 1995). Further defence mechanisms include free radical scavengers, such as vitamin C and E, which reduce the detrimental effects of ROS. However, the continued production of ROS, subsequent to further UV exposure, depletes these innate antioxidant defence mechanisms and physiological levels of free radical scavengers (Podda *et al.*,

1998). The continued generation of these endogenously synthesised ROS molecules elicit a plethora of biological effects including: (1) poly(ADP-ribose) polymerase (PARP) activation, resulting in energy depletion in the skin; (2) oxidative DNA damage; (3) lipid peroxidation and nitric oxide synthase activation leading to inflammation and further generation of ROS and nitrogen species from inflammatory cells; (4) immunosuppression (reviewed by Halliday, 2005). Moreover, the continued generation of ROS also causes a multiplicity of DNA base modifications, including DNA strand breaks, DNA-protein cross-links, and oxidised bases (8-hydroxy-deoxyguanosine). The mutagenic effect of UVA is typified by the chromosomal aberrations and point mutations observed in cultured human and mouse cells, following exposure to UVA (reviewed in Friedberg *et al.*, 2006). In addition to DNA damage, UVA irradiation impedes fundamental processes, which preserve cellular homeostasis. For example, the peroxidation of lipid constituents of cellular membranes causes structural modifications, resulting in disturbances to cellular transport mechanisms. Furthermore, lipid peroxidation causes the synthesis of prostaglandins (PG), such as PGE2, which causes inflammation of the skin (Hruza & Pentland, 1993).

Although UVB represents only 1-10% of the solar spectrum that penetrates the Earth's atmosphere (de Gruijl, 1999; Woodhead *et al.*, 1999), UVB is considered the most mutagenic wavelength, compared to UVA (Courdavault *et al.*, 2005), which is thought to be 1000-fold less damaging than UVB. DNA is the principle chromophore for UVB radiation (Rosenstein & Mitchell, 1987). Moreover, UVB radiation acts on DNA via the direct excitation of the nucleobases in an oxygen-independent manner. This results in the generation of dimeric photo lesions at bipyrimidine sites (discussed further in Sections 1.1.3 & 1.1.4). Conversely, the damaging effect of UVA on cellular DNA occurs via a photosensitisation reaction, as nucleobases weakly absorb wavelengths above 320 nm (reviewed by Cadet *et al.*, 2005). However, UVA and UVB radiation generate free radicals, such as OH radical, one-electron oxidation, oxidants and peroxynitrite that can damage DNA via the production of 8-hydroxyguanine, bass loss, single-strand breaks and protein-DNA cross linking (reviewed in Hildesheim & Fornace, 2004).

1.1.2 DNA lesions induced by UV irradiation

Following exposure to UV radiation, two principal mutagenic DNA lesions are generated: cyclobutane pyrimidine dimers (CPDs) and pyrimidine (6-4) pyrimidone (6-4PP) adducts (and their Dewar valence isomers), which account for a high proportion of the UV-induced lesions (~95%). Previous studies have demonstrated the involvement of these photoproducts in photocarcinogenesis, by the multitude of mutations identified at bipyrimidine sites in human cutaneous tumours (Agar *et al.*, 2004; Dumaz *et al.*, 1993; Ziegler *et al.*, 1993). In addition to 6-4PPs and CPDs, UV induces a multitude of DNA lesions, including cytosine photohydrates, oxidation of guanine into 8-oxo 7,8-dihydroguanine purine photoproducts and single stranded breaks (reviewed by Ravanat *et al.*, 2001). However, UV lesions involving purines equate to <1% of UV-induced photolesions (Friedberg, 2006). The ratio of induction of 6-4PP:CPD is 1:3 in human and hamster cells (Mitchell, 1988; Van Hoffen *et al.*, 1995; Balajee *et al.*, 1999).

1.1.3 Cyclobutane pyrimidine dimers (CPDs)

CPDs possess a high mutagenic potential. This is attributed to the high level of induction, reduced repair capacity and increased bypass tolerance (Pfeifer *et al.*, 1997; Johnson *et al.*, 1999; Smith *et al.*, 1998). Although DNA polymerase η (POLH) correctly bypasses 5'-TT sequences, within a CPD, a high frequency of C to T transition mutations at dipyrimidine sites have been observed (Pfeifer *et al.*, 2005). Two models involving bypass tolerance have been implicated, which drive UV-induced mutagenesis. Firstly, it has been speculated that a lesion is bypassed by an alternative error-prone polymerase, which incorporates an adenine opposite a cytosine or 5-methylcytosine within the CPD. However, the precise polymerase involved in this mechanism remains elusive. Alternatively, the second model involves the initial deamination of a cytosine or 5-methylcytosine within a CPD. This is followed by the correct bypass during DNA replication. In concordance, recent studies have shown that the deamination model contributes significantly to UVB-induced mutagenesis (Lee

et al., 2003; Tu *et al.*, 1998). More recently, You *et al.* (2001) showed that CPDs induced by UVB irradiation, are responsible for 80% of mutations in a mouse cell line harbouring the transgenic mutation reporter genes, *LacI* and *CII*. Whether this frequency occurs at different loci in human cells remains to be seen.

CPDs are generated by the covalent interaction between two adjacent pyrimidine bases. The saturation of the C5-C6 double bonds results in the formation of a four-membered cyclobutyl ring (Fig. 1.1A). CPDs can form between adjacent T<>T, C<>T, T<>C, or C<>C residues with a ratio of 68:13:16:3 in plasmid DNA. A similar trend has been observed in irradiated human cells (Mitchell *et al.*, 1992; Tornaletti *et al.*, 1993). However, the distribution of CPDs between pyrimidines depends on UV wavelength, dose of irradiation and adjacent sequence (Gillet & Schärer, 2006). Most frequently, however, the formation of CPDs occurs between adjacent thymine residues (T<>T) in DNA. By contrast, the lowest yield of CPDs is generated between two adjacent cytosine (C<>C) residues. Theoretically, the formation of CPDs can occur in twelve structural configurations. However, only four isomeric forms with the configurations *cis-syn*, *cis-anti*, *trans-syn* or *trans-anti* are found in significant yields (Fig. 1.1B; Friedberg *et al.*, 2006). Interestingly, it was initially thought that CPDs are distributed randomly throughout the genome, and that the formation of CPDs between two adjacent thymine residues occurs with equal probability. However, the generation of CPDs is dependent upon sequence content (discussed further in Section 1.1.6).

1.1.4 Pyrimidine (6-4) pyrimidone (6-4PPs) photoproducts

Following UV radiation, 6-4PPs are primarily found between thymine and cytosine bases. Prior to the formation of 6-4PPs, however, cycloaddition occurs between the C5-C6 bond of a 5' prymidine residue and the C4 carbonyl group of an adjacent 3' thymine (or the 4-imino group of the 3' cytosine), resulting in the creation of an oxetane intermediate (Fig. 1.1C). The subsequent formation of 6-4PPs, occurs via spontaneous rearrangement of the oxetane intermediate, resulting in the linkage between C6 position of the 5' pyrimidine and C4 position

of the adjacent 3' pyrimidine (Fig. 1.1D). Further exposure to UVB can induce further structural modifications, resulting in the generation of Dewar isomers (Ravanat *et al.*, 2001; Fig. 1.1E). These isomers are derivatives of 6-4PPs, generated by the photoisomerisation of 6-4PPs, following exposure to wavelengths longer than 290 nm, which corresponds to the maximum absorption peak of 6-4PPs. However, the precise biological relevance of Dewar isomer formation in relation to mutagenesis and carcinogenesis in human cells remains poorly understood.

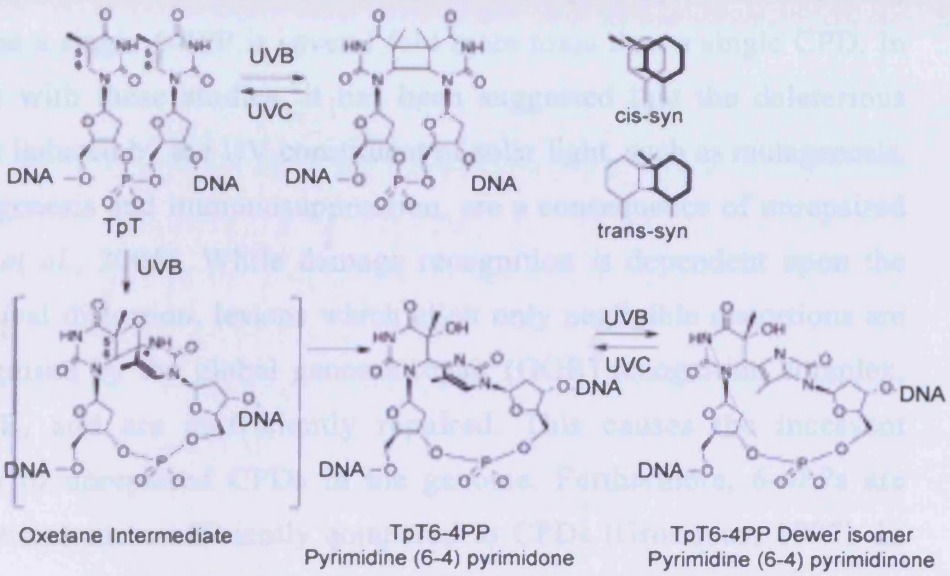

Figure 1.1. UV-induced photolesions of a TpT in DNA. (A) The structural formation of CPDs. (B) The different diastrereoisomers of the CPD within DNA. (C) Initial exposure of UV to two adjacent T residues, results in the formation of an oxetane intermediate. (D) Spontaneous rearrangement of the oxetane intermediate causes the formation of a 6-4PP. (E) Further UVB irradiation of the 6-4PP can lead to rearrangement of the 6-4PP, resulting in the formation of a Dewer isomer (adapted from Gillet & Scharer, 2006).

1.1.5 UV-induced damage and DNA structure

Both CPDs and 6-4PPs distort the structural configuration of DNA, inducing a bend of 7-9° and 44°, respectively (Friedberg *et al.*, 2006; Kim *et al.*, 1995). The formation of CPDs has a negligible effect on Watson-Crick base pairing. By contrast, the extensive distortion to the DNA backbone by 6-4PPs results in significant disruption to base pairing. So, although CPDs are the most prevalent and cytotoxic UV-induced lesion, 6-4PPs are potentially more mutagenic, as a result of increased helical distortion. In concordance, Nakajima *et al.* (2004) speculated that a single 6-4PP is several fold more toxic than a single CPD. In disagreement with these studies, it has been suggested that the deleterious consequences induced by the UV constituent of solar light, such as mutagenesis, photocarcinogenesis and immunosuppression, are a consequence of unrepaired CPDs (Jans *et al.*, 2005). While damage recognition is dependent upon the degree of helical distortion, lesions which elicit only negligible distortions are weakly recognised by the global genome repair (GGR) recognition complex, XPC-hHR23B, and are inefficiently repaired. This causes the incessant accumulation of unrepaired CPDs in the genome. Furthermore, 6-4PPs are removed 15 times more efficiently compared to CPDs (Grossman, 1997). In concordance, using liquid chromatography in combination with mass spectrometry, Courdavault *et al.* (2005), showed that CPDs are the most abundant and less efficiently repaired bipyrimidine photoproducts, irrespective of UV wavelength.

1.1.6 UV-induced damage and chromatin structure

The yield and distribution of CPDs and 6-4PPs is highly heterogeneous, and dependent upon DNA sequence, local DNA structure and the association between DNA and chromosomal proteins. Notably, the distribution of CPDs predominantly occurs at poly (dA.dT) tracts. Indeed, studies have implicated chromatin arrangement as having the most significant affect on photolesion formation in nucleosomes (Gale *et al.*, 1987; Pehrson, 1995). Interestingly, the interval between CPD distribution has been a periodicity of approximately 10.3

bps (Gale *et al.*, 1987). This suggests that CPD formation reflects the structural organisation of a nucleosomal unit. Furthermore, the formation of CPDs appears to preferentially occur at sites where the minor groove is positioned away from the core histone surface (Gale *et al.*, 1987; Pehrson, 1995). In contrast, 6-4PPs are dispersed randomly within nucleosome cores and preferentially in linker DNA nucleosome free regions of chromatin (Gale & Smerdon, 1990; Mitchell *et al.*, 1990).

1.1.7 A molecular model: the role of CPDs and 6-4PPs in UV-induced mutagenesis and photocarcinogenesis

The transition from a normal cell to a cancerous cell is a highly intricate and sequential process involving a multiplicity of genetic and epigenetic modifications, resulting in the emergence of clones with a selective growth advantage. Under normal physiological conditions, following UV exposure, epidermal keratinocytes containing unrepaired UV-induced lesions are removed by apoptosis. However, continued exposure to UV results in the accumulation of DNA damage and the initiation of photocarcinogenesis (reviewed by Melnikova & Ananthaswamy, 2005). This is attributed to the failure of DNA repair mechanisms to eliminate cells containing DNA damage. UV-induced lesions that are not repaired before DNA replication can generate mutations in cancer-associated genes, such as tumour suppressors and oncogenes. Although mutations in the tumour protein 53 (*TP53*) gene is a well-characterised prerequisite for the progression of cutaneous tumours, the precise molecular and cellular events remains poorly delineated. However, recent studies have implicated the activation of proto-oncogens such as *ras* and the inactivation of additional tumour suppressor genes, such as *PTCH* and *INK4a-ARF*, in the photocarcinogenic process (reviewed by Melnikova & Ananthaswamy, 2005).

A hallmark of UVC- and UVB-induced mutagenesis is a high frequency of transition mutations at dipyrimidine sequences containing cytosine. Approximately 35% of mutations identified in cutaneous malignancies occur as a result of transition mutations at dipyrimidines within the sequence 5'-TCG and

5'-CCG in the *TP53* gene (Pfeifer *et al.*, 2005). Interestingly, Tornaletti & Pfeifer (1994) also showed an association between *TP53* mutation hotspots and the slow removal of UV-induced CPDs in cutaneous malignancy. Indeed, based on the mutations observed in human premalignant actinic keratosis (AK) lesions and data from UV-induced carcinogenesis studies in mice, mutations in the *TP53* gene in epidermal keratinocytes is thought to promote the initiating event in skin tumorigenesis (Ziegler *et al.*, 1994; Brash *et al.*, 1996; Leffell & Brash, 1996). In concordance, Jiang *et al.* (1999) showed the rapid progression of UV-induced cutaneous tumours in $p53^{-/-}$ and $p53^{+/-}$ mice compared to wild-type mice.

Continued exposure to UV promotes dysregulation of the apoptotic pathway, causing aberrant proliferation and clonal expansion of premalignant apoptotic-resistant clones, possessing DNA damage, accumulated *TP53* gene mutations and the abolition of Fas-Fas ligand interaction. Repeated UV exposure facilitates further expansion of clones possessing additional UV-induced mutations in further genes, resulting in the inactivation of tumour suppressor genes or the activation of oncogenes. This ultimately results in the transition from a preneoplastic lesion, AK, to a carcinoma, such as SCC (Fig. 1.2).

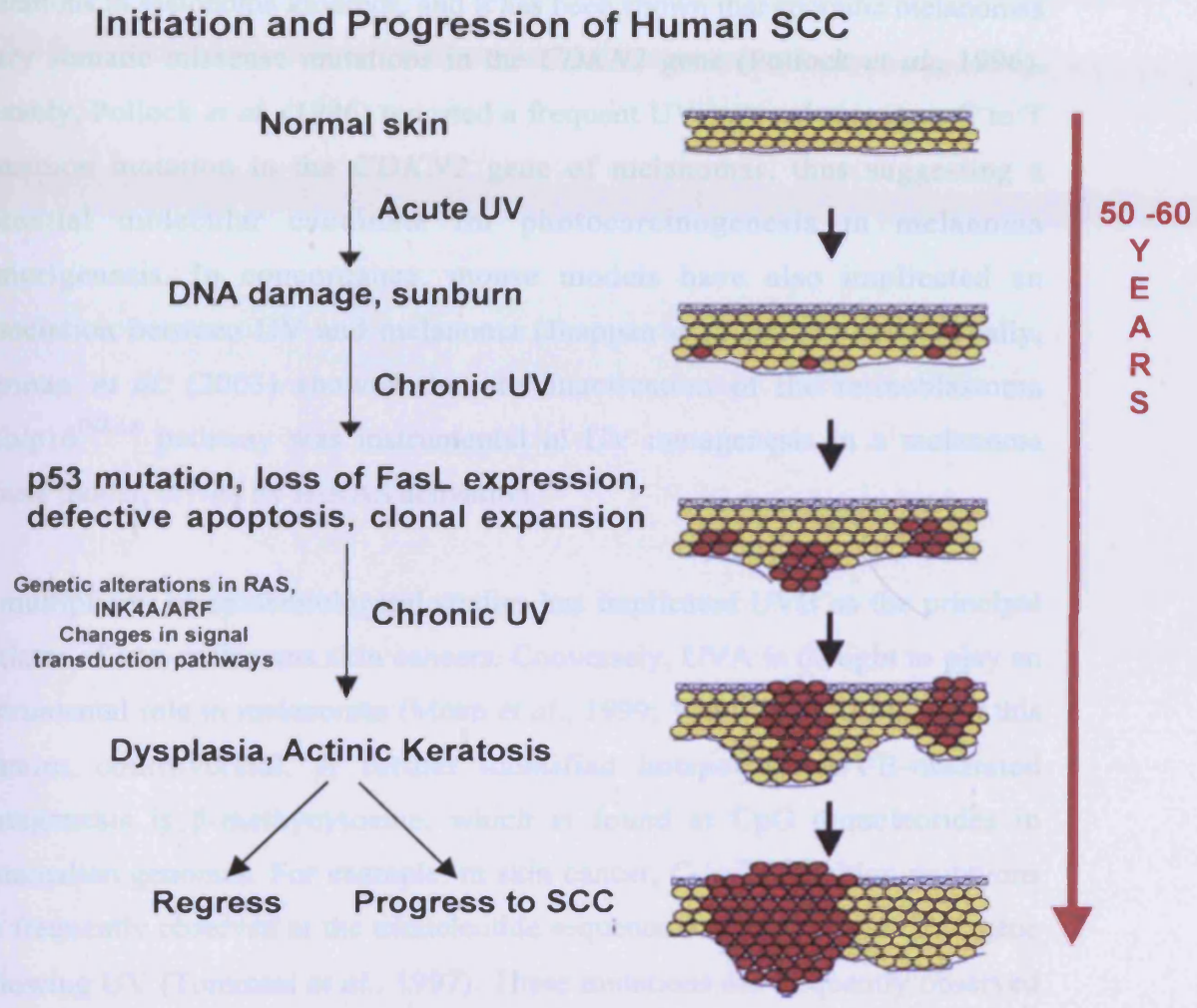

Figure 1.2. A model for UV-induced initiation and progression for SCC. Generation of DNA photoproducts by UVB and defects in DNA repair and re replication leads to the accumulation of mutations in the *TP53* tumour suppressor gene in keratinocytes, loss of Fas ligand expression and apoptosis resistance. After repeated exposure to UV, *TP53*-mutant cells undergo clonal expansion and accumulate mutations in other key genes such as $p16^{INK4A}$. Clones form preneoplastic lesions (actinic keratosis), and some of them progress into SCC (adapted from Melnikova & Ananthaswamy, 2005).

Although the relationship between UVB and non-melanoma cutaneous malignancies has been well documented (Kraemer, 1997; de Gruijl, 1999), the association between UV and the molecular targets in malignant melanoma remains poorly understood (Houghton & Polsky, 2002). Kamb *et al.* (1994) speculated that the *CDKN2* ($p16^{INK4A}$) tumour suppressor gene carries germ line mutations in melonoma kindreds, and it has been shown that sporadic melanomas carry somatic missense mutations in the *CDKN2* gene (Pollock *et al.*, 1996). Notably, Pollock *et al.* (1996) reported a frequent UV-induced signature C to T transition mutation in the *CDKN2* gene of melanomas, thus suggesting a potential molecular candidate for photocarcinogenesis in melanoma tumorigenesis. In concordance, mouse models have also implicated an association between UV and melanoma (Jhappan *et al.*, 2003). Additionally, Kannan *et al.* (2003) showed that the inactivation of the retinoblastoma pRb/$p16^{INK4A}$ pathway was instrumental in UV mutagenesis in a melanoma mouse model, driven by H-RAS activation.

A multiplicity of epidemiological studies has implicated UVB as the principal initiator of non-melanoma skin cancers. Conversely, UVA is thought to play an instrumental role in melanomas (Moan *et al.*, 1999; Wang *et al.*, 2001), but this remains controversial. A further identified hotspot for UVB-mediated mutagenesis is 5-methycytosine, which is found at CpG dinucleotides in mammalian genomes. For example, in skin cancer, C to T transition mutations are frequently observed at the trinucleotide sequence 5'-PyCG in the *TP53* gene following UV (Tommasi *et al.*, 1997). These mutations are frequently observed in the skin tumours of individuals with the UV sensitive syndrome, xeroderma pigmentosum (XP; Giglia-Mari & Sarasin, 2003).

1.2 UV exposure: The cellular response

Normal human skin provides a protective biological barrier against a multiplicity of exogenous stresses, including UV. Following exposure to UV, a series of primary cellular responses are elicited by the skin, such as induction of melanin pigmentation, immunomodulation and endocrine modulation, which is coupled

with vitamin D and neuropeptide synthesis (reviewed by Slominski & Pawelek, 1998; Slominski & Wortsman, 2000). The skin is regarded as a peripheral neuroendocrine organ, which elicits a multiplicity of defence mechanisms via a network of intracellular pathways; these are orchestrated by the local neuroendocrine-immune system (reviewed by Slominski & Wortsman, 2000). These intricate cellular responses require the co-ordinated regulation of hormones, neurotransmitters, neuropeptides, cytokines and their receptors. Consequently, it is essential that the expression of the respective network of genes regulating these pathways is hierarchical, coordinated and highly organised (Pisarchik *et al.*, 2004).

Despite these protective cellular responses, it has been estimated that acute exposure to the UV component of sunlight at a biologically relevant dose can induce approximately 100,000 CPDs per epidermal keratinocyte (Ichihashi *et al.*, 2003) and 40,000 damaged sites in exposed cells in the human epidermis in 1 hour, resulting from the absorption of UV (200-300 nm) radiation by DNA (Ura & Hayes, 2002). This can cause erythema, tanning and localised or systemic immuno-suppression. Continued exposure to UV, however, will have greater deleterious consequences, including premature aging and carcinogenesis, resulting from the accumulation of genetic modifications (as previously discussed). These molecular alterations facilitate selective growth and clonal expansion of cells with a mutator phenotype, which will ultimately promote tumorigenesis, resulting in the aggressive progression of UV-induced cutaneous malignancies, which are the most prevalent cancers in Caucasians (Kraemer *et al.*, 1997). In the UK, over 65,400 cases of non-melanoma skin cancers are diagnosed each year making it the most prevalent type of cancer. BCC is the most common type of skin cancer accounting for approximately 75% of all reported non-melanoma skin cancers, whereas SCC account for 20% of all non-melanoma skin cancers in the UK. Approximately 8,000 new cases of malignant melanoma are reported every year, which accounts for 3% of all reported cancers (http://www.cancerresearchuk.org).

1.3 DNA repair mechanisms

Mammalian cells possess an intricate network of DNA repair mechanisms, which function to reduce the detrimental effects of DNA damage, thereby preserving genome stability and reducing tumorigenesis. Approximately 130 human DNA repair genes have been cloned and sequenced (Ronen & Glickman, 2001; Wood *et al.*, 2001). These genes orchestrate cell signalling and the mechanistic functioning of distinct DNA repair mechanisms, including: nucleotide excision repair (NER), base excision repair (BER), mismatch repair (MMR) homologous recombination (HR) and non-homologous end joining (NHEJ; reviewed by Christmann *et al.*, 2003). However, the commencement of DNA repair also activates a series of DNA damage checkpoints to delay or arrest cell cycle progression.

1.3.1 Nucleotide excision repair (NER): genetic and structural characterisation of core repair factors in humans

Both prokaryotic and eukaryotic organisms adopt analogous NER repair factors and mechanistic strategies to eliminate and repair DNA lesions. NER repair genes in a multitude of organisms, such as bacteria, yeast, human and mouse have been identified. Furthermore, the advent of modern recombinant DNA techniques and *in vitro* reconstitution assays has resulted in the biochemical and functional characterisation of the corresponding NER proteins.

Over the past forty years, numerous experimental strategies have been exploited in the cloning of DNA repair genes. These methodologies have been based on: (1) the complementation of mutant rodent cells with human genomic DNA; (2) the transfection of cDNA libraries into human or rodent cells; (3) the transfection of microbial mutants with human cDNA; (4) antibody screening of bacterial expression libraries (5) degenerate primers based on peptide sequence; (6) library screening using homology-based probes; (7) homology comparison combined

with database analysis; (8) positional mapping strategies; (9) the yeast two-hybrid system; (10) protein interactions in mammalian cells.

The isolation of genes inactivated in human cells and subsequent assignment to the different XP groups was in part achieved on the basis of functional complementation, using mutant Chinese hamster ovary (CHO) cells that possess gene defects analogous to XP cells (Thompson, 1998; Bootsma, 2001). Like human XP cells, CHO cells were assigned to excision repair cross-complementation (*ERCC*) groups (Busch *et al.*, 1989) and, utilising recombinant DNA methodologies, were screened with libraries of human DNA fragments. This resulted in the identification of human DNA sequences, which causes UV survival in CHO cells previously exhibiting severe UV sensitivity. This technology facilitated the identification and cloning of the first *ERCC* human genes: *ERCC1* (Westerveld & Hoeijmakers, 1984), *ERCC2* (Weber *et al.*, 1888), *ERCC3* (Weeda *et al.*, 1990a), *ERCC4* (Thompson *et al.*, 1994) and *ERCC6* (Troelstra *et al.*, 1990). These were found to correct the corresponding UV-sensitive CHO cells complementation groups. Further analysis revealed that *ERCC2*, *ERCC3*, *ERCC4* and *ERCC6* complemented the human cells assigned to XP-D, XP-B, XP-F and CS-B complementation groups respectively. However, the first cloned DNA repair gene, *ERCC1*, failed to correct the UV sensitivity in any known XP complementation group, and for this reason retained its rodent name.

Alternative methods have been used to identify DNA repair genes. For example, the direct complementation of human cells is illustrated by the identification of the *XPA* gene, which was identified following large-scale screening of XP-A cells transfected with mouse genomic libraries (Tanaka, *et al.*, 1989; Tanaka *et al.*, 1990). Conversely, both *XPC* and *CSA* genes were identified by direct cloning from human cells, using episomally replicating plasmids containing viral replication systems and human cDNA libraries (Legerski & Peterson, 1992; Henning *et al.*, 1995). Genes such as *XPG* (MacInnes *et al.*, 1993; Scherly *et al.*, 1993), *XPF* (Sijbers *et al.*, 1996; Brookman *et al.*, 1996), *hHR23B* (Masutani *et al.*, 1994), and the more recently identified *TTDA* (Giglia-Mari *et al.*, 2004) were identified serendipitously or through sequence homology with repair genes

cloned in other organisms. The cloning of *XPG* was cloned by chance and was found to be equivalent to *ERCC5* (O'Donovan & Wood, 1993). Some investigators have adopted a reverse approach, whereby purification of the protein was achieved first. Subsequent microsequencing facilitated the generation of DNA primers, which resulted in the cloning of the corresponding gene by PCR amplification. This method was used for the identification of the DDB protein, which was initially elucidated as a DNA damage binding (DDB) factor absent in XP-E cells (Chu & Chang, 1988; Dualan *et al.*, 1995; Takao *et al.*, 1993). This technique was also adopted for the XPC protein, which was isolated by fractionation of cell extracts used to complement the activity XP-C cell extracts (Masutani *et al.*, 1994).

1.3.1.1 XPA

The human *XPA* gene was cloned through the complementation of UV sensitive XP-A cells; following transfection with total mouse genomic DNA (Tanaka *et al.*, 1989; Tanaka *et al.*, 1990). Cells lacking XPA protein exhibit no residual NER activity (Tanaka *et al.*, 1990). The *XPA* gene encodes a 273 amino acid 31 kDa protein. However, the separation of XPA on polyacrylamide gels most frequently results in the detection of multiple bands between 40-45 kDa. These additional bands do not correspond to posttranslational modifications, but occurs due to the formation of different denatured conformations. The initial indication that exogenous proteins can translocate into the nucleus of XP cells and correct their phenotype was first shown in XP-A and XP-C with cytoblasts from different repair-proficient cells (Giannelli *et al.*, 1982; Keijzer *et al.*, 1982).

XPA possesses a zinc finger motif, a nuclear localisation signal and four further domains, which facilitate the formation of protein-protein interactions with proteins of the NER machinery, such as transcription factor II H (TFIIH), ERCC1 and replication protein A (RPA; discussed in Section 1.6.4).

1.3.1.2 XPB (ERCC3)

The human *XPB* gene was cloned by complementation of the UV radiation sensitivity of cells derived from RGCG3 (Weeda *et al.*, 1990a). Mutational analysis of XP-B cells showed that *ERCC3* and *XPB* are synonymous (Vermeulen *et al.*, 1994; Weeda *et al.*, 1990b). *XPB* cDNA possesses an open reading frame (ORF) of 782 codons that encodes a protein of 89.2 kDa. Like XPD, the amino acid sequence shows that the XPB protein is a DNA helicase. XPB is a constituent of TFIIH (Schaeffer *et al.*, 1993) that has ATP-dependent DNA helicase activity with a 3'→5' polarity (Drapkin *et al.*, 1994; Ma *et al.*, 1994).

1.3.1.3 XPC-hHR23B

Legerski & Peterson (1992) characterised the molecular defect in human XP-C defective cells and isolated a partial *XPC*-complementing cDNA sequence. The subsequent cloning of the *XPC* cDNA was undertaken by the purification of the a 93 kDa XPC-complementing protein, derivation of partial amino acid sequence and the construction of DNA probes based on the amino acid sequence (Masutani *et al*, 1994). The *XPC* gene is located on chromosome 3p25, and the complete *XPC* ORF encodes a hydrophilic 940 amino acid polypeptide with an electrophoretic mobility of ca. 125 kDa (Masutani *et al.*, 1994).

Purification of the XPC protein resulted in the copurification of a further polypeptide of ca. 58 kDa, known as hHR23B (Masutani *et al.*, 1994). This polypeptide is a highly conserved ortholog of the yeast RAD23B protein. Humans contain a second ortholog, RAD23A (HR23A). Both the hHR23A and hHR23B proteins contain ubiquitin-like (UbL) and ubiqutin-associated (UbA) domains. Furthermore, one or more conserved regions in hHR23A and hHR23B are required for interactions with the C-terminal region of XP-C (Li *et al.*, 1997; Masutani *et al.*, 1997). In a reconstituted reaction, recombinant XPC protein displays weak NER efficiency without either hHR23 polypeptide. However, inclusion of the hHR23B protein stimulates NER (Sugasawa *et al.*, 1996).

Furthermore, although recombinant hHR23A or hHR23B can bind to XPC, the hHR23B protein is most often associated with XPC (Sugasawa *et al.*, 1997).

1.3.1.4 XPD (ERCC2)

The *XPD* gene was cloned from a cosmid that only corrects the cellular phenotype of CHO mutants derived from RGCG2 (Weber *et al.*, 1990). The *XPD* gene encodes a protein of 760 amino acids with a size of 87 kDa. Like *XPB*, the *XPD* gene product contains a DNA-dependent ATPase with DNA helicase activity (Sung *et al.*, 1993). XPD is an essential constituent of the TFIIH complex (Schaeffer *et al.*, 1994). This is exemplified in mice, as deletion of XPD results in embryonic lethality (de Boer *et al.*, 1998).

1.3.1.5 DNA damage-binding protein (DDB) complex (XPE)

DDB also referred to as UV-DDB was identified using electrophoretic mobility shift or filter-binding assays. The purification of DDB resulted in the detection of a heterodimer consisting of a 127 kDa subunit known as DDB1 and a 48 kDa subunit called DDB2 (Keeney *et al.*, 1993). Microinjection of purified DDB complex into XP-E cells results in the restoration of NER activity (Keeney *et al.*, 1994; Rapic-Otrin *et al.*, 1998). The *DDB* genes encoding both the DDB1 and DDB2 subunits were identified by Dualan *et al.* (1995) as previously discussed.

1.3.1.6 XPF (ERCC4)

The *XPF* gene was cloned by functional correction of a rodent cell line derived from RGCG4 (Brookman *et al.*, 1996). The *XPF* ORF encodes a 916 amino acid polypeptide with a molecular mass of 104 kDa.

1.3.1.7 ERCC1

The human *ERCC1* cDNA encodes a polypeptide of 297 amino acids with a molecular mass of 32.5 kDa (van Duin *et al.*, 1986), and complements the sensitivity of RGCG1 cells. The human *ERCC1* gene does not complement the UV sensitivity of cell lines derived from patients with the XP syndrome that are defective in NER (van Duin *et al.*, 1989). Early investigations showed that ERCC1 and XP-F mutant cell extracts did not complement one another for DNA repair when mixed *in vitro* (Biggerstaff *et al.*, 1993; van Vuuren *et al.*, 1993). The ERCC1 and XPF NER factors were shown to be part of a heterodimeric complex in human cells (Brookman *et al.*, 1996; Sijbers *et al.*, 1996). XPF-ERCC1 exhibits structure-specific nuclease activity, as it can cut DNA at junctions between a duplex and a single strand in a 5' to 3' direction (de Laat *et al.*, 1998a; Sijbers *et al.*, 1996).

1.3.1.8 XPG (ERCC5)

Somatic cell analysis showed that human chromosome 13q contained a gene capable of correcting the UV radiation sensitivity in cells derived from RGCG5 (Thompson *et al.*, 1987). Previous to these findings, MacInnes *et al.* (1984) showed that transfection of human genomic DNA corrected this phenotype in a group of 5 known mutants. However, the correcting activity was initially isolated as two overlapping cosmids that generated a functional 32 kb *ERCC5* gene only by intercosmid recombination (Mudgett & MacInnes, 1990). The human *XPG* cDNA was found to correct the UV radiation sensitivity of cells from individuals with XP-G (Scherly *et al.*, 1993). Furthermore, complementation of NER activity was absent when extracts of human XP-G and RGCG5 cells were combined (O'Donovan & Wood, 1993; Reardon *et al.*, 1993b). The isolation of the *ERCC5* cDNA (MacInnes *et al.*, 1993; Shiomi *et al.*, 1994), and *in situ* mapping of *XPG* cDNA to chromosome 13q33 (Samec *et al.*, 1994) to the same site that the *ERCC5* gene was mapped (Takahashi *et al.*, 1992) provided further evidence that *ERCC5* and *XPG* are identical.

XPG has an ORF of 1,186 codons, which encodes a polypeptide of 133 kDa. The amino acid sequence contains several possible nuclear localisation signals. Furthermore, XPG protein possesses endonuclease activity that cleaves several DNA structures containing junctions between unpaired and duplex DNA, cutting the strand in a 3'→5' polarity away from the junction (Cloud *et al.*, 1995; Evans *et al.*, 1997a; O'Donavan *et al.*, 1994).

1.3.1.9 CSA (ERCC8)

The human *CSA* (Cockayne syndrome type A) gene was originally cloned by functional complementation of the UV sensitivity of a *CSA* mutant cell line (Henning *et al.*, 1995). The *CSA* gene also corrects the UV sensitivity in the rodent cell line, US31. Furthermore, the defect is not corrected following fusion with CS-A cells after UV (Itoh *et al.*, 1996). *CSA* is located on chromosome 5 and encodes a 396 amino acid repeat protein that has a molecular weight of 44 kDa (Henning *et al.*, 1995). Investigations using the two-hybrid protein-protein interaction method found that the human CSA and CSB proteins form interactions and that CSA further binds with p44, a subunit of the TFIIH complex (Henning *et al.*, 1995). In contrast, cell fractionation studies found that CSA and CSB are present in separate multiprotein complexes (van Gool *et al.*, 1997). These conflicting findings have been attributed to the fact that CSA protein resides in the cytoplasm, but translocates to the nucleus following UV irradiation (Kamiuchi *et al.*, 2002).

1.3.1.10 CSB (ERCC6)

The *ERCC6* gene was originally identified by virtue of its ability to correct the UV sensitivity phenotype in rodent cells from the genetic complementation group 6. It was subsequently shown that *ERCC6* corrects the UV sensitivity observed in CS-B cells (Troelstra *et al.*, 1992), thus *ERCC6* was reassigned as *CSB*. The *CSB* gene also corrects the phenotype of defective transcription-coupled repair (TCR) in the CHO cell line, UV61 (Orren *et al.*, 1996). The *CSB* gene encodes a polypeptide of 168 kDa (Orren *et al.*, 1996). A noticeable

characteristic of the predicted amino acid sequence is the presence of an ATPase-helicase motif that is common to the SWI2/SNF2 ATPase superfamily (Orren *et al.*, 1996), which is frequently associated with chromatin remodelling. Although the CSB protein possesses consensus domains that are common to many DNA helicases, this activity has not been observed in the CSB protein (Citterio *et al.*, 1998; Licht *et al.*, 2003; Selby & Sancar, 1997b). However, Licht *et al.* (2003) reported the disruption of the RNA polymerase II (RNA Pol II) transcription complex by CSB. Significant homology has been observed between CSB and the *Escherichia coli* (*E.coli*) transcription-repair coupling factor (Selby & Sancar, 1993). The ATPase activity of CSB is stimulated by DNA (Selby & Sancar, 1997b; Tantin *et al.*, 1997). Moreover, the ATPase activity is more active when stimulated by double-stranded than single-stranded DNA. Interestingly, site-directed mutagenesis of highly conserved amino acid residues in the ATP-binding domain of the CSB protein results in the inactivation of the ATPase activity (Citterio *et al.*, 1998), which has also been shown to abolish the ability of CSB protein to correct the mutant phenotype displayed by CSB cells (Licht *et al.*, 2003). It is thought that the ATPase activity of CSB plays a role in chromatin remodelling during transcription and/or TCR. Citterio *et al.* (2000) showed that CSB alters the conformation of nucleosomes reconstituted on plasmid DNA in an ATP-dependent manner. They also found that CSB interacts with core histones.

1.3.1.11 XPA binding protein (XAB2)

The *XAB2* gene was first identified in a yeast two-hybrid screen for proteins that interact with XPA (Nakatsu *et al.*, 2000). The *XAB2* gene encodes an 855 amino acid protein, which is characterised by 15 tetratricopeptide repeat motifs (Nakatsu *et al.*, 2000). Furthermore, the XAB2 protein has been found to interact with CSA, CSB and RNA Pol II. Attempts to generate a mouse model defective in Xab2 has resulted in embryonic lethality, suggesting that the gene is indispensable (Nakatsu *et al.*, 2000).

1.4 Mechanistic action of NER in humans

NER is a ubiquitous and highly versatile mechanism, which has remained conserved between species, such as bacteria, yeast and mammalian cells. However, the repertoire of enzyme and protein constituents utilised during NER structurally and functionally differs between prokaryotic and eukaryotic organisms and exhibit minimal homology (Eisen & Hanawalt, 1999; Petit & Sancar, 1999; Zou & van Houten, 1999). NER orchestrates the elimination and repair of an array of structurally unrelated bulky DNA lesions, which induce helical distortions and modify DNA chemistry. These lesions are induced by a multiplicity of exogenous and endogenous sources of DNA damage, such as UV-induced photoproducts, electrophilic chemicals, adducts induced by polycyclic carcinogens (such as cisplatin and psoralens), crosslinks and oxidised bases. Additionally, previous *in vitro* studies have shown that NER can mediate the removal of lesions, which cause significantly less helical distortion, including AP sites and thymine glycols (Sancar, 1996; Reardon *et al.*, 1997).

Principally, NER orchestrates the removal of UV-induced photolesions, such as CPDs, 6-4PPs and Dewar valence isoforms. The initial discovery of NER in *E.coli* (Setlow & Carrier, 1964; Boyce & Howard-Flanders, 1964) provided a paradigm for the subsequent identification of NER in eukaryotes (Cleaver, 1968; Cleaver, 1969; Setlow *et al.*, 1969). This resulted in the serendipitous association between defective NER and the human hereditary, cancer prone, photosensitive syndrome, XP (Cleaver, 1968; Cleaver, 1969).

When operating on damage in naked DNA, approximately 30 polypeptides are required to orchestrate the six sequential mechanistic steps in NER (Aboussekhra *et al.*, 1995): (i) damage recognition; (ii) unwinding and formation of the preincision complex; (iii) stabilisation of the pre incision complex; (iv) bimodal incision and excision of an oligonucleotide fragment; (v) polymerisation by repair synthesis, using the complementary undamaged strand as a template; (vi) ligation of the remaining single-stranded nick. The intricate recruitment,

assembly and disassembly of the NER machinery is completed within ~4 minutes in human cells (Hoogstraten *et al.*, 2002).

The efficiency of NER varies throughout the entire genome, depending upon both the structural nature and precise location of the lesion. In particular, it has been previously shown that the repair rate of α-DNA is significantly impaired compared to the entire genome. This has been attributed to the complex chromatin structure in the repetitive centromeric DNA sequences and the presence of a multitude of DNA binding proteins (Zolan *et al.*, 1982; Cline & Hanawalt, 2003).

The most intricate rate-limiting mechanistic step in the NER pathway is the initial recognition of UV-induced photolesions. This is attributed to the differences in the complexity of chromatin structure in the transcribed and non-transcribed regions of the genome, and the requirement for different specific proteins.

Previous analysis of the repair of CPDs in transcriptionally active regions, compared to transcriptionally silent regions of the genome, and between the transcribed and non-transcribed strand of constitutively expressed genes, through the utilisation of strand-specific DNA repair assays (Bohr *et al.*, 1985; Mellon *et al.*, 1987; Mellon & Hanawalt, 1989; van Hoffen *et al.*, 1993), resulted in the discovery of two partially distinct mechanistic NER pathways. NER is subdivided into two overlapping recognition subpathways: global genome repair (GGR) and TCR. GGR is initiated by the recognition of UV-induced helical distorting lesions on the nontranscribed strand of transcriptionally active genes and transcriptionally silent regions of the genome. In contrast, TCR exclusively operates on the transcribed strand of transcriptionally active genes, probably following the recognition of an arrested RNA Pol II at a stalled transcription complex (Mellon & Hanawalt, 1989). Most importantly, following initial recognition of DNA damage *per se*, or the recognition of an arrested RNA Pol II, both GGR and TCR converge at a common node.

Differences in the dynamics of NER are observed between GGR and TCR. The temporal differences in lesion removal throughout the genome were explained by the preferential removal of lesions from the transcribed strand of transcriptionally active genes, by TCR, compared to the slower removal and repair of lesions by GGR in the remaining regions of the genome, including the nontranscribed strand of transcriptionally active genes (Hanawalt, 2002). Furthermore, the dynamics of lesion demarcation and repair by GGR is dependent upon the nature of the lesion. For instance, 6-4 PPs, which induce major structural distortions in the double helix compared to CPDs (Kim *et al.*, 1995), are eliminated five- to ten-fold faster than CPDs (Tornaletti & Hanawalt, 1999), while the latter are more prevalent in the genome, following UV irradiation (Mitchell *et al.*, 1989). It has been estimated that the NER apparatus removes CPDs at a rate of only 10-20% that of the removal of 6-4PPs (Ford & Hanawalt, 1997; Reardon & Sancar, 2003). However, it should be noted that repair rates of CPDs can vary enormously depending on sequence and chromatin.

1.5 Chromatin remodelling and NER in humans

The human genome is systematically organised in chromatin structures, which are further condensed and packaged into chromosomes. The spatial organisation of the genome operates at several levels of complexity. The genome is principally organised into linear chromosomes, which are packaged within the nucleus. In addition, the structural integrity of chromosomes is maintained by a series of structural constituents, such as centromeres, telomeres and repetitive DNA sequence. The second level of chromatin organisation necessitates the association between DNA and histone proteins. The structural composition of chromatin includes a nucleosomal core, which consists of approximately 147 bp of DNA wrapped around a histone octamer composed of H2A, H2B, H3 and H4 histone proteins. In addition, linker DNA binds two nucleosomes together via histones H1 & H5, which stabilises nucleosomal structures, thus further condensing the chromatin and reducing the accessibility to regulatory factors involved in DNA metabolism. Therefore, the *in vivo* initiation of processes of DNA metabolism, such as replication, recombination, transcription or repair,

necessitates decondensation of chromatin and chromatin re-modelling to permit chromatin relaxation, thereby increasing the accessibility to factors essential to these DNA metabolising processes. The final level of genome organisation is the three dimensional topology within the nucleus (reviewed by Reed, 2005).

A preliminary investigation by Smerdon & Lieberman (1978), showed an increase in the accessibility of nucleases to damaged DNA, during UV-induced repair synthesis. This indicated that highly condensed chromatin underwent significant nucleosomal rearrangement, in response to UV, thus permitting access of the entire repair apparatus to damaged sites. This led to the postulation of the 'access, repair, restore' (ARR) model for NER repair (Smerdon, 1991). In concordance, a battery of *in vitro* NER assays, using purified proteins and cell extracts, has shown that the repair rates of DNA damage is significantly compromised in nucleosomal structures compared to naked DNA, thus reiterating the importance of chromatin remodelling in NER (Araki *et al.*, 2000; Hara *et al.*, 2000; Sugasawa *et al.*, 1993; Ura *et al.*, 2001; Wang & Taylor, 1991).

Chromatin re-modelling occurs via two essential processes: (1) posttranslational modification of histone tails and (2) ATP-dependent chromatin re-modelling. Histone tails can undergo a multiplicity of modifications, such as methylation, acetylation, phosphorylation and ubiquitylation. In particular, histone acetylation has been detected subsequent to UV irradiation (Ramanathan & Smerdon, 1986). Furthermore, hyperacetylation of histones by inhibiting histone deacetylases (HDACs) augments the repair of UV-induced lesions (Dresler, 1985; Ramanathan & Smerdon, 1989; Smerdon *et al.*, 1982). A battery of histone acetyltransferases (HAT) have been implicated as accessibility factors during NER: STAGA (SPT3, $TAF_{II}31$-GCN5l acetylase), TFTC (TBP-free TAF_{II} complex) and p300 (reviewed in Gillet & Schärer, 2006). ATP-dependent chromatin remodelling has also been implicated in NER. A recent *in vitro* study has shown that the ATP-utilising chromatin assembly and re-modelling factor (ACF) enhances the removal of 6-4PPs from the linker DNA between two nuclosomes (Ura *et al.*, 2001). This suggests that ACF is a potential requisite for

histone octamer sliding, thereby increasing the accessibility to the lesion situated within the linker regions (Ura *et al.*, 2001).

Significant controversy, however, surrounds the precise mechanistic steps involved in chromatin remodelling prior to the initiation of NER, as both histone modifying enzymes and ATP-dependent chromatin remodelling factors do not possess a specific binding affinity for lesions located in nucleosomal DNA. It has been speculated, however, that NER factors play an instrumental role in chromatin accessibility. In particular, DDB1 has been isolated in several complexes involved in histone acetylation (as previously described): p300, STAGA or TFTC (reviewed by Gillet & Schärer, 2006). It was recently speculated that p53 acts as a global relaxer of chromatin through the activation of p300, which mediates the hyperacetylation of histones. This hyperacetylation of histones was proposed to elicit the initiation of GGR, but this maybe a considerable over interpretation (Rubbi *et al.*, 2003). Although the body of evidence implicates the DDB complex as the linking between NER and chromatin remodelling, *in vivo* evidence for this remains unreported. Furthermore, a paradox between damage recognition and chromatin remodelling becomes apparent, as the remodelling of chromatin is essential for the recognition of damage, while DNA damage recognition is a prerequisite for chromatin remodelling (reviewed by Gillet & Schärer, 2006).

Following the completion of NER, further chromatin remodelling is essential for the repositioning of nucleosomal structures, thus facilitating the restoration of chromatin structure to its original state (Gontijo *et al.*, 2003). The repositioning of core histones protects the repaired DNA patches from nuclease digestion within 20 minutes of the completion of NER. However, this immediate protection is followed by an extended period (1-24 hours) of nuclease sensitivity, which corresponds with the slow nucleosomal repositioning at exposed sites, containing newly synthesised DNA (Smerdon & Conconi, 1999). Numerous studies have implicated that the mechanistic function of chromatin assembly factor 1 (CAF-1) is essential in the reassembly of chromatin following NER (Gaillard *et al.*, 1996; Gaillard *et al.*, 1997; Moggs *et al.*, 1999).

1.6 Sequential assembly of the NER apparatus

In human cells, the sequential formation of the NER machinery necessitates a minimal set of protein constituents: XPA, XPC-hHR23B, XPG, RPA, ERCC1-XPF, TFIIH, proliferating cell nuclear antigen (PCNA), replication factor C (RCF), DNA polymerases δ or ε, and DNA ligase III (Fig. 1.3; Araujo *et al.*, 2000). These components are further divided into two mechanistic groups; the six core components required for the recognition and dual incision (hHR23B-XPC, RPA, XPA, XPG, ERCC1-XPF and TFIIH) and those required for repair synthesis and ligation (PCNA, RCF, DNA polymerase δ or ε, and DNA ligase III).

Following the initial *in vitro* reconstitution of the NER apparatus (Aboussekhra *et al.*, 1995), controversy surrounded the precise assembly of the NER machinery. Numerous models have been postulated for the recruitment of the NER apparatus and subsequent formation of a repair complex at the site of damage. Principally, two contrasting models have been proposed: (1) the existence of a pre-assembled repairosome complex; (2) the sequential assembly of repair factors at the lesion site. Initial yeast studies suggested that a pre-assembled repairosome complex was a prerequisite for proficient NER (Svejstrup *et al.*, 1995). However, Thoma & Vasquez (2003) has approximated that the assembled mammalian NER machinery has a mass of ~3 MDa. Therefore, the preassembled repairosome model presents numerous caveats, such as its large size and reduced mobility, thus making nuclear translocation problematic. Alternatively, from subsequent mammalian cell studies, Maldonado *et al.* (1996) speculated that the NER apparatus was a constituent of the RNA Pol II holoenzyme. Following further yeast studies, however, it has been widely accepted that the individual protein constituents of the NER apparatus undergo nuclear translocation and are sequestered to the site of damage, whereby they sequentially assemble to form a pre-incision complex (Guzder *et al.*, 1995). In concordance with these findings, Volker *et al.* (2001) showed no evidence for the existence of a pre-assembled repairosome complex, and favoured the sequential assembly of the NER machinery.

1.6.1 Global genome repair (GGR): damage recognition by XPC-hHR23B and the DDB complex

The recognition mechanisms involved in NER are highly intricate, necessitating systematic and complex interactions between a multitude of repair factors. To date, numerous models have been suggested for the initial recognition of UV-induced lesions in GGR, which involve the initial recruitment of several potential NER proteins: DDB, XPC-hHR23B, XPA and/or RPA. Alternatively, a further model termed the concerted or cooperative recognition model, suggests that the XPA, RPA and XPC-hHR23B proteins form a recognition complex that permits increasing selectivity for damaged DNA by amalgamating the specific selectivity of each constituent of the complex.

Initial experimentation involved the measurement of binding affinities between the various repair candidates and DNA. However, none of the candidates, such as DDB (Keeney *et al.*, 1993; Reardon *et al.*, 1993a; Fujiwara *et al.*, 1999), XPC-hHR23B (Batty *et al.*, 2000; Hey *et al.*, 2002; Sugasawa *et al.*, 1998; Sugasawa *et al.*, 2001), XPA (Li *et al.*, 1995a; Jones & Wood 1993; Buschta-Hedayat *et al.*, 1999) or RPA (He *et al.*, 1995; Burns *et al.*, 1996; Schweizer *et al.*, 1999) displayed preferential binding for damaged DNA, compared to undamaged DNA. Competition assays were subsequently utilised to elucidate the precise sequence of recruitment and interaction events of NER proteins at a lesion site. Sugasawa *et al.* (1998) showed that damaged plasmids, incubated with the heterodimeric XPC-hHR23B complex, preferentially binds to damaged DNA and facilitates the rapid removal and repair of DNA damage. By contrast, slower repair rates were observed in damaged plasmids incubated with the XPA-RPA heterodimeric complex alone. This supported a previous study by Evans *et al.* (1997b), who suggested that the XPA-RPA complex was instrumental for the stabilisation of the TFIIH apparatus, rather than the initiator of GGR. Further studies have supported these findings (Batty *et al.*, 2000; Reardon *et al.*, 1996), suggesting that the XPC-hHR23B complex is instrumental in initiating GGR and is a prerequisite for the recruitment of the NER apparatus. In particular, the

utilisation of reconstitution methodologies indicated that the presence of ATP was not necessary for the recruitment of XPC (Aboussekhra *et al.*, 1995; Mu *et al.*, 1995), while XPA (and the core NER apparatus) is sequestered to the site of damage only in the presence of ATP. This suggested that the ATP-dependent unwinding of DNA, by the TFIIH apparatus is a prerequisite for the subsequent recruitment of XPA (Riedl *et al.*, 2003). However, in contrast, Wakasugi & Sancar (1999) showed that preincubation of damaged DNA with XPA-RPA facilitates the rapid induction of repair, in comparison to preincubation of XPC-hHR23B with the damaged DNA substrate. The incongruity between these findings results from the inherent caveats associated with the *in vitro* biochemical assays adopted. In particular, *in vitro* assays do not reflect the complexity of chromatin structure. Moreover, the alteration in protein conformation and localisation *in vivo* may differ to an *in vitro* situation.

Alternative approaches were also adopted to determine the systematic assembly of the NER apparatus. For example, Volker *et al.* (2001) analysed the nuclear trafficking of each NER protein in living cells. This was accomplished by UV irradiating cells through isopore polycarbonate filters (with pores of 3 and 8 μm diameter), which facilitated the localisation of DNA damage at defined positions. This facilitated the detection of both DNA damage foci formation, using CPD- and 6-4PP-specific antibodies. Furthermore, the localisation of NER repair factors was determined, using corresponding antibodies targeting the NER factors. The migration of XPC-hHR23B and XPA from unirradiated regions of the nuclei to damaged foci was investigated by staining the damage (such as CPDs and 6-4PPs) and NER factors with fluorescently labelled antibodies. In agreement with previous studies, the XPC-hHR23B complex was found to accumulate at damaged foci. Interestingly, the recruitment of XPA was not observed in the absence of the XPC-hHR23B complex (Volker *et al.*, 2001). Adopting a similar experimental approach, using cells derived from other XP complementation groups, Rademakers *et al.* (2003) showed that both XPG and RPA are sequestered to the NER complex before and independently of XPA. More recently, biochemical analysis has shown that XPC orchestrates an instrumental role in opening the DNA surrounding the damaged site (Riedl *et al.*,

2003), and is therefore a prerequisite for the recruitment of the core NER apparatus (Tapias *et al.*, 2004).

Significant debate still surrounds the precise molecular mechanistic trigger for the initiation of GGR. Until recently, the body of evidence suggested that GGR was initiated following the recruitment, localisation and preferential binding of the XPC-hHR23B heterodimeric complex to the site of damage (Sugasawa *et al.*, 1998). More recently however, it has been suggested that DDB binding is a prerequisite to the binding of XPC-hHR23B (Fitch *et al.*, 2003b; Wakasugi *et al.*, 2002). Furthermore, it has been speculated that DDB is a prerequisite for histone acetylation, which is thought to augment NER, through its association with histone acetylase p300 (Datta *et al.*, 2001). The importance of DDB is also exemplified in rodents, where the p48 subunit is not upregulated in response to UV (Tan & Chu, 2002). This has been attributed to the absence of a p53-responsive element in the p48 promoter (Tan & Chu, 2002), as the upregulation of p48 occurs in a p53-dependent manner (Ford & Hanawalt, 1997; Hwang *et al.*, 1999). This causes the complete cessation of CPD repair on the nontranscribed strand (and silent regions of the genome) by GGR in rodents (Bohr *et al.*, 1985; Vreeswijk *et al.*, 1994). The binding of DDB, however, is not essential for the recognition of 6-4PPs by XPC-hHR23B (Hwang *et al.*, 1998), due to the significant helical distortion generated by 6-4PPs (Gunz *et al.*, 1996).

Interestingly, it has been shown that XPC-hHR23B selectively binds to helical distortions, regardless of whether they possess a UV-induced lesion (Hess *et al.*, 1997; Sugasawa *et al.*, 2001). For example, XPC-hHR23B binds to helical distortions generated by a 3-5 bp mispaired nucleotide bubble, despite the absence of a lesion (Sugasawa *et al.*, 2001). This suggests the possible requirement for a verification mechanism to ascertain whether the helical distortion detected by XPC-hHR23B is a permissible NER substrate (Hess *et al.*, 1997). It has been shown that the XPC-hHR23B complex preferentially binds 6-4PPs with high affinity (Hey *et al.*, 2002). Additionally, it has also been demonstrated that the XPC-hHR23B complex does not recognise CPDs (Kusumoto *et al.*, 2001), thus suggesting the requirement of additional recognition factor(s) to mediate the recognition of CPDs. However, conflicting

data has shown that XPC selectively repairs CPDs compared to 6-4PPs (Emmert *et al.*, 2000).

In addition to its DNA-damage binding properties, the XPC-hHR23B complex can be described as a multifaceted complex, orchestrating a multitude of functions, including the subsequent recruitment of the repair protein apparatus, thus facilitating the sequential assembly of the NER machinery. The hHR23A and hHR23B, human homologs of the yeast repair factor RAD23; appear to have a redundant role in NER (Ng *et al.*, 2003; Sugasawa *et al.*, 1997). Moreover, the stability of XPC is completely dependent on hHR23B, which is thought to protect it from proteolytic degradation (Ng *et al.*, 2003). Accordingly, XPC is found bound to the hHR23B protein (van der Spek *et al.*, 1996). Furthermore, a recent study has speculated that hHR23B enhances XPA/RPA-mediated displacement of XPC from damaged DNA (You *et al.*, 2003), thus suggesting that hHR23B is instrumental in regulating downstream NER events. More recently, the centrosomal protein, centrin 2 (caltractin 1), has been isolated bound to the XPC-hHR23B complex, and is thought to facilitate stabilisation of XPC by hHR23B. This may suggest a possible regulatory association between NER and cell division (Araki *et al.*, 2001). Both centrin 2 and hHR23B bind to the carboxy-terminal of XPC (Uchida *et al.*, 2002; Nishi *et al.*, 2005).

The damaged DNA binding protein (DDB), is a heterodimeric complex composed of two protein constituents, DDB1 (p127; Fu *et al.*, 2003) and DDB2 (p48), which belong to the XPE complementation group (as previously discussed). Hwang *et al.* (1999) previously reported that the mechanistic function of DDB is instrumental in the recognition of, and subsequent excision of CPDs *in vitro* with high efficacy. It is thought that DDB binds to CPDs, which induces further helical distortions, thus facilitating recognition by the GGR-specific heterodimeric complex, XPC-hHR23B (Fitch *et al.*, 2003b; Fujiwara *et al.*, 1999), thereby providing an accessory function to the XPC-hHR23B complex. Kusumoto *et al.* (2001) showed that the XPC-hHR23B complex possesses a reduced affinity for CPDs. Interestingly, like XPC, DDB2 exhibits an increased affinity for 6-4PP compared to CPDs (Keeney *et al.*, 1993; Fujiwara *et al.*, 1999; Batty *et al.*, 2000). More recently, however, Moser *et al.* (2005) showed that UV-

DDB accelerates the repair of 6-4PPs, while an increase in CPD repair was observed at later time points. They also showed that the proportion of 6-4PPs that is bound by UV-DDB is restricted by the presence of low physiological levels and rapid UV-dependent degradation. Even in the absence of UV-DDB, it was further shown that a slow XPC-hHR23B dependent pathway was capable of removing 6-4PPs and to some extent CPDs (Moser *et al.*, 2005).

The precise relationship between the two complexes (XPC-hHR23B and DDB1-DDB2) remains to be fully delineated. In addition, the elucidation of the mechanistic function of UV-DDB remains poorly understood. As the reconstitution of the repair reaction can be accomplished in the absence of UV-DDB (Aboussekra *et al.*, 1995). However, it has been shown that the inclusion of UV-DDB can stimulate repair up to 17-fold and ~2-fold for CPDs and 6-4PPs respectively (Wakasugi *et al.*, 2001; Wakasugi *et al.*, 2002). However, it has been suggested that the localisation of XPC is dependent upon the basal levels of DDB2, as the recruitment of XPC to damaged sites is hindered with reduced basal DDB2 levels. Conversely, XPC is rapidly sequestered when DDB2 is over-expressed (Fitch *et al.*, 2003b). Furthermore, cells deficient in DDB exhibit a deficiency in the GGR of CPDs, but maintain proficiency in TCR, thus resulting in the XP-E phenotype. Hwang *et al.* (1999) also showed that DDB has a $5x10^6$ fold preference for binding to damaged DNA compared to undamaged DNA. Therefore, it has been suggested that the initial binding of DDB facilitates the subsequent recruitment and binding of XPC-hHR23B to the lesion in the non-transcribed strand. To date, no interaction between the DDB and XPC-hHR23B heterodimeric complexes has been demonstrated (Batty *et al.*, 2000). However, the importance of both XPC and DDB2 in coordinating GGR has been exemplified in XP-C and XP-E cells, which are deficient in GGR, but proficient in TCR (Venema *et al.*, 1991; Hwang *et al.*, 1999).

Investigators have started to elucidate the precise mechanistic complexity of DDB. For example, DDB was found to interact with a multitude of proteins required for chromatin remodelling and ubiquitin ligation (Shiyanov *et al.*, 1999; Nag *et al.*, 2001). In addition, Groisman *et al.* (2003) isolated DDB as part of a

complex, containing Cullin4A (CUL4A), Roc1 and COP9 signalosome (CSN), which are constituents of ubiquitin ligase (discussed further in Section 1.8). More recently, Kulaksiz *et al.* (2005) showed that DDB2 exists in at least four forms within the cell: monomeric DDB2, DDB1-DDB2 heterodimer (UV-DDB) and as a protein associated with both the CUL4A complex and the CSN.

Following the recognition of lesions on the nontranscribed stand of transcriptionally active genes or transcriptionally silent regions of the genome by the GGR subpathway (Fig. 1.3), the XPC-hHR23B heterodimeric complex mediates the recruitment of the TFIIH complex, through protein-protein interactions with the XPB and p62 subunits of TFIIH (Yokoi *et al.*, 2000). Recently, it was shown that the carboxy-terminal domain of the XPC protein is required for the subsequent binding of TFIIH, as truncations in this region significantly impair the binding of TFIIH (Uchida *et al.*, 2002). The recruitment and binding of the TFIIH complex facilitates lesion demarcation and verification (discussed in Section 1.6.3).

1.6.2 Transcription-coupled repair (TCR): Recognition of stalled RNA Pol II

The recommencement of transcription following damage is essential for normal cellular functionality. Although bacterial TCR has been well characterised (reviewed by Saxowsky & Doetsch, 2006), the precise mechanistic action of TCR in mammalian cells remains poorly delineated. As previously discussed, the GGR subpathway has been extensively characterised due to the establishment of an *in vitro* reaction (Sibghat-Ullah *et al.*, 1989; Wood *et al.*, 1988) and reconstitution exploiting recombinant NER factors (Aboussekhra *et al.*, 1995). In contrast, the establishment of an *in vitro* TCR assay has remained unsuccessful, due to the mechanistic complexity of TCR.

TCR, first described by Mellon *et al.* (1987), specifically targets DNA lesions in the transcribed strand of transcriptionally active genes. Proficient TCR is not only paramount for the repair of cytotoxic lesions on the transcribed strand of

transcriptionally active genes, but also facilitates the rapid recovery and restoration of basal and/or inducible transcription. Furthermore, an arrested RNA Pol II at a stalled transcription fork elicits a cytotoxic stress signal, which initiates apoptosis in a p53-dependent and independent manner (Ljungman & Zhang, 1996). The importance of TCR as a prerequisite for the removal of UV-induced lesions on the transcribed strand and resumption of transcription is exemplified in cells derived from patients with CS, where the inhibition of transcription in certain genes, such as *DHFR* or glyceraldehyde-3-phosphate dehydrogenase (*GAPDH*), is abolished following UV irradiation (Proietti-De-Santis *et al.*, 2006). It was assumed this defect occurs for all RNA Pol II transcribed genes, but this may not be the case (see below). The defect has been attributed to a failure to assemble the transcription initiation complex at the promoter due to the abolition of TATA-binding protein (TBP), the failure to recruit TFIIB and aberrant histone H4 acetylation. Therefore, the mechanistic action of the TCR apparatus is paramount for the recognition of an arrested RNA Pol II at a stalled transcription fork, efficient recruitment of the NER apparatus and the subsequent recruitment of the transcription apparatus, thus permitting the resumption of transcription. This was further illustrated by van Oosterwijk *et al.* (1996), who suggest that CS gene products mediate the transition of the TFIIH apparatus from a repair mechanism to a transcription mechanism, thus protecting the cell from apoptosis, induced by transcription blocking lesions (Proietti-De-Santis *et al.*, 2002). More recently, McKay *et al.* (2004) suggested that transcription may regulate cellular homeostasis, by acting as a DNA-damage dosimeter.

The initiation of TCR is dependent upon the recognition of an arrested RNA Pol II at a stalled transcription fork, by an XPC-, XPE-independent mechanism (Kamiuchi *et al.*, 2002). It was previously shown that human cells, defective in XPC, retain the capacity to undertake TCR, thus suggesting that the XPC protein is superfluous for the preferential repair of lesions on the transcribed strand of transcriptionally active genes (Venema *et al.*, 1991; van Hoffen *et al.*, 1995; Mu & Sancar, 1997). In human cells, a multitude of proteins have been implicated in the mechanistic functioning of TCR, including: CSA, CSB, XPB, XPD, XPG, hMSH2 (Mellon *et al.*, 1996), hMLH1 (Mellon *et al.*, 1996) and XAB2 (Nakatsu

et al., 2000). However, the precise mechanistic function and relationship between these proteins remains unclear.

A stress signal initiated by an arrested RNA Pol II at a stalled transcription fork is thought to elicit the recruitment of the TCR-specific proteins, CSA and CSB (Fig. 1.3; Henning *et al.*, 1995; Troelstra *et al.*, 1992), which facilitates the subsequent assembly of the core NER apparatus. CSA is a 44 kDa protein, possessing seven WD-40 repeats, instrumental for protein-protein interactions, which provide a molecular scaffold for the stabilisation of further repair and/or transcription factors (Henning *et al.*, 1995). WD-repeat proteins have been implicated in a multiplicity of cellular processes, such as signal transduction, vesicular trafficking, cytoskeletal assembly, cell cycle regulation, RNA processing, transcriptional regulation and DNA repair. This suggests that CSA provides a regulatory function, as no WD-repeat proteins have been identified possessing catalytic activity. Previously, it has been shown that CSA interacts with XAB2, CSB and the p44 subunit of TFIIH (Nakatsu *et al.*, 2000; Henning *et al.*, 1995). More recently, it was shown that CSA associates with CUL4A containing the ubiquitin ligase (E3) complex, consisting of DDB1, CUL4A and ROC1/rbx1 proteins (Section 1.8; Groisman *et al.*, 2003).

The interaction between CSA and CSB has been shown by employing *in vitro* translated proteins in combination with the yeast two-hybrid system (Henning *et al.*, 1995). CSA and CSB have also been co-purified with large molecular weight complexes devoid of the other (van Gool *et al.*, 1997; Groisman *et al.*, 2003). Kamiuchi *et al.* (2002), however, has proposed that following UV, the CSA protein is translocated from the nucleoplasm to the nuclear matrix, by a CSB-dependent mechanism, whereby CSA colocalises with the hyperphosphorylated form of RNA Pol II, engaged in transcription elongation (Kamiuchi *et al.*, 2002). Originally, there was no evidence to suggest that CSA directly binds to RNA Pol II (Tantin, 1998), or displaces the arrested RNA Pol II from the elongation apparatus (Selby & Sancar, 1997b). However, Groisman *et al.* (2003) & Kamiuchi *et al.* (2002) showed that CSA physically associates with RNA Pol II in a UV-dependent manner.

The *CSB* gene encodes a 168 kDa protein that possesses a helicase domain (Troelstra *et al.*, 1992), and is a member of the SWI2/SNF2 family of DNA-dependent ATPases (Eisen *et al.*, 1995; Selby & Sancar, 1997b). It is found complexed with both RNA Pol I and II, and is thought to stimulate the enzymatic activity of both RNA polymerases (Bradsher *et al.*, 2002; van Gool *et al.*, 1997). The SWI2/SNF2 family have been implicated in a multitude of cellular processes, such as transcriptional regulation, chromosome stability and DNA repair (Eisen *et al.*, 1995). The DNA-dependent ATPase activity of CSB has been implicated in chromatin remodelling *in vitro*, and it has been suggested that it is required for the subsequent recruitment of the NER apparatus following TCR-specific recognition (Citterio *et al.*, 1998; Selzer *et al.*, 2002). It has been shown that CSB interacts with components of the NER apparatus, such as XPA (Selby & Sancar, 1997), XPG (Bradsher *et al.*, 2002; Iyer *et al.*, 1996) and TFIIH, which contains the XPB and XPD helicases (Selby & Sancar, 1997b; Bradsher *et al.*, 2002; Tantin, 1998). The precise role of CSB in transcription remains poorly delineated. Several studies have suggested that CSB promotes elongation by RNA Pol I (Bradsher *et al.*, 2002), II (Selby & Sancar 1997a; Tantin *et al.*, 1997) and III (Yu *et al.*, 2000a). Selby & Sancar (1997a) has also suggested that CSB counteracts the rescue of backtracked and arrested transcription complexes by the elongation factor TFIIS. Interestingly, a recent study undertaken by Proietti-De-Santis *et al.* (2006) has shown that CSB is dispensable for the transcription of p53-responsive genes, following DNA damage, both in wild-type and CSB cells, but is required for the resumption of transcription in p53-independent housekeeping genes.

Immediately after UV, transcription is globally downregulated to permit the recruitment of the NER machinery. The recovery of RNA synthesis occurs immediately following the completion of DNA repair. However, this recovery is not observed in CS cells (Rockx *et al.*, 2000). The abolition of transcription is thought to occur due to the reduction of hypophosphorylated RNA Pol II, which is required for entry into the pre-initiation complex situated at the promoter. Moreover, UV damage on the transcribed strand promotes hyperphosphorylation of the C-terminal domain (CTD) of unbound RNA Pol II, which inhibits its recruitment into new pre-initiation complexes. Under normal physiological

conditions hyperphosphorylated RNA Pol II is required for the transition of initiation to elongation. Interestingly, however, the level of inactive hyperphosphorylated RNA Pol II remains high in CS cells. In contrast, wild-type cells rapidly replenish their levels of the active hypophosphorylated form of RNA Pol II. This suggests that the cessation of RNA synthesis following UV irradiation, is not simply caused by blocked elongation at sites of lesions, but is also caused by the abolition of transcription initiation. In addition, it has been speculated that the TBP has a selective affinity for DNA containing UV-induced lesions, compared to undamaged DNA. This reduces the availability of TBP for transcription at the promoter site of undamaged DNA (Vichi *et al.*, 1997).

The displacement of an arrested RNA Pol II elongation complex from the transcribed strand, following UV damage, is a prerequisite for the initiation of TCR, sequential recruitment of core NER factors and repair. Single nucleotide resolution analysis has shown that initial rapid repair occurs near the promoter. This is followed by the initiation of CSA- and CSB-dependent TCR at the coding region of the *JUN* gene (Tu *et al.*, 1996; Tu *et al.*, 1997; Tu *et al.*, 1998). A recent study has shown that TFIIH dissociates from RNA Pol II as the polymerase passes the promoter 30-60 bases downstream of the transcription initiation site (Dvir *et al.*, 2001). From these findings, it has been speculated that this dissociation of TFIIH at the promoter explains the superfluous requirement of CSB for rapid TCR, adjacent to the point of transcription initiation (Svejstrup, 2002). However, the subsequent recruitment of CSB is necessitated further downstream in the coding region for the recruitment of TFIIH at the site of an arrested RNA Pol II (Tantin *et al.*, 1997; Tantin, 1998).

Although the mechanistic function of CSA and the functional relationship between CSA and CSB in TCR has remained enigmatic, several recent studies have established a link between the two TCR-specific factors. For example, Groisman *et al.* (2006) have shown that the degradation of CSB occurs in a proteasome- and CSA-dependent manner. Groisman *et al.* (2006) has speculated that this ubiquitin-dependent degradation of CSB is essential for the resumption of transcription following TCR. A further investigation undertaken by Fousteri *et al.* (2006), used an *in vivo* crosslinking approach coupled with chromatin

coimmunoprecipitation (ChIP) to shown that CSA and CSB differentially regulate the recruitment of chromatin remodelling and repair factors to stalled RNA Pol II *in vivo*. Fousteri *et al.* (2006), showed that CSB provides an essential role as a coupling factor, by attracting HAT p300 and core NER factors (excluding XPC-hHR23B) to the stalled RNA Pol IIo, whereas the CSA-DDB1 E3/CSN complex is required for the recruitment of the nucleosomal binding protein HMGN1, XAB2 and TFIIS. Interestingly, Fousteri *et al.* (2006) showed that lesion-stalled RNA Pol IIo does not dissociate from its template during the assembly of the TCR complex.

Several lines of evidence have resulted in the postulation of six models for TCR initiation, which necessitate the displacement or remodelling of RNA Pol II (reviewed by Svejstrup, 2002). Most of which require the SWI/SNF-mediated activity of CSB: (1) dissociation of RNA Pol II from damaged strand; (2) temporary displacement of RNA Pol II by retrograde motion; (3) remodelling of the RNA Pol II at a transcription-blocking DNA lesion, through the addition of a single nucleotide; (4) Accessory-factor-mediated lesion bypass; (5) Binding of repair factors to damaged site prior to the arrival of RNA Pol II; (6) Immediate degradation of a stalled RNA Pol II.

Following the initial recognition of UV-induced lesions on the transcribed strand of transcriptionally active genes by TCR-specific mechanisms, the subsequent processing of the lesion requires a series of sequential mechanistic steps identical to those necessitated for GGR (Fig. 1.3; discussed in Sections 1.6.3-1.6.6).

1.6.3 Lesion demarcation and verification: TFIIH

Following lesion recognition by the GGR- or TCR-specific pathway, the formation of an open complex through local unwinding of the DNA helix and demarcation of the lesion is essential for the recruitment of the core NER apparatus (TFIIH, XPA, RPA and XPG) and subsequent formation of the pre-incision complex (Fig. 1.3). The basal transcription factor, TFIIH, a multiprotein, multifunctional complex composed of ten subunits, is able to switch between

transcription and NER (Hoogstraten *et al.*, 2002). The structural composition of TFIIH is further divided into two complexes; the core complex (containing p8, p34, p44, p52, p62 and XPB) and the cdk-activating kinase (CAK) complex (containing cyclin-dependent kinase 7 (CDK7), cyclin H and MAT1). Both complexes are bound together through their association with XPD (Schultz *et al.*, 2000). In transcription, TFIIH facilitates the unwinding of DNA, which mediates the transition of RNA Pol II from initiation near the promoter to the elongation phase. In GGR, the TFIIH complex is sequestered to the damaged site by XPC-hHR23B in an ATP-independent manner. In both GGR and TCR, the XPB and XPD subunits, which possess DNA-dependent helicase activity, mediate the local unwinding of the DNA helix around the lesion, in a 3'→5' and 5'→3' polarity, respectively, in an ATP-dependent manner. It has been speculated that the XPB and XPD helicases transclocate with opposite polarities in the same direction on each strand of the antiparallel DNA helix (Dillingham *et al.*, 2003). The presence of a UV-induced lesion is thought to cause a strand-specific unilateral block of either the XPB or XPD helicase, whilst the other helicase continues to translocate along the undamaged strand. This is thought to generate distortion and bending in the DNA helix, which is essential for damage verification and the subsequent recruitment of the core NER apparatus (reviewed by Dip *et al.*, 2004).

In transcription, the helicase activity of TFIIH permits the unwinding of approximately 10-20 bp near the promoter region, thus facilitating the initiation of the nascent mRNA synthesis on the DNA template strand (Holstege *et al.*, 1996). In NER, the XPB and XPD helicases generates a demarcation around the lesion of similar size, 20-25 nucleotides (Evans *et al.*, 1997b), thus facilitating the recruitment of the endonucleases, XPG and XPF-ERCC1. Whilst the 3'→5' helicase activity of XPB is essential for transcription, XPD helicase activity is superfluous for *in vitro* basal transcription (Tirode *et al.*, 1999). The essential role of XPB in transcription is thought to explain the infrequency of XP-B phenotypes, compared to XP-D, where a battery of pathological phenotypes associated with *XPD* gene defects have been identified such as XP, TTD, XP-CS, and COFS syndrome (Section 1.9).

The precise mechanistic function of the core TFIIH constituents, such as p8, p34, p44, p52 and p62, are not well understood. However, recently, Ranish *et al.* (2004) and Giglia-Mari *et al.* (2004) identified a novel component of the TFIIH complex, TFB5 (p8), which is encoded by the *GTF2H5* gene. TFB5 is thought to stabilise the TFIIH complex and defects in the *GTF2H5* gene causes a global reduction in the levels of TFIIH, resulting in a TTD-A phenotype (discussed in Section 1.9.4). The p34 and p44 constituents are thought to possess Zn^{2+} motifs and putative DNA-binding capabilities (Humbert *et al.*, 1994). In addition, the N-terminal domain of p44 positively regulates the helicase activity of XPD. Conversely, the C-terminal end orchestrates a role in promoter escape (Tremeau-Bravard *et al.*, 2001). It has also been shown that p52 plays a role in facilitating the interaction between XPB and TFIIH. Unlike the core complex, the mechanistic functions of the CAK complex have been well characterised, and it promotes the phosphorylation of CDKs, which mediate the regulation of the cell cycle. The CAK complex is also required for the phosphorylation of the C-terminus end of RNA Pol II. Interestingly, the transient association of the CAK complex with TFIIH and its superfluous nature in NER provides further evidence for the existence of different modes of TFIIH specific for either transcription or repair (Svejstrup *et al.*, 1995).

1.6.4 Assembly of the preincision complex: RPA, XPA and XPG

Following the preliminary denaturation and unwinding of the DNA duplex by TFIIH, three further NER factors are sequestered to the site of damage, including RPA, XPA and XPG (Fig. 1.3). The recruitment of these factors is essential for the assembly of the preincision complex. The precise order of recruitment and assembly of these factors remains unclear, but it has been suggested that they assemble independently of each other. RPA is a trimeric complex composed of three subunits: 70, 32 and 14 kDa. The 70 kDa component possesses three DNA binding domains, which covers approximately 30 nucleotides of DNA during DNA repair. RPA is sequestered to the site of DNA damage devoid of XPA or XPG (Rademakers *et al.*, 2003). Furthermore, the colocalisation of XPA and

RPA can occur without recruiting XPG (Rademakers *et al.*, 2003), and the recruitment of XPG can take place without XPA (Volker *et al.*, 2001).

RPA is indispensable for DNA replication, recombination and repair. In NER, RPA is essential for both dual incision (Coverley *et al.*, 1992; Guzder *et al.*, 1995; Mu *et al.*, 1995) and the repair synthesis steps (Coverley *et al.*, 1991; Shivji *et al.*, 1995). In accordance, RPA exhibits two binding configurations, which occupy either 8-10 or ~30 nucleotides of single stranded (ss) DNA. RPA binds to the undamaged strand of the unwound DNA helix (Bochkarev *et al.*, 1997), thus facilitating the accurate positioning of the XPG and XPF-ERCC1 endonucleases. Similarly, Lee *et al.* (2003) showed that RPA preferentially interacts with the undamaged DNA strand. In addition, it has been speculated that RPA mechanistically functions as a recognition factor, through the detection of unwound ssDNA regions rather than lesion recognition *per se*. In agreement, Hermanson-Miller & Turchi (2002) demonstrated the strand-specific photo-cross-linking of RPA to damaged oligonucleotides. The mechanistic functioning of RPA is enhanced by the inclusion of XPA, suggesting that XPA and RPA function synergistically to ensure the correct positioning of RPA on the nondamaged strand of the DNA (Hermanson-Miller & Turchi, 2002).

XPA is a 31 kDa zinc metalloprotein, which forms associations with a multitude of NER factors, and exhibits a preference for damaged DNA. XPA is thought to undertake a structural role in the preincision complex by binding both to other NER factors (such as RPA, XPF-ERCC1, TFIIH and XPC-hHR23B) and to damaged DNA. XPA has a preferential affinity for binding distorted DNA in the absence of DNA lesions (Missura *et al.*, 2001). From these findings, it was speculated that XPA provides an essential role in the recognition of DNA kinks that are generated following lesion recognition by TCR or GGR, thus providing the common node between the GGR and TCR subpathways and facilitating the recruitment of the core NER apparatus. Moreover, it has been suggested that the XPA-RPA complex ensures the correct three-dimensional assembly of the NER apparatus, before endonucleolytic incision by XPG and XPF-ERCC1.

The N-terminal region of XPA binds to RPA32 and ERCC1 (Li *et al.*, 1994; Li *et al.*, 1995a; Park *et al.*, 1994), whereas the C-terminal domain targets TFIIH (Park *et al.*, 1995). The central zinc finger domain is required for the binding of RPA70 (Li *et al.*, 1995b). The formation of the heterodimeric XPA-RPA complex is essential for positioning the XPG and XPF-ERCC1 endonucleases for correct incision of damaged DNA (de Latt *et al.*, 1998a). The binding of XPA to RPA also contributes to the stabilisation of the incision complex by preventing the strand separation activity of RPA (Missura *et al.*, 2001).

Interestingly, XPA interacts with two recently identified proteins, XAB1 and XAB2, whose mechanistic function(s) in NER remain to be fully discovered (Nitta *et al.*, 2000; Nakatsu *et al.*, 2000). XAB1 is a GTPase protein found within the cytoplasm and is thought to provide an accessory role in the nuclear localisation of XPA (Nitta *et al.*, 2000). Conversely, XAB2 binds to CSA, CSB and RNA Pol II (Nakatsu *et al.*, 2000). The importance of XAB2 in both TCR and transcription was demonstrated by microinjecting XAB2-specific antibodies into fibroblasts. This caused the complete abolition of both processes (Nakatsu *et al.*, 2000). Intriguingly, a recent study has also identified functional association between NER, via XPA, and the DNA damage-induced ATR-dependent checkpoint pathway. Wu *et al.* (2006) showed that ATR modulates the cellular activity of NER through the phosphorylation of XPA at ser196, following UV-irradiation, thus providing evidence for a direct link between DNA damage signalling and NER.

Subsequent to damage verification, XPG is sequestered to the preincision complex via its interaction with TFIIH (Araujo *et al.*, 2001). A recent body of evidence has suggested that XPG interacts with TFIIH, prior to the recruitment of both XPA and XPF-ERCC1 (Araujo *et al.*, 2001; Volker *et al.*, 2001). Conflicting reports, however, suggest that XPA, RPA and XPG reciprocally stabilise their association with the NER complex (Reardon & Sancar, 2003; Riedl *et al.*, 2003). This suggests that these three NER proteins interact with DNA in a synergistic manner. It has also been shown that the removal of XPC-hHR23B from the preincision complex is essential for the binding of XPG (Riedl *et al.*, 2003; Wakasugi & Sancar, 1998). XPG is a member of the flap endonuclease 1

(FEN-1) family of structure-specific endonucleases, which incise flap or bubble DNA structures.

1.6.5 Dual incision and excision of the oligonucleotide fragment: XPG and XPF-ERCC1

Although both XPG and XPF-ERCC1 orchestrate the bimodal incision of the damaged DNA, the recruitment of both endonucleases occurs asynchronously. The recruitment of the XPF-ERCC1 heterodimeric complex completes the formation of the incision complex, prior to dual incision (Fig. 1.3). The XPF-ERCC1 heterodimeric complex is formed by the interaction between the 103 kDa XPF and the 33 kDa ERCC1 proteins, respectively (de Laat *et al.*, 1998b; Westerveld *et al.*, 1984). XPF-ERCC1 is sequestered to the NER incision complex, through the direct interaction between XPA and ERCC1. As previously discussed, the XPA protein is not required for the recruitment of XPG. However, the binding of XPG alone is insufficient to activate its endonuclease activity, which was previously shown in XP-A cells. Therefore, it has been speculated that the XPA-RPA complex is required to activate the endonuclease activity (de Laat *et al.*, 1998b). By contrast, the recruitment of XPF-ERCC1 requires the XPA protein (Volker *et al.*, 2001). Recently, Winkler *et al.* (2001) showed that TFIIH inhibits the endonuclease activity of XPG and XPF-ERCC1 in the absence of ATP. This regulation of endonuclease activity is thought to prevent inadvertent incision prior to the completion of lesion demarcation.

The dual incisions mediated by XPG and XPF-ERCC1 are made asymmetrically to the UV-induced lesion (Mu *et al.*, 1996). XPG cleaves 2-8 nucleotides 3' to the lesion, whereas XPF-ERCC1 cleaves 20-24 nucleotides 5' to the lesion. Following bimodal incision, a 15-24 bp oligonucleotide fragment is excised, containing the UV-induced lesion (Evans *et al.*, 1997b). Although XPG is sequestered to the NER complex prior to XPF-ERCC1, it has been speculated that the 5' incision made by XPF-ERCC1 occurs first (Gillet & Schärer, 2006). This results in the production of a free 3' hydroxyl group on the damaged DNA strand, which provides a primer site for the initiation of repair synthesis.

1.6.6 Polymerisation and ligation by repair synthesis: RPA, RFC, PCNA Pol δ/ε and DNA ligase III

Following dual incision by the XPG and XPF-ERCC1 endonucleases, the recruitment of additional factors, such as replication factor C (RFC), PCNA and DNA polymerases δ and ε, are essential for repair synthesis (Shivji *et al.*, 1995). As previously discussed, RPA is a central component of the DNA re-synthesis apparatus. RPA remains bound to the undamaged strand following dual incision, whilst the entire core NER machinery dissociate (Fig. 1.3). It is thought that RPA is required for the subsequent recruitment of RFC and PCNA (Yuzhakov *et al.*, 1999; Gomes & Burgers, 2001). Both RFC and PCNA provide accessory functions, which facilitate the assembly of the polymerases.

RFC is sequestered to the OH group at the 3'-termini, generated during dual incision by XPF-ERCC1, which provides a primer site for DNA polymerases δ and ε. The binding of RFC permits the subsequent loading of PCNA onto the DNA at the 3' termini, in an ATP-dependent manner. PCNA is a homotrimeric protein that possesses a ring-shaped clamp, which facilitates the sliding of PCNA along DNA whilst bound to DNA polymerase (Gulbis *et al.*, 1996). More recently, it has been shown that the recruitment of CAF-1, which is essential for chromatin restoration following NER, requires PCNA (Green & Almouzni, 2003). This further reiterates the association between repair synthesis and the reconstitution of chromatin following NER. Finally, ligation of the 5'-end of the newly synthesised DNA to the original sequence is completed by DNA ligase III (Tomkinson & Levin *et al.*, 1997). Interestingly, Barnes *et al.* (1992) reported an individual with mutations in the *DNA ligase III* gene, displaying sensitivity to UV.

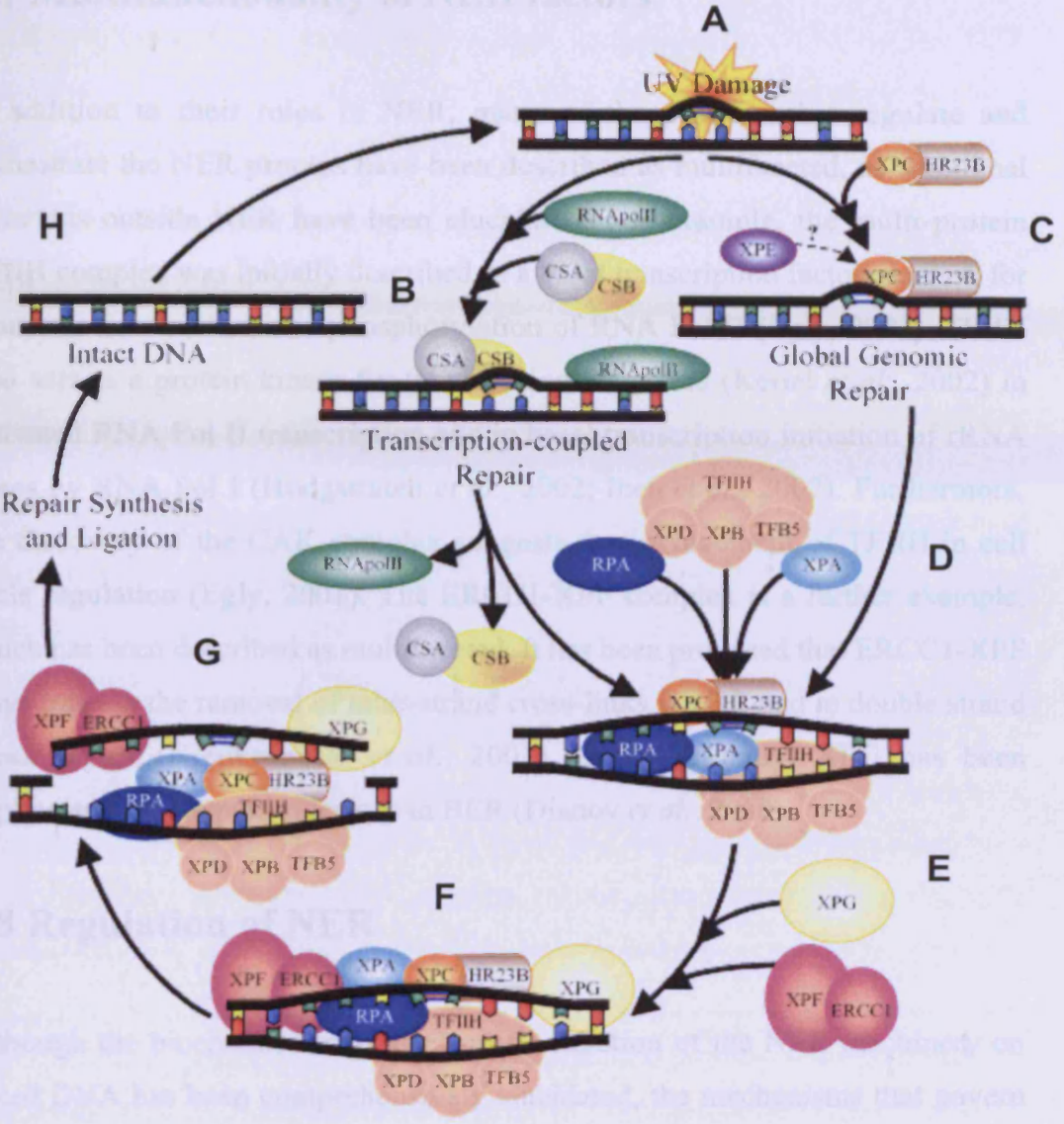

Figure 1.3. Schematic representation of the GGR- and TCR-NER mechanism. (A) UV lesions induce DNA helical distortion; (B) Arrested RNA Pol II on the transcribed strand of an active gene results in the recruitment of the CSA and CSB TCR-specific proteins, facilitating the displacement of the stalled RNA Pol II from the damaged site; (C) Recognition of a lesion on the non-transcribed strand of an active gene (and the transcriptionally silent regions of the genome) is undertaken by the recruitment of the XPC-hHR23B and XPE (DDB2) GGR-specific NER factors; (D) Lesion demarcation and verification is performed by the sequestration of the core NER apparatus including the bi-directional XPB/XPD helicase subunits of TFIIH, XPA (common node for GGR and TCR) and RPA; (E) Denaturation and unwinding of the DNA duplex (~20 bp) by XPB and XPD results in the recruitment of the XPG endonuclease. The recruitment of RPA, XPA and XPG mediate the formation of the preincision complex; (F) The XPF-ERCC1 heterodimeric complex joins the preincision complex and bimodal incision and excision (5' by ERCC1-XPF and 3' by XPG) occurs; (G) A 15-24 bp oligonucleotide fragment is excised, containing the UV lesion and RPA remains bound to the ssDNA, thus facilitating the transition to repair synthesis; (H) The subsequent recruitment of the Pol δ (or ε) supported by RFC and PCNA (not shown) orchestrate synthesis. Ligase III seals the remaining nick (adapted from http://ccr.coriell.org/nigms/pathways/ner.html).

1.7 Multifunctionality of NER factors

In addition to their roles in NER, many of the proteins that regulate and orchestrate the NER process have been described as multifaceted, as additional functions outside NER have been elucidated. For example, the multi-protein TFIIH complex was initially described as a basal transcription factor required for promoter demarcation and phosphorylation of RNA Pol II (Egly, 2001). TFIIH also acts as a protein kinase for transcription activators (Keriel *et al.*, 2002) in activated RNA Pol II transcription and in basal transcription initiation of rRNA genes by RNA Pol I (Hoogstraten *et al.*, 2002; Iben *et al.*, 2002). Furthermore, the discovery of the CAK complex suggests the involvement of TFIIH in cell cycle regulation (Egly, 2001). The ERCC1-XPF complex is a further example, which has been described as multifaceted. It has been proposed that ERCC1-XPF plays roles in the removal of inter-strand cross-links via HR and in double strand break repair (Niedernhofer *et al.*, 2001). Controversially, XPG has been implicated in the repair of lesions in BER (Dianov *et al.*, 2000).

1.8 Regulation of NER

Although the biochemical and mechanistic function of the NER machinery on naked DNA has been comprehensively elucidated, the mechanisms that govern NER remain poorly delineated. Indeed, the recognition of UV-induced photoproducts, subsequent recruitment and sequential assembly of the NER apparatus is an intricate process, requiring meticulous regulation. Our understanding of NER regulation has been made particularly problematic due to the intricate association between genomic DNA and histone complexes, which further fold to form nucleosomes. These highly ordered structures require mechanisms that orchestrate the remodelling of chromatin, thus permitting the NER apparatus to obtain access to the damaged bases. The accessibility of NER factors varies significantly within different regions of the genome (reviewed by Moggs & Almouzni, 1999). It has been suggested that the presence of the transcription machinery on the transcribed strand increases accessibility to the NER apparatus due to a more 'open' chromatin conformation (Friedberg, 1996).

Furthermore, the presence of TFIIH, which plays an indispensable role in both transcription and DNA repair, may further increase accessibility to the NER apparatus (Hoeijmakers *et al.*, 1996). Therefore, the remodelling of chromatin is a particularly fundamental prerequisite in transcriptionally silent regions of the genome.

A recent body of evidence, however, has identified the ubiquitin-proteasome pathway as an essential regulator in the co-ordinated assembly and disassembly of the NER apparatus (Sweder & Madura, 2002). The ubiquitin-proteasome pathway is instrumental in orchestrating a multiplicity of processes fundamental to normal cellular functionality, such as cell cycle progression, stress responses and cellular differentiation. Although ubiquitylation is most frequently associated with the targeted degradation of cellular proteins, via the proteasome, several non-degradative functions have been identified in NER (reviewed by Huang & D'Andrea, 2006; Sugasawa, 2006). Following the first association between DNA repair and ubiquitylation in yeast (Jentsch *et al.*, 1987), further associations have been characterised. Recent studies in yeast and humans have suggested both proteolytic and non-proteolytic functions of ubiquitin in modulating the NER pathway (Gillette *et al.*, 2006; Sweder & Madura, 2002).

Indeed, it has been previously demonstrated that proteins required for the recognition steps of both GGR and TCR undergo ubiquitylation. This suggests a regulatory role not only in NER *per se*, but that ubiquitylation is instrumental in modulating the GGR and TCR subpathways (Sweder & Madura, 2002; Svejstrup, 2003; Lommel *et al.*, 2002; Wang *et al.*, 2005b). In particular, recent evidence suggests that the XPC and DDB2 proteins provide the principal targets for ubiquitin-mediated regulation of the NER machinery, thus facilitating the assembly and degradation of the recognition apparatus. For example, the yeast homologue of XPC, Rad4, is ubiquitylated, following UV-irradiation, and elicits the targeted degradation of Rad4 by the 26S proteasome (Lommel *et al.*, 2002; Ramsey *et al.*, 2004). Conversely, the UV-induced ubiquitylation of XPC in human cells is reversible, and is not targeted by the ubiquitin-proteasome pathway (Sugasawa *et al.*, 2005; Wang *et al.*, 2005c). Additionally, the 26S

proteasome also operates as a molecular chaperone, which facilitates the disassembly of the NER apparatus (Sweder & Madura, 2002).

Recently, Groisman *et al.* (2003) showed that both the DDB2 and CSA proteins are incorporated in separate, but otherwise identical complexes, via the direct interaction with DDB1. Additionally, Groisman *et al.* (2003) found that both complexes possess CUL4A and Roc1, which are constituents of the E3 complex. Furthermore, both complexes were found to contain CSN, a negative regulator of cullin-based ubiquitin ligases. However, CSN differentially regulates the ubiquitin ligase activity of the DDB2 and the CSA complexes, following UV irradiation. Although the constituent proteins within both the DDB2 and CSA complex exhibit significant homology, they differ biochemically, which reflects the differential function of DDB2 and CSA in GGR and TCR, respectively. So, although both the DDB2 and CSA complexes contain CSN, UV-irradiation differentially modulates the interaction of CSN with both complexes. It has been shown that the CSN complex is displaced from the DDB2 complex following UV irradiation, which facilitates the modification of CUL4A by neuronal-precursor-cell-expressed developmentally downregulated protein-8 (NEDD8) through neddylation (Groisman *et al.*, 2003). This suggests that the E3 activity of the DDB2 complex is stimulated by UV irradiation. In contrast, UV irradiation initiates the rapid interaction between the CSA and CSN complex, which facilitates the suppression of the E3 activity. It has been further speculated by Groisman *et al.* (2003), that the CSA complex is incorporated into the transcription preinitiation complex, via its interaction with RNA Pol II. However, the mechanistic function of suppressed E3 activity in modulating TCR, following the detection of the stalled transcription apparatus, remains poorly understood. Although the DDB2 and CSA E3 complexes mediate different mechanistic functions in GGR and TCR, the similarity in the complexes provides a link between the two NER subpathways and the ubiquitin/proteasome pathway.

It has also been shown that the polyubiquitylation of DDB2, results in its rapid degradation by the ubiquitin-proteasome pathway (Fig. 1.4), which occurs following UV-irradiation (Rapic-Otrin *et al.*, 2002). In agreement, Fitch *et al.* (2003b) have shown that the degradation of DDB2 is inhibited following the

inclusion of proteasome inhibitors, thus further supporting the requirement of the ubiquitin-proteasome pathway in the regulation of GGR. Therefore, the ubiquitylation of DDB2 is orchestrated following the direct association between DDB1 and CUL4A, which possess E3 activity (Shiyanov *et al.*, 1999; Groisman *et al.*, 2003; Matsuda *et al.*, 2005). Furthermore, the importance of functional DDB has been shown by Shiyanov *et al.* (1999), who reported the abolition of co-immunoprecipitation between CUL4A and DDB in naturally occurring DDB mutants.

More recently, Kapetanaki *et al.* (2006) have shown that the DDB1-CUL4A^{DDB2} ubiquitin ligase complex is deficient in XP-E cells. Moreover, Kapetanaki *et al.* (2006) have implicated a novel function of the DDB1-CUL4A^{DDB2} ligase in histone modification facilitating subsequent chromatin remodelling from a condensed to a relaxed configuration, thus increasing the accessibility for the NER apparatus. It was also demonstrated that DDB1-CUL4A^{DDB2} E3 colocalises with CPDs and co-immunoprecipitates with monoubiquitylated H2A following UV-irradiation, which is also dependent upon functional DDB2. This suggests that DDB1-CUL4A^{DDB2} E3 targets histone H2A for ubiquitylation at UV-induced lesions, and that DDB2 mechanistically functions as a possible substrate receptor (Kapetanaki *et al.*, 2006).

The systematic modulation of GGR is further regulated by the post-translational modification of the XPC NER factor. The XPC protein displays significant modifications immediately following UV-irradiation, which is consistent with polyubiquitylation or sumoylation (Sugasawa *et al.*, 2005; Wang *et al.*, 2005c). These modifications to XPC do not cause protein degradation, but are reversed within two hours (Fig 1.4). Furthermore, these modifications are thought to stabilise the XPC protein, thus augmenting the recognition of CPDs. Recently, Sugasawa *et al.* (2005) showed that the DDB2 E3 complex is essential in orchestrating the subsequent polyubiquitylation of the XPC protein. Interestingly, however, unlike the targeted degradation of DDB2 by the proteasome, following DDB2-induced polyubiquitylation, the XPC protein potentiates the DNA-binding activity of XPC by displacing DDB (Sugasawa *et al.*, 2005). Furthermore, it has been speculated that the polyubiquitylation of the DDB ligase complex, CUL4A,

facilitates the dissociation of the complex from the lesion. This causes the subsequent cessation of the ubiquitin-proteasome pathway through deubiquitylating enzymes (DUBs), as opposed to targeted degradation through the proteasomal pathway. These modifications are reversed within two hours, following UV exposure.

Recent evidence presented by Wang *et al.* (2005c), suggests that XPC is covalently modified following UV, through both the small ubiquitin-related modifier-1 (SUMO-1) and ubiquitin. Furthermore, it was shown that in addition to the ubiquitin-proteasome system, both functional DDB2 and XPA are required for these XPC modifications, following UV-irradiation. From these data Wang *et al.* (2005c) further speculated that the UV-induced sumoylation of XPC is essential for the stabilisation of the XPC protein, thus preventing its degradation. Wang *et al.* (2005c) have also postulated that the sumoylation of XPC may abolish the affinity of the XPC protein to damaged sites, thus facilitating the dissociation of XPC from the NER apparatus, permitting the subsequent recruitment of further NER proteins. XPC-hHR23B is essential in the initial assembly of the preincision complex; however, XPC-hHR23B is superfluous during the formation of the dual incision complex (Wakasugi & Sancar, 1998).

Interestingly, it has been speculated that polyubiquitylated XPC is protected from proteasome-mediated degradation through its interaction with the ubiquitin-associated (UBA) domains of the hHR23A and hHR23B proteins, which protect XPC from degradation (Ng *et al.*, 2003; Okuda *et al.*, 2004). In agreement with these findings, further investigations in yeast have shown that the homologous protein, Rad23, regulates NER through its interaction with members of the proteasome (Russell *et al.*, 1999; Ortolan *et al.*, 2004; Heessen *et al.*, 2005; Gillette *et al.*, 2006).

Although basal levels of both DDB2 and p53 are required for the modifications exhibited by the XPC protein, it has been speculated that the ubiquitylation and subsequent degradation of DDB2 is also essential for the successful modification of the XPC protein (Ford *et al.*, 2005). In addition, however, it has been speculated that these modifications require both the ubiquitylation and

degradation of DDB2; the first to assist DDB-CUL4A mediated ubiquitylation of XPC, and the second to facilitate the displacement of DDB2 from a damaged site, thus permitting the subsequent recruitment of XPC. Additionally, the degradation of DDB2 is thought to facilitate the recruitment of NER proteins and increases the accessibility for the sequential assembly of the NER apparatus (Fig. 1.4).

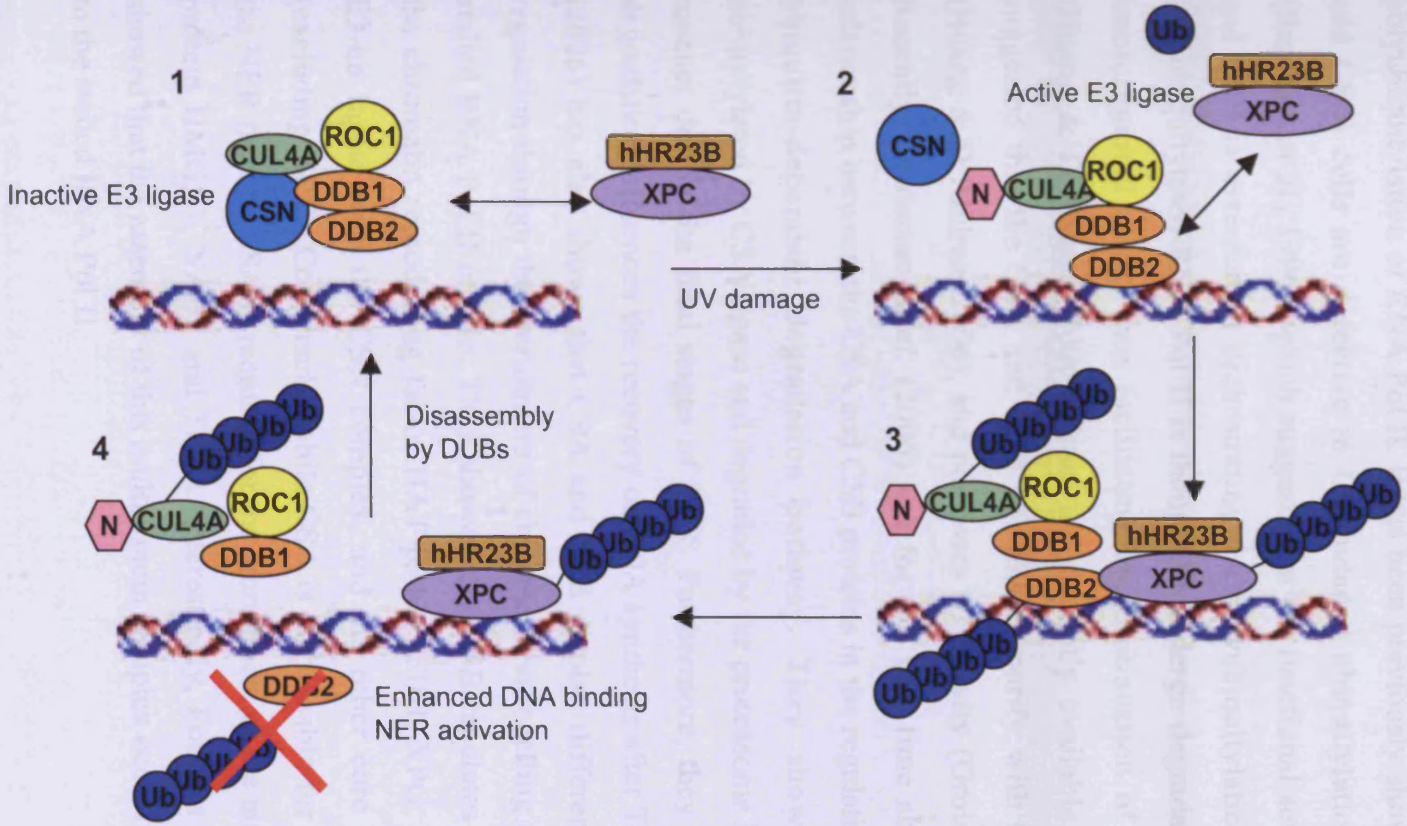

Figure 1.4. Regulation of GGR by the polyubiquitylation of XPC. In undamaged cells, the DDB E3-ligase complex (including DDB1-DDB2, CUL4A and ROC1) is in an inactive state, due to its interaction with the negative regulator, CSN. Furthermore, XPC is not ubiquitylated irrespective of its association with the DDB ligase complex (step 1). Following UV exposure, the DDB ligase complex translocates onto the DNA lesion, causing neddylation (N) of the CUL4A subunit and the disassociation of CSN. This results in the activation of the DDB ligase complex and the recruitment of XPC-hHR23B to the damaged DNA (step 2). XPC, DDB2 and CUL4A are polyubiquitylated by the DDB ligase complex (step 3). The polyubiquitylation of XPC potentates the DNA-binding and mechanistic action of XPC. Conversely, polyubiquitylation of DDB2 targets it for proteasomal-mediated degradation. The ubiquitylated DDB ligase complex mediates the displacement of the complex from the damaged site (step 4). The final abolition of this pathway may involve DUBs (adapted from Huang & D'Andrea, 2006).

As previously discussed, TCR preferentially repairs lesions on the transcribed strand of transcriptionally active genes, and is regulated through the polyubiquitylation of RNA Pol II. It has been previously shown that both CS-A and CS-B cells are defective in UV-induced ubiquitylation of RNA Pol II (Bregman *et al.*, 1996), which suggests that the functional activity of both CSA and CSB is essential in orchestrating the polyubiquitylation of RNA Pol II. Polyubiquitylated RNA Pol II is thought to undergo degradation or bypass the transcriptional block, thus facilitating the continuation of mRNA synthesis (Huang & D'Andrea, 2006). From the currently available data, it has been suggested that the CSA and CSB proteins co-purify with the CSN complex (Huang & D'Andrea, 2006), and possesses E3 activity (Groisman *et al.*, 2003). Recently, Groisman *et al.* (2006) has for the first time shown a functional relationship between the CSA and CSB proteins in the regulation of TCR, via the ubiquitin-dependent degradation pathway. They showed that CSB is ubiquitylated by CSA ligase and degraded by the proteasome in a UV-dependent manner during the final stages of TCR. Furthermore, they showed that CSB degradation influences the recovery of RNA synthesis after TCR. Fousteri *et al.* (2006) has also shown that CSA and CSB display differential roles in TCR regulation through the recruitment of chromatin remodelling or repair factors to stalled RNA Pol II *in vivo*. They showed that CSB regulates the recruitment of the chromatin remodelling factor HAT p300, TFIIH, XPG, RPA, CSA/DDB1 E3-ub ligase with the CSN complex, and the other core NER components (excluding XPC). Conversely, while CSA is dispensable for the recruitment of the NER factors, CSA is required for the recruitment of the nucleosomal binding protein HMGN1, XAB2 and TFIIS. Interestingly, Fousteri *et al.* (2006) also showed that the assembly of this multiprotein complex occurs without disruption to the stalled RNA Pol II.

The precise molecular function of ubiquitylated RNA Pol II has remains elusive. However, a recent study has suggested that the E3 complex facilitates the degradation of stalled RNA Pol II (Kleiman *et al.*, 2005). In support of these findings, previous yeast studies have shown that the yeast orthologue of CSB, Rad 26, interacts with Def1, which is essential in the ubiquitylation of RNA Pol II, following DNA damage. This interaction between Rad26 and Def1 is not

required for TCR (Woudstra *et al.*, 2002). By contrast, Rad26 is indispensable for TCR, but is not required for the degradation of RNA Pol II. Therefore, it has been speculated by Svejstrup *et al.* (2003), that the abolition of Rad26-dependent TCR of UV-induced damage, activates the targeted ubiquitylation and degradation of RNA Pol II through Def1. The targeted degradation of RNA Pol II is thought to initiate the removal of lesions from the transcribed strand by GGR.

1.9 Syndromes associated with defective NER

The importance of functional DNA metabolism and stress signalling/repair pathways, in maintaining genome stability and cellular homeostasis, has been exemplified by a series of human genetic disorders associated with defects in DNA repair and cellular signalling. Defects in approximately 35 distinct genes have been shown to cause 16 human genetic disorders, phenotypically presenting segmental progeria, a predisposition to tumorigenesis, or a complexity of both (Lehmann, 2003). In particular, defects in 11 distinct genes, which orchestrate the functioning of the NER pathway and/or basal transcription (and translesion synthesis), have been associated with autosomal recessive photosensitive syndromes: XP, XP with neurological deficiency and CS (Fig. 1.5). Additionally, less frequent photosensitive syndromes (<50 characterised individuals worldwide), include: trichothiodystrophy (TTD), combined xeroderma pigmentosum with Cockayne syndrome (XP-CS), combined xeroderma pigmentosum with trichothiodystrophy (XP-TTD), XP with DeSanctis-Cacchione syndrome (XP-DSC), cerebro-oculo-facio-skeletal syndrome (COFS) and UV-sensitive ($UV^{S}S$) syndrome (Fig. 1.5). Although XP, CS and TTD are genetic disorders of defective NER, the spectrum of clinical manifestations exhibited by these three syndromes differs significantly. Moreover, the more recent emergence of genotypes that exhibit the combined phenotypes (such as XP-CS, XP-TTD and XP-DSC) has further increased the clinical and molecular complexity of these syndromes (Fig. 1.5).

1.9.1 'Classical' xeroderma pigmentosum (XP)

XP, initially described in the late 19th century by Hebra & Kaposi, is a rare (approximately 1 in 250, 000 newborns) autosomal recessive hereditary human skin disease. XP is further classified into two distinct entities, known as "classical" and variant. Systematic analysis of classical XP, utilising cell fusion methodologies (de Weerd-Kastelein *et al.*, 1972), resulted in the elucidation of seven complementation groups designated XP-A to XP-G (Fig. 1.5; as described in section 1.1.4). Each corresponding to defects in the *XPA* to *XPG* genes, which perform vital functions during NER and transcription. Accordingly, abolition of GGR (with or without defects in TCR) causes XP. GGR has a greater influence on carcinogenesis compared to defective TCR. Evidence in support of this comes from human tumours where 90% of the G to T transversion mutations identified in the *TP53* tumour suppressor gene correspond to damage on the non-transcribed DNA strand (Denissenko *et al.*, 1998).

The heterogeneous nature of XP is typified by the multitude of clinical manifestations documented in ~1000 XP cases (Andressoo & Hoeijmakers, 2005). The hallmark clinical manifestations exhibited by XP patients include a severe photosensitivity to the UV constituent of sunlight and a marked predisposition to skin neoplasia, with a >2000-fold incidence of skin tumours (Stary & Sarasin, 2002). Initially, XP patients present extensive dermatitis solaris and freckling, subsequent to minimal exposure to sunlight. Dermatitis solaris may continue for weeks resulting in erythema. This is followed by the appearance of atypical UV-induced cutaneous hyperpigmentation with dry parchment-like skin. XP patients exhibit further atypical cutaneous alterations, including increased melanin production in the basal cell layer, loss of skin elasticity, actinic keratosis, poikiloderma and premature skin aging. Further pathophysiological disturbances to the skin include atrophy, scabbing and extensive scarring. This is followed by the progressive formation of cutaneous lesions, resulting in a multiplicity of cutaneous tumours. This is observed in XP patients as young as 3-5 years old, who present cutaneous tumours, including: BCC and SCC, resulting in extensive facial disfigurement. Conversely, the

occurrence of BCCs and SCCs in NER-proficient individuals is observed at a mean age of 50-60 years (Fig. 1.2; Daya-Grosjean & Sarasin, 2005). In XP patients under the age of 20 years, the incidence of pigmentary tumours, such as malignant melanoma, is >2000-fold higher than in age-matched NER-proficient individuals. BCCs and SCCs account for approximately 96% of sporadic skin cancers and malignant melanoma account for 4% in the general population. By contrast, approximately 22% of skin cancers in XP patients are malignant melanoma (Takebe *et al.*, 1989; Kraemer *et al.*, 1994). Further malignancies including keratoakanthomas and sarcoma have been reported (De Silva *et al.*, 1999). Additionally, the incidence of neoplasia in the oral mucosa and internal organs is significantly higher in XP compared to the general population. XP patients most frequently die prior to adulthood, as a result of metastatic dissemination (English & Swerdlow, 1987).

XP patients exhibit several other pathophysiological features associated with neurological degeneration (Fig. 1.5), resulting from the progressive accumulation of DNA base damage. Symptoms of motor impairment, such as reduced reflexes, ataxia and spasticity have been widely documented. In addition, mental retardation coupled with impaired speech development has been reported. The presentation of severe neurological abnormalities has been further termed as DeSanctis-Caccione syndrome (discussed in Section 1.9.6). These patients are characterised by severe growth retardation, spasticity and intellectual impairment. Further pathophysiological manifestations exhibited in DeSanctis-Caccione syndrome included segmental demyelination, microcephaly, deafness and epilepsy. Tumours of the central nervous system (CNS), including astocytomas, medulloblastomas, glioblastomas and malignant schwannoma, have been reported (Nakamura *et al.*, 1991).

Ophthalmological manifestations are a key pathophysiological feature, and have been documented in approximately 40% of XP patients. Conjunctival inflammation, blepharitis, ectropion, symblepharon, vascular pterygia, fibrovascular pannus formation and corneal ulcerations have been described (Goyal *et al.*, 1994). Benign lid papillomas, corneal dysplasias and ocular neoplasis have been observed.

1.9.2 Xeroderma Pigmentosum variant (XP-V)

Initially described as 'pigmented xerodermoid (Jung *et al.*, 1970), XP-V patients exhibit a phenotype frequently observed in classical XP, such as photosensitivity and a marked predisposition to cutaneous malignancy. However, the symptomatic presentation in XP-V patients is significantly milder than 'classical' XP and documented much later in life (~30 years of age). Furthermore, approximately only 20% of individuals with XP are assigned to the XP-V complementation group (reviewed by Gratchev *et al.*, 2003). Intriguingly, at the cellular and biochemical level, XP-V cells display proficient NER, but possess a defect in post replication repair following UV irradiation (Lehmann *et al.*, 1977). Therefore, XP-V cells are deficient in the ability to synthesise intact complementary daughter DNA on the UV damaged parental template strand. Furthermore, cultured fibroblasts, obtained from XP-V individuals, exhibit a mild sensitivity to the killing effects of UV, compared to 'classical' XP individuals, which display a severe hypersensitivity. Burk *et al.* (1971) reported that a patient exhibiting severe pathophysiological features of XP displayed normal NER in his fibroblasts, lymphocytes and neoplastic cells. Subsequent cases of pigmented xerodermoid and XP-V were reported as discrete entities; until Cleaver *et al.* (1980) substantiated that the biochemical and molecular defects in pigmented xerodermoid and XP-V were analogous (Fischer *et al.*, 1980).

Following extensive biochemical studies, Masutani *et al.* (1999) showed that a protein isolated from HeLa cells restored the capability of XP-V cells to replicate DNA containing CPDs, by bypassing a TT-dimer in a error-free manner, while incorporating two adenines opposite the TT-dimer. Sequencing of the isolated protein resulted in the subsequent cloning of a translesion DNA polymerase, referred to as polymerase eta (polη). Polη is a member of the Y-family polymerases, which facilitate error-free bypass of replication-blocking lesions, via a process called translesion synthesis (TLS). Additionally, the highly specialised properties of Y-family DNA polymerases (including high flexibility and low processivity) permits polη to bypass DNA lesions and rapidly dissociate,

thus facilitating the rapid resumption of the replication machinery and the continuation of the replicative polymerase (Ling *et al.*, 2001). Further studies have suggested that polη activity is perturbed by the presence of a 6-4PP. Following the misincorporation of a G opposite the 3' (only) T of the 6-4PP, polη is displaced from the DNA (Zhang *et al.*, 2000), thus suggesting an incapacity to bypass 6-4PPs. Additionally, this further suggests that polη is a highly specialised bypass DNA polymerase, which facilitates the repair of UV-induced CPDs in an error-free manner. Therefore, aberrant TLS explains the molecular characteristics of XP-V cells and the phenotypic features displayed by XP-V patients. As the accurate bypass activity of polη is abolished and TLS is undertaken by an alternative error-prone bypass polymerase(s), thus resulting in an increase in the number of mutagenic events in the genome. Additionally, the cessation of polη activity causes the attenuation of S phase progression and the formation of double strand breaks and sister chromatid exchange (Cordeiro-Stone *et al.*, 2002; Limoli *et al.*, 2000; Limoli *et al.*, 2002), which significantly contributes to the increased incidence of cutaneous malignancy.

1.9.3 Cockayne syndrome (CS)

CS, first described by Edward Alfred Cockayne (1936), is a rare autosomal recessive disease typically characterised by a severe photophobia to sunlight. At the molecular level, CS is characterised by the abolition of recovery of RNA synthesis, after UV exposure, despite the normal repair capacity displayed by the genome overall (Mayne & Lehmann, 1982; Proietti-De-Santis *et al.*, 2006). Like XP, the photosensitivity in CS is manifested as a severe rash, however, the hallmark characteristic of XP, a marked predisposition to skin neoplasia, is absent in CS. This is exemplified by the ~180 characterised CS patients, which have displayed no predisposition to cutaneous or internal neoplasia (Spivak & Hanawalt, 2006). An extensive review of the clinical manifestations exhibited by 140 CS cases suggests that growth failure is the most frequently observed feature, which is exhibited within the first year of life (Nance & Berry, 1992). Premature aging is a further cardinal pathophysiological feature exhibited in CS. The observation that CS cells exhibit a severe deficiency in the recommencement

of RNA synthesis following damage has resulted in CS being described as a 'transcription syndrome' in addition to a 'repair syndrome' (Bootsma & Hoeijmakers, 1993). It has been shown that cell extracts, derived from UV-irradiated CS cells, were unable to transcribe even though the DNA template was free of lesions (Rockx *et al.*, 2000). Additionally, both RNA Pol II and the associated basal transcription apparatus are not sequestered to the promoter sites of 'housekeeping' genes. It has also been suggested that the acetylation of H4 is severely compromised at transcription initiation sites. The deficiency in transcription suggests a reason for the complete absence of tumour predisposition, as a result of the elimination of damaged cells by UV-induced apoptosis (Ljungman & Zhang, 1996). Conversely, it has been shown that the presence of wild-type CSB is dispensable for the transcription of p53-responsive genes, following DNA damage (Proietti-De-Santis *et al.*, 2006).

Characteristically, normal *in utero* development is followed by a state of cachectic dwarfism, which progresses during the first year of life. Subsequently, CS patients present an atypical progeroid phenotype coupled with large ears and nose, sunken eyes, thinning of the skin and hair, and a curved standing posture. CS patients also demonstrate a thin appearance, resulting from the progressive loss of subcutaneous fat tissue (Nance & Berry, 1992). Further symptomology displayed in CS, includes an array of skeletal abnormalities such as a bird-like face, dental caries, kyphosis of the spinal cord and osteoporosis. In addition, progressive neurological degeneration is observed, coupled with delayed psychomotor development and mental retardation. Microcephaly is observed in CS patients over 2 years of age, and nerve biopsies frequently demonstrate myelination abnormalities. The postnatal neurological manifestations displayed by CS patients are thought to occur due to aberrant neuronal proliferation, migration and deployment (Rapin *et al.*, 2000). Moreover, the progressive accumulation in oxidative DNA damage may further explain the postnatal onset of CS. The early onset of cataracts coupled with marked neurological abnormalities and microcephaly, is frequently indicative of poor prognosis and survival. Further clinical features exhibited in CS include sensorineural hearing loss, progressive pigmentary retinopathy. CS patients also present impaired sexual development along with their postnatal growth failure. The failure to

thrive coupled with neurological degeneration is followed by pneumonia and respiratory infections, resulting in death at a mean age of 12.5 years. Historically, CS patients have been assigned to one of two classic complementation groups (Fig. 1.5), CS-A or CS-B (Troelstra *et al.*, 1992; Henning *et al.*, 1995). However, patients with mutations in three XP genes, *XPB*, *XPD* and *XPG* also exhibit clinical manifestations exhibited by CS patients, in addition to displaying features common to XP. Further classification of CS has resulted in the characterisation of a spectrum of distinct but associated syndromes differing in the underlying genetic defect and pathophysiological severity. These include CS type 1 (CS-A), CS type 2 (CS-B), COFS (discussed in section 1.9.7), Pena-Shokeir type 2, CS type 3, and XP-CS (discussed in Section 1.9.5).

1.9.4 Trichothiodystrophy (TTD)

TTD, first described by Price *et al.* (1980), is a rare autosomal recessive syndrome. Three genetic complementation groups have been identified, which correspond to mutations in the *XPB*, *XPD* and *TTDA* (*TFB5*) genes (Fig. 1.5), and all of which are constituents of the 11-subunit transcription/repair factor TFIIH apparatus. Therefore, the phenotypic characteristics exhibited by TTD patients are attributed to an impairment of the basal transcription machinery, in addition to the DNA repair defect. Therefore, like CS, TTD has been referred to as a 'transcriptional syndrome' (de Boer & Hoeijmakers, 2000; Bergmann & Egly, 2001). Like XP and CS, TTD is frequently characterised by a severe photophobia to sunlight. Unlike XP however, TTD patients do not display an atypical predisposition to skin neoplasia or pigmentary abnormalities. Indeed, many TTD patients exhibit varying degrees of photosensitivity and aberrant NER (Stefanini *et al.*, 1986). Furthermore, it has been previously shown that TTD patients exhibit a concordant relationship between photosensitivity and heterogeneous repair of UV-induced lesions (Broughton *et al.*, 1990; Stefanini *et al.*, 1992). However, some TTD patients do not display sensitivity to sunlight (Lehmann, 2001).

The cardinal manifestations of TTD include an atypical predisposition to sulphur-deficient brittle hair caused by a diminution of cysteine-rich matrix proteins within the hair shaft, resulting in trichoschisis. This is further typified by "tiger tail" patterns observed in the brittle hair fibres (Liang *et al.*, 2004). Further clinical features presented by TTD patients, include ichthyosis, mental and physical retardation. Due to the heterogeneous nature of TTD, a multiplicity of syndromes have been erroneously described as discrete entities (including Pollitt syndrome, Tay's syndrome, Amish brittle hair syndrome, Sabinas syndrome and Marinesco-Sjögren syndrome), which have subsequently been reassigned as TTD. Although infrequently documented, TTD patients display a pattern of mental development that is comparable to that of CS patients. Further symptomatic features include: low IQ, hyperreflexia, tremor and ataxia. In addition, microcephaly and neurodysmyelination of the cerebral white matter has been observed. Aberrant development of the reproductive system, such as hypogonadism and cryptorchidism has been reported, resulting in reduced fertility. As observed in CS, cachectic dwarfism is a feature frequently exhibited in TTD. However, the extent of cachexia varies considerably in TTD. Additionally, like CS, skeletal abnormalities are a further feature of TTD, including: a bird-like face, abating chin, delayed skeletal development, axial osteosclerosis and peripheral osteoporosis.

1.9.5 Combined XP-CS

A combined XP-CS phenotype has been documented in an infrequent number of photosensitive individuals (Lindenbaum *et al.*, 2001). These patients display the cutaneous disturbances (such as freckling, BCCs, SCCs and malignant melanomas) associated with XP, coupled with the progressive neurological abnormalities observed in CS. Pigmentary disturbances have been observed as early as 2 weeks of age, with cutaneous neoplasia displayed at 2.5 years of age. Among the 9 reported cases, the additional clinical manifestations displayed by combined XP-CS patients are extensively heterogeneous, as XP-CS patients exhibit a complexity of additional pathophysiological features, such as cachexia, dwarfism and pigmentary retinal degeneration. However, the clinical features

typically associated with CS are more prevalent in combined XP-CS patients. For example, in XP, the neurological abnormalities are attributed to primary neurological degeneration. By contrast, the neurological pathology observed in CS results from demyelinating neuropathy. At autopsy, like CS, combined XP-CS patient's present marked dysmyelination (Lindenbaum *et al.*, 2001). At the cellular level, however, XP-CS cells are analogous to XP cells, displaying attenuation in UDS and the complete abolition of photoproduct repair. This has been further associated with the generation of nicks in DNA subsequent to UV radiation. Intriguingly, Berneburg *et al.* (2000) established that the formation of nicks occurred at sites other than that induced by DNA damage. It has been speculated that the induction of nicks is caused by a defect in the TFIIH complex. This causes the NER apparatus to erroneously recognise a transcription initiation site as a damaged region, thus resulting in generation of DNA nick at a transcription initiation site.

To date, three complementation groups (XP-B, XP-D and XP-G) have been elucidated, which display a combined XP-CS phenotype (Fig. 1.5). Three patients have been identified with a point mutation in the *XPB* gene, and display a relatively mild CS phenotype. Two patients have been assigned to the XP-D complementation groups, whilst the remaining four patients possess mutations in the *XPG* gene (Lindenbaum *et al.*, 2001). The XPD-XPCS and XPG-XPCS patients presented severe phenotypes and all died before the age of seven.

1.9.6 Xeroderma pigmentosum with DeSanctis-Cacchione (XP-DSC) syndrome

XP-DSC was first identified by DeSanctis & Cacchione (1939), who reported the association between severe neurological abnormalities coupled with the dermatological manifestations of XP. Approximately 20% of XP patients display neurological abnormalities (Fig. 1.5). Whilst the formation and progression of cutaneous neoplasia in XP-DSC are comparable to that observed in XP, the average presentation of photosensitivity for XP-DSC is 6 months. Conversely, patients assigned to "classical" XP complementation groups display sensitivity to

sunlight at 2 years (Kraemer *et al.*, 1987). Although 80% of XP-DSC patients present severe mental retardation, less than 25% of patients exhibit concurrent microcephaly, growth retardation and gait disturbances, such as spasticity, and ataxia (Kraemer *et al.*, 1987; Itoh *et al.*, 1999; Brooks, 2002).

Interestingly, XP-DSC patients do not present demyelination of CNS and the peripheral nervous system (PNS), or retinal degeneration and calcification of the basal ganglia, typically associated with CS. However, XP-DSC patients display diminution of specific neuronal populations. In particular, extensive cell death occurs within the cortex and substantia nigra of the CNS, resulting in severe intellectual impairment and dementia (Brooks, 2002; Itoh *et al.*, 1999).

1.9.7 Cerebro-oculo-facial-skeletal (COFS) syndrome

Although COFS was first identified in 1971 (Lowry *et al.*, 1971), the multiplicity of clinical manifestations was not unequivocally documented until 1974 (Pena & Shokeir, 1974). COFS is an autosomal recessive hereditary syndrome with only approximately 50% of patients presenting a hypersensitivity to the UV constituent of sunlight. Until recently, COFS was considered a severe variant form of CS type II, as the phenotypic characterisation of cell lines ascertained from genotypically characterised COFS patients are indistinguishable from those cell lines derived from typical CS patients. However, the comprehensive analysis of a recently identified COFS patient resulted in the elucidation of a previously uncharacterised mutation in the *XPD* gene. This suggests that, the underlying molecular defect is not limited to a single gene mutation. The cardinal diagnostic features indicative of COFS includes skeletal defects at birth resulting from fetal immobility and cataracts. However, these two clinical features in isolation may not permit a definitive diagnosis (Bohr *et al.*, 2005). The differentiation between COFS and CS can be determined by the dissimilar ocular defects exhibited by the two syndromes. COFS patients present microcornea with optic atrophy. By contrast, CS patients exhibit less severe ocular defects and are most frequently associated with pigmentary retinopathy (Andressoo & Hoeijmakers, 2005). Further clinical manifestations of COFS include: reduced birth weight, loss of

subcutaneous fat, hypogonadism, microcephaly, cerebral atrophy, severe mental retardation, hypoplasia of the corpus callosum, progressive joint contractures and hypotonia (Pena & Shokeir, 1974).

Until recently, the underlying molecular defect in COFS has remained uncharacterised. However, recent reports have suggested that COFS is heterogeneous for mutations in the *XPD*, *XPG* and *CSB* genes (Fig. 1.5). For example, Graham *et al.* (2001) identified a point mutation in the *XPD* gene. Furthermore, Meira *et al.* (2000) documented a mutation in the *CSB* gene, resulting in a mild C-terminal truncation of the CSB protein.

1.9.8 UV-sensitive syndrome ($UV^{S}S$)

Unlike XP, CS and TTD, the identification of patients with $UV^{S}S$ remains extensively problematic, due to a relatively asymptomatic presentation and the complete absence of any distinguishing pathophysiological features. The first realisation that $UV^{S}S$ was a discrete entity was made by Cleaver & Thomas (1993), who took a large cohort of UV sensitive individuals and concluded that a subset were distinct from XP and CS. Initially, patients with $UV^{S}S$ present an atypical response to UV exposure similar to that exhibited by mild XP, resulting in acute sunburn, coupled with cutaneous photosensitivity (erythema) and mild pigmentary disturbances (skin dryness and extensive freckling), while the multiplicity of clinical manifestations observed in XP, CS and TTD are completely absent.

To date, $UV^{S}S$ has remained idiopathic, due to an insufficient number of patients and the erroneous assignment of previously documented cases to the CS-B and XP-E complementation groups (Miyauchi-Hashimoto *et al.*, 1998; Itoh *et al.*, 2000). However, more recent investigations have revealed that $UV^{S}S$ is attributed to a defect in the TCR of UV-induced cytotoxic lesions in the transcribed strand of transcriptionally active genes (Spivak *et al.*, 2002), whilst the GGR of UV-induced CPDs and 6-4PPs remains normal. Additionally, at the cellular and biochemical level, the responses elicited by $UV^{S}S$ and CS cells in

response to UV light are indistinguishable (Spivak *et al.*, 2002), which may explain the absence of cutaneous or internal tumours. Furthermore, $UV^{S}S$ cells exhibit a similar pattern of p53 accumulation to CS cells (Ohta *et al.*, 1999). $UV^{S}S$ cells, like CS cells, are defective in the recovery of RNA and DNA synthesis following UV damage. Interestingly, the cardinal hallmark characteristics of CS, including neurological and developmental abnormalities, are not observed. It has been speculated that the absence of neurological and developmental abnormalities in $UV^{S}S$ patients is attributed to the preservation of the proficient removal and repair of oxidative lesions, or in transcriptional bypass of these lesions (Spivak, 2004). In agreement with this, Spivak & Hanawalt (2006) have demonstrated that $UV^{S}S$, but not CS-B cells, are proficient in host cell reactivation of plasmids possessing oxidative DNA lesions.

To date, six patients with $UV^{S}S$ have been identified (Spivak, 2005), and assigned to one of two complementation groups and allocated the nomenclatures: $UV^{S}S$/CS-B and $UV^{S}S$/A. In concordance, cell fusion studies of cells obtained from $UV^{S}S$ patients, resulted in the complementation of cell lines derived from previously characterised XP and CS patients (Itoh *et al.*, 1995). Further experimentation has resulted in the identification of a *CSB* gene mutation specific for two $UV^{S}S$ patients and their reclassification to the $UV^{S}S$/CS-B complementation group. However, the gene defect in four $UV^{S}S$ patients remains uncharacterised ($UV^{S}S$/A).

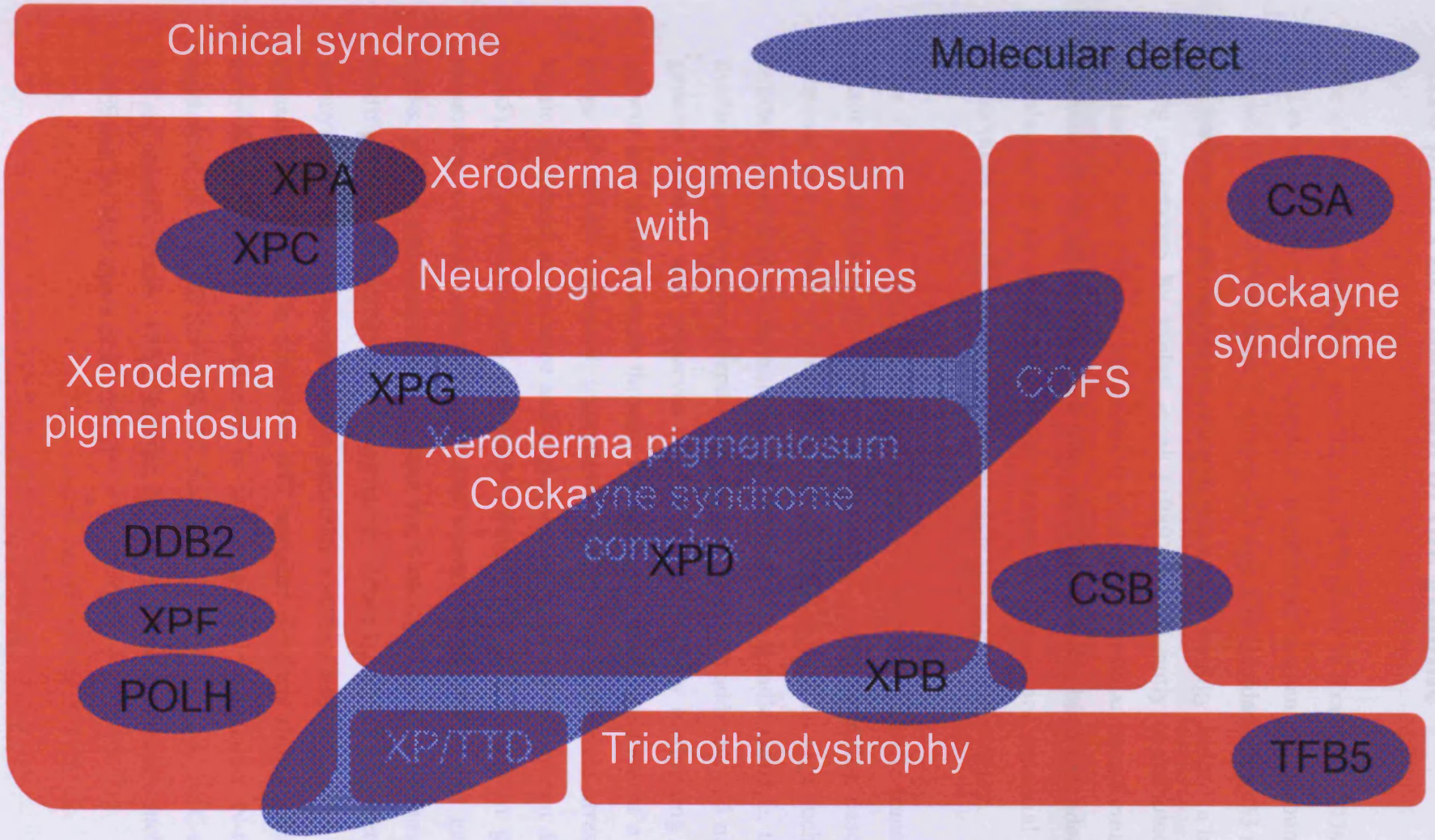

Figure 1.5. Phenotype-Genotype relationship between rare human diseases of NER and transcription associated with 11 different gene defects (Ovals). All seven syndromes (rectangles) display extreme photosensitivity, but exhibit a battery of additional clinical manifestations (adapted from Kraemer, 2004)

1.10 p53: The guardian of the genome

The p53 tumour suppressor, identified in 1979 (Lane & Crawford, 1979; Linzer & Levine, 1979), was first isolated in transformed human cells, bound to the simian virus 40 (SV40) large T antigen (LTAg). The elucidation of p53 structure and function has revolutionised research into tumour biology. Indeed, a landmark study undertaken by Finlay *et al.* (1989), significantly contributed to the realisation that p53 was an essential inhibitor of cellular transformation. In addition to its antiproliferative role, p53 function has been extended to the regulation of an array of cellular processes, which are essential for the preservation of cellular homeostasis and maintaining genome stability.

The *TP53* tumour suppressor gene encodes a sequence-specific transcription factor that regulates the activation of general stress signalling cascades in response to a plethora of exogenous and endogenous DNA damage such as UV, hypoxia, oxidative stress, nucleotide insufficiency, spindle damage, telomere dysfunction and hyperproliferative oncogenic signals. In addition, p53 maintains genome stability and preserves cellular homeostasis by modulating cellular growth and differentiation through the activation and regulation of a diverse range of cellular responses: transcriptional activation, cell cycle arrest, DNA repair, apoptosis, senescence and angiogenesis (reviewed by Latonen & Laiho, 2005). The dysregulation of these cellular processes results in genomic instability, cellular transformation and tumorigenesis. Following genotoxic stress, p53 is activated and stabilised via a multiplicity of posttranslational modifications including: phosphorylation, dephosphorylation, acetylation, sumoylation and glycosylation. This generates a sequence-specific DNA binding domain, which binds to consensus p53 response elements situated within the promoter or intronic constituents of target genes. In particular, N-terminal residues of p53 such as Ser15, Ser20, Ser33, Ser37, and Ser392 at the C-terminal end are phosphorylated within minutes, following genotoxic damage such as UV (reviewed by Melnikova *et al.*, 2005).

Essentially, the p53 tumour suppressor mechanistically functions as a transcription factor, which orchestrates the differential regulation of a multiplicity of downstream gene targets. Previously, Tokino *et al.* (1994) identified 57 tagged sequences from a human genomic library, which corresponded to p53 binding sites. Furthermore, Zhao *et al.* (2000) used oligonucleotide arrays to characterise p53 regulated gene expression and identified over one hundred downstream targets.

The importance of p53 in orchestrating cellular homeostasis and the antiproliferative machinery has been exemplified in human cancers. *TP53* mutations, resulting in aberrant functioning or complete abolition of p53 activity, are found in approximately 50% of all human cancers (Harris & Hollstein, 1993). Furthermore, 5% of *TP53* gene mutations have been identified in the regulatory domain, with 95% of the mutations occurring in the central DNA binding domain (Hoogervorst *et al.*, 2005). Furthermore, mutations in the *TP53* gene can result in the addition of oncogenic functions through a dominant-negative phenotype. The wild-type p53 protein, produced by the normal allele, is inactivated by hetrodimerization with the mutated p53 protein (Milner and Medcalf, 1991).

1.10.1 p53 structure

The *TP53* gene has remained relatively conserved throughout evolution (Soussi *et al.*, 1987; Soussi *et al.*, 1990). In human cells, p53 is found situated on the short arm of chromosome 17 (17p13). The human *TP53* gene encodes a nuclear phosphoprotein of 393 amino acids and possesses a molecular weight of 43.6 kDa. Like many transcription factors, p53 contains a series of functional domains, which tightly regulate the functional activity of its transcription factor activity and a multitude of downstream events. p53 contains five structurally and functional discrete domains: (1) amino-terminal (N-terminal domain); (2) proline-rich domain; (3) sequence-specific DNA binding domain; (4) oligmerisation domain; (5) carboxy-terminal (C-terminal) domain (Fig. 1.6). The N-terminus, also referred to as the transactivation domain (TAD), possesses an acidic domain (amino acids 1-42), which is essential for the interaction with

constituents of the transcriptional apparatus, such as TBP and TAFs, thus facilitating the transcriptional activation and repression of downstream target genes (Seto *et al.*, 1992; Xiao *et al.*, 1994; Lu & Lavine, 1995; Thut *et al.*, 1995; Chao *et al.*, 2000). Contiguous to the N-terminal domain is a proline-rich domain (amino acids 63-97), which contains five proline repeats. This region is instrumental in the regulation of the apoptotic pathway (Walker & Lavine, 1996; Sakamuro *et al.*, 1997; Venot *et al.*, 1998). Furthermore, the proline-rich domain has been implicated as a negative regulator of p53. The sequence-specific DNA binding domain (102-292) is composed of a DNA consensus sequence 5'-PuPuPuC(A/T)-(T/A)GPyPyPy-3' (Pu, purine; py, pyrimidine) that is located in the central region of the p53 protein (el-Deiry *et al.*, 1992). The oligomerisation domain (amino acids 323-356) is required for the formation of p53 tetramers, which permits the sequence-specific binding of p53 with DNA (Wang *et al.*, 1993; Friedman *et al.*, 1993). Finally, the C-terminal domain, which resides between amino acids 363-393, maintains p53 in an inactive state until posttranslational modifications (such as phosphorylation and acetylation) allosterically activate the protein (Fig. 1.6).

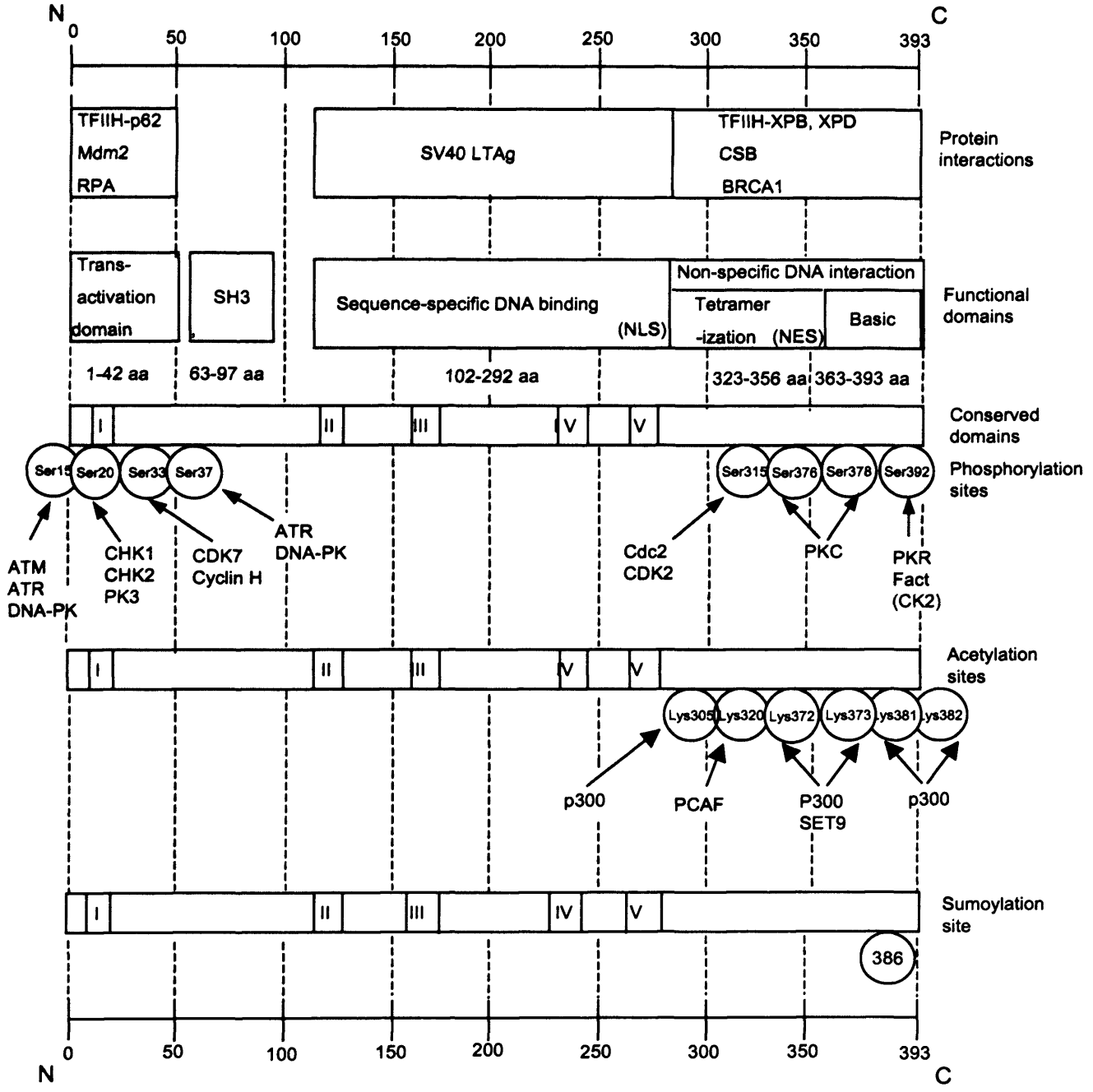

Figure 1.6. Schematic of human p53 protein structure. The p53 protein is composed of 393 amino acids. A multiplicity of factors interact with p53 and those that are of particular interest are highlighted. Normal p53 functionality is dependent upon a series of posttranscriptional modifications, such as phosphorylation, acetylation and sumoylation. The most significant and well-characterised residues that undergo posttranslational modification have been highlighted. *Abbreviations*: Lys, lysine; NES, nuclear export signal; NLS, nuclear localisation signal; Ser, serine; SH3, SRC homology 3-like.

1.10.2 Regulation of p53

Under normal physiological conditions, wild-type p53 is expressed at low basal levels in cells. The transient nature of p53 is attributed to a relatively short half-life of approximately 10-20 minutes, resulting from the rapid turnover of p53, mediated by the ubiquitin-proteasomal pathway (Giaccia and Kastan, 1998). However, exposure to a plethora of exogenous and endogenous agents, such as UV, IR, hypoxia, nucleotide imbalance, spindle damage or hyperproliferative signals (Levine, 1997), elicit the transient induction of nuclear p53 protein levels (Kastan & Kuerbitz, 1993), in a dose-dependent manner with negligible effect on p53 mRNA levels. The increased stability of the p53 protein occurs within minutes following DNA damage, due to a series of posttranslational modifications at the N-terminus (including Ser15, Ser20 and Ser33), which inhibits the interaction of proteins that regulate its degradation (Fig. 1.7), such as the transformed 3T3 cell double minute 2, p53 binding protein (Mdm2; Shieh *et al.*, 1997; Shieh *et al.*, 1999).

The ubiquitin-proteasome pathway mediates the degradation of p53 through the targeted action of the 26S proteasome complex (Rodriguez *et al.*, 2000). The ubiquitylation of p53 is initiated by the mechanistic action of the proto-oncogene, Mdm2, which possesses E3 activity (Yang *et al.*, 2004; Vargas *et al.*, 2003). Interestingly, Mdm2 is a transcriptional downstream target of p53 and a repressor of p53 function, thus resulting in the establishment of a negative autoregulatory feedback loop (Momand *et al.*, 1992; Wu *et al.*, 1993). Mdm2 binds the N-terminus of p53, thus preventing the subsequent interaction between p53 and the transcriptional apparatus. This results in the mono-ubiquitylation of p53, which mediates the nuclear export of Mdm2-bound p53 for subsequent degradation by the ubiquitin-mediated proteolytic pathway (Honda *et al.*, 1997; Freedman & Lavine, 1998). Furthermore, Mdm2 interacts with the p53 TAD, resulting in the abolition of p53-mediated transcriptional activation (Chen *et al.*, 1993). In addition to Mdm2, HAT p300 is required for p53 degradation (Grossman *et al.*, 1998; Zhu *et al.*, 2001), as Mdm2 can only monoubiquitinate p53 (Lai *et al.*, 2001). Following nuclear export, HAT mediates the polyubiquitylation of p53

(Grossman *et al.*, 2003), which results in the subsequent ubiquitylation of both p53 and Mdm2 (Honda *et al.*, 1997; Haupt *et al.*, 1997). However, the N-terminal phosphorylation of p53 abolishes its interaction with Mdm2, thus resulting in stabilisation of p53.

Subsequent to cellular stress (such as UV-irradiation), the dissociation of the p53-Mdm2 complex occurs, resulting in the accumulation of the p53 protein. The disruption of the p53-Mdm2 complex is mediated by the recruitment of interacting proteins, which preferentially binds to Mdm2. Alternatively, posttranslational modifications to the p53 and/or Mdm2 proteins, promotes the liberation of p53. For example, ARF (alternative reading frame; $p14^{ARF}$) interacts with the C-terminus of the Mdm2 protein, resulting in the relocation of Mdm2 to the nucleoli, thus inhibiting Mdm2-mediated ubiquitylation of p53 (reviewed by Sherr &Weber, 2000).

The functional activation of p53 occurs through posttranscriptional covalent modifications, at both the amino-terminal and the carboxyl-terminal domains via phosphorylation, acetylation and sumolation (Fig. 1.6). These modifications facilitate the subsequent regulation of p53 by promoting DNA binding, degradation, cellular localisation, oligomerisation and affiliation with cellular molecules.

1.10.3 p53 and cell cycle arrest

Following genotoxic damage, activation and accumulation of the p53 tumour suppressor signals the G_1 cell cycle checkpoint to inhibit the transition from G_1 to S phase. This increases the opportunity for the repair of DNA damage prior to the commencement of replication in S phase. This prevents the propagation of potentially mutagenic defects from parental to daughter cell populations. Cell-cycle arrest is mediated in part by the p53-dependent induction of $p21^{WAF1/CIP1}$ (Fig. 1.7), an inhibitor of CDKs, which abolishes the interaction between cyclin D/cdk4, cyclin D/cdk6 and cyclin E/cdk2 complexes (Harper *et al.*, 1993; El-Deiry *et al.*, 1993; Dulic *et al.*, 1994). The coupling of cyclin D to cdk4/6 causes

the phosphorylation of serine and threonine residues on the Rb tumour suppressor, this tethers Rb from the E-box factor 2 (E2F) transcription factor, thus permitting E2F-mediated activation of a multiplicity of downstream transcriptional gene targets required for S phase progression. However, the overexpression of $p21^{WAF1/CIP1}$ causes the accumulation of hypophosphorylated Rb (pRb) and the sequestration of E2F, resulting cell-cycle arrest.

1.10.4 The role of p53 in UV-induced NER

The p53 tumour suppressor protein mediates a series of cellular responses that inhibit photocarcinogenesis following UV, such as enhancing NER and inducing apoptosis (Hall *et al.*, 1993; Brash *et al.*, 1996). In addition to a high nuclear accumulation of p53 (Hall *et al.*, 1993), exposure to UV also causes the phosphorylation of p53 at Ser46 (Fig. 1.7), which regulates the activation of p53-dependent apoptotic genes (Oda *et al.*, 2000). Phosphorylation of p53 also occurs at Ser15 and Ser20 (Fig. 1.7), which regulate the transcriptional activation of G_1 checkpoint arrest genes, such as $p21^{WAF1/CIP1}$, and genes involved in DNA repair (reviewed by Adimoolam & Ford, 2003; Ford, 2005; Hanawalt, 2002; McKay *et al.*, 1999; Seo & Jung, 2004).

The systematic investigation into the mechanistic action and regulation of the NER machinery has resulted in the identification of key effector molecules, such as the p53 tumour suppressor, which coordinates the spatial and temporal regulation of the NER pathway. A recent body of evidence has shown that NER factors are upregulated in response to UV in a p53-dependent manner at both the transcriptome and proteome level (Adimoolam & Ford, 2002; Amundson *et al.*, 2002; Amundson *et al.*, 2003; Ng *et al.*, 2003).

Since the initial observation that p53 stabilisation occurs in nontransformed mouse cells subsequent to UV-irradiation (Maltzman *et al.*, 1984), it has been shown that the core domain of p53 contains 3'-5' exonuclease activity (Janus *et al.*, 1999). However, this remains poorly delineated. Numerous studies have also demonstrated that the C-terminal domain directly interacts with DNA lesions or

single-stranded DNA (Bakalkin *et al.*, 1995; Jayaraman & Prives, 1995; Lee *et al.*, 1997). Conversely, Jackson *et al.* (1994) has shown that p53 does not localise at sites of NER. Following further extensive investigation, however, p53 is now thought to regulate stress signalling pathways and modulate the NER machinery through the transcriptional activation of downstream gene targets. Alternatively, p53 modulates the NER machinery through direct interaction with proteins that coordinate the DNA damage response and the NER pathway, which are independent of transcriptional modifications.

The initial discovery that p53 orchestrates an essential function in NER regulation, was first identified in Li-Fraumeni syndrome (LFS) skin fibroblasts (Ford & Hanawalt, 1995). Cells derived from LFS patients possess germline mutations in the *TP53* gene, which phenotypically causes a marked predisposition to cancer. From studies utilising LFS cells, Ford & Hanawalt (1995) found that LFS cells possessing homozygous mutations for *TP53*, resulted in the attenuation of GGR. In contrast, LFS cells, heterozygous for *TP53* mutations, displayed levels of GGR comparable to normal cells. Additionally, using strand-specific DNA repair assays, based on Southern blot methodologies first described by Bohr *et al.* (1985), Ford & Hanawalt (1997) further reported that the abolition of p53 activity in LFS cells had no effect on the removal of CPDs by TCR. Furthermore, it has been shown that the abolition of p53 activity by viral proteins, such as the E6 constituent of the human papillomavirus (HPV)-16 virus, abrogates GGR (Ford *et al.*, 1998; El-Mahdy *et al.*, 2000). In concordance, other groups have shown that *TP53* mutations or disruption to p53 function cause a significant reduction in the removal of CPDs by GGR (Smith *et al.*, 1995; Zhu *et al.*, 2000). These findings were further substantiated by repair analysis at single nucleotide resolution, where Wani *et al.* (1999) showed that the removal of CPDs from the nontranscribed strand by GGR was attenuated in *TP53* mutant and null cell lines, compared to wild-type cells. In contrast, the removal of CPDs in the transcribed strand was similar in the *TP53* mutant, null and wild-type cells. Indeed, a multiplicity of studies has indicated that basal p53 levels are indispensable for the proficient repair of CPDs by GGR. However, it has been speculated that the regulation of GGR could occur via p53-independent mechanisms in a cell-type specific manner. For example, Oh & Yhe (2005) have

reported the proficient removal of CPDs in differentiated kerationcytes in the absence of detectable basal levels of p53.

Conflicting studies, however, have demonstrated that p53 modulates TCR (Wang *et al.*, 1995; Mirzayans *et al.*, 1996; Therrien *et al.*, 1999). In concordance with these reports, McKay & Ljungman (1999) have shown that the p53-deficient LFS cells utilised in previous studies (Ford & Hanawalt, 1995; Ford *et al.*, 1998) display a defect in the recovery of RNA synthesis, following UV-irradiation. This suggests that TCR is impaired in LFS cells. Whereas, Leveillard *et al.* (1996) reported that the inclusion of recombinant p53 protein *in vitro* did not enhance NER *per se*. These conflicting and controversial observations have been attributed to technical differences between studies, such as *in vitro* versus *in vivo* assays, cell-type used and the UV wavelength utilised. For example, it was shown that the requirement for functional p53 in TCR, but not in GGR, is dependent upon UV wavelength (Mathonnet *et al.*, 2003).

Recent studies have shown that functional p53 is a requisite for the NER of a multiplicity of DNA adducts (Lloyd & Hanawalt, 2000; Wani *et al.*, 2002a; Lloyd & Hanawalt, 2002), while other investigations have shown that the abolition of p53 activity inhibits the repair of certain UV-induced lesions. For example, Ford & Hanawalt (1997) adopted an immunoassay, utilising CPD- and 6-4PP-specific monoclonal antibodies, to measure the rate of CPD and 6-4PP removal by GGR. They found that *TP53* mutations had a negligible effect on the removal of 6-4PPs, compared to a complete cessation in CPD repair. Therefore, it has been suggested that functional p53 is indispensable for the proficient GGR of CPDs, but modulates the efficiency of GGR in the repair of both CPDs and 6-4PPs. From the multiplicity of studies, Ford & Hanawalt (1997) postulated that functional p53 regulates NER through the transcriptional activation of NER genes required for the GGR subpathway, but not TCR. However, Wang *et al.* (1995) has shown that p53 interacts directly with the XPB and XPD constituents of the TFIIH transcription apparatus, which are instrumental in the NER pathway.

Whilst it has been demonstrated that p53 is superfluous for proficient NER in *vitro* (Leveillard *et al*, 1996), it has been shown that p53 is required *in vivo* (Hwang *et al.*, 1999). Furthermore, recent evidence suggests that p53 orchestrates NER by modulating transcription and through direct interaction with constituents of the NER machinery (Hanawalt *et al.*, 2002). Recently, Chen *et al.* (2002) utilised a p53 null cell line, possessing regulated wild-type p53 expression, to characterise the transcriptional portrait of 23,000 genes in response to UV-irradiation. Interestingly, both the *XPC* and *DDB2* transcripts clustered with previously characterised p53 transcriptional targets. This confirmed a previous study, which identified a promoter region in *DDB2* that facilitates the preferential binding of p53 and subsequent transcriptional activation of *DDB2* (Tan *et al.*, 2002). These findings agree with Hwang *et al.* (1999), who demonstrated that DDB2 was transcriptionally regulated in a p53-dependent manner. More recently, Fitch *et al.* (2003a) has shown that the overexpression of DDB2 augments the removal of CPDs by GGR in the absence of p53.

The accumulation of p53 has been observed in NER-defective cells, in response to low doses of UV, compared to normal cells, which mirrors the progressive accumulation of unrepaired CPDs (Dumaz *et al.*, 1997). Although the precise function of p53 in orchestrating the mechanistic action of NER remains elusive, it has been speculated that the principal p53 transcriptional target of the NER machinery is the p48 constituent of the UV-DDB complex. However, it has also been reported that the rapid binding of both XPC and p48 to UV-induced lesions can occur in the absence of p53. The p53 tumour suppressor also transcriptionally activates the *XPC* gene, modulating both basal and inducible levels of mRNA and protein in a p53- and UV-dependent manner (Amundson *et al.*, 2002; Adimoolam & Ford, 2002).

The p53-dependent induction of DDB2 and XPC, following UV irradiation, facilitates the rapid accumulation of depleted levels, resulting from proteasomal degradation, following the recognition of UV-induced photolesions. Additionally, it has been speculated that the p53-dependent induction of XPC and DDB2 facilitates the recognition of CPDs that remain present within the genome following repair (Fitch *et al.*, 2003a). It has also been shown that the

basal levels of DDB2 and XPC are significantly reduced in p53 deficient cells, compared to cells exhibiting normal p53 activity (Hwang *et al.*, 1999; Fitch *et al.*, 2003a; Adimoolam & Ford, 2002). Interestingly, although p53 regulates the basal and inducible expression of the *p48* and *XPC* genes, it has been recently speculated that DDB2 may regulate p53 expression (Itoh *et al.*, 2003).

The first documented target of p53, growth arrest- and DNA damage-inducible 45 alpha (GADD45α), is upregulated in response to UV radiation. Furthermore, it has been shown that GADD45α is instrumental in modulating GGR, but is superfluous in TCR (Smith *et al.*, 2000), which further suggests that p53 is required for GGR. Additionally, it has been suggested that GADD45α binds to UV-damaged DNA, increasing the accessibility to the NER apparatus (Carrier *et al.*, 1999; Smith *et al.*, 2000). In addition to its functional role in the G_2/M arrest (Jin *et al.*, 2002), GADD45α is thought to facilitate NER through its interaction with PCNA, core histones and $p21^{WAF1/CIP1}$ (Smith *et al.*, 1994).

p53 regulates several of its regulatory effects indirectly through a p53-dependent manner, via the transcriptional activation of downstream effector molecules, such as the CDK inhibitor, $p21^{WAF1/CIP1}$ (El-Deiry *et al.*, 1993; Xiong *et al.*, 1993). Principally, $p21^{WAF1/CIP1}$ binds to CDKs, resulting in the attenuation of their activity (as previously discussed). This results in cell cycle arrest at G_1 and the inhibition of DNA replication, thus facilitating DNA repair before entry into S phase (Nakanishi *et al.*, 1995; Gu *et al.*, 1993). The transcriptional activation of $p21^{WAF1/CIP1}$, however, is not required for p53 to activate GGR, which suggests that the initiation of cell cycle arrest is superfluous for repair (Adimoolam *et al.*, 2001; Smith *et al.*, 2000). Furthermore, Adimoolam *et al.* (2001) has shown that the transactivation of $p21^{WAF1/CIP1}$ is not required for TCR. Interestingly, Loignon *et al.* (1997) previously showed that exposure to 254 nm UV resulted in the concurrent activation of the $p21^{WAF1/CIP1}$ protein and G_1 arrest in p53-deficient fibroblasts originating from LFS patients, thus suggesting that the induction of $p21^{WAF1/CIP1}$ can occur through a p53-independent mechanism.

Although extensive investigations have been undertaken, adopting numerous methodologies, the precise mechanistic functionality of $p21^{WAF1/CIP1}$ in modulating NER remains to be completely delineated, as conflicting reports have suggested a multiplicity of functions of p53-dependent activation of $p21^{WAF1/CIP1}$ in response to UV. It has been suggested that p53-dependent transactivation of $p21^{WAF1/CIP1}$ modulates the activity of NER through direct interaction with PCNA. Essentially, PCNA is a replication factor (Waga *et al.*, 1994), which is also thought to play a role in the modulation of NER. $p21^{WAF1/CIP1}$ inhibits PCNA activity, resulting in the inhibition of DNA replication (Sherr & Roberts, 1995). In addition to its mechanistic role in DNA replication, PCNA is also required for repair synthesis in NER. Exposure to UV promotes the translocation of soluble PCNA to an insoluble form, which is found coupled to chromatin (Otrin *et al.*, 1997), which further facilitates its interaction with DNA polymerase η (Haracska *et al.*, 2001). However, optimal DNA repair necessitates the ubiquitin-dependent degradation of $p21^{WAF1/CIP1}$, following exposure to low doses of UV (Bendjennat *et al.*, 2003). Furthermore, the interaction between PCNA and chromatin is sustained in cells possessing *TP53* gene mutations and in $p21^{WAF1/CIP1}$ null cells (Riva *et al.*, 2001; Stivala *et al.*, 2001). In concordance, Therrien *et al.* (2001) reported the enhancement of NER in p53-deficient cells with abolished $p21^{WAF1/CIP1}$ expression. From these studies it has been speculated that $p21^{WAF1/CIP1}$ has an inhibitory effect on the initial mechanistic steps of NER, but the subsequent induction of $p21^{WAF1/CIP1}$ is a prerequisite for the translocation of PCNA following post-incision repair synthesis (Latonen *et al.*, 2005). Conflicting reports, however, have suggested that $p21^{WAF1/CIP1}$ has either no effect on the modulation of NER (Li *et al.*, 1996; Shivji *et al.*, 1994; Wani *et al.*, 2002b), or has an inhibitory effect on NER functionality (Pan *et al.*, 1995). Conversely, it has been reported that $p21^{WAF1/CIP1}$ may regulate the NER apparatus in the repair of UV damage (Sheikh *et al.*, 1997).

Several studies have reported the direct protein-protein interaction between p53 and an array of DNA repair proteins required for NER, such as XPB, XPD and RPA (de Laat *et al.*, 1999). Additionally, studies have shown the direct interaction between p53 and the TCR specific protein, CSB (Wang *et al.*, 1995;

Yu *et al.*, 2000a). In addition, p53 interacts with other transcription factors, including TFIID and p300/CBP (Chen *et al.*, 1993; Wang *et al.*, 1995; Lill *et al.*, 1997). More recently, it was proposed that p53 assists GGR through sequestering HAT complexes to the site of DNA damage, thus permitting chromatin relaxation, required for maximal accessibility to DNA lesions, by the NER machinery (Rubbi & Milner, 2003).

Despite extensive investigation, the precise mechanistic function(s) of p53 in the regulation of GGR and/or TCR remains largely controversial. Investigators have argued against the role of UV-induced transactivation of p53 responsive genes in the regulation of NER, as UV-induced DNA damage blocks elongation of RNA Pol II. Therefore, the presence of photolesions will inhibit expression of p53-responsive genes. Moreover, reduced $p21^{WAF1/CIP1}$ mRNA and protein levels have been documented following UV irradiation in human cells (Gorospe *et al.*, 1998; McKay *et al.*, 1998). It has also been shown that the time required for the recovery of and induction of $21^{WAF1/CIP1}$ protein levels inversely correlates with the TCR capacity of cells (McKay *et al.*, 1998). It has therefore been argued that for UV-induced p53-dependent genes to contribute to DNA repair, the removal, modification or bypass of transcription blocking lesions would be required to allow the expression of these genes (Ljungman, 1999; McKay *et al.*, 1998). This would suggest that cells derived from a CS patient would be defective in GGR, as these cells are devoid of TCR and mRNA recovery. However, CS cells exhibit no defect in GGR, which implies that the recovery of transcription does not significantly contribute to GGR. These findings contradict the observations of a transactivation-dependent role of p53 in the induction of GGR and/or TCR after UV irradiation (McKay *et al.*, 1999). However, it has been further speculated that p53 may regulate the steady-state levels of proteins that are essential for the repair of UV-induced damage and/or the recovery of transcription (McKay *et al.*, 1999). For example, it has been shown that the basal level of p53-regulated proteins in cells under normal physiological conditions is affected by the basal levels of p53 (Tang *et al.*, 1998). Furthermore, Crowley & Hanawalt (1998) showed that the expression of the *p48* gene is regulated by wild-type p53 in the absence of damage. So, although the UV-induced expression of gene products that are required for NER and the recovery of transcription is not fast enough to

contribute to these processes immediately following UV-irradiation (McKay *et al.*, 1998), it has been argued that p53 regulates NER and the recovery of transcription by regulating the basal levels of DNA-damage response and/or repair proteins (McKay *et al.*, 1999).

1.10.5 p53 and Apoptosis

The accumulation of UV-induced DNA damage results in the induction of apoptosis in a p53-dependent manner (Ziegler *et al.*, 1994; Smith & Fornace, 1997). The role of p53 in apoptosis is both transcription-dependent and –independent (Fig. 1.7; Jimenez *et al.*, 2000; Chao *et al.*, 2000). For example, p53 directly induces the expression of proapoptotic genes, which mediate cytochrome *c* release from the mitochondria. This results in the interaction between cytochrome *c* and the apoptotic protease activating factor (Apaf-1), which initiates the recruitment of procaspase 9, activation of the apoptosomal complex, the processing of caspase 9 and the initiation of apoptosis. p53 is also essential for the transcriptional activation of a multiplicity of proapoptotic factors, such as the B-cell CLL/lymphoma 2 (Bcl-2) members: Bcl2-associated X protein (Bax), p53-upregulated modulator of apoptosis (PUMA), phorbol-12-myristate-induced protein 1 (PMAIP1/NOXA), p53-upregulated apoptosis-inducing protein 1 (p53AIP1) and PIGa (galectin-7). These proteins mechanistically function by interacting with the Bcl2 protein. This causes the abolition of its antiapoptotic function, resulting in the sequestration of Bcl2 to the mitochondria, where it induces the release of cytochrome *c* and apoptosis (reviewed by Melnikova & Ananthaswamy, 2005).

In addition, p53 can mediate the immediate disruption of the mitochondria via the upregulation of the death receptor TNF receptor superfamily member 6 (Fas/APO1), TNF receptor superfamily member 10a (KILLER/DR5) and leucine-rich repeats and death domain (PIDD). This promotes the cleavage of procaspase 8 and release of cytochrome c from the mitochondria, resulting in the subsequent activation of the Apaf1-caspase 9-caspase 3 pathway (reviewed by Melnikova & Ananthaswamy, 2005).

p53 can further elicit apoptosis by activating genes which repress survival signalling such as insulin-like growth factor-binding protein 3 (IGF-BP3), or by repressing the expression of survival-promoting or antiapoptotic genes including IGF-receptor 1, Bcl-2 and survivin (reviewed by Latonen & Laiho, 2005).

p53-mediated apoptosis is further enhanced by inhibitor of growth family member 1(p33ING1b), a splice variant of the tumour suppressor ING1. p33ING1b enhances apoptosis through its direct interaction with p53, which results in both the accumulation and activity of p53, by preventing Mdm2 binding. p33ING1b can further mediate the acetylation of p53 and transcriptionally activate the p53 homologues, p63α and p73α (reviewed by Latonen & Laiho, 2005).

Interestingly, p53 can promote apoptosis via the negative regulation of NER. The cessation of XPB and XPD helicase activity is mediated via the direct interaction of the p53 C-terminus (reviewed by Latonen & Laiho, 2005).

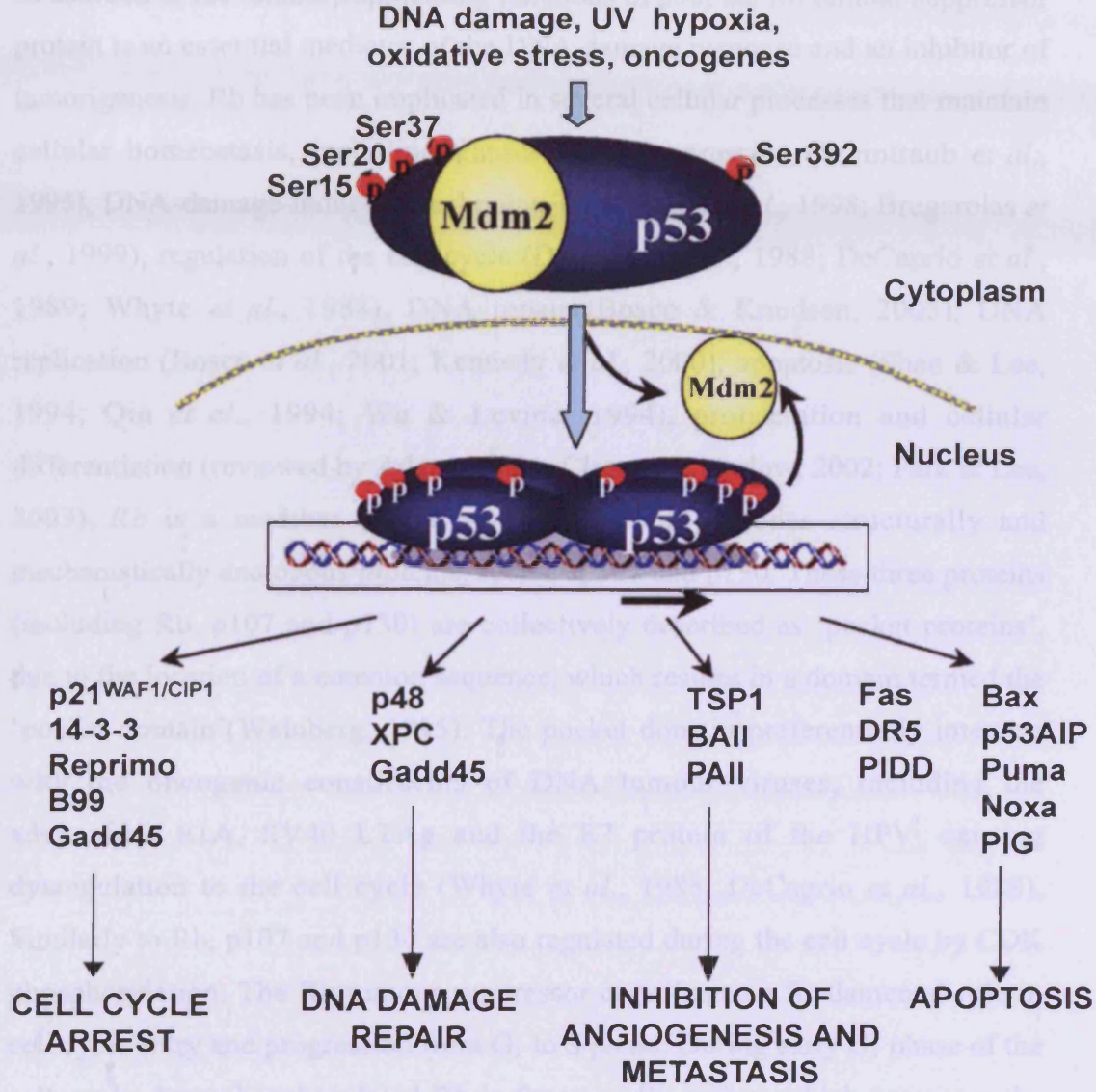

Figure 1.7. Functions of p53 tumour suppressor protein. In response to various stresses (such as UV), p53 is activated by the upstream mediators. The transcriptional modification of p53 may elicit cell cycle arrest at G_1/S or G_2/M checkpoints, initiate DNA repair, induce apoptosis and inhibit apoptosis (adapted from Melnikova & Anathaswamy, 2005).

1.11 Retinoblastoma (pRb) mediated tumour suppression

In addition to the tumour suppressing functions of p53, the Rb tumour suppressor protein is an essential mediator of the DNA damage response and an inhibitor of tumorigenesis. Rb has been implicated in several cellular processes that maintain cellular homeostasis, including transcriptional repression (Weintraub *et al.*, 1995), DNA-damage-induced checkpoints (Harrington *et al.*, 1998; Brugarolas *et al.*, 1999), regulation of the cell cycle (DeCaprio *et al.*, 1988; DeCaprio *et al.*, 1989; Whyte *et al.*, 1988), DNA repair (Bosco & Knudsen, 2005), DNA replication (Bosco *et al.*, 2001; Kennedy *et al.*, 2000), apoptosis (Shan & Lee, 1994; Qin *et al.*, 1994; Wu & Levine, 1994), proliferation and cellular differentiation (reviewed by Adams, 2001; Classon & Harlow, 2002; Park & Lee, 2003). *Rb* is a member of the gene family that encodes structurally and mechanistically analogous proteins, such as p107 and p130. These three proteins (including Rb, p107 and p130) are collectively described as 'pocket proteins', due to the location of a common sequence, which resides in a domain termed the 'pocket domain'(Weinberg, 1995). The pocket domain preferentially interacts with the oncogenic constituents of DNA tumour viruses, including the adenovirus E1A, SV40 LTAg and the E7 protein of the HPV, causing dysregulation to the cell cycle (Whyte *et al.*, 1988; DeCaprio *et al.*, 1988). Similarly to Rb, p107 and p130 are also regulated during the cell cycle by CDK phosphorylation. The Rb tumour suppressor coordinates a fundamental role in cell cycle entry and progression from G_1 to S phase. During early G_1 phase of the cell cycle, hypophosphorylated Rb is functionally active, which promotes the preferential binding to the E2F family of transcription factors and HDACs, thus negatively regulating both E2F and CDK function. The binding of Rb to E2F results in the formation of an Rb-E2F complex on the promoters of a multiplicity of E2F target genes. This represses the transcriptional activation of these E2F downstream gene targets that orchestrates cell cycle progression (such as cyclin A, cyclin E, cdc2, cdk2, p107, b-myb and DHFR), through the inactivation of promoter sites. In addition, Rb orchestrates the transcriptional repression of genes, which mediate DNA replication, including: PCNA, mini-chromosome

maintenance-7 (MCM-7), topoisomerase IIα and thymidine kinase. The indispensable nature of these Rb transcriptional targets, results in the inhibition of S-phase progression. In the presence of DNA damage, low serum or high cell confluency during culture, pRb is activated via its dephosphorylation (Buchkvoich *et al.*, 1989; DeCaprio *et al.*, 1989). Under normal physiological conditions, however, as cells progress through late G_1, the transcriptional activation and subsequent formation of cdk4/cyclin D1 and cdk2/cyclin E complexes orchestrate the phosphorylation and inactivation of Rb and dissociation of the Rb-E2F complex (Sherr, 1996; Weinberg, 1995). The cessation of repression of E2F regulated genes facilitates cell cycle progression through a G_1 exit and subsequent entry into S-phase.

The importance of Rb function is exemplified in the majority of human cancers where the functional inactivation of Rb has been reported. Furthermore, the cloning of the p*Rb1* tumour suppressor gene was undertaken by virtue of its association with the familial cancer, retinoblastoma, a tumour of the retina caused by germline mutations in the p*Rb1* gene (Lee *et al.*, 1987). Rb has also been implicated in further human malignancies, such as small-cell lung carcinoma and osteosarcoma. The abrogation of Rb results in the dysregulation of the G_1 CDK pathway and the subsequent initiation of tumorigenesis. This has been demonstrated in studies where the overexpression of *Rb* causes cells to undergo arrest in the G_1 phase of the cell cycle. Conversely, the abolition of Rb function promotes accelerated G_1 transition, which further supports the mechanistic function of Rb as an inhibitor of proliferation (Whyte *et al.*, 1988; DeCaprio *et al.*, 1988).

$p16^{INK4A}$, a cyclin D-CDK4/6 dependent kinase inhibitor, is an important regulator of the pRb pathway, and is upregulated in response to cellular stress, such as prolonged tissue culture and DNA damage, resulting in a G_1 cell cycle arrest (reviewed by Sherr & Roberts, 1999).

1.11.1 Role of Rb in response to UV

Following the exposure to exogenous and endogenous sources of DNA damage, such as UV, cells elicit signal transduction cascades, which promote a series of effector responses, thus maintaining genome stability. A multitude of checkpoint proteins play an instrumental role in mounting an appropriate DNA damage response. Subsequent to DNA damage, Rb is functionally activated through dephosphorylation, resulting in the abolition of cell cycle progression (Herrera *et al.*, 1996; Harrington *et al.*, 1998; Knudsen *et al.*, 1998). The hypophosphorylated state of Rb facilitates the formation of Rb-E2F complexes, which antagonises the binding of E2F transcription factor family members to their downstream transcriptional targets. In previous studies, accumulating evidence has implicated Rb as a mediator of DNA repair following UV or IR exposure, as several recently elucidated Rb/E2F transcriptional downstream gene targets have been implicated in the repair of UV- and IR-induced damage. Consequently, it has been suggested that the abolition of Rb function causes dysregulation of DNA repair, resulting in genome instability. More recently however, Bosco & Knudsen (2005) demonstrated that although temporally ablated *Rb* gene function compromised rapid cell cycle arrest following UV, Rb-deficient murine adult fibroblasts displayed an accelerated repair of 6-4 PPs. Furthermore, a body of evidence has shown that pRb regulates the expression of several NER repair factors such as FEN1, XPC, RPA2-3, RCF4 and PCNA (Cam *et al.*, 2004; Ishida *et al.*, 2001; Polager *et al.*, 2002; Markey *et al.*, 2002; Classon *et al.*, 2002). In accordance with these findings, Therrien *et al.* (1999) previously showed that HPV E7-expressing lung fibroblasts, which were compromised for pRb function, were defective in GGR (Section 4.1).

1.12 Replicative senescence

Human diploid fibroblasts possess a finite replicative capacity *in vitro*, following extensive subcultivation (Hayflick & Moorhead, 1961; Hayflick, 1965). This has been attributed to a state of permanent and irreversible growth arrest, a phenomenon known as replicative senescence, the Hayflick limit (Shay &

Wright, 2000), or mortality stage 1 (M1) (Fig. 1.8; Wright *et al.*, 1989). In addition, to human diploid fibroblasts, replicative senescence has also been reported in a number of cell types *in vitro*, including glial cells, keratinocytes (Rheinwald, 1975), vascular smooth muscle cells (Bierman, 1978), lens cells (Tassin *et al.*, 1979), endothelial cells (Mueller *et al.*, 1980) and lymphocytes (Tice *et al.*, 1979).

Indeed, the progressive attenuation of proliferative capacity has also been observed *in vivo*, thus signifying similarities in replicative capacity between *in vitro* culture models and *in vivo*. However, only a limited number of reports have observed reductions in telomere length in proliferating and non-proliferating tissues *in vivo* (Allsopp *et al.*, 1992; Frenck *et al.*, 1998; Kveiborg *et al.*, 1999; Aikata *et al.*, 2000). In contrast, Kang *et al.* (2003) showed a correlation between telomere length attrition and increasing donor age in oral keratinocytes, but not in oral fibroblasts *in situ*. By contrast, many reports have failed to demonstrate a relationship between donor age and proliferative capacity *in vitro* (Goldstein *et al.*, 1978; Cristofalo *et al.*, 1998a,b; Smith *et al.*, 2002). Thus, the extrapolation of *in vitro* culture models to *in vivo* aging has been extensively problematic and controversial. This is thought to be attributed to selection pressures placed upon slower proliferating cells present within the culture.

It was postulated that senescence is initiated by the progressive erosion of telomeric ends (Olovnikov, 1973; Harley *et al.*, 1990), thus suggesting that telomere shortening functions as a mitotic "clock" (Harely, 1991). During the replicative lifespan of normal diploid somatic cells, telomere attrition is thought to occur at approximately 50-200 base pairs (bp) per cell division (Harley *et al.*, 1990). The progressive attrition of hexameric telomeric sequence (5'-TTAGGG-3') has been attributed to the incapability of DNA polymerase to replicate the ends of chromosomal DNA during lagging strand synthesis (Olovnikov, 1973; Harley, 1991). This phenomenon, first postulated by Olovnikov (1971), known as the end replication problem, occurs when somatic diploid fibroblasts undergo each cell division. Olovnikov (1971, 1973) showed that the presence of an RNA primer at the 5' end is a prerequisite for the initiation of lagging strand synthesis by DNA polymerase. The subsequent displacement of the RNA primer,

following the completion of DNA replication, elicits the progressive loss of telomeric ends. Cells obtained from older individuals displayed a restricted replicative capacity and attenuation in telomeric length, compared to cells derived from younger donors (Harley *et al.*, 1990; Hastie *et al.*, 1990).

Whilst previous evidence suggests that progressive telomeric erosion remains the speculated "replicometer" mechanism of replicative senescence (Wright & Hayflick, 1975; Muggleton-Harris & Hayflick, 1976; Wright & Shay, 1992; Bodnar *et al.*, 1998), the precise molecular trigger(s) that initiate replicative (M1) senescence, following critical telomeric shortening, remain(s) elusive. Current models of (M1) replicative senescence initiation, associated with aberrant telomeres include; telomere positioning effects (Baur *et al.*, 2001; Koering *et al.*, 2002; Shay *et al.*, 2000), DNA damage signalling induced by telomere attrition (d'Adda *et al.*, 2003; Zou *et al.*, 2004; Sedelnikova *et al.*, 2004; Gire *et al.*, 2004; Herbig *et al.*, 2004) and loss of the 3' G-rich telomeric overhang (Stewart *et al.*, 2003).

The limited replicative capacity of normal diploid cells provides an innate mechanism, which prevents malignant transformation and indefinite proliferation (immortalisation), thus inhibiting tumorigenesis (Reddel, 2000; Campisi, 2000; Campisi, 2001). Conversely, Krtolica *et al.* (2001) has argued that senescent dermal fibroblasts incite premalignant and malignant epithelial cells to proliferate *in vitro* and promote tumorigenesis in mice.

Whilst the hallmark of replicative senescence is the cessation of responsiveness to mitogens (Seshadri & Campisi, 1990), the senescent phenotype is typically characterised by marked alterations in growth kinetics, morphological appearance and dysregulation of biological processes. Senescent cells maintained under routine culture conditions are morphologically characterised by an increase in cell size, with a marked flattened and vacuolated appearance coupled with an associated increase in nucleus and nucleoli size (Cristofalo & Kritchevsky, 1969; Greenberg *et al.*, 1977; Mitsui & Schneider, 1976). A marked increase in the number of lysosomes and golgi (Cristofalo & Kabakjian, 1975; Maciera-Coelho *et al.*, 1971) and a pronounced increase in the number of cytoplasmic

microfilaments are also features indicative of replicative senescence (Brandes *et al.*, 1972; Comings & Okada, 1970; Lipetz & Cristofalo, 1972). In addition to the morphological alterations, senescent cell populations exhibit a pronounced increase in the number of multinucleated cells (Galloway & Buckton, 1978; Matsumura, 1980; Matsumura *et al.*, 1979; Yanishevsky & Carrano, 1975) and heterochromatic foci are observed (Narita *et al.*, 2003). Although in a nonproliferative state, senescent cells remain metabolically active. Furthermore, the progressive accumulation of senescent cells causes attenuation in tissue function (Dimri *et al.*, 1995; Fenton *et al.*, 2001; Minamino *et al.*, 2002). For example, investigators have shown that the NER repair of UV-induced lesions is severely compromised in senescent cells compared to their young isogenic counterparts (Boyle *et al.*, 2005; discussed further in Chapter 4).

The complete cessation of proliferation in senescent fibroblasts in associated with alterations in gene expression patterns and posttranslational modifications in a cell-type specific manner, resulting in an altered phenotype compared to their young isogenic counterparts (Cristofalo *et al.*, 1998; Park *et al.*, 2001; Shelton *et al.*, 1999). For example, altered patterns of gene expression are seen in the transduction and secretory pathways. In particular, the differential regulation of proteases and constituents of the extracellular matrix, such as extracellular matrix (ECM)-degrading secreted proteases, collagenase (Millis *et al.*, 1992a,b; West *et al.*, 1989), tissue plasminogen activator (West *et al.*, 1996; Zeng & Millis, 1994) ECM-modifying proteins (matrix metalloproteinases (MMPs), tissue inhibitor of metalloproteinase family), growth factors and inflammatory cytokines have been reported (Campisi, 1998; Faragher & Kipling, 1998; Shay & Wright, 2005). Additionally, senescent fibroblasts express reduced levels of MMP inhibitors, tissue inhibitor of metalloproteinase (TIMP1) and Ras-related C3 botulinum toxin substrate 1 (MIG5; Wick *et al.*, 1994), a reduction in ECM components, including elastin, laminin (Linskens *et al.*, 1995) and constituents of collagen (Furth, 1991). These modifications in cellular homeostasis have been shown to facilitate the acceleration of tumorigenesis by promoting the survival, metastasis and proliferation of pre-malignant cells.

Historically, cellular senescence *in vitro* is determined experimentally by the staining of senescence associated-β-galactosidase (SA-βG). β-galactosidase (βG) functions as a hydrolase, which is found localised in the lysosome. βG enzymatically cleaves β-D-galactose residues in β-D-galactosides. Dimri *et al.* (1995) first reported that senescent cells express SA-βG, which optimally functions at pH 6. Apart from the exit of the cell cycle, the SA-βG assay has become the most frequently utilised marker to characterise cellular senescence in culture. For example, SA-βG staining has been implemented to investigate the accelerative ageing effects of homocysteine (Xu *et al.*, 2000), ceramide (Mouton & Venable, 2000), oxidative stress (Dumont *et al.*, 2000) and cardiolipin (Arivazhagan *et al.*, 2004). However, despite the extensive application of the SA-βG assay as an indicator of senescence, the validity and reliability of the assay has been challenged, due to the lack of specificity. An increase in SA-βG staining has been reported in immortalised cells subsequent to serum starvation (Yegorov *et al.*, 1998), oxidative treatment with H_2O_2 and in confluent primary fibroblast cultures grown *in vitro* (Severio *et al.*, 2000). Most recently, Yang & Hu (2005) also found that in addition to cellular ageing and cell confluency, serum starvation and H_2O_2 also increased SA-βG activity.

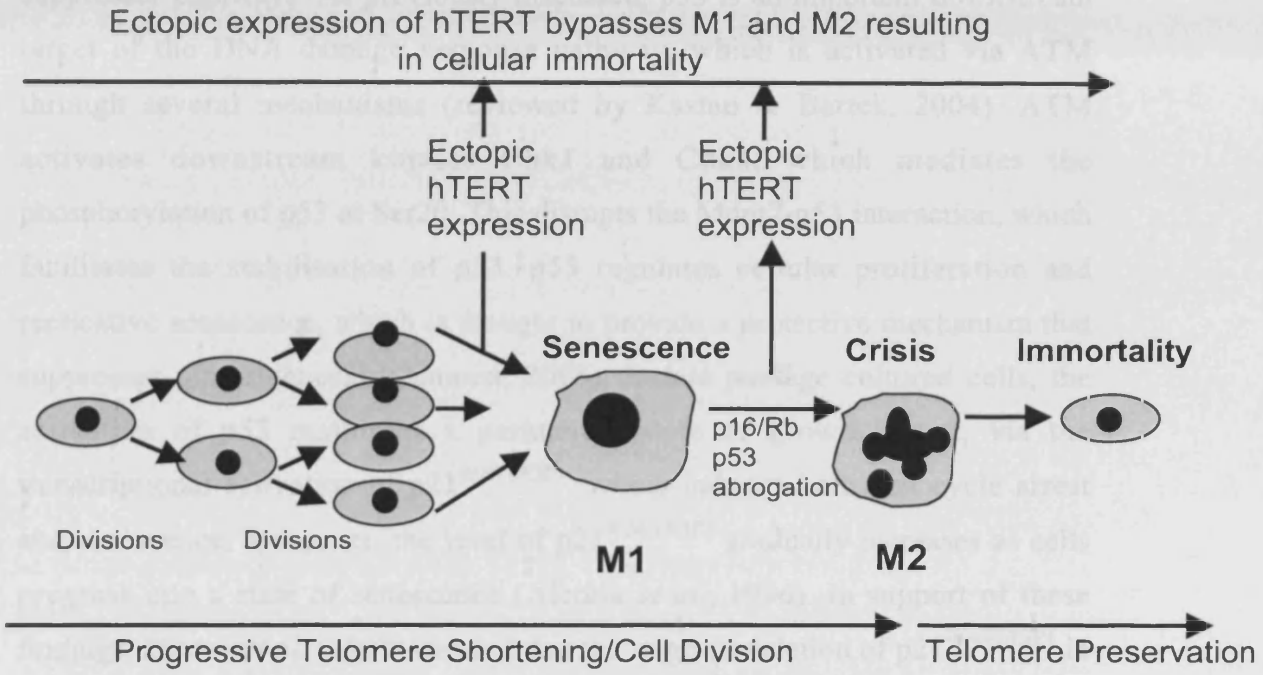

Figure 1.8. The ectopic expression of the catalytic subunit of telomerase, hTERT, results in the immortalisation of human cells. The ectopic expression of telomerase can facilitate the bypass of senescence (M1) and crisis (M2), as hTERT expression either before M1 or after M1 results in cellular immortalisation (adapted from Shay & Wright, 2005).

1.12.1 Replicative senescence: activation through the DNA damage response pathways

Although the precise mechanism(s) that recognise critically short telomere lengths remain poorly delineated, short telomeres are thought to serve as a DNA-damage like signal. Two pathways have been implicated in the activation of cellular senescence; including the p53/p21$^{WAF1/CIP1}$ and pRb/p16^{INK4A} tumour suppressor pathways. As previously discussed, p53 is an important downstream target of the DNA damage response pathway, which is activated via ATM through several mechanisms (reviewed by Kastan & Bartek, 2004). ATM activates downstream kinases Chk1 and Chk2, which mediates the phosphorylation of p53 at Ser20. This disrupts the Mdm2-p53 interaction, which facilitates the stabilisation of p53. p53 regulates cellular proliferation and replicative senescence, which is thought to provide a protective mechanism that suppresses tumorigenesis (Campisi, 2005). In late passage cultured cells, the activation of p53 maintains a permanent state of growth arrest, via the transcriptional activation of p21$^{WAF1/CIP1}$, which induces both cell cycle arrest and senescence. Moreover, the level of p21$^{WAF1/CIP1}$ gradually increases as cells progress into a state of senescence (Alcorta *et al.*, 1996). In support of these findings, Brown *et al.* (1997) showed that the targeted deletion of p21$^{WAF1/CIP1}$ in fibroblasts resulted in the bypass of cellular senescence. Collectively, these findings suggest that the p53/p21$^{WAF1/CIP1}$ and pRb/p16^{INK4A} pathways orchestrate cellular senescence in response to telomere shortening.

1.12.2 Replicative senescence and DNA repair

Although initial observations suggest that replicative senescence occurs as a result of telomere shortening (Harley *et al.*, 1990) during semi-conservative replication (Olovnikov, 1973, Watson 1972), recent finding suggest that cellular senescence can be triggered by DNA damage (reviewed by Lou & Chen, 2006). Indeed, as previously mentioned, both telomere dysfunction- and DNA-damage-induced replicative senescence elicit the same mechanism, the DNA damage response pathway (d'Adda di Fagagna *et al.*, 2003; von Zglinicki *et al.*, 2005).

Mutations in many constituents of DNA repair pathways have been associated with cellular senescence (reviewed by Lou & Chen, 2006). For example, mouse embryonic fibroblasts (MEFs) defective in Ku70, Ku80, XRCC4 and DNA ligase IV fail to repair double-strand breaks (DSBs) by NHEJ, and enter a state of accelerated premature senescence (Lombard *et al.*, 2005). A further link between HR mutation and cellular senescence and aging has been identified in BRCA1. In BRCA1Δ^{11}/Δ^{11} MEFs, a deficiency in BRCA1 causes impaired HR-mediated DSB repair and premature senescence, as indicated by β-galactosidase activity (Cao *et al.*, 2003). As previously discussed, defects in *XPD* causes TTD, while mutations in *CSA* and *CSB* result in CS (Mitchell *et al.*, 2003). Although both TTD and CS patients exhibit premature aging phenotypes, the role of *XPD* and *CSA* mutations in accelerated cellular senescence (if any) remains unknown.

In addition to factors directly involved in DNA repair, further factors are involved in other aspects of the DNA damage response, including signal transduction and checkpoint activation. ATM elicits the entire damage response pathway and activates a multitude of downstream substrates. Defects in ATM cause ataxia-telangiectasia (AT), resulting in neurodegeneration, immunodeficiency and premature aging. Fibroblasts derived from AT patients enter a state of premature senescence. H2AX and MDC1 function downstream to ATM. H2AX, a histone variant, rapidly phosphorylates at regions flanking DSBs (Rogakou *et al.*, 1999). Phospho-H2AX (γH2AX) provides a molecular docking site for sequestered DNA repair factors. MDC1 binds γH2AX resulting in further H2AX phosphorylation (Stucki *et al.*, 2005). Therefore, H2AX and MDC1 provide a positive feedback loop to amplify the ATM-mediated DNA damage response (Lou *et al.*, 2006). It has been shown that H2AX$^{-/-}$ and MDC1$^{-/-}$ MEFs grow slowly *in vitro* and enter a state of premature senescence (reviewed by Lou & Chen, 2006). Collectively, these data suggest that, similar to telomere dysfunction, genome instability induced by defects in the DNA damage response pathway further contribute to cellular senescence and premature aging.

Like DNA damage, telomere dysfunction results in the exposure of DNA ends, thus resulting in the elicitation of the DNA damage response. Numerous studies

have provided evidence for the involvement of the DNA damage response in both telomere dysfunction- and DNA-damage-induced cellular senescence. For example, Takai *et al.* (2003) showed that overexpression of mutant telomeric repeat binding factor 2 (TRF2) resulted in t-loop uncapping, telomere shortening and replicative senescence. Furthermore, overexpression of mutant TRF2 induces γH2AX foci formation (Takai *et al.*, 2003), which is indicative of DSB formation. It has been shown that, DNA damage factors such as tumour protein p53 binding protein 1 (53BP1), mediator of DNA damage checkpoint 1 (MDC1), phospho-ATM, Nibrin (NBS1) and Rad17, have been found to accumulate at mutant TRF2-induced foci (d'Adda di Fagagna *et al.*, 2003). From these findings, it can be speculated that telomere shortening, like DNA damaging agents, elicit DNA damage responses.

1.12.3 Telomere-independent senescence

In addition to telomere-dependent replicative senescence, further mechanisms that elicit a permanent state of growth arrest, which recapitulates the morphological and biological characteristics exhibited by telomere-dependent senescence, have been described. The most frequently reported causes of telomere-independent senescence include; oxidative damage (Parrinello *et al.*, 2003), genotoxic damage (Schmitt *et al.*, 2002) and oncogene dysregulation (Serrano *et al.*, 1997). It is thought that ROS causes DNA damage and elicits the progressive acceleration of telomere attrition (von Zglinicki *et al.*, 1995: Forsyth *et al.*, 2003; Parrinello *et al.*, 2003). For example, mortality stage 0 (M0) senescence is frequently observed in keratinocytes and mammary epithelial cells *in vitro*, due to the activity of the $p16^{INK4A}$/pRb pathway (Brenner *et al.*, 1998; Kiyono *et al.*, 1998). However, it is thought that M0 may be an artifactual consequence of continued *in vitro* cultivation, resulting in a delayed response to insufficient culture conditions, rather than a physiological process. Most recently, Ramirez *et al.* (2001) found that culturing keratinocytes and mammary epithelial cells on feeder layers can circumvent M0 senescence. This reiterates the requirement for fully optimised culture conditions, in order to maintain a viable culture and the establishment of permanent cell lines. Post-mitotic, terminally

differentiated cells also possess a senescence-associated phenotype, due to the complete cessation of proliferative capability following differentiation, such as neuronal cells. Furthermore, the inability to recapitulate an *in vivo* environment can be problematical *in vitro*, such as hepatocytes, thus resulting in premature senescence.

1.13 Telomeres, telomerase and immortalisation

1.13.1 Telomeres: An essential genomic element

Telomeres, the DNA-protein structures that cap the ends of eukaryotic liner chromosomes, protect chromosomal ends from normal cellular activity and genome instability promoting events (Muller, 1938; McClintock, 1941). Telomeres form a higher-order chromatin structure that physically hides the 3'-overhang. This is achieved by the 3'-overhang, which folds back and invades the double-stranded region of the telomere, resulting in the formation of the T-loop, which is displaced to form the D-loop. This structure performs a minimum of three essential roles in chromosome preservation. Firstly, capping allows the cell to differentiate chromosome ends from DSBs in the genome. Uncapped chromosome ends can have catastrophic consequences for the cell, as uncapped telomeres are susceptible to degradation, recombination or fusion of the DNA ends by NH and/or end-joining DNA repair mechanisms. Chromosome degradation causes loss of genetic information, resulting in cell death. Recombination causes rearrangements or a reduction or increase in telomere length, which can cause the premature onset or delay on cellular senescence. Telomere fusion results in the formation of dicentric chromosomes, which break during mitosis, thus resulting in the formation of additional DSBs, further cycles of breakage and fusion, resulting in genome instability. Secondly, telomeres facilitate the attachment of chromosomes to the nuclear envelope during meiosis. Finally, the replication of chromosome ends (reviewed by Davis & Kipling, 2005). Therefore, the loss of telomeres ultimately results in the loss, rearrangement or destabilisation of genetic information (Shore, 1997; Blackburn, 2000; Gasser, 2000). There are three rudimentary requisites essential for the

protective function of telomeres: (1) a minimum length of TTAGGG repeats (Moyzis *et al.*, 1988); (ii) the telomere-binding proteins; (iii) the integrity of the G-strand overhang.

1.13.2 Immortalisation using telomerase

Telomerase, a cellular reverse transcriptase, provides the main regulator of telomere length and facilitates the replication of telomeric DNA via the addition of TTAGGG repeats onto pre-existing telomeres. Telomerase is composed of two essential constituents, the reverse transcriptase subunit, human telomerase reverse transcriptase (hTERT), and the RNA component, human telomerase RNA component (hTERC), which contains the template for the synthesis of new tandem telomeric repeats (reviewed by Blasco, 2003). As previously mentioned, most human normal somatic cells do not possess sufficient telomerase activity to retain telomere length, thus resulting in telomere attrition (Harley *et al.*, 1990). Most normal primary human somatic cells either completely lack telomerase activity or possess residual levels that are insufficient for telomere maintenance (Kim *et al.*, 1994).

The isolation and subsequent cloning of the *hTERT* gene (Nakamura *et al.*, 1997; Meyerson *et al.*, 1997; Harrington *et al.*, 1997; Kilian *et al.*, 1997), has revolutionised the development of *in vitro* culture models. As the exploitation of hTERT facilitates the establishment of immortalised cell lines with a relatively impervious phenotype, which resemble their primary isogenic counterparts. Therefore, unlike conventional methods adopted to establish immortalised cell lines, such as the expansion of tumour biopsies or the utilisation of oncogenic viral proteins, the utilisation of hTERT permits an extension of proliferative lifespan, remain diploid, differentiated, contact-inhibited, nontumorigenic and anchorage dependent. More importantly, hTERT-immortalisation facilitates the maintenance of normal p53/p21$^{WAF1/CIP1}$ and pRb/p16^{INK4A} functionally, thus sustaining genome preservation, without inducing cancer-associated alterations (discussed in Chapter 4).

The ectopic expression of hTERT cDNA in normal fibroblasts and retinal pigment cells has been shown to facilitate senescence bypass (Bodnar *et al.*, 1998; Vaziri & Benchimol, 1998) and immortalisation, without inducing alterations that resemble a malignant phenotype (Jiang *et al.*, 1999; Morales *et al.*, 1999; Vaziri *et al.*, 1999). In stark contrast, telomerase-mediated immortalisation alone does not extend the proliferative lifespan of a multiplicity of epithelial cells maintained under certain culture conditions, unless the pRb/$p16^{INK4A}$ pathway is abrogated (Kiyono *et al.*, 1998; Farwell *et al.*, 2000; Kim *et al.*, 2002; Toouli *et al.*, 2002). Further strains of lung (MacKenzie *et al.*, 2000; Franco *et al.*, 2001), mammary (O'Hare *et al.*, 2001 and periodontal ligament (Tsutsui *et al.*, 2002) fibroblasts require further loss of $p16^{INK4A}$ function in conjunction with hTERT expression for immortalisation.

1.14 Aims

To date, the availability of permanent human *in vitro* models of defective NER are limited to those derived from characterised human genetic diseases, such as XP, CS and TTD, which have been established by *in vitro* transformation using viral oncogenes. These cell lines are compromised by an undesirable legacy of immortalisation, namely disruption of the p53/p21$^{WAF1/CIP1}$ and pRb/p16^{INK4A} tumour suppressor pathways, which are instrumental in the elicitation of a DNA damage response and efficient NER. Therefore, in the cell lines currently available a critical response to DNA damage is missing. Telomerase-mediated immortalisation, however, provides an alternative for the establishment of permanent cell lines defective in NER, as their primary NER defect is preserved, while retaining both p53/p21$^{WAF1/CIP1}$ and pRb/p16^{INK4A} function. Currently, the availability of telomerised cells, defective in NER, is limited to cell lines derived from XP-E, XP-V and CS-B individuals.

Cells derived from XP-C and CS-A individuals, which are defective in the *XPC* and *CKN1* genes respectively, represent defects in the GGR and TCR subpathways of NER. For that reason, primary XP-C (GM02996, XP8CA) and CS-A (GM01856, CS3BE) dermal fibroblasts were selected for subsequent investigation.

In the present study, the first aim was to characterise the underlying molecular defect in XP-C and CS-A fibroblasts (Chapter 3) and establish permanent *in vitro* XP-C and CS-A culture models with an extended proliferative lifespan. This was achieved by transducing primary XP-C and CS-A fibroblasts with a retroviral vector expressing the catalytic subunit of telomerase, *hTERT* (Chapter 4). Additional requisites to the establishment of permanent telomerised XP-C and CS-A cell lines included the preservation of the phenotypic characteristics observed in their primary isogenic counterparts and the maintenance of the p53/p21$^{WAF1/CIP1}$ and pRb/p16^{INK4A} pathways. Following the establishment of telomerised XP-C and CS-A cell lines, three representative clone of each cell line was maintained in continuous culture for ~100 PDs, thereby allowing the

conformation of immortality. Once immortality was confirmed, the removal of damage was assessed in the XP-C and CS-A cell lines, using DNA repair assays. Furthermore, the preservation of p53/p21$^{WAF1/CIP1}$ and pRb/p16^{INK4A} pathways was addressed at the translational level. In particular, p53 activation and stabilisation is a well-documented response to DNA damage, but the nature of its activation in terms of post-translational modifications is poorly understood. Hence, a further aim was to characterise these responses.

To date, our current understanding of the UV-induced global transcriptional response in NER-defective cell lines remains limited. Therefore, once telomerised XP-C and CS-A cell lines were established, a further aim was to utilise Affymetrix™ microarrays to dissect the global UV-induced transcriptional response of telomerised XP-C and CS-A cells (Chapter 5). The transcription expression responses of telomerised XP-C and CS-A cells were compared to the transcriptional profile of normal telomerised MRC-5 fibroblasts previously generated in our laboratory. Transcription profiling in the different genetic backgrounds permitted the identification of genes differentially regulated in response to UV and what aspect of defective DNA repair blocks their expression. Furthermore, gene expression profiling facilitated the identification of cell-type-specific transcriptional 'signatures' in telomerised XP-C and CS-A cells. This will further assist in unravelling any underlying molecular defects, which contribute to the neoplastic and progeroid phenotypes observed in XP and CS patients, respectively. Following transcription profiling, a further aim was to validate the Affymetrix™ data, at the transcriptional level, by qRT-PCR. Additionally, validation was undertaken at the protein level by Western blotting and immunocytochemisty, to substantiate whether changes at the protein level reflect those changes observed at the mRNA level (Chapter 5).

As previously mentioned, the availability of permanent cell lines defective in NER are limited to rare human genetic diseases such as XP, CS and TTD, which are defective in a subset of DNA repair genes. Therefore, a further aim of this investigation was to demonstrate the applicability of RNAi in investigations of DNA repair by transiently ablating *XPC* or *CSA* function in normal telomerised

MRC-5 cells, by transfection with siRNAs specific to *XPC* or *CSA* mRNA (Chapter 6). A further aim was to create a permanent XPC^{KD}/CSA double knockdown phenotype by transducing the telomerised CS-A cell line with a retroviral vector expressing an *XPC*-targeted shRNA construct (Chapter 6). Logic dictates that complete ablation of *XPC* and *CKN1* would result in the removal of the GGR and TCR subpathways that feed into the convergence point of NER where XPA co-ordinates excision of damage. One might expect that an XPC^{KD}/CS-A null cell would exhibit the UV-induced DNA damage response and repair kinetics of an *XPA* null cell. However, this is by no means a certainty as the *rad16* (GGR) and *rad26* (TCR) *S. cerervisiae* double mutant is less sensitive than the *rad14* (XPA) mutant, which is completely defective in NER (Verhage *et al.*, 1996). Additionally, attempts have been made to establish a double $Csa^{-/-}Xpc^{-/-}$ transgenic model (van der Horst *et al.*, 2002). However, double mutants are severely runted and die within a month of birth. Once the establishment of the XPC^{KD}/CS-A phenotype was confirmed at the protein level by Western blotting and immunocytochemistry (ICC), a further aim was to assess the biological effect of the *XPC* shRNA construct. To address this, immuno-slot-blot assays were undertaken to determine whether knocking down XPC in a *CSA* null background had a biological effect on the global repair of UV-induced damage. The successful establishment of NER defective cell lines, through the exploitation of RNAi technology, will provide an alternative to the establishment of cell lines derived from donors with defined genetic backgrounds such as XP, CS and TTD.

Chapter 2

Materials and Methods

All general chemicals were purchased from Fisher and all molecular biology grade chemicals and reagents were obtained from Sigma® (Chemical Co., Dorset, UK) unless otherwise stated. Water was prepared by reverse osmosis (Millipore). Further diethyl pyrocarbonate (DEPC) treatment of water was performed were stated.

2.1 Cell strains and routine culture conditions

Normal human diploid MRC-5 fibroblasts, derived from lung tissue of a 14-week-old male foetus (ECACC No. 84101801), were purchased from the European Collection of Cell Culture (ECACC). These were grown in monolayers at 37°C in a humidified incubator (95% air), 5% CO_2 atmosphere in Eagle's minimum essential medium with Earle's salts (EMEM; Invitrogen™, Life Technologies) and supplemented with 10% foetal calf serum (FCS; Imperial Laboratories, London), 1X MEM non-essential amino acids (NEAA) without L-glutamine (Sigma®), 2 mM MEM L-glutamine (Invitrogen™), 0.002% $NaHCO_3$ (Invitrogen™), 10 mM Hepes (Sigma®). The pH was adjusted to 7.2 using 10 N NaOH (~100 µl/100 ml). All growth media were supplemented with 10,000 U/ml penicillin (Sigma®) and 10 µg/ml streptomycin (Sigma®). Medium was made to the correct concentration with autoclaved milli Q H_2O. Fibroblasts were subcultured at subconfluence (~80-90% confluent) and reseeded in T75 cm^2 flasks at a density of ~1 X 10^5-4 X 10^5. Cells were refed with 10 ml of EMEM medium approximately every 3-4 days.

DNA repair-deficient primary and SV40-transformed human dermal fibroblast cell lines were purchased from the National Institute of General Medical Sciences (NIGMS) Human Genetic Mutant Cell Repository (Coriell Institute for

Medical Research, Camden, NJ). The following cell lines were used: primary XP-A human fibroblasts (catalogue No.: GM05509, patient No.: XP12BE); primary XP-C human fibroblasts (GM02996, XP8CA); primary CS-A (CKN1) human fibroblasts (GM01856, CS3BE); isogenic SV40-transformed XP-A human fibroblasts (GM04429, XP12BE); isogenic SV40-transformed CS-A (CKN1) human fibroblasts (GM16094, CS3BE.s3g1). The donor for the GM05509 (and GM04429) cells was a 17-year-old Caucasian female, cells of strain GM02996 were from a skin biopsy of 7-week-old Caucasian Egyptian male, and the cells of strain GM01856 (and GM16094) were derived from a 13-year-old Caucasian male. All primary and SV40-transformed DNA repair-defective human fibroblasts were grown under identical condition in medium recommended by the NIGMS Human Genetic Mutant Cell Repository. Briefly, cultures were grown in growth medium previously described, supplemented with 1X vitamins (Invitrogen™) and 10 mM Hepes was omitted from the medium.

Fibroblasts were trypsinised and subcultured close to confluence (~80-90%). Briefly, the medium was aspirated from the flask and washed with 2 ml of 1X trypsin/ethylenediamine tetracetate (EDTA; Invitrogen™) to remove any residual medium. The trypsin was discarded and a further 2 ml of fresh trypsin was added. The fibroblasts were incubated at 37°C for approximately 5-15 minutes, depending on cell-type. Once the cells had detached from the surface of the flask, they were resuspended in 8 ml of medium and transferred to a 15 ml Falcon tube (Becton Dickinson). Total cell counts were determined by counting the total number of cells distributed over the top-left and bottom-right primary squares of a Neubauer ruled haemocytometer (Hawksley). Approximately 10 µl of the cell suspension was pipetted onto a haemocytometer. Fibroblasts that were within, or that touched the right or bottom periphery of the primary squares were counted, whereas fibroblasts that touched, or were outside the upper, or left periphery was excluded from the cell count. The number of cells counted within two primary squares were added together and divided by two, to give the mean number of cells per ml of cell suspension. The total cell count was obtained by multiplying the number of cells per ml by ten (10 ml). The number of population doublings (PDs) for each passage (P) was calculated from the cell count by comparing the

total cell count following trypsinisation with the initial number of cells seeded. For cumulative PDs, the number of PDs calculated following each subcultivation was added to the total number of PDs accumulated whilst in culture.

For routine passing of cells, fibroblasts were reseeded into a fresh T75 cm^2 flask approximately every 7 days at a density of between 1 X 10^5 – 4 X 10^5, which equated to approximately 1-2ml of cell suspension in 8-9 ml of fresh medium. All cell strains were grown in this manner. However, for specific experimentation, cells were grown in a range of different sized flasks or dishes, and cells were re-seeded and refed with the appropriate volume of medium and cell densities were modified accordingly.

Primary XP-C (XP8CA, GM02996) and CS-A (CS3BE, GM01856) dermal fibroblasts that were first seeded for subsequent retroviral infection with hTERT were assigned PD 0. During the exponential phase of growth, fibroblasts that were not re-seeded were frozen and stored as viable stocks. Briefly, once an appropriate volume of cell suspension had been reseeded, the remaining cells were centrifuged at 90 g for 5 minutes at room temperature in a Centaur 2 centrifuge (Sanyo). The supernatant was discarded and the cell pellet was re-suspended in 1 ml of 1X Cell Freezing Medium-Glycerol (Sigma®), thus permitting the cryopreservation of cell cultures. The cell suspension was transferred to a freezing CryoTube™ (Nunc™, Denmark) and stored at -80°C in a storage box, containing isopropanol, for a minimum of 2 hours, before transferring the ampoule to liquid nitrogen. When recovering viable cell cultures from liquid nitrogen, the ampoule was rapidly thawed in a 37°C sterile water bath. Once thawed, the cell suspension was transferred to a 15 ml Falcon tube. Subsequently, 9 ml of warm medium was pipetted into the Falcon tube in a drop-wise manner. The cell suspension was gently mixed by pipetting up and down. To remove any residual Cell Freezing Medium-Glycerol, the cell suspension was centrifuged at 90 g for 5 minutes at room temperature. The supernatant was carefully aspirated and 10 ml of fresh EMEM medium was added. The cell suspension was transferred to a T75 cm^2 flask.

2.2 hTERT-immortalisation of primary XP-C and CS-A human dermal fibroblasts with ψCRIP-pBABE-neo-hTERT

All manipulations during the retroviral infection procedure were undertaken with significant caution and in accordance with the Advisory committee on Genetic Modification (ACGM) guidelines. Briefly, all procedures involving the transfer and filtration of retroviral-containing supernatants were performed using a sterile plastic kwill and syringe. All pipette tips and stripettes were thoroughly rinsed with neat bleach. All retroviral-containing supernatants were aspirated from cell cultures into a retroviral trap, containing neat bleach. All disposable plastics including filters, kwills and syringes were re-sheathed to minimise potential generation of aerosols. All retroviral waste was placed in a specially designated metal container and all retroviral waste was autoclaved.

A retrovirus co-expressing the catalytic subunit of telomerase, hTERT, and the neomycin phosphotransferase selectable (G418) gene marker was previously constructed in the laboratory and made available as a general reagent. The pBABE-neo-hTERT construct was transduced into primary XP-C (GM02996, XP8CA) and CS-A (GM01856, CS3BE) human dermal fibroblasts, using this amphotropic retroviral vector. In addition, an empty pBABE-neo vector without the hTERT insert was used as a control. For retroviral infection, primary XP-C and CS-A dermal fibroblasts were plated out in three 60 mm dishes/cell type, containing 2 ml of fresh non-selective EMEM medium (without G418), at a density of 2.8 X 10^5 and 2.7 X 10^5 cells/dish, respectively. One day later and 1 hour prior to infection, the fibroblasts were refed with 4 ml of fresh non-selective medium, containing 40 µl of (10 µg/ml) polybrene (Aldrich Chemical Company, Inc.). Immediately prior to infection, amphotropic retroviral supernatants, previously harvested from near confluent ψCRIP producer cells, were rapidly thawed at 37°C. Using a sterile plastic 5 ml syringe (Tyco HealthCare Ltd., UK) and Avon kwill filling Tube (127 mm; Sims™ Portex, UK), the supernatants were drawn up, and the kwill was replaced with a sterile plastic 0.45 µm

Acrodisc syringe membrane filter (Pall Cor., MI, USA). The supernatant was filtered through the 0.45 μm membrane filter into a bijou. A 1/100 volume of 100X polybrene was added to the filtered supernatant to give a final concentration of 1X polybrene (8 μg/ml). The non-selective medium (containing 10 μg/ml of polybrene) was aspirated from the 60 mm dishes. The fibroblasts were exposed to either 2 ml of retrovirus-containing medium from near-confluent producer cells expressing ψCRIP-pBABE-neo-hTERT or 2ml of retrovirus-containing harvest medium expressing the empty pBABE-neo control vector, or mock treated with non-selective medium alone (containing polybrene). The dishes were incubated at 37°C for 4 hours. Following incubation, 3 ml of non-selective medium was added to the dishes. The fibroblasts were incubated overnight (16-18 hours) at 37°C in a humidified incubator. The next day, the retroviral-containing medium was aspirated and cells were refed with non-selective medium and incubated for a further 24 hours.

Fibroblasts infected with the ψCRIP-pBABE-neo-hTERT were trypsinised, serially diluted in non-selective medium and seeded in 100 mm Petri dishes at densities appropriate for the production of polyclonal and monoclonal populations. The dilutions that were used included: 1/2, 1/10, 1/50, 1/100, 1/250 and 1/500. Fibroblasts infected with an empty pBABE-neo retroviral control vector or mock infected without retroviral supernatant were trypsinised and transferred directly from the 60 mm dish to a T75 flask and maintained under routine culture conditions as a polyclonal population. Fibroblasts infected with the ψCRIP-pBABE-neo-hTERT vector, empty pBABE-neo vector, or mock infected were refed 24 hours post dilution with selective medium, containing G418 at a concentration of 400 μg/ml. The 100 mm dishes were frequently analysed for colony formation and refed with selective medium every 3-4 days. Individual colonies were selected by trypsinisation, using autoclaved cloning rings. Selected clones were subsequently transferred to a 24 well plate. Once monoclonal populations were transferred to a 24 well plate the culture was denoted as passage 1 (P1) post retroviral infection. Confluent monoclonal populations were passaged into 35 mm dishes followed by T25 cm^2 flasks. A cell count was obtained from confluent T25 flasks and cumulative PDs were

calculated post infection. A fraction of the culture was passaged into a T75 flask (as described above). Both monoclonal and polyclonal populations were maintained under routine culture conditions and routinely subcultivated in T75 flasks.

Monoclonal XP-C and CS-A populations, infected with the ψCRIP-pBABE-neo-hTERT retroviral supernatant, were isolated and maintained under routine culture conditions for approximately 25-30 PDs. Three monoclonal populations, derived from each cell-type (XP-C and CS-A), which exhibited the best growth characteristics, were maintained under routine culture conditions for a further 70 PDs, as immortality was defined as ≥100 PDs. A single hTERT-immortalised XP-C (clone 19) and CS-A (clone 3) monoclonal population was selected from the three clones for all subsequent experimentation. The XP-C and CS-A polyclonal populations were maintained under routine culture conditions for ≥100 PDs and stored in liquid nitrogen as viable cultures.

2.3 Transfection of *XPC* and *CSA* short interfering RNA (siRNA) duplexes

Three 21mer siRNA sequences, targeting different regions of the *XPC* and *CKN1* mRNA gene transcript were designed using the Qiagen siRNA design tool (http://www.qiagen.com/Products/GeneSilencing/CustomSiRnaDesigner.aspx) and were synthesised and purified by Qiagen. The sequences of the siRNAs were: 5'-AAG TGG CCA AGG TGA CTG TTA-3' (*XPC*#1), 5'-AAG CAT AGC TGG TAT AGA CCA-3' (*XPC*#2), 5'-AAT TCA AAG ACG TGC TCC TGA-3' (*XPC*#3), 5'-AAG CAG TGT GTT CCA TTG GCA-3' (*CKN1*#1), 5'-AAT CGA ATG AGG CTC TGG AAT-3' (*CKN1*#2) and 5'-AAT CAC AAT TAA ATC CGG CCT-3' (*CKN1*#3). All siRNA sequences were confirmed by submitting the sequences to a BLAST search (using the National Centre for Biotechnology Information (NCBI) database) against the human genome sequences, thereby ensuring that the target-specific siRNAs only targeted the *XPC* or *CSA* gene.

Exponentially growing human hTERT-immortalised MRC-5 lung fibroblasts (previously established in the laboratory) were cultured in EMEM medium supplemented with 10% FCS (as previously described). Cells were seeded in 60 mm dishes, at a density of 2 X 10^5 cells/60 mm dish, 24 hours prior to transfection. Three 60 mm dishes were seeded/*XPC* (or *CSA*) siRNA duplex. Three further 60 mm dishes were seeded at a density of 2 X 10^5 cells for transfection of the scramble control. At the time of the initial transfection (treatment 1), the cell density was approximately 4 X 10^5 cells/60 mm dish. For each 60 mm dish, solution A was prepared as a master mix for the appropriate number of samples (X1) by combining 24 μl of 20 μM stock siRNA solution/60 mm dish with 400 μl of 1X serum-free Opti-MEM (Invitrogen)/60 mm dish in a plastic Bijou. Solution B was also prepared as a master mix for the appropriate number of samples X1 by combining 24 μl of Oligofectamine™ Reagent (Invitrogen™)/60 mm dish with 96 μl of serum-free Opti-MEM/60 mm dish in a plastic bijou. Solutions A and B were allowed to equilibrate at room temperature for 10 minutes. Solutions A and B were combined and incubated for a further 25 minutes at room temperature. Following incubation, 256 μl of Opti-MEM/60 mm dish was added to the combined solution A and B master mix. During the preparation of the transfection mix, the 60 mm dishes were washed with EMEM medium omitting penicillin (10,000 U/ml) and streptomycin (10 μg/ml). 3 ml of fresh EMEM was added to each 60 mm dish followed by 800 μl of the resulting transfection mixture and incubated overnight at 37°C. Following overnight incubation, the medium containing the transfection mix was aspirated, and the cells were refed with 4 ml of EMEM, containing penicillin (10,000 U/ml) and streptomycin (10 μg/ml). The hTERT-immortalised MRC-5 lung fibroblasts were treated with three treatments of *XPC*- or *CSA*-specific siRNAs (or control scramble) during a nine day treatment cycle (Fig. 2.1). Whole cell extracts (WCEs) were prepared following each siRNA treatment and western blot analysis was performed (Sections 2.9.0-2.9.5).

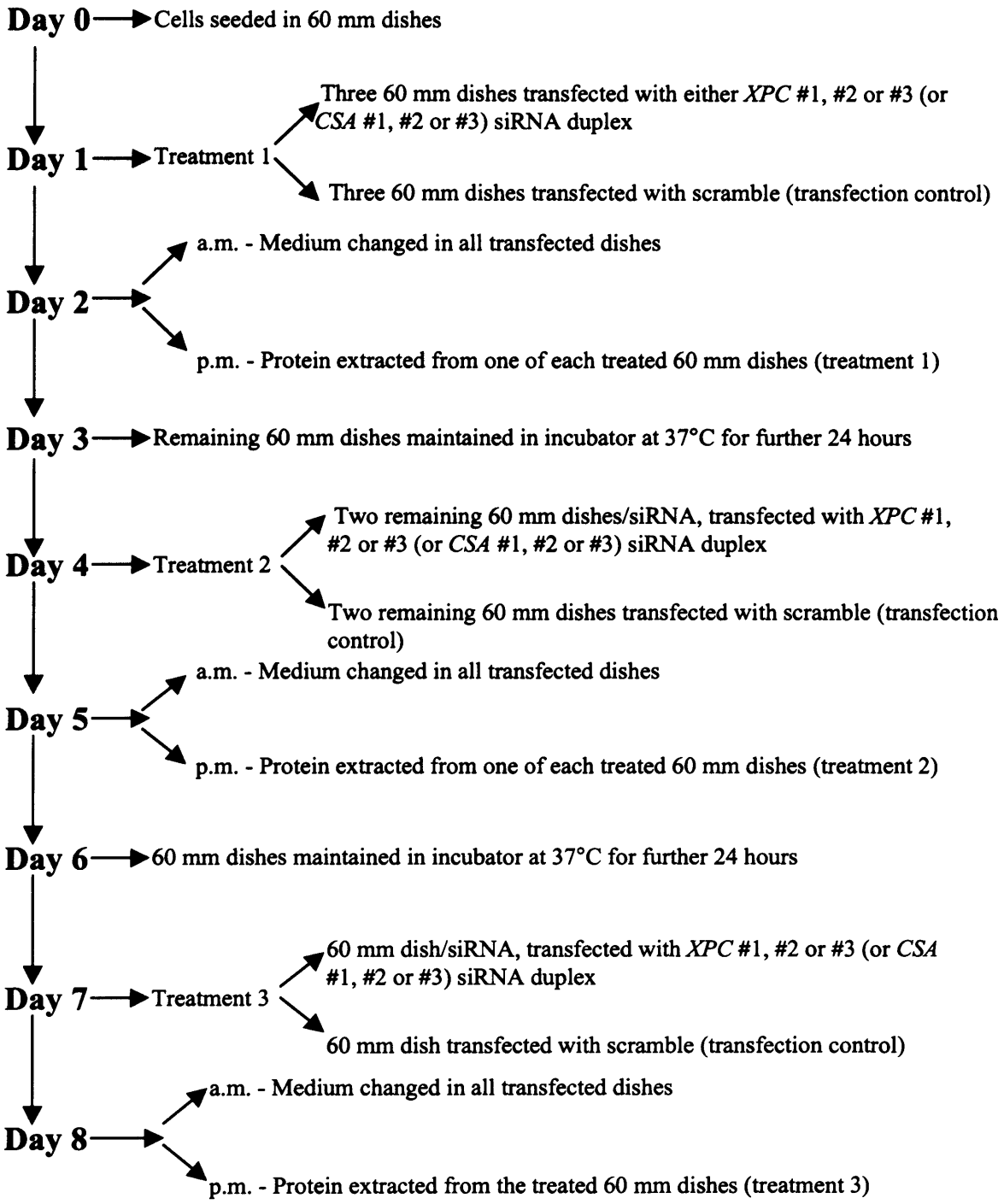

Figure 2.1. Experimental methodology adopted for the transient knockdown of *XPC* or *CSA* in normal MRC-5 fibroblasts, using *XPC*- or *CSA*-targeted siRNA duplexes.

2.4 Creation of permanent and stable double *XPC*^{KD}/*CS-A* and *XPA*^{KD}/*CS-A* cell lines using the CRUK pSUPER RNAi library

2.4.1 Background to the pSUPER RNAi ™ system

The human SUPER RNAi™ library, utilised in the creation of a permanent and stable *XPC*^{KD}/CS-A double knockdown, was based on the pSUPER RNAi system (Fig. 2.2), first described by Brummelkamp *et al.* (2002) and the human SUPER RNAi™ library (NKi library) described by Berns *et al.* (2004). The complete CRUK SUPER RNAi™ library was made available within eighty-three 96 well plates.

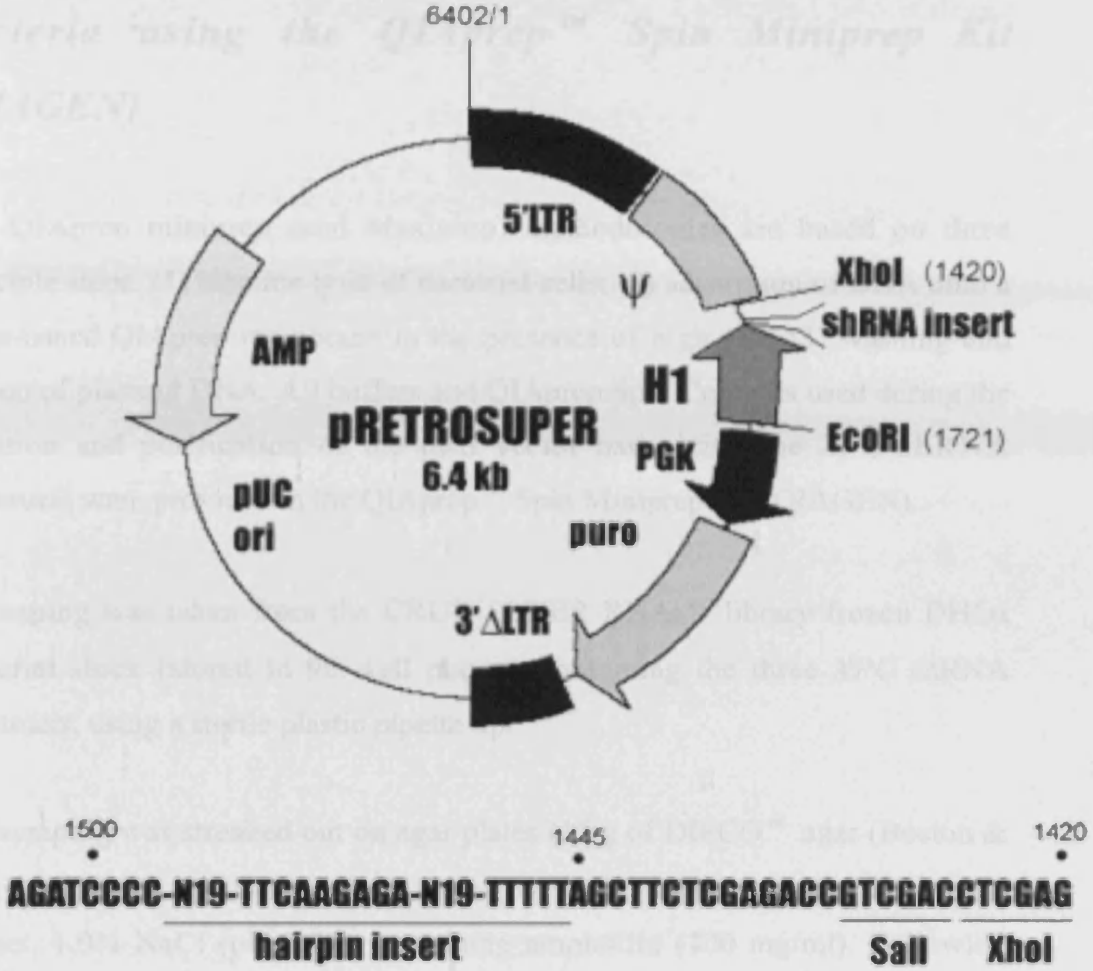

Figure 2.2. Schematic of pRETROSUPER vector derived from pMSCV. The 59mer hairpin oligonucleotides were cloned downstream of the polymerase III Histone H1-RNA promoter (H1; 1506-1721). The phosphoglycerate kinase promoter (PGK; 1721-2229) drives the expression of the puromycin resistance gene (puro; 2255-2854) in eukaryotic cells. The pRETROSUPER plasmid was propagated in *E.coli* under ampicillin (AMP; 5468-4611) selection.

2.4.2 Isolation of XPC shRNA constructs from DH5α bacteria using the QIAprep™ Spin Miniprep Kit (QIAGEN)

The QIAprep miniprep (and Maxiprep) methodologies are based on three principle steps: (1) alkaline lysis of bacterial cells; (2) adsorption of DNA onto a silica-based QIAprep membrane in the presence of high salt; (3) washing and elution of plasmid DNA. All buffers and QIAprep Spin Columns used during the isolation and purification of the pRS vector harbouring the *XPC* shRNA constructs were provided in the QIAprep™ Spin Miniprep Kit (QIAGEN).

A scraping was taken from the CRUK SUPER RNAi™ library frozen DH5α bacterial stock (stored in 96 well plates), containing the three *XPC* shRNA constructs, using a sterile plastic pipette tip.

The scraping was streaked out on agar plates (15 g of DIFCO™ agar (Becton & Dickinson)/l of Luria Bertani (LB) broth (containing 1.0% tryptone, 0.5% yeast extract, 1.0% NaCl (pH 7.0)), containing ampicillin (100 mg/ml). Following overnight incubation at 37°C, 20 individual colonies were selected with a sterile plastic pipette tip and placed in 5 ml culture tubes, containing 3 ml of L-broth and ampicillin (100 mg/ml). The cultures were incubated in an Orbital incubator (Sanyo) at 37°C overnight with agitation at 250 rpm.

After overnight incubation, 1.5 ml of the DH5α bacterial cultures, harbouring the *XPC* shRNA constructs, was added to a 1.5 ml Eppendorf tube, whilst the remaining 1.5 ml of the overnight cultures were stored at 4°C. The Eppendorf tubes were centrifuged at 13,400 g for 1 minute at room temperature in a Centra-M2 centrifuge (International Equipment Company, USA). The supernatant was decanted from the 1.5 ml Eppendorf tube, and the bacterial pellet was resuspended in 250 μl of buffer P1. Following complete resuspension, 250 μl of buffer P2 was added. The samples were mixed by gently inverting 4-6 times. 350 μl of buffer N3 was added and the tubes were mixed by gently inverting 4-6

times, or until the sample appeared cloudy. The tubes were centrifuged for 10 minutes at 13,400 g in a Centra-M2 centrifuge. The supernatant was decanted into a QIAprep Spin Column. The QIAprep Spin Columns were centrifuged for 1 minute at 13,400 g in a Centra-M2 centrifuge. Following centrifugation, the flow-through was discarded from the QIAprep Spin Column. The QIAprep Spin Columns were washed by adding 750 µl of buffer PE, and centrifuged for 1 minute at 13,400 g in a Centra-M2 centrifuge. The flow-through was discarded, and the QIAprep Spin Column was centrifuged for a further minute at 13,400 g in a Centra-M2 centrifuge to remove any residual wash buffer. The QIAprep Spin Column was placed in a fresh 1.5 ml Eppendorf tube. The purified pRS retroviral vector, containing the *XPC* expression cassette was eluted by adding 50 µl of buffer EB to the centre of each QIAprep spin column, whilst avoiding direct contact between the pipette tip and the column surface. The column was left to stand for 1 minute and centrifuged for 1 minute at 13,400 g in a Centra-M2 centrifuge.

Following isolation and purification of the pRETROSUPER plasmid DNA, containing the *XPC*-specific shRNA cassette, a double EcoRI/XhoI digest was performed on the 20 isolated clones. The double EcoRI/XhoI digests were performed in a final reaction volume of 20 µl, containing 2 µl of plasmid DNA, 2 µl of 10X buffer H (Promega), 1 µl of EcoRI (Promega), 1 µl of XhoI (Promega) and 14 µl of water. The double EcoRI/XhoI digests were incubated for 1 hour at 37°C. Following digestion, 10 µl of each digest, containing 2 µl of bromophenol blue, was electrophoresied on a 0.7% agarose gel (containing 2.5 µl ethidium bromide /50 ml agarose) for approximately 2 hours at 120 volts (V) in TBE (Tris-base, boric acid, EDTA) buffer. The expected size of the shRNA hairpin insert was 301 bp.

2.4.3 Identification of XPC shRNA sequences

The sequencing reactions were undertaken in a final reaction volume of 10 µl, containing 1 µl of miniprep DNA, 1 µl of the pRS sequencing primer 5'-GCT GAC GTC ATC AAC CCG CT-3' (3.3 pmol/µl), 4 µl of ABI PRISM® BigDye® Terminator v3.1 Cycle Sequencing Reaction Ready Kit (Applied Biosystems), and 4 µl of water. Sequencing reactions were prepared using a GRI MJ Tetrad Thermocycler. The sequencing conditions were 24 cycles of 96°C for 30 seconds, 50°C for 15 seconds and 60°C for 4 minutes. Following the completion of the sequencing reactions, a further 10 µl of water was added to each reaction to give a total volume of 20 µl.

2.4.4 Sequence reaction cleanup using the DyeEx™ Spin Kit

The sequencing reactions were subsequently purified, using the DyeEx™ 2.0 Spin Kit (Quiagen). The DyeEx™ 2.0 Spin Kit uses gel-filtration technology for the rapid removal of unincorporated dye terminators directly from sequencing. Spin columns provided with the DyeEx™ Spin Kit, were vortexed to resuspend the resin. The cap of the column was loosened and the bottom closure of the spin column was removed. The spin column was placed in a 2 ml collection tube and centrifuged for 3 minutes at 101 g using a Micro Centaur bench-top centrifuge (Sanyo). The collection tube was discarded and the spin column was transferred to a fresh collection tube. The sequencing reaction (20 µl) was applied to the gel bed with a pipette, whilst avoiding direct contact with the resin. The sequencing reaction product was collected by further centrifugation for 3 minutes at 101 g in a Micro Centaur bench-top centrifuge. Sequencing reactions were sent to the in-house Central Biotechnology Service (CBS; www.cardiff.ac.uk/cbs), where sequence analysis was undertaken using an automated ABI PRISM 3100 Genetic Analyser. Data was received as text files and electropherograms.

After sequencing and conformation of the successful isolation of the pRS vector harbouring the *XPC* shRNA constructs, 1 ml of the overnight 3 ml culture, previously stored at 4°C, was pipetted into 500 ml of L-broth, containing ampicillin (100 mg/ml). The cultures were incubated in a 2 l conical flask at 37°C overnight (16-18 hours) with agitation at 250 rpm in an Orbital incubator.

2.4.5 Maxiprep of XPC shRNA overnight 500 ml culture using the QIAGEN plasmid Maxi Kit

Following incubation, the 500 ml overnight cultures were divided into two 250 ml fractions and transferred to two 500 ml bacterial containers. An SLA-3000 rotor was chilled to 4°C and the two fractions were pelleted by centrifugation at 6,000 g for 15 minutes at 4°C using a Sorvall® Evolution RC refrigerated centrifuge. After centrifugation, the supernatant was aspirated.

One of the pelleted bacterial fractions was resuspended in 10 ml of buffer P1. The sample was transferred to the second container, containing the second fraction. The two fractions of the same sample were resuspended and 10 ml of buffer P2 was added. The samples were mixed gently by inverting 4-6 times, and incubated at room temperature for 5 minutes. Buffer P3 was chilled to 4°C, and 10 ml was added to each sample. The samples were mixed immediately by inverting 4-6 times and incubated on ice for 20 minutes. The samples were centrifuged at 6000 g for 30 minutes at 4°C. The supernatant, containing the plasmid DNA, was transferred to a 30 ml Sorvall tube. A SS-34 rotor was chilled and the Sorvall tubes were centrifuged at 9,000 g for 15 minutes at 4°C, using a Sorvall® Evolution RC centrifuge. A Qiagen-tip 500, provided in the Qiagen kit, was equilibrated by applying 10 ml of buffer QBT and the column was allowed to empty by gravity flow. The supernatant, containing the plasmid DNA, was applied to the Qiagen-tip and allowed to enter the resin by gravity flow. The Qiagen-tip was washed twice with 30 ml of buffer QC. The plasmid DNA was eluted from the Qiagen-tip with 15 ml of buffer QF into a fresh Sorvall tube. The plasmid DNA was precipitated by adding 10.5 ml (0.7 volumes) of isopropanol to the eluted DNA. The plasmid DNA was mixed and centrifuged immediately at

9,000 g for 30 minutes at 4°C. The supernatant was carefully decanted from the 30 ml Sorvall tube. The isolated plasmid DNA was washed with 5 ml of 70% ethanol and centrifuged at 9,000 g for 10 minutes at 4°C. The supernatant was decanted from the Sorvall tube. The pellet was air-dried for 10 minutes and resuspended in 400 µl of TE (10 mM Tris-Cl, 1 mM EDTA) buffer.

10 µl of each plasmid DNA, harbouring the *XPC* shRNA construct, was diluted in 990 µl of water. The diluted plasmid DNA samples were quantified, using an UltraSpec 31000 PRO spectrophotometer (Amersham Biosciences). To ensure that the isolated plasmid DNA harboured the *XPC* shRNA construct, a double EcoRI/XohI digest was performed as previously described. Following digestion, 10 µl of each digest, containing 2 µl of bromophenol blue, was electrophoresied on a 0.7% agarose gel (as previously described). To ensure that the sequence of the maxipreped plasmid DNA corresponded to the minipreped DNA, 1 µl of each plasmid DNA sample, prepared by the Maxiprep kit, was used to prepare sequencing reactions. The sequencing reactions were purified using the DyeEx™ Spin Kit (as previously described in Sections 2.4.5-2.4.6) and sequencing was performed (as before) by the CBS on an ABI PRISM 3100 Genetic Analyser.

2.4.6 Calcium phosphate transfection of XPC, XPA shRNA or an empty pBABE-puro plasmid DNA into FLY A13 cells

The *XPA* shRNA (isolated from the CRUK human SUPER RNAi™ library) and the pBABE-puro plasmid DNA, used as transfection controls, were previously prepared in the laboratory and made available as a general reagent.

Subconfluent FLY A13 human epithelial cells (retroviral packaging cell line), derived from fibrosarcoma tissue (Cosset *et al.*, 1995), were trypsinised from a T75 flask and seeded in 60 mm dishes at a density of 1 X 10^5 cells/dish. The cells were allowed to equilibrate overnight (16-18 hours) at 37°C in a humidified incubator (with 95% air, 5% CO_2 atmosphere). The next day and four hours prior to infection, the cells were re-fed with 3.6 ml of fresh non-selective Dulbecco's

modified Eagle's medium (DMEM; without puromycin) supplemented with 10% FCS, L-glutamine, 10,000 U/ml penicillin and 10 μg/ml streptomycin. The *XPC* and *XPA* shRNA plasmid DNA, previously prepared by the Quiagen maxi prep kit, was transferred from the 30 ml Sorvell tubes to 1.5 ml Eppendorf tubes. The tubes were centrifuged at 13,400 g for 10 minutes at room temperature in a Micro Centaur bench-top centrifuge, to remove residual proteins and cell debris. The supernatants were transferred to fresh 1.5 ml Eppendorf tubes. For each 60 mm dish transfected, 20 μg of plasmid DNA (containing either *XPC/XPA* shRNA or the pBABE-puro construct) was mixed with 200 μl of 0.25 M $CaCl_2$ (solution A). Solution B was prepared for each 60 mm dish to be transfected, by adding 200 μl of (2X) Hepes-buffered saline (HBS) solution (pH 7.05-7.12) to a sterile universal container. Solution A was taken up in a 200 μl plugged sterile pipette tip and pipetted drop by drop into solution B, whilst simultaneously blowing air through a 1 ml plastic stripette into solution B. The combined solution was incubated at room temperature for 25 minutes to allow the formation of a precipitate. The precipitate was gently resuspended and added drop-wise to the 60 mm dishes, containing the FLY A13 epithelial cells, using a 1 ml plugged sterile pipette tip and Gilson. The 60 mm dishes were transferred to an incubator and maintained under routine culture conditions overnight (16-18 hours). Following overnight incubation, the medium was aspirated from the 60 mm dishes and discarded. The 60 mm dishes were refed with fresh non-selective DMEM medium and incubated for 24 hours under routine culture conditions. Following incubation, the retroviral supernatant containing the retroviral virions was collected using a sterile plastic kwill and 5 ml syringe. The harvested supernatants were snap frozen in liquid nitrogen for 5 minutes and transferred to a -80°C freezer. The cells were refed with non-selective DMEM medium and incubated for a further 24 hours under routine culture conditions. Supernatants were harvested as previously described 48 hours post feeding.

2.4.7 Retroviral infection of hTERT-immortalised CS-A human dermal fibroblasts with XPC/XPA shRNA constructs or an empty pBABE-puro vector

The transfection (pBABE-puro) control supernatant was generated (during the calcium phosphate transfection of the shRNA constructs) from previously prepared plasmid DNA. In addition, pBABE-puro supernatant, previously generated in the laboratory was also obtained and used in the retroviral infection, thus providing an infection control.

For retroviral infection, hTERT-immortalised CS-A dermal fibroblasts were plated out in six 60 mm dishes, containing 2 ml of fresh non-selective medium (without puromycin), at a density of $1x10^5$ cells/dish. Retroviral infection of hTERT-immortalised CS-A dermal fibroblasts with the *XPC/XPA* shRNA constructs, the empty pBABE-puro control plasmid vector, or mock-infected (nontransduced) was performed as previously described (Section 2.2). Fibroblasts infected with the shRNA constructs or empty pBABE-puro vector were serially diluted in non-selective medium and seeded in 100 mm dishes at densities appropriate for the production of monoclonal populations (as previously described). The 60 mm dish infected with either the pBABE-puro supernatant (previously generated in the lab) or mock-infected (nontransduced) were transferred directly to a T75 flask and maintained in culture as polyclonal populations. Fibroblasts infected with the *XPC* or *XPA* shRNA vectors, empty pBABE-puro vector, or mock-infected were refed 24 hours post dilution with selective medium, containing puromycin at a concentration of 1 μg/ml. Monoclonal populations of hTERT-immortalised CS-A dermal fibroblasts, infected with either the *XPC* (or *XPA*) shRNA constructs, or the empty pBABE-puro vector were selected (as previously described in Section 2.2).

2.5 Plating efficiency

Prior to cell survival determination by colony forming ability, plating efficiencies were undertaken. Fibroblasts were seeded at densities of 1 X 10^2, 5 X 10^2, 1 X 10^3 and 5 X 10^3 in triplicate 100 mm Petri dishes, and were maintained under routine culture conditions for 10-16 days (depending upon cell-type). Following incubation, cells were washed twice in phosphate-buffered saline (PBS) and fixed for 15 minutes with methanol: acetic acid (3:1) and left to dry for 30 minutes at room temperature. The plates were subsequently stained in Giemsa's solution: Sorenson's buffer (pH 6.8; BDH, Poole, Dorset). Purple colonies with a minimum of 50 cells were scored. Plating efficiency was calculated as a percentage of the number of colonies formed compared to the initial number of cells seeded.

2.6 Cell survival determination by colony forming ability

Sub-confluent, exponentially growing human fibroblasts were trypsinized from T75 flasks and 5 X 10^2 to 2 X 10^3 cells were seeded in 100 mm Petri dishes, and allowed to attach overnight (16-18 hours), prior to UV-C irradiation (254 nm). For UV treatment, a UVP germicidal lamp (UVP, Ltd., Cambridge), emitting UV-C light, was calibrated using a UVX digital radiometer (UVP, Ltd., Cambridge) to emit an incident fluence rate of 1 J/m^2/s. Cells were washed twice with prewarmed (37°C) Hank's balanced salt solution (Sigma®) and irradiated with 0-10 J/m^2 in increments of 2 J/m^2. Fibroblasts were refed with fresh medium and maintained in culture for 7-14 days at 37°C in a humidified atmosphere containing 5% CO_2. Mock-irradiated (0 J/m^2) cells were treated as previously described, however, irradiation was omitted. At the end of the experiment, dishes were stained and scored (as above) to determine the clonogenic survival of cells. Survival values were calculated as a percentage of the number of colonies from irradiated cells compared to non-irradiated cells. Three data points (UV-irradiations) were obtained per experiment, which was

performed in triplicate. Therefore, each data point is representative of nine replicates.

2.7 Immuno-slot-blot assay

The immuno-slot-blot assay facilitated the detection of DNA damage following exposure to UV radiation, through the detection of both CPDs and 6-4PPs in genomic DNA, using specific mouse monoclonal antibodies, raised against either CPDs or 6-4PPs, respectively.

Exponentially growing hTERT-immortalised MRC-5, XP-C (GM02996, XP8CA), CS-A (GM01856, CS3BE) and double *XPC*^{KD}/CS-A knockdown fibroblasts were seeded in 4-8 100 mm culture dishes/time point at a density of $1x10^6$ cells/100 mm dish. Cells were irradiated with 10 J/m^2 (as previously described) and incubated under routine culture conditions for an indicated period of time following UV-irradiation. Genomic DNA was isolated (as described below) and stored at -20°C.

The Bio-Dot SF Microfiltration apparatus (BioRad) was assembled and a Vacugene pump (Pharmacia Biotech, UK) was attached to the outlet valve. Two layers of Whatman paper (Whatman International Ltd., UK) were placed on the blot machine as a base. This was followed by a piece of GeneScreenPlus nylon membrane (NEN Life Sciences Products, Inc., USA), soaked in a 0.4N NaOH solution. The lid was positioned and secured tightly. The vacuum pump was started and allowed a pressure of 40-50 mbar. Once the desired pressure was reached, 1 μg of DNA from each sample (in TE buffer) was loaded into each well and left for 5 minutes under pressure. Once the DNA had absorbed into the membrane, a final rinse of the individual wells was performed, by applying 200 μl of 0.4N NaOH. The membrane was removed from the Bio-Dot SF Microfiltration apparatus and washed once with 1X TBST (containing 100 mM Tris-base (pH 8), 500 mM NaCl, Tween 20 made up in water) solution for 5 minutes at room temperature. The membrane was blocked overnight (16-18 hours) at 4°C, in 1X TBST/3% non-fat milk (Marvel). The membrane was placed

in a plastic bag and was incubated with either 2 μg of CPD- (TDM-2) or a 6-4PP- (64M-2) specific monoclonal mouse antibody (both purchased from MBL® International Corporation; Mori *et al.*, 1991) in 10 ml of 1X TBST/3% non-fat milk solution. The membrane was incubated with agitation on a Gyro-Rocker® STR9 (Stuart) for 1 hour at room temperature. This was followed by three 15 minute washes in fresh 1X TBST solution. The membrane was incubated in 0.5 μl of the alkaline phosphatase-linked anti-mouse secondary antibody provided in the ECF™ (enhanced chemifluorescence) Western Blotting Analysis system Kit (Amersham Pharmacia Biotech), diluted in 10 ml of 1X TBST/3% non-fat milk solution, for 1 hour with agitation at room temperature. Residual secondary antibody was removed by extensive washing with 1X TBST solution as previously described. The ECF detection solution, provided with the ECF™ Western Blotting Analysis system, was prepared by adding 36 mg of ECF substrate to 60 ml of ECF dilution buffer. The ECF detection solution was pipetted onto Clingfilm, and the membrane was placed on top of the solution, with the side harbouring the DNA samples facing the detection solution. The membrane was incubated for 2 minutes at room temperature. The fluorescent emission from the samples bound to the membrane was detected using a STORM 860 phosphorimager (Molecular Dynamics, Inc.) and quantification was performed using ImageQuant software (Molecular Dynamics, Inc.). The percentage of lesions remaining at each time point was calculated in comparison to the lesions present immediately (0 hours) after UV-irradiation. Three biological replicates were performed for each indicated time point.

2.8 Detection of telomerase activity by the Telomeric repeat amplification protocol (TRAP) assay

The TRAP assay is a two-stage methodology used to detect telomerase activity in cell extracts of cultured cells or tumour samples. Stage 1 requires a nontelomeric TS oligonucleotide, which is extended by the synthesis of telomeric (TTAGGG) repeats, as a result of telomerase activity. The second step involves

the PCR amplification of the extension products, using the downstream CX primer and the presence of the upstream TS primer. Amplification products are resolved on a polyacrylamide gel and detected by fluoro-imaging. The TRAP assay was performed in accordance to the methodology first described by Kim *et al.* (1994), and undertaken in an RNase-free environment. All tubes were DEPC treated and solutions were made using DEPC treated water. All glassware used to prepare stock solutions was baked with a metal lid at 200°C for 2 hours and sealed with parafilm when cooled. In addition, to avoid contamination, all manipulations were performed in a PCR hood, using RNase-free pipette tips.

2.8.1 Preparation of S100 cell extracts

Following the selection of monoclonal and polyclonal populations of fibroblasts infected with hTERT, exponentially growing fibroblast cell cultures were trypsinised and resuspended in 8 ml of medium and counted (as previously described in Section 2.1). The cells were centrifuged at 277 g for 5 minutes at room temperature and the medium was discarded. The cell pellets were resuspended and washed in 10 ml of 1X sterile PBS. The cells were centrifuged at 202 g for a further 5 minutes at room temperature and the supernatant was aspirated. The pellets were resuspended in 1 ml of 1X PBS and transferred to a 1.5 ml RNase-free Eppendorf tube. The samples were centrifuged at 15,000 g for 2 minutes at 4°C in a OLE DICH Type 154.RF cooling centrifuge (Camlab Ltd., Cambrige, UK) and the supernatant was discarded. The pellets were stored at -80°C.

The cells were thawed on ice and resuspended in 1 ml of wash buffer (containing 100 µl 0.1 M Hepes-KOH, 1.5 µl 1 M $MgCl_2$, 1 µl 1 M KCl, made up to 1 ml with DEPC treated water) with 1 µl of 1 M dithiothreitol (DTT) added immediately prior to use. The cell suspension was centrifuged at 15,000 g for 2 minutes at 4°C and the supernatant aspirated. Fresh lysis buffer was prepared by adding 3 µl of 10% β-mercaptoethanol (diluted 1/10 in DEPC treated water) and 2 µl of 0.5 M phenylmethylsulphonyl fluoride (PMSF; diluted in methanol) to 500 µl of lysis buffer (100 µl 0.1 M Tris-HCl (pH 8.3), 1.5 µl 1 M $MgCl_2$, 10 µl

0.1 M ethyleneglycol tetraacetic acid (EGTA), 100 µl glycerol, 100 µl 5% chapso (CHAPS; Pierce) made up to 1 ml with DEPC water, immediately prior to use. The cell pellets were resuspended in 20 µl of lysis buffer and incubated on ice for 30 minutes. During incubation, a S150AT rotor was placed in a RCI50GX micro-ultracentrifuge (Sorvall) and cooled to 4°C under vacuum. The cell suspension was transferred to cooled DEPC-treated polycarbonate centrifuge tubes (Sorvall) during the 30 minutes incubation on ice. Lysates were centrifuged at 100,000 g for 30 minutes at 4°C in a RC M150 GX ultracentrifuge. Supernatants were aliquoted into fresh DEPC-treated polycarbonate tubes. The supernatants were snap frozen on dry ice and stored at -80°C. All cell lysates, including positive cell extract 293 (derived from adenovirus transformed human embryonic kidney cells (HEK 293; Graham, 1977)), were thawed on ice, and further diluted in lysis buffer to give approximately 5000 cell equivalents/µl.

2.8.2 Pre-treatment of TRAP assay lysates

To prepare negative controls (and destroy telomerase activity), the diluted cell lysates (prepared in 2.8.1) were divided into two equal aliquots by transferring half the cell lysate to a fresh RNase free 0.5 ml microcentrifuge tube. One aliquot from each sample was incubated at 85°C for 10 minutes to destroy telomerase activity, thus providing a negative control for the detection of possible contamination within the assay. The other aliquot of each sample was placed on ice for 10 minutes.

2.8.3 TRAP assay – Stage 1 (extension of TS primer)

TRAP assay reactions were prepared by transferring 1 µl of each heat-treated and non-heat treated cell extract to a fresh 0.5 ml RNase-free microcentrifuge tube incubated on ice, containing 50 µl 1X reaction buffer (20 mM Tris-HCl (pH 8.3), 1.5 mM $MgCl_2$, 63 mM KCl, 0.005% Tween 20, 1 mM EGTA (pH 8), 50 µM dNTP's (Promega), 0.1 mg/ml bovine serum albumin (BSA; acetylated: nuclease free: Promega). In addition, 1 µg of the single-stranded DNA (ssDNA) binding

protein T4 Gene 32 protein (New England BioLabs, Inc.), 100 ng TS (5'-AATCCGTCGAGCAGAGTT-3') primer (MWG Biotech) was added to each reaction immediately prior to extension. The samples were capped with mineral oil (Sigma®), transferred to a GRI MJ Tetrad Thermocycler, and incubated for 30 minutes at 30°C. The temperature was increased to 92°C in preparation for stage 2.

2.8.4 TRAP assay – Stage 2 (PCR amplification)

Extension products generated in stage 1 are undetectable by conventional methods. Therefore, products were amplified by PCR. Following the initial extension, 100 ng of CX (5'-CCCTTACCCTTACCCTTACCCTAA-3') primer (MWG Biotech), 2.5 U of *Taq* polymerase (Promega) and 0.5 X 10^{-18} g (0.5 µl/reaction) of the internal telomerase amplification standard (ITAS) PCR control was added to each reaction at 92°C. PCR amplification was performed in a GRI MJ Tetrad Thermocycler. The amplification conditions were 31 cycles of denaturation (92°C, 30 seconds), annealing (50°C, 30 seconds) and extension (72°C, 90 seconds). Following PCR amplification, the reaction mix (approximately 50 µl) was carefully transferred to a fresh microcentrifuge tube, without carrying over mineral oil. 10 µl of 6X xylene cyanol/bromophenol blue (0.25% xylene cyanol (Sigma®), 0.25% bromophenol blue (Sigma®), 15% Ficoll (Pharmacia) dissolved in water) was added to each sample. 20 µl of each sample was electrophoresed at 300 V on a 10% polyacrylamide 20 cm Protean II gel (containing 45 ml distilled water, 30 ml 5X TBE buffer (54 g Tris base, 27.5 g boric acid and 20 ml 0.5 M EDTA made up to 1 litre with water), 25 ml acrylamide (19:1 bis: acrylamide; BIO-RAD Laboratories, Inc.), 500 µl 100 mg/ml ammonium persulphate (APS) and 100 µl N, N, N,' N,'-tetramethylethylenediamine (TEMED)) in a tank containing 1.5X TBE buffer, for approximately 4 hours or until the bromophenol blue electrophoresed to ~ 3 cm from the bottom of the gel. The gel was incubated in SybrGold (Cambridge Bioscience) diluted 1:10,000 in water for 10 minutes at room temperature with agitation. The gel was washed for 5 minutes in water at room temperature to remove excess SybrGold. After washing, the gel was scanned on STORM

(Amersham Biosciences), employing the blue fluorescence mode. A DNA ladder of 6 bp increments typified a telomerase positive extract.

2.9.0 Western blotting

2.9.1 Sample preparation and protein extraction

Fibroblasts were seeded in 100 mm Petri dishes or 60 mm dishes at a density of ~1 X 10^6 cells/dish or ~2 X 10^5/dish, respectively, and maintained under routine culture conditions for 1-3 days (depending on cell-type and experimental procedure) prior to extraction. For UV-irradiated and mock-irradiated samples, fibroblasts were seeded in multiple 100 mm Petri dishes/time point and allowed to equilibrate overnight at 37°C under routine culture conditions. Dishes were UV treated as previously described (Section 2.6) and maintained in culture at 37°C for the indicated period of time. Total protein was harvested at the indicated time point (hours) post UV-irradiation (as described below). Mock-irradiated samples were prepared in an identical manner, omitting UVC-irradiation.

Subconfluent (~80-90% confluence) dishes were washed twice with 5 ml ice-cold sterile 1X PBS. The cells were incubated and policed off with 1 ml ice-cold sterile STE buffer (containing 10 mM Tris; pH 8, 150 mM NaCl, 1 mM EDTA (pH 8)) and transferred to a 15 ml Falcon tube. This was repeated for each dish with a further 1 ml of STE buffer. The cells were centrifuged at 123 g for 5 minutes at 4°C in a refrigerated Falcon 6/300 (Sanyo). Following centrifugation, the supernatant was aspirated and discarded. The total cell volume was estimated, and WCEs were prepared by resuspending pellets in 2.5 packed cell volumes of 1 X lysis buffer (150 mM NaCl, 50 mM Tris, 5 mM EDTA and 1% nonident P40 (NP40)), containing protease inhibitors; 100 mM PMSF dissolved in propan-2-ol, 20 μg/ml Aprotinin and 10 μg/ml Leupeptin (all Sigma®) were both added to the lysis buffer. For the analysis of phosphorylated proteins, additional phosphatase inhibitors were added, including 200 μM sodium

orthovanadate and 50 mM sodium fluoride. WCEs were centrifuged at 20,000 g for 30 minutes at 4°C in an OLE DICH Type 154.RF cooling centrifuge. Following centrifugation, supernatants were transferred to a fresh 0.5 ml microcentrifuge tube and stored at -80°C.

2.9.2 Protein quantification

Total protein lysates were quantified by the Bradford colormetric method, using the Coomassie® Plus Protein Assay Reagent (Pierce). Lysis buffer, previously used to obtain the WCEs, was diluted 1/10 with sterile water, and used to dilute a stock solution of Comassie® Plus – The Better Bradford Assay™ Kit BSA reagent (Pierce, Ltd., UK) at a concentration of 2 mg/ml (stored at 4°C). A series of BSA standards were prepared in triplicate with final concentrations in the range of 0-400 μg/ml, in increments of 100 μg/ml. 5 μl of each WCE was diluted in 45 μl of water to give a 1/10 dilution. 40 μl of each WCE and BSA standard was transferred to a 1.6 ml plastic cuvette, before adding 1 ml of Coomassie Plus Protein Assay Reagent (Pierce). The Coomassies® Plus Protein Assay Reagent and WCEs or BSA standards were mixed thoroughly by vigorous pipetting. A 1/10 dilution of the lysis buffer (diluted with sterile water) was also prepared as a reference for subsequent spectrophotometric analysis. The OD (at 595 nm) of WCEs and BSA standards was determined using an UltraSpec 31000 PRO (Amersham Biosciences). Each BSA standard was assayed in triplicate and a mean value was calculated. Linear regression analysis of the BSA standards was used to calculate the concentration of protein (μg/μl) present in each WCE.

2.9.3 SDS-PAGE electrophoresis and transfer

A Biorad mini-protean II electrophoresis cell system was used to separate and transfer protein lysates to a polyvinylidene difluoride (PVDF) Immobilon™-P membrane (Millipore). WCEs were run on 8-12 % polyacrylamide, sodium dodecyl sulphate (SDS) resolving gels (containing 40% acrylamide:bis (29:1) 1.5 M tris (pH 8.8), 10% SDS, 10% APS and TEMED), depending upon the

molecular weight of the protein of interest (Table 2.1). The resolving gel was pipetted directly between the glass plates of the mini gel apparatus, using a Pasteur pipette, to approximately 2 cm from the top of the glass plates. Sterile water was subsequently pipetted directly on top of the resolving gel to promote polymerisation. Following polymerisation (approximately 1 hour at room temperature) of the resolving gel, the water was decanted from the gel apparatus, and any residual moisture was removed with 3 MM paper (Whatman). The stacking gel (2.5 ml 0.5 M Tris (pH 6.8), 1.25 ml 40% acrylamide:bis 29:1 (BIO-RAD Laboratories, Inc.), 100 µl 10% SDS, 50 µl 10% APS, 10 µl TEMED in 6.25 ml water) was pipetted directly onto the resolving gel between the glass plates of the minigel apparatus, using a Pasteur pipette. A plastic 10 lane (0.75 mm) comb was inserted into the stacking gel. The SDS-PAGE gels were allowed to stand at room temperature for a further 30 minutes to permit polymerisation of the stacking gel. Aliquots, containing 20 µg of the soluble WCEs was made up to the maximum allowable volume of 18 µl with sterile water and 9 µl of 3X loading buffer (for 960 µl stock: 300 µl 0.5 M Tris (pH 6.8), 300 µl glycerol, 300 µl 10% SDS, 60 µl 1% bromophenol blue and 30 µl β-mercaptoethanol) was added to give a total volume of 27 µl. 8 µl of 1 µg/µl High Molecular Weight Rainbow™ coloured marker (Amersham Pharmacia Biotech) was made up to 30 µl with 1X loading buffer. The WCEs and rainbow marker were denatured at 100°C for 5 minutes in a boiling water bath, and centrifuged at 12,000 g for 1 minute in a OLE DICH Type 154.RF cooling centrifuge, and loaded using "duck bill" tips. The High Molecular Weight Rainbow™ marker was also loaded in parallel to confirm the precise location of the protein of interest. 30 µl of 1X loading buffer was loaded in empty lanes to prevent the uneven electrophoresis of the protein extracts. Protein extracts were electrophoresed and separated at 100 V for 1 hour (or until the loading buffer migrated to the bottom of the SDS-PAGE gel) in 1X SDS running buffer (containing 15 g of Tris base, 94 g of glycine and 5 g of SDS made up to 1 litre with water, ~pH 8.3) using a vertical Biorad Mini-Protean II Electrophoresis Cell.

Following electrophoresis, the SDS-PAGE gel was removed from the Biorad Mini-Protean II electrophoresis cell, and the separated proteins were transferred

from the SDS-PAGE gel to a (0.45 μm) PVDF Immobilon™-P membrane, using a Mini Trans-blot Electrophoresis Transfer Cell (BIO-RAD Laboratories, Inc.). Preceding transfer, the PVDF membrane was prepared by immersing in methanol for 3 seconds. The membrane was washed in sterile de-ionised water for 2 minutes, thus removing any residual solvent from the membrane. The PVDF membrane was transferred and maintained in transfer buffer (containing 3.03 g Tris base, 14.4 g glycine, 200 ml methanol, made up to 1 litre with water, pH 8.1-8.4) to prevent drying and facilitate equilibration between the transfer buffer and membrane, until the assembly of the Mini Trans-blot Electrophoresis Transfer Cell was completed. In addition to the PVDF membrane, the Mini Trans-blot electrophoresis transfer pads and 3 MM filter paper were equilibrated in transfer buffer prior to transfer. Following electrophoresis, the Biorad Mini-Protean II Electrophoresis Cell was disassembled and the SDS-PAGE gel was carefully removed from the gel plates. The gel was washed and allowed to equilibrate in transfer buffer. The Trans-blot electrophoresis apparatus was assembled by transferring the PVDF membrane to a piece of 3 MM filter paper prior to positioning the SDS-PAGE gel onto the PVDF membrane. A further piece of 3 MM filter paper was positioned on top of the SDS-PAGE gel. The gel and PVDF membrane was secured by the Mini Trans-blot electrophoresis clamps and transferred to a Mini Trans-blot electrophoresis tank. Transfer buffer was poured into the electrophoresis tank, and a stir bar was added. In addition, an ice block was inserted into the Mini Trans-blot electrophoresis tank to prevent the electrophoresis tank from overheating. The electrophoresis tank was placed on a stirrer and transfer of the separated proteins was performed at 100 V for 1 hour.

2.9.4 Immunoprobing

PVDF membranes were blocked by overnight incubation at 4°C in 1X PBS, containing 5% non-fat milk and 0.2% Tween 20 (Sigma®). Following overnight incubation, the PVDF membrane was incubated with the primary antibody (Table 2.1) in a 30 ml Sorvall tube for 1 hour at room temperature (unless where otherwise stated) on a Roller Mixer SRT2 (Stuart Scientific, UK) in (a minimum volume of 2 ml) 1X PBS containing 5% non-fat milk/1% BSA/0.2% Tween 20,

or TBS. The PVDF membrane was washed with 1% Tween 20 in PBS, at room temperature on a Gyro-Rocker® STR9 (Stuart Scientific, UK) for 15 minutes. This was followed by three further 5 minute washes with fresh 1% Tween 20 in PBS. The PVDF membrane was transferred to a fresh 30 ml Sorvall tube before incubating with a rabbit anti-mouse (RAM) or goat anti-rabbit (GAR) horseradish peroxidase (HRP)-conjugated secondary antibody (Table 2.1) supplied with the ECL™ (enhanced chemiluminescence) Western Blotting Analysis system (Amersham Pharmacia Biotech), or with a peroxidase-conjugated rabbit anti-goat (RAG) immunoglobulin (Dako). The secondary HRP-coupled antibody was diluted as before in (a minimum volume of 2 ml) 1X PBS, containing 5% non-fat milk/1% BSA/0.2% Tween 20 (Table 2.1). The PVDF membrane was incubated with the secondary HRP-coupled antibody for 1 hour at room temperature on a Roller Mixer SRT2. The PVDF membrane was washed with 1% Tween 20 in 1X PBS, as previously described. The protein-antibody complexes were detected using the ECL™ Western Blotting Analysis system (Amersham Pharmacia Biotech) and was used according to the manufacturers recommendations. Briefly, ECL Reagents A (luminol) & B (enhancer) were equilibrated at room temperature, and 1 ml of each reagent was pipetted into a Bijou and mixed. Residual wash buffer was removed from the PVDF membrane by blotting, and the combined solution of reagents A & B was pipetted onto the PVDF membrane at a recommended (by Amersham Pharmacia Biotech) volume of 1 ml of combined reagent per 8 cm^2 (or 0.125 ml/cm^2) of PVDF membrane. The PVDF membrane was incubated at room temperature for 1 minute, and any residual reagent was blotted from the membrane. The membrane was tightly wrapped in Saran wrap. Protein bands, immobilised on PVDF membranes, were visualised by exposing the membrane to autoradiography hyperfilm (Amersham Pharmacia Biotech) for 5-120 minutes. After exposure, the autoradiography hyperfilm was developed and fixed using a XOGRAPH Compact X4 Automatic X-ray Film Processor (X-Ograph Imaging System, Ltd., Gloucestershire, UK).

2.9.5 Verification of equal protein loading

To account for differences in cell size (and therefore differences in the total amount of certain cellular proteins), India ink staining was used to verify equal protein loading of the WCEs.

Following visualisation of the hyperfim, equal loading of the WCEs was verified by washing the PVDF membrane with 0.2% Tween 20 in 1X PBS for 15 minutes, at room temperature with agitation on a rotator. The membrane was stained with 100 µl of India ink (Windsor & Newton) diluted in 100 ml of 0.2% Tween 20 in 1X PBS. To remove excess India ink residue, the PVDF membrane was washed with 0.2% Tween 20 in 1X PBS as previously stated. The membrane was subsequently dried at room temperature.

Table 2.1. Antibodies used during Western blot analysis and optimised immunoblot conditions (where the antibody concentration was not available the antibody dilution has been provided).

Antibody	Resolving gel (%)	1° antibody	Con.	Diluent	2° antibody	Con.	Diluent
ATF-3 C-terminus	12	ATF-3 (C-19):sc-188 (Santa Cruz Biotechnology, Inc)	1 µg/ml	PBS	GAR	1/2000	PBS
CSA C-terminus	12	CSA (W16): sc-10997 (Santa Cruz Biotechnology, Inc)	2 µg/ml	PBS	RAG	1/1000	PBS
FDXR Full-length	12	FDXR [6C2] (ab16810) (Abcam)	1 µg/ml	PBS	RAM	1/2000	PBS
GADD45α N-terminus	12	GADD45 (AB3863) (Chemicon International)	4 µg/ml	PBS	GAR	1/1000	PBS
PMAIP1 (NOXA)	12	NOXA [114C307] (ab13654) (Abcam)	1.25 µg/ml	PBS	RAM	1/2000	PBS
p16 (DCS50) C-terminus	12	Calbiochem®	2.5 µg/ml	PBS	RAM	1/1000	PBS

Table 2.1. *Continued.*

Antibody	Resolving gel (%)	1° antibody	Con/	Diluent	2° antibody	Con.	Diluent
p21 (sdi1/6B6)	12	Pharmingen (Cat No. 554228)	2 μg/ml	PBS	RAM	1/2000	PBS
p38	12	Cell Signalling (Cat No. 9212)	1/250	TBS	GAR	1/2000	PBS
p53 (aa 21-25)	12	DO-1 (Ab6) (Calbiochem)	0.1 μg/ml	PBS	RAM	1/2000	PBS
Phospho-p53 (Ser-15)	12	Phospho-p53 16G8 (Cell Signalling)	1/1000	TBS	RAM	1/2000	PBS
RB (aa 332-344)	7	RB (G3-245): 554136 BD Pharmingen	2 μg/ml	PBS	RAM	1/10,000	PBS
XPA (12F5)	12	Abcam (Cat No. ab2352)	2 μg/ml	PBS	RAM	1/1000	PBS
XPC	8	Abcam XPC [3.26] (ab6264)	2 μg/ml	PBS	RAM	1/1000	PBS

Abbreviations: ATF-3, activating transcription factor 3; Con., concentration; CSA, Cockayne syndrome A; FDXR, ferredoxin reductase; GADD45α, growth arrest and DNA-damage-inducible, alpha; GAR, goat anti-rabbit; PBS, phosphate-buffered saline; Phospho, phosphorylated; PMAIP1 (NOXA), phorbol-12-myristate-13-acetate-induced protein 1; RAG, rabbit anti-goat; RAM, rabbit ant-mouse; Rb, retinoblastoma; Ser, serine; XPA, xeroderma pigmentosum A; XPC, xeroderma pigmentosum group C; TBS, tris-buffered saline.

2.10 Immunocytochemistry (ICC)

The VECTRASTAIN® ABC system (Vector Laboratories, Peterborough, UK) utilises an immunoperoxidase system, which facilitates the immunocytochemical detection through: (1) binding of a primary antibody; (2) subsequent binding of a biotinylated secondary antibody; (3) formation of an Avidin and Biotinylated horseradish peroxidase macromolecular Complex (ABC). The horseradish peroxidase is visualised by the development of a peroxidase substrate that generates a brown reaction product.

Cells used for XPC labelling were plated onto Thermanox coverslips (which were previously attached to 35 mm culture dishes) at a density of 1 X 10^5 cells/35 mm dish. The dishes were allowed to equilibrate and attach to the surface of the coverslips in a humidified incubator at 37°C for 48 hours, prior to 4% paraformaldyhyde fixation and antibody labelling (as described below). For $p21^{WAF1/CIP1}$ labelling, following UV-irradiation, cells were plated onto Thermanox coverslips at a density of 1 X 10^5/35 mm dish (as previously described) and allowed to equilibrate and attach to the surface of the coverslips for 48 hours before UV treatment. The 35 mm dishes were irradiated (or not) as previously described (Section 2.6). Cells were fixed with 4% paraformaldyhyde at the indicated time points, post UV-C irradiation or mock-irradiation and labelled with the appropriate antibodies (as described below).

Following irradiation (or not), growth medium was aspirated and the 35 mm dishes were washed twice with 2 ml 1X PBS. The fibroblasts were fixed in 2 ml of 4% paraformaldehyde in 1X PBS for 10 minutes at room temperature. The paraformaldyhyde was aspirated and the coverslips were washed twice with 1X PBS. The dishes were stored in 2 ml 1X PBS at 4°C for up to 48 hours prior to undertaking ICC. To quench, the 1X PBS was decanted and the culture dishes were incubated with 2 ml of 50 mM glycine in 1X PBS for 10 minutes at room temperature. The glycine was decanted, and the dishes were washed three further times in 1X PBS. The dishes were incubated with 2 ml of 0.2% Triton X-100 in 1X PBS for 10 minutes at room temperature, and washed three times in 1X PBS.

The dishes were incubated for 3 minutes with 0.3% hydrogen peroxide (H_2O_2) in water and washed three further times in 1X PBS. To block, the dishes were incubated with 2% horse serum in 1X PBS for 10 minutes at room temperature. Coverslips were incubated for 1 hour at room temperature in a humidified chamber with 50 µl of either the anti-XPC (1/200) or anti-$p21^{WAF1/CIP1}$ (1/500) mouse monoclonal primary antibody, which was diluted in 2% horse serum 1X PBS. Coverslips were washed three times in 1X PBS, and incubated for 10 minutes at room temperature in a humidified chamber with 50 µl of the anti-mouse biotinylated secondary antibody (1/200) provided in the Vectastain® Elite® ABC Kit diluted in 2% horse serum/1X PBS. Coverslips were placed in a clean 24 well culture dish and washed in 1X PBS. The ABC reagents, supplied with the Vectastain® Elite® ABC Kit, was prepared by adding 2 µl of avidin solution DH (solution A)/100 µl 2% horse serum in 1X PBS, followed by 2 µl of biotinylated enzyme (solution B)/100 µl 2% horse serum in 1X PBS, containing solution A. Coverslips were incubated for 5 minutes at room temperature with 50 µl of the solution A and B mix and transferred to a clean 24 well dish and washed in 1X PBS. After washing, coverslips were incubated with 50 µl of diaminobenzidine (DAB) solution (containing 1 ml DAB/9 ml 1X PBS and 3.4 µl H_2O_2) for 5 minutes at room temperature, transferred to a clean 24 well plate and washed in distilled water. To enhance visualisation of the cells, coverslips were counter-stained with haematoxylin for 45 seconds and rinsed in tap water. Coverslips were dehydrated in 100% ethanol and xylene, mounted onto square coverslips using DPX (BDH), and left to dry overnight. Once dry, the coverslips were further mounted onto glass microscope slides, using DPX. Positive cells exhibited brown nuclei that were indicative of a peroxidase reaction product. By contrast, negative cells displayed blue nuclei, under a light microscope. For $p21^{WAF1/CIP1}$ ICC, the percentage of positively labelled nuclei was ascertained from a count of 500 cells/coverslip.

2.11 Characterisation of *XPC* and *CKN1* gene variants

2.11.1 Genomic DNA isolation & purification

The pellet was resuspended in 400 µl of digestion buffer (containing 100 mM NaCl, 10 mM Tris·Cl (pH 8), 25 mM EDTA and 0.5% SDS). 2.5 µl of 20 mg/ml RNase (Sigma®) was added, and the samples were incubated for 1 hour at 37°C in a water bath before adding 5 µl of 20 mg/ml proteinase K (Sigma®). The samples were incubated at 50°C in a water bath overnight (16-18 hours). Following overnight incubation, an equal volume of phenol (200 µl) and chloroform/isoamyl alcohol (200 µl) at a ratio of 25:24:1 was added, and the samples were mixed thoroughly by repeated inversion. The samples were emulsified by mixing gently on a ROTATOR DRIVE STR4 (Stuart Scientific, UK) at room temperature for 15 minutes. The centrifuge tubes were centrifuged at 13,400 g for 10 minutes in a bench-top Micro Centaur (Sanyo) centrifuge at room temperature. The upper aqueous layer, containing genomic DNA, was carefully transferred to a fresh 1.5 ml DNase-free Eppendorf tube, using a wide bore pipette tip. A 1/10 volume (40 µl) of 3 M sodium acetate (pH 5.2) was added, and the samples were mixed gently before adding 2.5 volumes (1000 µl) of ice cold absolute (100%) ethanol. The samples were mixed gently and incubated for a minimum of 20 minutes at -20°C. The samples were centrifuged at 20,000 g for 10 minutes at 4°C in an OLE DICH Type 154.RF cooling centrifuge. The ethanol was carefully aspirated from the Eppendorf tube. The pellet was washed with 500 µl of 70% ethanol, and the samples were incubated on ice for 5 minutes. The samples were centrifuged at 20,000 g for 5 minutes at 4°C in an OLE DICH Type 154.RF cooling centrifuge, and the supernatant was decanted. The pellet was air-dried for 5-10 minutes to remove any residual ethanol before resuspending the pellet in an appropriate volume of TE buffer to give a concentration of approximately 1-2 µg/µl. The genomic DNA was stored at 4°C overnight to redissolve. The DNA concentration was determined by measuring the absorbance at 260 nm (A_{260}) in an UltraSpec 31000 PRO

spectrophotometer (Amersham Biosciences), using a quartz cuvette. In addition, the purity was determined by the 260 nm and 280 nm ratio (A_{260}/A_{280}). Following quantification, genomic DNA was stored at -20°C.

2.11.2 PCR amplification of XPC & CKN1 gene fragments from isolated genomic DNA

To reduce the risk of contamination, PCR reaction mixes were prepared in a laboratory separate from PCR product analysis. All subsequent manipulations were performed in a sterile laboratory dedicated to genomic DNA amplification. In addition, all procedures were undertaken in a DNase-free environment, using DNase-free pipette tips and microcentrifuge tubes.

PCR primer sets, used to amplify the *XPC* (Table 2.2) and *CKN1* (Table 2.3) coding regions and sequences flanking the intron-exon boundaries, from isolated XP8CA and CS3BE genomic DNA, respectively, were devised using NCBI sequences, NT_0.22517.17 and NT_006713.14 (respectively). Genomic DNA, isolated from XP-C (XP8CA) and CS-A (CS3BE) dermal fibroblasts, was thawed on ice and diluted to give a final concentration of 5 ng/µl. PCR amplification was performed in a final reaction volume of 25 µl, containing 2.5 µl of GeneAmp® 10X PCR Gold Buffer (containing 150 mM Tris-HCl (pH 8.0), 500 mM KCl and 25 mM $MgCl_2$), 0.5 µl of each forward and reverse primer (25 pmol), 0.1 µl of (5 U/µl) AmpliTaq Gold® polymerase (Applied Biosystems), 0.5 µl of dNTP mix (10 pmol for each dNTP) and 15.9 µl of water. The PCR reaction mix was prepared as a master mix for the appropriate number of samples (X1). The PCR reaction mix was gently mixed and pulsed in a bench-top centrifuge, and 20 µl of reaction mix was aliquoted into Thermo Hybaid 96 well plates for subsequent thermocycling on a GRI MJ Tetrad thermocycler. Finally, 5 µl of XP8CA or CS3BE (5 ng/µl) genomic DNA was added to each individual well and 5 µl of dH_2O was added to a well containing only PCR reaction mix, thus providing a negative control. The Thermo Hybaid 96 well plate was spun in a salad spinner. PCR amplification was performed on a GRI MJ Tetrad

thermocycler. Amplification conditions were 95°C for 12 minutes, followed by 33-35 cycles of 30 seconds each at 94°C, the primer specific annealing temperature (Tables 2.2 & 2.3), and 72°C, ending with a final 10 minute extension step at 72°C. The PCR amplification of *XPC* exon 1 required the inclusion of 4% dimethyl sulphoxide (DMSO).

Table 2.2. Forward and reverse primer sets for *XPC* amplification from genomic DNA isolated from human XP-C (XP8CA) dermal fibroblasts.

Exon	Sequence	Direction	Annealing temp. (°C)	Product size (bp)
1	5′-TGA CTA GGC CTC CAA CGA AG-3′	F	60	
1	5′-TAC GCA GGA GCT TGG ATC G-3′	R	60	453
2	5′-ATA AGC TGC ACT GCC TCC AC-3′	F	62	
2	5′-GAT CCA ATC TTC CAT GGA CC-3′	R	62	371
3	5′-GCT TGA ATG GAA CAC TAG G-3′	F	62	
3	5′-TAG TGA TCT GAC TCC AAA CAG-3′	R	62	257
4	5′-TGA TTC TGT TCA GTA CAG TAG C-3′	F	62	
4	5′-CAA AGT CCT CCT AAG CAG C-3′	R	62	308
5	5′-GAG GAG AAG GAA TTG CCT G-3′	F	62	
5	5′-AGC ACA AGC TCT TTG CAC C-3′	R	62	224
6	5′-CAT GTC TTG ACT TTG GCA GC-3′	F	62	
6	5′-CTG TGG AAG TGA CCT GAA CC-3′	R	62	325
7	5′-CTT GGC TGG AAA TGA AAA TTC C-3′	F	62	
7	5′-GCA CAT GGC TGC CAT TAT C-3′	R	62	257
8	5′-TTC TTA GGA TAA CTA TGT TCT TCC-3′	F	58	
8	5′-ACT CCG TGA ATA CCA GCT C-3′	R	58	232
9.1	5′-CTC TAG CTG GTG ACT TAA CC-3′	F	62	
9.1	5′-CTT GAA GAG CTT GAG GAT GC-3′	R	62	453
9.2	5′-GCT CTG ATT TTG AGC TCT CC-3′	F	62	
9.2	5′-CCT GAC TGT GTC TTG GAG C-3′	R	62	588
10	5′-GTC TAA GGA TCA TCT CCC TC-3′	F	62	
10	5′-TGC TGT CCA GTC AGA TGA GC-3′	R	62	344
11	5′-ACG TTC AAG GCT GTT TGC C-3′	F	62	
11	5′-GCT CAT CAT CAC TTC TCT GC-3′	R	62	344
12/13	5′-TGA GGA ACT GGA TGC CTT TG-3′	F	62	
12/13	5′-TGA AAA TTG GAG CCA CCA GG-3′	R	62	558
14	5′-CAC TGT CTT CCA CAA ACT GG-3′	F	62	
14	5′-TGT ATT CAG TGC TCG CTC C-3′	R	62	333
15	5′-ACTTGGTGTGAAGGAGAGGC-3′	F	62	
15	5′-CCT TTC TGA GCT GCA TCT CC-3′	R	62	291
16	5′-GAA CTT GCT GCC TCT TCA TGG-3′	F	62	
16	5′-TGC CTT CTC AGC AGA GAA GC-3′	R	62	416

Table 2.3. Forward and reverse primer sets for *CKN1* amplification from genomic DNA isolated from human CS-A (CS3BE) dermal fibroblasts.

Exon	Sequence	Direction	Annealing temp. (°C)	Product size (bp)
1	5'-GAC TCT GCT GTT CCA GTC C-3'	F	60	
1	5'-CAA AGC TTA CAG TCA TTG GTC C-3'	R	60	220
2	5'-TAC GTT AGG ATG TGT GGT AG-3'	F	60	
2	5'-ATG CCA GAT TCA AAA ATG CTA C-3'	R	60	500
3	5'-TGA AGT CTG TGT TAT TGA GG-3'	F	60	
3	5'-CAG TCA AGT GAA TGG GTC AA-3'	R	60	363
4	5'-ATG TGA TCT CGG TTT GGC-3'	F	55	
4	5'-GGA TTA AAT TCT CCT TTA TCC TAC-3'	R	55	302
5	5'-TGT TTA AGT TGA ATT GCT AAC AGT C-3'	F	60	
5	5'-TTG TGA TAT TCC TCT GGG-3'	R	60	316
6	5'-TTC TGC ATG GAT ACA GTG AAA ATG-3'	F	60	
6	5'-TGA GTC TCA ACA ACC AGC AC-3'	R	60	302
7	5'-CAC TTT CTT CAG AAT CAG GC-3'	F	60	
7	5'-GGA AGA TTT CTT TTG GTG ACA-3'	R	60	367
8	5'-TAA CGA GAC CTC TGT GTG CCA-3'	F	60	
8	5'-GAA AGT GAT ATA CGA TGA ATG CC-3'	R	60	342
9	5'-GTA ACT CAA GTA GTT GTC CT-3'	F	60	
9	5'-ATC AAG TGT ATG TCA CAG ATC -3'C	R	60	295
10	5'-AGT ATT TCT CCT AGG CTT TGT TGT G-3'	F	60	
10	5'-ACA TAT AAC TGG TCT GGC AAG C-3'	R	60	334
11	5'-ATT GGC CTA GTT TCT TTA GGG AG-3'	F	60	
11	5'-TAA GCT TTA GAA GTC ACT GTA CC-3'	R	60	299
12	5'-TTT TCT TCC AAA ATA ATG TAA TTG CT-3'	F	60	
12	5'-CTG TAT GGT CTA TTC CTG AC-3'	R	60	235

2.11.3 Exonuclease I, Shrimp Alkaline Phosphatase (EXOSAP) treatment: post PCR reaction purification protocol

Exonuclease I (New England Biolabs, Ipswich, MA, USA) and Shrimp alkaline phosphatase (Amersham Pharmacia Biotech, Sweden) were utilised following PCR amplification, to remove single stranded DNA, such as excess oligonucleotides, and unincorporated dNTPs in preparation for Sanger dideoxy sequencing. Exonuclease I and Shrimp Alkaline Phosphatase were thawed on ice. Following PCR, 0.5 µl of Exonucelase and 1 µl of Shrimp alkaline phosphatase was added to 5 µl of the amplification product. The samples were incubated at 37°C for 15 minutes and immediately incubated at 85°C for 15 minutes in the GRI MJ Tetrad Thermocycler.

2.11.4 Screening XPC and CKN1 for genomic DNA variants by fluorescent, Sanger dideoxy sequencing

PCR amplification products were prepared for sequencing using the ABI PRISM® BigDye® Terminator v3.1 Cycle Sequencing Reaction Ready Kit (Applied Biosystems), and sequencing was performed in both forward and reverse directions, using the *XPC*- and *CKN1*-specific primers (Tables 2.2 & 2.3). Briefly, sequencing was performed in a final reaction volume of 10 µl, containing 1.5 µl of 5X sequencing buffer, 0.75 µl of ABI PRISM® BigDye® Terminator Mix (Applied Biosystems) and 5.75 µl of water. 1 µl of the *XPC* or *CKN1* forward or reverse primer, and 1 µl of the PCR product was added to a fresh Thermo Hybaid 96 well plate. A master mix was prepared and 8 µl of the reaction mix was aliquoted into allocated wells in the Thermo Hybaid 96 well plate, containing both the primer and PCR product. The Thermo Hybaid 96 well plate was sealed and placed on the GRI MJ Tetrad Thermocycler. Sequencing conditions were 25 cycles of 10 seconds at 96°C, 5 seconds at 50°C and 4 minutes at 60°C.

2.11.5 Millipore Montáge sequence reaction cleanup

The Montáge SEQ_{96} Sequencing Reaction Cleanup Kit (Millipore) facilitated the elimination of contaminating salts and excess unincorporated dye terminators (generated during the preparation of the DNA sequencing reactions) through a vacuum-based size exclusion separation platform. The Montage Seq_{96} Sequence Reaction was undertaken by adding 20 µl of injection solution to each 10 µl sequence reaction, using a multi-well pipette. The 30 µl of mix was transferred to the relevant wells of a Montage plate, avoiding direct contact between the pipette tip and the membrane. The plate was placed onto the Millipore vacuum manifold and the vacuum was adjusted to 17"Hg. The vacuum was allowed to run for approximately 3 minutes, or until all of the liquid had been drawn through the plate. Once the wells of the plate had dried, the vacuum was disconnected and the plate was removed from the manifold. The plate was placed onto the manifold and 25 µl of injection solution was added to the relevant wells. The vacuum was reconnected for a further 3 minutes at 17"Hg. Once the relevant wells had dried, the vacuum was disconnected, and the plate was removed from the manifold. A further 25 µl of injection fluid was added to the relevant wells and the lid was placed on the plate. The plated was subsequently placed into the plate holder of the Vortex Genie and was vortexed on setting 3 for 10 minutes. The samples were prepared for analysis on the ABI PRISM 3100 Genetic Analyser by removing the plate from the shaker. Approximately 10 µl of the solution from each sample was transferred to a fresh 96 well ABgene, semi-skirted plate.

2.11.6 Sequence analysis

For each sequence reaction, a minimum of 10 µl of the purified sequence product, present in the relevant wells of an ABgene, semi-skirted plate (AB-0999) from the Montáge Sequence Reaction Clean up, was required for subsequent sequence analysis, using the automated ABI PRISM 3100 Genetic Analyser. The ABI PRISM 3100 Genetic Analyser parameters for RunModule 1 RapidSeq36_Pop6DefaultModule used for sequence analysis were as followed:

Temperature – 55.0°C

Current – 100 uAmps

Voltage – 1 Kvolt

Injection time – 22 seconds

Run time – 2400 seconds

Following data acquisition, *XPC* and *CKN1* gene variants were identified by direct comparison with consensus cDNA sequences obtained from NCBI, using Sequencher™ Version 4.5 software (Gene Codes Corp.).

2.12 Analysis of CS3BE CKN1 mRNA

Total RNA was extracted using TRIzol reagent (Invitrogen™) and reverse transcribed with SuperScript II (Invitrogen™) in accordance to the manufacturers recommendations (as described below). PCR amplification of CS3BE cDNA was performed in a final reaction volume of 50 µl, containing 5 µl of (10X) *Taq* DNA polymerase magnesium free reaction buffer (Promega; containing 100 mM Tris-HCl (pH 9), 500 mM KCl and 1% Triton® X-100), 3 µl of 25 mM $MgCl_2$, 1 µl of each *CKN1*-specific forward 5'-GGT TTT TGT CCG CAC GCC AA-3' and reverse 5'-GTG GAG ACC AGG AAA CTG CT-3' primers (25 pmol; MWG), 0.5 µl of (5 U/µl) *Taq* DNA polymerase (Promega), 1 µl of dNTP mix (10 mM/dNTP) and 34.5 µl of water. The PCR reaction was prepared as a master mix for the appropriate number of samples (X1). The PCR reaction mix was gently mixed and pulsed in a bench top centrifuge, and 49 µl of reaction mix was aliquoted into thin-walled PCR tubes. Finally, 1 µl of CS3BE or MRC-5 (control) *CKN1* cDNA was pipetted into the PCR tubes, containing the reaction mix. In addition, 1 µl of H_2O was added to a PCR tube containing only PCR reaction mix, thus providing a negative control. PCR amplification was performed on a GRI MJ Tetrad thermocycler. Amplification conditions were 94°C for 3 minutes, followed by 29 cycles of 1 minute each at 94°C, 63°C and 72°C, ending with a final 10 minute extension step at 72°C. Following PCR amplification, 10 µl of each reaction was electrophorised for approximately 2

hours at 120 V in TBE buffer (as previously described). The expected size of the *CKN1* cDNA amplification product was 567 bp.

2.12.1 TA cloning

Following PCR amplification of CS3BE and MRC-5 (control) *CKN1* cDNA, 10 µl ligation reactions were prepared on ice, containing 5 µl sterile water, 1 µl of 10X ligation buffer (60 mM Tris-HCl (pH 7.5), 60 mM $MgCl_2$, 50 mM NaCl, 1 mg/ml BSA, 70 mM β-mercaptoethanol, 1 mM ATP, 20 mM DTT and 10 mM spermidine; Invitrogen™), 2 µl of 25ng/µl pCR®2.1 vector (Invitrogen™; Fig. 2.3), 1 µl of fresh PCR product (~10 ng) and 1 µl of T4 DNA ligase (4.0 Weiss units/µl; Invitrogen™). A self-ligation control reaction was further prepared, omitting the 1 µl of fresh PCR product. The ligation reaction was incubated overnight (16-18 hours) at 14°C in a PTC-200 Peltier MJ Tetrad Thermocycler (GRI). The overnight ligation reactions were briefly centrifuged and placed on ice. For One Shot® chemical transformation, a 50 µl vial of frozen INVαF' *Escherichia coli* One Shot® Competent cells/transformation was thawed on ice, and 2 µl of each ligation reaction was pipetted directly into the vial of competent cells. Gentle stirring with the pipette tip facilitated complete mixing of the ligation reaction and competent cells. The vials were incubated on ice for 30 minutes, and heat shock was performed for 30 seconds at 42°C in a prewarmed water bath. The vials were immediately transferred to ice, and 250 µl of room temperature super optimal catabolite (SOC) medium (containing 2% tryptone, 0.5% yeast extract, 10 mM NaCl, 2.5 mM KCl, 10 mM $MgCl_2$, 10 mM $MgSO_4$ and 20 mM glucose) provided in the TA Cloning® Kit (Invitrogen™), was added to each vial. The vials were shaken horizontally at 37°C for 1 hour at 225 rpm in an Orbital shaking incubator. After transformation, 50 µl and 200 µl from each transformation vial (including the self-ligation control) was spread onto LB agar plates and incubated overnight at 37°C. The LB agar plates (containing 100 µg/ml ampicillin) were previously prepared by spreading each plate with 40 µl of (40 mg/ml) 5-bromo-4-chloro-3-indolyl-β-D-galactopyranoside (X-Gal) and allowed to equilibrate at 37°C for 30 minutes, prior to overnight incubation.

After overnight incubation, the plates were stored at 4°C for 3 hours to facilitate complete colour development. For plasmid isolation, 60 white colonies theoretically harbouring the PCR amplified *CKN1* cDNA were selected from CS3BE, using a sterile pipette tip, and transferred to a 5 ml culture tube, containing 3 ml of LB (containing 100 μg/ml ampicillin). Additionally, ten white clones were selected from the wild-type MRC-5 control sample. The isolated colonies were expanded by incubating at 37°C overnight at 225 rpm in a shaking incubator.

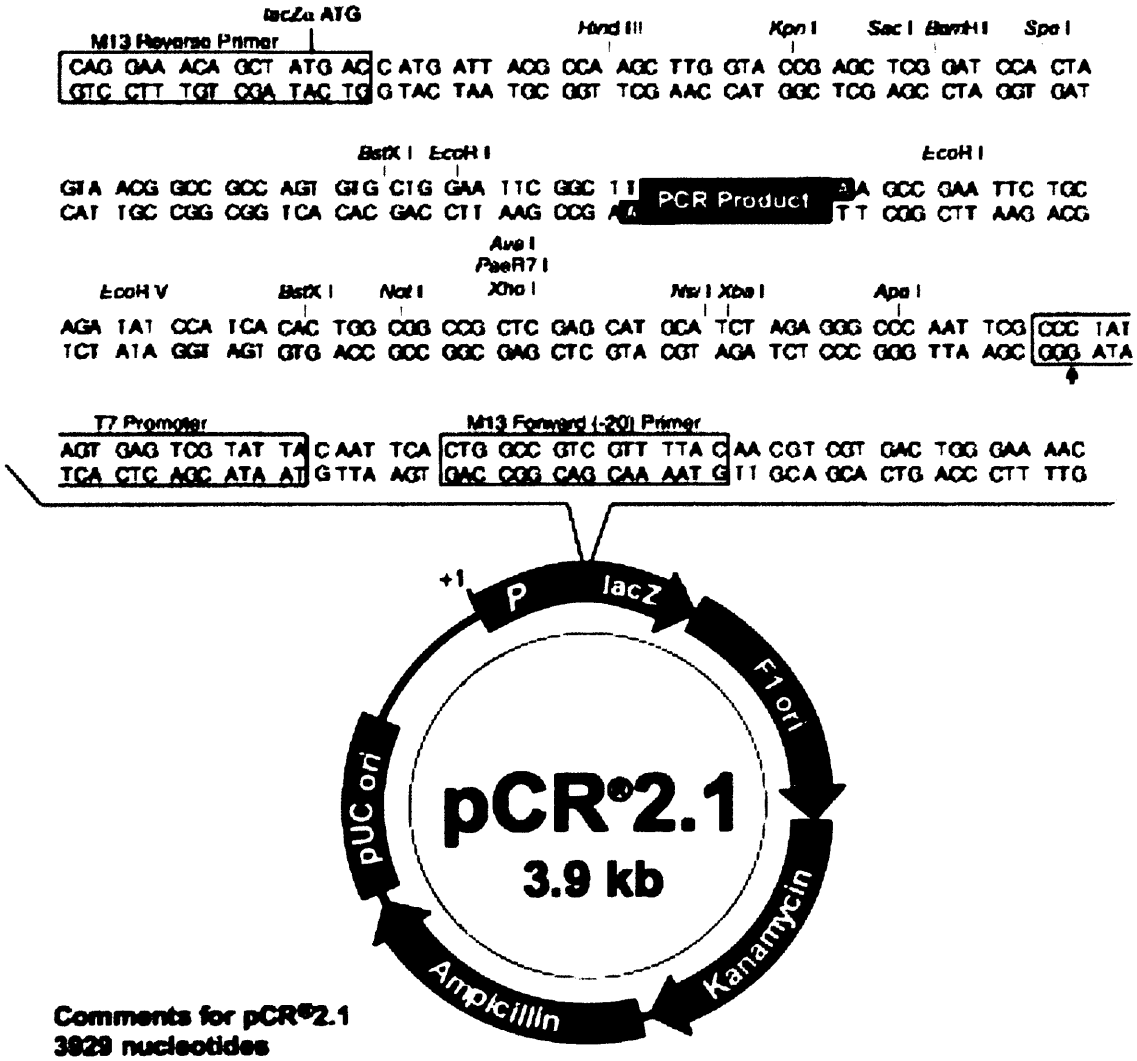

Comments for pCR®2.1
3929 nucleotides

***LacZα* gene: bases 1-545**
M13 Reverse priming site: bases 205-221
T7 promoter: bases 362-381
M13 (-20) Forward priming site: bases 389-404
f1 origin: bases 546-983
Kanamycin resistance ORF: bases 1317-2111
Ampicillin resistance ORF: bases 2129-2989
pUC origin: bases 3134-3807

Figure 2.3. Schematic of the linearised TA cloning vector, pCR®2.1. The arrow indicates the start of transcription for the T7 RNA polymerase (taken from the TA Cloning® Kit Version V Manual, Invitrogen™).

2.12.2 Plasmid isolation

The isolation and purification of the pCR®2.1 plasmid, harbouring the amplified *CKN1* cDNA PCR product, was undertaken using the QIAprep Spin Miniprep Kit protocol (as previously described in Section 2.4.4). To confirm the ligation of the *CKN1* cDNA product into pCR®2.1 and subsequent transformation into INVαF' *E.coli* One Shot cells, an EcoRI digest was performed in a final reaction volume of 20 µl, containing 2 µl of 10X buffer H, 1 µl of EcoRI, 2 µl of pCR®2.1 plasmid DNA (harbouring the amplified *CKN1* cDNA) and 15 µl of water. The EcoRI digests were incubated for 1 hour at 37°C. Following digestion, 10 µl of each digest was electrophoresed on a 0.7% agarose gel. The expected size of the *CKN1* cDNA insert was 582 bp.

2.12.3 Sequencing

To further analyse isolated clones, harbouring the *CKN1* cDNA amplified PCR product, 10 µl sequencing reactions were prepared, containing 1 µl of plasmid DNA, 1 µl of (3.3 pmol/µl) M13 forward (-20) (5'd[GTA AAA CGA CGG CCA G]-3') or M13 reverse (5'd[-CAG GAA ACA GCT ATG AC]-3') sequencing primers (both purchased from Invitrogen™), 4 µl of ABI PRISM BigDye® Terminator v3.1 Cycle Sequencing Reaction Ready Kit and 4 µl of sterile water. Thermocycling was performed on a GRI MJ Tetrad Thermocycler. Standard amplification conditions were used to sequence *CKN1* cDNA: 24 cycles of 96°C for 30 seconds, 50°C for 15 seconds and 60°C for 4 minutes. Following amplification, 10 µl of sterile water was added to each reaction to give a final volume of 20 µl and the DyeEx™ Spin Kit was used to purify sequencing reactions (as previously described in Sections 2.4.5-6). Sequencing reactions were sent to the in-house CBS sequencing facility, where sequence analysis was performed, using the automated ABI PRISM 3100 Genetic Analyser. Data was received as text files and electropherograms.

2.13.0 Transcription expression profiling using the Affymetrix™ GeneChip® array platform

2.13.1 Sample preparation for Affymetrix™ GeneChip® analysis

Exponentially growing hTERT-immortalised XP-C (GM02996, XP8CA) and CS-A (GM01856, CS3BE) dermal fibroblasts were seeded in three 60 mm culture dishes/time point (hours) at a density of 5 X 10^5 cells/60 mm dish. The cells were allowed to equilibrate overnight (16-18 hours) at 37°C in a humidified incubator containing 5% CO_2. UV-C (254 nm) irradiation was performed on 80-90% confluent cultures. A UVP germicidal lamp, emitting UV-C light (254 nm), was calibrated using a UVX digital radiometer to emit an incident fluence rate of 1 J/m^2/s (as previously described in Section 2.6). For UV treatment, cells were washed twice with 2 ml of warm (37°C) Hank's balanced salt solution and irradiated with 10 J/m^2. After irradiation, the cells were refed with fresh pre-warmed (37°C) EMEM medium and maintained at 37°C in a humidified incubator containing 5% CO_2 for the indicated period of time. Three independent biological replicates of UV-treated fibroblasts were performed at the indicated time points for the hTERT-immortalised XP-C (XP8CA) and CS-A (CS3BE) dermal fibroblasts. Samples were processed for subsequent Affymetrix™ GeneChip probe array analysis, utilising the Affymetrix™ platform (as described below in Section 2.13.2).

2.13.2 Total RNA isolation and purification

All procedures involved in total RNA extraction were undertaken in an RNase-free environment, using RNase-free, DNase-free pipette tips (Fisher) and microcentrifuge tubes. All solutions used for RNA isolation and purification was prepared using purchased sterile RNase-free water (Fresenius Kabi Inc., France), and all manipulations were performed in a laboratory dedicated for total RNA

isolation and purification. All surfaces were treated with RNaseZap® (Ambion®) to reduce RNase contamination.

Total RNA was isolated from fibroblasts using the TRIzol® reagent (Invitrogen™) in accordance to the manufacturers recommendations. Following incubation at the indicated time points after UV treatment or mock-irradiation (as previously described in Section 2.13.1), 1.5 ml of ice-cold TRIzol® reagent was added to each 60 mm culture dish. After 15 minutes incubation at room temperature, the cells were scraped off the 60 mm culture dishes, using a Nunc Cell Scraper (Nalge Nunc, Intl.). The cell lysates were pipetted and aspirated several times to ensure complete homogenisation. The cell lysate was divided into two 750 µl fractions, and transferred to 1.5 ml RNase-free centrifuge tubes and 175 µl of chloroform (Sigma®) was added to each sample fraction. The chloroform and TRIzol® were mixed thoroughly by repeated inversion. The chloroform/TRIzol® mix was transferred to a Heavy Phase Lock Gel™ (PLG; Eppendorf), which had been previously centrifuged in a microcentrifuge at 13,400 g for 25 seconds at room temperature in a bench top Sorvall® Pico centrifuge. The heavy PLG, containing the chloroform/TRIzol® mix, was subsequently centrifuged in a microcentrifuge at 13,400 g for 2 minutes at room temperature in a bench top Sorvall® Pico centrifuge. The upper colourless aqueous layer was transferred to a fresh 1.5 ml RNase-free Eppendorf tube. Total RNA was recovered from the aqueous phase by precipitating with 500 µl of isopropanol and 1 µl of 5 mg/ml glycogen (Ambion®), followed by incubation at room temperature for 10 minutes. Total RNA was precipitated by centrifugation at 12,000 g for 10 minutes at 4°C in a refrigerated ROTINA 35R centrifuge (Hettich Zentrifugen). The supernatant was aspirated and the pellet was washed with 500 µl of 75% ethanol (EtOH). The tubes were centrifuged at 7,500 g for 5 minutes at 4°C in a refrigerated ROTINA 35R centrifuge, and the supernatant was discarded. The RNA pellets were briefly air-dryed for 10 minutes and resuspended in 50 µl of RNase-free water. The RNA pellet was heated at 65°C for 10 minutes, using a Techne DRI-Block® DB-2D (JENCONS-PCS). Following resuspension, the RNA was rehydrated on ice for 1 hour. Fractions of the same sample were recombined to give a total volume of 100 µl. Total RNA

(1 µl) was assessed for purity by A_{260}/A_{280} (1.9-2) and quantified using the NanoDrop® ND-1000 spectrophotometer (NanoDrop Technologies, USA). For overnight EtOH precipitation, a $1/10^{th}$ volume (10µl) of 3M sodium acetate, 2.5 volumes (250 µl) of 100% EtOH and 1 µl of glycogen was added to the RNA. The tubes were mixed thoroughly by repeated inversion, and precipitated at -20°C overnight. Following overnight precipitation, the samples were centrifuged at 12,000 g for 20 minutes at 4°C in a ROTINA 35R centrifuge. The supernatant was aspirated and the pellet was washed twice with 500 µl of 80% EtOH. The samples were centrifuged at 12,000 g for 10 minutes at 4°C between each 80% EtOH wash. The supernatant was removed and the pellet was air-dried for 10 minutes at room temperature and resuspended in the required volume of RNase-free water to give a final RNA concentration of ~2 µg/µl. The RNA pellet was redissolved by placing the centrifuge tube on a Techne DRI-Block® DB-2D at 65°C for 10 minutes. Rehydration of the RNA was undertaken by incubating the centrifuge tubes on ice for 30 minutes. Following incubation on ice, RNA isolated from the three 60 mm dishes/time point were pooled and 1 µl of each total RNA sample was diluted in 1 µl of RNase-free water. To ascertain the final concentration of total RNA, following overnight precipitation, a 1 µl aliquot of the diluted sample was used for quantification using a NanoDrop® ND-1000 spectrophotometer (as above). The final 1 µl fraction was used to assess the integrity of the post EtOH total RNA by capillary electrophoresis, using the Agilent 2100 Bioanalyzer. Total RNA was subjected to subsequent labelling and hybridisation only if the 18S/28S ratio was approximately 2.

2.13.3 Reverse transcription (RT) by cDNA synthesis

An appropriate volume of total RNA, to give 10 µg RNA, was added to RNase-free water (if required) in a 0.5 ml RNase-free microcentrifuge tube, to make up to the maximum allowable volume of 9 µl for a cDNA synthesis reaction, containing 10 µg total RNA. First strand cDNA synthesis was undertaken by adding 2 µl of the (50 mM) chimeric T7-Oligo(dT) promoter primer, 5'-GGC CAG TGA ATT GTA ATA CGA CTC ACT ATA GGG AGG CGG-$(dT)_{24}$-3'

(Affymetrix™, Inc.), to the 10 μg of total RNA, which was subsequently incubated at 70°C in an PTC-200 Peltier MJ Tetrad thermocycler (GRI) for 10 minutes. Following hybridisation of the T7-Oligo(dT) promoter primer, the samples were incubated on ice for 2 minutes and pulsed down in a bench top Sorvall® Pico microcentrifuge. A master mix, containing 4 μl of 5X first strand synthesis buffer (250 mM Tris-HCl (pH8.3), 375 mM KCl, 15 mM $MgCl_2$; Invitrogen™), 2 μl of 0.1 M DTT (Invitrogen™) and 1 μl of 10 mM 2'-deoxynucleoside 5'-triphosphate (dNTP) mix (Invitrogen™, Life Technologies) per reaction (X1) was prepared, and 7 μl of the master mix was added to each sample on ice. The samples were incubated at 42°C for 2 minutes, using an MJ Tetrad Thermocycler. Following the 2 minute incubation, the samples were retained in the MJ Tetrad thermocycler, and 2 μl of SuperScript II reverse transcriptase (Invitrogen™) was added to each reaction. The samples were incubated in the GRI MJ Tetrad Thermocycler for 1 hour at 42°C. First strand synthesis reactions were placed on ice and pulsed down. For second strand synthesis, a master mix containing 91 μl RNase-free water, 30 μl 5X second strand synthesis buffer (100 mM Tris-HCl (pH 6.9), 23 mM $MgCl_2$, 450 mM KCl, 0.75 mM β-NAD^+, 50 mM $(NH_4)_2SO_4$; Invitrogen™), 3 μl 10 mM dNTP mix (Invitrogen™), 1 μl of 10 U/μl *E.coli* DNA ligase (Invitrogen™), 4 μl of 10 U/μl *E.coli* DNA polymerase I (Invitrogen™) and 1 μl of 2 U/μl *E.coli* RNase H (Invitrogen™) per reaction was prepared, and 130 μl of the master mix was added to each reaction on ice. The samples were incubated for 2 hours at 16°C, using an MJ Tetrad thermocycler. Following the 2 hour incubation, 2 μl of 5 U/μl *E.coli* T4 DNA polymerase (Invitrogen™) was added to the reactions and incubated in the MJ Tetrad thermocycler at 16°C for a further 5 minutes. The reaction was terminated by the addition of 10 μl of 0.5 M EDTA (Sigma®). The cDNA was purified by adding 162 μl phenol:chloroform:IAA (Invitrogen™) to the cDNA. The sample was mixed thoroughly by vortexing, using a Vortex Gene® 2 (Jencons-PLS) and was transferred to a fresh pre-spun light PLG (Eppendorf), which had been previously spun at 13,400 g for 25 seconds in a bench top Sorvall® Pico microcentrifuge. The light PLG, containing the cDNA and phenol:chloroform:IAA, was centrifuged at 13,400 g for 2 minutes at room

temperature in a bench top Sorvall® Pico microcentrifuge. The upper resultant aqueous layer, containing the cDNA, was transferred to a fresh RNase-free 1.5 ml centrifuge tube. To precipitate the cDNA, 0.5 volumes (80 µl) of 7.5 M NH_4 acetate (Sigma®), 2.5 volumes (400 µl) of 100% EtOH, and 1 µl of (5 mg/ml) glycogen was added. The samples were precipitated at -20°C overnight. Following precipitation, the samples were centrifuged at 12,000 g for 20 minutes at 4°C. The supernatant was aspirated, and the pellet was washed twice with 500 µl of 80% EtOH. The sample was centrifuged at 12,000 g for 5 minutes at 4 °C between each wash. The supernatant was discarded and the pellet was air-dried for 10 minutes at room temperature. The cDNA pellet was resuspended in 10 µl of RNase-free water and heated to 65°C for 5 minutes, using a Techne DRI-Block® DB-2D. The cDNA was incubated on ice for 1 hour to rehydrate. The samples were stored at -20°C.

2.13.4 cRNA synthesis by in vitro transcription (IVT)

Biotin-labelled cRNA was prepared by *in vitro* transcription from a bacteriophage T7 RNA polymerase promoter by T7 RNA polymerase and biotin-labelled nucleotides, using the ENZO BioArray™ High Yield™ RNA Transcript Labelling Kit (Enzo Lifesciences, Farmingdale, NY, USA). Synthesised cDNA and the first three components of the ENZO BioArray™ High Yield™ RNA Transcript Labelling Kit were allowed to equilibrate to room temperature. These components included: 10X hybridisation buffer, 10X biotin-labelled ribonucleotides and 10X DTT. The 10X RNase inhibitor mix and 20X T7 RNA polymerase were left on ice. Once the cDNA and the reagents from the ENZO BioArray™ High Yield™ RNA Transcript Labelling Kit had equilibrated to room temperature, a master mix was prepared containing 12 µl RNase-free water (to give a final volume of 40 µl), 4 µl of 10X hybridisation buffer, 4 µl 10X biotin-labelled ribonucleotides, 4 µl of 10X DTT, 4 µl of 10X RNase inhibitor mix and 2 µl of T7 RNA polymerase per sample. 30 µl of the pre-prepared IVT master mix was added to 10 µl of cDNA, previously prepared by reverse transcription (Section 2.13.3). The samples were incubated at 37°C in a

Thermomixer Comfort mixer (Eppendorf) for 6 hours. The mixer was programmed to agitate the samples every 30 minutes for 30 seconds. Following the 6 hour incubation, the IVT reactions were made up to 50 µl by adding 10 µl of RNase-free water, and left on ice. A BD Chroma Spin™ Column (BD Biosciences Clontech) was prepared per reaction, by inverting the column several times to ensure complete resuspension of the gel matrix. The end of the column was snapped off and the lid was removed. The column was placed in a 2 ml collection tube (provided in the BD Chroma Spin™ Column kit) and centrifuged at 700 g for 5 minutes at 4°C in a refrigerated ROTINA 35R centrifuge. The 2 ml collection tube was discarded and the Chroma Spin column was placed in a fresh 2 ml collection tube. The IVT reaction (50 µl) was applied to the centre of the Chroma Spin column gel bed, while avoiding direct contact between the pipette tip and the gel bed. The Chroma Spin column was centrifuged at 700 g for 5 minutes at 4°C in a refrigerated ROTINA 35R centrifuge. Following centrifugation, 50 µl of RNase-free water was pipetted into the centre of the column gel bed. The Chroma Spin column was centrifuged at 700 g for a further 5 minutes at 4°C in a refrigerated ROTINA 35R centrifuge. The cRNA (100 µl) was transferred from the 2 ml collection tube to a fresh 1.5 ml RNase-free centrifuge tube. The cRNA was precipitated by adding 50 µl (0.5 volumes) of RNase-free 7.5 M ammonium acetate (Sigma®), 250 µl (2.5 volumes) of 100% EtOH and 1 µl of 5 mg/ml glycogen. The samples were mixed thoroughly by repeated inversion, and the samples were precipitated overnight at -20°C. Following overnight precipitation, the samples were centrifuged at 20,000 g for 30 minutes at 4°C in a refrigerated ROTINA 35R centrifuge. The cRNA pellet was washed twice with 80% EtOH, and centrifuged at 12,000 g for 10 minutes at 4°C in a refrigerated ROTINA 35R centrifuge, following each EtOH wash. The EtOH was aspirated and the pellet was air-dried at room temperature for 10 minutes, and resuspended in 34 µl of RNase-free water. The samples were incubated at 65°C for 5 minutes on a Techne DRI-Block® DB-2D, and left on ice for 1 hour to rehydrate. 1 µl of the resuspended cRNA was quantified, using the NanoDrop® ND-1000 spectrophotometer. The integrity of the cRNA was assessed by capillary electrophoresis, using the Agilent 2100 Bioanalyzer.

2.13.5 Calculated adjusted cRNA yield and cRNA fragmentation

Prior to cRNA fragmentation, the adjusted cRNA yield was calculated by subtracting the quantity of cRNA measured subsequent to the IVT reaction (in μg) from the amount of total RNA used in the cDNA synthesis reaction, and multiplied by the fraction of the synthesised cDNA used in the IVT reaction. The adjusted cRNA yield was calculated to take into account the presence of residual total RNA. To reduce the frequency of secondary structure formation, the cRNA samples were fragmented, thus enabling the production of cRNA fragments between 50-200 bases in length. cRNA fragmentation was undertaken in a 0.5 ml RNase-free microcentrifuge tube, by adding the appropriate volume (in μl) of cRNA to give a total of 15 μg of cRNA and 8 μl of 5 X fragmentation buffer, containing 40 mM Tris-acetate (pH 8.1), 100 mM potassium-acetate and 30 mM magnesium-acetate. The reaction was made up to a final volume of 40 μl with RNase-free water. The samples were incubated at 94°C for 35 minutes and placed on ice. After cRNA fragmentation, a 1 μl aliquot of the cRNA sample was applied to the Agilent 2100 Bioanalyzer (Agilent). The fragmented cRNA was stored at -80°C.

Following sample preparation (Sections 2.13.1-2.13.6), all subsequent procedures performed using the Affymetrix™ GeneChip® platform was undertaken by our in-house CBS facility (Sections 2.13.6).

2.13.6 Microarray hybridisation, staining, washing and scanning of HG-U133A probe arrays

All solutions and buffers used in the following procedures were prepared in a DNase- and RNase-free environment, using molecular biology grade water.

Hybridisation to and scanning of the Affymetrix™ HG-U133A oligonuclotide arrays was performed by our core in-house microarray facility provided by the CBS, and was undertaken in accordance to the manufacturers guidelines (http://www.affymetrix.com/support/technical/manual/expression_manual.affx).

The hybridisation cocktail was prepared for each reaction (in accordance to the recommendations for a 49 format array) by adding 15 μg (0.5 μg/μl) of fragmented cRNA to 5 μl of (3 nM) control oligonucleotide B2 (50 pM), 15 μl of 20X eukaryotic hybridisation control BioB (1.5 pM, equating to three transcripts per cell), BioC, BioD and CreX (5, 25 and 100 pM, respectively; Affymetrix™ GeneChip® Eukaryotic Hybridisation Control Kit), 3 μl of (10 mg/ml) Herring sperm DNA (0.1 mg/ml; Promega, Cor.), 3 μl of (50 mg/ml) acetylated BSA (0.5 mg/ml; Invitrogen™), 150 μl of 2X hybridisation buffer (at a final concentration of 100 mM MES (2[N-Morpholino] ethanesulfonic acid), 1 M [Na^+], 20 mM EDTA and 0.01% Tween 20). The hybridisation cocktail was preheated to 99°C for 5 minutes in a heat block, then transferred to a 45°C heat block for a further 5 minutes. Meanwhile, the Affymetrix™ GeneChip® Human HG-U133A probe arrays (Affymetrix™) were equilibrated to room temperature and 200 μl of 1X hybridisation buffer was pipetted through the septa of the array, using a micropipettor. The probe array was then incubated at 45°C for 10 minutes with rotation at 60 rpm. The hybridisation cocktail was centrifuged at 13,400 g for 5 minutes in a Sorvall® Pico microcentrifuge to remove insoluble matter from the hybridisation mixture. The buffer solution was removed from the probe array cartridge and was filled with 200 μl of hybridisation cocktail. The probe arrays were transferred to a preheated Affymetrix™ GeneChip® hybridisation oven 640 and hybridised at 45°C for 16 hours with rotation at 60 rpm. After hybridisation,

HG-U133A arrays were prepared for scanning using the Affymetrix™ wash protocols on an Affymetrix™ Fluidics Station FS 450 under the control of Affymetrix™ GeneChip Operation software. Briefly, an initial wash of 10 cycles of 2 mixes was performed with the non-stringent wash buffer A (containing 6X SSPE and 0.01% Tween 20) at 25°C. This was followed by 4 cycles of 15 mixes with the stringent wash buffer B (containing 100 mM MES, 0.1 M [Na^+] and 0.01% Tween 20) at 50°C. The probe array was incubated for 10 minutes with Streptavidin Phycoerythrin (SAPE) solution (containing 1X MES stain buffer, 2 mg/ml acetylated BSA and 10 μg/ml SAPE) at 25°C. A post stain wash of the arrays was undertaken for 10 cycles of 4 mixes with the non-stringent wash buffer A at 25°C. The probe array was incubated for 10 minutes in antibody solution (containing 1X MES stain buffer, 2 mg/ml acetylated BSA, 0.1 mg/ml Normal Goat IgG and 3 μg/ml biotinylated antibody) at 25°C. A final incubation of the probe array was performed for 10 minutes in SAPE solution at 25°C (as above). This was followed by a final wash for 15 cycles of 4 mixes with wash buffer A at 30°C. The HG-U133A arrays were scanned using an Affymetrix™ GeneChip® Scanner 3000 System. Image scanning and data pre-processing to obtain transcript measurements were performed using Affymetrix™ MAS 5.0.

2.14 Validation of UVC inducible genes by real-time quantitative reverse transcriptase polymerase chain reaction (qRT-PCR)

The TaqMan® real-time qRT-PCR system exploits fluorogenic-labelled probes that utilise the 5' nuclease activity of *Taq* DNA polymerase to detect and quantify a specific PCR amplification product, as it accumulates throughout the PCR reaction. A gene-specific oligonucleotide probe is constructed, which possesses a reporter fluorescent dye on the 5' end and a quencher dye on the 3' end. The proximity of the quencher dye reduces the fluorescence emitted by the reporter dye by fluorescence resonance energy transfer (FRET). However, in the presence of the target sequence, the probe anneals downstream from one of the

primer sites and is cleaved by the 5' nuclease activity of *Taq* DNA polymerase as the primer extends. The cleavage of the probe separates the reporter dye from the quencher dye, which increases the reporter dye signal. Therefore, the increase in fluorescence intensity is proportional to the amount of amplicon generated during the PCR reaction.

Real-time qRT-PCR analysis was undertaken, using the TaqMan® 7000 detection system, to independently validate differentially regulated gene candidates at the transcriptome level, identified following transcription expression profiling, using the Affymetrix™ GeneChip® system.

2.14.1 Sample preparation

Exponentially growing hTERT-immortalised XP-C (GM02996, XP8CA) and CS-A (GM01856, CS3BE) dermal fibroblasts were seeded in three 60 mm culture dishes/time point (hours) at a density of 5 X 10^5 cells/60 mm dish (as previously described in Section 2.13.1). In addition, exponentially growing hTERT-immortalised MRC-5 fibroblasts were also seeded (as described) for the subsequent construction of a standard curve for relative quantification. For real-time qRT-PCR experiments, fibroblasts were subjected to the identical UV treatment (10 J/m^2) and incubated for the indicated periods of time as in the Affymetrix™ microarray experiments (previously described in Sections 2.6 and 2.13.1). In addition, time-matched mock-irradiated controls were performed in parallel. The time matched non-irradiated controls were processed in an identical manner to the experimental cultures, and maintained under routine culture conditions for 0, 6, 12 or 24 hours. However, mock-irradiated cultures were not exposed to UVC radiation. Three independent biological replicates of UV-treated and time-matched, mock-irradiated fibroblasts were performed at the indicated time points for each cell line and processed for subsequent real-time qRT-PCR (Section 4.14.2), utilising the ABI Prism 7000 Detection System (PE Applied Biosystems).

2.14.2 Total RNA isolation and first-strand cDNA synthesis for qRT-PCR

Total RNA was isolated at the indicated time points using TRIzol® reagent according to the manufacturers recommendations (and as previously described in Section 2.13.2). RNA isolated from three 60 mm dishes/time point was pooled and first-strand cDNA synthesis was performed using SuperScript II (Invitrogen™). Briefly, 5 μg of total RNA, isolated from the irradiated or mock-irradiated samples, was reverse transcribed by adding 1 μl of (500 μg/μl) Oligo(dT) primer (Invitrogen™) and 1 μl of 10 mM dNTP mix to the 5 μg of RNA in a 0.5 ml nuclease-free microcentrifuge tube. The sample was made up to 13 μl with sterile water. The reaction mixture was heated to 65°C for 5 minutes, using a GRI MJ Tetrad Thermocycler. The samples were placed on ice for 2 minutes and the contents was collected by brief centrifugation. After centrifugation, 4 μl of 5X first-strand buffer and 2 μl of 0.1 M DTT was added. The contents was gently mixed and incubated at 42°C for 2 minutes in a GRI MJ Tetrad Thermocycler. 1 μl of (200 U) SuperScript II was added to the reaction and mixed by pipetting gently up and down. The reactions were incubated at 42°C for 50 minutes in a GRI MJ Tetrad Thermocycler. The reaction was inactivated by heating at 70°C for 15 minutes in a GRI MJ Tetrad Thermocycler. The resulting XP-C and CS-A cDNA was diluted 1 in 25 by adding 480 μl of sterile water. cDNA generated from the irradiated and mock-irradiated hTERT-immortalised MRC-5 fibroblasts (at the indicated time points) was pooled, thus providing a stock of cDNA standard, which was used to construct a standard curve for relative quantification.

2.14.3 qRT-PCR assay using the ABI PRISM® 7000 Sequence Detector

For real-time qRT-PCR, 5 μl of the diluted first-strand cDNA product, generated by reverse transcription, was used as the template. Each cDNA was amplified in triplicate using gene-specific primers (Table 2.4) and the TaqMan® Universal

PCR Master Mix (2X) No AmpErase® UNG (PE Applied Biosystems), according to the manufacturer's recommendations. Briefly, 5 μl of the cDNA sample was pipetted into the appropriate well of a MicroAmp™ Optical 96-Well Reaction Plate (PE Applied Biosystems). Amplification was performed in a final reaction volume of 20 μl containing 10 μl of (2X) TaqMan® Universal PCR Reaction Mix, 1 μl of Assay on Demand (Table 2.4; PE Applied Biosystems), and 4 μl of sterile water. A master mix was prepared and 15 μl was pipetted down the wall of the appropriate well of the MicroAmp™ Optical 96-well reaction plate, containing the 5 μl of cDNA, using a Finnpipette® Novus-Single Channel Pipette (Thermo electron Cor.) A MicroAmp™ Optical Adhesive Film (PE Applied Biosystems) was firmly attached to the MicroAmp™ Optical 96-Well Reaction Plate, using a MicroAmp™ Adhesive Film Applicator (PE Applied Biosystems). A MicroAmp™ Optical Film compression Pad (PE Applied Biosystems) was subsequently placed over the MicroAmp™ Optical Adhesive Film, providing a thermal seal between the thermal cycler and the reaction plate. The MicroAmp™ Optical 96-Well Reaction Plate was loaded and run on an ABI PRISM® 7000 system. The amplification reaction was undertaken in an ABI PRISM® 7000 Sequence Detector (PE Applied Biosystems), using the following amplification conditions: an initial hot start incubation at 95°C for 10 minutes (AmpliTaq Gold® enzyme activation cycle), followed by 40 cycles of denaturation at 95°C for 15 seconds and annealing/extension at 60°C for 1 minute. *GAPDH* was used as an endogenous control and the level of expression of each gene was normalised against these *GAPDH* levels, employing the standard curve method. *GAPDH* levels were determined for each irradiated and mock-irradiated sample at the indicated time points, by performing a *GAPDH* only RT-PCR assay in separate 96-well reaction plates for each cell line (XP8CA and CS3BE). In addition to preparing three independent biological replicates for UV-treated and time-matched mock-irradiated control samples, all RT-PCR reactions were performed in triplicate. Therefore, each expression value was representative of nine replicates. A PCR reaction, containing TaqMan® Universal PCR Master Mix and gene-specific probe in the absence of template cDNA, was performed in each assay, thus permitting the detection of contaminating products.

Table 2.4. Gene-specific TaqMan® Gene Expression Assays used in real-time qRT-PCR.

Gene symbol	Gene Name	TaqMan® Gene Expression Assay ID
ATF-3	Activating transcription factor 3	Hs00231069
CDKN1A (p21)	Cyclin dependent kinase inhibitor 1A	Hs00355782
Ccng2	Cyclin G2	Hs01548160
DDB2	Damage-specific DNA binding protein 2	Hs00172068
DTR	Heparin-binding EGF-like Growth Factor	Hs00181813
FDXR	Ferredoxin reductase	Hs01031621
GAPDH	Glyceraldehyde-3-phosphate dehydrogenase	HS99999905
GDF15	Growth differentiation factor 15	Hs00171132
PMAIP1 (NOXA)	Phorbol-12-myristate-13-acetate-induced protein 1	Hs00382168
PPM1D (wip1)	Protein 1D magnesium-dependent	Hs00186230
SAT	Spermidine/spermine N1-acetyl transferase 1	Hs00971735

2.14.4 Data acquisition, analysis and normalisation

The relative quantification of gene expression was undertaken using a standard curve methodology in accordance to the manufacturer's recommendations (PE Applied Biosystems). During the run, the ABI PRISM® 7000 instrument was used to record the fluorescence emission. After the run, the ABI PRISM® 7000 SDS software was used to process the raw fluorescence data to produce threshold cycle (C_T) values of the diluted standards. Relative quantities were obtained for the unknown experimental samples based on their C_T values. For comparison of transcript levels between control (mock-irradiated) and UVC-irradiated samples at the indicated time points and between hTERT-immortalised XP-C and CS-A dermal fibroblasts, a standard curve of C_Ts for several serial dilutions of MRC-5 cDNA was constructed for each RT-PCR assay (as previously discussed). The standard curve was used to calculate the relative abundance of mRNA for each gene studied. The expression values for each gene, generated from UVC-irradiated and mock-irradiated samples at the indicated time points, were normalised to the relative amounts of *GAPDH* mRNA. The expression level of each gene-specific mRNA was determined relative to the *GAPDH* mRNA levels of the same sample by dividing the C_T value obtained for the gene of interest by the C_T value obtained for *GAPDH*.

Chapter 3

Characterisation of Novel Mutations in Cockayne Syndrome type A and Xeroderma Pigmentosum Group C Subjects

[Published in **J. Hum. Genet.** (2005) 50: 151-154]

3.1 Introduction

XP is characterised by hyperphotosensitivity to the UV constituent of sunlight. The clinical hallmarks of XP include initial pigmentation disturbances followed by a marked predisposition to skin neoplasia, with a >1000-fold incidence of UV-induced cutaneous neoplasia, such as SCC, BCC and malignant melanoma (Section 1.9.1). Seven 'classical' XP complementation groups have been characterised, each corresponding to mutations in one of seven genes, *XPA-XPG,* involved in NER (Section 1.9.1). The XP-C complementation group is the most prevalent form of the XP syndrome (Khan *et al.*, 1998; Kraemer *et al.*, 1987). Patients from this complementation group exhibit skin abnormalities with no associated neurological abnormalities (Section 1.9.1). To date, mental retardation has been described in patient XP1MI (Li *et al.*, 1993). The differences in cutaneous manifestations between XP-C patients depend on age, climate and life-style. At the cellular level, cultured fibroblasts from XP-C patients display partial UV-induced DNA repair synthesis, which range between 10-20% of normal, and are only defective in GGR. Indeed, XP-C cells are fully proficient in the removal

of lesions from the transcribed strand of active genes (Kantor *et al.*, 1990; Venema *et al.*, 1991; van Hoffen *et al.*, 1995), as TCR activity is retained. Initial complementation studies (Legerski & Peterson, 1992), by transfecting partial but fully active *XPC* cDNA, resulted in phenotypic correction of XP-C cells. This led to the subsequent purification and cloning of the XPC-hHR23B complex (Masutani *et al.*, 1994). The full-length *XPC* cDNA is 3558 nucleotides long and encodes a 940 amino acid polypeptide of 106 kDa (Fig 3.1). The XPC protein is composed of three principle binding regions, which facilitate binding to DNA, hHR23B and TFIIH (Fig. 3.1). XPC forms a heterodimeric complex with hHR23B (XPC-hHR23B). The XPC domain that facilitates the interaction with hHR23B has been mapped to the evolutionary conserved carboxy-terminal region. Interestingly, the carboxy-terminal 125 aa's are superfluous for both DNA and hHR23B binding. However, interactions with TFIIH are disturbed by truncation of this domain (Uchida *et al.*, 2002).

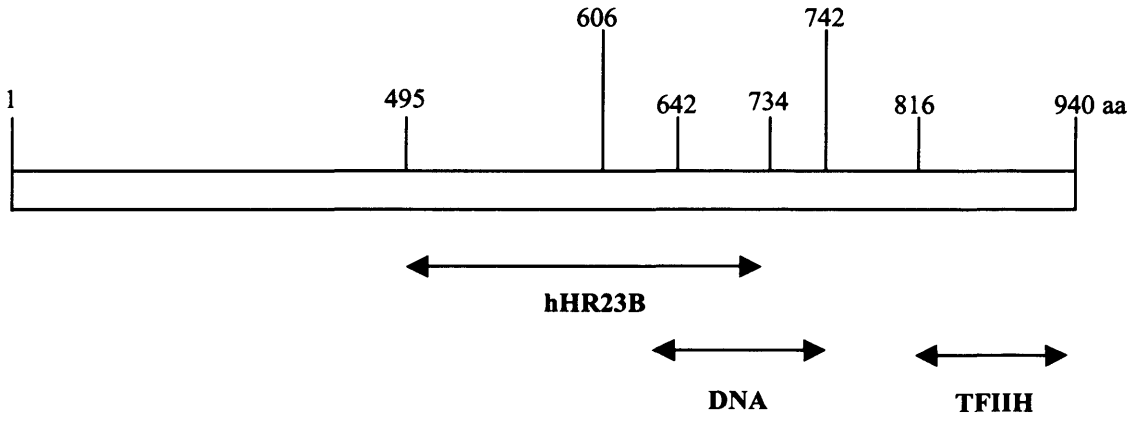

Figure 3.1. Schematic of the domain structure of human XPC protein (adapted from Dip *et al.*, 2004).

Unlike XP, CS patients do not display a predisposition to UV-induced skin neoplasia, but exhibit a battery of other clinical manifestations (Section 1.9.3). Principally, segmental progeria is the hallmark clinical pathophysiological manifestation exhibited by CS patients (Nance & Berry, 1992). Further clinical features include; cachetic dwarfism, deafness, retinal degeneration, neurological dysfunction and skeletal-associated abnormalities, such as osteoporosis and a

bird-like face (Section 1.9.3). Death occurs at a mean age of 12 years. Mutations in the *CKN1* (*CSA*) and *CSB* genes are responsible for CS.

Whilst CS and XP cells have defective NER, the striking differences between the syndromes are explained by the fact that the NER mechanism is divided into two distinct sub-pathways, GGR and TCR (Sections 1.6.1-1.6.2). GGR facilitates the removal of lesions from the non-transcribed strand and transcriptionally silent regions of the genome. Conversely, TCR preferentially removes lesions from the transcribed strand of active genes. In GGR, the recruitment of the 106 kDa XPC protein, complexed with the 43 kDa hHR23B protein, allows interaction with damaged DNA, facilitating the recognition of UV-induced lesions (Sugasawa *et al.*, 1998). Conversely, the arrest of an elongating RNA polymerase II at a lesion on the transcribed strand of an active gene is considered to elicit the recruitment of TCR-specific proteins, including CSA. The 44 kDa CSA protein is encoded by the *CKN1* gene and contains multiple WD-40 repeats (Henning *et al.*, 1995). The two NER sub-pathways converge at the point where the presence of a lesion is confirmed. Excision, resynthesis and ligation follow using a common mechanism (Sections 1.6.3-1.6.6)

3.2 Aims

Both *XPC* and *CKN1* genes were previously cloned as a result of screening cDNA libraries for genes that corrected the UV sensitivity of XP-C and CS-A cell lines (Legerski & Peterson, 1992; Henning *et al.*, 1995). Interestingly, the mutations present in the original CS-A line (CS3BE) used for library screening have not previously been identified (Henning *et al.*, 1995), although it was reported that the cell line appeared to produce no CSA protein (van Gool *et al.*, 1997). Furthermore, although the XP-C line, derived from donor XP8CA, has been extensively used in previous structural, biochemical and functional studies (Baxter & Smerdon, 1998; Azzam *et al.*, 2002; Hashem *et al.*, 1980), the underlying genetic defect remains uncharacterised. Therefore, genetic analysis was undertaken to identify the *XPC* and *CKN1* genomic DNA variants in patients

XP8CA (GM02996) and CS3BE (GM01856), respectively, and to confirm that the cultures had the desired genetic defects required for subsequent analysis.

3.3 Materials and methods

Primary XP-C (GM02996, XP8CA) and CS-A (CKN1; GM01856, CS3BE) human dermal fibroblasts were purchased from the NIGMS Human Genetic Mutant Cell Repository (Coriell Institute for Medical Research, Camden, NJ). Genomic DNA was isolated and purified by proteinase K digestion, followed by a phenol/chloroform extraction (Section 2.11.1). PCR amplification of *XPC* and *CSA* gene fragments from isolated XP8CA and CS3BE genomic DNA, respectively, was performed on a GRI MJ Tetrad Thermocycler. Sequence analysis was undertaken by the Wales Gene Park, using an automated ABI PRISM 3100 Genetic Analyser (Sections 2.11.2-2.11.6). *XPC* and *CSA* genomic DNA variants were identified using Sequencher™ Version 4.5 software (Gene Codes Corp.).

Total RNA was extracted from CS-A human dermal fibroblasts, using the TRIzol® reagent according to the manufacturers recommendations (Section 2.13.2) and reverse transcribed using SuperScript II (Section 2.13.3). Amplification of *CKN1* cDNA was performed by PCR (Section 2.12) and amplification products were ligated into the TA cloning vector, pCR2.1, and transformed into INVαF' *E.coli* One Shot cells (Section 2.12.1). Individual colonies were isolated, expanded and sequenced in both directions, using M13 forward and reverse primers (Sections 2.12.2-3). Sequence analysis was performed by our in-house CBS facility, using an automated ABI PRISM 3100 Genetic Analyser.

Immunoblotting was performed using a Biorad Mini-Protean II Electrophoresis Cell System. Briefly, WCEs were prepared as previously described (Sections 2.9.1-2.9.2). Proteins were separated on SDS-PAGE gels (Section 2.9.3), transferred to PVDF membranes (Section 2.9.3) and exposed to either an anti-XPC mouse monoclonal antibody or an anti-CSA goat polyclonal antibody

(Table 2.1, Section 2.9.4). Blots were visualised using an appropriate HRP-coupled secondary antibody and an ECL system using Hyperfilm (Table 2.1, Section 2.9.4). Equal protein loading was confirmed by staining the PVDF membrane with India ink (Section 2.9.5).

For the immunocytochemical detection of XPC, the VECTRASTAIN® ABC system (Vector Laboratories, Peterborough, UK) was used as previously described (Section 2.10).

3.4 Results

3.4.1 Identification of XPC and CKN1 genomic DNA gene variants

The causative mutations in the *XPC* and *CKN1* gene were identified by isolating genomic DNA from patients XP8CA and CS3BE, respectively, and the 16 exons of *XPC* and 12 exons of *CSA* were amplified by PCR. The PCR products were sequenced and base changes identified by comparing to consensus cDNA sequences (NM_000082 [*CKN1*]; NM_004628 [*XPC*]) obtained from NCBI.

In patient XP8CA, a homozygous 2 bp TG deletion (del) was identified in codon 547 at position 1639 (1639delTG) in exon 9 (Fig. 3.2*A*). This creates a frame shift and a premature termination at codon 572, resulting in a predicted protein of 63.4 kDa. Two homozygous missense mutations were identified. The first, a 2061A>G transition in exon 11 (R687R; Fig. 3.2*B*), resulted in no change to the amino acid sequence, as the single base change also encoded an Arg residue. In addition, patient XP8CA displayed a further missense mutation consisting of a 2815A>C transversion in exon 16 (Fig. 3.2*C*), which caused an amino acid substitution at position 939 from Lys to Gln (K939Q). Notably, the location of both the homozygous missense variants (2061A>G and 2815A>C) lie 3' to the 2 bp TG deletion (1639delTG), therefore these variants would not appear in the

final translated protein product. Accordingly, these missense variants should not contribute to the XP-C phenotype presented by patient XP8CA.

Patient CS3BE, assigned to CS complementation type A, was a compound heterozygote for mutations in *CKN1*, the gene encoding the CSA protein (MIM 216400). The first heterozygous mutation found, was a previously described nonsense mutation consisting of a G to T transversion (37G>T) at position 37 (Fig. 3.3*A*). This nonsense mutation caused a change at aa 13 from Glu to a non-coding codon (E13X). In addition, patient CS3BE displayed a novel missense mutation consisting of a C to T transition at position 479 (479C>T; Fig. 3.3*B*), resulting in a change in aa 160 from Ala to Val (A160V).

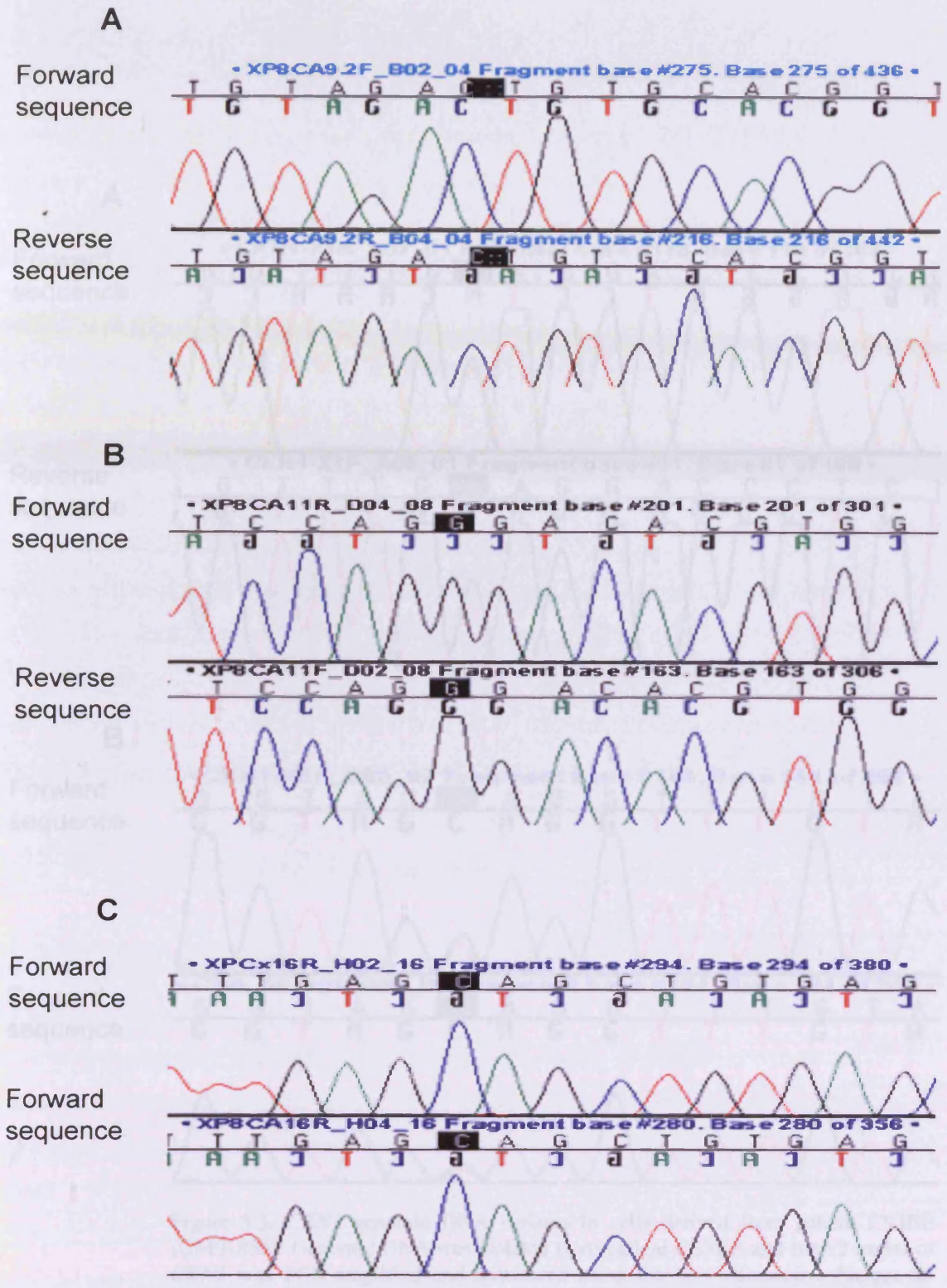

Figure 3.2. *XPC* genomic DNA variants in cells derived from patient XP8CA (GM02996). Genomic DNA was isolated from patient XP8CA and the 16 exons of *XPC* was PCR amplified and sequenced, using the non-radioactive Sanger di-deoxy protocol. Patient XP8CA was homozygous for a (A) 2 bp TG deletion at codon 547 . Two further homozygous missense variants were identified; (B) 2061A>G and (C) 2815A>C.

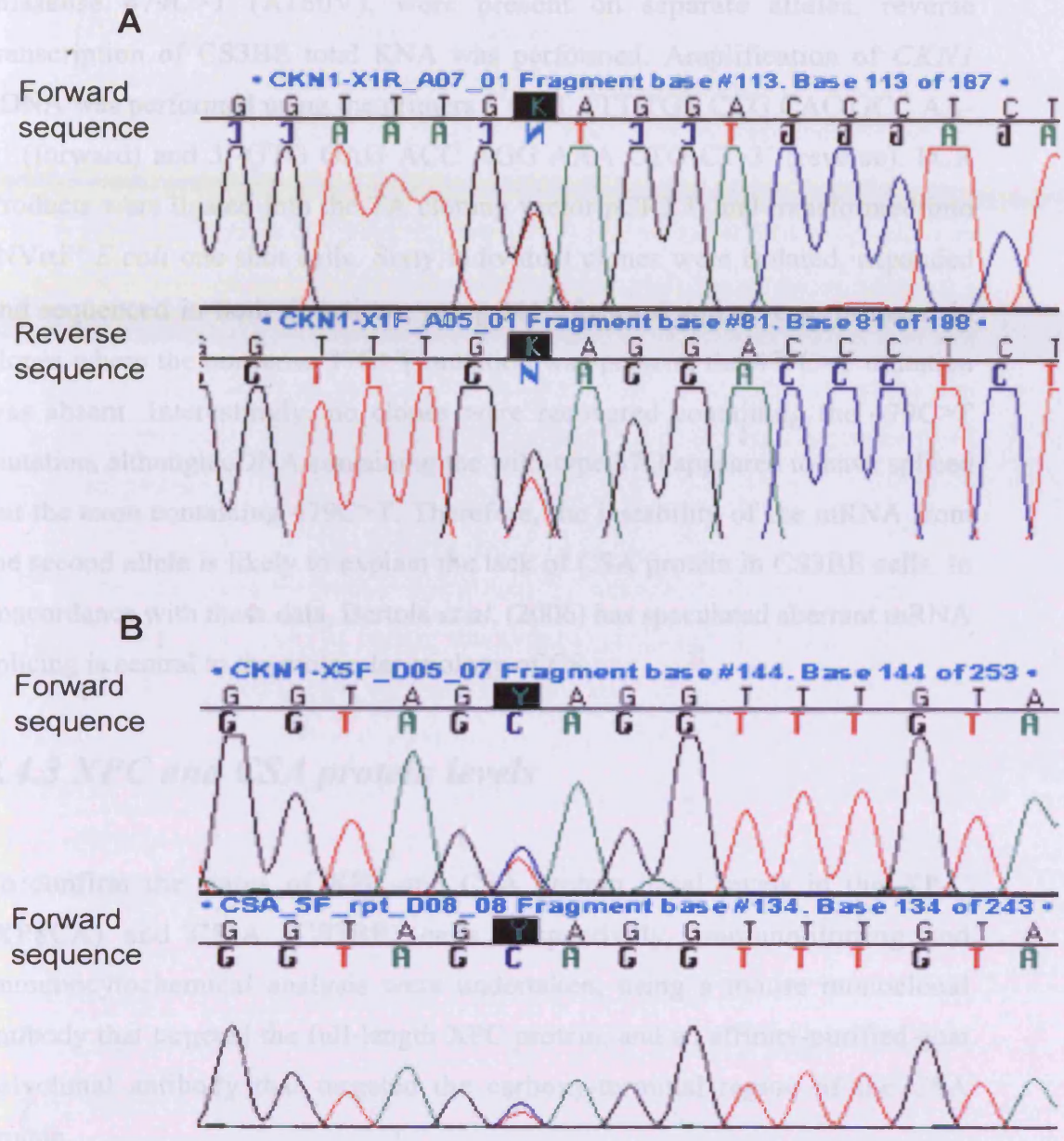

Figure 3.3. *CKN1* genomic DNA variants in cells derived from patient CS3BE (GM01856). Genomic DNA was isolated from patient CS3BE and the 12 exons of *CKN1* was PCR amplified and sequenced using the non-radiaoactive Sanger di-deoxy protocol. Pateint CS3BE was a compound heterozygote for *CKN1* mutations (A) 37G>T and (B) 479C>T.

3.4.2 Analysis of CS3BE mRNA

To confirm that the two heterozygous variants, nonsense 37G>T (E13X) and missense 479C>T (A160V), were present on separate alleles, reverse transcription of CS3BE total RNA was performed. Amplification of *CKN1* cDNA was performed using the primers 5'GGT TTT TGT CCG CAC GCC AA-3' (forward) and 5'-GTG GAG ACC AGG AAA CTG CT-3' (reverse). PCR Products were ligated into the TA cloning vector pCR2.1, and transformed into INVαF' *E.coli* one shot cells. Sixty individual clones were isolated, expanded and sequenced in both directions, using M13 forward and reverse primers. In clones where the nonsense 37G>T mutation was present, the 479C>T mutation was absent. Interestingly, no clones were recovered containing the 479C>T mutation, although cDNA containing the wild-type 37G appeared to have spliced out the exon containing 479C>T. Therefore, the instability of the mRNA from the second allele is likely to explain the lack of CSA protein in CS3BE cells. In concordance with these data, Bertola *et al.* (2006) has speculated aberrant mRNA splicing is central to the molecular etiology of CS.

3.4.3 XPC and CSA protein levels

To confirm the status of XPC and CSA protein basal levels in the XP-C (XP8CA) and CS-A (CS3BE) cells, respectively, immunoblotting and immunocytochemical analysis were undertaken, using a mouse monoclonal antibody that targeted the full-length XPC protein, and an affinity-purified goat polyclonal antibody that targeted the carboxy-terminal region of the CSA protein.

As expected, XPC protein was clearly visible in the WCE derived from wild-type, hTERT-immortalised MRC-5 fibroblasts (Fig. 3.4*A*, lane 1). Moreover, immunoblotting confirmed the presence of XPC protein in WCEs derived from hTERT-immortalised, DNA repair-defective XP-A (XP12BE) and CS-A (CS3BE) dermal fibroblasts (Fig. 3.4*A*, lanes 2 & 4). In subject XP8CA, the homozygous 2 bp TG deletion causes a frame shift and creates a premature

termination codon that predicts the translation of a protein product of 63.4 kDa. However, immunoblotting, using the XPC-specific antibody confirmed the absence of full-length protein in the cell extract derived from patient XP8CA (Fig. 3.4*A*, lane 3). Interestingly, XPC protein levels were slightly reduced in the CS-A cell extract, with apparently equal protein loading. These data are in concordance with a recent study undertaken by Adimoolam & Ford (2002), who reported that XPC is an inducible protein regulated in a p53-dependent manner, and the lower expression in CS3BE cells may reflect the different steady state level compared to other cell lines. Alternatively, the reduced protein levels may have been attributed to a global reduction in transcription, which is frequency observed in CS cells. Furthermore, the presence of a further mutation at K939 in subject XP8CA is likely to have no effect because firstly, translation terminates prior to the mutation, and secondly, K939 is adjacent to the final amino acid of the normal protein.

XPC protein levels were further confirmed by immunocytochemical staining, using the same XPC-specific mouse monoclonal antibody. This resulted in the detection of a nuclear brown peroxidase reaction product in hTERT-immortalised normal MRC-5 fibroblasts (Fig. 3.5A) indicative of XPC expression. However, XPC expression was not detected in hTERT-immortalised XP-C (XP8CA) fibroblasts (Fig. 3.5B). These data recapitulated data obtained from Western blotting for both hTERT-immortalised MRC-5 and XP-C fibroblasts (Fig. 3.4A).

Western blot analysis of MRC-5 and CS-A (CS3BE) WCEs, using an anti-CSA goat polyclonal antibody, resulted in the detection of a lower non-specific, cross-reacting band in both cell extracts (Fig. 3.4*B*, lanes 1 & 2, respectively). However, an upper band corresponding to the CSA protein was present in MRC-5 (Fig. 3.4*B*, lane 1) and absent in CS3BE (Fig. 3.4*B*, lane 2). This indicated that the CSA protein in patient CS3BE either was not present or lacked the COOH-terminal region that was used to raise the CSA antibody. These data complemented an earlier report that the CSA protein was not expressed in the CS3BE cell line (van Gool *et al.*, 1997).

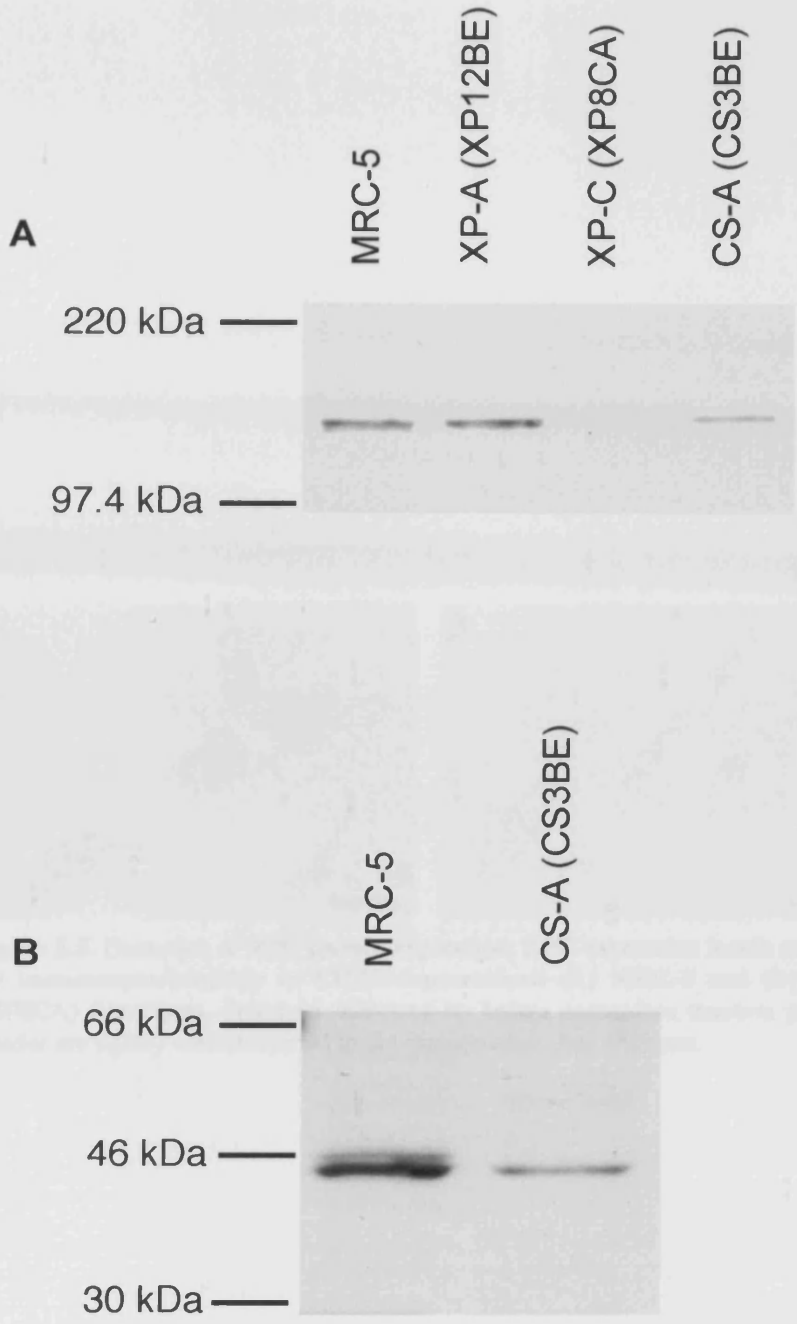

Figure 3.3. Loss of expression of XPC and CSA proteins in mutant cell lines. (A) Protein extracts from a normal (MRC-5) and DNA repair-defective XP-A, XP-C and CS-A cell lines were seperated on SDS-PAGE gels, transferred and membranes probed with an anti-XPC antibody. A band of approximately 125 kDa corresponding to XPC protein was absent in XP8CA. (B) Protein extracts from MRC-5 and CS3BE (CS-A) were seperated as above and transferred protein probed with an anti-CSA antibody. CS3BE cell extracts showed no expression of a protein of approximately 44 kDa (*upper band*) that was present in MRC-5 extracts.

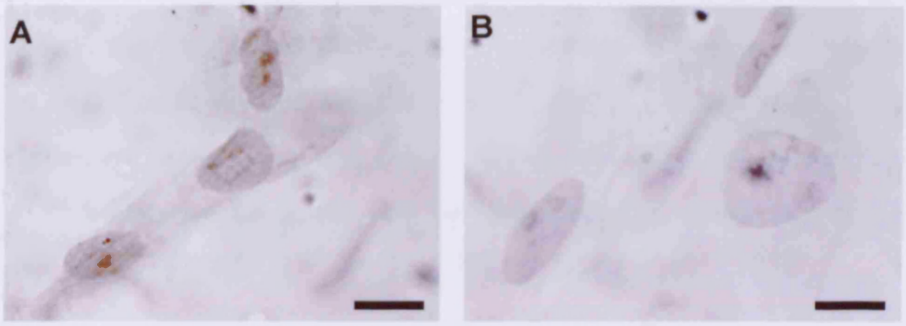

Figure 3.5. Detection of XPC protein expression. XPC expression levels analysed by immunocytochemistry in hTERT-immortalised (A) MRC-5 and (B) XP-C (XP8CA) fibroblasts. Positivity indicated by brown peroxidase reaction product. Nuclei are lightly counterstained to aid visualisation. Bar = 25 µm.

3.5 Discussion

As the mutations within the XP-C and CS-A repair-defective cell lines were previously uncharacterised, genetic analysis was undertaken to confirm that the cultures had the postulated genetic defects.

In this investigation we screened an XP-C (XP8CA, GM02996) and a CS-A (CS3BE, GM01856) cell line for *XPC* and *CKN1* genomic DNA variants, respectively, by amplifying *XPC* and *CKN1* coding regions and the intron-exon boundaries from XP8CA and CS3BE genomic DNA. The original assignments of subjects XP8CA to XP complementation group C and subject CS3BE to the Cockayne syndrome type A complementation groups were previously made on the basis of cell fusion studies (Hashem *et al.*, 1980; Tanaka *et al.*, 1981). Subsequent cloning of the *XPC* and *CKN1* genes was achieved as a result of screening cDNA libraries for genes that corrected the UV sensitivity of XP-C and CS-A cell lines (Legerski & Peterson, 1992; Henning *et al.*, 1995).

While the XP-C complementation group remains the most prevalent XP group found in North America and Europe (Kahn *et al.*, 1998; Kraemer *et al.*, 1987), only a limited number of causative mutations, resulting in an XP-C phenotype, have been published in the literature (Chavanne *et al.*, 2000; Cleaver *et al.*, 1999; Gozukara *et al.*, 2001; Khan *et al.*, 1998; Khan *et al.*, 2004; Li *et al.*, 1993; Slor *et al.*, 2000). From these studies, 17 inactivating mutations, which include 9 frameshifts, 3 nonsense and 3 splice site mutations, have been described. Interestingly, only two inactivating missense mutations have been characterised: Pro 334 His in patient XP1MI (Li *et al.*, 1993) and Trp 690 Ser in patient XP13PV (Chavanne *et al.*, 2000). Until recently, the body of evidence suggested that mutations characterised in the *XPC* gene are distributed throughout the gene, with no evidence of hotspots or founder effects (Chavanne *et al.*, 2000). However, a more recent study undertaken by Khan *et al.* (2006), reported a battery of novel *XPC* genomic variants, including 5 nonsense, 2 frameshifts and 3 splice mutations, all resulting in a classical XP-C phenotype. Notably, Khan *et al.* (2006) identified a 1744-5delTG in exon 8 common to 4 kindreds (XP16VI,

XP664VI, XP132BE and XP30BE), which was previously reported in patients XP4PA (Li *et al.*, 1993) and XP26PV (Chavanne *et al.*, 2000), thus suggesting a possible hotspot. From this body of evidence, Khan *et al.* (2006) speculated that this region was highly susceptible to polymerase slippage, as the deleted TG (1744-5) is situated in a run of 3 TGs. Conversely, Chavanne *et al.* (2000) has suggested that the presence of the 1643-44delTG at the 3' end of exon 8 may interfere with normal splicing, thus resulting in the partial activation of a cryptic donor site at position 1627. This will result in the appearance of a transcript where the final 246 nucleotides of exon 8 are lost. Alternatively, Khan *et al.* (2006) speculated that the 1744-5delTG may have been attributed to a founder mutation, as two of the families in their study, and the previously described patient, XP4PA (Li *et al.*, 1993), originated from North Africa.

The data presented here, suggest that the previously uncharacterised XP-C subject (XP8CA) was homozygous for mutations in the *XPC* gene. XP8CA was homozygous for a 2 bp TG deletion at codon 547 (1639delTG). This nonsense mutation would result in a frame shift and cause a premature termination at codon 572. The homozygous missense variant, identified in patient XP8CA (Ridley *et al.*, 2005), consisting of a 2815A>C transversion in exon 16, which caused a change in 939 aa from a Lys to a Gln (K939Q) was previously described by Li *et al.* (1993) as a second putative mutation in patient XP8BE. However, in disagreement with these findings (Li *et al.*, 1993), more recent analysis undertaken by Chavanne *et al.* (2000) has revealed that the 2815A>C variant is actually a polymorphism.

It is apparent from the literature, that the 1639delTG in exon 9 reported in this study (Ridley *et al.*, 2005), is identical to the 1744-5delTG in exon 8, previously identified in patients XP4PA (Li *et al.*, 1993), XP26PV (Chavanne *et al.*, 2000), and more recently in patients XP16VI, XP664VI, XP132BE and XP30BE (Khan *et al.*, 2006). The incongruity in the TG position between the various mutation reports can be attributed to the difference in base and exon nomenclature within the literature. For example, Khan *et al.* (2002) identified a 1.6 kb intron within exon 5 between nucleotides 726 and 727. Accordingly, a recent paper published by Khan *et al.* (2006) describes exon 5 as exons 5.1 and 5.2. Conversely, the

NCBI data bank and the data presented here (Ridley *et al.*, 2005) describe exons 1 to 16 and have assigned exons 5.1 and 5.2 as exons 5 and 6 respectively. Therefore, the 1639delTG in exon 9 described herein, corresponds to the 1744-5delTG in exon 8 reported elsewhere (Chavanne *et al.*, 2000; Li *et al.*, 1993; Khan *et al.*, 2006).

As previously discussed, Khan *et al.* (2006) describes the TGdel as occurring at position 1744-1745. Conversely, the same TGdel reported herein, has been described as occurring at position 1639 (Ridley *et al.*, 2005). Khan *et al.* (2006) describes the A residue from the methionine (AUG) initiation signal as being at base position 106, whereas in this study the same A residue is described as position 1 of exon 1, thus suggesting that Khan *et al.* (2002) have included part of the 5'-untranslated region (5'-UTR). This results in a 105 base discrepancy between the two reported nomenclatures, thus explaining the difference between the 1744-5delTG reported by Khan *et al.* (2006) and the 1639delTG described in this study (Ridley *et al.*, 2005). Taking this into account, the 1639delTG reported herein, provides additional evidence for the existence of a hotspot, as speculated by Khan *et al.* (2006). Although Khan *et al.* (2006) has also speculated a founder effect as being a possible cause for the 1744-5delTG, as two of the affected families originate from South Africa, patient XP8CA reported herein originates from Egypt. Furthermore, the precise relationship between subjects XP8CA and XP4PA is unknown, although they were originally identified in different laboratories.

Recently, Khan *et al.* (2006) speculated that mutant *XPC* mRNA transcripts, resulting from the creation of a premature termination codon (PTC) in the *XPC* gene, are degraded by the nonsense-mediated mRNA decay (NMD) pathway. It is thought that the degradation of *XPC* transcripts, possessing pre-termination signals, is a protective biological process that inhibits the expression of low levels of mutant *XPC* mRNA. Therefore, preventing the translation of truncated proteins, which may have a significantly more deleterious consequence on normal cellular functionality, compared to the complete lack of XPC protein (reviewed by Amrani *et al.*, 2006).

As expected, XPC protein was detected by Western blotting in normal hTERT-immortalised MRC-5 and DNA repair-defective XP-A (XP12BE) and CS-A (CS3BE) fibroblasts (Fig. 3.4A). Conversely, neither full-length nor truncated XPC protein was detected in WCEs derived from patient XP8CA (Fig. 3.4A), thus suggesting that the truncated XPC protein product is either expressed at low levels undetected by Western blotting or is unstable. This finding is consistent with a previous study by Chavanne *et al.* (2000), where no full-length or truncated XPC protein was detected in cells derived from twelve XP-C patients. All twelve XP-C patients where XPC protein was not detected possessed frame-shifts, deletion or aberrant splicing mutations. A low level of XPC protein, however, was detected in patient XP13PV, who displayed a missense 2069G>C transversion, which resulted in the aa change at position 690 from Trp to Ser (Chavanne *et al.*, 2000). Trp-690 is conserved in five XPC homologues (human, mouse, *Drosophila melanogaster*, *S. cerevisiae* and *Schizosaccharomyces pombe*) and the position of this residue is embedded within an α-helix. Therefore, the aa change from Trp to Ser is thought to abolish the α-helical conformation, thus inducing a modification to the secondary structure of the XPC protein. The presence of the missense 2069G>C transversion, thus resulted in the detection of dysfunctional XPC protein. Moreover, from these findings, Chavanne *et al.* (2000) speculated that XPC is dispensable for proliferation and cell viability. Additionally, Khan *et al.* (2006) has suggested that the mutated XPC proteins, produced by frame-shifts, deletions or aberrant splicing would cause the loss of the COOH-terminus, which possesses domains essential for the recruitment of the TFIIH factor to the preincision NER complex (Uchida *et al.*, 2002).

Like XPC, a multiplicity of protein truncations caused by frame-shifts, deletions and abnormal splicing have been described elsewhere in other nonessential DNA damage signalling and repair genes, such as *ATM* (Rotman & Shiloh, 1998), *CSB* (Colella *et al.*, 1999; Mallery *et al.*, 1998) and *XPA* (Cleaver *et al.*, 1999; Kuraoka *et al.*, 1996; Sato *et al.*, 1996; states *et al.*, 1998). Another NER factor, XPD, is an indispensable constituent of the basal transcription factor, TFIIH. Therefore, nonsense mutations in *XPD* are incompatible with life, and all gene

variants characterised in *XPD,* that result in XP, XP/CS, TTD or COFS are missense mutations (Cleaver *et al.*, 1999; Lehmann, 2001; Graham *et al.*, 2001), which preserve some XPD protein function for its transcriptional role (Cleaver *et al.*, 1999; Lehmann, 2001).

Chavanne *et al.* (2000) have speculated that missense mutations that cause negligible structural modifications to XPC may cause a mild clinical phenotype that remains undiagnosed. From the current data, the complete abolition of XPC protein and the presence of dysfunctional protein both result in an identical clinical phenotype, which display similar levels of photosensitivity and DNA repair, as determined by UDS. Chavanne *et al.* (2000) described 10 of the 12 diagnosed XP-C cases as presenting clinical features indicative of XP-C. Indeed, XP-C individuals are a genotypically diverse group, but the clinical manifestations are homogeneous. At the time of biopsy, patient XP8CA (described in this study) was 2 months old, and exhibited no clinical symptoms, but fibroblasts were defective in DNA repair. At 4 months, however, patient XP8CA displayed cutaneous symptoms, such as erythema and a single large (2 to 5 mm in diameter) pigment patch on the bridge of the nose (Hashem *et al.*, 1980).

Although a multiplicity of recent studies have identified several key mechanistic roles of XPC in the NER pathway (Section 1.6.1), the continued characterisation of the molecular defects in XP-C patients will assist in the elucidation of XPC function, and the identification of functional domains within the XPC protein. Furthermore, recent investigations into the association between phenotype-genotype in XP patients, have suggested that variations in NER capacity may have significant implications regarding cancer predisposition in heterozygotes and the general population. Studies undertaken by Olsen *et al.* (2001) and Gruber *et al.* (2002) showed an association between increased cancer incidence and heterozygotes with mutations in other DNA repair disease genes, such breast cancer in ataxia-telangiectasia and colon cancer in Bloom syndrome.

A frequently observed single nucleotide polymorphism (SNP) in the *XPC* gene (Khan *et al.*, 2000; Khan *et al.*, 2002), has been associated with a reduced DNA

repair capacity and increased risk of SCC of the head and neck (SCCHN; Shen *et al.*, 2001) and of the lung (Marin *et al.*, 2004) in the general population. A reduction in *XPC* mRNA levels has also been associated with an increase in SCCHN (Yang *et al.*, 2005). In addition to *XPC*, several SNPs have been identified in a number of genes involved in NER including *ERCC1* (Yu *et al.*, 1997; Yu *et al.*, 2000b), *XPD* (Broughton & Steingrimsdottir, 1996), *hHR23B* (Millikan *et al.*, 2005), *XPF* (Millikan *et al.*, 2005; Winsey *et al.*, 2000), *XPG* (Emmert *et al.*, 2001) and *XPA* (Mellon *et al.*, 2002). The role of these SNPs in influencing NER remains poorly delineated. It has been speculated, however, that SNPs of NER genes may be utilised as a predictive marker for cancer susceptibility in the general population (Gillet & Schärer, 2006). Interestingly, NER is known to provide a protective effect against DNA damaging anti-cancer treatments. Therefore, it has been speculated that the information on SNPs in NER genes could be exploited to predict the efficacy of specific agents, thus facilitating the development of tailored anti-cancer therapies.

To date, the data on *CKN1* mutations is limited because, although mutations in the *CKN1* gene account for approximately 20% of CS (Stefanini *et al.*, 1996), only 13 have been characterised (Cao *et al.*, 2004; Ren *et al.*, 2003; Bertola *et al.*, 2006). Here, we report a third novel missense mutation C479T in *CKN1*, which resulted in a change in aa 160 from Ala to Val (A160V). Interestingly, the Utah Genome Center single nucleotide SNP database (http://www.genome.utah.edu/genesnps) and a previous study (Cao *et al.*, 2004) indicate that this 479C>T variant is not a SNP. Moreover, the availability of genomes from other species has shown that the CSA protein is highly conserved (http://www.ensemble.org). In particular, Ala-160 is conserved in all species known to possess a CSA homologue (Table 3.1). The two previously reported missense mutations, Q106P and A205P (Ren *et al.*, 2003; Cao *et al.*, 2004), lie within the WD-40 region. The A160V mutation reported here lies between the second and third WD-40 repeats. If undetectably low levels of full-length protein are expressed in subject CS3BE, this is likely to be inactive as the sites of all three missense mutations (Q106, A205 and A160) are highly conserved in mammalian, chicken and puffer fish CSA protein homologues (Table 3.1).

Unlike Q106 and A205, A160 is also retained in *Schizosaccharomyces pombe* and *Arabidopsis thaliana* (Table 3.1).

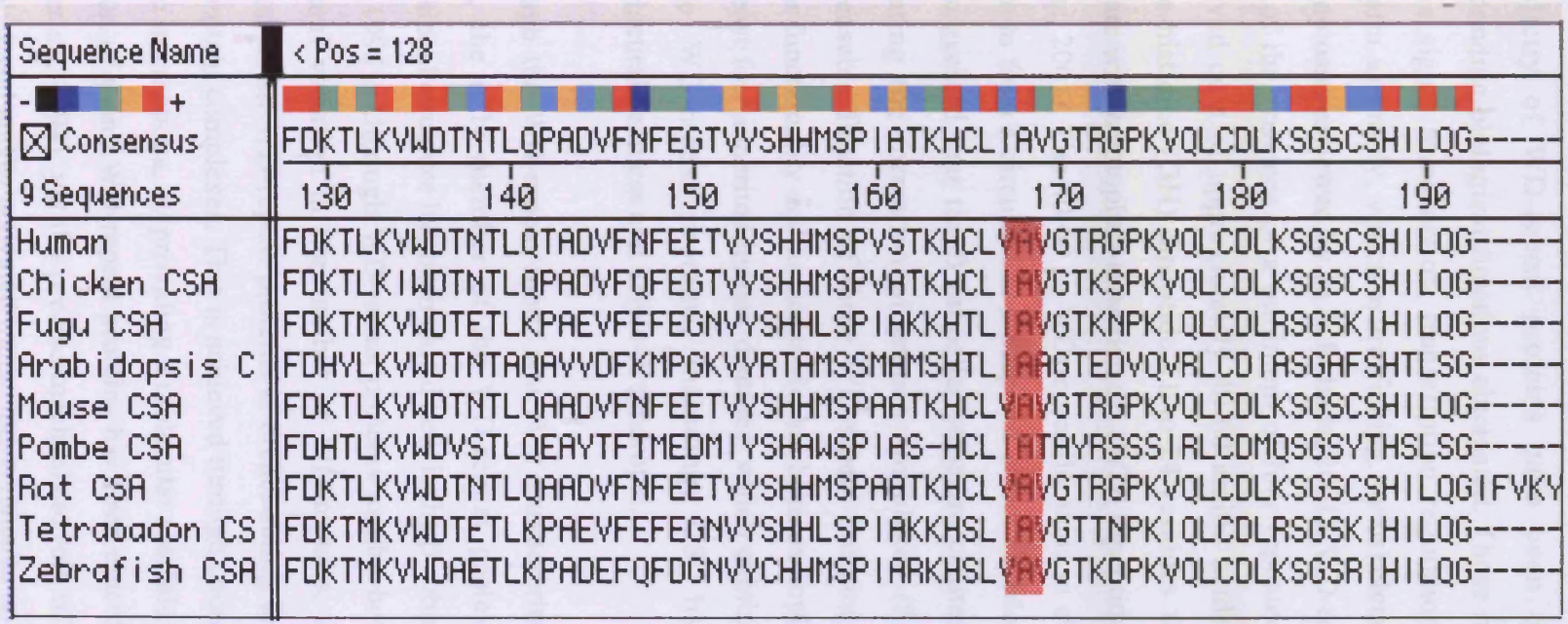

Table 3.1. Amino acid sequence alignment of all species known to possess a *CKN1* gene homologue, using the MegAlign component of the Lasergene software suite. The position of A160 is highlighted.

The *CKN1* gene encodes a 396 aa protein, which is considered a member of the WD-repeat family, due to the presence of seven WD-40 repeats. To date, a multiplicity of WD-repeat proteins have been characterised and their corresponding biological functions elucidated. These include cellular processes such as signal transduction, transcription regulation, cell cycle regulation, chromatin assembly, vesicular trafficking, cytoskeletal assembly, DNA repair and apoptosis (reviewed by Li & Roberts, 2001). WD-repeat proteins, defined by virtue of the presence of a minimum of four repeated units, contain a highly conserved core of approximately 40-60 amino acids, that are initiated by a glycine-histidine (GH) dipeptide 11 to 24 residues from the N terminus and terminate with tryptophan-aspartic acid (WD) dipeptide at the C terminus (Li & Roberts, 2001). The 40-60 aa WD-repeat domains in all WD-repeat proteins are thought to form a circularised β propeller structure. Molecular modelling studies have suggested that the β propeller structure creates a stable platform, thus facilitating the formation of protein complexes (Smith *et al.*, 1999). The indispensable function of these WD-repeat proteins, in maintaining normal cellular functionality and homeostasis, has been exemplified in their involvement in at least four inherited human diseases, which exhibit mutations in genes that encode WD-repeat proteins, including; CS, lissencephaly, late-onset sensorineural deafness and Triple-A syndrome.

Although the WD-repeat motif was first characterised in 1986 (Fong *et al.*, 1986), the only member of the WD-repeat protein family, whose three-dimensional structure has been elucidated, is the β subunit of the G protein (Wall *et al.*, 1995). Although WD-repeat proteins exhibit both sequence diversity and structural variation in the number of WD-repeats, the common mechanistic function of all WD-repeat proteins is orchestrating the sequential assembly of multiprotein complexes. This is achieved through coordinating multiple protein-protein interactions, by providing a molecular scaffold. Indeed, the mechanistic function of many WD-repeat proteins has been elucidated (Smith *et al.*, 1999; Neer *et al.*, 1994), yet the precise mechanistic role of CSA in DNA repair and possibly basal and/or activated transcription remains poorly understood (Henning *et al.*, 1995). Therefore, the existence of this highly conserved WD-repeat region,

within CSA, provides a possible avenue for elucidating the precise mechanistic function of this protein. However, it should be noted that the assignment of WD-repeat proteins to specific functional groups has been extensively problematic, as the WD-repeat domain is devoid of catalytic activity and does not possess a functional domain. Therefore, the elucidation of further structural, functional or binding domains is essential in the assignment of some WD-repeat proteins. Ren *et al.* (2003) has speculated that the 42A>C transversion they identified, resulting in an amino acid substitution (Q106P), may modify the β propeller structure of the WD-40 repeat domain in CSA, causing the defect in TCR.

As discussed in Chapter 1, in addition to the indispensable role of CSA in TCR, recent studies have elucidated further roles of CS-A. For example, Groisman *et al.* (2003) demonstrated the essential function of CSA in the modulation of NER, through the ubiquitin-proteasome pathway. It is thought that, following UV-irradiation, CSN rapidly associates with the CSA complex, resulting in the suppression of the ubiquitin ligase activity. However, the precise mechanistic function of this complex remains poorly understood. More recently, Groisman *et al.* (2006) has shown that the degradation of CSB occurs in a proteasome- and CSA-dependent manner, thus for the first time providing evidence for a functional relationship between CSA and CSB. Fousteri *et al.* (2006) has shown that functional CSA is dispensable for the recruitment of NER proteins to lesion-stalled RNAPIIo, but is essential for the recruitment of HMGN1, XAB2 and TFIIS.

Unlike XP, it appears that there are no apparent phenotype-genotype differences between characterised CS subjects displaying different mutations in the *CKN1* gene. Recently, Bertola *et al.* (2006) reported no phenotypical differences between eight Brazilian CS-A patients with splicing and frameshift mutations. However, as indicated by Bertola *et al.* (2006), the mutation studies undertaken on affected CS-A subjects so far have been performed in the absence of the correlation of phenotype to genotype (Bertola *et al.*, 2006; Cao *et al.*, 2004; Komatsu *et al.*, 2004; Ren *et al.*, 2003; Ridley *et al.*, 2005). This further emphasises the requirement for additional clinical investigation, into the

phenotype-genotype relationship exhibited by CS-A subjects. This will improve our understanding of the association between genotype and clinical symptomology exhibited by CS patients. Furthermore, extensive clinical investigation will facilitate the elucidation of the precise mechanistic function of CSA in TC-NER and basal and/or activated transcription.

Chapter 4

Establishment of hTERT-immortalised XP-C (XP8CA) and CS-A (CS3BE) Human Dermal Fibroblast Cell Lines

4.1 Introduction

The complete cessation of cellular proliferation due to telomere-dependent senescence provides the principle obstacle for the immortalisation of primary human cells. Prior to the emergence of telomerase-based immortalisation strategies, the generation of cell lines involved the selection of rare clonal populations that arose as a consequence of loss of tumour suppressor gene function and subsequent genome instability. The availability of established cell lines, derived from individuals with syndromes of genomic instability, are limited to those created through clonal expansion of tumour derived cells, due to the loss of p53 function following spontaneous mutation (Honda *et al.*, 1996), or alternatively through the transduction of primary cells with viral oncogenes, such as the HPV16 E6/E7 oncoproteins or the SV40 LTAg (Lin & Simmons, 1991). Several studies have reported the successful application of the SV40 LTAg in the establishment of immortalised cell lines, derived from individuals with defects in DNA repair, such as XP, CS, TTD, XP/CS and UV^{S}S (Yagi & Takebe, 1983; Merk & Speit, 1997; Mayne *et al.*, 1986; Tanaka *et al.*, 1985; Eveno *et al.*, 1995; Ellison *et al.*, 1998). Moreover, the SV40 LTAg has been successfully exploited to immortalise DNA repair-defective cells, which have subsequently been recipients for cDNA library screening for the elucidation of DNA repair genes (Tanaka *et al.*, 1990; Itoh & Yamaizumi *et al.*, 2000). Unfortunately, however, although these cell lines retain their original DNA repair defect, they exhibit an altered karyotype due to the genome instability that occurs during crisis.

Although many phenotypic characteristics are retained following SV40-transformation (reviewed by Bryan & Reddel, 1994), the well-documented interaction between the SV40 LTAg and p53 during immortalisation (Lane & Crawford, 1979; Linzer & Levine, 1979), suggests that SV40-transformation may result in the modification of various p53-dependent biological processes fundamental to normal cellular functionality (previously discussed in Sections 1.10.3-5). Although an increase in p53 levels has been reported following SV40 LTAg/or HPV16 E6 transformation, the apparent stabilisation of p53 levels results in the abolition of many p53-dependent functions, such as tumour suppression (Moore *et al.*, 1992), site-specific DNA binding (Bargonetti *et al.*, 1992), transactivation of downstream transcriptional gene targets (Mietz *et al.*, 1992; Segawa *et al.*, 1993), and regulation of DNA recombination (Mekeel *et al.*, 1997). In addition to the abrogation of the p53 tumour suppressor pathways (Merk & Speit, 1997), the abolition of the pRb/p16^{INK4A} tumour suppressor pathway has also been observed. Furthermore, previous reports suggest that the inactivation of p53 function, either through mutation, such as that found in p53-deficient cells derived from individuals with Li-Fraumeni syndrome (Ford & Hanawalt, 1995; Ford & Hanawalt, 1997), or by oncogenic transformation, through the exploitation of the SV40 LTAg or HPV E6/E7 viral oncoproteins, abrogates the GGR-NER pathway (Bowman *et al.*, 2000; El-Mahdy *et al.*, 2000; Ford *et al.*, 1998; Therrien *et al.*, 1999). Similarly, numerous studies have shown that the transcriptional activation of the GGR-specific genes, *XPC* and *p48* (DDB2/XP-E), which are essential for the recognition of 6-4PPs and CPDs respectively, require functional p53 (Bowman *et al.*, 2000; Amundson *et al.*, 2002; Porter *et al.*, 2006; Hwang *et al.*, 1999). Several studies have shown that the *p48* and *XPC* gene possess p53 response elements (Itoh *et al.*, 2003; Tan *et al.*, 2002; Adimoolam & Ford, 2002), and are thus regulated in a p53-dependent manner (Hwang *et al.*, 1999; Adimoolam & Ford, 2002). In agreement with these findings, Wei *et al.* (2005) exploited ChIP coupled with a paired-end ditag sequencing strategy to elucidate a whole-genome map of transcription-factor binding sites; among the p53 target genes identified were the GGR-specific genes *XPC* and *p48*. It has also been suggested that p21$^{WAF1/CIP1}$ plays an important role in NER, following the recruitment of PCNA to DNA repair sites (Stivala *et al.*, 2001). The precise role of p53/p21$^{WAF1/CIP1}$ in TCR, however,

remains controversial. Collectively, these findings reiterate the importance of p53/p21$^{WAF1/CIP1}$ preservation when establishing *in vitro* culture models of NER.

It has been shown that cell lines established through HPV E6 or E7 transformation display varying levels of NER. For example, HPV E6 transformation functionally inhibits p53 and causes a reduction in both GGR and TCR. Conversely, HPV E7-mediated transformation inactivates pRb and abrogates GGR only, thus suggesting a mechanistic function for pRb in GGR (Therrien *et al.*, 1999). As a result, the utilisation of transformed cells lines for long-term *in vitro* analysis of stress signalling pathways and the mechanistic functioning of NER has been problematic, particularly with cell lines derived from human syndromes already compromised in genome stability. Interestingly, a more recent study showed that the abrogation of GGR by the HPV E6 or E6/E7 oncoproteins occurs in a cell-type-specific manner (Ferguson & Oh, 2005). This reiterates the requirement of an alternative immortalisation system, as a critical response to DNA damage, namely p53, is missing. Moreover, subtle differences in NER may be attributed to a modulation in GGR by oncogenic protein transformation rather than the phenotypical characteristics of the cell.

The preservation of the p53/p21$^{WAF1/CIP1}$ and pRb/p16^{INK4A} tumour suppressor pathways is particularly important, as mutations and the subsequent loss of p53 and p16^{INK4A} function has been implicated as important targets in the molecular pathogenesis of cutaneous malignancy in both the normal population and in XP patients (reviewed by Daya-Grosjean & Sarasin, 2005; Melnikova & Ananthaswamy, 2005; Pfeifer *et al.*, 2005). Although Ferguson & Oh (2005) have recently reported proficient GGR in human keratinocytes defective in p53, a growing body of evidence has shown that preservation of p53 and pRb is indispensable for the GGR of CPDs and other DNA lesions in non-keratinocyte cells (Bowman *et al.*, 2000; El-Mahdy *et al.*, 2000; Ford & Hanawalt, 1995; Ferguson & Oh, 2005; Ford & Hanawalt, 1997; Ford *et al.*, 1998; Lloyd & Hanawalt, 2000; Therrien *et al.*, 1999; Wani *et al.*, 2002b), although the abolition of 6-4PP repair resulting from abolished p53 function has been documented less frequently (Ford *et al.*, 1998). Despite the role of p53/p21$^{WAF1/CIP1}$ being well

characterised, the precise role of pRb in the repair of UV-induced lesions remains controversial.

Indeed, extensively characterised primary human cell cultures, defective in DNA repair, derived from several genome instability syndromes such as XP, CS and TTD donors, which retain normal p53 functionality, are widely available and provide an alternative *in vitro* culture model to transformed cell lines that recapitulate their primary isogenic counterpart. However, the long-term *in vitro* genetic, biochemical and functional analysis of primary cultures is hindered by limited proliferative lifespan (and therefore limited cell numbers) and the confounding effects of cellular senescence. For example, investigations into DNA damage signalling and tumour suppressor function is significantly compromised by the alterations in the basal state of p53 activation. Moreover, the induction of both the p53/p21$^{WAF1/CIP1}$ and pRb/p16^{INK4A} anti-proliferative pathways occur as a result of stress signalling induced by double-stranded DNA breaks and the uncapping of telomeres. In stark contrast, Goukassian *et al.* (2000) have shown an association between a reduction in both the basal and activated levels of p53 protein with an increase in chronological age of the donor.

The limited expansion of primary cells in culture provides the principle obstacle when undertaking genetic manipulations that require subsequent clonal expansion. For example, the creation of stable and permanent *in vitro* gene knockout models, through homologous recombination or the exploitation of shRNA technologies, requires the extensive propagation of cells during the establishment of clones. Furthermore, slowly dividing primary cells derived from genome instability syndromes are resistant to transfection.

A multiplicity of conflicting *in vitro* studies have shown either insignificant or no modulation in the repair capacity of various DNA repair pathways in young or senescent cells (Painter *et al.*, 1973; Clarkson & Painter, 1974; Merkle *et al.*, 2004). In congruence, Christiansen *et al.* (2000) adopted strand-specific DNA repair assays to demonstrate that gene-specific NER of CPDs was not compromised in senescent human dermal fibroblasts or trabecular osteoblasts. More recently, however, Boyle *et al.* (2005) utilised an anti-CPD monoclonal

antibody in combination with an *in situ* immunochemical method, to show that senescent cells are compromised in the excision of CPDs following UV-irradiation, compared to their young isogenic counterpart. These widely conflicting findings have been attributed to differences in culture conditions (Al-Baker *et al.*, 2005). It is thought that young cultures grown under high serum concentrations (10%) contain cells that are at different phases of the cell cycle. In contrast, senescent cultures grown under identical culture conditions contain fewer than 4% proliferating cells. This has significant implications for DNA repair studies, as damage will occur to young proliferating cells in G_1, S and G_2 phases of the cell cycle, while damage to senescent cultures will predominantly occur to cells in G_1. It has been previously shown that cells in G_1 are more susceptible to DNA damage than cells in S and G_2 phases of the cell cycle (Watanabe & Horikawa, 1974).

A reduction in NER capacity would be particularly problematic when undertaking long-term *in vitro* NER assays, as a reduction in NER may be attributed to the phenotypical characteristics of the cell, or simply due to the onset of replicative senescence.

The initial cloning of the *hTERT* gene (Nakamura *et al.*, 1997), has provided an alternative system for the establishment of permanent cell lines with an unlimited proliferative potential (Bodnar *et al.*, 1998; Viziri & Benchimol, 1998), which phenotypically resemble their primary isogenic counterpart, without displaying the cancer-associated alterations displayed by transformed cell lines (Jiang *et al.*, 1999; MacKenzie *et al.*, 2000; Morales *et al.*, 1999; Morales *et al.*, 2003), or a protracted proliferative capacity exhibited by primary cultures. Initially, it was demonstrated that expressing *hTERT* restored telomerase activity in normal somatic cells (Nakayama *et al.*, 1998; Vaziri & Benchimol, 1998; Weinrich *et al.*, 1997). Subsequent to the initial demonstrations that the transient and stable transduction of the catalytic subunit of telomerase (hTERT), resulted in the reconstitution of telomerase activity, elongation of telomeres and an extended replicative capacity (Bodnar *et al.*, 1998; Steinert *et al.*, 2000; Vaziri & Benchimol, 1998; Wang *et al.*, 1998), several reports have exploited telomerase-mediated immortalisation to extend the proliferative lifespan, without

compromising the phenotypic characteristics of the cell or inducing changes associated with a malignant phenotype, such as growth in soft agar and tumour formation *in vivo* (Jiang *et al.*, 1999; MacKenzie *et al.*, 2000; Morales *et al.*, 1999; Morales *et al.*, 2003). Furthermore, it was shown that human skin fibroblasts displaying reconstituted telomerase activity retained normal growth regulation in response to serum depletion, high confluency, G_1 or G_2 phase inhibitors and spindle inhibitors (Jiang *et al.*, 1999). In addition to an unlimited proliferative capacity, hTERT-immortalised cells retain the characteristics associated with normal diploid primary fibroblasts cultured *in vitro*, such as contact inhibition, non-tumorigenicity, anchorage dependence, a normal karyotype, chromosomal stability and fully functional tumour suppression including p53/p21$^{WAF1/CIP1}$ and pRb /p16^{INK4A} activity.

Although the ectopic expression of hTERT alone is sufficient to reconstitute telomerase activity, elongate telomeres, and extend proliferative lifespan in primary human fibroblasts and epithelial cells (Bodnar *et al.*, 1998; Nakayama *et al.*, 1998; Vaziri & Benchimol, 1998; Weinrich *et al.*, 1997), conflicting studies have shown that several cell types require further manipulation in addition to telomerase reactivation.

Interestingly, numerous reports describe the stable and permanent establishment of hTERT-immortalised cell lines derived from genetically compromised phenotypes, without resulting in alterations associated with oncogenic transformation, including the abrogation of the p53/p21$^{WAF1/CIP1}$ and pRb/p16 ^{INK4A} pathways, which are known to elicit cellular senescence (Bond *et al.*, 1999; Hara *et al.*, 1996; Shay *et al.*, 1991). These include cells derived from Werner syndrome (WS), AT, Roberts's syndrome (RBS), XP-E, XP-V, CS-B, Bloom syndrome (BLM), Hutchinson-Gilford progeria syndrome (HGPS) and Nijmegen breakage syndrome (NBS) (Wyllie *et al.*, 2000; Ouellette *et al.*, 2000; Newman *et al.*, 2006; Wood *et al.*, 2001; Ranganathan *et al.*, 2001).

It has been speculated that hTERT functions in several cellular responses independent of telomere length. Recent studies have shown that the interaction between hTERT and telomeres increases genome stability and enhances DNA

repair (Sharma *et al.*, 2003; Shin *et al.*, 2004). Sharma *et al.* (2003) speculated that the increased DNA repair capacity was attributed to the stabilisation of telomeres at the nuclear matrix, resulting in the down regulation of senescence-associated gene expression and an upregulation of DNA repair-associated genes. Conversely, Shin *et al.* (2004) postulated that hTERT directly mediates the recruitment of DNA repair proteins to the site of damage. Interestingly, Gorbunova *et al.* (2002) showed that the expression of hTERT in fibroblasts confers resistance to UV-induced apoptosis.

In contrast, however, several conflicting studies have shown that hTERT-immortalised fibroblasts progressively acquire features closely associated with a transformed phenotype. For example, Milyavsky *et al.* (2003) showed that hTERT-immortalised cells remain phenotypically similar to primary cells during the first 150 PDs, however, the long-term propagation (≤500 PDs) of hTERT-immortalised cells in culture, resulted in the appearance of clones harbouring potentially malignant alterations. Although the long-term cultures retained both intact p53/p21$^{WAF1/CIP1}$ and pRb-mediated checkpoints, numerous studies have reported conflicting findings for the preservation of p14^{ARF} and p16^{INK4A}. For example, Jiang *et al.* (1999) showed that telomerised BJ foreskin fibroblasts display no alterations in a p16^{INK4A} response to a cell-cycle checkpoint arrest compared to parental non-hTERT expressing cells. Conflicting studies, however, have reported fluctuations in p16^{INK4A} basal protein levels, following continuous growth of telomerised cells in culture. Milyavsky *et al.* (2003) observed a significant induction in p16^{INK4A} at both the transcriptional and translational levels in telomerised WI-38 fibroblasts soon after the cells passed the replicative senescence barrier. This resulted in a reduction in colony formation and a subsequent senescence-like arrest. A similar induction of p16^{INK4A} in hTERT-immortalised fibroblasts has been reported elsewhere (Wei *et al.*, 2001). Milyavsky *et al.* (2003) also reported a subsequent decline and loss of p16^{INK4A} expression following prolonged culture of telomerised WI-38 fibroblasts, which resulted in loss of contact inhibition. Milyavsky *et al.* (2003) proposed that the stable changes in p16^{INK4A} expression were due to epigenetic events. The loss of p16^{INK4A} during telomerase-mediated immortalisation has been reported in

several other fibroblast strains (Kiyono *et al.*, 1998; Tsutsui *et al.*, 2002). Consistent with these data, gene expression profiling of normal human fibroblasts and endothelial cells immortalised with hTERT revealed a dramatic down-regulation in *CDKN2A*, the gene that encodes $p16^{INK4A}$ (Kumazaki *et al.*, 2004). It is of note that the pattern of initial $p16^{INK4A}$ induction immediately after telomerase-mediated immortalisation followed by the gradual disappearance during an accelerated growth phase appears to be a frequently reported phenomenon among fibroblast strains (Milyavsky *et al.*, 2003; Noble *et al.*, 2004; van Waarde-Verhagen *et al.*, 2006).

Moreover, the long-term propagation of hTERT-immortalised fibroblasts resulted in the overexpression of the *c-myc* and *Bmi-1* oncogenes. Similarly, a number of studies have reported epigenetic and genetic changes associated with alterations in the $p53/p21^{WAF1/CIP1}$ and $pRb/p16^{INK4A}$ pathways, following extensive *in vitro* subcultivation of hTERT-immortalised cells (Farwell *et al.*, 2000; Nobel *et al.*, 2004; van Waarde-Verhagen *et al.*, 2006; Wang *et al.*, 2000). Interestingly, transcription expression profiling revealed significant differences between the profiles of normal (nontransduced) and isogenic hTERT-immortalised fibroblasts (Lindvall *et al.*, 2003). In particular, epiregulin, a growth factor of the EGF family was significantly upregulated in hTERT-immortalised cells. Epiregulin is thought to play a role in the maintenance of continued proliferation (Toyoda *et al.*, 1997). Conversely, it has been speculated that excessive telomerase activity induces a senescent-like phenotype (Gorbunova *et al.*, 2003), as elevated telomerase activity acts as a hyperproliferative signal in a similar manner to that observed following overexpression of oncogenic Ras, Raf and E2F1.

Although the ectopic expression of hTERT permits the extension of proliferative capacity in primary cells derived from donors of genome instability syndromes, a recent study has shown that hTERT does not circumvent stress-induced premature senescence (SIPS), irrespective of extensions on telomere length (Naka *et al.*, 2004). In addition to telomere-dependent replicative senescence, fibroblasts undergo SIPS in response to DNA damage induced by oxidative stress, UV or ionising radiation. Naka *et al.* (2004) showed that exposure of

hTERT-immortalised AT fibroblasts to x-rays or H_2O_2, resulted in SIPS. This suggests that SIPS is not exclusively triggered by telomere shortening, but also occurs via a telomere-independent pathway. Therefore, the cessation of cellular proliferation may occur subsequent to the ectopic expression of hTERT.

As previously mentioned, the long-term genetic, biochemical and structural *in vitro* analysis of normal NER was restricted to cell lines created by the expansion of clones following spontaneous mutation or by oncogenic transformation, as the establishment of normal telomerase-immortalised cell lines exhibiting unaltered NER remained unreported. However, several investigators have successfully established hTERT-immortalised normal fibroblast cultures, which exhibit unaltered levels of UV sensitivity and confer normal levels of NER to their primary isogenic counterparts (Bates *et al.*, 2005; Ouellette *et al.*, 2000; Porter *et al.*, 2006). Moreover, hTERT-immortalisation maintains cell-cycle checkpoint controls and permits the continued preservation of genome stability. In concordance, Cordeiro *et al.* (2002) used previously established hTERT-immortalised XP-V fibroblasts (Ouellettee *et al.*, 2000), which displayed S phase fractions similar to its primary isogenic counterparts, to evaluate checkpoint responses. In addition, the utilisation of telomerase-immortalised XP-V cells allowed Cordeiro *et al.* (2002) to substantiate whether the abolition of pol η activity in XP-V cells increases the risk for accumulating UVC-induced chromosomal aberrations.

All previous investigations of CSB function in immortal cells were performed using CS-B cell lines established through SV40-transformation (Troelstra *et al.*, 1992). However, in addition to the known interactions between the SV40 LTAg and p53 (Pipas & Levine), studies have shown that p53 directly interacts with CSB *in vitro* and possibly *in vivo* (Yu *et al.*, 2000a; Wang *et al.*, 1995). Therefore, to avoid the confounding functional interactions between SV40 LTAg and CSB, Newman *et al.* (2006) established a permanent CS-B fibroblast cell line through telomerase-mediated immortalisation. This provided a control for the isogenic SV40-transformed CS-B cell line and allowed Newman *et al.* (2006) to characterise CSB-dependent transcription expression responses, by expression

profiling telomerised CS-B fibroblasts that possessed intact tumour suppressor pathways.

Therefore, the exploitation of telomerase will provide an invaluable tool in the establishment of novel *in vitro* model systems of ageing, carcinogenesis and tumorigenesis, when compared to the conventional exploitation of cell lines established by oncogenic transformation. Furthermore, the indefinite expansion of human fibroblasts by hTERT reconstitution can provide unlimited access to biological material for long-term genetic, biochemical and physiological analysis of normal growth and differentiation, without exhausting the proliferative capacity of the culture.

Pirzio *et al.* (2004) reported low frequencies of chromosomal aberrations and the maintenance of karyotypic stability in human fibroblasts immortalised through the ectopic expression of telomerase, and speculated that reconstituted telomerase activity contributed to genome stability via a telomere-independent mechanism, suggesting the potential exploitation of hTERT-immortalised human fibroblasts in gene targeting studies.

In accordance, Jiang *et al.* (1999) speculated that the ectopic expression of hTERT *per se* does not elicit oncogenic transformation, as both germ cells and stem cells exhibit telomerase activity (Wright *et al.*, 1996), whilst remaining functionally normal. Furthermore, a preliminary study undertaken by Morales *et al.* (1999) suggests that in addition to reconstitution of telomerase activity and extension of replicative lifespan, the ectopic expression of telomerase facilitates the preservation of the p53-mediated cell cycle checkpoint in response to UV. Morales *et al.* (1999) further demonstrated a UV-dependent induction of $p21^{WAF1/CIP1}$ in response to UV, which is indicative of normal p53 functionality. Also, they showed that UV-irradiated cells, transformed with HPV E6, are devoid of a UV-induced p53-dependent induction of $p21^{WAF1/CIP1}$ protein levels, due to E6-mediated degradation of p53. So, although several caveats have been associated with hTERT-immortalisation, the current literature suggests that the exploitation of hTERT in the establishment of permanent cell lines provides a superior alternative for the long-term *in vitro* propagation of cell cultures and

investigations into the DNA damage response and repair mechanisms (Bates *et al.*, 2005; Cordeiro *et al.*, 2002; Ouellette *et al.*, 2000; Porter *et al.*, 2006).

The mutator phenotype exhibited by XP cells is exemplified by the high levels of UV-specific changes observed in key regulatory genes in XP skin tumours. These modifications are also observed in the same genes modified in sporadic skin cancer in NER-proficient individuals. This reiterates the relevance of using XP as an *in vitro* model for dissecting the molecular pathogenesis underlying cutaneous malignancy (reviewed by Daya-Grosjean & Sarasin, 2005). Since the initial association between defective NER and the XP syndrome (Cleaver, 1968; Cleaver, 1969), cells derived from XP patients, have been characterised and established as permanent cell lines by oncogenic transformation, thereby providing *in vitro* culture models of carcinogenesis.

Currently, established cell lines derived from syndromes of genome instability such as XP, CS and TTD, are predominantly limited to those created by SV40 LTAg, or through HPV 16 E6/E7 oncogenic viral protein transformation. Although these cell lines were satisfactory for complementation studies and elucidating the mechanistic function of the NER machinery, as they retained their DNA repair defect, investigations at the molecular level are problematic due to the abrogation of the p53/p21$^{WAF1/CIP1}$ and pRb/p16^{INK4A} pathways. This not only results in the removal of the DNA damage response, but is also thought to severely compromise the NER pathway. Therefore, the application of cell lines established through oncogenic transformation for long-term *in vitro* NER studies, involving genetic manipulation or molecular analysis has a multiplicity of associated caveats. From the body of evidence, there is a need for immortalised cell lines that retain DNA damage response mechanisms and reflect the NER capacity displayed by their primary isogenic counterpart, but are devoid of the compounding genetic changes frequently observed in cancer-derived cell lines.

To date, alternative XP and CS cell lines, established by telomerase-immortalisation, remains limited to XP-E (GM01389), XP-V (GM02359, XP115LO) and CS-B (GM00739B, CS1AN) fibroblasts (Ouellette *et al.*, 2000; Newman *et al.*, 2006). The telomerase-mediated immortalisation of primary cells

derived from the XP and CS complementation groups such as XP-C and CS-A, respectively, remains unreported. Furthermore, although Ouellette *et al.* (2000) & Newman *et al.* (2006) demonstrated the successful establishment of telomerase-immortalised XP-E, XP-V and CS-B cells, the p53/p21$^{WAF1/CIP1}$ and pRb/p16^{INK4A} pathways were never characterised. Moreover, the applicability of currently available telomerase-immortalised cell lines, as *in vitro* culture models of genome instability, has remained poorly delineated. More importantly, the ability to recapitulate their *in vivo* phenotype such as DNA repair capacity remains relatively unknown.

4.2 Aims

To address the lack of robust *in vitro* XP-C and CS-A culture models with retained tumour suppressor function and an NER capacity reflecting their primary isogenic counterpart, the aim of this investigation was to establish novel hTERT-immortalised XP-C (GM02996, XP8CA) and CS-A (GM01856, CS3BE) human dermal fibroblasts possessing: (1) reconstituted telomerase (hTERT) activity; thereby removing p53 activating senescence signals; (2) an extended proliferative lifespan; (3) retained p53/p21$^{WAF1/CIP1}$ pRb/p16^{INK4A} tumour suppressor function; (4) repair capacity that recapitulates their primary isogenic counterparts. A further aim was to evaluate their potential applicability in *in vitro* NER assays.

The successful establishment of these cell lines will permit the preservation of a relatively 'normal' phenotype that resembles their primary isogenic counterpart, thereby providing a biologically pertinent *in vitro* cell culture model for NER studies. The extension of proliferative lifespan will permit clonal expansion for subsequent long-term genetic, biochemical and functional *in vitro* DNA repair assays.

4.3 Materials and methods

Primary human dermal fibroblasts, derived from XP-C and CS-A individuals were purchased from the NIGMS Human Genetic Mutant Cell Repository (Coriell Institute for Medical Research, Camden, NJ) and the *XPC* and *CKN1* gene variants were characterised, respectively, as previously described (Chapter 3; Ridley *et al.*, 2005).

Retroviral supernatants, containing pBABE-neo-hTERT was previously prepared and made available as a general reagent for the laboratory (Section 2.2). The catalytic sub-unit of telomerase, hTERT, was transduced into primary XP-C (GM02996, XP8CA) and CS-A (GM01856, CS3BE) human dermal fibroblasts, using an amphotropic retroviral vector (ψCRIP-pBABE-neo-hTERT), co-expressing hTERT and the neomycin phosphotransferase selectable (G418) gene marker or an empty pBABE-neo vector, as previously described (Section 2.2). To confirm telomerase activity approximately 5000 cell equivalents/μl was assayed using the TRAP assay (Sections 2.8.1-4).

For the detection of p53, p53(Ser15), $p21^{WAF1/CIP1}$, pRb and $p16^{INK4A}$ protein, immunoblotting was performed using a Biorad Mini-Protean II Electrophoresis Cell System. Briefly, cells were irradiated or mock-irradiated (Section 2.6) and WCEs were prepared as previously described (Sections 2.9.1-2.9.2). Proteins were separated on SDS-PAGE gels (Section 2.9.3), transferred to PVDF membranes (Section 2.9.3) and exposed to the appropriate primary antibody (Section 2.9.4 & Table 2.1). Blots were visualised using an appropriate HRP-coupled secondary antibody (Section 2.9.4 & Table 2.1) and an ECL system using Hyperfilm (Section 2.9.4). Equal protein loading was confirmed by staining the PVDF membrane with India ink (Section 2.9.5).

For the immunocytochemical detection of $p21^{WAF1/CIP1}$, the VECTRASTAIN® ABC system (Vector Laboratories, Peterborough, UK) was used as previously described (Section 2.10).

For colony forming ability assays, initial plating efficiencies were undertaken for each cell line (Section 2.5). UV survival curves were constructed by seeding cells in 100 mm dishes at varying cloning densities between 5 X 10^2-2 X 10^3 (depending upon cell-type) to produce monoclonal populations. Dishes were irradiated with 0-10 J/m^2 in increments of 2 J/m^2 as previously described (Section 2.6). Cells were incubated for the indicated time period (days), fixed with methanol: acetic acid (3:1) and stained in Giemsa's solution. Purple colonies with a minimum of 50 cells were scored. Three data points (UV-irradiations) were obtained per experiment, which was performed in triplicate. Therefore, each data point is representative of nine replicates.

The global repair of CPDs and 6-4PPs was measured using a standard immuno-slot-blot assay. Briefly, 1 X 10^6 cells were seeded into multiple 100 mm Petri dishes and subconfluent hTERT-immortalised MRC-5, XP-C (GM02996, XP8CA) and CS-A (GM01856, CS3BE) fibroblasts were irradiated with UVC (10 J/m^2). Dishes were maintained under routine culture conditions for an indicated period of time (hours). Genomic DNA was isolated and purified, using RNase A treatment and overnight proteinase K digestion, followed by phenol/chloroform extraction (Section 2.11.1). For each time point 500 or 1000 ng of DNA was used for the detection of UV-induced photolesions. DNA was denatured and the immuno-slot-blot assay was undertaken by Dr. Shirong Yu, using the Bio-Dot SF Microfiltration apparatus (Section 2.7). The detection of CPDs or 6-4PPs was performed by incubating the membrane with either the H3 CPD- or 6-4PP-specific monoclonal mouse antibodies (Mori *et al.*, 1991). The membrane was incubated with an alkaline phosphatase-linked anti-mouse secondary antibody and detection was performed using the ECF™ Western Blotting Analysis System Kit. The fluorescent emission from the samples bound to the membrane was detected using a STORM 860 phosphorimager and quantification was performed using ImageQuant software. The percentage of lesions remaining at each time point was calculated in comparison to the lesions present immediately (0 hours) after UV-irradiation. Three biological replicates were performed for each indicated time point.

4.4 Results

4.4.1 Ectopic expression of the catalytic subunit of telomerase, hTERT, in XP-C and CS-A primary dermal fibroblasts resulted in the reconstitution of telomerase activity

XP-C and CS-A human fibroblasts were transduced at PDs 17 and 1, respectively, with a replication-defective amphotropic pBABE retroviral vector co-expressing hTERT cDNA, and the neomycin (G418) resistance gene. In parallel, primary XP-C and CS-A fibroblasts were also infected with an empty pBABE-neo (control) vector, or mock-infected (nontransduced). XP-C and CS-A cells transduced with the amphotropic retroviral vector, expressing hTERT, or the empty control vector were assigned as 0 PD post infection. Two days posttransduction, XP-C and CS-A dermal fibroblasts, infected with ψCRIP-pBABE-neo-hTERT, were serially diluted in non-selective medium and seeded at densities appropriate for the generation of polyclonal and monoclonal populations. Primary XP-C and CS-A fibroblasts, infected with the empty amphotropic (control) vector or mock-infected (nontransduced), were propagated as polyclonal populations. Fibroblasts infected with the ψCRIP-pBABE-neo-hTERT vector, empty pBABE-neo vector, or mock infected (nontransduced) were refed 24 hours post dilution with selective medium, containing G418 at a concentration of 400 μg/ml. After serial dilution of transduced cells, 29 XP-C and 21 CS-A monoclonal populations, each derived from a single cell, were isolated and expanded in culture, and passaged continuously with G418 drug selection.

Both the hTERT transduced primary XP-C and CS-A fibroblasts were assayed for telomerase activity through the utilisation of the TRAP assay (Kim *et al.*, 1994). In addition, negative controls were prepared for each lysate (as previously described in Section 2.8.2), by incubating an aliquot of each sample at 85°C for 10 minutes to destroy telomerase activity. In addition, cell extracts, prepared

from the adenovirus 5-transformed 293 cell line, derived from HEK cells and known to express telomerase, were used as a positive control. TRAP reaction products appear as a ladder of bands with a periodicity corresponding to the size of the 6 bp tandem telomeric repeat sequence, TTAGGG. This confirmed the reconstitution of telomerase activity following the ectopic expression of hTERT.

As shown in Fig. 4.1, the retroviral infection of primary XP-C fibroblasts with the empty pBABE-neo vector did not confer telomerase activity (Fig. 4.1, lanes 1 & 2). Conversely, telomerase activity was detected in the non heat-treated extract prepared from the polyclonal population of XP-C fibroblasts, infected with pBABE-neo-hTERT (Fig. 4.1, lanes 21). As expected, telomerase activity was not detected in the heat-treated sample (Fig. 4.1, lane 22). In addition to the control extracts, 9 representative monoclonal populations of XP-C cells, infected with pBABE-neo-hTERT, were assayed for telomerase activity by the TRAP assay (Fig. 4.1, lanes 3-20). The majority of non heat-treated extracts, prepared from the monoclonal populations of XP-C fibroblasts, infected with pBABE-neo-hTERT, displayed similar levels of telomerase activity. As expected, all heat-treated XP-C extracts, prepared from the monoclonal populations, were negative for telomerase activity.

Telomerase activity was found to be absent in both the heat-treated and non heat-treated cell extract, prepared from the polyclonal population of human CS-A fibroblasts, infected with the empty pBABE-neo vector (Figs. 4.2A-C, lanes 3 & 4). Conversely, telomerase activity was detected in the cell extract prepared from the polyclonal population of CS-A fibroblasts, infected with pBABE-neo-hTERT (Figs. 4.2A-C, lane 5), while telomerase activity was absent in all heat-treated samples. All non heat-treated cell extracts, prepared from 14 representative monoclonal populations of CS-A fibroblasts at various PDs, following retroviral infection of pBABE-neo-hTERT, displayed telomerase activity (Figs. 4.2A-C). Moreover, the level of telomerase activity detected in the monoclonal populations of CS-A fibroblasts, infected with hTERT, was comparable to the telomerase activity detected in cell extracts prepared from control 293 cells (Figs. 4.2A-C, lane 1). The data presented here, suggests that the ectopic expression of

the catalytic unit of telomerase, hTERT, is sufficient to restore telomerase activity *in vitro* in both the primary XP-C and CS-A fibroblasts.

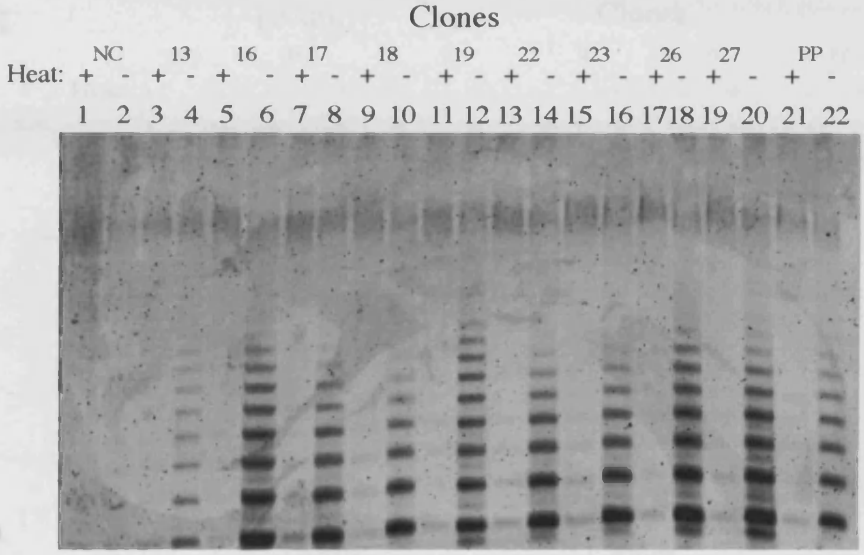

Figure 4.1. Reconstitution of telomerase activity in primary XP-C (GM02996, XP8CA) human dermal fibroblasts following retroviral infection with pBABE-neo-hTERT or an empty pBABE-neo vector. TRAP assays were performed as previously described (Kim *et al.*, 1994). Lanes 1 & 2, NC (negative control); cell extracts derived from polyclonal population infected with an empty pBABE-neo vector; lanes 3-20, cell extracts prepared from monoclonal populations infected with pBABE-neo-hTERT; lanes 21-22, cell extracts obtained from polyclonal population (PP) infected with pBABE-neo-hTERT. Each sample was assayed with (+) or without (-) prior heat treatment (85°C for 10 minutes).

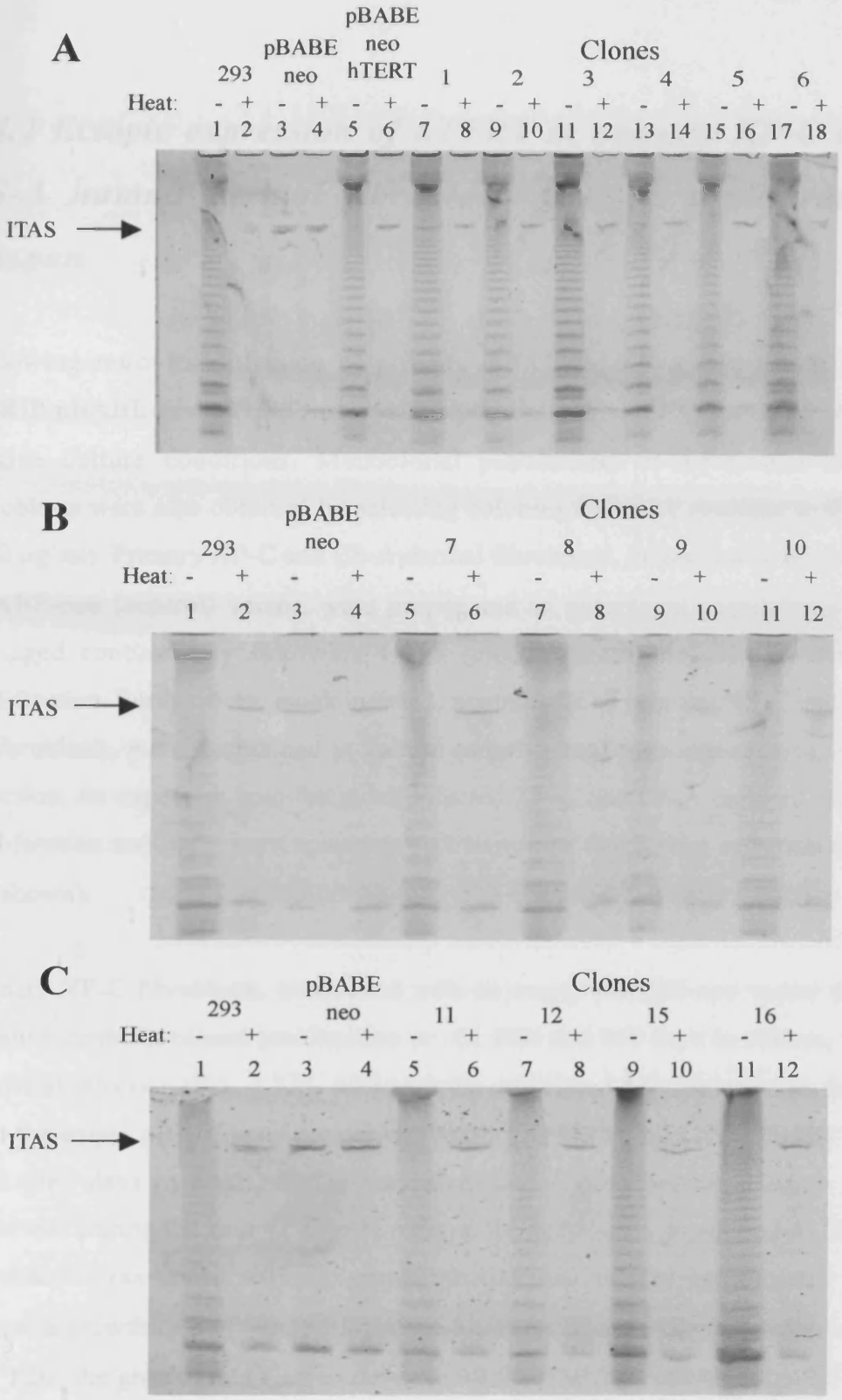

Figure 4.2. Determination of telomerase activity by TRAP assay in CS-A primary human fibroblasts (GM01856, CS3BE) following retroviral infection with pBABE-neo-hTERT. Each sample was assayed with (+) or without (-) prior heat treatment (85°C for 10 minutes). The immortal human epithelial cell line, 293, was included as a positve control. The arrows represent the position of the internal telomerase amplification standard (ITAS) as a control for inhibition during the PCR reaction. (A) Epithelial cell line 293, CS-A pBABE-neo (negative control) and CS-A pBABE-neo-hTERT polyclonal populations, CS-A pBABE-neo-hTERT - clones 1-6. (B) Epithelial cell line 293, CS-A pBABE-neo and CS-A pBABE-neo-hTERT polyclonal population, CS-A pBABE-neo-hTERT clones 7-10. (C) Epithelial cell line 293, CS-A pBABE-neo and CS-A pBABE-neo-hTERT polyclonal populations, CS-A pBABE-neo-hTERT clones 11, 12, 15 & 16.

4.4.2 Ectopic expression of hTERT in primary XP-C and CS-A human dermal fibroblasts extends proliferative lifespan

Following retroviral infection of primary XP-C and CS-A fibroblasts with ψCRIP-pBABE-neo-hTERT, polyclonal populations were propagated under routine culture conditions. Monoclonal populations of XP-C and CS-A fibroblasts were also obtained by selecting colonies that were resistant to G418 (400 μg/ml). Primary XP-C and CS-A dermal fibroblasts, infected with an empty pBABE-neo (control) vector, were propagated as polyclonal populations and passaged continuously following G418 selection until the cultures ceased proliferation. Furthermore, mock infected, nontransduced primary XP-C and CS-A fibroblasts, were maintained in culture as polyclonal populations with G418 selection. As expected, both the mock-infected XP-C and CS-A cultures ceased proliferation and underwent apoptosis ~11 days post G418 drug selection (data not shown).

Primary XP-C fibroblasts, transduced with an empty pBABE-neo vector (NC; negative control), ceased proliferation at ~31 PDs and 258 days in culture, post retroviral infection (Fig. 4.3A). Although the polyclonal population (transduced with the empty pBABE-neo vector) was maintained in culture for a further 129 days (387 days in total), no further extension on proliferative lifespan was observed. During the first 41 days in culture, the polyclonal population of XP-C fibroblasts (transduced with the empty pBABE-neo vector) accumulated ~12 PDs at a growth rate of ~0.36 PDs/day. However, after 64 days in culture and ~17 PDs, the growth rate slowed down to ~0.07 PDs/day between days 65-258 post retroviral infection. Between days 259 and 387 the polyclonal population of XP-C cells (infected with the empty pBABE-neo vector) remained stationary at ~31 PDs. The culture ceased proliferation and appeared to enter a state of permanent growth arrest, which is the principle hallmark indicative of cellular senescence. Conversely, the polyclonal population of XP-C fibroblasts, infected with pBABE-neo-hTERT, was propagated continuously for ~138 PDs and 387

days in culture (Fig. 4.3A; MP). This culture displayed a logarithmic growth pattern during the propagation period in culture, and displayed a growth rate of ~0.36 PDs/day. At the point at which the culture was terminated (387 days post retroviral infection) and stored as a viable culture, the polyclonal population of XP-C fibroblasts (infected with pBABE-neo-hTERT) displayed no decline in growth rate.

The 29 monoclonal populations of XP-C fibroblast cultures, infected with pBABE-neo-hTERT, which exhibited resistance to G418, were maintained in culture for a minimum of ~23 PDs (Figs. 4.3B-F, 4.4A-F and 4.5A-C). The three monoclonal populations of XP-C fibroblasts (clones 16, 19 & 30), which exhibited the best growth characteristics, were maintained in culture for an additional ≥70 PDs (Fig. 4.3B), as immortality was defined at ≥100 PDs. This is the point at which a normal adult dermal *in vitro* culture, expressing HPV E6/E7, would typically reach a state of M2 'crisis' (Bond *et al.*, 1999). For this reason, any fibroblast culture continuing to proliferate ≥100 PDs was considered as immortal. Like the polyclonal population of XP-C cells, infected with pBABE-neo-hTERT, the monoclonal populations of XP-C cells (clones 16, 19 and 30) displayed a logarithmic growth pattern whilst in culture. XP-C pBABE-neo-hTERT clones 16, 19 and 30 exhibited comparable growth rates during propagation. Clones 16 and 30 accumulated ~98 and ~100 cumulative PDs in 247 days, respectively, while clone 19 accumulated ~106 PDs in 249 days (Fig. 4.3B).

As shown in Fig. 4.6A (NC), the transduction of primary CS-A fibroblasts, with an empty pBABE-neo vector, resulted in no extension of proliferative lifespan, and ceased proliferation after ~1.5 cumulative PDs and 21 days following retroviral infection. Conversely, the polyclonal population (PP) of isogenic primary CS-A fibroblasts, transduced with ψCRIP-pBABE-neo-hTERT (Fig. 4.6A), were propagated and grown continuously for 38 days under routine culture conditions post drug (G418) selection. Moreover, the polyclonal population continued to proliferate to the point at which the culture was terminated at ~16 PDs (Fig. 4.6A). The 21 monoclonal populations of CS-A

fibroblast cultures, infected with pBABE-neo-hTERT, which exhibited resistance to G418, were maintained in culture for a minimum of 19 PDs post retroviral infection (Figs. 4.6B-F & 4.7A-E). Following the confirmation of telomerase activity by the TRAP assay, three monoclonal cell cultures (clones 2, 3 and 8), infected with pBABE-neo-hTERT, which exhibited the best growth characteristics, were maintained under routine culture conditions for a further ~70 PDs to confirm the immortalised phenotype (Fig. 4.6B). Both CS-A (pBABE-neo-hTERT) clones 2 and 3 continued to display a logarithmic growth pattern, accumulating ~113 and ~116 PD respectively (Fig. 4.6B). Furthermore, both CS-A clones 2 and 3 continued to exhibit a logarithmic growth pattern until the point at which both cultures where terminated at 302 days post retroviral infection (Fig. 4.6B). Interestingly, however, a reduction in growth rate was observed in clone 8, which only accumulated ~77 cumulative PDs following 303 days in culture, at which point the culture was terminated and stored as a viable stock (Fig. 4.6B). The data presented here, suggests that the ectopic expression of hTERT not only resulted in the reconstitution of telomerase activity, but also extended the proliferative lifespan of the selected clones.

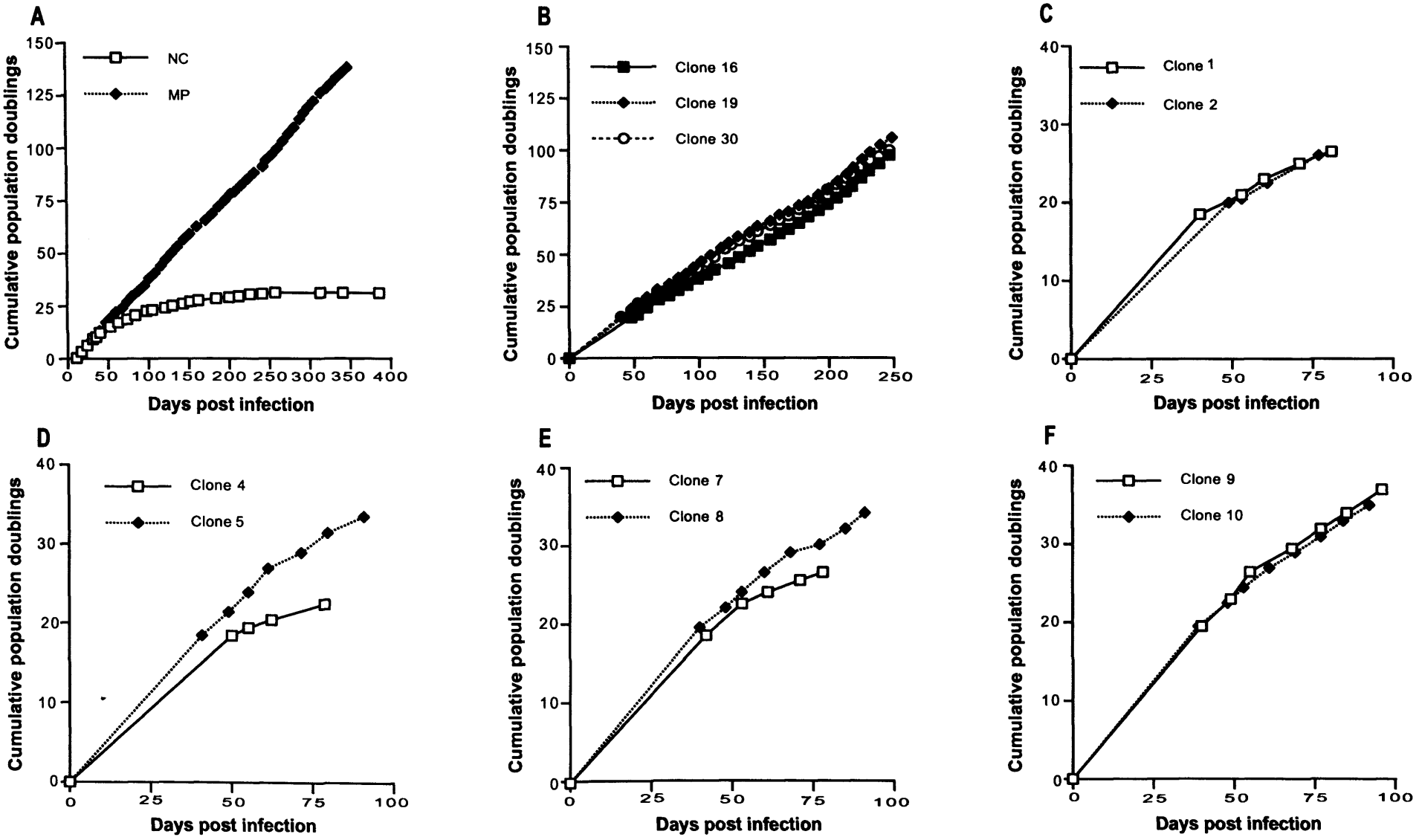

Figure 4.3. Extension of proliferative lifespan in monoclonal and polyclonal populations of XP-C (GM02996, XP8CA) human dermal fibroblasts following the ectopic expression of hTERT or an empty pBABE-neo vector. *Abbreviations*: NC, negative control; MP, mixed population.

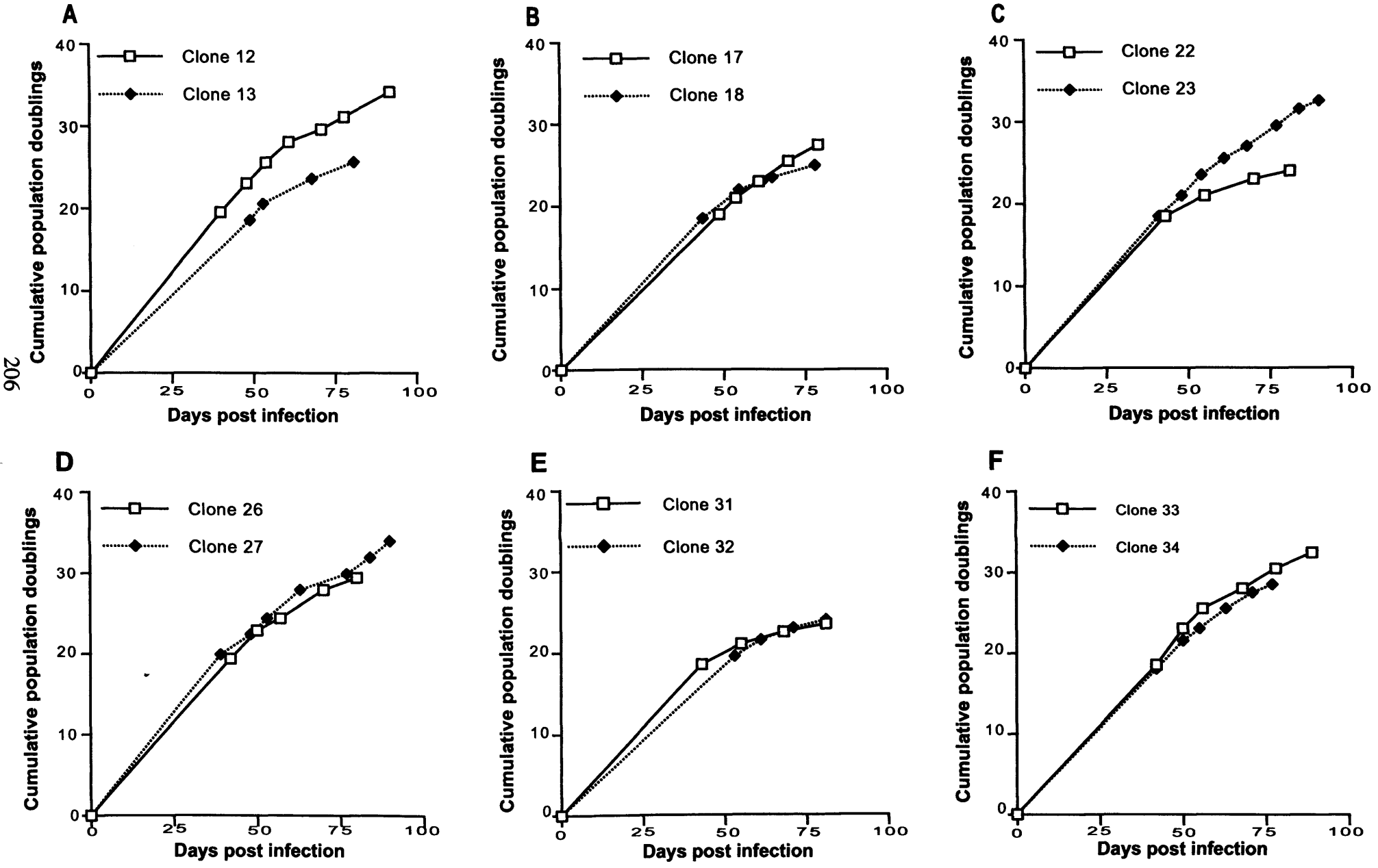

Figure 4.4. Proliferative lifespan of monoclonal populations of XP-C (GM02996, XP8CA) human dermal fibroblasts following the ectopic expression of hTERT.

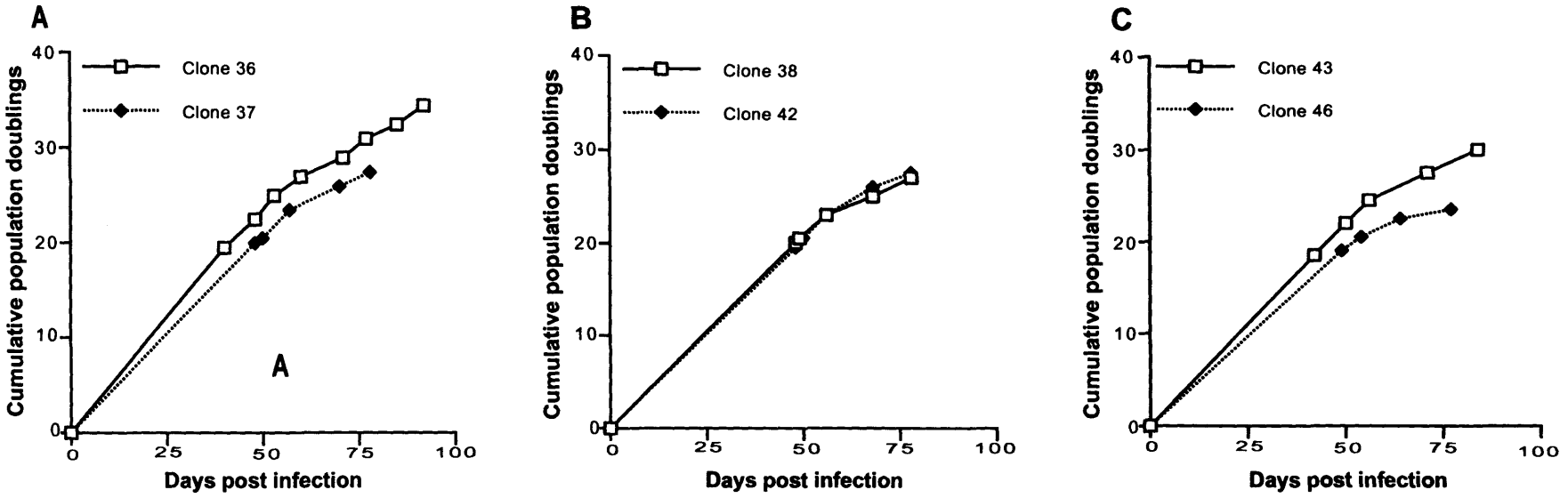

Figure 4.5. Proliferative lifespan of monoclonal populations of XP-C (GM02996, XP8CA) human dermal fibroblasts following the ectopic expression of hTERT.

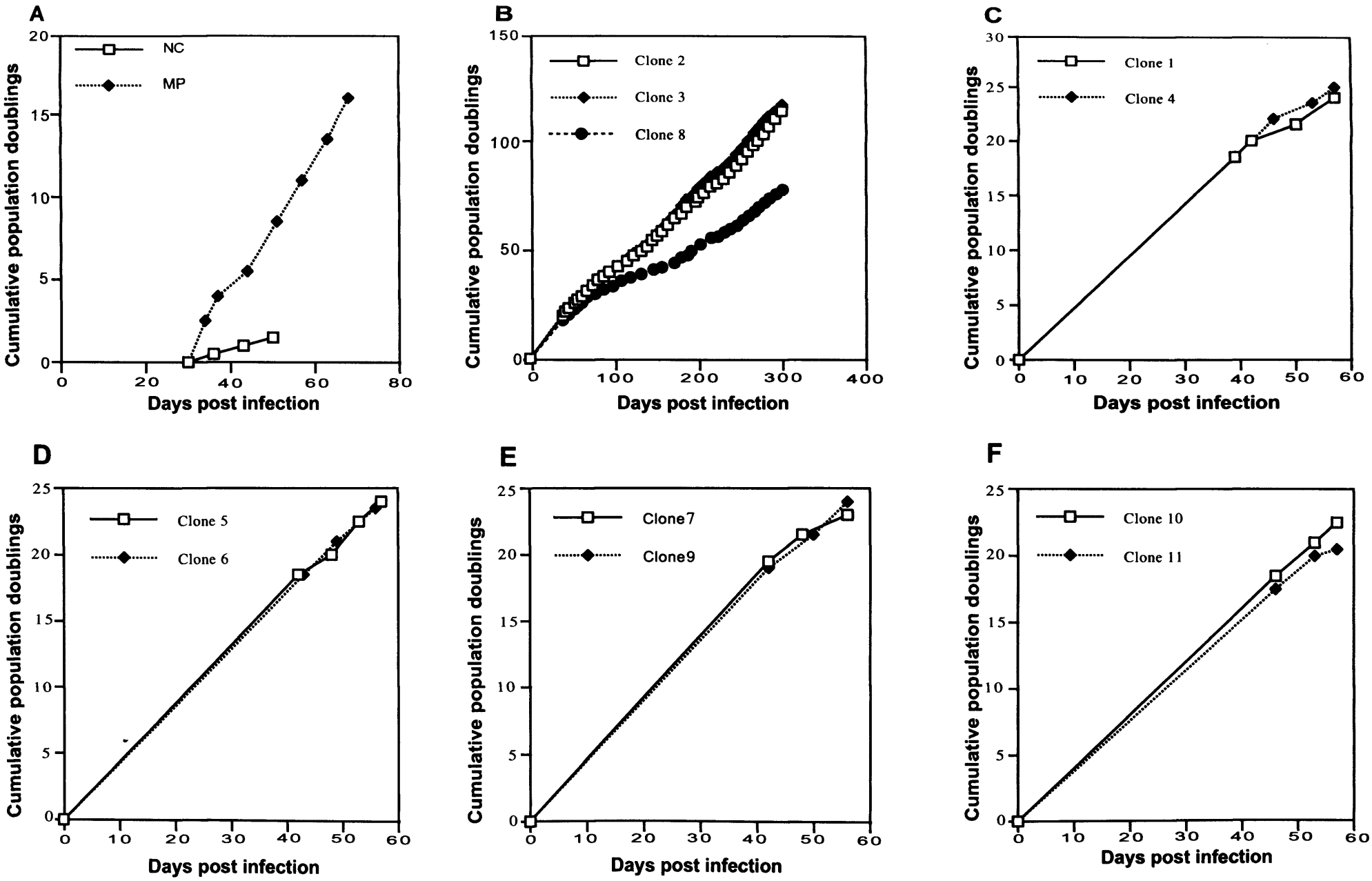

Figure 4.6. Extension of proliferative lifespan of CS-A (GM01856, CS3BE) human dermal fibroblasts following the ectopic expression of hTERT or an empty pBABE-neo vector. *Abbreviations*: NC, negative control; MP, mixed population.

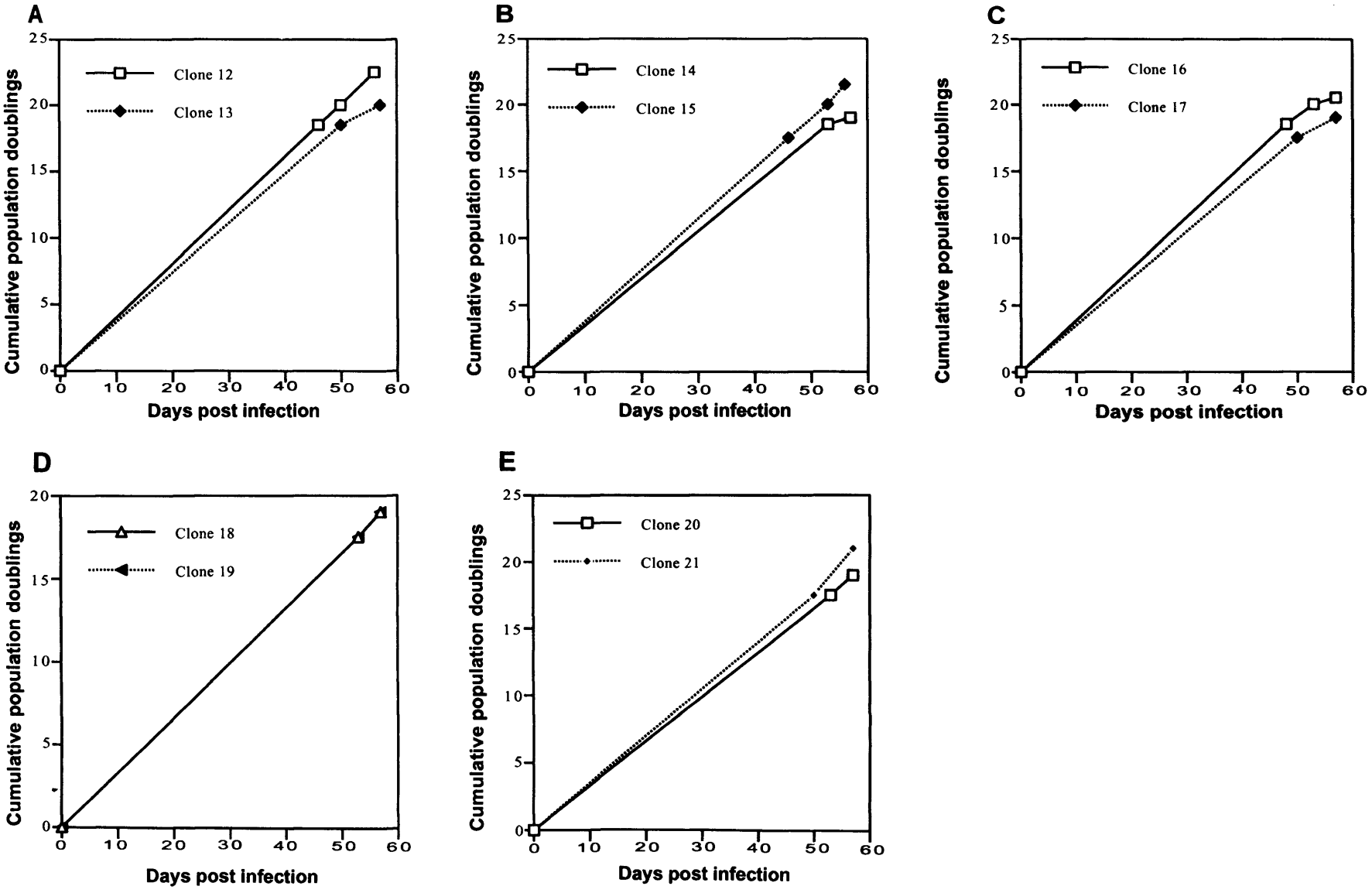

Figure 4.7. Extension of proliferative lifespan of monoclonal populations of CS-A (GM01856, CS3BE) human dermal fibroblasts following the ectopic expression of hTERT.

4.4.3 Morphological appearance of XP-C and CS-A human dermal fibroblasts following ectopic expression of hTERT

At various PDs, after the retroviral transduction of ψCRIP-pBABE-neo-hTERT or the empty pBABE-neo (control) vector, photomicrographs of the XP-C and CS-A fibroblasts where taken.

Primary XP-C fibroblasts, infected with an empty pBABE-neo (control) vector, exhibited a relatively normal morphology at PD 24 and 122 days in culture post retroviral infection (Fig. 4.8A). However, at PD 31 and 387 days in culture, the primary XP-C fibroblasts, infected with the empty pBABE-neo (control) vector, displayed an altered morphological appearance, consistent with changes typically exhibited by fibroblasts undergoing replicative senescence *in vitro*. The polyclonal population of XP-C cells appeared enlarged and flattened with a concomitant increase in the nucleus (Fig. 4.8B). The cells also appeared granulated, nonrefractile and exhibited a large number of stress fibres, all of which are hallmarks of cellular senescence. Further morphological alterations observed in the XP-C fibroblasts, infected with the empty pBABE-neo vector, included the appearance of cylindrical cytoplasmic cell surface projections and thin peripheral sheet structures frequently associated with cellular senescence, such as filopodia, lamellipodia and membrane ruffles (Fig. 4.8B). Conversely, the polyclonal population of XP-C fibroblasts transduced with ψCRIP-pBABE-neo-hTERT was morphologically characteristic of young dermal fibroblasts in culture at ~63 PDs (Fig. 4.8C). Similarly, the three monoclonal XP-C dermal fibroblast cultures (transduced with ψCRIP-pBABE-neo-hTERT) including clones, 16, 19 and 30, that were isolated and maintained in culture for ~98, ~106 and ~100 PDs, respectively, displayed a morphology indicative of young dermal fibroblasts growing exponentially *in vitro* (Figs. 4.8D, E & F, respectively). Although clones 16, 19 and 30 where photographed at various PDs (~68, ~74 and ~75, respectively), the monoclonal populations were morphologically similar, exhibiting minimal differences between clones.

Immediately following retroviral transduction (~1 PD), primary CS-A fibroblasts, infected with an empty pBABE-neo (control) vector, exhibited morphologic features, typically observed in senescent fibroblasts *in vitro* (Fig. 4.9A). Interestingly, however, the senescent morphological appearance exhibited by the CS-A fibroblasts was significantly more pronounced compared to the morphology displayed by senescent XP-C cells at later PDs (24 & 31) that were transduced with an empty pBABE-neo vector (Figs. 4.8A & B, respectively). The CS-A fibroblasts morphologically appeared enlarged, flattened and nonrefractile with an increased cytoplasmic to nuclear ratio. A significantly large proportion of the CS-A cells within the polyclonal population also displayed a fan-like shape. The CS-A fibroblasts exhibited fewer senescence-associated appendages, such as filopodia, which was significantly less pronounced, compared to XP-C pBABE-neo fibroblasts. However, morphologic features such as lamellipodia and membrane ruffles were exhibited by the CS-A pBABE-neo fibroblasts. Furthermore, a marked increase in the number of actin filament bundles (or 'stress' fibers) were observed in the cell body, compared to the XP-C fibroblasts, infected with the empty pBABE-neo vector. Conversely, the polyclonal population of CS-A dermal fibroblasts infected with ψCRIP-pBABE-neo-hTERT, exhibited a morphology indicative of young fibroblasts (Fig. 4.9B), compared to its isogenic counterpart infected with an empty pBABE-neo vector. Similarly, the isolated and expanded monoclonal CS-A cell populations, including clones 2, 3, and 8 (Figs. 4.9C, D & E, respectively), infected with pBABE-neo-hTERT, displayed a morphological appearance characteristic of young proliferating dermal fibroblasts.

Although clones 2, 3 and 8 exhibited reconstituted telomerase activity (Fig. 4.2A & B), an extended proliferative capacity (Fig. 4.6B) and a relatively normal morphological appearance (Figs. 4.9C, D & E, respectively), compared to the polyclonal population of primary CS-A fibroblasts infected with the empty pBABE-neo vector (Fig. 4.9A), a sub-population of cells within the monoclonal populations in the hTERT-immortalised cultures, displayed a senescent-like morphology. This was particularly evident in clone 8, where a large proportion of the cell population appeared to display a marked senescent-like phenotype (Fig.

4.9E), which was similar to its isogenic primary counterpart, transduced with the empty pBABE-neo vector (Fig. 4.9A).

The data presented here, suggests that the telomerised XP-C cells do not (by definition) enter growth arrest, nor do they take on the characteristic enlarged and vacuolated appearance observed in their primary isogenic senescent counterpart, transduced with the empty pBABE-neo vector. In contrast, although CS-A cells, infected with ψCRIP-pBABE-neo-hTERT, display a marked difference in morphological appearance compared to their isogenic primary counterpart infected with the empty pBABE-neo vector, a sub-population of cells displayed a senescent-like morphology.

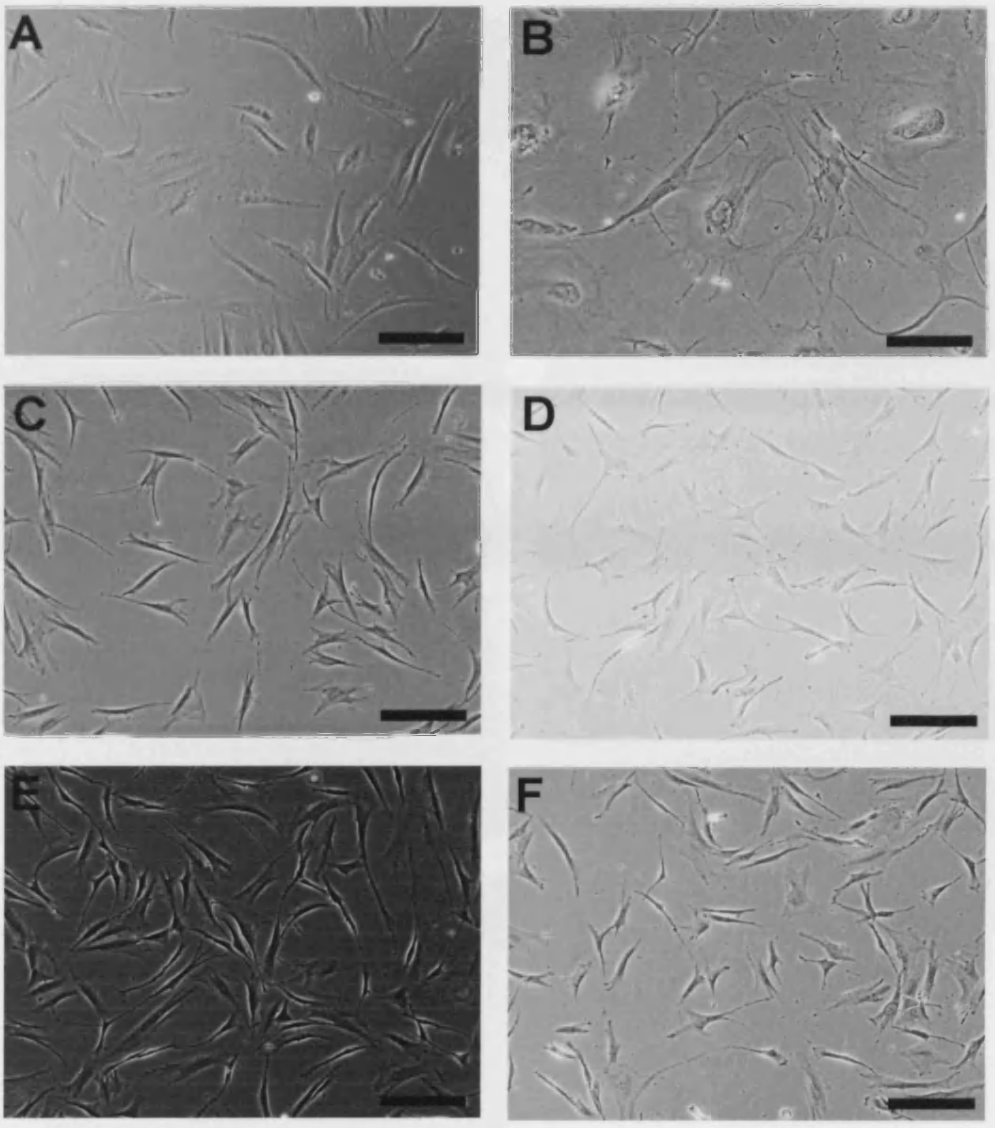

Figure 4.8. Morphological appearance of primary XP-C (XP8CA) dermal fibroblasts following retroviral transduction of ψCRIP-pBABE-neo-hTERT. Representative photomicrographs of polyclonal populations of primary XP-C dermal fibroblasts infected with an empty pBABE-neo control vector at (A) PD 24 & (B) PD 31.25, or (C) ψCRIP-pBABE-neo-hTERT (PD 62.5), or monoclonal populations (D) clone 16 (PD 68), (E) clone 19 (PD 73.5), (F) clone 30 (PD 74.5) infected with ψCRIP-pBABE-neo-hTERT. Bar = 100 μm.

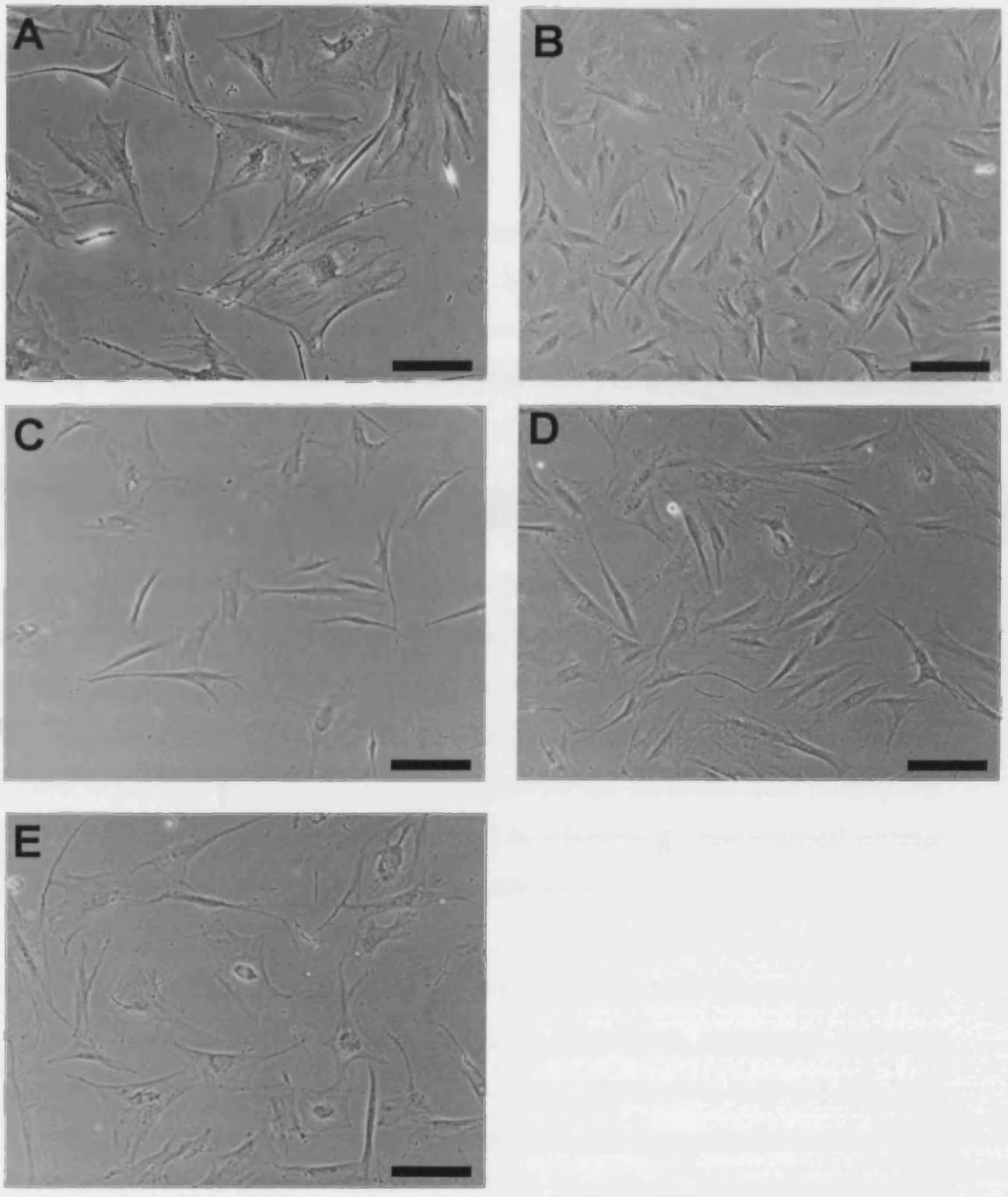

Figure 4.9. Morphological appearance of primary CS-A (CS3BE) dermal fibroblasts following retroviral transduction of ψCRIP-pBABE-neo-hTERT. Representative photomicrographs of polyclonal populations of primary CS-A dermal fibroblasts infected with (A) an empty pBABE-neo control vector (PD 0.5), or (B) ψCRIP-pBABE-neo-hTERT (PD 11), or monoclonal populations, (C) clone 2 (PD 49), (D) clone 3 (PD 45.5), (E) clone 8 (PD 38.5) infected with ψCRIP-pBABE-neo-hTERT. Bar = 100 μm.

4.4.4 Retained basal and inducible p53/p21$^{WAF1/CIP1}$ tumour suppressor function in hTERT-immortalised XP-C and CS-A human dermal fibroblasts

In addition to extended proliferative capacity, a further reason for the establishment of telomerase-immortalised XP-C and CS-A cell lines was the preservation of functional p53/p21$^{WAF1/CIP1}$mediated responses to DNA damage. Therefore, constitutive levels and the kinetics of UVC-induced, time-dependent accumulation of p53 and p21$^{WAF1/CIP1}$ protein was characterised in monoclonal populations of telomerase-immortalised XP-C (clone 19) and CS-A (clone 3) fibroblasts (transduced with hTERT) by Western blotting and immunocytochemical analysis. p53 expression was detected using an N-terminus antibody (DO-1), which binds to an epitope that targets amino acids 21-25. The basal level of p53 protein expression was determined over a 24 hour time-course at the indicated time points, via time-matched (non-irradiated) controls, examined in parallel to the UV-treated samples (at the indicated time points). As a control, p53 status was also characterised in telomerase-immortalised normal MRC-5 fibroblasts, which were previously established in our laboratory.

Basal levels of p53 protein expression in hTERT-immortalised normal MRC-5 and DNA repair-detective XP-C and CS-A fibroblasts remained constant throughout the time course and displayed minimal fluctuation between the time points following mock-irradiation (Figs. 4.10A-C). As expected, the level of p53 protein in telomerised MRC-5, XP-C and CS-A fibroblasts remained unchanged at 0 hours after UV (Figs. 4.10A-C), compared to their time-matched (0 hour) non-irradiated control. In contrast, p53 induction was observed at 6 hours in hTERT-immortalised MRC-5, XP-C and CS-A fibroblasts following a UVC dose of 10 J/m^2 (Fig. 4.10A-C). The high level of p53 protein was sustained throughout the time course and no further increase in p53 protein was observed at ~12 and ~24 hours in the MRC-5, XP-C or CS-A cells after UV (Figs. 4.10A-C).

Following DNA damage, cells elicit a multiplicity of cellular responses through the posttranslational modification and stabilisation of the p53 protein. In particular, phosphorylation of p53 at Ser15, located at the N-terminus, is a well-characterised posttranslational target, following UV exposure. To verify the preservation of p53 posttranslational modifications in response to UV, following the ectopic expression of hTERT, p53(Ser15) phosphorylation was evaluated by Western blot analysis, using a phospho-specific antibody.

Similarly to p53 accumulation, phosphorylation of p53 at Ser15 occurred in a time-dependent manner after treatment with UV (10 J/m^2). As expected, phosphorylation of p53 at Ser 15 was not observed in the time-matched, non-irradiated hTERT-immortalised MRC-5, or XP-C fibroblasts (Figs. 4.11A & B, respectively). However, the phosphorylation of p53 at Ser15 was observed in the time-matched, non-irradiated hTERT-immortalised CS-A fibroblasts (Fig. 4.11C). The phosphorylation of p53 at Ser15 reached a peak at ~6 hours, which subsequently decreased at ~12 and ~24 hours, following mock-irradiation (Fig. 4.11C).

As expected, phosphorylation at Ser15 was not detected in WCE prepared from telomerised MRC-5, XP-C and CS-A cells immediately after (0 hours) UV (Figs. 4.11A-C). Unlike the accumulation of p53 protein, the kinetics of p53 stabilisation at Ser15 occurred in a genotype-specific manner. Phosphorylation of p53 at Ser15 was observed in hTERT-immortalised MRC-5 fibroblasts at ~6 hours following UV treatment. The level of phosphorylation at Ser15 peaked at ~12 hours after UV-irradiation and was not detected at ~24 hours following UV-irradiation (Fig. 4.11A). In contrast, phosphorylation of p53 at Ser15 paralleled p53 accumulation in hTERT-immortalised XP-C fibroblasts in response to UV-irradiation (Fig. 4.11B). Similarly to p53 accumulation, phosphorylation of p53 at Ser15 was detected at ~6 hours. The level of phosphorylation at Ser15 remained elevated at ~12 hours and reached a peak at ~24 hours after UV. Similarly, phosphorylation of p53 at Ser15 in hTERT-immortalised CS-A fibroblasts was observed at ~6 hours following UV-irradiation (Fig. 4.11C). Like p53 accumulation, phosphorylation at Ser15 remained elevated at ~12 and ~24

hours after UV. However, further increases in phosphorylation at Ser15 were not observed. These data indicate that the posttranslational modification at Ser15, which facilitate the stabilisation of p53, has remained intact following the ectopic expression of hTERT.

Posttranslational modifications of p53, such as phosphorylation at Ser15, permit p53 to function as a transcription factor and regulate the transcriptional activation of downstream target genes. For example, p53-dependent cell cycle arrest at G_1 is partly regulated by the transcriptional activation of the downstream CDK inhibitor, $p21^{WAF1/CIP1}$, thus $p21^{WAF1/CIP1}$ activity can be used as an indirect functional marker of p53. Therefore, the kinetics of $p21^{WAF1/CIP1}$ accumulation was monitored over a 24 hour time course in response to UV, to further confirm normal p53 functionality.

Western blot analysis revealed that the level of $p21^{WAF1/CIP1}$ protein remained at basal levels in the time-matched, non-irradiated MRC-5 fibroblasts throughout the time course (Fig. 4.12A). Conversely, a fluctuation in $p21^{WAF1/CIP1}$ expression was observed in both the time-matched, non-irradiated XP-C and CS-A fibroblasts. In XP-C cells, high levels of $p21^{WAF1/CIP1}$ expression were observed at 0 and ~6 hours (Fig. 4.12B). Similarly, elevated levels of $p21^{WAF1/CIP1}$ were also detected in CS-A cells at 0 and ~6 hours (Fig. 4.12C). Following UV-irradiation, similar analysis revealed a gradual increase in $p21^{WAF1/CIP1}$ accumulation in hTERT-immortalised MRC-5 fibroblasts. $p21^{WAF1/CIP1}$ protein expression was induced at ~6 hours, and further increases were observed at both ~12 and ~24 hours following irradiation (Fig. 4.12A). In contrast, $p21^{WAF1/CIP1}$ induction reached a peak at ~6 hours in XP-C cells, while further increases in $p21^{WAF1/CIP1}$ protein levels were not observed at ~12 and ~24 hours. Like XP-C cells, induction of $p21^{WAF1/CIP1}$ was observed at ~6 hours in CS-A cells, following UV. Moreover, further increases in $p21^{WAF1/CIP1}$ expression were observed at ~12 and ~24 hours, where $p21^{WAF1/CIP1}$ levels appeared to peak at ~24 hours (Fig. 4.12C). The data presented here, show that $p21^{WAF1/CIP1}$ accumulation correlated with both p53 accumulation and phosphorylation at Ser15 in the hTERT-immortalised XP-C and CS-A fibroblasts following UV.

Interestingly, although $p21^{WAF1/CIP1}$ protein levels corresponded to the accumulation of p53 in hTERT-immortalised MRC-5 fibroblasts, a concomitant increase in p53 phosphorylation at Ser15 was not observed. Accordingly, these data suggest that the transcriptional activation of downstream target genes by p53, such as *CDKN1A*, is preserved following the ectopic expression of hTERT in MRC-5, XP-C and CS-A fibroblasts.

In concordance with the Western blot data (Figs. 4.12A-C), the $p21^{WAF1/CIP1}$ protein levels, detected by immunocytochemistry, recapitulated the UV-induced time-dependent accumulation of $p21^{WAF1/CIP1}$ (Figs. 4.13-15) that was observed in hTERT-immortalised MRC-5, XP-C and CS-A fibroblasts. However, due to the heterogeneous nature of $p21^{WAF1/CIP1}$ staining, the images presented here (Figs. 4.13-15), are not necessarily a precise representation of the percentage counts of $p21^{WAF1/CIP1}$ positive cells (obtained following immunocytochemical analysis; n=500 cells counted/coverslip).

In hTERT-immortalised MRC-5 cells, $p21^{WAF1/CIP1}$ expression remained at basal levels in the time-matched, mock-irradiated controls at all time points. The level of $p21^{WAF1/CIP1}$ was between 20-24% at 0, ~6, ~12 and ~24 hours (Figs. 4.13A, C, E & G, respectively). As expected, the level of $p21^{WAF1/CIP1}$ remained at basal levels immediately (0 hours) following UV (Fig. 4.13B). In stark contrast, a marked induction in $p21^{WAF1/CIP1}$ expression was observed at 6 hours post UV, with 37% of MRC-5 cells staining positive for $p21^{WAF1/CIP1}$ (Fig. 4.13D). This was indicated by the visualisation of a brown peroxidase reaction product. Dramatic increases of 70% and 81% were observed at ~12 and ~24 hours, respectively, after UV treatment (Figs. 4.13F & H, respectively). Immunocytochemical analysis resulted in the detection of $p21^{WAF1/CIP1}$ protein at 0 and ~6 hours in the hTERT-immortalised XP-C fibroblasts after mock-treatment, with 24% and 25% of cells staining positive for $p21^{WAF1/CIP1}$ (Figs. 4.14A & C, respectively). This was followed by a reduction in $p21^{WAF1/CIP1}$ levels at ~12 and ~24 hours, with 12% and 6%, respectively, staining positive (Figs. 4.14E & G). The higher levels of $p21^{WAF1/CIP1}$ detected at 0 and ~6 hours in the non-irradiated controls were comparable to the levels observed by Western

blot analysis (Fig. 4.12B). A small increase in $p21^{WAF1/CIP1}$ was observed at ~6 hours after UV, with 27% of cells staining positive for $p21^{WAF1/CIP1}$ (Fig. 4.14D). A marked increase was observed at ~12 and ~24 hours after UV treatment with 40% and 51%, respectively, of XP-C cells staining positive for $p21^{WAF1/CIP1}$ (Figs. 4.14F & H, respectively).

Interestingly, like XP-C, hTERT-immortalised CS-A fibroblasts exhibited a marked level of $p21^{WAF1/CIP1}$ staining in the time-matched non-irradiated controls. Approximately 21% and 39% of hTERT-immortalised CS-A fibroblasts were immunopositive for $p21^{WAF1/CIP1}$ staining at 0 and ~6 hours respectively, after mock-irradiation (Figs. 4.15A & C). In contrast, 13% and 14% of CS-A cells were immunopositive for $p21^{WAF1/CIP1}$ staining at ~12 and ~24 hours, respectively, after mock-irradiation (Figs. 4.15E & G). As expected, a marked increase in $p21^{WAF1/CIP1}$ staining was not observed at 0 hours (30%) after UV (Fig. 4.15B). No notable increase in $p21^{WAF1/CIP1}$ protein expression was observed at ~6 hours after UV with only 34% of CS-A cells staining positive for $21^{WAF1/CIP1}$ (Fig 4.15D). At ~12 hours and ~24 hours after UV, $p21^{WAF1/CIP1}$ staining dramatically increased with ~48% and ~64% of CS-A cells immunopositive for $p21^{WAF1/CIP1}$ (Figs. 4.15F & H).

In summary, the data presented here suggest that there was a time-dependent decrease in $p21^{WAF1/CIP1}$ expression in the hTERT-immortalised XP-C and CS-A cells, following mock-irradiation. Moreover, induction of p53, $p21^{WAF1/CIP1}$ and phosphorylation of p53 at Ser15 occurred in hTERT-immortalised MRC-5, XP-C and CS-A fibroblasts, in a time-dependent manner following 10 J/m^2 of UVC. Although the accumulation of p53 was comparable between the cell lines, the phosphorylation of p53 at Ser15 occurred in a genotype-specific manner and was more apparent in the hTERT-immortalised XP-C and CS-A cells, compared to the MRC-5 fibroblasts. Interestingly, Western blot analysis suggested that $p21^{WAF1/CIP1}$ accumulation was higher in the XP-C and CS-A cells, compared to the normal MRC-5 fibroblasts. However, immunocytochemical analysis suggested that higher $p21^{WAF1/CIP1}$ levels were observed in MRC-5 fibroblasts.

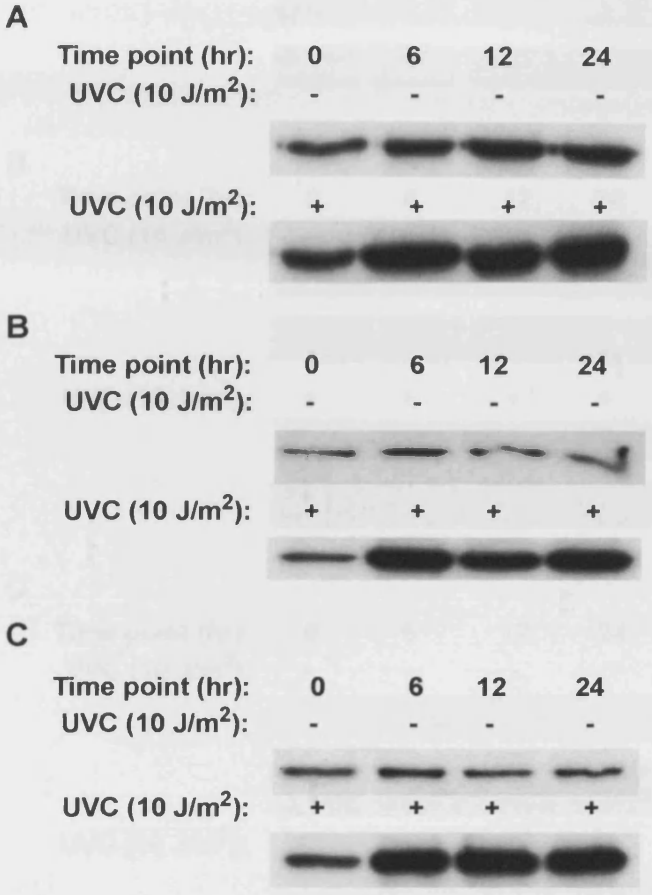

Figure 4.10. Western blot analysis of UVC-induced time-dependent induction of p53 protein, using an anti-p53 (DO-1) mouse monoclonal antibody (1:1000). Time course of p53 induction following mock-irradiation (-) or exposure to 10 J/m^2 (+) UVC in hTERT-immortalised (A) MRC-5, (B) XP-C (GM02996, XP8CA) and (C) CS-A (GM01856, CS3BE) fibroblasts (20 μg of WCE per lane).

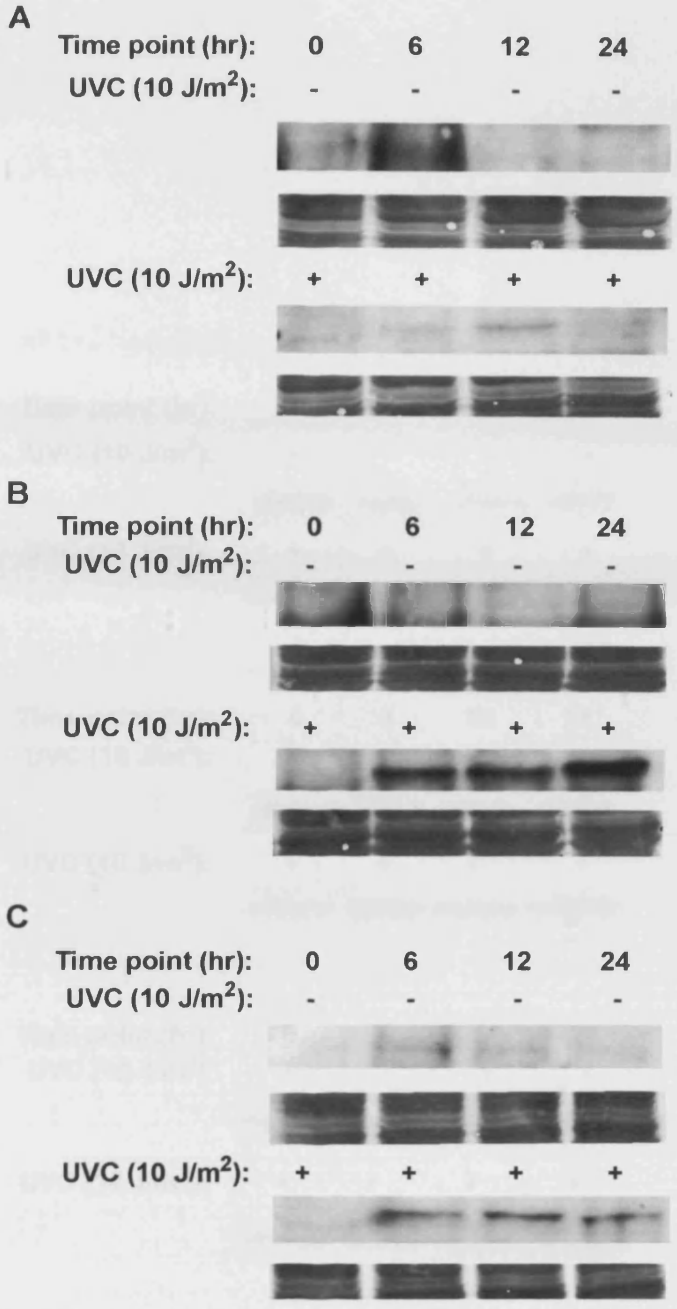

Figure 4.11. Western blot analysis of UVC-induced time-dependent phosphorylation of p53 on Ser15, using an anti-p53 (Ser15) mouse monoclonal antibody (1:1000). Time couse of p53 phosphorylation at Ser15 following mock-irradiation (-) or exposure to 10 J/m^2 (+) UVC in hTERT-immortalised (A) MRC-5, (B) XP-C (GM02996, XP8CA) and (C) CS-A (GM01856, CS3BE) fibroblasts (20 µg of WCE per lane). Equal protein loading was confirmed by India ink staining (*lower panel of each blot*).

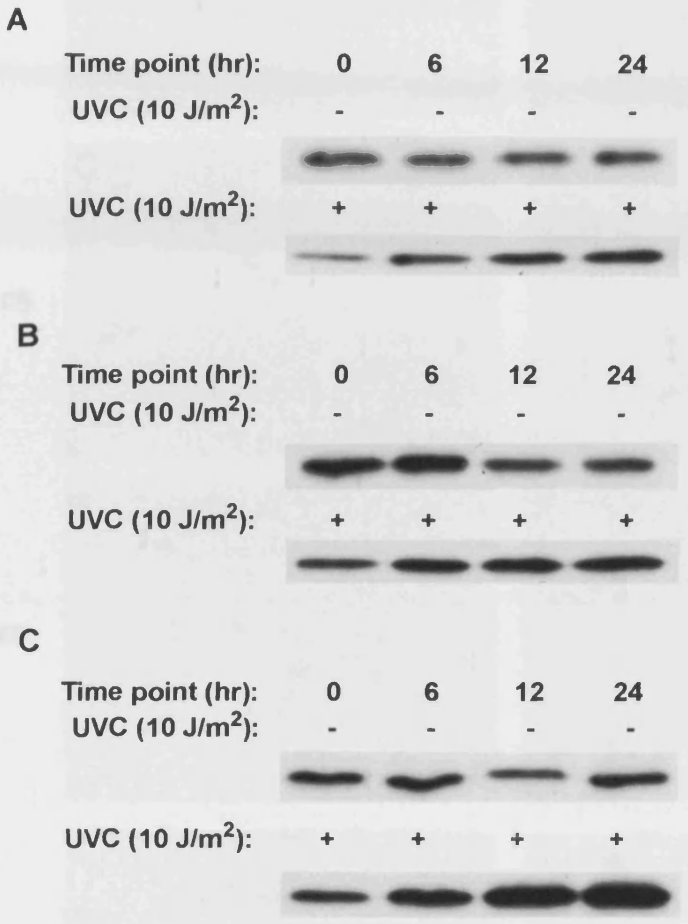

Figure 4.12. Western blot analysis of UVC-induced, time-dependent induction of $p21^{WAF1/CIP1}$ protein, using an anti-p21 mouse monoclonal antibody (1:250). Time couse of $p21^{WAF1/CIP1}$ induction following mock-irradiation (-) or exposure to 10 J/m^2 (+) UVC in hTERT-immortalised (A) MRC-5, (B) XP-C (GM02996, XP8CA) and (C) CS-A (GM01856, CS3BE) fibroblasts (20 μg of WCE per lane).

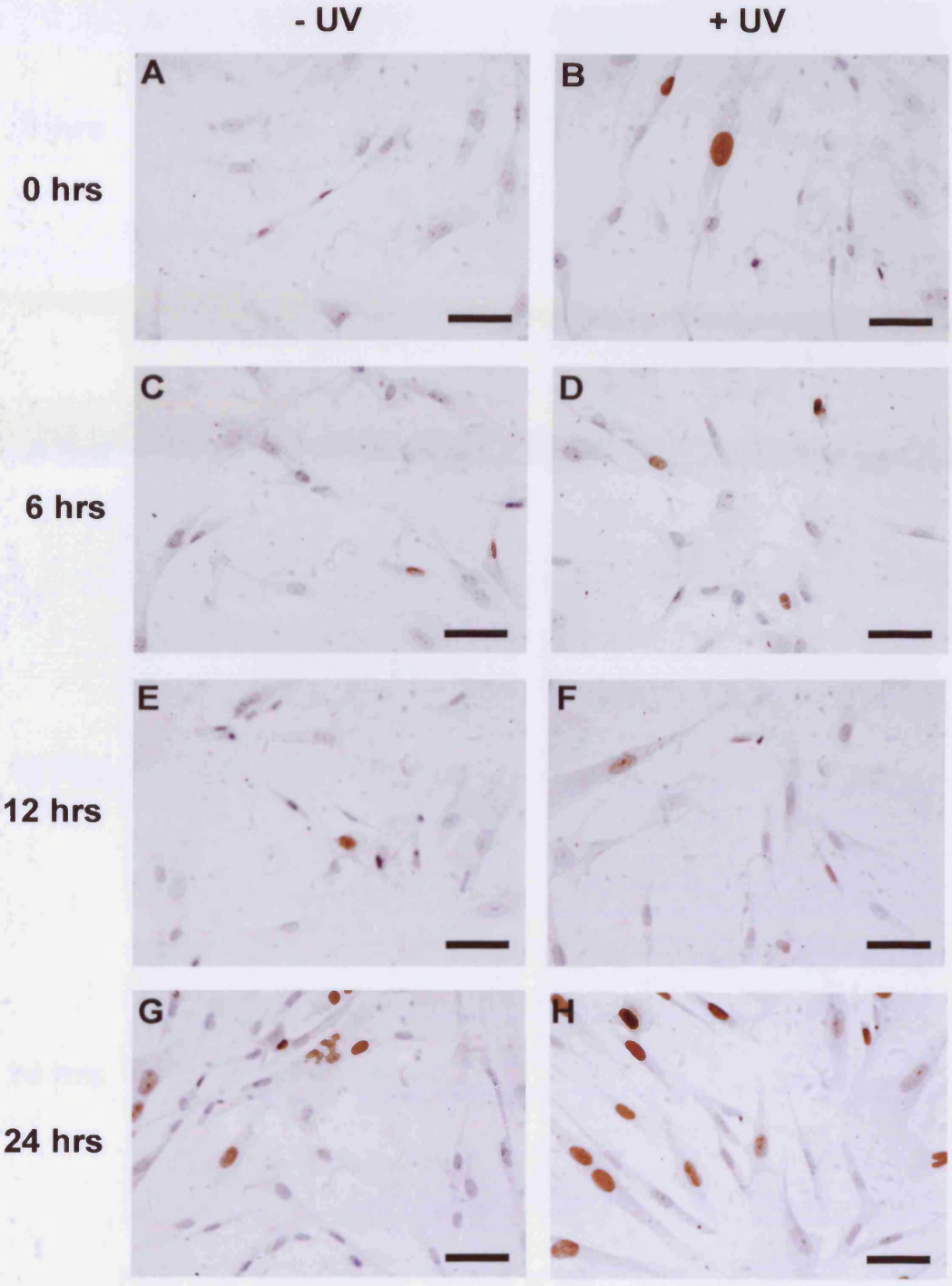

Figure 4.13. Time-dependent induction of $p21^{WAF1/CIP1}$ in hTERT-immortalised MRC-5 human lung fibroblasts in response to UVC-irradiation (10 J/m^2) or mock-irradiated (0 J/m^2), measured by ICC analysis, using a p21-specific antibody. Time course of $p21^{WAF1/CIP1}$ induction at (A) 0 hours, 0 J/m^2, (B) 0 hours, 10 J/m^2, (C) 6 hours, 0 J/m^2, (D) 6 hours, 10 J/m^2, (E) 12 hours, 0 J/m^2, (F) 12 hours, 10 J/m^2, (G) 24 hours, 0 J/m^2, (H) 24 hours, 10 J/m^2. Positivity indicated by a brown peroxidase reaction product. Nuclei were counterstained with haematoxylin to aid visualisation. Bar = 100 μm.

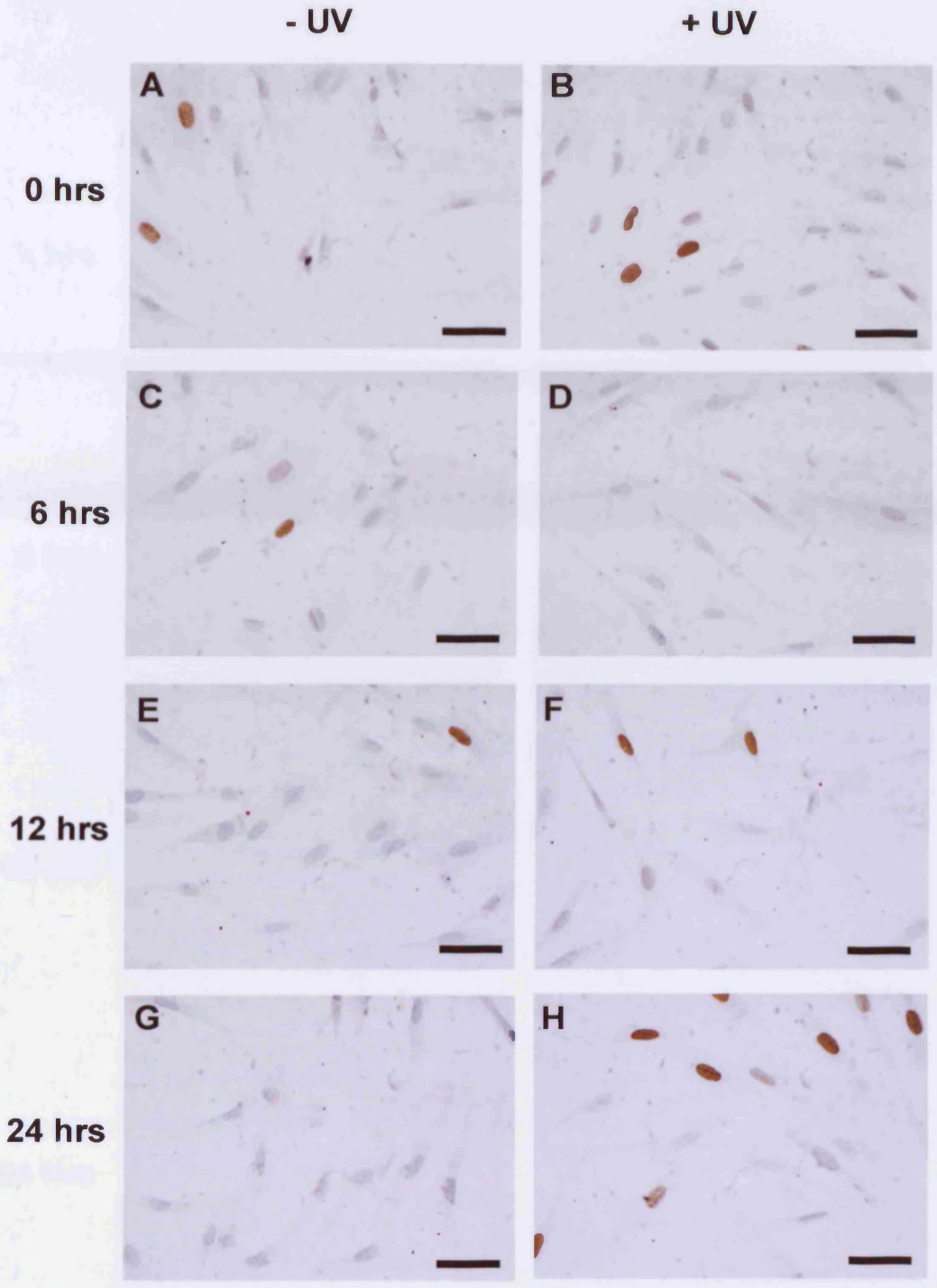

Figure 4.14. Time-dependent induction of $p21^{WAF1/CIP1}$ in hTERT-immortalised XP-C (GM02996, XP8CA) human dermal fibroblasts in response to UVC-irradiation (10 J/m^2) or mock-irradiated (0 J/m^2), measured by ICC analysis, using a p21-specific antibody. Time course of $p21^{WAF1/CIP1}$ induction at (A) 0 hours, 0 J/m^2, (B) 0 hours, 10 J/m^2, (C) 6 hours, 0 J/m^2, (D) 6 hours, 10 J/m^2, (E) 12 hours, 0 J/m^2, (F) 12 hours, 10 J/m^2, (G) 24 hours, 0 J/m^2, (H) 24 hours, 10 J/m^2. Positivity indicated by a brown peroxidase reaction product. Nuclei were counterstained with haematoxylin to aid visualisation. Bar = 100 μm.

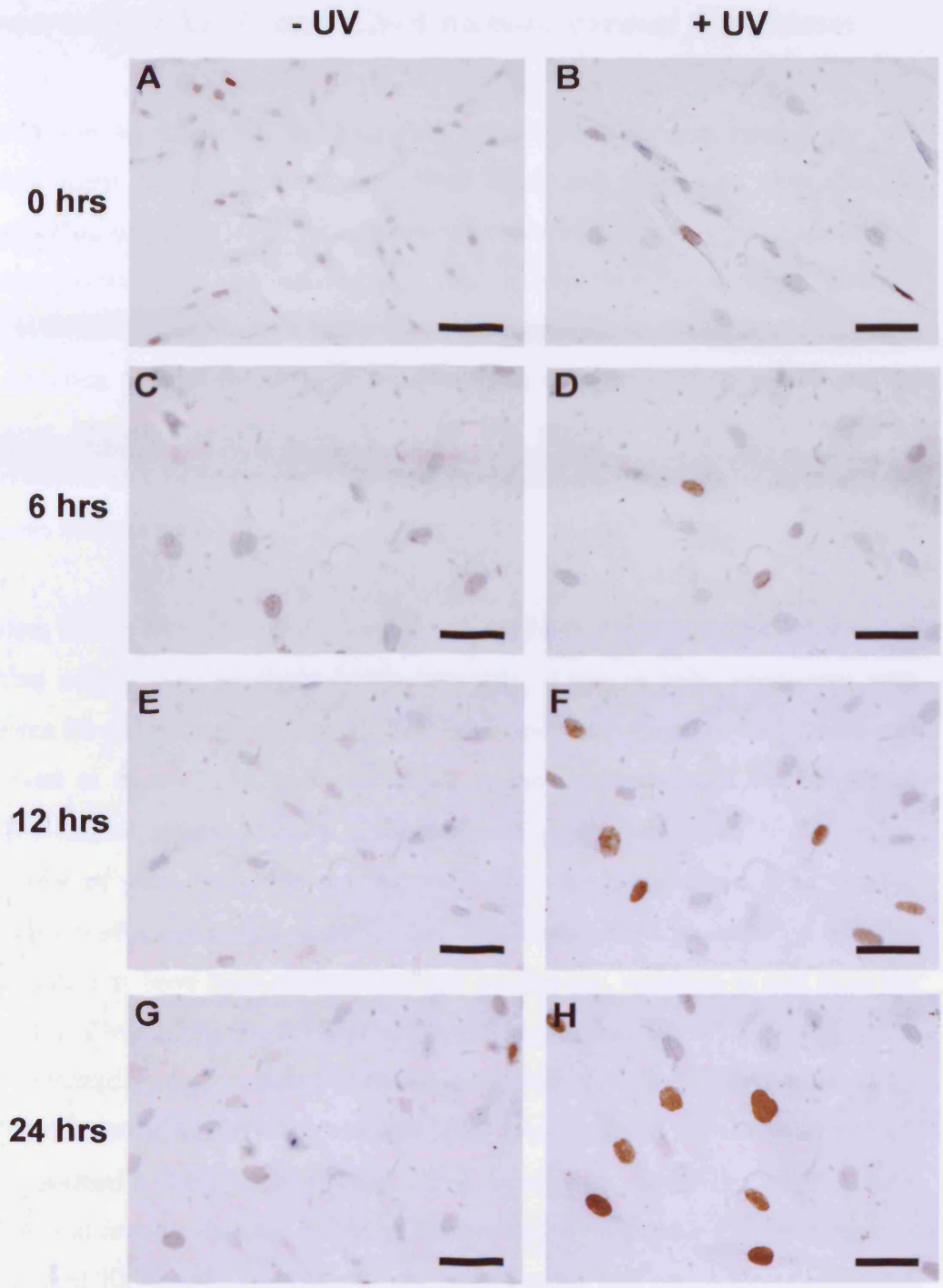

Figure 4.15. Time-dependent induction of $p21^{WAF1/CIP1}$ in hTERT-immortalised CS-A (GM01856, CS3BE) human dermal fibroblasts in response to UVC-irradiation (10 J/m^2) or mock-irradiated (0 J/m^2), measured by ICC analysis, using a p21-specific antibody. Time course of $p21^{WAF1/CIP1}$ induction at (A) 0 hours, 0 J/m^2, (B) 0 hours, 10 J/m^2, (C) 6 hours, 0 J/m^2, (D) 6 hours, 10 J/m^2, (E) 12 hours, 0 J/m^2, (F) 12 hours, 10 J/m^2, (G) 24 hours, 0 J/m^2, (H) 24 hours, 10 J/m^2. Positivity indicated by a brown peroxidase reaction product. Nuclei were counterstained with haematoxylin to aid visualisation. Bar = 100 μm (except A = 200 μm).

4.4.5 Retained pRb/p16^{INK4A} function in hTERT-immortalised XP-C and CS-A human dermal fibroblasts

In addition to extended proliferative capacity, a further reason for the establishment of telomerase-immortalised XP-C and CS-A cell lines was the preservation of pRb/p16^{INK4A} tumour suppressor activity. In order to establish whether constitutive and induced pRb protein expression was intact, Western blot analysis was performed using an anti-Rb-specific antibody that facilitated the detection of both the active hypophosphorylated form of Rb (pRb) and the inactive hyperphosphorylated form of Rb (ppRb). The preservation of constitutive and induced p16^{INK4A} protein expression was also confirmed by Western blot analysis.

Western blot analysis, using the Rb-specific antibody, resulted in the detection of Rb that migrated as multiple bands between ~110-116 kDa, consistent with different Rb phosphorylation states. Both pRb and ppRb forms of Rb protein was observed at 0, ~6, ~12 and ~24 hours in the time-matched, non-irradiated hTERT-immortalised MRC-5 fibroblasts (Fig. 4.16A). The lower band, indicative of pRb, appeared more intense than the upper band. The notable increase in pRb compared to ppRb that was observed in telomerised MRC-5 fibroblasts may have been attributed to cell confluency, resulting in exit from the cell cycle. Conversely, the level of ppRb was higher than the level of pRb in the time-matched, non-irradiated hTERT-immortalised XP-C fibroblasts (Fig. 4.16B). Similarly, a marked increase in ppRb was observed in the time-matched, non-irradiated hTERT-immortalised CS-A fibroblasts, while the level of pRb remained at low levels (Fig. 4. 16C). The increased ppRb/pRb ratio observed in telomerised XP-C and CS-A fibroblasts corresponded to a concomitant reduction in the cyclin-dependent kinase inhibitor, p21$^{WAF1/CIP1}$, which occurred at ~12 and ~24 hours (Fig. 4.12B & C). The reduced p21$^{WAF1/CIP1}$ expression and the increased level of ppRb observed in this study suggest that both the telomerised XP-C and CS-A fibroblasts were progressing through the G_1 to S cell cycle transition.

pRb and ppRb remained unchanged in telomerised MRC-5 fibroblasts at 0 hours following UV (Fig. 4.16A), compared to the levels observed in the time-matched, non-irradiated telomerised MRC-5 cells. A slight reduction in both pRb and ppRb was observed at ~6 and ~12 hours following UV, compared to the levels of pRb and ppRb observed at 0 hours (Fig. 4.16A). However, it is possible that this reduction was attributed to a slight reduction in the amount of protein present within the sample, as a reduction in band intensity was observed at ~6 hours following India ink staining (Fig. 4.16A, *lower panel*). Although slight differences in protein levels were observed, a reduction in the levels of pRb and ppRb at ~6 and ~12 hours after UV was also observed compared to the time-matched, non-irradiated controls. Although the ratio between pRb and ppRb remained similar, a concomitant increase was observed in both pRb and ppRb at ~24 hours post UV, compared to the levels observed at ~6 and ~12 hours following UV. However, the levels of both pRb and ppRb at ~24 hours after UV, appeared similar to those observed at ~24 hours, following mock-irradiation. The reduction in inactive hyperphosphorylated Rb at ~6 and ~12 hours, suggested that the MRC-5 cells entered a state of growth arrest at G_1 after UV. However, the subsequent accumulation of inactive ppRb at ~24 hours indicated that MRC-5 cells were committed to cell cycle progression, thereby completing the transition from the G_1 checkpoint arrest to S-phase.

A marked reduction in both pRb and ppRb was observed in hTERT-immortalised XP-C fibroblasts after UV, compared to the time-matched non-irradiated controls (Fig. 4.16B). Furthermore, telomerised XP-C fibroblasts exhibited a gradual reduction in the level of ppRb following UV (Fig. 4.16B), compared to the level of pRb, which remained unchanged. Similarly, the level pRb and ppRb was lower in irradiated telomerised CS-A fibroblasts, compared to the levels observed in the time-matched non-irradiated controls (Fig. 4.16C). Like XP-C fibroblasts, CS-A cells displayed a reduction in the level of ppRb at ~6, ~12 and ~24 hours after UV, compared to the time-matched non-irradiated controls. Interestingly, a marked reduction in both pRb and ppRb was observed at ~24 hours in telomerised CS-A cells after UV, compared to that observed at 0, ~6 and ~12 hours following UV, and the time-matched non-irradiated samples (Fig.

4.16C). The data presented here suggested that, Rb remained in an active dephosphorylated state in telomerised XP-C and CS-A fibroblasts following UV, thereby resulting in delayed G_1/S cell cycle progression.

$p16^{INK4A}$ protein levels remained unchanged throughout the time course in non-irradiated hTERT-immortalised MRC-5 fibroblasts (Fig. 4.17A). Although $p16^{INK4A}$ protein levels appeared unchanged in MRC-5 cells at 0 hours following UV-irradiation (Fig. 4.17A), a slight increase was observed at ~6 and ~12 hours. Moreover, the level of $p16^{INK4A}$ appeared to peak at ~24 hours, as a further increase was observed at ~24 hours post UV. Similarly, the constitutive expression of $p16^{INK4A}$ remained constant throughout the time course in non-irradiated hTERT-immortalised XP-C fibroblasts (Fig. 4.17B). In contrast, a progressive reduction in $p16^{INK4A}$ expression was observed at ~12 and ~24 hours in the time-matched, UV-irradiated hTERT-immortalised XP-C fibroblasts (Fig. 4.17B). $p16^{INK4A}$ levels remained unchanged in mock-irradiated hTERT-immortalised CS-A fibroblasts and following UV at all time points (Fig. 4.17C). Collectively, the data presented herein, suggested that although constitutive $p16^{INK4A}$ protein expression was observed in all telomerised cell lines following the ectopic expression of hTERT, a UV-induced induction of $p16^{INK4A}$ was limited to telomerised MRC-5 fibroblasts.

In summary, these data suggest that the elevated level of pRb, observed in non-irradiated MRC-5 fibroblasts was indicative of a G_1/S phase cell cycle arrest. UV-irradiation appeared to affect the pRb/ppRb ratio in telomerised XP-C and CS-A cells, as a reduction in ppRb was observed in both cell lines following UV. This suggested that both XP-C and CS-A cells entered a state of cell cycle arrest following UV. The levels of $p16^{INK4A}$ remained at basal levels in the non-irradiated controls. Interestingly, although an increase in the level of $p16^{INK4A}$ was observed in telomerised MRC-5 fibroblasts after UV, similar increases were not observed in both telomerised XP-C and CS-A fibroblasts. This suggested that $p16^{INK4A}$ was not UV inducible in both telomerised XP-C (GGR-defective) and CS-A (TCR-defective) cell lines.

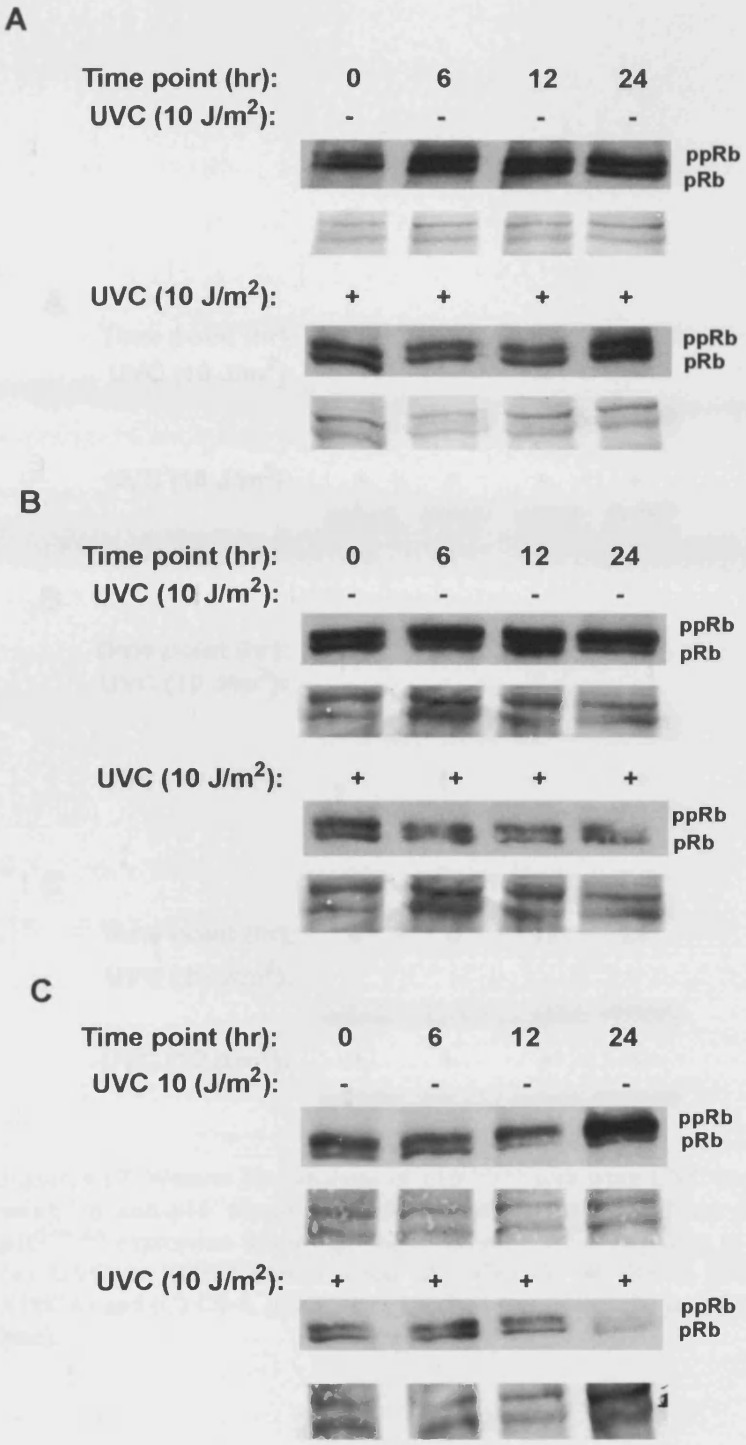

Figure 4.16. Western blot analysis of pRb following UV-irradiation, using an anti-pRb mouse monoclonal antibody (1:250). Time couse of pRb induction following mock-irradiation (-) or exposure to 10 J/m^2 (+) UVC in hTERT-immortalised (A) MRC-5, (B) XP-C (GM02996, XP8CA) and (C) CS-A (GM01856, CS3BE) fibroblasts (20 µg of WCE per lane). Equal protein loading was confirmed by India ink staining (*lower panel of each blot*). *Abbreviations*: pRb, hypophosphorylated Rb (*lower band*); ppRb, hyperphosphorylated (*upper band*).

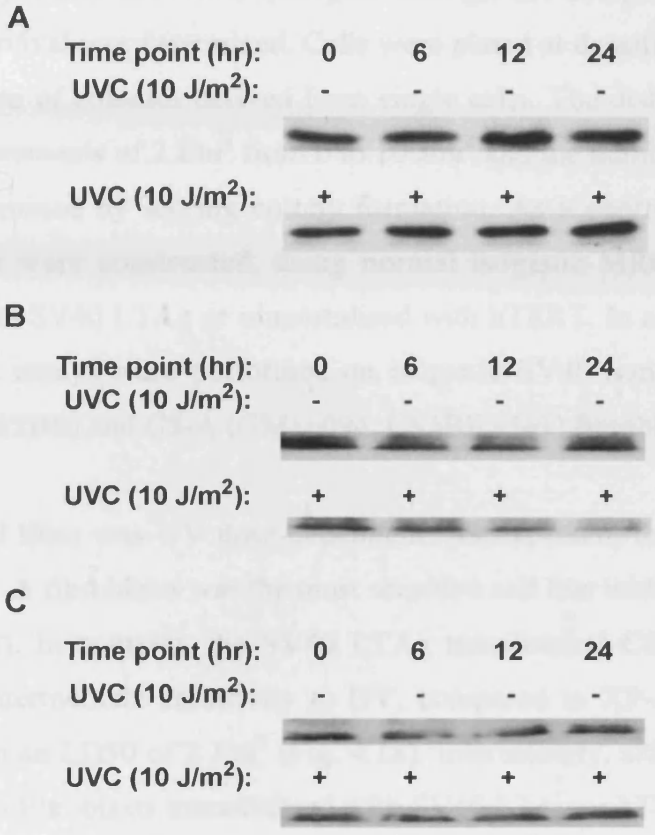

Figure 4.17. Western blot analysis of $p16^{INK4A}$ following UVC-irradiation, using an anti-p16 mouse monoclonal antibody (1:40). Time couse of $p16^{INK4A}$ expression following mock-irradiation (-) or exposure to 10 J/m^2 (+) UVC in hTERT-immortalised (A) MRC-5, (B) XP-C (GM02996, XP8CA) and (C) CS-A (GM01856, CS3BE) fibroblasts (20 µg of WCE per lane).

4.4.6 Survival curves of SV40-transformed fibroblasts following UV- irradiation

To establish whether there was a notable difference between the colony forming ability of asynchronous cultures of normal or repair-defective human fibroblasts, immortalised by either the SV40 LTAg or through the ectopic expression of hTERT, UV survival was determined. Cells were plated at densities that resulted in the production of colonies derived from single cells. The dishes were UVC-irradiated in increments of 2 J/m^2 from 0 to 10 J/m^2 and the number of surviving cells was determined by scoring colony formation. As a control, preliminary survival curves were constructed, using normal isogenic MRC-5 fibroblasts transformed with SV40 LTAg or immortalised with hTERT. In addition, colony forming ability assays were performed on isogenic SV40-transformed XP-A (GM04429, XP12BE) and CS-A (GM16094, CS3BE.s3g1) fibroblasts.

Survival of cell lines was UV dose-dependent. As expected, the SV40 LTAg transformed XP-A fibroblasts was the most sensitive cell line with a LD50 of 0.8 J/m^2 (Fig. 4.18). In contrast, the SV40 LTAg transformed CS-A fibroblasts displayed an intermediate sensitivity to UV, compared to XP-A and MRC-5 fibroblasts, with an LD50 of 2 J/m^2 (Fig. 4.18). Interestingly, although both the isogenic MRC-5 fibroblasts immortalised with SV40 LTAg or hTERT, produced survival curves typical of NER proficient cells, a modest but notable difference was observed between the two MRC-5 cultures, with an LD50 of 6.3 and 4.9 J/m^2, respectively (Fig. 4.18). Attempts were made to construct survival curves using a similar approach for the primary XP-C (XP8CA) and CS-A (CS3BE) fibroblasts transduced with pBABE-neo-hTERT (clones 19 and 3, respectively). Additionally, a monoclonal population of primary isogenic XP-A (XP12BE) fibroblasts (clone 13), which were previously transduced with pBABE-neo-hTERT in the laboratory and made available, was included as a control. Surprisingly, survival data was not obtained for the hTERT-immortalised XP-C, CS-A or XP-A dermal fibroblasts. During incubation after UV, the cells appeared to migrate across the dish and were unable to form distinct scorable colonies.

Although colony formation is frequently used to assess cell survival, these assays also give an indication on the NER capacity of *in vitro* cell cultures. Therefore, due to the absence of colony formation obtained for the hTERT-immortalised cell lines, an alternative repair assay was adopted based on an immuno-slot-blot methodology, which used CPD- and 6-4PP-specific antibodies (Section 4.4.7).

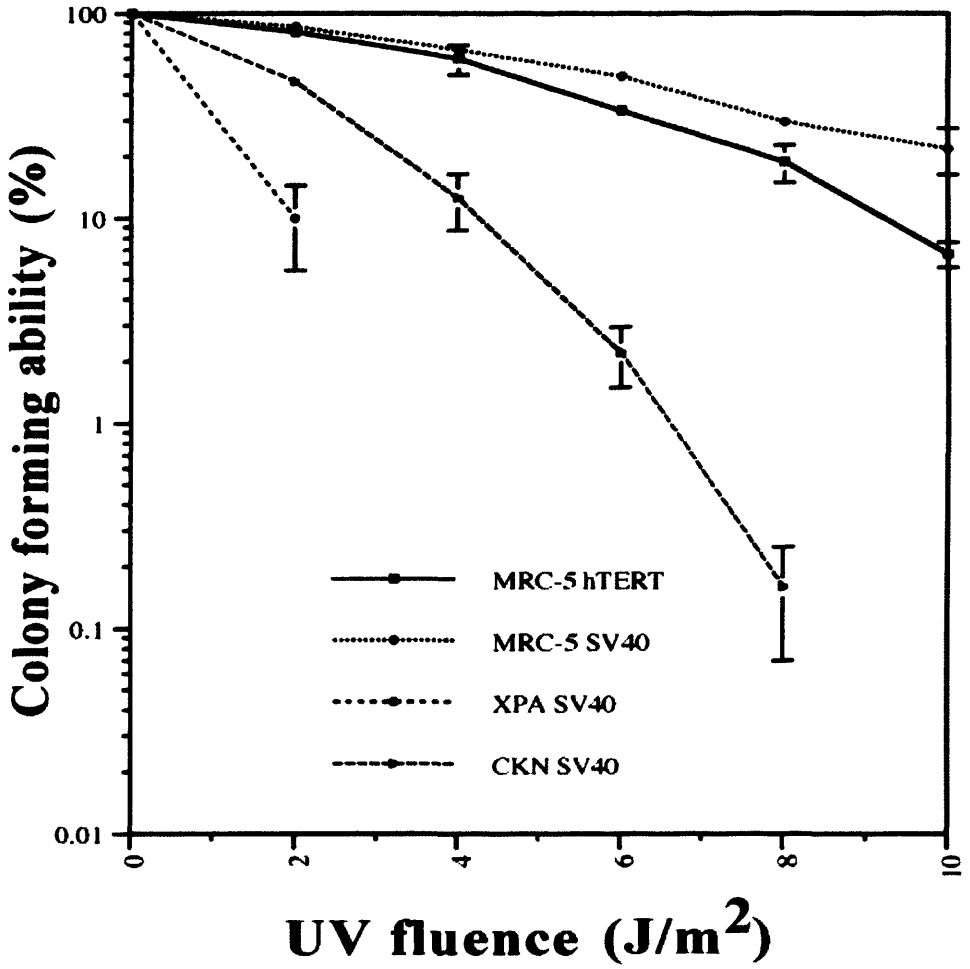

Figure 4.18. Survival after exposure to UVC (254 nm) radiation of the hTERT-immortalised repair-proficient and SV40-transformed repair-proficient and DNA repair-defective cell lines. hTERT-immortalised MRC-5 lung fibroblasts (closed square); SV40-transformed MRC-5 lung fibroblasts (closed circle); SV40-transformed XP-A (XP12BE) dermal fibroblasts (open circle); SV40-transformed CKN1 (CS-A) dermal fibroblasts (closed triangle). Points represent an average of three independent biological replicates and triplicate dishes were performed for each biological replicate. Bars represent standard error of the mean.

4.4.7 Global repair of CPDs and 6-4PPs in hTERT-immortalised XP-C and CS-A dermal fibroblasts

To investigate whether the removal of UV-induced lesions from the global genome was affected by the ectopic expression of hTERT, immunological slot blot assays were undertaken. This assay measures the removal of CPDs or 6-4PPs from genomic DNA, using specific monoclonal antibodies raised against these photolesions (Mori *et al.*, 1991). Cells were irradiated with UV-C (10 J/m^2) and genomic DNA was isolated immediately after treatment (0 hours) or ~6, ~12 and ~24 hours post UV. The band intensity measured at 0 hours was defined as 100% lesions for each cell line, and the lesions removed at each time point (at ~6, ~12 and ~24 hours) was calculated as a percentage of lesions present immediately (0 hours) after UV.

Figures 4.19A and B show representative slot blots of the kinetics of the removal of 6-4PPs (Fig. 4.19A) and CPDs (Fig. 4.19B) in the global genome in hTERT-immortalised MRC-5 (wild-type) and repair-defective XP-C and CS-A fibroblasts at the indicated time points after UV (10 J/m^2). As expected, only ~49.8% of CPDs were removed from the overall genome by MRC-5 cells at ~6 hours, and a modest but notable removal of 62.6% and 73.1% was observed at ~12 and ~24 hours after UV (Fig. 4.20). hTERT-immortalised CS-A (CKN) fibroblasts, which are defective in TCR, displayed similar levels of CPD removal to the MRC-5 cells. The CS-A cells exhibited a slightly higher (55.6%) level of CPD removal at ~6 hours compared to the MRC-5 cells (Fig. 4.20). However, the removal of CPDs at ~12 hours (58.5%) and ~24 hours (74.1%) closely resembled the levels observed in MRC-5 cells (Fig. 4.20). In contrast, there was a marked reduction in the removal of CPDs in hTERT-immortalised XP-C cells, compared to the MRC-5 and CS-A cells. Only 26% and 31.9% of CPDs were removed from the overall genome by XP-C cells at ~6 and ~12 hours, respectively, after UV. Moreover, XP-C cells displayed a protracted half-life of ~24 hours for the removal of CPDs (Fig. 4.20).

Immunological slot-blot analysis revealed that both hTERT-immortalised MRC-5 and CS-A fibroblasts removed 6-4PPs from the global genome with comparable levels of efficiency (Fig. 4.20). At ~6 hours after UV treatment, both cell lines had removed almost all 6-4PPs. In contrast, hTERT-immortalised XP-C fibroblasts demonstrated a marked (3-4 fold) reduction in the removal of 6-4PPs. At 6 hours, only 21.5% of 6-4PPs were removed, while only 33.4% of 6-4PPs were removed at ~12 hours and 46% of 6-4PPs were removed at ~24 hours post UV (Fig. 4.20).

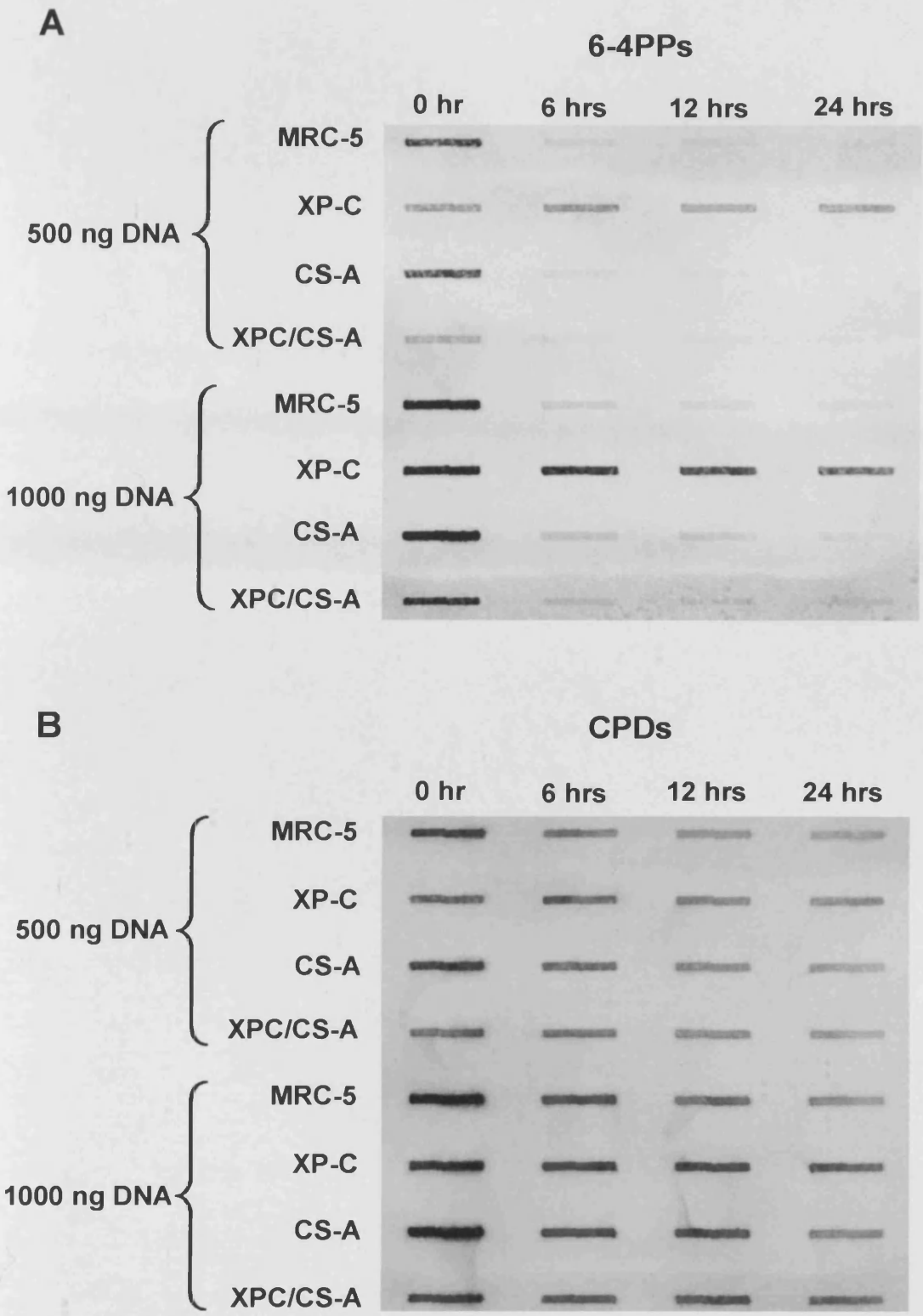

Figure 4.19. Kinetics of the removal of 6-4PPs and CPDs from the overall genome in esablished hTERT-immortalised cell lines (MRC-5, XP-C (GM02996, XP8CA), CS-A (GM01856, CS3BE) and hTERT-immortalised CS-A dermal fibroblasts infected with a pRETROSUPER retroviral vector expressing an *XPC*-specific shRNA construct) irradiated with UV-C (254 nm; 10 J/m^2). Representative immuno-slot-blots of the removal of (A) [6-4] photoproducts or (B) CPDs, using monoclonal [6-4] photoproduct- and CPD-specific antibodies, respectively. Immuno-slot-blot assays were undertaken using 500 ng or 1000 ng of genomic DNA isolated at the indicated time points, following exposure of cells to UV.

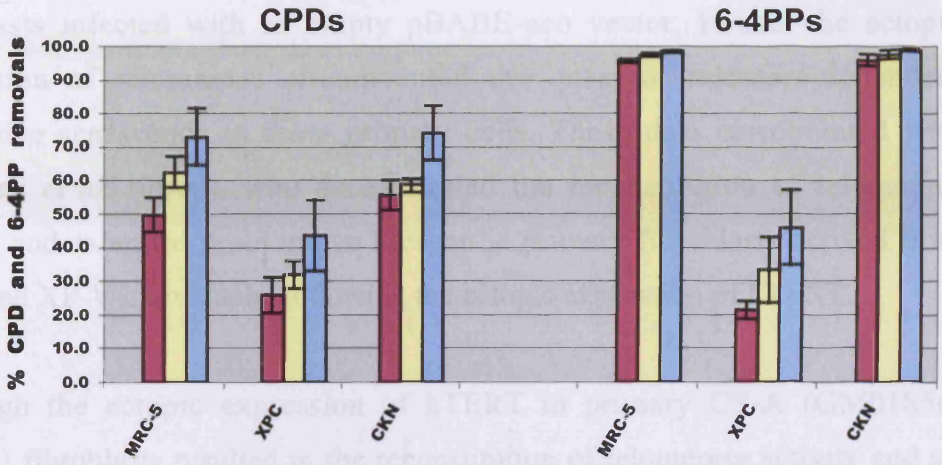

Figure 4.20. Time-course of removal of CPDs or 6-4PPs from the overall genome in hTERT-immortalised (MRC-5, XP-C (GM02996, XP8CA) and CKN (CS-A; GM01856, CS3BE)) cell lines irradiated with UV-C (254 nm; 10 J/m^2). Removal of CPDs or 6-4PPs was measured at 6 hrs (purple), 12 hrs (yellow) or 24 hrs (blue) following UV treatment, using monoclonal CPD- or 6-4PP-specific antibodies, respectively. Immuno-slot-blot assays were undertaken using 1000 ng of genomic DNA isolated at each time point. Each point represents the mean of three independent biological replicates.

4.5 Discussion

The present investigation demonstrated, for the first time, that the ectopic expression of the catalytic subunit of telomerase, *hTERT*, in primary XP-C (GM02996, XP8CA) and CS-A (GM01856, CS3BE) human fibroblasts, resulted in reconstituted telomerase activity and a significant extension on proliferative lifespan (≥100 PDs). This was not observed in primary XP-C and CS-A fibroblasts infected with an empty pBABE-neo vector. Hence, the ectopic expression of telomerase circumvented the onset of telomere-dependent replicative senescence in these primary cells. These data corroborated with Oullettee *et al.* (2000), who demonstrated the reconstitution of telomerase activity and extended proliferative lifespan in primary fibroblasts derived from XP-E and XP-V individuals, following the ectopic expression of hTERT.

Although the ectopic expression of hTERT in primary CS-A (GM01856, CS3BE) fibroblasts resulted in the reconstitution of telomerase activity and an extension on proliferative lifespan, a slower growth rate was observed in clone 8 at ~30 PDs. The slow growth rate observed in telomerase-immortalised CS-A cells (compared to XP-C cells) reflected the reduced growth rate displayed by their primary isogenic counterpart prior to the transduction of hTERT (data not shown). Furthermore, the slower growth rate was not simply due to clonal variability, as the three telomerase-immortalised CS-A clones exhibited a slower growth rate compared to telomerase-immortalised MRC-5 (data not shown) and XP-C cell lines. From these data, it can be speculated that cell lines established by telomerase-mediated immortalisation reflect the growth kinetics displayed by their primary isogenic counterpart, prior to the onset of replicative senescence. Interestingly, however, MacKenzie *et al.* (2000) showed that while telomerase reconstitution extended cellular lifespan, telomerase-immortalised cells become unstable after prolonged periods of culture and undergo crisis as early as 36 PDs after hTERT transduction. They speculated that, although hTERT expression extends prolifarative capacity, immortality is not the universal outcome of hTERT expression. Interestingly, Gorbunova *et al.* (2003) reported the isolation of telomerase-immortalised fibroblast populations that contained 3-20% of cells

with a senescent morphology. Further analysis revealed that these subpopulations exhibited elevated basal levels of $p21^{WAF1/CIP1}$ and pRb. These authors also showed that telomerase activity in these populations was significantly elevated, thus suggesting overexpression of hTERT provided a hyperproliferative signal that induced a senescent-like phenotype. This is thought to provide a protective mechanism that prevents uncontrolled cellular proliferation. However, the precise mechanism(s), that signal growth arrest and ultimately crisis following telomerase-mediated immortalisation remain unknown.

As previously reported in normal fibroblasts (Bodnar *et al.*, 1998; Vaziri & Benchimol, 1998), the ectopic expression of hTERT resulted in primary XP-C human dermal fibroblasts displaying a morphology typically observed in young fibroblasts growing *in vitro*. In contrast, a sub-population of cells within the polyclonal and monoclonal populations of CS-A cells retained a morphological appearance typical of senescent dermal fibroblasts *in vitro*, following telomerase reactivation. This was particularly evident in the CS-A (clone 8) monoclonal population, where a large subset of fibroblasts displayed morphological features typically associated with a senescent phenotype. Similarly, Davis *et al.* (2006) showed that primary WS cells retain a senescent morphology, following ectopic expression of hTERT. Although telomere length was not investigated in the present study, it was previously shown by terminal restriction fragment (TRF) length analysis, that telomerase-mediated immortalisiation of WS cells resulted in an extension on telomere length (Wyllie *et al.*, 2000). This suggests that the senescent-like phenotype exhibited by both WS and possibly CS-A cells is attributed to a telomere-independent stress-induced pathway.

An essential requisite to the establishment of DNA repair-defective XP-C and CS-A dermal fibroblast cell lines was the preservation of both the $p53/p21^{WAF1/CIP1}$ and $pRb/p16^{INK4A}$ tumour suppressor pathways. According to the data presented here and in agreement with previously published findings (Jiang *et al.*, 1999; Milyavsky *et al.*, 2003; Morales *et al.*, 1999), the reconstitution of telomerase activity through the ectopic expression of hTERT did not affect the constitutive expression of p53 in telomerase-immortalised fibroblasts. A high basal level of p53 protein was observed in telomerase-

immortalised normal MRC-5 and NER-defective XP-C and CS-A fibroblasts over a period of 24 hours, thus suggesting the preservation of constitutive p53 expression. However, unlike in previous studies (Milyavsky *et al.*, 2003; Noble *et al.*, 2004; van Waarde-Verhagen *et al.*, 2006), the constitutive p53 status was not assessed frequently while in culture. Therefore, the high constitutive level of p53 observed in this study may have resulted from an artifactual consequence of prolonged culture, resulting from the accumulation of endogenous DNA damage (such as ROS) caused by normal cellular metabolism (van Waarde-Verhagen *et al.*, 2006), rather than a true reflection of p53 status. Several conflicting studies have shown that p53 status during the *in vitro* proliferative lifespan of telomerase-immortalised cells is significantly more complex (Noble *et al.*, 2004; Milyavsky *et al.*, 2003; Waarde-Verhagen *et al.*, 2006). Numerous studies have shown that the prolonged culture of normal hTERT-immortalised fibroblasts has no effect on basal or UV-induced expression of p53 (Jiang *et al.*, 1999; Milyavsky *et al.*, 2003; Morales *et al.*, 1999; Porter *et al.*, 2006), but other investigators have reported that prolonged culture (>100 PDs) of telomerase-immortalised cells results in an increase in the constitutive expression of p53 (Kampinga *et al.*, 2004; Noble *et al.*, 2004; van Waarde-Verhagen *et al.*, 2006). Overexpression of p53 has been attributed to mutations in the *TP53* gene locus, rendering the gene inactive, thus resulting in complete loss of wild-type p53 activity. This is frequently observed in many human cancers (Lane & Benchimol, 1990; Soussi & Lozano, 2005). In support of these findings, Noble *et al.* (2004) reported the presence of mutations in the *TP53* gene in telomerase-immortalised human foreskin fibroblasts, which are also frequently reported in numerous tumours (Olivier *et al.*, 2002).

Although many studies have confirmed the preservation of constitutive p53 expression following telomerase-mediated immortalisation, few have reported the maintenance of a DNA damage p53-mediated response, such as that observed following UV irradiation (Gorbunova *et al.*, 2002; Morles *et al.*, 2000; Porter *et al.*, 2006). In concordance with Porter *et al.* (2006), a UVC-induced time-dependent accumulation of p53 was observed in MRC-5 telomerase-immortalised cells. Moreover, the time-dependent accumulation of p53 was of similar magnitude to that observed in telomerase-immortalised XP-C and CS-A

fibroblasts at the indicated time points over a 24 hour period. In agreement with Porter *et al.* (2006), a UV-dependent induction of p53 was observed in telomerase-immortalised cells as early as 6 hours after UV treatment. Therefore, the data presented here, suggests that a UV-induced p53-dependent DNA damage response remained intact in MRC-5, XP-C and CS-A fibroblasts, following telomerase-mediated immortalisation. It has been shown that NER-defective XP-A cells in G_1 phase require a 10-fold lower UV dose to induce p53 to the same level as wild-type cells in G_1 phase (Ljungman & Zhang, 1996). Interestingly, Porter *et al.* (2006) observed a reduction in p53 and a concomitant appearance of morphological features indicative of apoptosis at ~36 hours after UV. This was not seen during the present study, as p53 levels were monitored for up to 24 hours post UV. Although p53 status in response to different doses of UV was not addressed in this study, it has been shown that the accumulation of p53 in telomerase-immortalised fibroblasts can also occur in a UV dose-dependent manner (Porter *et al.*, 2006).

As previously mentioned, the stabilisation and activation of p53 occurs in response to UV damage, via a series of posttranslational modifications. For example, the phosphorylation of Ser15 at the N-terminus has been a well-documented target following UV (Bean & Stark, 2001; Prives, 1998; Shieh *et al.*, 1997; Webley *et al.*, 2000); and is mediated by the phosphoinositide 3-kinase-related superfamily member, ATR kinase (Tibbetts *et al.*, 1999). Phosphorylation at Ser15 is thought to induce a conformational change and disrupt mdm2 binding, thereby inhibiting the degradation of p53 (Shieh *et al.*, 1997). In this study, like p53 accumulation, phosphorylation at Ser15 occurred in a time-dependent manner in telomerised MRC-5, XP-C and CS-A fibroblasts after exposure to 10 J/m^2 of UV. Similarly, Porter *et al.* (2006) reported the time-dependent phosphorylation of p53 at Ser15 in telomerase-immortalised cells following UV. Hence, it appears that the UV-induced stabilization of p53 by ATR remained intact. Interestingly, the magnitude of Ser15 phosphorylation was significantly higher in telomerase-immortalised XP-C cells, compared to normal MRC-5 and DNA repair-defective CS-A cells. Conversely, Ljungman *et al.* (2001) found that the accumulation of Ser15-modified p53 protein occurred in

CS cells. They suggested that the accumulation of phosphorylated p53 at Ser15 occurred due to a UV-induced inhibition of transcription during RNA Pol II elongation.

The stabilisation of p53 facilitates the transcriptional activation of the downstream CDK inhibitor, $p21^{WAF1/CIP1}$, a key regulator of G_1 cell cycle arrest. Moreover, Bean & Stark (2001) showed that following UV, phosphorylation of p53 at Ser15 is required to maintain basal levels of $p21^{WAF1/CIP1}$. Therefore, the analysis of $p21^{WAF1/CIP1}$ provided an indirect measure of p53 function. In concordance with numerous studies (Farwell *et al.*, 2000; Milyavsky *et al.*, 2003) the data presented here suggests that $p21^{WAF1/CIP1}$ remained at low basal levels in the telomerase-immortalised normal (MRC-5) fibroblasts during the first 100 PDs. In disagreement, other studies revealed significant variations in constitutive $p21^{WAF1/CIP1}$ expression between populations of fibroblasts immortalised with hTERT following extended (>100 PDs) growth in culture (Kampinga *et al.*, 2004; Noble *et al.*, 2004; van Waarde-Verhagen *et al.*, 2006). As previously discussed, Gorbunova *et al.* (2003) found that 3-20% of telomerase-immortalised cells displayed a senescent-like phenotype. This subpopulation also exhibited elevated $p21^{WAF1/CIP1}$ levels. Unlike MRC-5 cells, both telomerised XP-C and CS-A fibroblasts displayed heterogeneous basal levels of $p21^{WAF1/CIP1}$. The variable level of $p21^{WAF1/CIP1}$ expression in XP-C and CS-A cells, during the 24 hour time course, may have been attributed to the generation of ROS, which may accumulate in culture due to defective GGR and TCR, respectively.

Like p53, the preservation of a UV-induced $p21^{WAF1/CIP1}$ response, following telomerase-mediated immortalisation has remained poorly documented (Gorbunova *et al.*, 2002; Morales *et al.*, 1999; Porter *et al.*, 2006). In this study, an increase in $p21^{WAF1/CIP1}$ protein expression was observed in both the telomerase-immortalised normal MRC-5 and NER-defective XP-C and CS-A fibroblasts after UV. Moreover, in agreement with Porter *et al.* (2006), $p21^{WAF1/CIP1}$ protein levels correlated with the accumulation of p53 after UV. Therefore, the UV-induced phosphorylation of p53 at Ser15, and accumulation of

$p21^{WAF1/CIP1}$ observed in this study, provides evidence that p53 activation and stabilisation is preserved following telomerase-mediated immortalisation.

Consistent with these data, previous studies reported an induction of $p21^{WAF1/CIP1}$ in human or mouse primary cells after UV (Itoh *et al.*, 2003; Itoh *et al.*, 2004; Itoh & Linn, 2005; Li *et al.*, 1996; Poon *et al.*, 1996). This further supports the exploitation of telomerase as a vehicle for establishing permanent cell lines. In contrast, however, other investigators reported a reduction in $p21^{WAF1/CIP1}$ protein levels following UV (Allan & Fried, 1999; Butz *et al.*, 1998; Maki & Howley, 1997; Rieber & Strasberg, 2000; Schoenfeld *et al.*, 2000; Wang *et al.*, 1999). Moreover, Bendjennat *et al.* (2003) reported the UV-induced ubiquitin-dependent degradation of $p21^{WAF1/CIP1}$. More recently, Itoh & Linn (2005) suggested that the marked difference in $p21^{WAF1/CIP1}$ expression was attributed to experimental variability. In particular, many of the studies that reported significant decreases in $p21^{WAF1/CIP1}$ levels used cancer cell lines (Allan & Fried, 1999; Butz *et al.*, 1998; Maki & Howley, 1997; Rieber & Strasberg, 2000; Schoenfeld *et al.*, 2000; Wang *et al.*, 2000). This further reiterates the importance of using nontransformed cell lines, as cell cycle regulation and apoptosis in response to DNA damaging agents, such as UV, are disrupted in cancer cell lines. Furthermore, the precise mechanistic function of $p21^{WAF1/CIP1}$ in NER remains controversial, as conflicting studies have proposed both inhibitory and stimulatory roles in NER (Cooper *et al.*, 1999; Sheikh *et al.*, 1997).

pRb phosphorylation is required for progression through S phase (Buchovitch *et al.*, 1989; DeCaprio *et al.*, 1989), and is regulated by the cell cycle proteins CDK4, cyclin D and $p16^{INK4A}$ (Weinberg, 1995). To delineate the consequences of telomerase-mediated immortalisation on the pRb/$p16^{INK4A}$ pathway, both pRb and $p16^{INK4A}$ protein expression was investigated. The data suggest that, although both inactive hyperphosphorylated and active hypophosphorylated forms of Rb were observed in telomerised non-irradiated MRC-5 fibroblasts, a slight increase in pRb was observed. This is consistent with the high proliferative capacity of telomerised MRC-5 fibroblasts, which resulted in the culture reaching confluency and the possible exit from the cell cycle. In agreement with these data, Jiang *et al.* (1999) and Morales *et al.* (1999) showed that the pRb response

to high cell density remained intact in telomerase-expressing cells. In contrast, pRb was predominantly in a hyperphosphorylated state in the non-irradiated telomerised XP-C and CS-A fibroblasts at all time points. This was attributed to the reduced proliferative capacity observed in both telomerised XP-C and CS-A cells lines, compared to the MRC-5 cells. Therefore, it can be speculated the XP-C and CS-A cells remained in a subconfluent state throughout the time course, thus progressing through the G_1/S phase transition. In agreement with these data, Jiang *et al.* (1999) and Morales *et al.* (1999) showed that Rb remained in a hyperphosphorylated state in subconfluent telomerised cells. Unfortunately, pRb status or functionality was not investigated in non-telomerised MRC-5, XP-C or CS-A fibroblasts in this study. Therefore, the precise effect of telomerase-mediated immortalisation on these cell lines remains unknown. However, from previous studies (Jiang *et al.*, 1999; Morales *et al.*, 1999) it can be speculated that, telomerase-mediated immoralisation had no affect on the state of pRb in telomerised MRC-5, XP-C and CS-A cells. Furthermore, it can be speculated that the G_1 to S phase transition remained intact. However, further assessment of cell proliferation and pRb functionality is required to support this.

After UV, a global reduction in Rb protein levels was seen in telomerised MRC-5, XP-C and CS-A cells. However, an increased level of pRb and marked reduction in ppRb was observed in both telomerised XP-C and CS-A fibroblasts following UV. Therefore, it can be speculated that regulation of the G_1 to S phase transition, following DNA damage, by the pRb/$p16^{INK4A}$ pathway remained intact. Consistent with previous studies (Jiang *et al.*, 1999; Morales *et al.*, 1999), it can be speculated that telomerase-mediated immortalisation does not abolish the integrity of the pRb checkpoint. However, further investigation into the translational and posttranslational modifications of G_1 to S phase regulators that lie downstream to pRb, such as E2F target genes that are involved in cell cycle progression (including cyclin A, cyclin E, cdc2 and cdk2) is required.

The basal level of $p16^{INK4A}$ remained constant in telomerised MRC-5, XP-C and CS-A fibroblasts, over a 24 hour period. In agreement, Jiang *et al.* (1999) showed that telomerised BJ foreskin fibroblasts displayed no alterations in a $p16^{INK4A}$ response to cell-cycle checkpoint arrest compared with parental non-

telomerised cells. Unlike previous studies (Milyavsky *et al.*, 2003; Noble *et al.*, 2004; van Waarde-Verhagen *et al.*, 2006), however, the constitutive expression of $p16^{INK4A}$ was not addressed during the period of continuous growth in culture prior to termination (~100 PDs).

Previously, it was shown that $p16^{INK4A}$ accumulates in keratinocytes that are grown in an inadequate culture environment (Ramirez *et al.*, 2001). This has led to the assumption that $p16^{INK4A}$ is a general mediator of the stress response. In agreement, a UV-induced time-dependent upregulation of $p16^{INK4A}$ was observed in telomerised MRC-5 fibroblasts following UV in this study. However, in agreement with Gorbunova *et al.* (2002) a UV-induced up-regulation of $p16^{INK4A}$ was not observed in telomerised XP-C and CS-A fibroblasts. In disagreement with these findings, Wang *et al.* (1996) showed that $p16^{INK4A}$ accumulates following UV, and correlates with a late S to G_2 phase cell cycle arrest. Interestingly, Milligan *et al.* (1998) reported that melanoma cells that are devoid of $p16^{INK4A}$ activity show no delay in G_2 after UV, suggesting that inactivation of the $p16^{INK4A}$ gene, *CDKN2A*, causes the abolition of a $p16^{INK4A}$-dependent G_2 cell cycle checkpoint arrest. These findings indicate that the preservation of $p16^{INK4A}$ is important following DNA damage. It is possible that alterations in $p16^{INK4A}$ occurred in the telomerised XP-C and CS-A fibroblast cell lines.

As previous studies have reported the establishment of permanent telomerase-immortalised cell lines in the absence of changes in $p53/p21^{WAF1/CIP1}$ and $pRb/p16^{INK4A}$ status (Jiang *et al.*, 1999; Morales *et al.*, 1999), it has been suggested that the manipulation of these pathways is not required in telomerase-mediated immortalisation (Noble *et al.*, 2004). As a result, it has been speculated that the emergence of clones with altered tumour suppressor responses, following prolonged (>100 PDs) growth (van Waarde-Verhagen *et al.*, 2006; Milyavsky *et al.*, 2003), is a stochastic process (van Waarde-Verhagen *et al.*, 2006). Clones with altered $p53/p21^{WAF1/CIP1}$ and/or $pRb/p16^{INK4A}$ responses are selected during continuous growth *in vitro*. Moreover, the abolition of these pathways increase the probability that these cells continue to cycle, while their normal counterparts undergo a G_1 arrest. This permits the accumulation of further genetic changes,

thereby resulting in the selection of clones possessing a selective growth advantage, malignant phenotype and increased growth rate (Noble *et al.*, 2004). Clonogenic survival following UV is frequently used to confirm the NER capacity of *in vitro* cell cultures. As expected, the SV40-transformed XP-A (XP12BE) fibroblasts displayed the highest level of UV sensitivity and the lowest colony forming ability. Correspondingly, Ouellette *et al.* (2000) observed a similar level of survival in an unrelated SV40-transformed XP-A (XP12RO) fibroblast cell line. The isogenic SV40-transformed CS-A (CS3BE.s3g1) cell line exhibited a UV sensitivity that was intermediate to XP-A and MRC-5. In agreement with the data presented here, Henning *et al.* (1995) previously observed an identical pattern of clonogenic survival in the SV40-transformed CS-A (CS3BE.s3g1) cell line. The UV survival curves obtained for both the isogenic MRC-5 SV40-transformed and hTERT-immortalised fibroblasts were indicative of DNA repair-proficient cells. Furthermore, the UV survival observed for telomerised normal MRC-5 fibroblasts in this study, were similar to those reported elsewhere in the literature for NER-proficient fibroblasts (Bates *et al.*, 2005; Ouellette *et al.*, 2000; Porter *et al.*, 2006). In the present study, however, there was a distinct difference between the SV40–transformed and telomerised MRC-5 cell lines. The SV40-transformed MRC-5 fibroblasts displayed a slightly increased colony forming ability compared to the telomerase-immortalised MRC-5 cells. Previously, it was show that GGR is abrogated in SV40-transfomed cells (Bowman *et al.*, 2000), due to the inhibition of normal p53 function by LTAg. This abolishes the transcriptional activation of several downstream transcriptional gene targets that mediate GGR such as *DDB2* (Hwang *et al.*, 1999), *XPC* (Adimoolam & Ford, 2002) and *GADD45α* (Smith *et al.*, 2000). In accordance, Porter *et al.* (2006) showed that the inactivation of p53 expression, through the exploitation of p53-targeted siRNAs, resulted in the down regulation of DDB2 protein expression and an increased colony forming ability of normal diploid human fibroblasts, following UV radiation. This further supported the mounting evidence that suggests p48 activation occurs in a p53-dependent manner (Hwang *et al.*, 1999). Although, GGR is compromised in SV40-transformed cells, the increased clonogenic survival in the SV40 LTAg MRC-5 fibroblasts, observed in this study, was possibly attributed to the

abolition of p53-dependent G_1 cell cycle arrest and apoptosis. In support of these findings, Ljungman & Zhang (1996) reported that the induction of apoptosis correlated with the induction of p53 and to the abolition of mRNA synthesis.

To determine whether the ectopic expression of hTERT influenced colony forming ability, clonogenic survival assays were also undertaken on telomerase-immortalised XP-C, CS-A and XP-A cell lines. Surprisingly, data were not obtained for these assays due to the absence of colony formation. Conflicting studies, reported the construction of clonogenic survival curves and have shown that UV dose-dependent survivals obtained for normal primary and telomerase-immortalised fibroblasts were indistinguishable, reflecting levels of DNA repair typical for proficient cells (Bates *et al.*, 2005; Newman *et al.*, 2006; Ouellette *et al.*, 2000; Porter *et al.*, 2006). Furthermore, Ouellette *et al.* (2000) constructed survival curves for XP-E and XP-V fibroblasts, and showed that the constitutive expression of hTERT had no affect on fibroblast survival.

In the present investigation, the data suggest that telomerase-mediated immortalisation had no effect on the repair phenotype for CPDs or 6-4PPs in telomerised NER-proficient MRC-5 or GGR-deficient XP-C or TCR-deficient CS-A fibroblasts following UV. Unlike CPDs, which are repaired at heterogeneous rates in different genomic regions, 6-4PPs are rapidly removed from the overall genome without any preference towards transcriptionally active regions of the genome (reviewed by Balajee & Bohr *et al.*, 2000). Therefore, as expected, telomerised MRC-5 fibroblasts removed ~98.4% of 6-4PPs within 24 hours. In stark contrast, telomerised MRC-5 cells removed significantly fewer CPDs. In agreement with these findings, Van Hoffen *et al.* (1995) previously showed that the removal of 6-4PPs is at least five-fold faster than that of CPDs. Consistent with these findings, numerous studies have adopted strand-specific repair assays and ligation-mediated PCR (LMPCR) to show that NER of UV-induced photolesions is preserved at the global, strand and nucleotide resolution in normal fibroblasts, following telomerase-mediated immortalisation (Bates *et al.*, 2005; Porter *et al.*, 2006). In stark contrast, numerous studies have suggested

that DNA repair is enhanced following telomerase-mediated immortalisation (Sharma *et al.*, 2003; Shin *et al.*, 2004).

The removal of CPDs and 6-4PPs from the global genome by telomerised XP-C cells was identical. Furthermore, the data herein, showed that the global genomic removal of CPDs and 6-4PPs was unaffected in the telomerised GGR-proficient, TCR-deficient CS-A cells, as the repair rates were similar to those observed in the telomerised normal MRC-5 fibroblasts. This observation may have occurred due to several reasons. Firstly, only ~1% of the genome is coding sequence (Lander *et al.*, 2001; Venter *et al.*, 2001), which is actively transcribed. However, the assay adopted in this study to assess repair, measured global repair (GGR and TCR) rather than TCR alone. Therefore, it is possible that the TCR defect was not observed, as the CS-A cells were GGR-proficient. Therefore, the exploitation of strand-specific DNA repair assays (Bohr *et al.*, 1985) would address this issue. Alternatively, it has been shown by numerous investigators that lesions that efficiently block transcription may also be efficiently recognised by GGR, as a result of local disruption to base paring at the site of the lesion (Hess *et al.*, 1997), thus the slow GGR apparatus may override TCR and repair photolesions present on the transcribed strand (de Boer & Hoeijmakers 2000; Queille *et al.*, 2001; Van Hoffen *et al.*, 1995). This may explain the efficient removal of both CPDs and 6-4PPs from the telomerised TCR-deficient CS-A fibroblasts observed in this study. As previously mentioned, the removal of 6-4PPs is five-fold faster than the removal CPDs, and it thought to occur within the first few hours following UV. In this study, however, the repair of CPDs and 6-4PPs was assessed at a limited number of time points (0, ~6, ~12 and ~24 hours) post UV. Therefore, it is possible that assessing repair at earlier time points (between 0.5-4 hours) after UV would have resulted in the detection of slower repair of 6-4PPs in the telomerised TCR-deficient CS-A fibroblasts compared to the TCR-proficient MRC-5 fibroblasts.

Although this investigation has demonstrated the successful establishment of novel hTERT-immortalised XP-C (GM02996, XP8CA) and CS-A (GM01856, CS3BE) human dermal fibroblasts, through the ectopic expression of *hTERT*

cDNA, significant caution should be applied when undertaking long-term genetic, biochemical and functional *in vitro* assays. Previously, Milyavsky *et al.* (2003) showed that hTERT-immortalised WI-38 fibroblasts exhibit similar characteristics as their primary isogenic counterparts, during the first 150 PDs, following retroviral infection with *hTERT* cDNA. However, the long-term (≥200 PDs) *in vitro* growth of telomerase-immortalised cultures, resulted in a gradual reduction in both $p16^{INK4A}$ and $p14^{ARF}$ expression. In contrast, an alteration in p53 and $p21^{WAF1/CIP1}$ expression was not observed, following extensive subcultivation.

It was initially believed that the ectopic expression of hTERT resulted in the establishment of telomerase-immortalised cells, which possessed an infinite proliferative capacity and an unaltered phenotype that recapitulated their primary isogenic counterpart (Bodnar *et al.*, 1998; Jiang *et al.*, 1999; Morales *et al.*, 1999; Nakamura *et al.*, 2002; Vizari & Benchimol, 1998). The exploitation of hTERT, however, in the establishment of permanent cell lines remains relatively controversial, as more recent studies have shown that telomerase reactivation merely extends the proliferative lifespan of primary cells to 100-200 PDs (Di Donna *et al.*, 2003; MacKenzie *et al.*, 2000) rather than the creation of permanent cell lines with infinite proliferative potential. In stark contrast, conflicting reports have observed the emergence of cultures which display alterations frequently associated with cell lines established through oncogenic transformation, such as loss of the p53/$p21^{WAF1/CIP1}$ and/or pRb/$p16^{INK4A}$ pathways (Milyavsky *et al.*, 2003; Noble *et al.*, 2004; van Waarde-Verhagen *et al.*, 2006). Furthermore, the overexpression of oncogenes such as c-*myc* and *Bmi-1* has been reported (Milyavsky *et al.*, 2003).

In summary, the data presented in this thesis, for the first time, shows that the ectopic expression of hTERT in primary XP-C (GM02996, XP8CA) and CS-A (GM01856, CS3BE) human dermal fibroblasts resulted in the reconstitution of telomerase activity, extension of proliferative capacity (≥100 PD) and the preservation of the p53/$p21^{WAF1/CIP1}$ and pRb/$p16^{INK4A}$ tumour suppressor pathways. This suggests that the reconstitution of telomerase activity confers XP-

C and CS-A dermal fibroblasts with the potential of infinite proliferation. Moreover, the telomerase-mediated extension of proliferative lifespan did not require additional genetic manipulation, as previously reported by other investigators. Collectively, these data suggest that, with the exception of extended proliferative capacity, the cellular phenotypes remained unaltered following the ectopic expression of hTERT, while the DNA damage responses remained intact. The absence of the XP-C and CS-A proteins (Chapter 3) in the telomerised XP-C (GM02996, XP8CA) and CS-A (GM01856, CS3BE) fibroblasts respectively, indicate that the cells retain the defect that causes the syndromes. In agreement with the data presented in this thesis, a growing body of evidence suggests that NER remains intact and that no differences are observed between telomerase-immortalised normal fibroblasts and their primary isogenic (non-telomerised) counterparts. The data presented here, strongly supports the use of telomerase-mediated immortalisation as an alternative and more robust system to oncogenic-mediated transformation, for studying genetic and biochemical events including NER, when the use of primary cells is experimentally disadvantageous, due to the caveats associated with cellular senescence. Moreover, the stable clonal expansion of telomerised cells provides an excellent tool for the dissection of transcriptional responses by transcription expression profiling and the selective abrogation of gene expression, using RNAi technologies. However, the altered phenotypes observed elsewhere in telomerised cells following continuous growth in culture, reiterates the importance of continuous monitoring of these cultures for genomic instability and changes in the p53/p21$^{WAF1/CIP1}$ and pRb/p16^{INK4A} pathways.

Chapter 5

Expression Profiling and Validation of Transcriptional Responses in hTERT-immortalised XP-C and CS-A Human Dermal Fibroblasts Following UVC-irradiation

5.1 Introduction

The principles of microarray technology are based on Watson-Crick base pairing (Watson & Crick, 1953) and the process of hybridisation, which have been exploited extensively in established techniques such as Southern and Northern blotting (Southern, 1975). The emergence of microarray technologies has significantly contributed to our understanding of the intricate networks and pathways that regulate fundamental biological processes, thereby facilitating the elucidation of gene function and the underlying cause of disease. Furthermore, microarrays have permitted the identification of cell-type-specific transcriptional portraits and complex expression signatures unique to defined genetic backgrounds.

The characterisation of the cellular response to UV has advanced rapidly since the advent of microarrays (Schena *et al.*, 1995). Exposure to UV results in responses involving several DNA damage-induced signalling cascades such as the signalling kinases ATR/Chk1, c-jun N-terminal kinase and the p38 kinase pathway, which results in the activation of NER and recovery mechanisms through the transcription factors: inhibitor of DNA binding 1 (Id1), Noct-3, Rho GTPase activating protein 24 (p73), p53, nuclear factor of kappa light

polypeptide gene enhancer in B-cells (NF-κB), AP-1, activating transcription factor 3 (ATF-3) and cAMP response element binding protein, Mift (reviewed by Bender *et al.*, 1997; Yang *et al.*, 2003; Zhou *et al.*, 2000). The activation of these factors results in a complex transcriptional response of the cells, resulting in the transcriptional activation of downstream target effector molecules that regulate DNA damage repair (GADD45α, DDB2 and XPC), cell cycle regulation ($p16^{INK4A}$, GADD45α and $p21^{WAF1/CIP1}$) and apoptosis (Bax, Bcl-2 and NOXA; Gentile *et al.*, 2003). The interactions between these known and as yet-to-be identified constituents define the programme of set transcriptional responses in the cell. Furthermore, mutations, altered patterns of expression or dysregulation of many of these molecules or entire pathways have been implicated in the molecular pathogenesis of cutaneous malignancy.

To dissect the temporal and functional relationships of these UV-induced transcriptional responses in telomerised XP-C and CS-A cell lines; Affymetrix™ GeneChip® technology was used. This system offers extensive coverage of the human genome, and is based on oligonucleotides. Light-mediated DNA synthesis is exploited to construct high-density arrays using a combination of two techniques, namely photolithography and solid-phase DNA synthesis. This facilitates the deposition of several hundred thousand 25mer oligos on the surface of a prefabricated oligonucleotide GeneChip® array. Approximately 11 to 20 independent perfect match (PM; perfectly complementary to the mRNA of a gene) oligos (probes) are designed to hybridise to different regions of the same gene. An additional level of complexity comes from the inclusion of mismatch (MM) control probes that are identical to the PM partners, except for a single base difference located at the central position (usually at nt 13), where one nucleotide has been changed to its complementary nucleotide. The MM probes provide controls for specific hybridisation and facilitate direct subtraction of background and cross-hybridisation signals (reviewed by Hardiman, 2004). The HG-U133A arrays used in this investigation contain 22,283 probe sets, which represent 13,387 human genes.

Numerous investigators have exploited various microarray platforms such as cDNA microarrays or Affymetrix™ GeneChip® arrays to delineate the transcriptional response to genotoxic stress such as UV. To date, the transcriptional responses to genotoxic stress have been characterised in yeast (Birrell *et al.*, 2001; Chen *et al.*, 2003; Gasch *et al.*, 2000; Mercier *et al.*, 2001), *E.coli* (Courcelle *et al.*, 2001), mouse dermal fibroblasts (MDF; Garinis *et al.*, 2001) and rat cardiac myocytes (Boerma *et al.*, 2005). The transcriptional response of human epidermis *in vivo* and various cultured normal human cell types of the skin has been extensively investigated, following exposure to different UV wavelengths. For example, the global transcriptional response to UVA has been investigated in keratinocytes, melanocytes, epithelial cells, fibroblasts and an MCF-7 breast cancer cell line (Abe *et al.*, 2003; Andley *et al.*, 2004; He *et al.*, 2004; Jean *et al.*, 2001; Koch-Paiz *et al.*, 2004). Further investigations have been undertaken to dissect the transcriptional response in intact human epidermis, keratinocytes, melanocytes and an MCF-7 breast cancer cell line after UVB irradiation (Becker *et al.*, 2001; Catani *et al.*, 2001; Dazard *et al.*, 2003; Enk *et al.*, 2004; Enk *et al.*, 2006; Li *et al.*, 2001; Lee *et al.*, 2005; Murakami *et al.*, 2001; Howell *et al.*, 2004; Koch-Paiz *et al.*, 2004; Pisarchik *et al.*, 2004; Sesto *et al.*, 2001; Takao *et al.*, 2002; Valéry *et al.*, 2001; Yang *et al.*, 2006). The UVC-induced transcriptional responses in fibroblasts, lymphoblastoid cells, HeLa cells, colon carcinoma EB-1 cells and an MCF-7 breast cancer cell line have also been well documented (Gentile *et al.*, 2003; Guo *et al.*, 2002; Koch-paiz *et al.*, 2004 McKay *et al.*, 2004; Rieger & Chu, 2004; Wano *et al.*, 2004; Zhao *et al.*, 2000).

In general, these various cell types display similar patterns of differential regulation, which involve genes that regulate DNA-damage-repair, cell cycle arrest and apoptosis. Among these studies, a large number of differentially regulated genes have also been identified that regulate the expression of transcription factors, cytoskeletal proteins, secreted signalling molecules and controlling cellular functions such as signal transduction and terminal differentiation. However, the regulation of immunomodulatory factors appears overlapping but distinct, suggesting that there is a cell-type-specific response of skin as an organ to UV (reviewed by Latonen & Laiho, 2005). Interestingly,

different UV doses eliciting either cell cycle arrest or apoptosis induce highly divergent transcriptional responses (Gentile *et al.*, 2003; McKay *et al.*, 2004). However, as these studies differ considerably in terms of time kinetics, UV dose, light source and microarray technologies applied, it has been difficult to generate a comprehensive and coherent model that gives a detailed and definitive global picture of the complex transcriptional programme in response to UV.

Several investigators have also reported highly specialised cell-type-specific UV responses among various skin cells. For example, Yang *et al.* (2006) showed that epidermal melanocytes execute specific physiological programmes in response to UV. These melanocytic responses include increased dendrite formation and enhanced melanogenesis/melanisation, all of which are thought to influence the ability of melanocytes to survive and attenuate the deleterious consequences of UV. Cell-type-specific transcription expression patterns have also been observed in keratinocytes. For example, using a novel skin organ culture model, Li *et al.* (2001) showed that epidermal keratinocytes displayed three distinct patterns of differential gene expression following exposure to UVB. The first contained transcription factors, signal transducers and cytoskeletal proteins that modify the cell phenotype from a normal, fast-growing cell to an activated, arrested cell. The second contained secretory growth factors, cytokines and chemokines, thus alerting the surrounding tissue to UV damage. The third wave of differential gene expression included the cell-type-specific response, in which constituents of the cornified envelope were up-regulated, thus permitting ketatinocytes to enhance the epidermal protective covering.

Despite extensive investigation into the UV-induced transcriptional response of various normal cell types in response to different wavelengths, a limited number of studies have characterised the UV-induced transcriptional response of cells derived from individuals defective in NER or cell signalling. To date, studies have remained limited to cell lines derived from XP-C, XP/CS, CS-B, TTD or AT donors (Chang *et al.*, 2003; Newman *et al.*, 2006; da Costa *et al.*, 2005; Heinloth *et al.*, 2003). Therefore, the well-characterised UV-induced transcriptional responses in normal cells such as DNA repair, cell cycle arrest and apoptosis, remain poorly delineated in cells defective in NER. For example,

although CS has been extensively investigated and much is known about the genetic defects and cellular functionality of the *CSA* and *CSB* genes, which are responsible for the syndrome, the precise nature of the molecular defect(s) that cause the CS phenotype remains poorly understood. Furthermore, the CSA and CSB proteins have been implicated, alone or in various combination with other proteins in numerous cellular functions such as TCR of UV-induced lesions (Cleaver *et al.*, 1999; Venema *et al.*, 1990), removal of oxidative damage (Tuo *et al.*, 2002), transcription initiation by RNA Pol I (Bradsher *et al.*, 2002; Iben *et al.*, 2002) and RNA Pol II (Dubaele *et al.*, 2002), elongation by RNA Pol II (Lee *et al.*, 2002; Selby & Sancar, 1997a), transcription of induced genes (Kyng *et al.*, 2003), protein ubiquitylation (Groisman *et al.*, 2003), and recruitment of chromatin remodelling and repair factors (Fousteri *et al.*, 2006). Kyang *et al.* (2003) exploited microarray technology to show that the transcriptional response, after oxidative stress, was defective in CS-B cells, thus implicating oxidative damage as playing a possible role in the pathogenesis of CS. More recently, Groisman *et al.* (2006) has established a functional relationship between CSA and CSB through the CSA-dependent degradation of CSB by the ubiquitin-proteasome pathway. Furthermore, Proietti-De-Santis *et al.* (2006) has shown that CSB is essential for initiating the transcriptional programme of non p53-responsive genes, but is dispensable for the transcription of p53-responsive genes. In order to delineate these mechanistic functions further and elucidate how defects in *CSB* cause the molecular defect(s) in CS, Newman *et al.* (2006) used expression microarrays to identify genes regulated by CSB in the absence of stress (such as UV), as previous transcription expression studies, although comprehensive, failed to provide definitive conclusions (Selzer *et al.*, 2002). Furthermore, investigators previously focused on the role of CSB in the transcriptional response to oxidative or UV DNA damage (Kyng *et al.*, 2003; da Costa *et al.*, 2005), rather than determining the precise function of CSB in cells not receiving exogenous DNA damage.

Newman *et al.* (2006) found that CSB causes significant changes in gene expression in the absence of UV. They showed that patterns of gene deregulation in CS-B cells resembled those induced by agents that disrupt chromatin structure or modifications. Interestingly, however, Newman *et al.* (2006) showed that CSB

does not appear to affect the expression of chromatin modifiers, such as HATs or methytransferases. From these findings, they concluded that although CSB does not regulate chromatin modifying factors, it plays a direct role in facilitating chromatin modification, possibly by increasing accessibility of histones to modifying enzymes, by transiently moving or displacing nucleosomes, or by remodelling histone-histone or histone-DNA interactions. To date, similar attempts to dissect and elucidate the global transcriptional responses of genes regulated by CSA under normal physiological conditions or after stress (such as UV) have remained elusive. More importantly, investigators have failed to characterise the differences in UV-induced transcriptional responses between genetic backgrounds that display differences in NER capacity, such as those observed in XP, CS and TTD, which are defective in GGR and/or TCR. Although recent investigations have used expression arrays to characterise the UVC-specific transcriptional signatures in cell lines displaying an XP-C, XP/CS or TTD phenotype (Chang *et al.*, 2003; da Costa *et al.*, 2005), these cell lines were severely compromised. Moreover, several caveats have been identified with both the experimental design and statistical approaches adopted in these studies (discussed below).

Microarray analysis of the UV-induced transcriptional response in normal human cells has been well documented. However, a multiplicity of caveats has been identified in the experimental design of many studies due to the limited number of samples. This is particularly problematic, as large datasets generated by microarray experiments require the inclusion of several replicates to ensure statistical validity (Rieger & Chu, 2004). Several studies have used only duplicates (Sesto *et al.*, 2002), while other investigators have interrogated data from single array experiments (Li *et al.*, 2001). Although many investigators have addressed this by the inclusion of additional biological replicates, many studies have prepared replicates derived from a single cell line (Becker *et al.*, 2001; Catani *et al.*, 2001; Chang *et al.*, 2003; da Costa *et al.*, 2005; Gentile *et al.*, 2003; Guo *et al.*, 2002; He *et al.*, 2004; Kock-Paiz *et al.*, 2004; Li *et al.*, 2001; McKay *et al.*, 2004; Murakami *et al.*, 2001; Park *et al.*, 2002; Sesto *et al.*, 2002; Wano *et al.*, 2004; Zhao *et al.*, 2000) or donor (Howell *et al.*, 2004; Jean *et al.*, 2001; Lee *et al.*, 2005), thus failing to account for variation among individuals. A

limited number of studies have extended transcription expression profiling to multiple cell lines or cells derived from multiple donors (Rieger & Chu *et al.*, 2004; Yang *et al.*, 2006), while others have tried to address the problem of inter individual variability by using a polygenic (pooled) cell population (or RNA samples) derived from several donors (Enk *et al.*, 2004; Enk *et al.*, 2006; Valéry *et al.*, 2001). Although the use of polygenic samples addresses the problem of inter individual variability, further caveats have been associated with this method.

Several studies have characterised the UV-induced transcriptional response in primary cell cultures (Andley *et al.*, 2004; Becker *et al.*, 2001; Enk *et al.*, 2006; Gentile *et al.*, 2003; Howell *et al.*, 2004; Jean *et al.*, 2001; Li *et al.*, 2001; Murakami *et al.*, 2001; Pisarchik *et al.*, 2004; Sesto *et al.*, 2002; Yang *et al.*, 2006), as they are thought to best recapitulate the responses of their *in vivo* isogenic counterpart. However, the use of primary cells in long-term studies is problematic due to the limited proliferative capacity of primary cultures (discussed in Chapter 4). Therefore, the establishment of permanent cell lines provides an alternative for unlimited clonal expansion of *in vitro* cultures. Despite numerous studies demonstrating the disruption of GGR and/or TCR subpathways of NER following oncogenic-mediated transformation (Bowman *et al.*, 2000; El-Mahdy *et al.*, 2000; Ford *et al.*, 1998; Therrien *et al.*, 1999), investigators have continued to exploit SV40-transformed cell lines in the characterisation of transcription responses in NER-defective cells, following exposure to UV or oxidative damage (Chang *et al.*, 2003; da Costa *et al.*, 2005; Kyng *et al.*, 2003). The use of transformed, NER-defective cell lines in transcription expression profiling studies is particularly disadvantageous, as it is difficult to substantiate whether the expression profiles displayed by these cell lines is attributed to their repair-defective phenotype or loss of p53/p21$^{WAF1/CIP1}$ and/or pRb/p16^{INK4A} function during the establishment of these cell lines. As previously discussed (Chapter 4), the ectopic expression of hTERT provides a superior alternative for the establishment of permanent cell lines, which not only extends prolierative capacity (Bodnar *et al.*, 1998), but also retains NER function (Bates *et al.*, 2005; Oullette *et al.*, 2000; Porter *et al.*, 2006). Limited studies have realised the potential of telomerase-mediated immortalisation in the

characterisation of the *in vitro* UV-induced transcriptional response in cells defective in NER. To avoid possible confounding affects of SV40 LgTA on TCR function, and to provide a well controlled isogenic pair of cell lines for analysing *CSB*-dependent gene expression, Newman *et al.* (2006) established hTERT-immortalised isogenic CS-B lines in addition to a CS-B SV40 cell line, derived from the same primary CS-B fibroblast culture (GM00739B, CS1AN).

A further caveat in expression studies is the use of artificial systems. For example, one of the initial transcription expression profiling studies used a pre-existing p53 null colon cancer cell line, compared with a derivative that expressed p53 in response to zinc (Zhao *et al.*, 2000). This produced a set of p53-inducible genes; these were in turn spotted to form a second, custom array that was interrogated using RNA derived from cancer cell lines damaged by UV or IR. The list of differentially regulated genes identified in this study is questionable, as p53 expression in this system was artificially induced. Moreover, the cell lines analysed, although wild type for p53, contained pre-existing mutations.

Many studies have restricted their analysis to a limited number of time points following UV, thus preventing the identification of time-dependent transcriptional responses. This is exemplified in many studies that have characterised the portrait of transcriptional responses to UV after a single time point: 4 hours (Catani *et al.*, 2001; Valéry *et al.*, 2001), 6 hours (Heinloth *et al.*, 2003; McKay *et al.*, 2004; Takao *et al.*, 2002; Zhao *et al.*, 2000) or 24 hours (Becker *et al.*, 2001; Enk *et al.*, 2004; Rieger & Chu, 2004). Several studies, however, have assessed the UV-induced transcriptional response at multiple time points up to 24 hours after UV (Andley *et al.*, 2004; da Costa *et al.*, 2005; Gentile *et al.*, 2003; Lee *et al.*, 2005; Li *et al.*, 2001; Pisarchik *et al.*, 2004), while few have extended the time course up to 72 hours post UV (Enk *et al.*, 2006; Murakami *et al.*, 2001).

A further obstacle in the experimental design of microarray studies is the selection of appropriate and statistically robust methods for the identification of differentially regulated genes. Numerous investigators have implemented flawed

analytical methods to interrogate large datasets generated by microarrays. For example, several studies have deemed a gene to be significantly induced or repressed if an R-fold change is observed (Becker *et al.*, 2001; da Costa *et al.*, 2005; Enk *et al.*, 2004; Enk *et al.*, 2006; Gentile *et al.*, 2003; Li *et al.*, 2001; McKay *et al.*, 2004; Murakami *et al.*, 2001; Pisarchik *et al.*, 2004; Sesto *et al.*, 2002; Zhao *et al.*, 2000), where R represents the ratio of differential gene expression between two states (i.e. treated Vs non treated). This method does not account for the variability in gene expression across the entire sample (array), and results in the biased selection of genes with apparent changes in expression that are not necessarily statistically significant (Tusher *et al.*, 2001). Several investigators have realised the limitations to fold-change and adopted more robust statistical approaches to the identification of differentially regulated genes, such as principle component analysis (PCA), analysis of variance (ANOVA), Student *t* test, the test statistic and significance analysis of microarrays (SAM) (Chang *et al.*, 2003; Guo *et al.*, 2002; He *et al.*, 2004; Howell *et al.*, 2004; Newman *et al.*, 2006; Reiger & Chu, 2004).

A major drawback common to almost all transcription expression profiling studies discussed here is that they were performed on cultured cells under *in vitro* conditions. This is particularly problematic, as skin tissue cultures differ considerably compared to their intact isogenic *in vivo* counterpart that they are supposed to phenotypically resemble. For example, keratinocyte cultures are usually supplemented with hormones and growth factors that might affect cell cycle regulation, stress response and apoptosis (Gibbs *et al.*, 1998). Furthermore, the confluency of an *in vitro* cell culture can affect the regulation of UV-induced apoptosis. Carvalho *et al.* (2003) showed that confluent GGR-defective XP-C and GGR- and TCR-defective TTD primary dermal fibroblasts displayed a decreased level of UV-induced apoptosis compared to subconfluent cultures. They suggested that *in vitro* cultures of confluent cells may better reflect how cells behave *in vivo*, as skin fibroblasts *in vivo* have a quiescent metabolism and reduced turnover similar to that observed in confluent *in vitro* cultures. A further caveat associated with *in vitro* culture models is that the cultures are usually derived from a homogeneous population of cells that lack the additional cellular components of intact skin, which assist in orchestrating a response to UV

through the expression of signalling molecules, such as cytokines. Consequently, although transcription expression profiling of cultured cells has contributed to our understanding of UV-induced stress responses, significant caution should be applied when extrapolating from findings based on cultured cells to transcriptional responses that occur *in vivo*. A recent study undertaken by Enk *et al.* (2006) showed for the first time that, the UVB-induced transcriptional profiles of human epidermis *in vivo* significantly differed from that of cultured epidermal keratinocytes. They found that the expression profiles between human epidermis *in vivo* and cultured epidermal kerationcytes differed by 1931 genes. Moreover, the expression profile of intact epidermis was predominantly associated with DNA repair, while cultured epidermal keratinocytes responded by activating genes associated with cell cycle arrest and apoptosis. However, several experimental caveats have been associated with this study. For example, although the profiling of the *in vivo* intact human epidermis and *in vitro* monolayer of keratinocytes was performed in the same laboratory, they were not performed in parallel. Furthermore, different Affymetrix™ GeneChip® arrays were used for profiling both the *in vivo* and *in vitro* models.

Early attempts at delineating the systematic programme of UV-induced transcriptional responses by microarray were limited by the restricted coverage of the human genome. However, the recent availability of high-density oligonucleotide arrays, more thorough annotation of the human genome and more advanced technological platforms for the analysis and interpretation of array data has permitted the expression profiling of the entire human genome in response to UV. Currently, however, only a limited number of studies have used the new high-density oligonucleotide arrays (such as the HG-U133 Set/Plus 2.0 microarrays) to characterise the UV-induced response (Newman *et al.*, 2006; Yang *et al.*, 2006).

5.2 Aims

Primary XP-C (GM02996, XP8CA) and CS-A (GM01856, CS3BE) human dermal fibroblasts were previously characterised (Chapter 3) and immortalised by transducing the catalytic sub-unit of telomerase (hTERT) into primary XP-C and CS-A fibroblasts (Chapter 4).

To date, information regarding the global transcriptional response to UV remains limited in NER-defective cells. Furthermore, most of the genome-wide studies that have been undertaken on NER-defective *in vitro* cell models (with exception to Newman *et al.*, 2006) have been compromised by the undesirable legacy of immortalisation, namely loss of tumour suppressor function (such as the p53/p21$^{WAF1/CIP1}$ and pRb/p16^{INK4A} pathways), due to the utilisation of cell lines created through transduction with viral oncogenes (previously discussed in Chapter 4). The establishment of hTERT-immortalised XP-C and CS-A cell lines, now permit the genome-wide analysis of NER-defective cell lines in response to UV, whilst retaining the DNA damage response, which lies upstream of DNA repair.

To understand the mechanisms underlying the UV-C transcriptional response in the different NER-defective backgrounds, transcription expression profiling was undertaken on telomerised XP-C and CS-A human dermal fibroblasts at the genome-wide level, using Affymetrix™ GeneChip® HG-U133A probe arrays, with the aim to: (1) identify differentially regulated genes (up-regulated or down-regulated) and pathways; (2) dissect the global transcriptional response to the initiation of DNA repair, in addition to characterising the primary transcriptional stress response to DNA damage *per se*; (3) identify possible UVC-induced, cell-type-specific expression signatures between the telomerised XP-C and CS-A fibroblasts.

The transcription expression profiles obtained for the telomerised XP-C and CS-A cell lines were compared to the wild-type transcriptional response, used as a baseline dataset previously characterised in telomerised NER-proficient MRC-5

fibroblasts. This allowed the identification of genes that fail to be up- or down-regulated in the NER-defective backgrounds, thus further facilitating the identification of genes that are differentially regulated not as a direct result of DNA damage, but as a consequence of the commencement of DNA repair. Transcription expression profiling in the different repair-defective backgrounds would potentially allow the delineation of repair genes that are activated immediately after UV damage and identify what aspect of defective NER repair blocks their expression.

To confirm the validity of the UV-induced transcription expression profile data generated by the Affymetrix™ GeneChip® HG-U133A arrays, a further aim was to validate differentially regulated genes identified in the telomerised XP-C and CS-A cell lines, at both the transcriptome and translational levels by RT-PCR (using the TaqMan platform) and by Western blot analysis, respectively. The rationale behind gene candidate selection for subsequent validation at both the mRNA and protein levels were as followed:

- Selection of genes that orchestrate a diverse range of biological functions in response to UV, such as transcription, stress signalling, cell cycle regulation, DNA repair and apoptosis.

- Demonstrate the establishment of p53/p21$^{WAF1/CIP1}$, pRb/p16^{INK4A} proficient, hTERT-immortalised NER repair-defective XP-C (GM02996, XP8CA) and CS-A (GM01856, CS3BE) fibroblast cell lines (Chapter 4).

- Select genes that exhibited genotype-specific signatures between the hTERT-immortalised NER repair-defective XP-C and CS-A fibroblast cell lines.

- Ascertain whether expression at the translational level recapitulated the transcriptome data obtained from the Affymetrix™ microarrays and quantitative RT-PCR.

5.3 Materials & Methods

Telomerised XP-C (GM02996, XP8CA) and CS-A (GM01856, CS3BE) fibroblasts were prepared by seeding 5 X 10^5 cells in three 60 mm dishes/time point and allowed to equilibrate overnight (Section 2.13.1). For UV treatment, cells (at ~80-90% confluency) were UVC irradiated for 10 seconds with a germicidal lamp (254 nm) at a fluence of 1 J/m^2/s to a dose of 10 J/m^2 (Sections 2.6 & 2.13.1).

Cells were harvested at the indicated time points and total RNA was isolated, using TRIzol reagent, according to the manufacturer's recommendations (Section 2.13.2). Total RNA quantity and quality was assessed, using the NanoDrop® ND-1000 spectrophotometer and Agilent 2100 Bioanalyser (Section 2.13.2). 10 μg of total RNA was reverse transcribed and double-stranded cDNA was synthesised, using a T7-Olio(dT) promoter primer and SuperScript II (Section 2.13.3). After second strand synthesis, IVT was performed and single stranded, biotin-labelled cRNA was prepared, using the ENZO BioArray™ High Yield™ RNA Transcript Labelling Kit (Section 2.13.4). Unincorporated biotinylated nucleotides were removed using a BD Chroma Spin™ Column Kit (Section 2.13.4). Following IVT, the quantity and integrity of the cRNA was assessed as above (Section 2.13.4). The adjusted cRNA yield was calculated and 15 μg of adjusted cRNA was fragmented (Section 2.13.5). The fragmented cRNA was assessed using the Agilent 2100 Bioanalyser as above (Section 2.13.2). Microarray hybridisations were performed by our in-house array service (Sections 2.13.6), using the Affymetrix™ HG-U133A GeneChip® probe arrays.

cRNA samples prepared from telomerised MRC-5 fibroblasts were used to generate the "gold standard" NER proficient transcriptional response, and were used as a baseline data set. They were processed by Dr. M. Peake (DNA Repair Group, Dept. Pathology, Cardiff Uni.) in an identical manner (as described in this thesis). The hybridisations were undertaken by our in-house array service (as above).

The output files generated by the scanned images were analysed using Affymetrix™ Microarray Suite 5 (MAS 5.0) software (Section 5.4.2), and global scaling to a target intensity of 100 was applied (Section 5.4.4). In addition, probe arrays were verified using data obtained for the spiked-in-control probes (BioB, BioC, BioD and CreX) and the housekeeping (GAPDH and β-actin) probe controls (Section 5.4.3).

For validation of *ATF3*, *CDKN1A*, *Ccng2*, *DDB2*, *DTR*, *FDXR*, *GDF15*, *PMAIP1*, *PPM1D* and *SAT* at the mRNA level, by qRT-PCR, cells were UV-irradiated and prepared in an identical manner to the microarray studies (Section 2.13.1). In addition, time-matched mock-irradiated controls were also prepared in an identical manner and in parallel with the irradiated samples, except UV treatment was omitted (Section 2.14.1). Total RNA was extracted at the indicated time points following UV (or mock-irradiation) as previously described (Section 2.13.2) and reverse transcribed using SuperScriptII (Section 2.14.2). RT-PCR was performed using gene-specific primers (Table 2.4, Chapter 2) and TaqMan® Universal PCR Master Mix No AmpErase® UNG in accordance to the manufacturer's recommendations (Section 2.14.3). The amplification reaction was undertaken using an ABI® PRISM® 7000 Sequence Detector (Section 2.14.3). In parallel to the gene-specific assays, *GAPDH* levels were determined for each irradiated and mock-irradiated sample at the indicated time points, by performing a *GAPDH* only RT-PCR assay. The expression value for each gene studied was normalised to the relative amounts of *GAPDH* mRNA present within the same sample. In addition to undertaking three independent biological replicates (performed on different days), each PCR reaction was performed in triplicate. The relative quantification of gene expression was determined using a standard curve methodology (Section 2.14.4).

For validation of ATF3, $p21^{WAF1/CIP1}$ (Chapter 4), GADD45α, PMAIP1 and FDXR at the protein level, immunoblotting was performed using a Biorad Mini-Protean II Electrophoresis Cell System. Briefly, cells were seeded in multiple 100 mm Petri dishes at a density of 1 X 10^6 cells/100 mm dish (Section 2.9.1) and UV irradiated (Section 2.6). WCEs were prepared and quantified as

previously described (Sections 2.9.1-2.9.2). Proteins were separated on SDS-PAGE gels (Section 2.9.3), transferred to PVDF membranes (Section 2.9.3) and exposed to the appropriate primary antibody (Table 2.1, Section 2.9.4). Immuno complexes were detected using an appropriate HRP-coupled secondary antibody, and the blots were visualised using an ECL system and Hyperfilm (Section 2.9.4). Equal protein loading was confirmed by staining the PVDF membrane with India ink (Section 2.9.5).

5.4 Results

5.4.1 The experimental in vitro NER-defective model systems

To investigate the global transcriptional responses in *in vitro* XP-C and CS-A dermal fibroblast cultures following UVC exposure, immortalised XP-C and CS-A cell lines were constructed by transducing primary human XP-C and CS-A fibroblasts with hTERT (Chapter 4). This ensured the preservation of the DNA damage and stress signalling pathways, p53/p21$^{WAF1/CIP1}$ and pRb/p16^{INK4A}. For microarray experiments, telomerised XP-C and CS-A cells were grown to near confluence (~80-90%) in 10% FCS prior to irradiation. A UV wavelength (UVC; 254 nm) and dose (10 J/m^2) was selected that was in line with other studies (Gentile *et al.*, 2003; McKay *et al.*, 2004; Reiger & Chu, 2004). This dose has been shown to have significant biological impact and induce apoptosis in <20% of UV-irradiated primary human fibroblasts or most other DNA-repair proficient human cell lines (Ljungman & Zhang, 1996; McKay & Ljungman, 1999; McKay *et al.*, 1998; Queille *et al.*, 2001; McKay *et al.*, 2002; McKay *et al.*, 2000) and yields ~2.4 lesions per strand of an average gene (McKay *et al.*, 2004; van Hoffen *et al.*, 1995). To analyse the UVC regulated expression patterns, cells were harvested at 0, ~6 ~12 and ~24 hours post UVC irradiation. Total RNA was extracted from the cells and was further processed and hybridised to Affymetrix™ HG-U133A GeneChip® oligonucleotide arrays as described in Materials and Methods. Three independent biological replicates were prepared

for each time point and cell line. Each biological replicate represented independent RNA isolations, cRNA synthesises and hybridisations, using the same stable telomerised cell line (and clone) at different PDs; each biological replicate used for microarray analysis did not exceed 100 cumulative PDs. In addition, for each time point and each independent biological replicate, three separate RNA isolations were performed (on three separate UVC irradiated 60 mm dishes) which where eventually pooled following RNA isolation. The incorporation of multiple dishes and biological replicates addressed any possible variability that occurred within the experimental design such as variation in the UV light source (such as fluctuations in fluence), RNA isolation, cRNA labelling, array hybridisations or variability in the scanner.

5.4.2 Initial data analysis of transcriptional regulation of gene expression in telomerised XP-C and CS-A fibroblasts

The image output data files (.DAT) generated from the scanned images were processed and analysed by the probe level software package, Affymetrix™ MAS 5.0 (Affymetrix™, 2001). This facilitated the conversion of the image data file to a CHP file. The CHP file provided the raw signal intensity value for each of the 22,283 probe sets present on the array, where an absent, present or marginal call was assigned to each probe. Subsequent analysis of the data was undertaken using the R environment for statistical computing (Gentlemen *et al.*, 2004) along with the '*affy*', '*affyPLM*' and '*simpleaffy*' analysis packages downloaded from http://www.bioconductor.org. The .CEL intensity data was analysed to produce a single expression value for each probe set using the MAS 5.0 statistical algorithm (Affymetrix™, 2002).

5.4.3 Quality control (QC) parameters

The Affymetrix™ platform has a number of built-in QC metrics, which are generated from the MAS 5.0 algorithm, that facilitate the assessment of array quality and identification of defective arrays. Therefore, several QC metrics

(Wilson & Miller, 2005) recommended by Affymetrix™ were assessed. These are described in detail in their 'Expression Analysis Technical Manual' (http:/ www.affymetrix.com/support/technical/mannual/expression_mannual.affx).

To determine whether there was any significant difference in cRNA quality between biological replicates used in each array experiment, a series of RNA degradation plots were constructed to assess the integrity of the cRNA between samples. RNA degradation, or problems during cRNA labelling can cause under representation at the 5' end. Therefore, the ratio between signals from the 5' and 3' probe sets were used to assess RNA quality. RNA degradation plots generated using the '*affy*' software package, display expression as a function of 5'-3' position of probes. For each array and within each probe set, probes are arranged by their proximity to the 5' end of the gene. Each line of the RNA degradation plots corresponds to an array and the slope of its trend indicates potential RNA degradation of the cRNA sample. Additionally, RNA degradation plots assess the efficiency of cDNA synthesis and the IVT of biotin labelled cRNA. As expected, following the labelling and hybridisation processes, within each probe set, the probes matching close to the 5'end of the gene had lower intensity measures than that of the probes matching closer to the 3' (Figs. 5.1A & B). Moreover, the individual lines (representing either an XP-C or CS-A sample) lie parallel to each other, which suggests that the degradation patterns between the arrays were similar (Figs. 5.1A & B).

The percentage of genes that call present on a given array is referred to as the percent present value and represents the percentage of probe sets called present on an array. This is dependent upon multiple factors including cell/tissue type, biological or environmental stimuli, and overall quality of the RNA sample and the probe array type. The Present/Marginal/Absent cells are calculated from the differences between PM and MM values for each probe pair in a probe set (described in Section 5.1). Probe sets are deemed marginal or absent when the PM values for each Probe set are not significantly above the MM probes. Replicate samples, however, should display a similar percent present value, as large variations in present calls between similar samples usually suggest that varying amounts of cRNA have hybridised to the array. Extremely low percent

present values are usually indicative of poor sample quality. The percent present values for all the arrays performed on the telomerised XP-C and CS-A samples, at the indicated time points ranged between 40-50% (Figs. 5.2A & B, respectively). Although the absolute % present value is generally not a good QC metric, as some cell types naturally express more genes than others, the values obtained in this study fall within the expected range for the HG-U133A array.

The average background should be similar across all arrays. Significant variations in background has been attributed to several factors such as different amounts of cRNA present in the hybridisation cocktail, varying hybridisation efficiencies, incorporation of more label or manufacturing variances producing a "brighter chip". Although there are no official guidelines regarding background, Affymetrix™ has found that typical average background values range from 20 to 100 for arrays scanned with the GeneChip® Scanner 3000. As shown by the quality control metrics in Figure 5.2, the background values for the hybridisations were within the normal range for both the XP-C and CS-A arrays (Figs. 5.2A & B, respectively).

By comparing the amount of signal from the 3' probe set to the 5' probe set, it is possible to assess the quality of the cRNA hybridised to the array, as high ratios signify the presence of truncated transcripts. Therefore, as a further internal quality control and to assess RNA integrity, GAPDH and β-actin ratios were calculated for each individual array. Both GAPDH 3':5' (circles) and β-actin 3':5' (triangles) ratios were plotted for the telomerised XP-C and CS-A samples (Figs. 5.2A and B, respectively). GAPDH ratios were ≤1 and well below the suggested maximum of 1.25 (Wilson & Miller, 2005). As β-actin is a longer gene, Affymetrix™ recommend that the 3':5' ratios should be below 3. As shown in Figures 5.2A and 5.2B the ratios for β-actin were <3 for the XP-C and CS-A samples, respectively.

The spike-in hybridisation BioB control was found to be present on all arrays, while BioC, BioD and CreX were also present in increasing intensity.

In summary, the quality control metrics assessed on the probe arrays presented here displayed no abnormalities, and were therefore subjected to further statistical analysis.

5.4.4 Data normalisation

Although the Affymetrix™ GeneChip® system is a robust platform, differences in signal intensity can occur due to experimental variability such as pipetting error, hybridisation efficiency, washing and staining efficiency, which are independent of relative transcript concentration. Therefore, a method of normalisation was required to standardise the target intensity (mean expression signal) of each experiment. The target signal was set to TGT= 100. Affymetrix™ stipulates that scale factors applied to expression values obtained from their GeneChips® should fall within a 3-fold range, as discrepancies in the scale factors (≥3 fold) usually indicate variability or cRNA degradation. The quality control plots confirm that all XP-C and CS-A arrays were within the recommended limits (Figs. 5.2A & B, respectively).

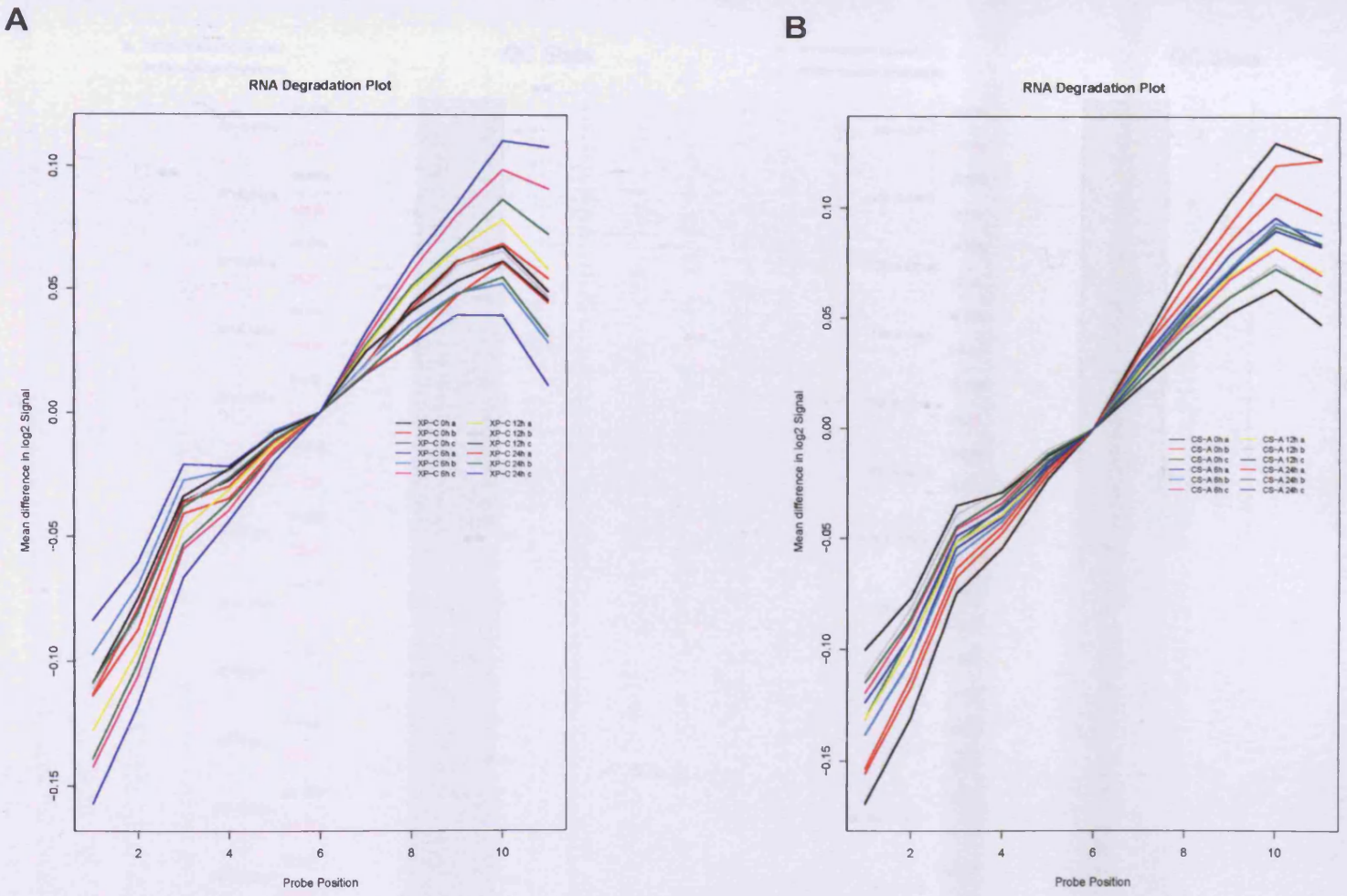

Figure 5.1. RNA degradation plots for GeneChip data from telomerised (A) XP-C (XP8CA) and (B) CS-A (CS3BE) dermal fibroblasts following UVC-irradiation (254 nm) at the indicated time points (h, hour).

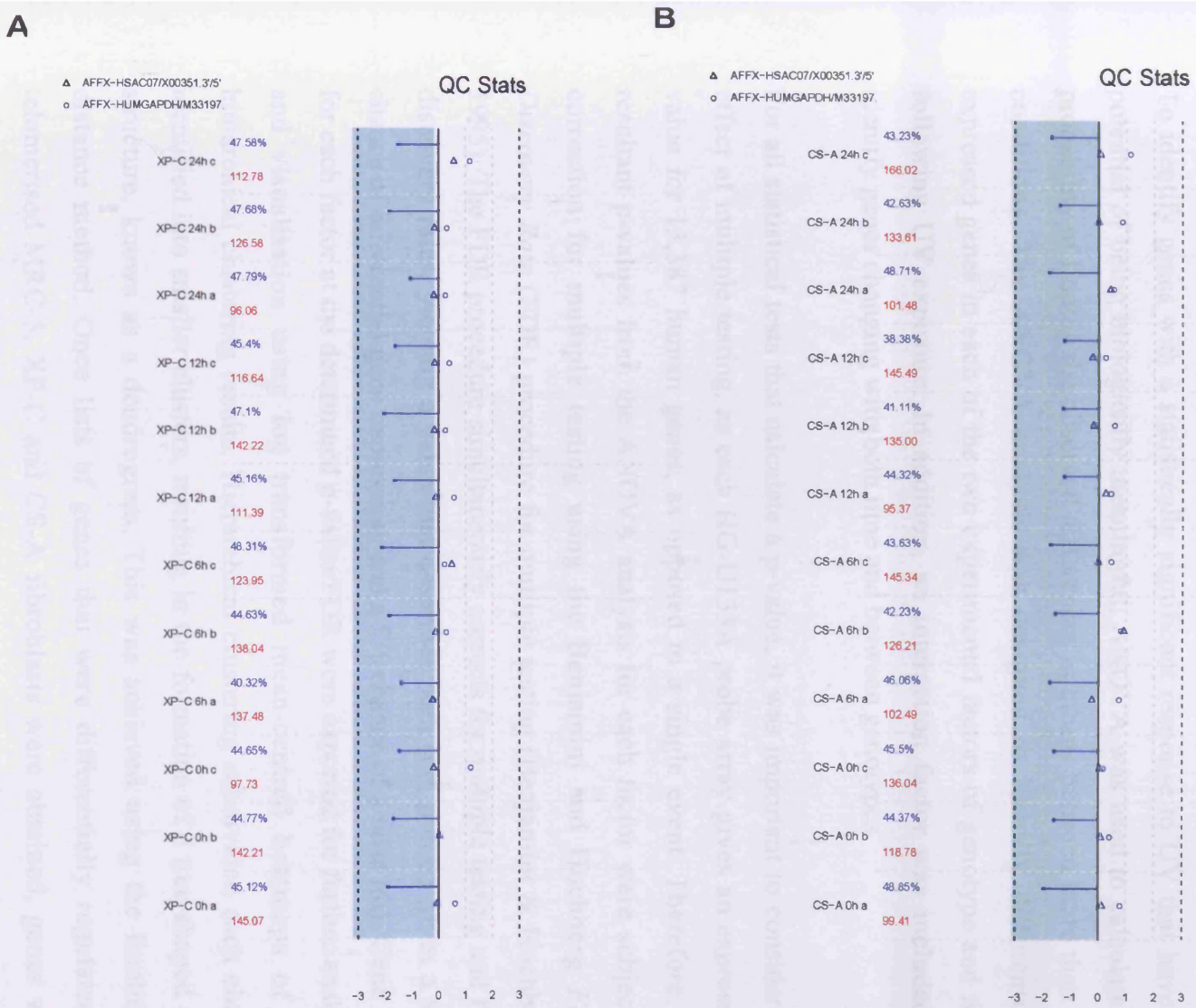

Figure 5.2. SimpleAffy quality control plots for array data from telomerised (a) XP-C (XP8CA) and (B) CS-A (CS3BE) dermal fibroblasts

5.4.5 Analysis of variance (ANOVA)

Statistical analysis was undertaken by Dr. Peter Giles (bioinformaticians), a member of our in-house array service.

To identify genes with a statistically significant response to UV that have the potential of being biologically meaningful, ANOVA was used to calculate the probability of finding the observed differences in means between more than two conditions. The ANOVA analysis was designed to identify differentially expressed genes in each of the two experimental factors of genotype and time, following UV exposure. In addition, an interaction factor was included to identify genes changing with both time and between genotypes.

For all statistical tests that calculate a p-value, it was important to consider the effect of multiple testing, as each HG-U133A probe array gives an expression value for 13,387 human genes, as opposed to a single event. Therefore, the resultant p-values from the ANOVA analysis for each factor were subject to correction for multiple testing using the Benjamini and Hochberg *False Discovery Rate* (FDR) procedure for multiple testing (Benjamini & Hochberg, 1995). The FDR procedure simultaneously corrects for multiple testing and false discovery rates, yielding a value that describes both (i.e. p=0.05 gives a 95% chance of differential gene expression, and a 5% chance of a false hit). Gene lists for each factor at the determined p-value/FDR were exported for further analysis and visualisation using log transformed mean-centred heatmaps of the hierarchical clustering results. Hierarchical clustering subdivided each cluster identified into smaller clusters, resulting in the formation of a tree-shaped data structure, known as a dendrogram. This was achieved using the Euclidean distance method. Once lists of genes that were differentially regulated in telomerised MRC-5, XP-C and CS-A fibroblasts were obtained, genes were individually assessed for their significance in response to UV.

5.4.6 Transcription profiles of un-irradiated telomerised XP-C and CS-A dermal fibroblasts

In the present study, an important step in the experimental design was the selection of appropriate controls, as time-matched, non-irradiated controls for comparative analysis with each irradiated sample was beyond the scope of this investigation, due to the cost of Affymetrix™ HG-U133A high-density oligonucleotide GeneChip® arrays. Therefore, all XP-C and CS-A irradiated samples at the indicated time points (~6, ~12 and ~24 hours) were compared to irradiated samples extracted immediately after UV (0 hours). However, the immediate effects of UV on telomerised XP-C and CS-A fibroblasts were unknown. Therefore, three biological replicates were prepared (in an identical manner as the irradiated samples except UV was omitted) immediately following mock-irradiation for each of the telomerised XP-C and CS-A fibroblast cell lines at different PDs. The HG-U133A arrays prepared from mock-irradiated cells were compared to the probe arrays prepared immediately after UV. The data revealed no significant differences between the mock-irradiated and irradiated samples prepared at 0 hours (data not shown). This suggested that UV had no immediate effect (at 0 hours) on the transcriptome. Therefore, the irradiated samples prepared at 0 hours were used as the control for comparative analysis with the corresponding MRC-5, XP-C and CS-A samples prepared at 6, 12 and 24 hours after UVC treatment.

5.4.7 Genotype-specific modulation of the telomerised MRC-5, XP-C and CS-A cell transcriptome

Significant changes in transcriptional modulation were observed in hTERT-immortalised MRC-5, XP-C and CS-A fibroblasts. ANOVA analysis revealed that, of the 22,283 probe sets on the Affymetrix™ HG-U133A GeneChip® array, 705 probes sets (at an FDR= 0.0000001%), which represented 567 genes, were identified as being differentially regulated in a genotype-specific manner (Fig. 5.3). Subsequent hierarchical clustering of the 705 differentially regulated probe sets resulted in the formation of a dendogram which revealed five principle clusters according to the pattern of differential regulation. The five clusters displayed different kinetics of high and low expression levels of probe sets in the telomerised MRC-5, XP-C and CS-A fibroblasts at 0, ~6, ~12 and ~24 hours following UVC exposure (Fig. 5.4). Table 5.1 summarises the number of differentially regulated probe sets identified in this study, which occurred in a genotype-specific manner. The probe sets identified in each cluster were categorised according to biological function (Appendix 1). Because many of the genes present on the HG-U133A array were represented by multiple probe sets, several of the 567 genes appear more than once in the gene lists. The five clusters displayed differential patterns of expression, which represented a diverse range of biological functions, few changes in gene expression appeared UV-dependent. For example, the 351 differentially regulated probe sets in cluster 1 were repressed in telomerised MRC-5 fibroblasts throughout the entire time course at 0, ~6, ~12 and ~24 hours following UV. In contrast, although the telomerised XP-C and CS-A fibroblasts displayed a differential pattern of expression compared to the telomerised MRC-5 cells, both the telomerised XP-C and CS-A fibroblasts exhibited a similar programme of transcriptional responses for the 351 probe sets (Fig. 5.4, cluster 1). Generally, the 351 probe sets identified in cluster 1 were upregulated in both XP-C and CS-A cell lines (this was signified by an increase in intensity). Moreover, minimal fluctuations in the kinetics of differential regulation occurred between the 351 transcripts throughout the time course in MRC-5, XP-C and CS-A cells. Notably, however, a small subset of probe sets within cluster 1, displayed a further marked

induction in the telomerised CS-A cells compared to the XP-C cells (Fig. 5.4, cluster 1). The 351 differentially regulated probe sets represented gene transcripts from a diverse range of functional categories that regulate a multiplicity of pathways that maintain normal cellular homeostasis (Appendix 1). In addition to the identification of genotype-specific patterns of differential regulation observed in cluster 1, the kinetics of gene expression appeared to be similar throughout the time course and displayed minimal changes at 0, ~6, ~12 and ~24 hours following UVC irradiation. This suggested that the differential regulation of gene expression identified in telomerised MRC-5, XP-C and CS-A cell lines, occurred independent of UV-irradiation.

Similar to cluster 1, the patterns of differential gene expression observed among the 74 probe sets identified in cluster 2 occurred in a UV-independent manner. Unlike cluster 1, however, more than half (45) of the probe sets were deemed upregulated in the telomerised MRC-5 cells. In contrast, the 74 probe sets appeared to be repressed in telomerised XP-C cells, while the CS-A cell line displayed a heterogeneous level of differential gene expression for the same probe sets over the time course.

Interestingly, although the expression pattern of the 54 probe sets in cluster 3 appeared to be genotype-specific, the differential gene expression appeared to also occur in a UV-dependent manner (Fig. 5.4, cluster 3). For example, 36 of the 54 probe sets were significantly repressed in the CS-A cells at ~6 and ~12 hours following UVC-irradiation, compared to the level of expression observed at 0 and ~24 hours post UV-irradiation. Conversely, 18 probe sets were repressed throughout the entire time course, thus further suggesting a genotype-specific UV-independent response. In contrast, a large number of the probe sets were up-regulated at 0 hours post UV followed by rapid down regulation at 6 hours in telomerised MRC-5 cells. The probe sets displayed subsequent induction at ~12 and ~24 hours post UV. This suggested that UV caused a repression of these probe set in the MRC-5 cell line. However, without time-matched, mock-irradiated samples, it can only be speculated that these changes observed in cluster 3 for CS-A and MRC-5 occurred as a result of UV-irradiation. The

telomerised XP-C cells exhibited a heterogeneous level of expression for the same 54 probe sets in cluster 3 (Fig. 5.4, cluster 3).

Cluster 4 contained 193 probe sets that presented higher levels in MRC-5 compared to the XP-C and CS-A cell lines. Notably, the higher levels of expression continued throughout the time course at ~6, ~12 and ~24 hours. This suggested that the induction of the 193 probe sets identified in cluster 4 in MRC-5 cells, occurred in a genotype-specific and UV-independent manner (Fig. 5.4, cluster 4). Conversely, the 193 differentially regulated probe sets identified in cluster 4, exhibited heterogeneous levels patterns of expression in both telomerised XP-C and CS-A cell lines, but displayed no obvious patterns of induction or repression. This further suggested that the genotype-specific transcriptional responses were UV-independent.

Interestingly, the 33 differentially regulated probe sets in cluster 5 were significantly induced throughout the time course at 0, ~6, ~12 and ~24 hours in telomerised XP-C cells, irrespective of UV exposure (Fig. 5.4, cluster 5). The identical kinetics of induction that were observed at ~6, ~12 and ~24 hours compared to those observed at 0 hours, indicated that the transcriptional responses in XP-C cells were also genotype-specific, rather than UV-dependent. In contrast to clusters 1-4, heterogeneous patterns of expression was observed for the 33 probe sets in cluster 5 in MRC-5 cells. Similarly, CS-A cells displayed a heterogeneous level of expression for the 33 probe sets identified in cluster 5 (Fig. 5.4, cluster 5).

Although several differentially regulated probe sets identified in the five genotype-specific clusters represented biological functions in the cell cycle (such as *ABL1*, *CCND1*, *DUSP6*, *EREG*, *G0S2* and *PML*), regulation of proliferation (such as *CDKN2A*, *CREG1*, *FTH1*, *HOXC10*, *IGFBP6*, *IGFBP7*, *PPAP2A*, *TNFSF9* and *TP53I11*) and apoptosis (such as *BAG1*, *CASP1*, *CASP4* and *PPP2R1B*), which are pathways closely associated with the DNA damage response, a large number of probe sets represented several other functional groups. These common functional groups represented by the 705 differentially

regulated probe sets identified in clusters 1-5 included: membrane-associated, protein binding, nucleus, cytoplasm, metal ion binding, signal transduction and transcription factor activity (Table 5.1). Only three probe sets identified in cluster 1 represented genes that are directly involved in DNA repair (*ELN*, *MGMT* and *PML*). Two further probe sets identified in cluster 4 represented DNA repair genes (*PARP4* and *POLB*). Notably, however, non of the DNA repair genes identified here were associated with the core NER apparatus.

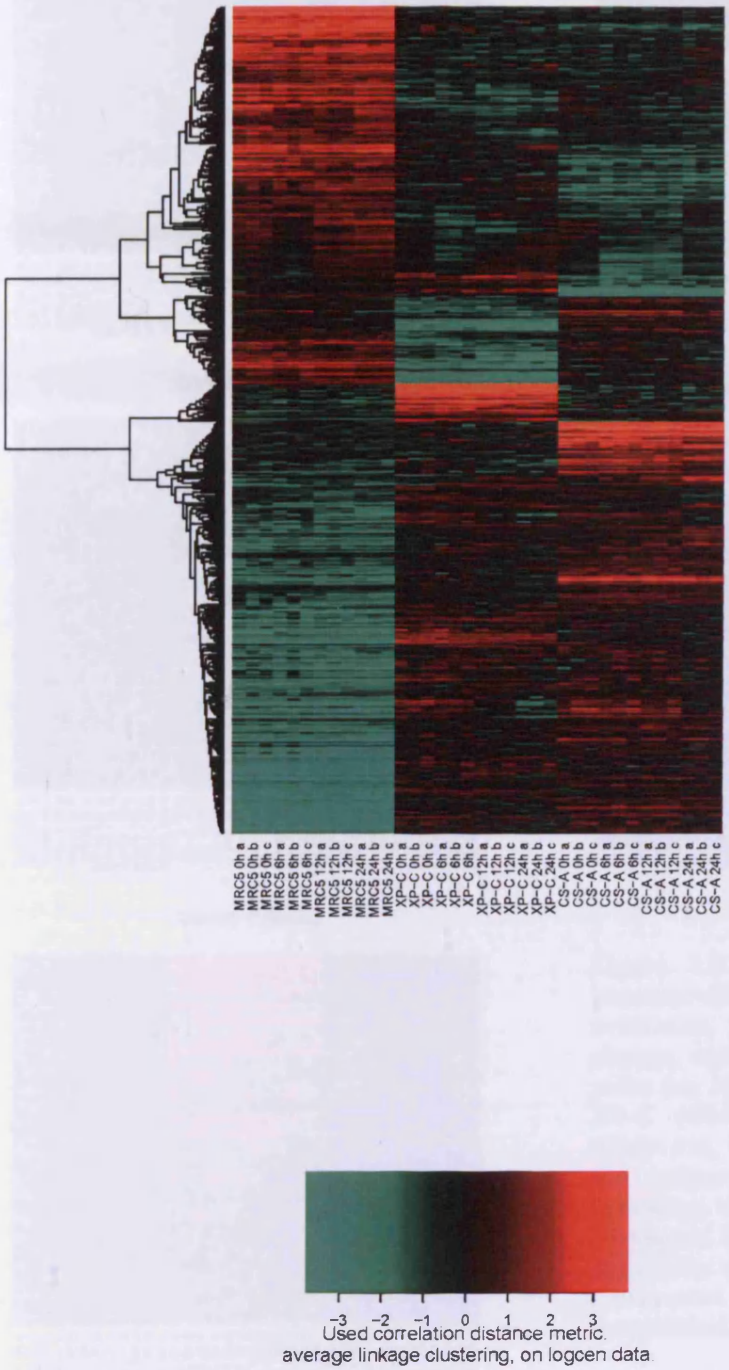

Figure 5.3. ANOVA of genotype-specific changes in gene expression. Hierarchical clustering depicting the genotype-specific transcriptional changes of 705 differentially regulated probe sets, whose levels of expression altered in a genotype-specific manner in telomerised MRC-5, XP-C (GM02996, XP8CA) and CS-A (GM01856, CS3BE) fibroblast cell lines, following UVC (254 nm), at the indicated time points (h, hour). The columns correspond to the cell lines and the rows to each gene transcript. The altered expression levels are represented in colour and red signifies upregulation, while green, downregulation.

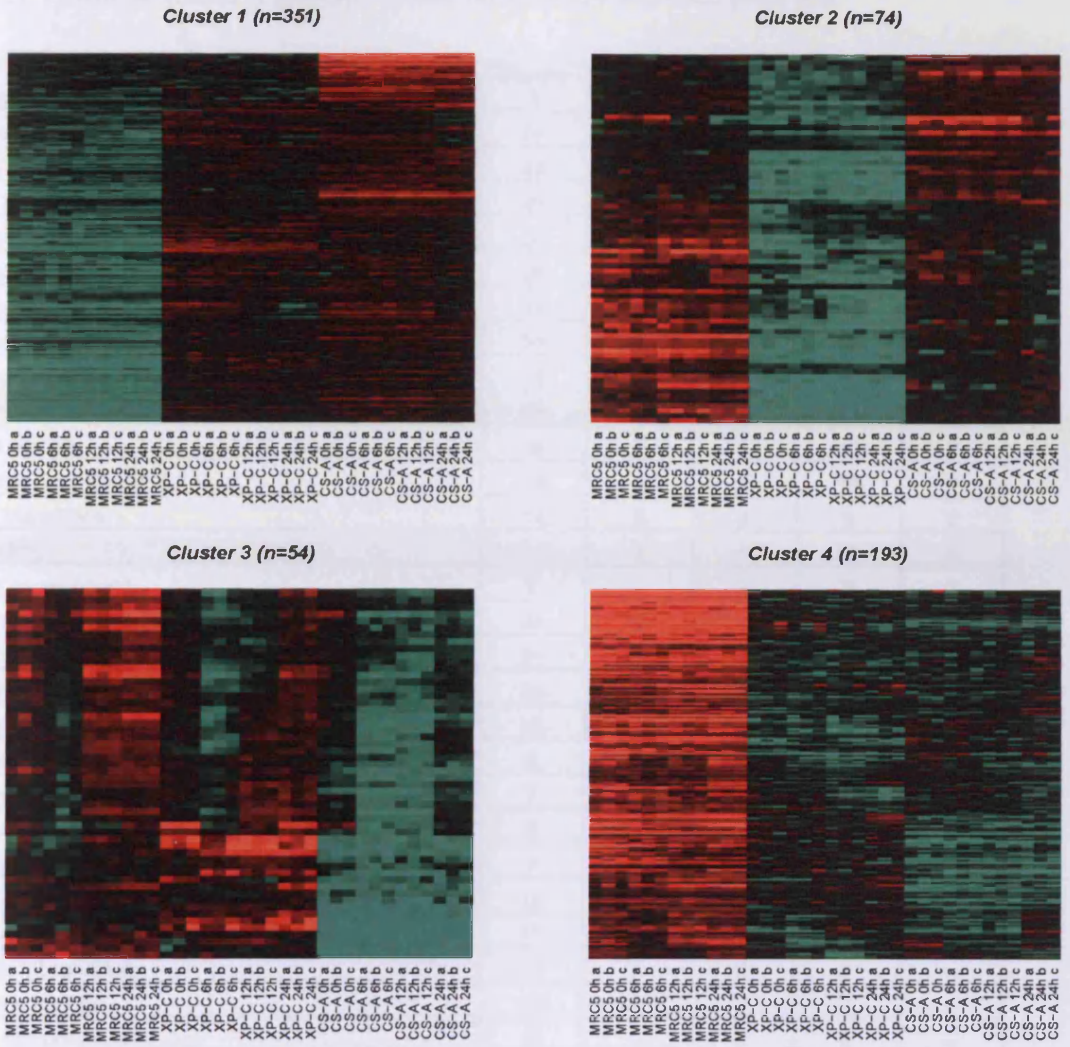

Figure 5.4. Hierarchical clustering of genotype-specific genes following UVC-irradiation. The data depicts five distinct clusters, which show differentially regulated probe sets identified in telomerised MRC-5, XP-C (GM02996, XP8CA) and CS-A (GM01856, CS3BE) fibroblast cell lines at the indicated time points (h, hour), following UV-C treatment. The columns correspond to the cell lines and the rows to each probe set. The change in expression is represented in colour and red signifies upregulation, while green, downregulation.

Table 5.1. Functional classes of genotype-specific differentially expressed probe sets.

GO Category	Cluster 1	Cluster 2	Cluster 3	Cluster 4	Cluster 5
Membrane	64	22	4	43	6
Integral to membrane	49	11	3	24	4
Protein binding	46	12	13	30	7
Nucleus	35	8	19	25	8
Cytoplasm	24	5	5	12	3
Metal ion binding	24	9	5	10	3
Signal transduction	21	5	9	23	5
Transcription factor activity	19	3	8	16	4
Regulation of transcription, DNA-dependent	19	4	10	12	4
Zinc ion binding	16	4	5	10	2
Nucleotide binding	15	6	8	13	2
Plasma membrane	14	5	2	9	2
ATP binding	11	3	5	10	2
Skeletal development	9	--	2	2	2
Cell adhesion	24	8	--	8	4
Receptor activity	21	8	--	16	2
Extracellular matrix (sensu Metazoa)	20	3	--	3	3
Calcium ion binding	16	4	--	11	3
Cell proliferation	8	2	--	2	2
Structural molecule activity	7	2	--	4	3
Cytoskeleton	6	--	--	5	3
Structural constituent of cytoskeleton	2	--	2	--	2
Development	18	4	2	10	--
Molecular function unknown	17	2	2	5	--
Endoplasmic reticulum	12	2	2	3	--
Membrane fraction	10	5	3	9	--
Cellular component unknown	16	--	2	5	--
Transferase activity	12	--	6	6	--
Transcription	8	--	6	8	--
Kinase activity	5	--	2	4	--
Regulation of transcription from RNA polymerase II promoter	5	--	2	3	--
RNA polymerase II transcription factor activity	3	--	2	2	--
Signal transducer activity	3	--	2	6	--
Ubiquitin cycle	3	--	3	4	--
Protein amino acid phosphorylation	3	--	6	6	--
Transcription from RNA polymerase II promoter	2	--	2	2	--
Regulation of progression through cell cycle	2	--	2	5	--
Transcription coactivator activity	2	--	2	3	--
Binding	2	--	2	2	--
Protein serine/threonine kinase activity	2	--	3	2	--
Integral to plasma membrane	25	9	--	25	--
Oxidoreductase activity	20	4	--	4	--
Extracellular space	19	6	--	6	--
Extracellular region	18	3	--	10	--

Table 5.1. *Continued*

Proteolysis and peptidolysis	15	2	--	8	--
Biological process unknown	15	2	--	8	--
Cell differentiation	10	4	--	2	--
Hydrolase activity	10	3	--	8	--
Electron transporter activity	9	2	--	2	--
Cell-cell signaling	9	6	--	5	--
Neurogenesis	7	4	--	5	--
Growth factor activity	6	2	--	4	--
Soluble fraction	6	2	--	4	--
lysosome	5	2	--	2	--
Transport	5	2	--	9	--
Morphogenesis	5	2	--	5	--
Immune response	5	2	--	4	--
carbohydrate metabolism	2	3	--	2	--
Extracellular matrix structural constituent	19	--	--	4	--
G-protein coupled receptor protein signaling pathway	11	--	--	13	--
Metabolism	10	--	--	4	--
Negative regulation of cell proliferation	8	--	--	2	--
Phosphate transport	8	--	--	4	--
Apoptosis	8	--	--	2	--
Mitochondrion	7	--	--	4	--
GTP binding	7	--	--	2	--
Golgi stack	7	--	--	2	--
Collagen	7	--	--	4	--
Regulation of cell growth	6	--	--	3	--
Cell cycle	6	--	--	3	--
Magnesium ion binding	6	--	--	3	--
Protein modification	6	--	--	2	--
Transmembrane receptor protein tyrosine kinase signaling pathway	5	--	--	2	--
Visual perception	5	--	--	2	--
Catalytic activity	5	--	--	3	--
Cytosol	5	--	--	5	--
Actin binding	5	--	--	2	--
Rhodopsin-like receptor activity	5	--	--	10	--
Serine-type endopeptidase inhibitor activity	4	--	--	2	--
Blood coagulation	4	--	--	6	--
Circulation	4	--	--	2	--
Insulin-like growth factor binding	4	--	--	3	--
Peptidase activity	4	--	--	5	--
Negative regulation of progression through cell cycle	4	--	--	2	--
Cell motility	4	--	--	3	--
Angiogenesis	4	--	--	2	--
Aminopeptidase activity	4	--	--	2	--
Positive regulation of cell proliferation	4	--	--	3	--
Intracellular	3	--	--	3	--

Table 5.1. *Continued*

Regulation of apoptosis	3	--	--	2	--
DNA repair	3	--	--	2	--
Sensory perception	2	--	--	4	--
Lipid metabolism	2	--	--	2	--
Protein complex assembly	2	--	--	3	--
Membrane alanyl aminopeptidase activity	2	--	--	2	--
Metallopeptidase activity	2	--	--	2	--
Positive regulation of I-kappaB kinase/NF-kappaB cascade	2	--	--	3	--
Receptor binding	2	--	--	2	--
Extracellular matrix organization and biogenesis	2	--	--	2	--
Vascular endothelial growth factor receptor activity	2	--	--	2	--
GTPase activity	2	--	--	2	--
Induction of apoptosis	2	--	--	2	--
Calmodulin binding	2	--	--	2	--
Transporter activity	2	--	--	6	--
ATPase activity	--	2	--	3	--
Cation transport	--	2	--	2	--
RNA binding	--	--	2	4	--
Protein amino acid dephosphorylation	--	--	2	6	--
Ubiquitin thiolesterase activity	--	--	2	2	--
DNA binding	6	--	5	--	--
Intracellular signaling cascade	5	--	3	--	--
Transcription corepressor activity	3	--	2	--	--
Chromosome organization and biogenesis (sensu Eukaryota)	2	--	2	--	--
Response to stress	2	--	2	--	--
ilon ion binding	6	2	--	--	--
Cell surface receptor linked signal transduction	3	2	--	--	--
Hormone activity	3	2	--	--	--
Cell surface	2	2	--	--	--
Perception of sound	2	3	--	--	--
Cytokine activity	2	2	--	--	--
Growth	2	2	--	--	--
Axon guidance	2	2	--	--	--
Protein folding	10	--	--	--	--
Ion transport	9	--	--	--	--
Electron transport	8	--	--	--	--
Organogenesis	8	--	--	--	--
Pregnancy	7	--	--	--	--
Muscle development	5	--	--	--	--
Defense response	5	--	--	--	--
Heparin binding	5	--	--	--	--
Copper ion binding	5	--	--	--	--
Isomerase activity	5	--	--	--	--
Neuropeptide signaling pathway	5	--	--	--	--
Nucleic acid binding	5	--	--	--	--
Microsome	4	--	--	--	--

Table 5.1. *Continued*

Basement membrane	4	--	--	--	--
Unfolded protein binding	4	--	--	--	--
Actin cytoskeleton organization and biogenesis	4	--	--	--	--
Ligase activity	4	--	--	--	--
Sugar binding	4	--	--	--	--
Synaptic transmission	4	--	--	--	--
Potassium ion transport	4	--	--	--	--
Response to unfolded protein	4	--	--	--	--
Cytoskeleton organization and biogenesis	4	--	--	--	--
Anti-apoptosis	4	--	--	--	--
Epidermis development	3	--	--	--	--
Neutral amino acid transporter activity	3	--	--	--	--
Coated pit	3	--	--	--	--
Transcription regulator activity	3	--	--	--	--
Regulation of transcription	3	--	--	--	--
Collagen binding	3	--	--	--	--
Ion channel transport	3	--	--	--	--
Central nervous system development	3	--	--	--	--
Nucleoside metabolism	3	--	--	--	--
Chemotaxis	3	--	--	--	--
Ion channel activity	3	--	--	--	--
Protein transport	3	--	--	--	--
Voltage-gated ion channel activity	3	--	--	--	--
Potassium channel activity	3	--	--	--	--
Voltage-gated potassium channel complex	3	--	--	--	--
Potassium ion binding	3	--	--	--	--
Cell cycle arrest	3	--	--	--	--
Cell-cell adhesion	3	--	--	--	--
Endonuclease activity	3	--	--	--	--
Rho protein signal transduction	3	--	--	--	--
Peptidyl-prolyl cis-trans isomerase activity	3	--	--	--	--
GTP biosynthesis	2	--	--	--	--
Intermediate filament	2	--	--	--	--
Enzyme inhibitor activity	2	--	--	--	--
Amino acid metabolism	2	--	--	--	--
Amino acid transport	2	--	--	--	--
Amino acid permease activity	2	--	--	--	--
Endocytosis	2	--	--	--	--
Microtubule	2	--	--	--	--
SH3 domain binding	2	--	--	--	--
Guanyl-nucleotide exchange factor activity	2	--	--	--	--
Cytochrome-b5 reductase activity	2	--	--	--	--
Aldehyde dehydrogenase [--D(P)+] activity	2	--	--	--	--
Aldehyde metabolism	2	--	--	--	--
Small GTPase mediated signal transduction	2	--	--	--	--
Collagen type I	2	--	--	--	--

Table 5.1. *Continued*

Structural constituent of bone	2	--	--	--	--
Heme binding	2	--	--	--	--
Nucleosome	2	--	--	--	--
Chromosome	2	--	--	--	--
Nucleosome assembly	2	--	--	--	--
ER-Golgi intermediate compartment	2	--	--	--	--
Metalloendopeptidase activity	2	--	--	--	--
integrin-mediated signaling pathway	2	--	--	--	--
Transferase activity, transferring glycosyl groups	2	--	--	--	--
Collagen type V	2	--	--	--	--
Microfibril	2	--	--	--	--
Calcium-mediated signaling	2	--	--	--	--
Protein-lysine 6-oxidase activity	2	--	--	--	--
Transmembrane receptor activity	2	--	--	--	--
iIntracellular protein transport	2	--	--	--	--
Enzyme activator activity	2	--	--	--	--
Peptide hormone processing	2	--	--	--	--
Receptor mediated endocytosis	2	--	--	--	--
Chloride transport	2	--	--	--	--
Postsynaptic membrane	2	--	--	--	--
Protein targeting	2	--	--	--	--
Protein secretion	2	--	--	--	--
Amino acid biosynthesis	2	--	--	--	--
Acyltransferase activity	2	--	--	--	--
Protein homodimerization activity	2	--	--	--	--
Cell-matrix adhesion	2	--	--	--	--
Neuropeptide hormone activity	2	--	--	--	--
Sarcoglycan complex	2	--	--	--	--
GTPase activator activity	2	--	--	--	--
G1/S transition of mitotic cell cycle	2	--	--	--	--
Cell division	2	--	--	--	--
Protein kinase C activation	2	--	--	--	--
Protein binding, bridging	2	--	--	--	--
Lipid raft	2	--	--	--	--
Nucleotide metabolism	2	--	--	--	--
Negative regulation of adenylate cyclase activity	2	--	--	--	--
Ossification	2	--	--	--	--
Integrin binding	2	--	--	--	--
Dipeptidyl-peptidase IV activity	2	--	--	--	--
Prolyl oligopeptidase activity	2	--	--	--	--
lLmellipodium	2	--	--	--	--
Motor activity	2	--	--	--	--
Protein self binding	2	--	--	--	--
Regulation of heart contraction rate	2	--	--	--	--
Positive regulation of cell migration	2	--	--	--	--
Mesoderm development	--	2	--	--	--

Table 5.1. *Continued*

Symporter activity	--	2	--	--	--
Ubiquitin-dependent protein catabolism	--	--	3	--	--
Protein-tyrosine kinase activity	--	--	2	--	--
Protein kinase cascade	--	--	2	--	--
Negative regulation of transcription	--	--	2	--	--
Transcriptional repressor activity	--	--	2	--	--
Negative regulation of transcription, DNA-dependent	--	--	2	--	--
Ribonucleoprotein complex	--	--	2	--	--
JNK cascade	--	--	2	--	--
Cysteine-type endopeptidase activity	--	--	2	--	--
Inflammatory response	--	--	--	4	--
Protein tyrosine phosphatase activity	--	--	--	4	--
Collagen type IV	--	--	--	4	--
Response to drug	--	--	--	3	--
Elevation of cytoplasmic calcium ion concentration	--	--	--	3	--
Serine-type endopeptidase activity	--	--	--	3	--
Steroid hormone receptor activity	--	--	--	3	--
Protein serine/threonine phosphatase activity	--	--	--	3	--
Aldehyde dehydrogenase (--D) activity	--	--	--	2	--
Plasminogen activator activity	--	--	--	2	--
Inactivation of MAPK activity	--	--	--	2	--
Regulation of cell adhesion	--	--	--	2	--
Negative regulation of cell growth	--	--	--	2	--
Protein heterodimerization activity	--	--	--	2	--
MAPKKK cascade	--	--	--	2	--
ATPase activity, coupled to transmembrane movement of substances	--	--	--	2	--
Sodium ion binding	--	--	--	2	--
RNA processing	--	--	--	2	--
Caspase activator activity	--	--	--	2	--
Response to nutrients	--	--	--	2	--
Prostaglandin E receptor activity	--	--	--	2	--
G-protein signaling, coupled to cAMP nucleotide second messenger	--	--	--	2	--
Bradykinin receptor activity	--	--	--	2	--
Activation of MAPK activity	--	--	--	2	--
Adenylate cyclase activation	--	--	--	2	--
Transcription factor complex	--	--	--	2	--
Cation channel activity	--	--	--	2	--
Ligand-regulated transcription factor activity	--	--	--	2	--
Cysteine-type peptidase activity	--	--	--	2	--
Caspase activity	--	--	--	2	--
Ubiquitin-protein ligase activity	--	--	--	2	--
Heterogeneous nuclear ribonucleoprotein complex	--	--	--	2	--

5.4.8 UVC-induced time-dependent modulation of the telomerised MRC-5, XP-C and CS-A cell transcriptome

Exposure of telomerised MRC-5, XP-C and CS-A fibroblasts to UV, resulted in the time-dependent transcriptional modulation of 763 probe sets (at an FDR of 0.001%), out of the 22,283 probe sets present on the HG-U133A GeneChip® array, (Fig. 5.5). The 763 differentially regulated probe sets, which represented 612 genes, were further organised by hierarchical clustering into five distinct clusters, according to the level and pattern of mRNA expression (Fig. 5.6).

Although many of the differentially regulated probe sets identified in the five clusters were common to telomerised MRC-5, XP-C and CS-A cell lines and displayed similar levels of induction and/or repression, the differentially regulated UV-responsive probe sets displayed marked differences in the kinetics of induction and/or repression between the cell lines over the time course.

The kinetics of transcriptional modulation in the 367 probe sets identified in cluster 1 was similar for both telomerised MRC-5 and XP-C cells following UV exposure (Fig. 5.6). The majority of probe sets within this cluster were highly expressed in both MRC-5 and XP-C cells at 0 hours. This was followed by kinetics of repression at ~6 hours in response to UV. The 367 probe sets were induced at both ~12 and ~24 hours post UV. Similarly, the CS-A cell line displayed similar kinetics of transcriptional modulation at 0 hours. However, the 367 probe sets were repressed at ~6 and ~12 hours following UV. A large number of probe sets remained downregulated at ~24 hours posts UV, while a subset of probe sets were induced at 24 hours (Fig. 5.6, cluster 1).

Similar to cluster 1, the kinetics of the 152 differentially regulated probe sets in cluster 2 was similar in both MRC-5 and XP-C cells. Both cell lines displayed kinetics of repression at 0 hours post UV. This was followed by an immediate upregulation at ~6 hours, which was maintained at ~12 hours after UV. The MRC-5 and XP-C cells displayed heterogeneous levels of transcriptional modulation at ~24 hours, as the probe sets showed high and low levels of

expression. These data suggest that, the probe sets differentially induced in the MRC-5 and XP-C cell lines reached a peak level of induction at ~6 hours after UV, and although the kinetics of induction was sustained at ~12 hours, no further increases in induction was observed. Like MRC-5 and XP-C cells, the 152 probe sets were repressed at 0 hours. However, unlike the early kinetics of induction observed in the MRC-5 and XP-C cells at ~6 hours, the CS-A cells presented a delayed pattern of induction. The pattern of transcription observed at ~6 hours was similar to that seen at 0 hours post UV. A gradual induction of the 152 probe sets was observed at ~12 hours. However, unlike the MRC-5 and XP-C cell lines, a further upregulation of the probe sets occurred at ~24 hours after UV. These data indicate that the UV-induced, time-dependent transcriptional response of the 152 probe sets was protracted in the CS-A cell line, compared to the MRC-5 and XP-C cell lines.

Cluster 3 (162 probe sets) comprises genes whose expression profiles vary significantly between the telomerised MRC-5, XP-C and CS-A cells (Fig. 5.6). Unlike clusters 1 and 2, the differentially regulated probe sets observed in cluster 3 displayed no common pattern of expression between these. In MRC-5, the 162 probe sets displayed high levels of expression at 0 hours. However, the probe sets displayed kinetics of downregulation at ~6 and ~12 post UV, while induction was observed at ~24 hours. Similarly, the 162 probe sets displayed high levels of expression in XP-C cells at 0 hours, followed by a slight downregulation at ~6 hours. A further global downregulation was observed at ~12 hours. However, the transcriptional modulation of the 162 probe sets at ~24 hours post UV exhibited no clear pattern of expression, except for a subset of probe sets which displayed a further downregulation in expression. CS-A cells presented similar kinetics of transcriptional modulation at 0 and ~6 hours post UV to MRC-5 and XP-C cells. However, a global repression of the probe sets was observed at ~12 and ~24 hours (Fig. 5.6, cluster 3).

Cluster 4 (81 probe sets) contained probe sets that displayed well-defined and similar patterns of transcriptional kinetics between the MRC-5, XP-C and CS-A cell lines (Fig. 5.6, cluster 4). The cluster included genes that were

predominantly induced at 0 and ~6 hours after UV. Moreover, the level of induction appeared similar between the two time points. Conversely, the 81 probe sets displayed a generalised pattern of repression at ~12 and ~24 hours after UV. In contrast, the induction of the 81 probe sets in the CS-A cell line was sustained at ~12, and kinetics of global repression was only observed at ~24 hours post UV.

The differentially regulated probe sets identified in the five time-dependent clusters represented biological functions typically associated with a DNA damage response such as proliferation, positive and negative regulators of the cell cycle and apoptosis. However, differentially regulated probe sets identified in clusters 1-4 represented a diverse range of functional groups associated with the nucleus, protein binding and regulation of transcription (Appendix 2). In contrast to the genotype-specific changes, however, several probe sets associated with DNA repair were differentially regulated. For example, *CDK7*, *CSNKID*, *NCOA6*, *PARP2*, *PML*, *POLB*, *RAD17* and *REV3C* were identified in cluster 1. Additionally, *BTG2*, *GADD45α*, *KCTD13*, *POLG2* and *SFPQ* were differentially regulated in cluster 2 (Appendix 2). Interestingly, *DDB2*, an important constituent of the GGR subpathway was upregulated in cluster 2.

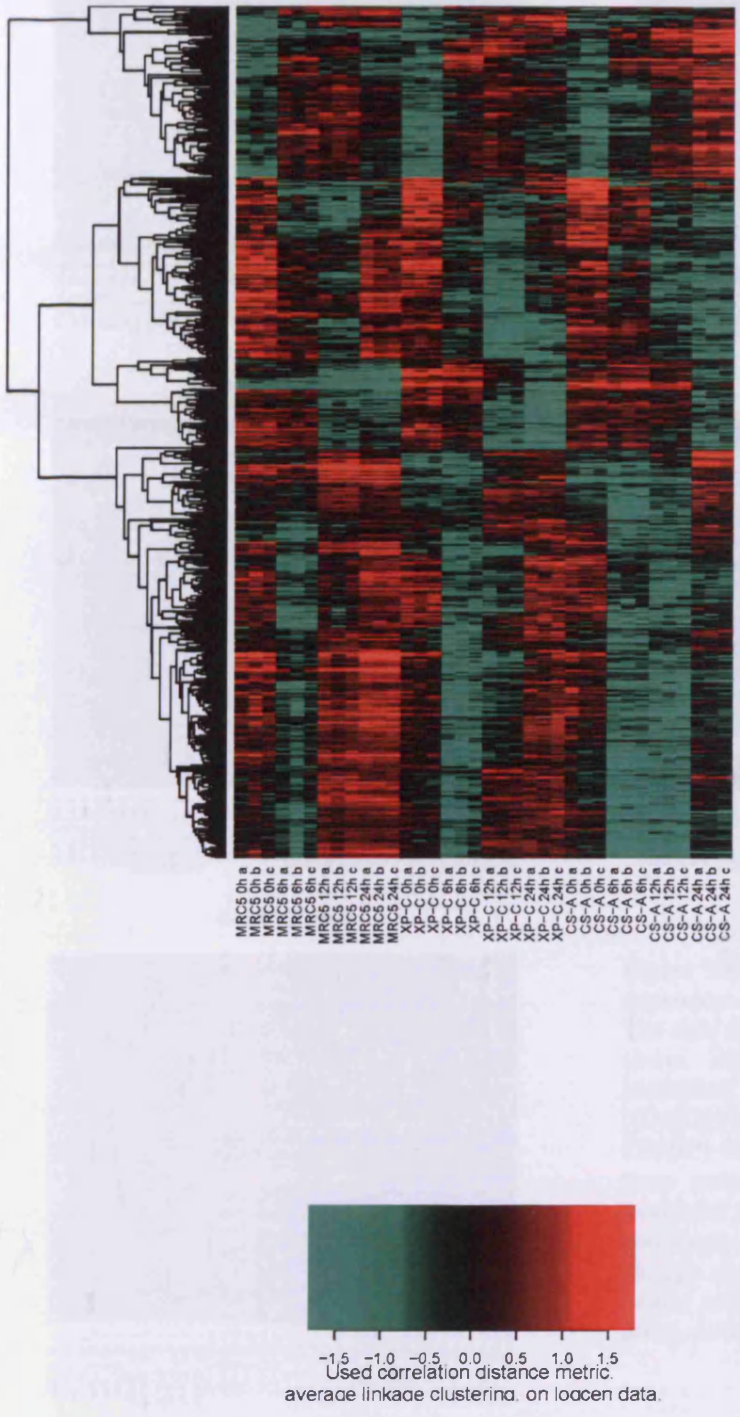

Figure 5.5. ANOVA of time-dependent changes in gene expression. Hierarchical clustering depicting the time-dependent transcriptional changes of 763 differentially regulated probe sets, whose levels of expression altered in a time-dependent manner in telomerised MRC-5, XP-C (GM02996, XP8CA) and CS-A (GM01856, CS3BE) fibroblast cell lines, following UVC (254 nm), at the indicated time points (h, hour). The columns correspond to the cell lines and the rows to each gene transcript. The altered expression levels are represented in colour and red means upregulation, while green, downregulation.

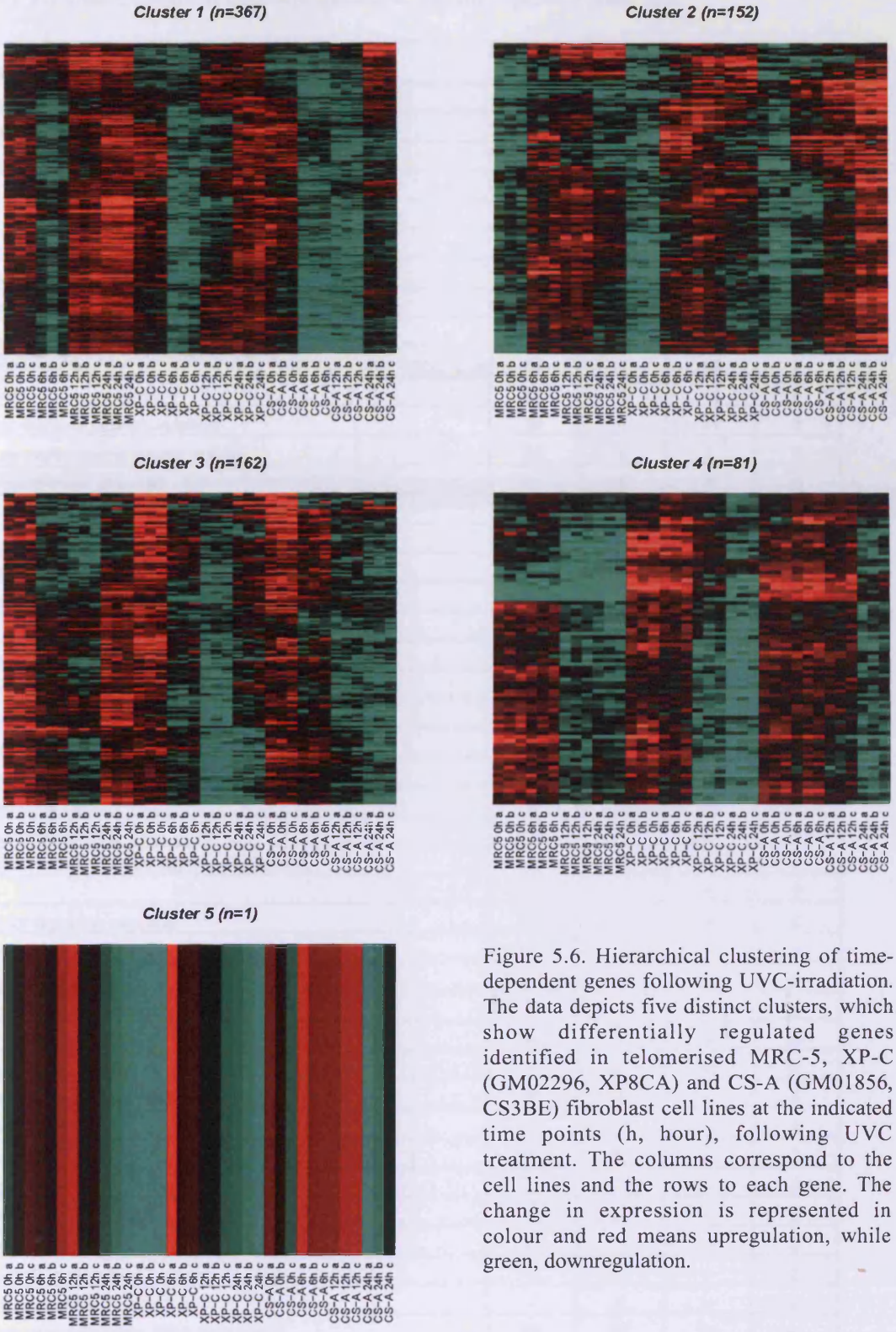

Figure 5.6. Hierarchical clustering of time-dependent genes following UVC-irradiation. The data depicts five distinct clusters, which show differentially regulated genes identified in telomerised MRC-5, XP-C (GM02296, XP8CA) and CS-A (GM01856, CS3BE) fibroblast cell lines at the indicated time points (h, hour), following UVC treatment. The columns correspond to the cell lines and the rows to each gene. The change in expression is represented in colour and red means upregulation, while green, downregulation.

Table 5.2. Functional classes of time-dependent differentially expressed probe sets.

GO Category	Cluster 1	Cluster 2	Cluster 3	Cluster 4
Nucleus	116	48	30	9
Protein binding	90	26	32	9
Transcription	50	16	9	2
Zinc ion binding	49	15	15	7
Nucleotide binding	48	19	21	8
Metal ion binding	48	14	10	5
ATP binding	38	11	18	6
Transferase activity	35	14	20	8
Membrane	32	18	22	13
Signal transduction	28	8	10	6
Cytoplasm	25	7	12	6
Protein amino acid phosphorylation	24	4	11	4
Protein serine/threonine kinase activity	22	4	7	3
Cellular component unknown	21	8	7	5
Integral to membrane	19	9	13	5
Molecular function unknown	17	5	7	4
Biological process unknown	16	4	7	2
Hydrolase activity	11	4	11	4
Integral to plasma membrane	9	5	5	5
Receptor activity	8	6	2	3
Guanyl-nucleotide exchange factor activity	6	2	2	2
Golgi stack	6	2	4	3
Mitochondrion	5	7	13	2
Kinase activity	4	3	3	3
Magnesium ion binding	4	3	6	2
Oxidoreductase activity	2	2	2	4
Cell surface receptor linked signal transduction	2	3	2	2
Binding	17	--	5	2
Intracellular signaling cascade	9	--	9	2
Cytoskeleton	7	--	2	3
Calcium ion binding	7	--	13	4
Protein amino acid dephosphorylation	6	--	6	2
Plasma membrane	3	--	5	3
GTPase activator activity	3	--	5	2
Regulation of progression through cell cycle	6	3	--	3
Cell adhesion	2	2	--	4
Neurogenesis	6	--	--	3
Protein transport	6	--	--	3
Proteolysis and peptidolysis	4	--	--	2
Cell differentiation	2	--	--	2
Carbohydrate metabolism	2	--	--	2
Protein biosynthesis	--	7	--	2
Regulation of transcription, DNA-dependent	60	17	10	--
DNA binding	35	15	7	--
Transcription factor activity	26	9	3	--

Table 5.2. *Continued*

Nucleic acid binding	19	3	7	--
Cell cycle	17	6	5	--
Ubiquitin cycle	15	3	2	--
Transcription coactivator activity	14	3	3	--
RNA binding	13	7	5	--
Development	13	2	2	--
Signal transducer activity	12	2	3	--
Intracellular	10	3	2	--
Transcription from RNA polymerase II promoter	8	3	2	--
Transport	7	2	3	--
Apoptosis	7	2	2	--
Cytosol	5	2	3	--
Protein self binding	3	2	2	--
Electron transport	2	2	2	--
Membrane fraction	2	2	3	--
Cell-cell signaling	2	2	2	--
Regulation of transcription from RNA polymerase II promoter	11	--	3	--
Intracellular protein transport	10	--	3	--
Cell proliferation	7	--	2	--
Metabolism	6	--	4	--
Ligase activity	6	--	3	--
Cell division	5	--	2	--
Endocytosis	5	--	4	--
Regulation of transcription	4	--	5	--
Transporter activity	4	--	3	--
Protein complex assembly	4	--	3	--
Acyltransferase activity	4	--	2	--
Protein-tyrosine kinase activity	4	--	4	--
Catalytic activity	4	--	4	--
Transcription regulator activity	4	--	2	--
Transferase activity, transferring glycosyl groups	4	--	2	--
Positive regulation of transcription, DNA-dependent	3	--	2	--
Protein kinase cascade	3	--	2	--
Nucleoplasm	3	--	3	--
Ribonucleoprotein complex	3	--	2	--
G-protein coupled receptor protein signaling pathway	3	--	2	--
Protein serine/threonine phosphatase activity	2	--	2	--
Protein tyrosine phosphatase activity	2	--	2	--
Diacylglycerol binding	2	--	3	--
Phosphoprotein phosphatase activity	2	--	2	--
Regulation of GTPase activity	2	--	2	--
Calmodulin binding	--	3	2	--
Lyase activity	--	2	2	--
DNA repair	8	5	--	--
Transcription corepressor activity	6	3	--	--

Table 5.2. *Continued*

Nuclear mRNA splicing, via spliceosome	6	3	--	--
Negative regulation of cell proliferation	5	5	--	--
Endoplasmic reticulum	5	4	--	--
Small GTPase mediated signal transduction	5	2	--	--
DNA replication	5	3	--	--
RNA splicing	4	2	--	--
Immune response	4	4	--	--
Regative regulation of transcription from RNA polymerase II promoter	4	3	--	--
Positive regulation of cell proliferation	4	2	--	--
Protein folding	3	3	--	--
Response to unfolded protein	3	3	--	--
mRNA processing	3	2	--	--
Protein dimerization activity	2	3	--	--
Nucleosome	2	3	--	--
Nucleosome assembly	2	3	--	--
Transmembrane receptor protein tyrosine kinase signaling pathway	2	2	--	--
DNA-dependent DNA replication	2	2	--	--
Regulation of cyclin dependent protein kinase activity	2	2	--	--
Chromosome organization and biogenesis (sensu Eukaryota)	2	3	--	--
Protein kinase activity	2	2	--	--
Regulation of apoptosis	2	2	--	--
General RNA polymerase II transcription factor activity	2	2	--	--
Nnucleolus	2	5	--	--
Cell cycle arrest	2	3	--	--
Positive regulation of I-kappaB kinase/NF-kappaB cascade	2	3	--	--
Translation initiation factor activity	2	3	--	--
RNA polymerase II transcription factor activity	12	--	--	--
Soluble fraction	7	--	--	--
Ubiquitin-dependent protein catabolism	7	--	--	--
Regulation of translation	6	--	--	--
Ubiquitin-protein ligase activity	6	--	--	--
Microtubule	5	--	--	--
Peptidase activity	5	--	--	--
Induction of apoptosis	5	--	--	--
Negative regulation of progression through cell cycle	5	--	--	--
Ubiquitin thiolesterase activity	5	--	--	--
Microtubule associated complex	4	--	--	--
Chromatin modification	4	--	--	--
Protein phosphatase type 2A complex	4	--	--	--
Protein phosphatase type 2A regulator activity	4	--	--	--
Protein transporter activity	4	--	--	--
Histone acetyltransferase activity	4	--	--	--
Specific RNA polymerase II transcription factor activity	4	--	--	--
Cysteine-type peptidase activity	4	--	--	--
Response to stress	4	--	--	--
Positive regulation of transcription from RNA polymerase II promoter	4	--	--	--

Table 5.2. *Continued*

Transcriptional repressor activity	4	--	--	--
Cysteine-type endopeptidase activity	4	--	--	--
Ion transport	3	--	--	--
Structural molecule activity	3	--	--	--
Nuclear pore	3	--	--	--
Protein heterodimerization activity	3	--	--	--
Androgen receptor signaling pathway	3	--	--	--
Androgen receptor binding	3	--	--	--
JAK-STAT cascade	3	--	--	--
Chromatin	3	--	--	--
Chromatin binding	3	--	--	--
SH3/SH2 adaptor activity	3	--	--	--
JNK cascade	3	--	--	--
Negative regulation of transcription, DNA--dependent	3	--	--	--
Transcriptional activator activity	3	--	--	--
ATP-dependent helicase activity	3	--	--	--
Ubiquitin ligase complex	3	--	--	--
Negative regulation of transcription	3	--	--	--
Transcription initiation from RNA polymerase II promoter	3	--	--	--
Wnt receptor signaling pathway	3	--	--	--
Manganese ion binding	3	--	--	--
Lipid metabolism	2	--	--	--
Cell motility	2	--	--	--
Mitosis	2	--	--	--
Outer membrane	2	--	--	--
Phosphoinositide binding	2	--	--	--
Response to hypoxia	2	--	--	--
Homeostasis	2	--	--	--
DNA-directed RNA polymerase activity	2	--	--	--
Inositol or phosphatidylinositol phosphatase activity	2	--	--	--
Protein phosphatase type 2A activity	2	--	--	--
Lysosome	2	--	--	--
Estrogen receptor binding	2	--	--	--
Response to DNA damage stimulus	2	--	--	--
Microtubule motor activity	2	--	--	--
Insulin receptor signaling pathway	2	--	--	--
mRNA splice site selection	2	--	--	--
Vesicle-mediated transport	2	--	--	--
Inactivation of MAPK activity	2	--	--	--
Regulation of Wnt receptor signaling pathway	2	--	--	--
Negative regulation of cell growth	2	--	--	--
Organogenesis	2	--	--	--
Electron transporter activity	2	--	--	--
MAPKKK cascade	2	--	--	--
Chromatin assembly or disassembly	2	--	--	--
frizzled signaling pathway	2	--	--	--

Table 5.2. *Continued*

Spliceosome complex	2	--	--	--
Transcription cofactor activity	2	--	--	--
Sodium ion binding	2	--	--	--
Ras protein signal transduction	2	--	--	--
Double-stranded DNA binding	2	--	--	--
Rho GTPase activator activity	2	--	--	--
Inflammatory response	2	--	--	--
Heart development	2	--	--	--
Helicase activity	2	--	--	--
Receptor binding	2	--	--	--
Endosome	2	--	--	--
Response to virus	2	--	--	--
DNA damage response, signal transduction by p53 class mediator resulting in induction of apoptosis	2	--	--	--
mRNA nucleus export	2	--	--	--
Apoptotic program	2	--	--	--
Caspase activity	2	--	--	--
G1/S transition of mitotic cell cycle	2	--	--	--
Establishment and/or maintenance of chromatin architecture	2	--	--	--
DNA recombination	2	--	--	--
Thyroid hormone receptor binding	2	--	--	--
Protein ubiqutylation	2	--	--	--
PML body	2	--	--	--
Isomerase activity	2	--	--	--
Transforming growth factor beta receptor activity	2	--	--	--
GTP binding	--	5	--	--
Structural constituent of ribosome	--	4	--	--
Extracellular space	--	4	--	--
Unfolded protein binding	--	3	--	--
Ribosome	--	3	--	--
Growth factor activity	--	3	--	--
Chromosome	--	3	--	--
rRNA processing	--	2	--	--
Translational initiation	--	2	--	--
Transcription factor TFIID complex	--	2	--	--
Cyclin-dependent protein kinase inhibitor activity	--	2	--	--
Transmembrane receptor activity	--	2	--	--
GTPase activity	--	2	--	--
Potassium ion transport	--	2	--	--
Voltage-gated potassium channel complex	--	2	--	--
Cytokine activity	--	2	--	--
Transcription from RNA polymerase I promoter	--	2	--	--
Motor activity	--	--	2	--
Actin binding	--	--	2	--
Myosin	--	--	2	--
ilon ion binding	--	--	2	--
phospholipase C activation	--	--	2	--

Table 5.2. *Continued*

Mitochondrial inner membrane	--	--	2	--
mRNA 3'-UTR binding	--	--	2	--
Exonuclease activity	--	--	2	--
Positive regulation of apoptosis	--	--	2	--
Embryonic development	--	--	2	--
Hindbrain development	--	--	2	--
Regulation of transcriptional preinitiation complex formation	--	--	2	--
Visual perception	--	--	2	--
Golgi apparatus	--	--	2	--
Protein tyrosine/serine/threonine phosphatase activity	--	--	2	--
Centrosome	--	--	2	--
NF-kappaB binding	--	--	2	--
Coated pit	--	--	2	--
Transcription factor binding	--	--	2	--
Tight junction	--	--	2	--
Ras GTPase binding	--	--	2	--
Heat shock protein binding	--	--	2	--
Axonogenesis	--	--	2	--
Actin cytoskeleton	--	--	--	2
Intergrin-mediated signaling pathway	--	--	--	2
Transmembrane receptor protein tyrosine phosphatase activity	--	--	--	2
Ribonucleoside monophosphate biosynthesis	--	--	--	2
Muscle development	--	--	--	2
Synaptic transmission	--	--	--	2
Perception of sound	--	--	--	2
Protein modification	--	--	--	2

5.4.9 Combined UVC-induced time-dependent and genotype-specific modulation of telomerised MRC-5, XP-C and CS-A cell transcriptome

The data presented in Sections 5.4.7 and 5.4.8 describe the effects of the two independent variables, namely cell type and time after UV-irradiation. However, to determine the combined effect of both genotype and time on the pattern of differential gene expression, a two-factor ANOVA was performed. To achieve this, an interaction factor was incorporated into ANOVA to facilitate the identification of genes that were differentially regulated with both time and genotype. The ANOVA revealed that of the 22,283 probe sets present on the Affymetrix™ HG-U133A GeneChip® array, 442 probe sets (at an FDR = 0.01%), which represented 377 genes, were differentially regulated in both a genotype- and time-dependent manner and they represented a diverse range of functional groups (Table 5.3). Subsequent hierarchical clustering resulted in the generation of three distinct clusters that represented different kinetics of transcriptional activation and/or repression.

Cluster 1 (270 probe sets) represented kinetics of downregulation at ~6 hours in both MRC-5 and XP-C cells. In contrast, both induction and repression of the 270 probe sets was observed in CS-A cells at ~6 hours post UV. At ~12 and ~24 hours, a marked upregulation was observed in MRC-5 cells. However, the kinetics of transcriptional modulation in XP-C cells at ~12 and ~24 hours was more complex (Fig. 5.8, cluster 1). The majority of probe sets remained downregulated at ~12 hours, while a subset of probe sets were upregulated. Conversely, most of the probe sets identified in cluster 1 were upregulated at ~24 hours in XP-C cells. However, a subset of downregulated genes (at ~12 hours) remained in a repressed state at 24 hours. The downregulated pattern of expression observed at ~6 hours in CS-A was sustained throughout the time course at ~12 and ~24 hours post UV.

After UV, the kinetics of transcriptional modulation of the 153 probe sets identified in cluster 2 was similar in both the telomerised MRC-5 and XP-C cells. At 0 hours, the 153 probe sets were repressed in both MRC-5 and XP-C. Rapid induction was observed at ~6 hours in both cell lines. Moreover, the level of induction was sustained at ~12 hours post UV in both MRC-5 and XP-C cells. A subsequent downregulation of the probe sets occurred at ~24 hours in both cell lines. In contrast, the 153 probe sets remained repressed at 0 and ~6 hours post UV in telomerised CS-A cells, while both induction and repression of the probe sets was observed at ~12 hours post UV. This was followed by a global upregulation of the probe sets at ~24 hours. These data suggested that the kinetics of UV-induced transcription was delayed in the telomerised CS-A cell line when compared to the MRC-5 and XP-C cells (Fig. 5.8).

Cluster 3 (19 probe sets) exhibited no obvious patterns of differential gene expression (Fig. 5.8). However, a global downregulation of the probe sets was observed throughout the time course in MRC-5 cells after UV. Conversely, the XP-C cell line displayed a pattern of moderate induction throughout the time course following UV. Although significant levels of induction and repression were displayed by CS-A, the heat map revealed no global pattern of expression between the 19 differentially regulated probe sets in cluster 3 (Fig. 5.8).

The differentially regulated probe sets identified following two-factor analysis resulted in the identification of several functional groups typically associated with a DNA-damage response such as proliferation, positive and negative regulators of the cell cycle and apoptosis (Appendix 3). However, a large number probe sets represented several functional groups that were previously identified (Sections 5.4.7 & 5.4.8) and associated with the nucleus, protein binding, nucleotide binding, membrane, signal transduction and transcription. Several probe sets identified in cluster 1 (*MNAT1*, *PARP4* and *XRCC4*) and cluster 2 (*BTG2*, *CSNK1D*, *GADD45α*, *HUS1*, *KCTD13*, *RBM14* and *UBE2B*) is closely associated with DNA repair.

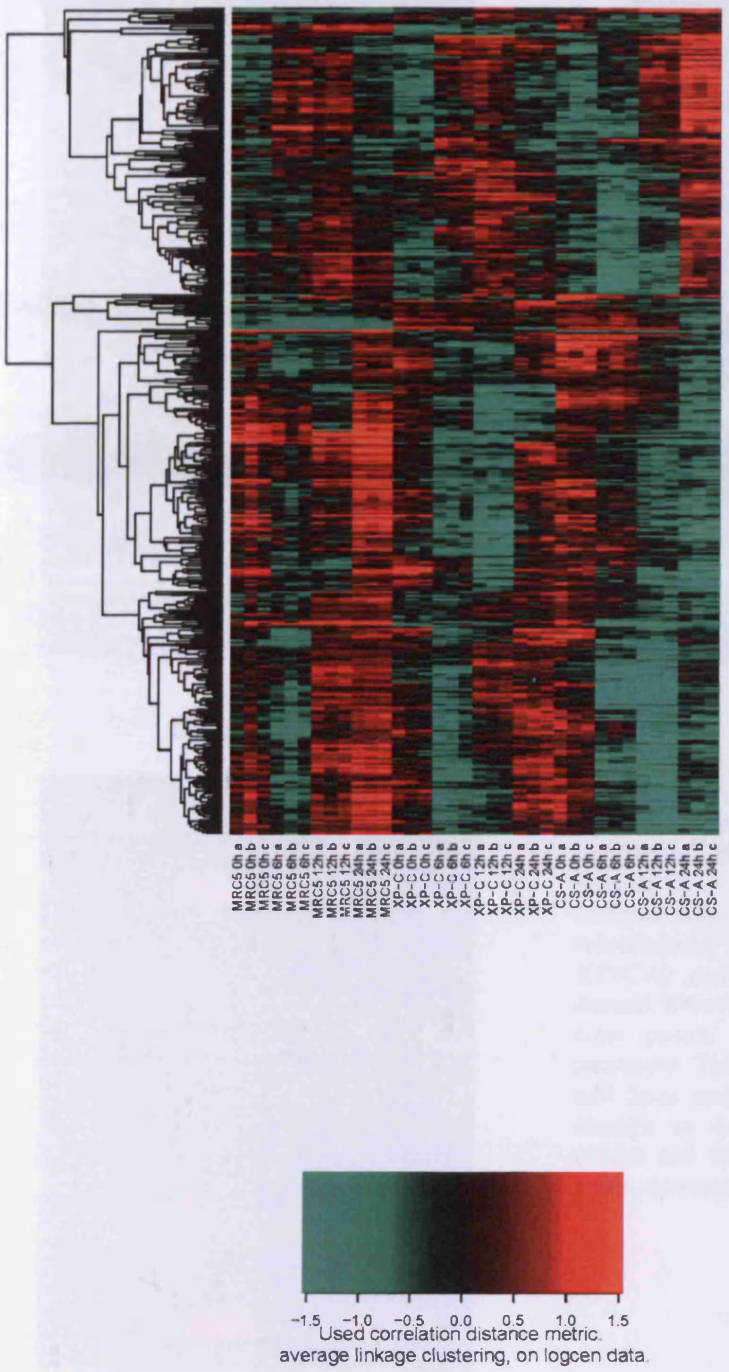

Figure 5.7. Hierarchical clustering depicting the transcriptional response to UVC radiation. The expression pattern of 442 differentially regulated genes, whose levels of expression altered after interaction analysis in telomerised MRC-5, XP-C (GM02996, XP8CA) and CS-A (GM01856, CS3BE) dermal fibroblast cell lines, following UVC (254 nm), at the indicated time points (h, hour). The columns correspond to the cell lines and the rows to each gene transcript. The altered expression levels are represented in colour and red means upregulation, while green, downregulation.

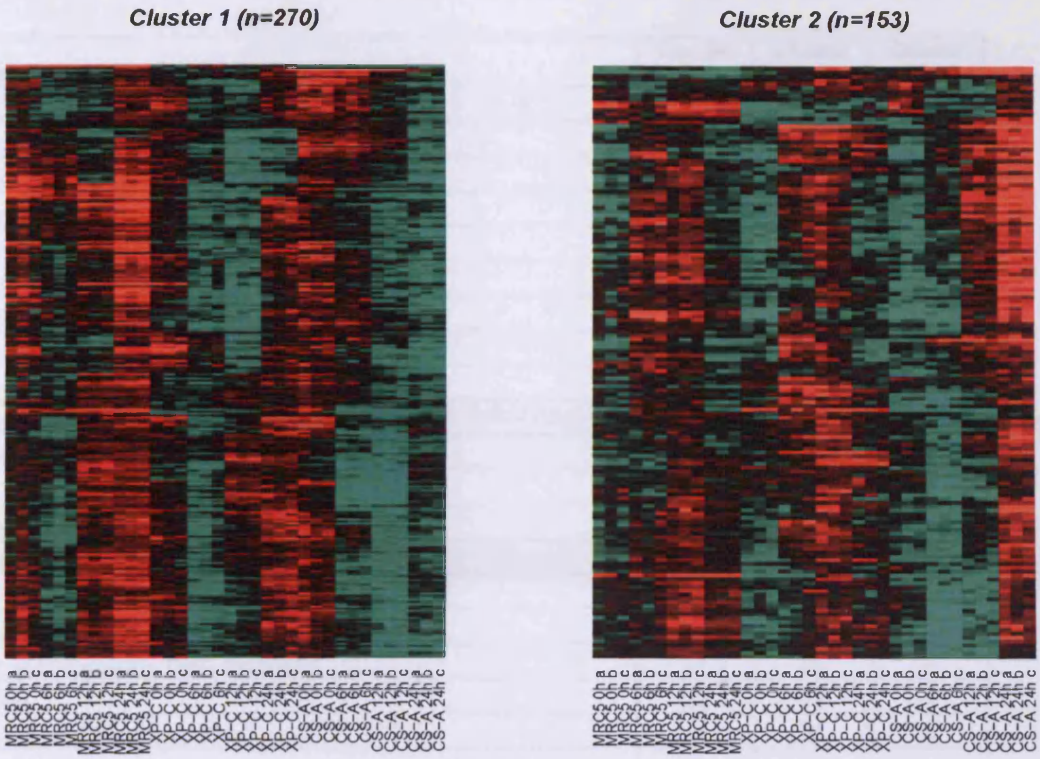

Figure 5.8. Hierarchical clustering of damage-responsive genes following UVC-irradiation (interaction term). The data depicts three distinct clusters, which show differentially regulated genes identified in telomerised MRC-5, XP-C (GM02996, XP8CA) and CS-A (GM01856, CS3BE) dermal fibroblast cell lines at the indicated time points (h, hour), following UVC treatment The columns correspond to the cell lines and the rows to each gene. The change in expression is represented in colour and red means upregulation, while green, downregulation.

Table 5.3. Functional classes of differentially expressed probesets following interaction analysis.

GO Category	Cluster 1	Cluster 2	Cluster 3
Nucleus	71	63	2
Protein binding	56	27	3
Membrane	28	15	2
Signal transduction	27	9	2
Zinc ion binding	27	19	2
Metal ion binding	23	19	2
Cytoplasm	21	8	3
Golgi stack	8	2	2
Biological process unknown	7	5	2
Metabolism	5	2	2
Cytoskeleton	10	--	2
Integral to plasma membrane	9	--	2
Skeletal development	2	--	2
Nucleotide binding	40	24	--
ATP binding	26	8	--
Transferase activity	24	10	--
Regulation of transcription, DNA-dependent	21	25	--
Transcription	19	22	--
Protein amino acid phosphorylation	18	5	--
Binding	16	2	--
Transcription factor activity	14	16	--
RNA binding	14	13	--
DNA binding	14	12	--
Hydrolase activity	14	8	--
Protein serine/threonine kinase activity	13	5	--
Nucleic acid binding	12	9	--
Signal transducer activity	12	5	--
Cell cycle	11	6	--
Integral to membrane	11	7	--
Cellular component unknown	11	7	--
Ubiquitin cycle	10	3	--
Cell proliferation	10	2	--
Protein transport	9	2	--
Cytosol	9	3	--
Intracellular	9	6	--
Ligase activity	8	2	--
Development	8	2	--
Molecular function unknown	8	11	--
Mitochondrion	8	6	--
GTP binding	7	5	--
Transport	7	3	--
Protein amino acid dephosphorylation	7	2	--
Endoplasmic reticulum	7	2	--
Apoptosis	7	7	--
Nuclear mRNA splicing, via spliceosome	5	6	--

Table 5.3. *Continued*

Neurogenesis	5	2	--
Small GTPase mediated signal transduction	5	3	--
Soluble fraction	5	3	--
Negative regulation of progression through cell cycle	5	2	--
Transcription coactivator activity	5	5	--
Magnesium ion binding	5	4	--
Proteolysis and peptidolysis	5	2	--
Transcription from RNA polymerase II promoter	4	3	--
Protein complex assembly	4	2	--
GTPase activity	4	2	--
RNA splicing	4	4	--
Response to stress	4	2	--
Immune response	4	2	--
Cell differentiation	3	3	--
Double-stranded RNA binding	3	2	--
Regulation of translation	3	2	--
DNA repair	3	7	--
Rbonucleoprotein complex	3	2	--
Protein kinase cascade	3	2	--
Negative regulation of transcription from R-- polymerase II promoter	3	4	--
RNA processing	3	2	--
Regulation of progression through cell cycle	3	5	--
Positive regulation of I-kappaB kinase/NF-kappaB cascade	3	4	--
Negative regulation of cell proliferation	2	7	--
Endonuclease activity	2	2	--
Negative regulation of cell growth	2	3	--
Regulation of apoptosis	2	2	--
Regulation of transcription	2	3	--
Manganese ion binding	2	2	--
Transcription corepressor activity	2	3	--
Calcium ion binding	10	--	--
Intracellular signaling cascade	10	--	--
Ubiquitin-dependent protein catabolism	9	--	--
Ubiquitin-protein ligase activity	8	--	--
Membrane fraction	7	--	--
Receptor activity	7	--	--
Nuclear pore	6	--	--
RNA polymerase II transcription factor activity	6	--	--
Intracellular protein transport	6	--	--
Regulation of GTPase activity	6	--	--
Regulation of transcription from RNA polymerase II promoter	6	--	--
GTPase activator activity	6	--	--
Cell adhesion	5	--	--
Guanyl-nucleotide exchange factor activity	5	--	--
Protein-tyrosine kinase activity	5	--	--
Protein transporter activity	4	--	--

Table 5.3. *Continued*

Cysteine-type endopeptidase activity	4	--	--
Ubiquitin thiolesterase activity	4	--	--
G-protein coupled receptor protein signaling pathway	4	--	--
Transcription factor binding	4	--	--
Protein phosphatase type 2A complex	4	--	--
Protein phosphatase type 2A regulator activity	4	--	--
ER to Golgi transport	4	--	--
Plasma membrane	4	--	--
Kinase activity	4	--	--
Mitosis	3	--	--
Lipid metabolism	3	--	--
Cell growth	3	--	--
Peptidase activity	3	--	--
Inflammatory response	3	--	--
Protein serine/threonine phosphatase activity	3	--	--
Calmodulin binding	3	--	--
Protein tyrosine phosphatase activity	3	--	--
MAPKKK cascade	3	--	--
Protein self binding	3	--	--
ATP-dependent helicase activity	3	--	--
Ubiquitin conjugating enzyme activity	3	--	--
Nuclear membrane	2	--	--
Microtubule	2	--	--
Microtubule associated complex	2	--	--
Cell motility	2	--	--
Cell division	2	--	--
Protein-nucleus import, docking	2	--	--
Small GTPase regulator activity	2	--	--
Ran GTPase binding	2	--	--
Protein complex	2	--	--
Muscle development	2	--	--
Oxidoreductase activity	2	--	--
Cell death	2	--	--
Epidermis development	2	--	--
Transporter activity	2	--	--
Vesicle-mediated transport	2	--	--
Actin cytoskeleton	2	--	--
Structural molecule activity	2	--	--
Motor activity	2	--	--
Actin binding	2	--	--
Androgen receptor signaling pathway	2	--	--
tTansferase activity, transferring glycosyl groups	2	--	--
NLS-bearing substrate-nucleus import	2	--	--
Nuclear localization sequence binding	2	--	--
Autophagy	2	--	--
Protein amino acid ADP-ribosylation	2	--	--

Table 5.3. *Continued*

Response to drug	2	--	--
Fatty acid catabolism	2	--	--
Iron ion binding	2	--	--
Response to DNA damage stimulus	2	--	--
SH3/SH2 adaptor activity	2	--	--
Epidermal growth factor receptor signaling pathway	2	--	--
Phospholipase C activation	2	--	--
Blood coagulation	2	--	--
Diacylglycerol binding	2	--	--
Vascular endothelial growth factor receptor activity	2	--	--
Transmembrane receptor protein tyrosine kinase signaling pathway	2	--	--
Chromatin	2	--	--
JNK cascade	2	--	--
Double-stranded DNA binding	2	--	--
Single-stranded DNA binding	2	--	--
Caspase activator activity	2	--	--
DNA recombination	2	--	--
Protein modification	2	--	--
Intracellular transporter activity	2	--	--
Negative regulation of signal transduction	2	--	--
integrin-mediated signaing pathway	2	--	--
MAP kinase phosphatase activity	2	--	--
Heterogeneous nuclear ribonucleoprotein complex	2	--	--
Wnt receptor signaling pathway	2	--	--
Angiogenesis	2	--	--
Positive regulation of cell proliferation	2	--	--
Calcium ion transport	2	--	--
Phosphoinositide binding	2	--	--
Centrosome	2	--	--
Golgi membrane	2	--	--
mRNA processing	--	5	--
Induction of apoptosis	--	4	--
DNA replication	--	4	--
Anti-apoptosis	--	3	--
Isomerase activity	--	3	--
Translation initiation factor activity	--	3	--
mRNA nucleus export	--	3	--
mRNA catabolism, nonsense-mediated decay	--	2	--
RNA splicing factor activity, transesterification mechanism	--	2	--
Mitochondrial outer membrane	--	2	--
Protein heterodimerization activity	--	2	--
Pseudouridylate synthase activity	--	2	--
Nucleoplasm	--	2	--
rRNA processing	--	2	--
Protein biosynthesis	--	2	--
Extracellular space	--	2	--

Table 5.3. *Continued*

Protein dimerization activity	--	2	--
DNA-directed RNA polymerase activity	--	2	--
Transcription factor complex	--	2	--
Positive regulation of transcription from RNA polymerase II promoter	--	2	--
Transmembrane receptor activity	--	2	--
Cell-cell signaling	--	2	--
Growth factor activity	--	2	--
Cell surface receptor linked signal transduction	--	2	--
Extracellular matrix structural constituent	--	--	2
Extracellular matrix (sensu Metazoa)	--	--	2

5.4.10 Data annotation and biological relevance

Following the identification of differentially regulated genes in telomerised MRC-5, XP-C and CS-A fibroblasts by ANOVA and hierarchical clustering, genes were individually assessed for their biological relevance in response to UV. This was undertaken using the Microarray Data Review and Annotation System (MADRAS; http://madras.uwcm.ac.uk), a web-based software package developed in-house by the Microarray Bioinformatics Group at Cardiff University. MADRAS provides a single accessible system, which facilitates the storage and sharing of gene lists whilst allowing the simultaneous visualisation of data and annotation of probes. MADRAS encompasses several web-based databases of descriptive annotation such as **Locuslink** (http://www.ncbi.nlm.nih.gov/entrez/query.fcgi?db=gene), **Homologene** (http://www.ncbi.nlm.nih.gov/entrez/query.fcgi?db=homologene), **OMIM** (http://www.ncbi.nlm.nih.gov/entrez/query.fcgi?db=OMIM), **PubMed** (http://www.ncbi.nlm.nih.gov/entrez/query.fcgi?DB=pubmed) and pathway packages such as **Biocarta** (http://www.biocarta.com/), **GenMAPP** (http://www.genmapp.org/links.html), **KEGG** (http://www.genome.jp/kegg/) and AmiGO (Gene Ontology; http://www.Geneontology.org/; Gene Ontology Consortium). The incorporation of these databases by MADRAS facilitates the acquisition of knowledge on gene functionality and its interaction with other genes and/or pathways. In addition, MADRAS facilitated the visualisation of kinetics for each individual probe set by single gene graphing.

To further investigate the precise relationship and biological relevance between differentially regulated probe sets identified on the HG-U133A array in telomerised MRC-5, XP-C and CS-A fibroblast cells and to obtain a more coherent view of the transcriptional changes that occurred in response to UV, over-representation analysis was performed using MADRAS. The probe IDs from each cluster that presented a change in expression in a time- or genotype-dependent manner or a combination of both (interaction term) was interrogated. Over-representation was performed using term-enrichment, which relied upon membership of a pathway, Gene Ontology terms and word present within the

functional summary. Although a large number of differentially regulated genes were identified in this investigation, none of the functional groups or pathways was significantly represented in a time- or genotype-dependent manner (Tables 5.4 & 5.5, respectively). Furthermore, term-enrichment using MADRAS, failed to identify any significantly over-represented terms or pathways following two-factor ANOVA analysis (Table 5.6).

Table 5.4. Over-representation analysis of genotype-specific transcriptional changes using term-enrichment.

Pathway	Probe list	Global	p-value
Cluster 1			
BioCarta pathway			
Biosynthesis of arginine in bacteria	1 / 290	3 / 12986	0.02
BTG family proteins and cell cycle regulation	2 / 290	12 / 12986	0.05
GeneMAPP			
Extracellular matrix Sensu Metazoa	19 / 290	227 / 12986	1.00E-05
KEGG			
ECM-receptor interaction	13 / 290	179 / 12986	0.002
Ascorbate and aldarate metabolism	3 / 290	19 / 12986	0.026
Words in Official Gene Name			
Pregnancy	7 / 290	21 / 12986	4.00E-08
27kda	3 / 290	8 / 12986	3.00E-04
Cathepsin	4 / 290	20 / 12986	0.005
Collagen	8 / 290	81 / 12986	0.009
Homeo	7 / 290	65 / 12986	0.01
Neuromedin	2 / 290	6 / 12986	0.011
Negative	3 / 290	3 / 290	0.027

Table 5.4. *Continued*

Pathway	Probe list	Global	p-value
Cluster 2			
BioCarta pathway			
Role of parkin in the ubiquitin-proteasomal pathway	1/63	5 / 12986	0.002
Msp/Ron receptor signaling pathway	1/63	7 / 12986	0.006
Adhesion and diapedesis of granulocytes	1/63	10 / 12986	0.014
Adhesion and diapedesis of lymphocytes	1/63	10 / 12986	0.014
Mechanism of acetaminophen activity and toxicity	1/63	11 / 12986	0.017
Y branching of actin filaments	1/63	12 / 12986	0.021
Low-density lipoprotein (LDL) pathway during atherogenesis	1/63	13 / 12986	0.025
Aspirin blocks signaling pathway involved in platelet activation	1/63	16 / 12986	0.04
GeneMAPP			
Hs 1-tissue-muscle fat and connective	4/63	105 / 12986	0.01
KEGG			
Galactose metabolism	2/63	37 / 12986	0.02
Words in official gene name			
Activin	2/63	15 / 12986	0.001
A activin	2/63	15 / 12986	0.001
Homeo	3/63	65 / 12986	0.007
Homeo box	3/63	65 / 12986	0.007

Table 5.4. *Continued*

Pathway	Probe list	Global	p-value
Cluster 3			
BioCarta pathway			
proteolysis and signaling pathway of notch	1/53	6 / 12986	0.003
Generation of amyloid B-peptide by PS1	1/53	9 / 12986	0.009
G-secretase mediated ErbB4 signaling pathway	1/53	9 / 12986	0.009
AKAP95 role in mitosis and chromosome dynamics	1/53	10 / 12986	0.011
Rho-selective guanine exchange factor AKAP13 mediates stress fiber formation	1/53	12 / 12986	0.017
Presenilin action in notch and Wnt signaling	1/53	14 / 12986	0.024
Protein kinase A at the centrosome	1/53	15 / 12986	0.027
IL 4 signaling pathway	1/53	17 / 12986	0.036
Growth hormone signaling pathway	1/53	18 / 12986	0.041
Multiple antiapoptotic pathways from IGF-1R signaling lead to BAD phosphorylation	1/53	18 / 12986	0.041
KEGG			
Notch signaling pathway	3/53	77 / 12986	0.004
Words in official gene name			
Ubiquitin	4/53	183 / 12986	0.03
Gene ontology terms			
RRNA modification	2/53	16 / 12986	2.00E-04

Table 5.4. *Continued*

Pathway	Probe list	Global	p-value
Cluster 4			
BioCarta pathway			
Extrinsic prothrombin activation pathway	3 / 156	12 / 12986	7.00E-05
Fibrinolysis pathway	2 / 156	6 / 12986	2.00E-04
Acute myocardial infarction	2 / 156	10 / 12986	0.002
Role of PPAR-gamma coactivators in obesity and thermogenesis	1 / 156	5 / 12986	0.023
Basic mechanism of Action of PPARa, PPARb(d) and PPARg and effects on gene expression	1 / 156	6 / 12986	0.038
Visceral fat deposits and the metabolic syndrome	1 / 156	6 / 12986	0.038
GenMAPP			
Hs complement and coagulation cascades KEGG	6 / 156	73 / 12986	0.003
KEGG			
Complement and coagulation cascades	7 / 156	95 / 12986	6.00E-04
Retinol metabolism	1 / 156	5 / 12986	0.05
Words in official gene name			
Bradykinin	2 / 156	2 / 12986	<2e-16
Pepsinogen	2 / 156	2 / 12986	<2e-16
Secreted	3 / 156	24 / 12986	0.02
Tissue	3 / 156	26 / 12986	0.02

Table 5.4. *Continued*

Pathway	Probe list	Global	p-value
Plasminogen	2 / 156	12 / 12986	0.03
Coagulation	3 / 156	28 / 12986	0.03
Multiple	4 / 156	50 / 12986	0.03
Cluster 5			
BioCarta pathway			
Biosynthesis of glycine and serine	1/30	3 / 12986	3.00E-05
Snf1 in Yeast glucose repression/derepression	1/30	6 / 12986	3.00E-04
Regulation of MAP kinase pathways through dual specificity phosphatases	1/30	15 / 12986	0.002
Rho cell motility signaling pathway	1/30	21 / 12986	0.005
Eicosanoid metabolism	1/30	38 / 12986	0.016
KEGG			
O-glycan biosynthesis	1/30	32 / 12986	0.03
Dentatorubropallidoluysian atrophy (DRPLA)	1/30	41 / 12986	0.05
Words in official gene name			
Homeobox	2/30	67 / 12986	0.005

Table 5.5. Over-representation analysis of time-dependent transcriptional changes by term-enrichment.

Pathway	Probe list	Global	p-value
Cluster 1			
BioCarta pathway			
Degradation of the RAR and RXR by the proteasome	1 / 327	1 / 12986	<2e-16
D4-GDI signaling pathway	1 / 327	3 / 12986	0.05
The information-processing pathway at the IFN-beta enhancer	1 / 327	3 / 12986	0.05
Words in official gene name			
Meis1	2 / 327	2 / 12986	<2e-16
Itam	2 / 327	4 / 12986	<2e-16
And itam	2 / 327	4 / 12986	<2e-16
Vps9	2 / 327	4 / 12986	<2e-16
Pumilio	2 / 327	5 / 12986	0.005
Ecotropic	3 / 327	13 / 12986	0.021
Enhancing	2 / 327	7 / 12986	0.043
Gene ontology			
Binding	5 / 327	36482 / 12986	NA
Cluster 2			
BioCarta pathway			
Regulation of EIF2	1 / 134	6 / 12986	0.04
Eukaryotic protein translation	1 / 134	7 / 12986	0.05

Table 5.5. *Continued*

Pathway	Probe list	Global	p-value
KEGG			
Lysine biosynthesis	1 / 134	6 / 12986	0.02
Words in offficial name			
Torsin	3 / 134	8 / 12986	6.00E-06
Maturation	2 / 134	5 / 12986	1.00E-04
120kda	2 / 134	5 / 12986	1.00E-04
1 120kda	2 / 134	5 / 12986	1.00E-04
Nucleolar	3 / 134	38 / 12986	0.05
Cluster 3			
BioCarta pathway			
Activation of PKC through G protein coupled receptor	1 / 147	2 / 12986	<2e-16
PKC-catalyzed phosphorylation of inhibitory phosphoprotein of myosin phosphatase	1 / 147	2 / 12986	<2e-16
G-protein signaling through tubby proteins	1 / 147	5 / 12986	0.03
Neuropeptides VIP and PACAP inhibit the apoptosis of activated T cells	1 / 147	6 / 12986	0.05
Regulation of EIF2	1 / 147	6 / 12986	0.05
Words in official gene name			
Acids	2 / 147	12 / 12986	0.02
Gene ontology			
Binding	2 / 147	36482 / 12986	NA

Table 5.5. *Continued*

Pathway	Probe list	Global	p-value
Cluster 4			
BioCarta pathway			
Neuropeptides VIP and PACAP inhibit the apoptosis of activated T cells	1/72	6 / 12986	0.003
Internal ribosome entry pathway	1/72	9 / 12986	0.007
Role of EGF receptor transactivation by GPCRs in cardiac hypertrophy	1/72	18 / 12986	0.035
Words in official gene name			
Branching	2/72	4 / 12986	<2e-16
Glycogen	2/72	14 / 12986	0
Cluster 5			
GenMAPP			
Hs 1-tissue-blood and lymph	1/1	271 / 12986	<2e-16

Table 5.6. Over-representation analysis of genotype- and time-dependent transcriptional changes by term-enrichment.

Pathway	Probe list	Global	p-value
Cluster 1			
BioCarta pathway			
Degradation of the RAR and RXR by the proteasome	1 / 327	1 / 12986	<2e-16
D4-GDI signaling pathway	1 / 327	3 / 12986	0.05
The information-processing pathway at the IFN-beta enhancer	1 / 327	3 / 12986	0.05
Words in official gene name			
Meis1	2 / 327	2 / 12986	<2e-16
Itam	2 / 327	4 / 12986	<2e-16
And Itam	2 / 327	4 / 12986	<2e-16
Vps9	2 / 327	4 / 12986	<2e-16
Pumilio	2 / 327	5 / 12986	0.005
Ecotropic	3 / 327	13 / 12986	0.021
Enhancing	2 / 327	7 / 12986	0.043
Gene ontology			
Binding	5 / 327	36482 / 12986	NA
Cluster 2			
BioCarta pathway			
Regulation of EIF2	1 / 135	6 / 12986	0.04
Eukaryotic protein translation	1 / 135	7 / 12986	0.05

Table 5.6. *Continued*

Pathway	Probe list	Global	p-value
KEGG			
Lysine biosynthesis	1 / 135	6 / 12986	0.02
Words in official gene name			
Torsin	3 / 135	8 / 12986	6.00E-06
Maturation	2 / 135	5 / 12986	1.00E-04
120kda	2 / 135	5 / 12986	1.00E-04
1 120kda	2 / 135	5 / 12986	1.00E-04
Nucleolar	3 / 135	38 / 12986	0.05
Cluster 3			
BioCarta pathway			
Activation of PKC through G protein coupled receptor	1 / 217	2 / 12986	<2e-16
PKC-catalyzed phosphorylation of inhibitory phosphoprotein of myosin phosphatase	1 / 217	2 / 12986	<2e-16
Neuropeptides VIP and PACAP inhibit the apoptosis of activated T cells	2 / 217	6 / 12986	9.00E-04
Words in official gene name			
Branching	2 / 217	4 / 12986	<2e-16
Glycogen	3 / 217	14 / 12986	0.004
Quinone	2 / 217	8 / 12986	0.016
Gene ontology			
Binding	2 / 217	36482 / 12986	NA

5.4.11 Validation of Affymetrix™ HG-U133A GeneChip® array data by qRT-PCR and Western blotting

To confirm the validity of the transcriptome data, quantitative RT-PCR was performed (using the ABI PRISM® 7000 System) on a selection of differentially regulated genes detected on the HG-U133A GeneChip® arrays. Genes were selected that lie downstream to p53 transactivation such as *CDKN1A*, the gene that encodes the $p21^{WAF1/CIP1}$ tumour suppressor. Genes were selected that represented a diverse range of distinct or overlapping biological functions that are known to orchestrate several well-characterised DNA-damage responses, such as transcription (*ATF3*), stress signalling (*CDKN1A* and *PPM1D*), cell cycle regulation (*Ccng2* and *CDKN1A*), growth (*DTR*), differentiation (*GDF15*), DNA repair (*DDB2* and *GADD45α*), apoptosis (*FDXR*, *PMAIP1* and *SAT*) and energy metabolism (*FDXR* and *SAT*). Moreover, many of these genes were selected due to their UV-induced genotype-specific signatures displayed by the telomerised MRC-5, XP-C and CS-A cell lines.

To increase the statistical validity of the RT-PCR assays, three independent biological replicates were prepared by performing additional UV-irradiations, RNA isolations and cDNA synthesis, independent of the samples processed for microarray analysis. In addition to the UV-irradiated samples, RT-PCR was performed on time-matched, non-irradiated controls, which were prepared in parallel to the irradiated samples and in an identical manner (except UV-irradiation was omitted).

Although Affymetrix™ microarrays and RT-PCR measured the changes in response to UV at the mRNA level, it is changes at the protein level that ultimately orchestrates cell function. To address this, changes at the protein level was investigated for $p21^{WAF1/CIP1}$ (Chapter 4), ATF3, FDXR, GADD45α and PMAIP1 (NOXA), by undertaking Western blot analysis.

In Chapter 4, data was presented that confirmed the preservation of the $p53/p21^{WAF1/CIP1}$ and $pRb/p16^{INK4A}$ tumour suppressor pathways, following the

ectopic expression of hTERT. In addition to confirming stabilisation, the functional activity of p53 was assessed indirectly by measuring the levels of the p53 downstream CDK inhibitor, $p21^{WAF1/CIP1}$, at the protein level by Western blotting and ICC. Global gene expression profiling presented in this Chapter, using the Affymetrix™ platform, revealed that *CDKN1A* was a UV-responsive gene that displayed kinetics of induction following UV at the transcriptome level in telomerised MRC-5, XP-C and CS-A cell lines (Fig. 5.9). To validate the Affymetrix™ data at the transcriptome level and confirm the functional activity of p53, *CDKN1A* was validated at the mRNA level by RT-PCR, using the TaqMan® platform.

Figure 5.10 clearly shows that the UV-induced transcriptional response of *CDKN1A* in telomerised XP-C and CS-A, measured by RT-PCR, recapitulated the kinetics of *CDKN1A* measured by Affymetrix™ HG-U133A GeneChip® arrays (Fig. 5.9). In agreement with the Affymetrix™ data, RT-PCR showed that *CDKN1A* was rapidly induced in XP-C at ~6 hours after UV (Fig. 5.10A). Although this response was sustained throughout the time course at ~12 and ~24 hours post UV, a further significant increase in the *CDKN1A* mRNA transcript was not observed in the telomerised XP-C cells (Fig. 5.10A). In addition, the RT-PCR data revealed that there was a ~2-3 fold induction of *CDKN1A* in the telomerised XP-C cells in response to UV, compared to the time-matched, non-irradiated controls (Fig. 5.10A). Conversely, and in concordance with the array data (Fig. 5.9), RT-PCR revealed that unlike the XP-C cell line, telomerised CS-A cells exhibited kinetics of a gradual induction of *CDKN1A* over the time course (Fig. 5.10B). The level of *CDKN1A* was ~1-3 fold higher at ~6 and ~12 hours, compared to the time-matched, non-irradiated controls (Fig. 5.10B). The level of *CDKN1A* appeared to peak at ~24 hours, displaying a ~7-fold induction, compared to the time-matched, non-irradiated control (Fig. 5.10B). Notably, a slight induction was observed at ~6 hours following mock-irradiation in the telomerised CS-A cell line (Fig. 5.10B). This may have been attributed to a serum response following feeding with fresh medium after mock-irradiation. However, the level of *CDKN1A* mRNA in the time-matched, non-irradiated telomerised XP-C and CS-A cell lines remained relatively constant throughout

the time course, displaying minimal fluctuations between the time points (Figs. 5.10A & B, respectively).

The kinetics of $p21^{WAF1/CIP1}$ induction in the UV-irradiated telomerised XP-C and CS-A cell lines at the protein level, recapitulated the kinetics of *CDKN1A* induction at the mRNA level (Figs. 4.12B & C, respectively). As previously discussed (Chapter 4), Western blot analysis and ICC revealed that the level of $p21^{WAF1/CIP1}$ protein in XP-C rapidly accumulated at ~6 hours post UV and was sustained at high levels throughout the time course at ~12 and ~24 hours (Figs. 4.12B & 4.14). Conversely, both Western blotting and ICC showed that $p21^{WAF1/CIP1}$ protein levels gradually accumulated over the time course in the telomerised CS-A cell line, with an increase in $p21^{WAF1/CIP1}$ observed at ~6, ~12 and ~24 hours post UV (Figs. 4.12C & 4.15). In summary, Western blotting, Affymetrix™ and RT-PCR data presented here, clearly showed that accumulation of $p21^{WAF1/CIP1}$ protein levels reflected the levels of *CDKN1A* mRNA in telomerised XP-C and CS-A cell lines following UV-irradiation. Notably, the levels of *CDKN1A* mRNA remained relatively constant in XP-C and CS-A throughout the time course in the time-matched, non-irradiated controls (Figs. 5.10A & B, respectively). In contrast, marked fluctuations were observed in $p21^{WAF1/CIP1}$ protein levels in both telomerised XP-C and CS-A cell lines, with high protein levels detected at 0 and ~6 hours, compared to the low levels observed at ~12 and ~24 hours (Figs. 4.12B & C, respectively).

Figure 5.9. Analysis of the transcriptional response of *CDKN1A* in response to UV-C radiation, using Affymetrix™ GeneChip® HG-U133A arrays. Graphical representation (using MADRAS) of the kinetics of the transcriptional response of *CDKN1A* over 24 hours in telomerised NER-proficient MRC-5, GGR-defective XP-C (GM02996, XP8CA) and TCR-defective CS-A (GM01856, CS3BE) fibroblasts, following exposure to 10 J/m^2 UV-C (254 nm) radiation. The incubation times are indicated. Differential regulation of expression is represented in colour and red represents upregulation, while green, downregulation. *Abbreviations*: hrs, hours.

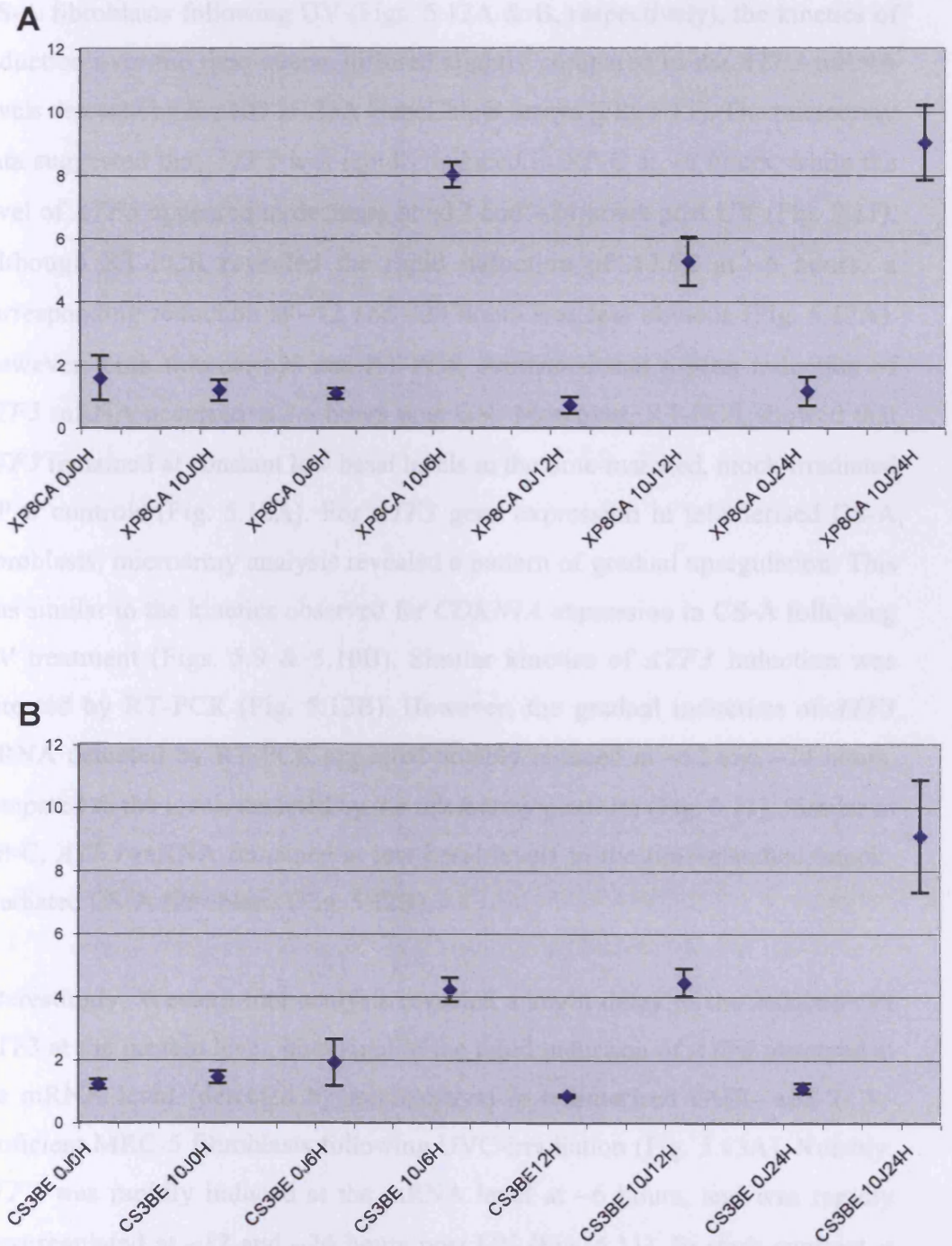

Figure 5.10. Verification of *CDKN1A* mRNA by quantitative RT-PCR. RT-PCR of *CDKN1A* in hTERT-immortalised (A) XP-C (GM02996, XP8CA) and (B) CS-A (GM01856, CS3BE) dermal fibroblasts at the indicated time points following UVC-irradiation (10 J/m^2) or mock-irradiation (0 J/m^2). The amplification of *GAPDH* was performed to normalise expression levels (not shown).

Although RT-PCR confirmed the induction of *ATF3* in telomerised XP-C and CS-A fibroblasts following UV (Figs. 5.12A & B, respectively), the kinetics of induction over the time course differed slightly compared to the *ATF3* mRNA levels detected by the HG-U133A GeneChip® arrays (Fig. 5.11). The microarray data suggested that *ATF3* was rapidly induced in XP-C at ~6 hours, while the level of *ATF3* appeared to decrease at ~12 and ~24 hours post UV (Fig. 5.11). Although RT-PCR revealed the rapid induction of *ATF3* at ~6 hours, a corresponding reduction at ~12 and ~24 hours was less obvious (Fig. 5.12A). However, both microarrays and RT-PCR confirmed that a peak induction of *ATF3* mRNA occurred at ~6 hours post UV. Moreover, RT-PCR showed that *ATF3* remained at constant low basal levels in the time-matched, mock-irradiated XP-C controls (Fig. 5.12A). For *ATF3* gene expression in telomerised CS-A fibroblasts, microarray analysis revealed a pattern of gradual upregulation. This was similar to the kinetics observed for *CDKN1A* expression in CS-A following UV treatment (Figs. 5.9 & 5.10B). Similar kinetics of *ATF3* induction was detected by RT-PCR (Fig. 5.12B). However, the gradual induction of *ATF3* mRNA detected by RT-PCR appeared notably reduced at ~12 and ~24 hours, compared to the levels detected by the microarray platform (Fig. 5.11). Similar to XP-C, *ATF3* mRNA remained at low basal levels in the time-matched, mock-irradiated CS-A fibroblasts (Fig. 5.12B).

Interestingly, Western blot analysis revealed a slight delay in the induction of ATF3 at the protein level, compared to the rapid induction of *ATF3* observed at the mRNA level (detected by microarrays) in telomerised GGR- and TCR-proficient MRC-5 fibroblasts following UVC-irradiation (Fig. 5.13A). Notably, *ATF3* was rapidly induced at the mRNA level at ~6 hours, and was rapidly downregulated at ~12 and ~24 hours post UV (Fig. 5.11). In stark contrast, a delay in ATF3 induction was observed at ~12 hours, which reached a peak at ~24 hours after exposure to UV (Fig. 5.13A). A subsequent decrease in ATF3 protein was not seen in MRC-5 fibroblasts during the time course in this investigation. Conversely, the accumulation of ATF3 protein in telomerised GGR- (XP-C) and TCR-deficient (CS-A) fibroblasts appeared to recapitulate the kinetics of *ATF3* induction at the mRNA level at ~6, ~12 and ~24 hours after UV

(Figs. 5.13B & C, respectively). For example, a rapid induction of ATF3 protein was observed at ~6 hours in XP-C, and was sustained at ~12 and ~24 hours (Fig. 5.13B). In contrast, a gradual accumulation of ATF3 protein occurred in the telomerised CS-A fibroblasts (Fig. 5.13C), and peaked at ~24 hours after UV. This pattern of kinetics for ATF3 protein induction in CS-A reflected the gradual accumulation of *ATF3* observed at the mRNA level.

Notably, although the level of *ATF3* mRNA remained constant in the time-matched, mock-irradiated controls in the telomerised XP-C and CS-A fibroblasts (Figs. 5.12A & B, respectively), a slight induction of ATF3 protein was seen in telomerised XP-C cells. The level of ATF3 peaked at ~6 hours and was subsequently reduced at ~12 and ~24 hours. A similar increase was not observed in telomerised MRC-5 and CS-A fibroblasts (Figs. 513A & C, respectively). Therefore, the induction of ATF3 at the mRNA and protein levels was UV-dependent. Furthermore, the telomerised NER-proficient (MRC-5), GGR-deficient (XP-C) and TCR-deficient (CS-A) cells exhibited genotype-specific kinetics for the differential regulation of ATF3 at both the transcriptome and proteome level. At the mRNA level both MRC-5 and XP-C cells displayed kinetics of rapid induction of *ATF-3* followed by downregulation, while CS-A fibroblasts exhibited a gradual upregulation of *ATF3* throughout the time course. This suggested a possible delay in the transcriptional expression of *ATF3* in CS-A cells. Similarly, a gradual delay in the induction of ATF3 protein was observed in CS-A, and this further supported these findings.

Figure 5.11. Analysis of the transcriptional response of *ATF3* in response to UVC-irradiation, using Affymetrix™ GeneChip® HG-U133A arrays. Graphical representation (using MADRAS) of the kinetics of the transcriptional response of *ATF3* over 24 hours in telomerised NER-proficient MRC-5 and GGR-defective XP-C (GM02996, XP8CA) and TCR-defective CS-A (GM01856, CS3BE) fibroblasts, following exposure to 10 J/m^2 UV-C (254 nm) radiation. The incubation times are indicated. Differential regulation of expression is represented in colour and red represents upregulation, while green, downregulation. *Abbreviations*: hrs, hours.

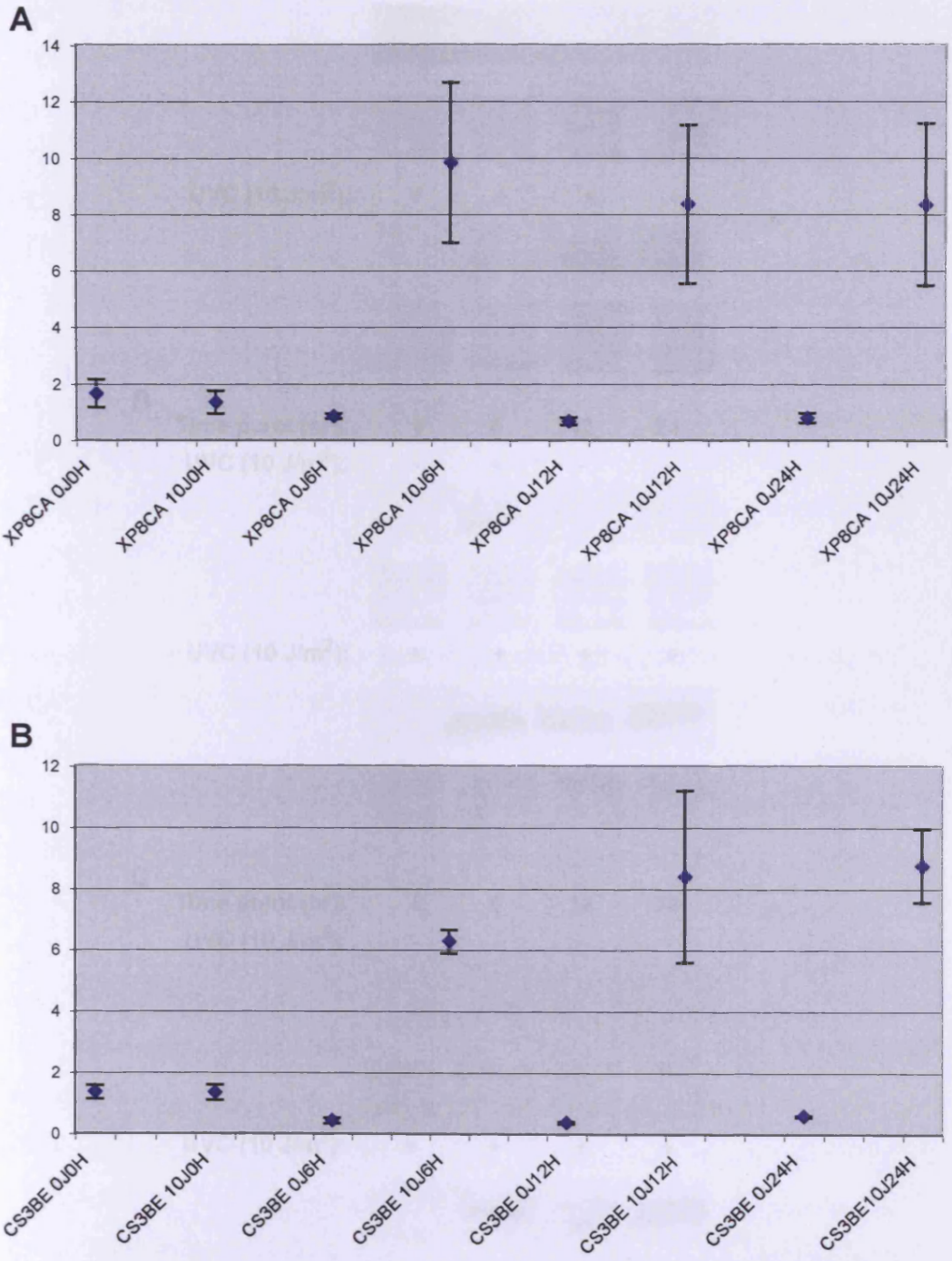

Figure 5.12. Verification of *ATF3* mRNA by quantitative RT-PCR. RT-PCR of *ATF3* in hTERT-immortalised (A) XP-C (GM02996, XP8CA) and (B) CS-A (GM01856, CS3BE) dermal fibroblasts at the indicated time points following UVC-irradiation (10 J/m^2) or mock-irradiation (0 J/m^2) . The amplification of *GAPDH* was performed to normalise *ATF3* expression levels (not shown).

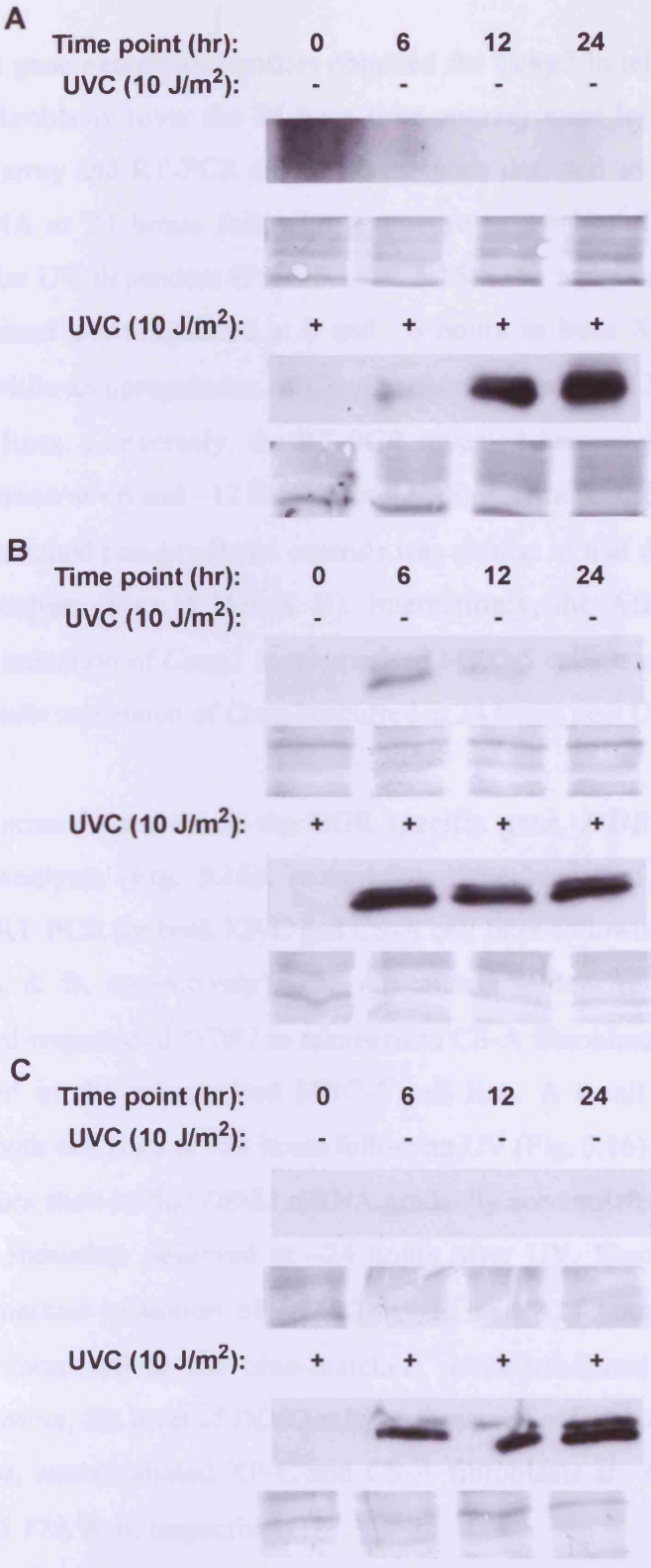

Figure 5.13. Induction of ATF3 protein following exposure to UVC-irradiation. Varification of microarray results at the protein level by Western blot analysis of UVC-induced time-dependent upregulation of ATF3, using an anti-ATF3 mouse monoclonal antibody (1:200). Time couse of ATF3 following mock-irradiation (-) or exposure to 10 J/m^2 (+) UV-C in hTERT-immortalised (A) MRC-5, (B) XP-C (GM02996, XP8CA) and (C) CS-A (GM01856, CS3BE) fibroblasts at the indicated time points (20 µg of WCE per lane). Equal protein loading was confirmed by India ink staining (*lower panel of each blot*).

Although the gene expression profiles obtained for *Ccng2* in telomerised XP-C and CS-A fibroblasts (over the 24 hour time course) were largely discordant between the array and RT-PCR data, both methods detected an upregulation in *Ccng2* mRNA at 24 hours following exposure to 10 J/m^2 UV, and which appeared to be UV-dependent (Figs. 5.14 & 5.15). The array data showed that *Ccng2* remained downregulated at 0 and ~6 hours in both XP-C and CS-A fibroblasts, while an upregulation of *Ccng2* was observed at ~12 and ~24 hours in both cell lines. Conversely, the RT-PCR revealed heterogeneous levels of *Ccng2* expression at ~6 and ~12 hours post UV. Furthermore, the level of *Ccng2* in the time-matched non-irradiated controls was similar to that displayed by the irradiated samples (Figs. 5.15A & B). Interestingly, the Affymetrix™ data showed that induction of *Ccng2* in telomerised MRC-5 cells was upregulated at ~12 hours, while repression of *Ccng2* occurred at 24 hours post UV (Fig. 5.14).

The transcriptional kinetics of the GGR-specific gene, *DDB2*, detected by microarray analysis (Fig. 5.16), recapitulated the levels of *DDB2* mRNA obtained by RT-PCR for both XP-C and CS-A cell lines following UV exposure (Figs. 5.17A & B, respectively). The Affymetrix™ data revealed that the transcriptional response of *DDB2* in telomerised CS-A fibroblasts was similar to that observed in the telomerised MRC-5 cell line. A small induction was observed in both cell lines at ~24 hours following UV (Fig. 5.16). In contrast, the microarray data showed that *DDB2* mRNA gradually accumulated in XP-C cells, with a peak induction observed at ~24 hours after UV. Similarly, RT-PCR revealed a marked induction of *DDB2* at ~12 and ~24 hours in the XP-C fibroblasts, compared to the time-matched, mock-irradiated controls (Fig. 5.17A). Moreover, the level of *DDB2* mRNA remained at low basal levels in the time-matched, non-irradiated XP-C and CS-A fibroblasts at ~6, ~12 and ~24 hours (Figs. 5.17A & B, respectively).

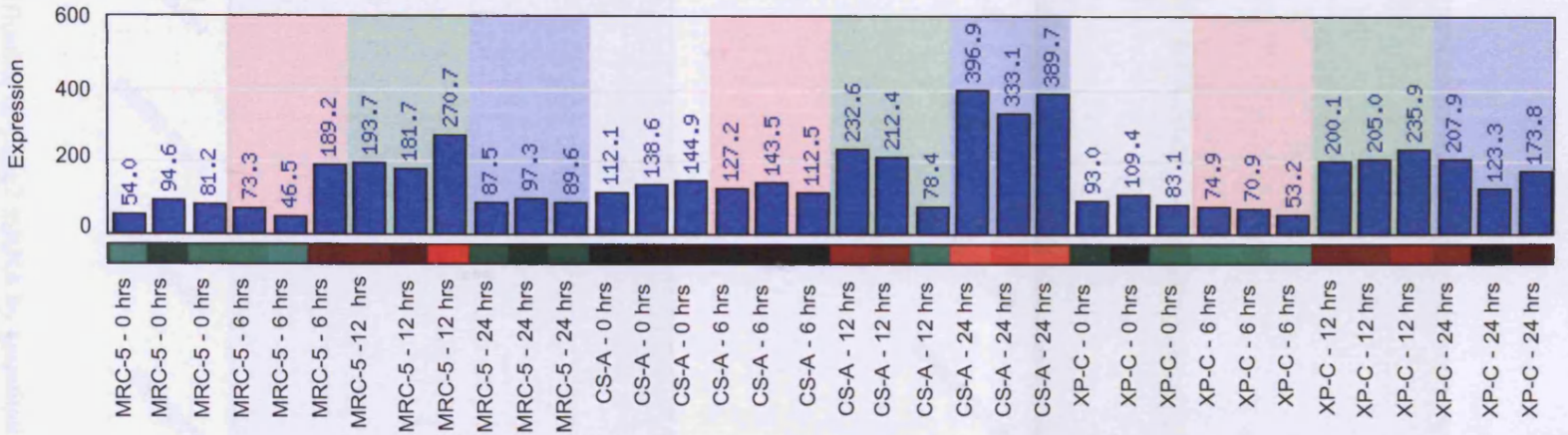

Figure 5.14. Analysis of the transcriptional response of *Ccng2* in response to UVC-irradiation, using Affymetrix™ GeneChip® HG-U133A arrays. Graphical representation (using MADRAS) of the kinetics of the transcriptional response of *Ccng2* over 24 hours in telomerised NER-proficient MRC-5 and GGR-defective XP-C (GM02996, XP8CA) and TCR-defective CS-A (GM01856, CS3BE) fibroblasts, following exposure to 10 J/m^2 UV-C (254 nm) radiation. The incubation times are indicated. Differential regulation of expression is represented in colour and red represents upregulation, while green, downregulation. *Abbreviations*: hrs, hours.

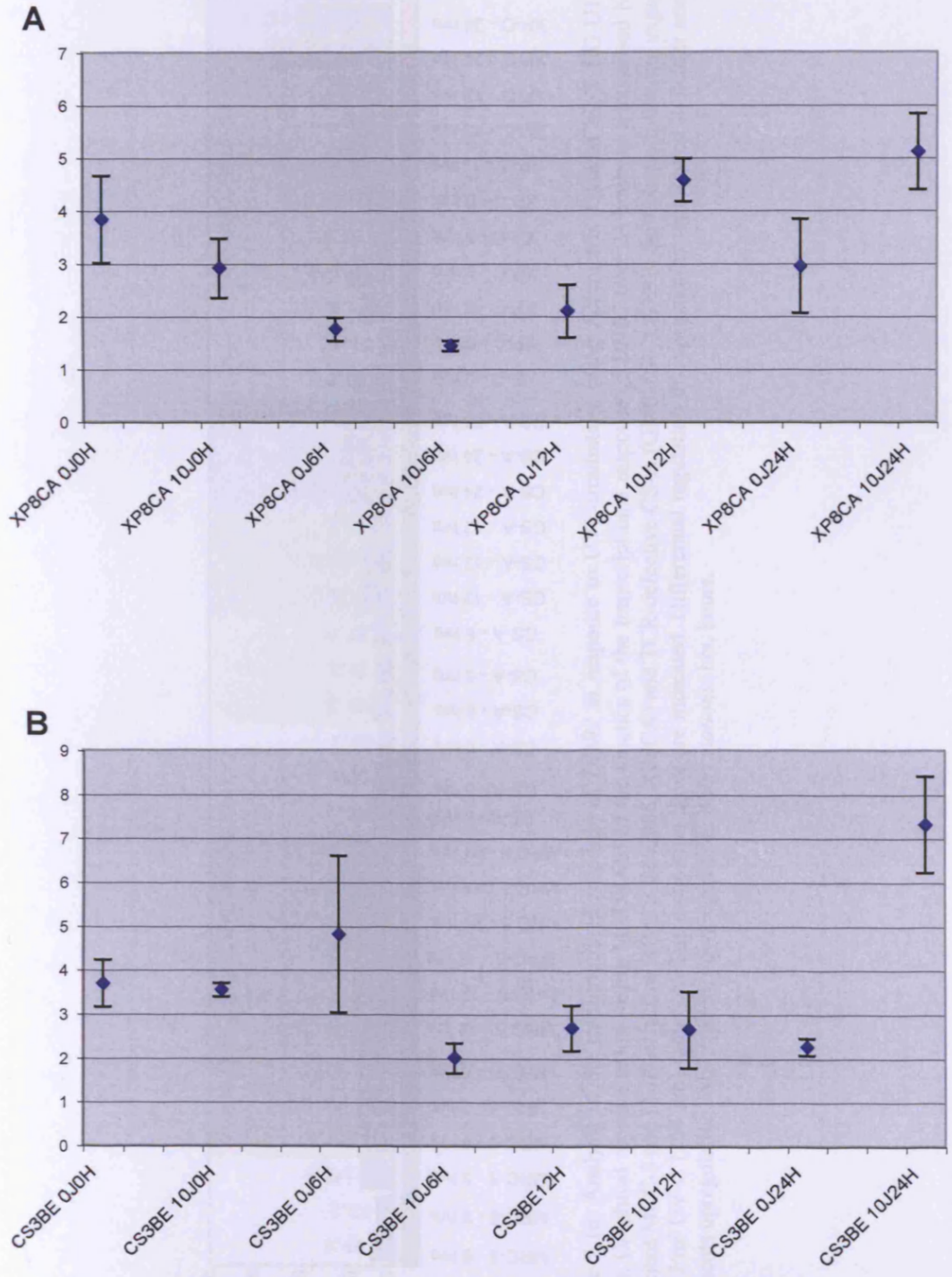

Figure 5.15. Verification of *Ccng2* mRNA by quantitative RT-PCR. RT-PCR of *Ccng2* in hTERT-immortalised (A) XP-C (GM02996, XP8CA) and (B) CS-A (GM01856, CS3BE) dermal fibroblasts at the indicated time points following UV-irradiation (10 J/m^2) or mock-irradiation (0 J/m^2). The amplification of *GAPDH* was performed to normalise *Ccng2* expression levels (not shown).

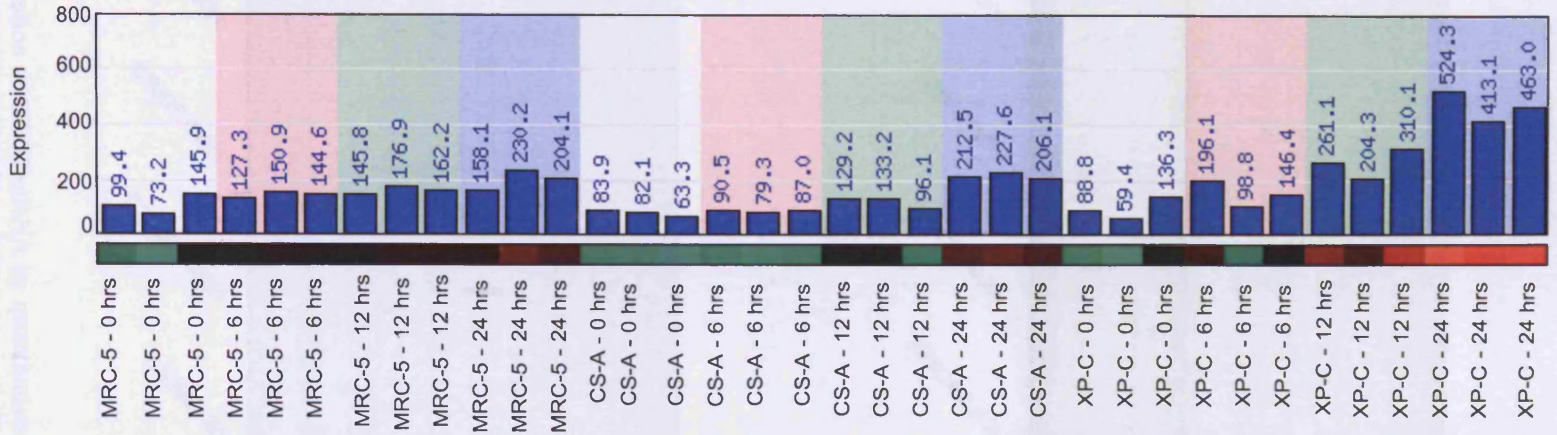

Figure 5.16. Analysis of the transcriptional response of *DDB2* in response to UVC-irradiation, using Affymetrix™ GeneChip® HG-U133A arrays. Graphical representation (using MADRAS) of the kinetics of the transcriptional response of *DDB2* over 24 hours in telomerised NER-proficient MRC-5 and GGR-defective XP-C (GM02996, XP8CA) and TCR-defective CS-A (GM01856, CS3BE) fibroblasts, following exposure to 10 J/m^2 UV-C (254 nm) radiation. The incubation times are indicated. Differential regulation of expression is represented in colour and red represents upregulation, while green, downregulation. *Abbreviations*: hrs, hours.

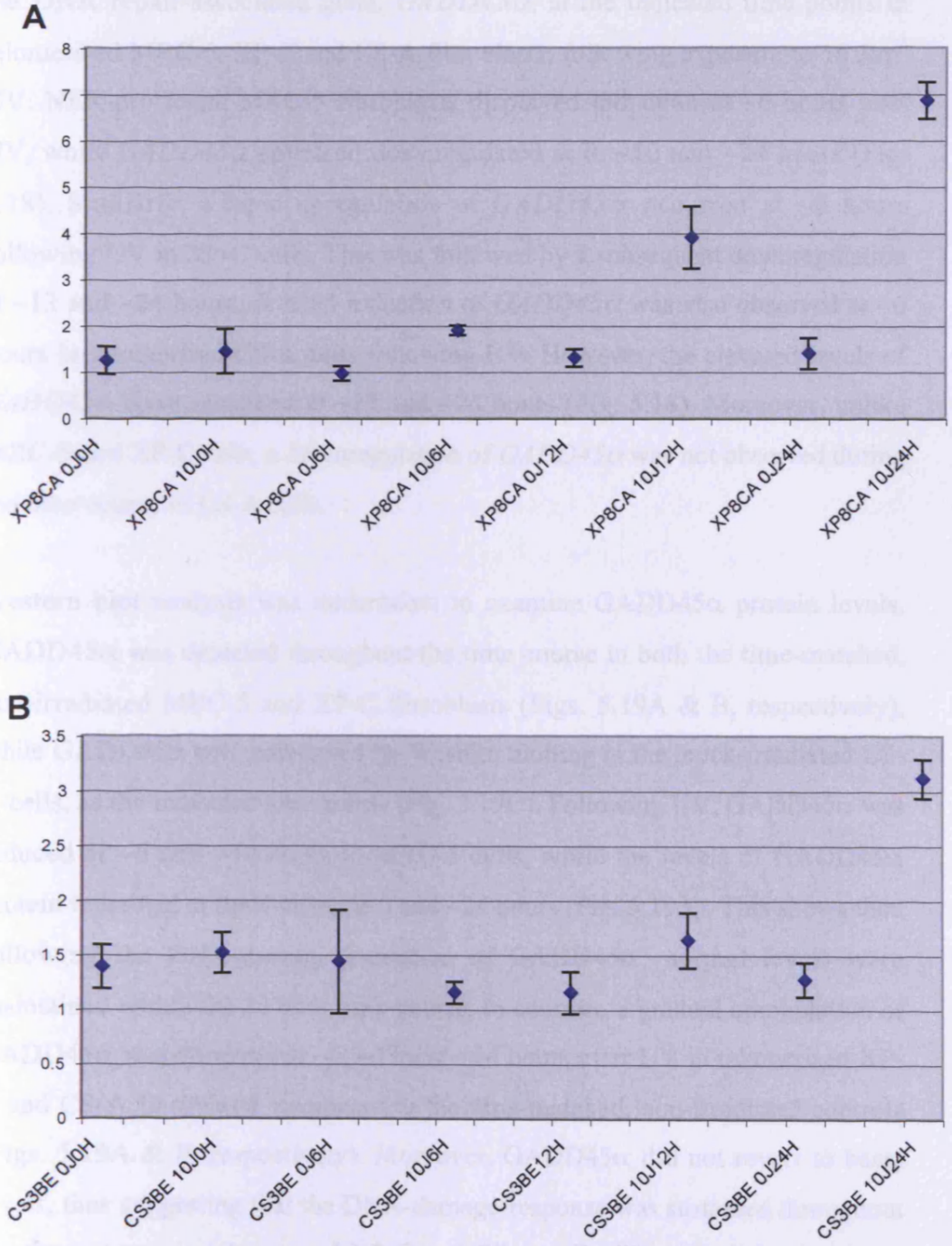

Figure 5.17. Verification of *DDB2* mRNA by quantitative RT-PCR. RT-PCR of *DDB2* in hTERT-immortalised (A) XP-C (GM02996, XP8CA) and (B) CS-A (GM01856, CS3BE) dermal fibroblasts at the indicated time points following UV-irradiation (10 J/m^2) or mock-irradiation 0 J/m^2). The amplification of *GAPDH* was performed to normalise *DDB2* expression levels (not shown).

Figure 5.18 shows the transcriptional profile (obtained by microarray analysis) of the DNA repair-associated gene, *GADD45α*, at the indicated time points in telomerised MRC-5, XP-C and CS-A fibroblasts, following exposure to 10 J/m^2 UV. NER-proficient MRC-5 fibroblasts displayed induction at ~6 hours post UV, while *GADD45α* appeared downregulated at 0, ~12 and ~24 hours (Fig. 5.18). Similarly, a rapid upregulation of *GADD45α* occurred at ~6 hours following UV in XP-C cells. This was followed by a subsequent downregulation at ~12 and ~24 hours. A rapid induction of *GADD45α* was also observed at ~6 hours in telomerised CS-A cells following UV. However, the elevated levels of *GADD45α* were sustained at ~12 and ~24 hours (Fig. 5.18). Moreover, unlike MRC-5 and XP-C cells, a downregulation of *GADD45α* was not observed during the time course in CS-A cells.

Western blot analysis was undertaken to examine GADD45α protein levels. GADD45α was detected throughout the time course in both the time-matched, non-irradiated MRC-5 and XP-C fibroblasts (Figs. 5.19A & B, respectively), while GADD45α was undetected by Western blotting in the mock-irradiated CS-A cells, as the indicated time points (Fig. 5.19C). Following UV, GADD45α was induced at ~6 and ~12 hours in MRC-5 cells, while the levels of GADD45α protein remained at basal levels at 0 and ~24 hours (Fig. 5.19A). This shows that, following the DNA-damage induction of GADD45α; normal levels were maintained within the 24 hour time course. In contrast, a gradual upregulation of GADD45α was observed at ~6, ~12 and ~24 hours after UV in telomerised XP-C and CS-A fibroblasts, compared to the time-matched, non-irradiated controls (Figs. 5.19A & B, respectively). Moreover, GADD45α did not revert to basal levels, thus suggesting that the DNA-damage-response was sustained throughout the time course in telomerised XP-C and CS-A cells. The data presented here, suggests that the accumulation of GADD45α protein recapitulated the induction of its mRNA. However, the data also suggested that there was a slight delay in kinetics, as peak *GADD45α* mRNA levels were observed at ~6 hours in MRC-5, XP-C and CS-A cells, while peak GADD45α protein levels were not observed until between 12-24 hours post UV (Figs. 9.19A-C).

The Affymetrix™ data suggested that the pro-apoptotic gene, *PMAIP1* (*NOXA*), was rapidly induced at ~6 hours in telomerised MRC-5 fibroblasts following UV (Fig. 5.20). A slight induction was also observed in telomerised XP-C cells following UV (Fig. 5.20). Like in MRC-5, *PMAIP1* was downregulated in XP-C cells at ~12 and ~24 hours after UV. In contrast, CS-A displayed kinetics of induction that were similar to that observed for *CDKN1A* and *ATF3* (Figs. 5.9 & 5.11, respectively). A gradual upregulation of *PMAIP1* was observed at ~6 and ~12 hours post UV, while *PMAIP1* reached a peak at ~24 hours. In disagreement with these data, RT-PCR suggested that *PMAIP1* was rapidly induced at ~6 hours in XP-C cells, which was sustained at ~12 and ~24 hours (Fig. 5.21A). Conversely, RT-PCR revealed a slight induction of *PMAIP1* at ~6 hours in CS-A cells that was followed by a marked upregulation ~12 hours (Fig. 5.21B). This was followed by a slight downregulation at ~24 hours (Fig. 5.21B). *PMAIP1* mRNA levels remained low in the time-matched, non-irradiated telomerised XP-C and CS-A controls (Figs. 5.21A & B, respectively).

Notably, Figure 5.22A shows that PMAIP1 protein levels were elevated in both UV- and mock-irradiated MRC-5 cells. Although PMAIP1 was observed at ~6 hours in non-irradiated XP-C cells, PMAIP1 protein levels (Fig. 5.22B), detected by Western blotting, appeared to reflect the Affymetrix™ data (Fig. 5.20). A slight increase was observed in XP-C cells at ~6 hours post UV. This was followed by a decrease at ~12 and ~24 hours. Similarly, the PMAIP1 protein levels recapitulated the *PMAIP1* mRNA levels in CS-A cells following UV (Fig. 5.22C). An increase of PMAIP1 was observed at ~6 hours, followed by a further accumulation at ~12 and ~24 hours (Fig. 5.22C).

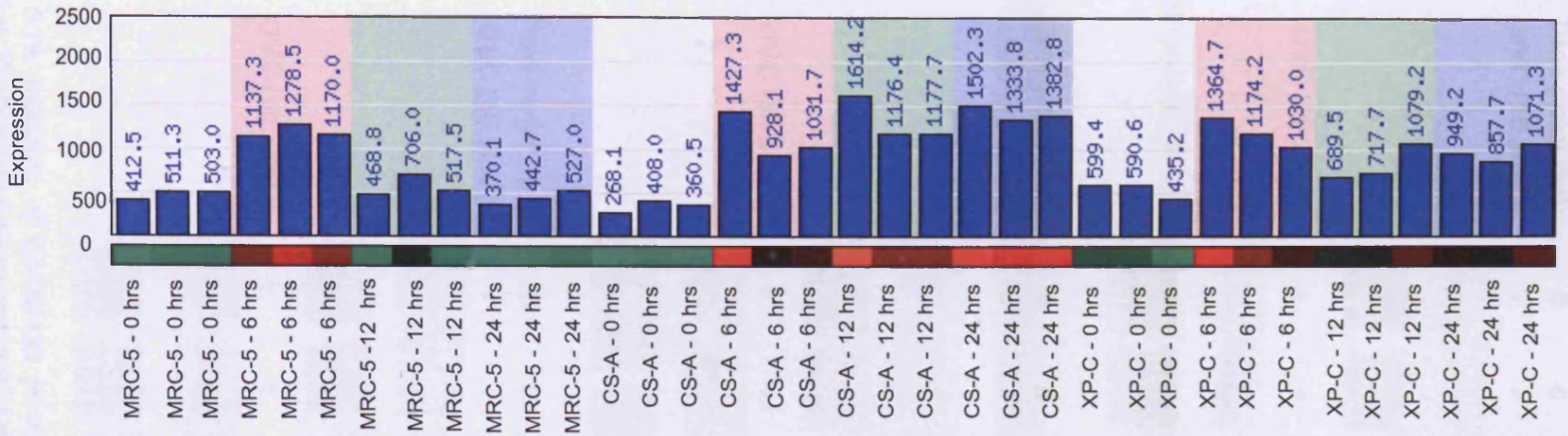

Figure 5.18. Analysis of the transcriptional response of *GADD45α* in response to UVC-irradiation, using Affymetrix™ GeneChip® HG-U133A arrays. Graphical representation (using MADRAS) of the kinetics of the transcriptional response of *GADD45α* over 24 hours in telomerised NER-proficient MRC-5 and GGR-defective XP-C (GM02996, XP8CA) and TCR-defective CS-A (GM01856, CS3BE) fibroblasts, following exposure to 10 J/m^2 UV-C (254 nm) radiation. The incubation times are indicated. Differential regulation of expression is represented in colour and red represents upregulation, while green, downregulation. *Abbreviations*: hrs, hours.

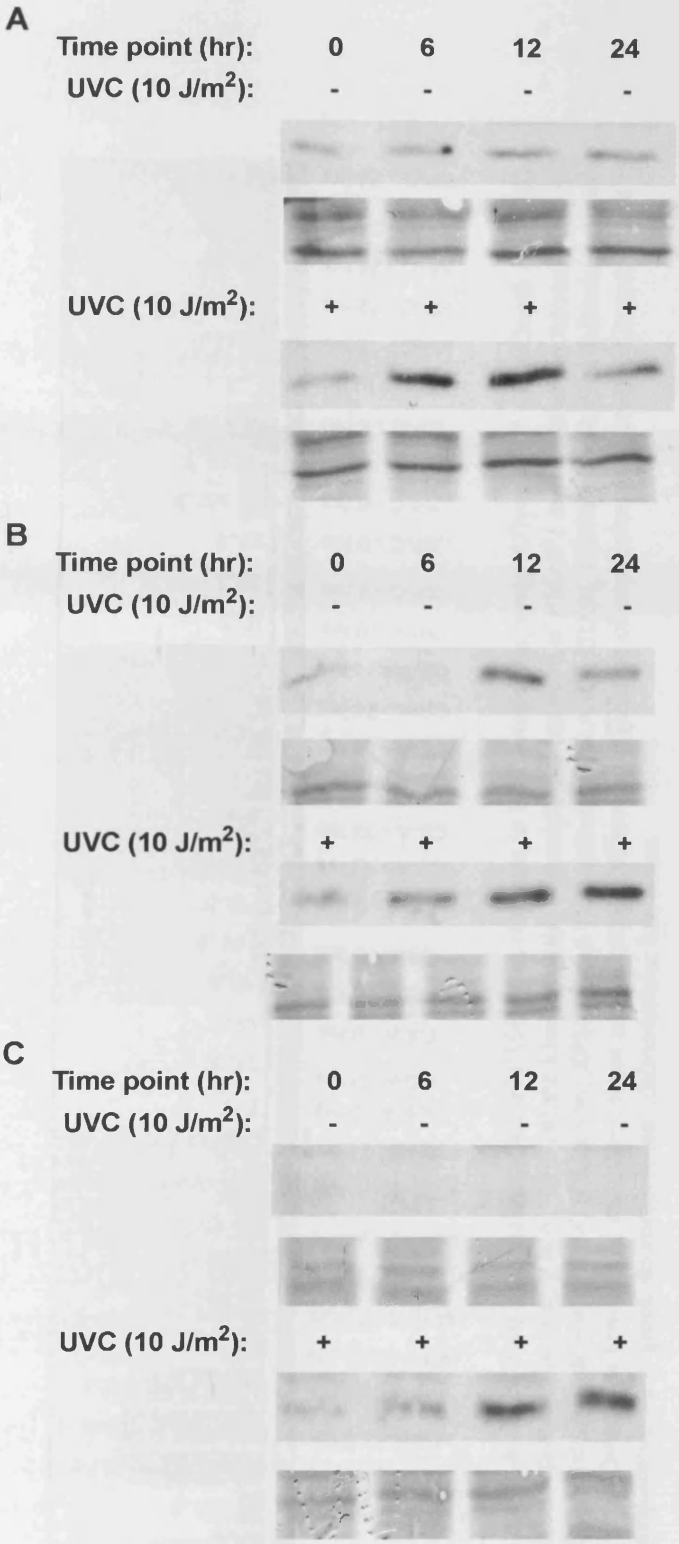

Figure 5.19. Induction of GADD45α protein following exposure to UVC-irradiation. Varification of microarray results at the protein level by Western blot analysis of UVC-induced time-dependent upregulation of GADD45α, using an anti-GADD45α mouse monoclonal antibody (1:250). Time couse of GADD45α following mock-irradiation (-) or exposure to 10 J/m^2 (+) UV-C in hTERT-immortalised (A) MRC-5, (B) XP-C (GM02996, XP8CA) and (C) CS-A (GM01856, CS3BE) fibroblasts at the indicated time points (20 µg of WCE per lane). Equal protein loading was confirmed by India ink staining (*lower panel of each blot*).

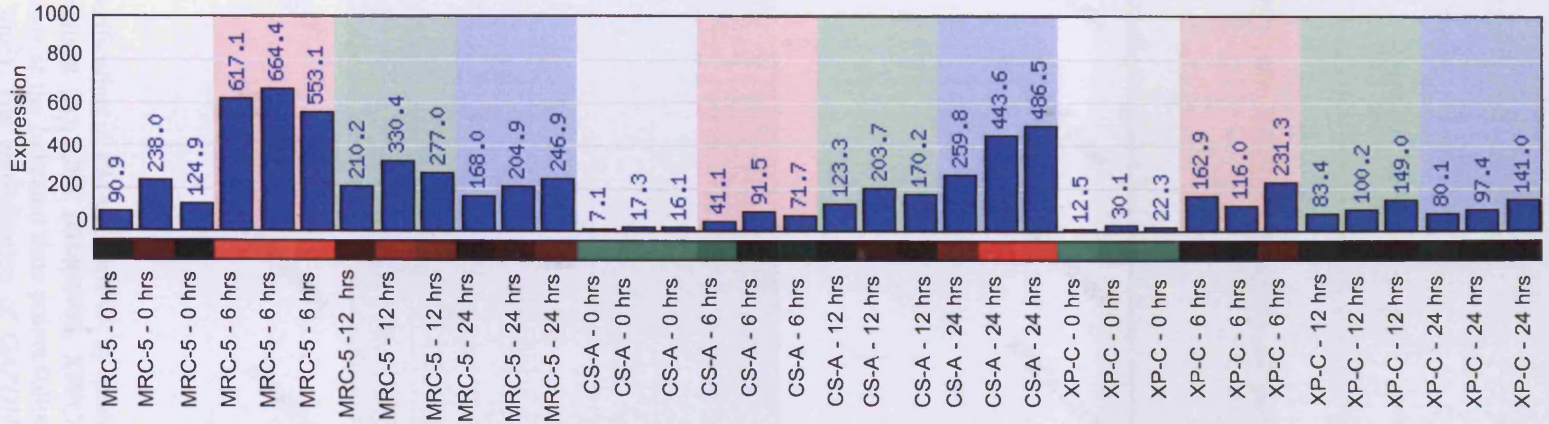

Figure 5.20. Analysis of the transcriptional response of *PMAIP1* in response to UVC-irradiation, using Affymetrix™ GeneChip® HG-U133A arrays. Graphical representation (using MADRAS) of the kinetics of the transcriptional response of *PMAIP1* over 24 hours in telomerised NER-proficient MRC-5 and GGR-defective XP-C (GM02996, XP8CA) and TCR-defective CS-A (GM01856, CS3BE) fibroblasts, following exposure to 10 J/m^2 UV-C (254 nm) radiation. The incubation times are indicated. Differential regulation of expression is represented in colour and red represents upregulation, while green, downregulation. *Abbreviations*: hrs, hours.

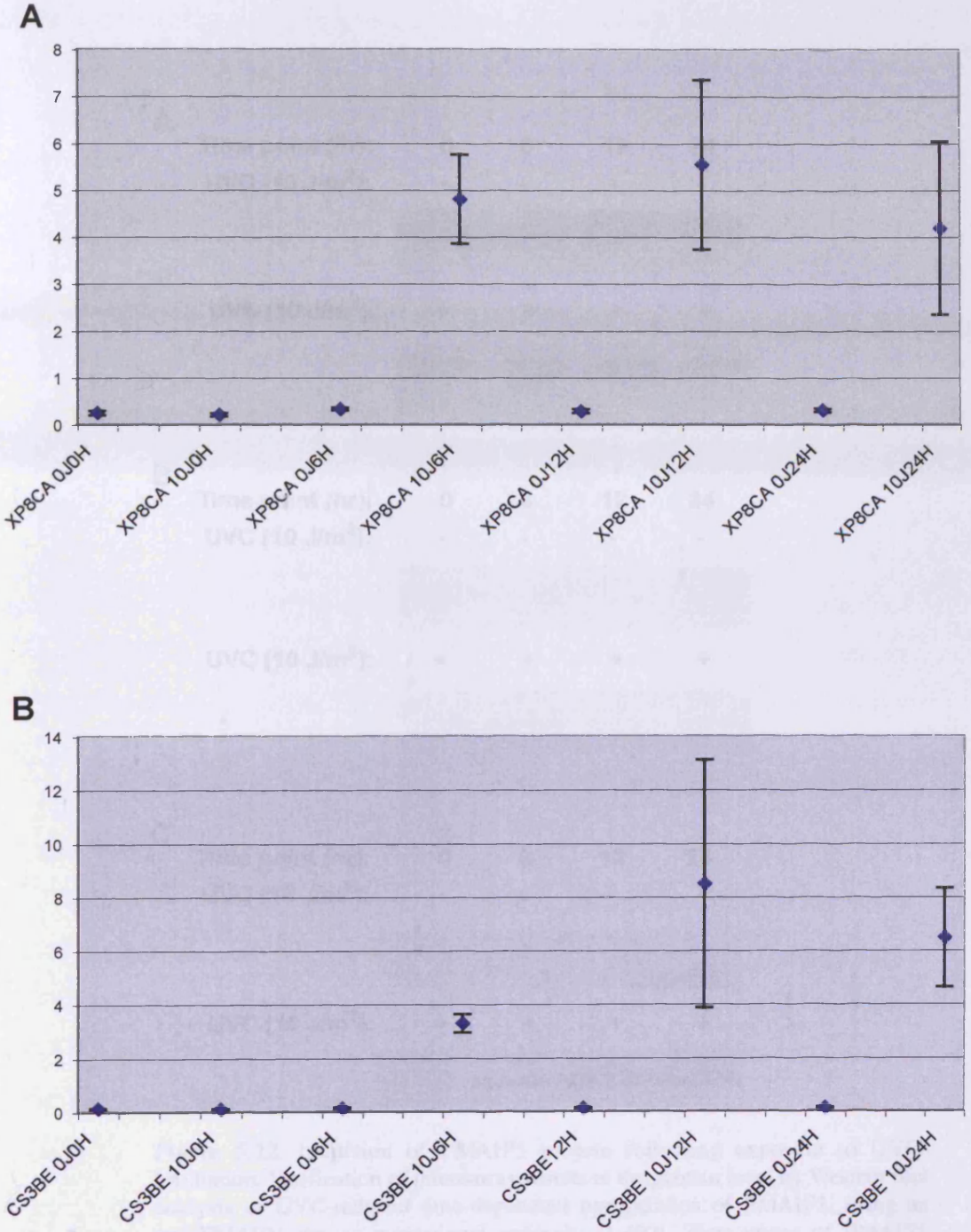

Figure 5.21. Verification of *PMAIP1* mRNA by quantitative RT-PCR. RT-PCR of *PMAIP1* in hTERT-immortalised (A) XP-C (GM02996, XP8CA) and (B) CS-A (GM01856, CS3BE) dermal fibroblasts at the indicated time points following UV-irradiation (10 J/m^2) or mock-irradiation (0 J/m^2). The amplification of *GAPDH* was performed to normalise *PMAIP1* expression levels (not shown).

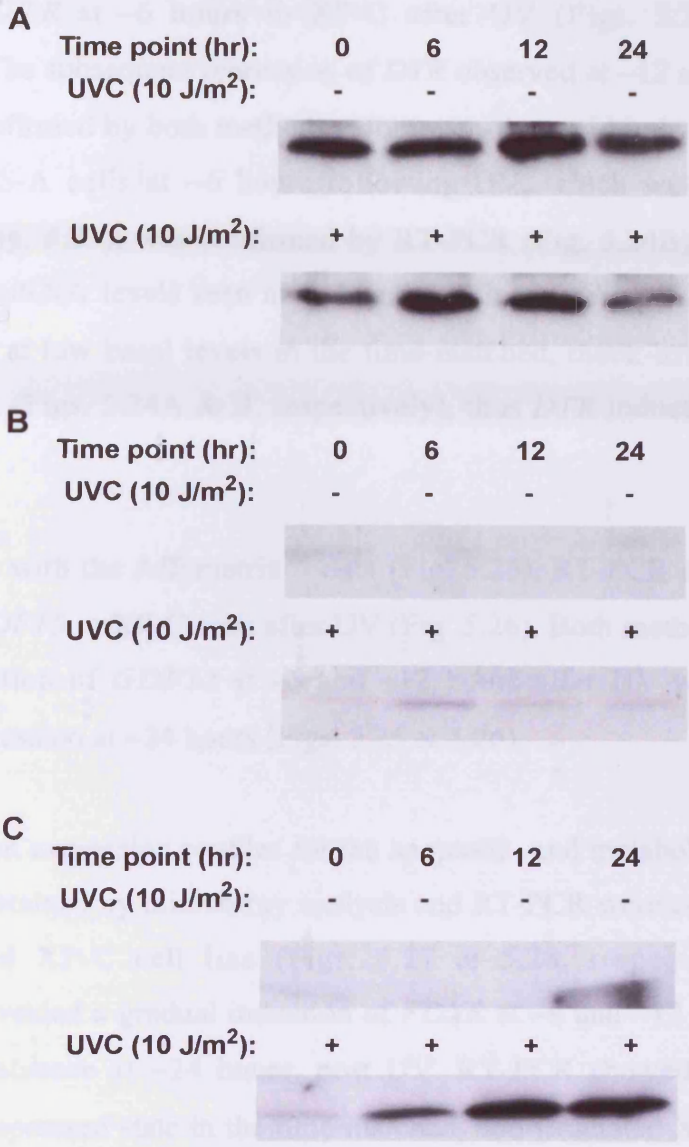

Figure 5.22. Induction of PMAIP1 protein following exposure to UVC-irradiation. Varification of microarray results at the protein level by Western blot analysis of UVC-induced time-dependent upregulation of PMAIP1, using an anti-PMAIP1 mouse monoclonal antibody (1:400). Time couse of PMAIP1 following mock-irradiation (-) or exposure to 10 J/m^2 (+) UVC in hTERT-immortalised (A) MRC-5, (B) XP-C (GM02996, XP8CA) and (C) CS-A (GM01856, CS3BE) fibroblasts at the indicated time points (20 µg of WCE per lane).

The expression profiles of *DTR* induction in telomerised XP-C and CS-A cells following UV, obtained by microarrays and RT-PCR were concordant (Figs. 5.23 & 5.24, respectively). Both microarrays and RT-PCR revealed a rapid induction of *DTR* at ~6 hours in XP-C after UV (Figs. 5.23 & 5.24A, respectively). The subsequent repression of *DTR* observed at ~12 and ~24 hours was further confirmed by both methods. Moreover, the rapid induction of *DTR*, observed in CS-A cells at ~6 hours following UV, which was detected by microarrays (Fig. 5.23), was confirmed by RT-PCR (Fig. 5.24B), as were the elevated *DTR* mRNA levels seen at ~12 and ~24 hours (Figs. 5.23 & 5.24B). *DTR* remained at low basal levels in the time-matched, mock-irradiated XP-C and CS-A cells (Figs. 5.24A & B, respectively), thus *DTR* induction was UV-dependent.

In concordance with the Affymetrix™ data (Fig. 5.25), RT-PCR confirmed the induction of *GDF15* in XP-C cells after UV (Fig. 5.26). Both methods showed a slight upregulation of *GDF15* at ~6 and ~12 hours after UV with a further increase in expression at ~24 hours (Figs. 5.25 & 5.26).

The transcription expression profiles for the apoptotic- and metabolic-associated gene, *FDXR*, obtained by microarray analysis and RT-PCR were concordant for the telomerised XP-C cell line (Figs. 5.27 & 5.28, respectively). Both technologies revealed a gradual induction of *FDXR* at ~6 and ~12 hours, which continued to increase at ~24 hours, post UV. RT-PCR showed that *FDXR* remained in a repressed state in the time-matched, non-irradiated XP-C controls (Fig. 5.28).

Western blot analysis on UV- and mock-irradiated telomerised MRC-5, XP-C and CS-A WCEs, revealed marked variations in FDXR expression. For example, relatively high levels of FDXR protein were detected in the time-matched, non-irradiated MRC-5, XP-C and CS-A controls, thus suggesting that FDXR was maintained at high basal levels (Figs. 5.29A-C, respectively). A slight induction of FDXR protein occurred at ~12 and ~24 hours in MRC-5 following UV compared to time-matched, non-irradiated MRC-5 cells (Fig. 5.29A). This

recapitulated the transcriptome data obtained by expression profiling (Fig. 5.27). However, although gradual *FDXR* induction was observed at the transcriptome level in UV-irradiated XP-C cells (Figs. 5.27 & 5.28), FDXR protein levels remained at similar levels to the untreated controls (Fig. 5.29B). In contrast, an accumulation of FDXR protein was detected in telomerised CS-A cells at ~6, ~12 and ~24 hours after UV exposure when compared to the untreated XP-C cells (Fig. 5.29C). Hence, the induction of FDXR at the protein level recapitulated the induction of *FDXR* at the mRNA level in CS-A fibroblasts (Figs. 5.29C and 5.27, respectively).

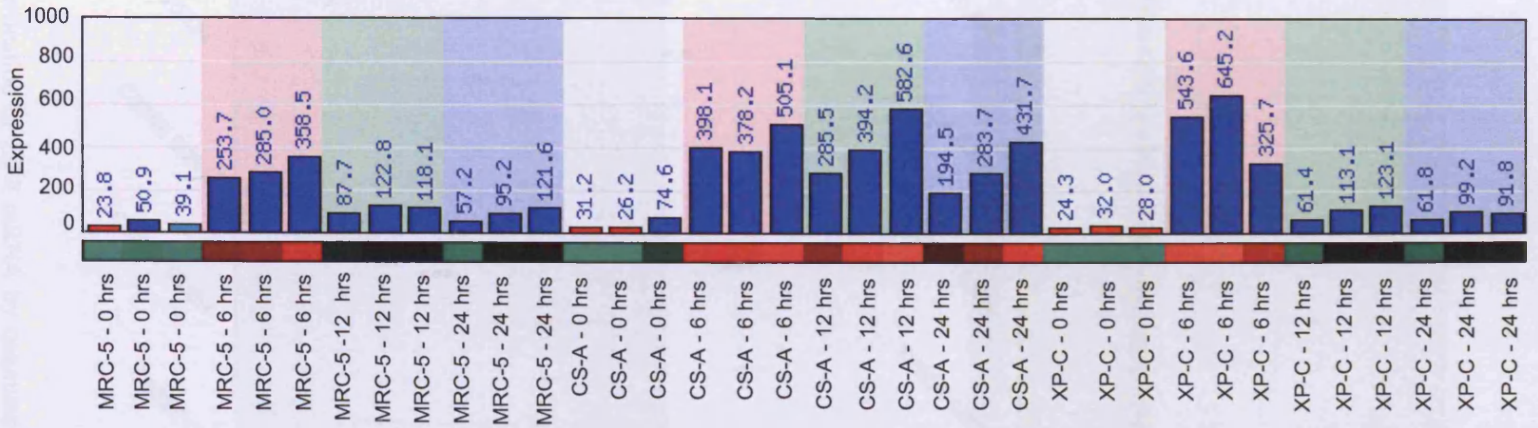

Figure 5.23. Analysis of the transcriptional response of *DTR* in response to UVC-irradiation, using Affymetrix™ GeneChip® HG-U133A arrays. Graphical representation (using MADRAS) of the kinetics of the transcriptional response of *DTR* over 24 hours in telomerised NER-proficient MRC-5 and GGR-defective XP-C (GM02996, XP8CA) and TCR-defective CS-A (GM01856, CS3BE) fibroblasts, following exposure to 10 J/m^2 UV-C (254 nm) radiation. The incubation times are indicated. Differential regulation of expression is represented in colour and red represents upregulation, while green, downregulation. *Abbreviations*: hrs, hours.

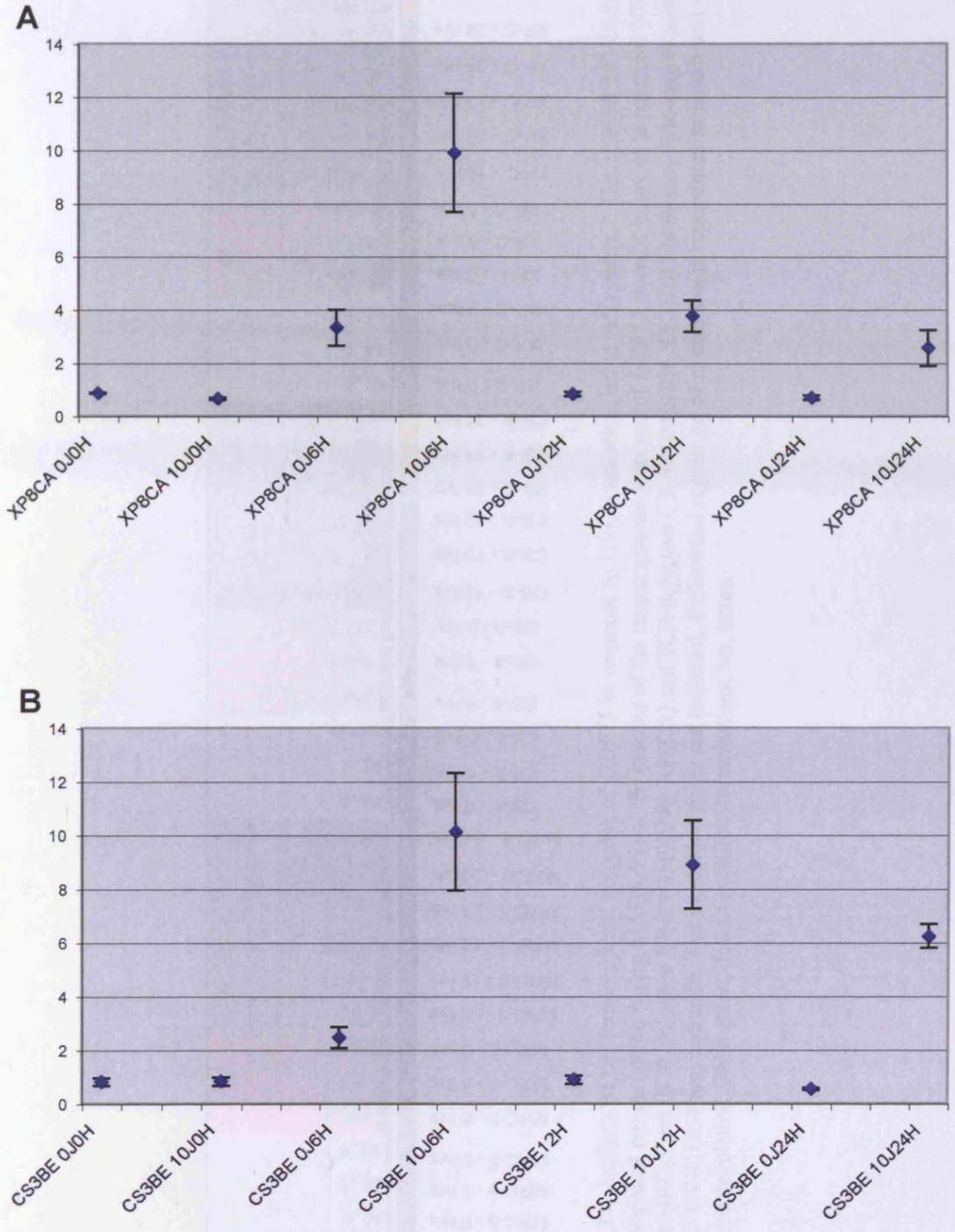

Figure 5.24. Verification of *DTR* mRNA by quantitative RT-PCR. RT-PCR of *DTR* in hTERT-immortalised (A) XP-C (GM02996, XP8CA) and (B) CS-A (GM01856, CS3BE) dermal fibroblasts at the indicated time points following UV-irradiation (10 J/m^2) or mock-irradiation (0 J/m^2). The ampification of *GAPDH* was performed to normalise *DTR* expression levels (not shown).

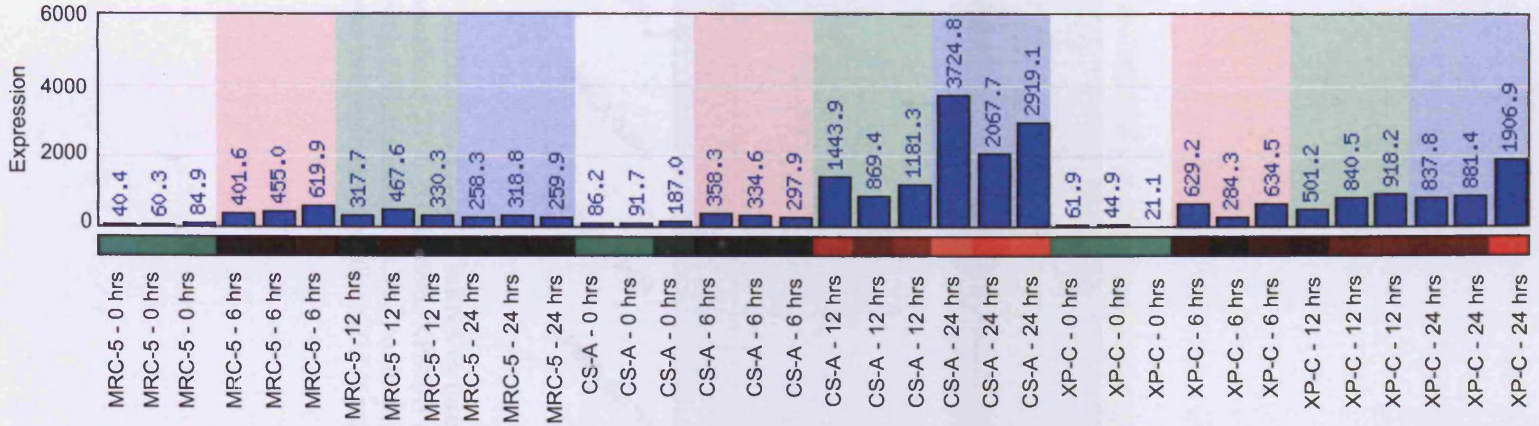

Figure 5.25. Analysis of the transcriptional response of *GDF15* in response to UVC-irradiation, using Affymetrix™ GeneChip® HG-U133A arrays. Graphical representation (using MADRAS) of the kinetics of the transcriptional response of *GDF15* over 24 hours in telomerised NER-proficient MRC-5 and GGR-defective XP-C (GM02996, XP8CA) and TCR-defective CS-A (GM01856, CS3BE) fibroblasts, following exposure to 10 J/m^2 UV-C (254 nm) radiation. The incubation times are indicated. Differential regulation of expression is represented in colour and red represents upregulation, while green, downregulation. *Abbreviations*: hrs, hours.

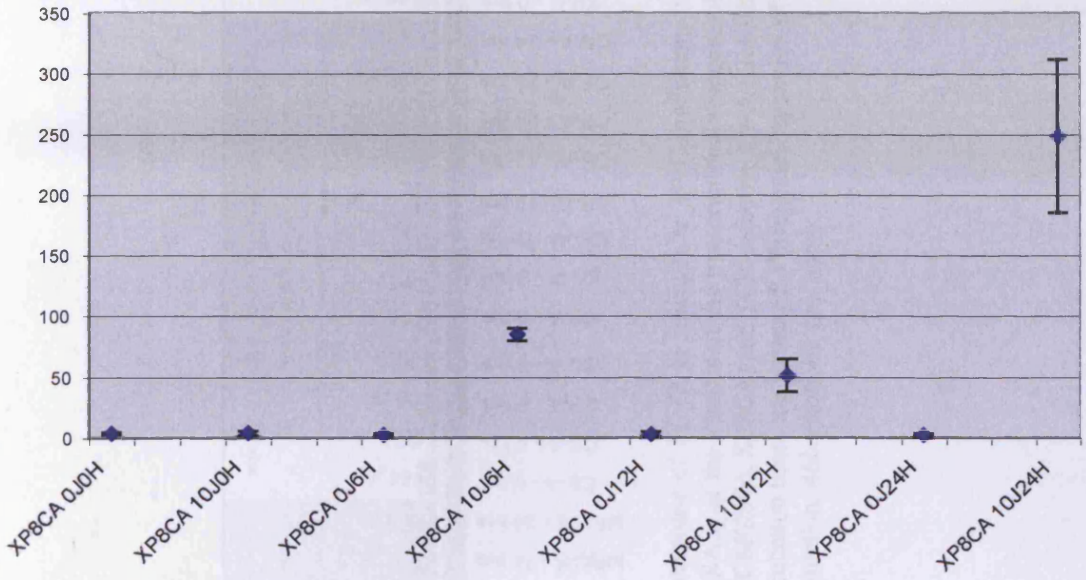

Figure 5.26. Verification of *GDF15* mRNA by quantitative RT-PCR. RT-PCR of *GDF15* in hTERT-immortalised XP-C (GM02996, XP8CA) dermal fibroblasts at the indicated time points following UV-irradiation (10 J/m^2) or mock-irradiation (0 J/m^2) . The amplification of *GAPDH* was performed to normalise *GDF15* expression levels (data not shown).

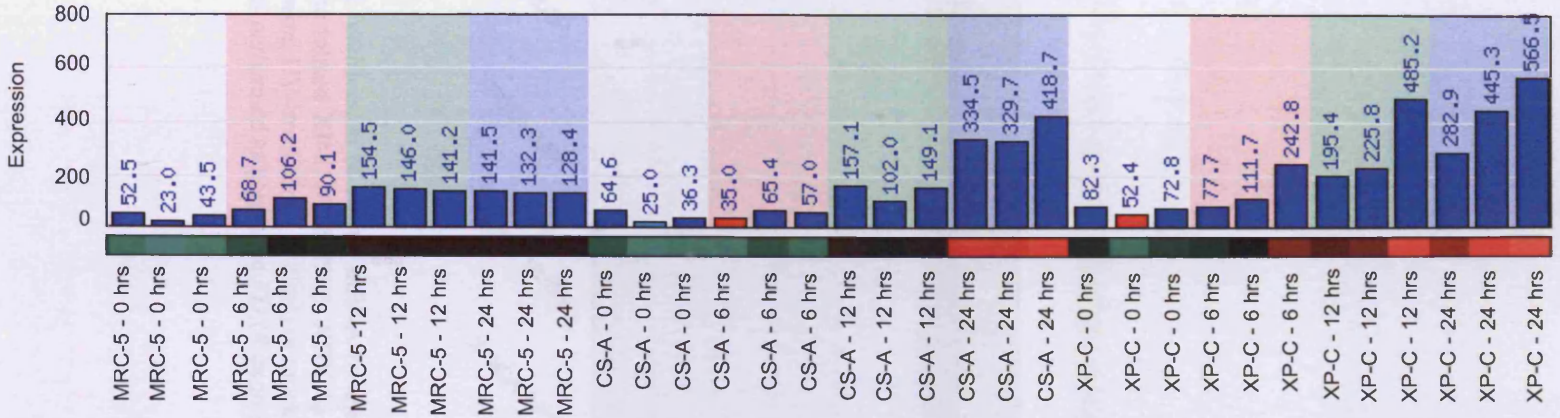

Figure 5.27. Analysis of the transcriptional response of *FDXR* in response to UVC-irradiation, using Affymetrix™ GeneChip® HG-U133A arrays. Graphical representation (using MADRAS) of the kinetics of the transcriptional response of *FDXR* over 24 hours in telomerised NER-proficient MRC-5 and GGR-defective XP-C (GM02996, XP8CA) and TCR-defective CS-A (GM01856, CS3BE) fibroblasts, following exposure to 10 J/m^2 UV-C (254 nm) radiation. The incubation times are indicated. Differential regulation of expression is represented in colour and red represents upregulation, while green, downregulation. *Abbreviations*: hrs, hours.

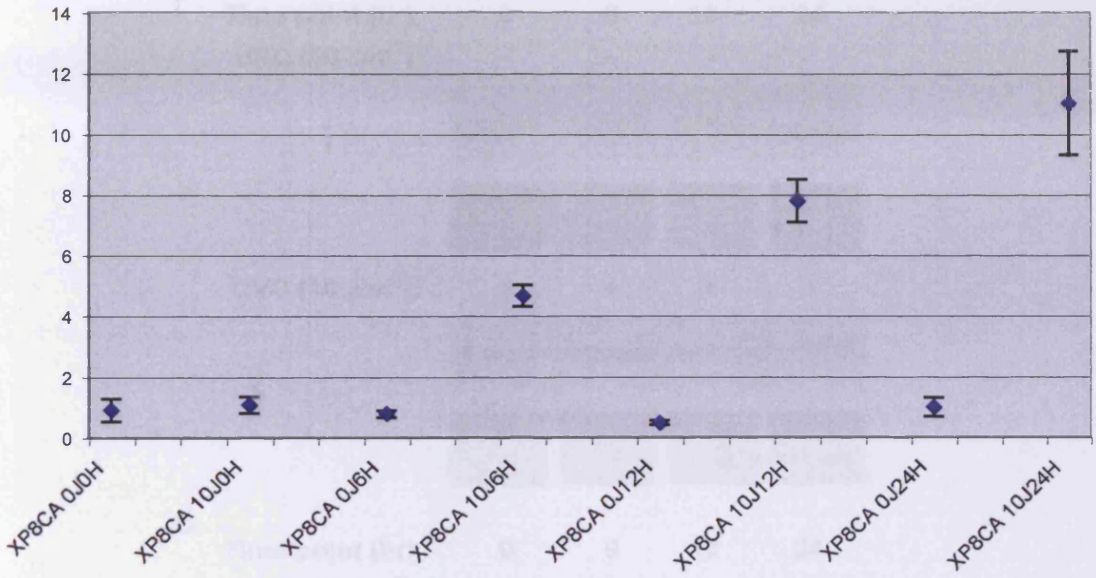

Figure 5.28. Verification of *FDXR* mRNA by quantitative RT-PCR. RT-PCR of *FDXR* in hTERT-immortalised XP-C (GM02996, XP8CA) dermal fibroblasts at the indicated time points following UV-irradiation (10 J/m^2) or mock-irradiation (0 J/m^2). The amplification of *GAPDH* was performed to normalise *FDXR* expression levels (data not shown).

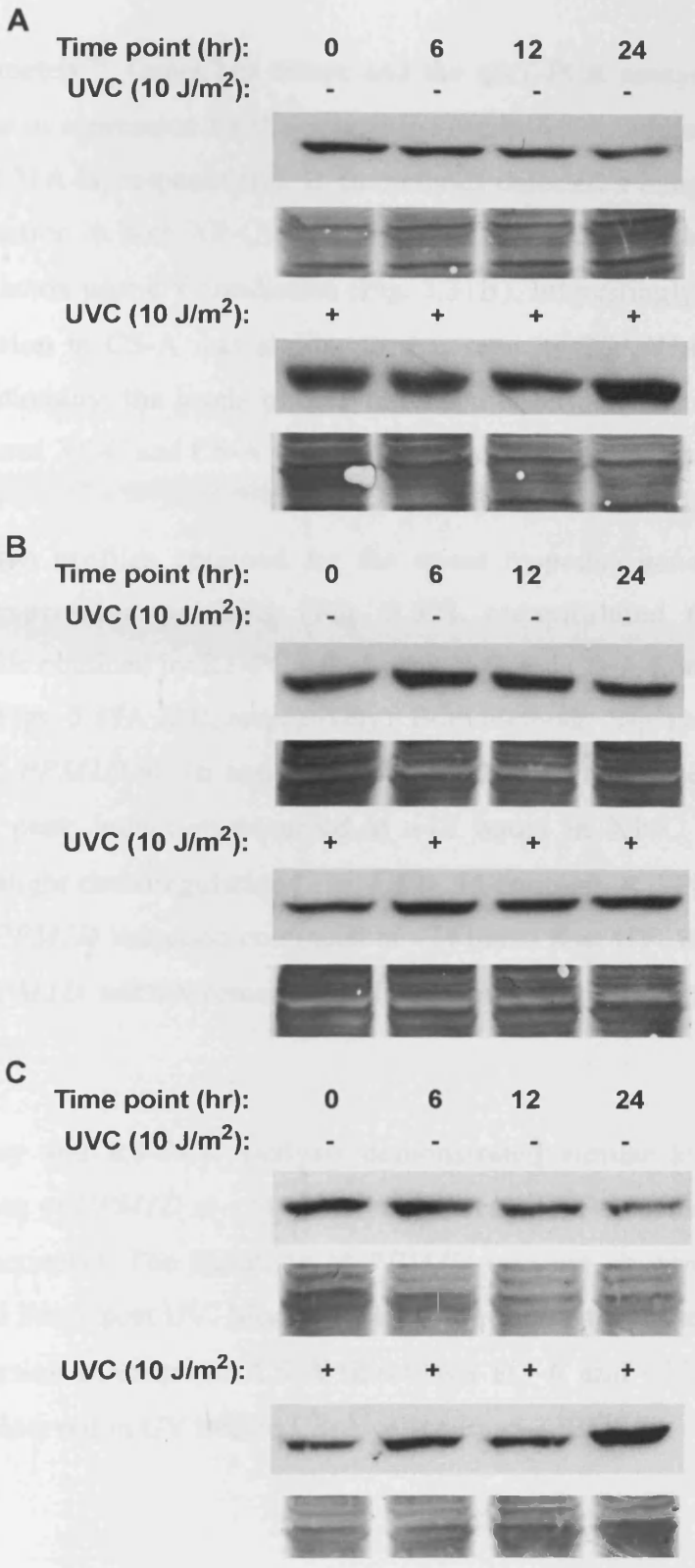

Figure 5.29. Expression of FDXR protein following UVC-irradiation. Varification of microarray results by Western blot, using an anti-FDXR mouse monoclonal antibody (1:1000). Time couse of FDXR following mock-irradiation (-) or exposure to 10 J/m^2 (+) UV-C in hTERT-immortalised (A) MRC-5, (B) XP-C (GM02996, XP8CA) and (C) CS-A (GM01856, CS3BE) fibroblasts at the indicated time points (20 µg of WCE per lane). Equal protein loading was confirmed by India ink staining (*lower panel of each blot*).

Both the Affymetrix™ GeneChip arrays and the qRT-PCR assays detected a gradual increase in expression for the polyamine catabolic-associated gene, *SAT* (Figs. 5.30 & 5.31A-B, respectively). Both methods detected a temporal pattern of gradual induction in both XP-C and CS-A cells at ~6 and ~12 hours, which peaked at ~24 hours post UV-irradiation (Fig. 5.31B). Interestingly, the pattern of *SAT* expression in CS-A was similar to that seen in *CDKN1A*, *ATF3* and *PMAIP1*. Additionally, the levels of *SAT* remained at basal levels in the time-matched, untreated XP-C and CS-A fibroblasts (Figs. 5.31A & B, respectively).

The transcription profiles obtained for the stress response gene, *PPM1D*, obtained by expression profiling (Fig. 5.32), recapitulated the *PPM1D* expression profile obtained by RT-PCR for both XP-C and CS-A fibroblasts after UV treatment (Figs. 5.33A & B, respectively). Both methods displayed a gradual upregulation of *PPM1D* at ~6 and ~12 hours in XP-C cells. The array data suggested that peak induction occurred at ~12 hours in XP-C fibroblasts, followed by a slight downregulation (Fig. 5.32). In contrast, RT-PCR analysis suggested that *PPM1D* induction continued at ~24 hours post UV. RT-PCR also showed that *PPM1D* mRNA remained at low basal levels in untreated XP-C cells (Fig. 5.33A).

Both microarray and RT-PCR analysis demonstrated similar kinetics of a delayed induction of *PPM1D* at ~24 hours in UV treated CS-A cells (Figs. 5.32 & 5.33B, respectively). The induction of *PPM1D* was not observed in CS-A fibroblasts at ~6 hours post UV. Moreover, RT-PCR showed that the kinetics of *PPM1D* expression in untreated CS-A fibroblasts at ~6 and ~12 hours was similar to that observed in UV treated CS-A cells (Fig. 5.33B).

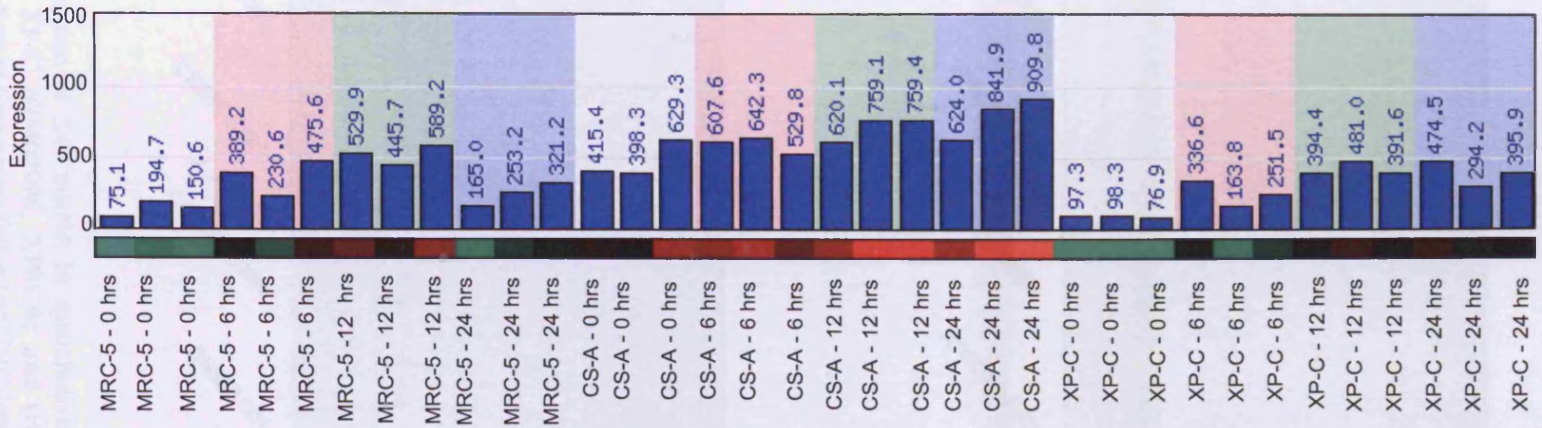

Figure 5.30. Analysis of the transcriptional response of *SAT* in response to UVC-irradiation, using Affymetrix™ GeneChip® HG-U133A arrays. Graphical representation (using MADRAS) of the kinetics of the transcriptional response of *SAT* over 24 hours in telomerised NER-proficient MRC-5 and GGR-defective XP-C (GM02996, XP8CA) and TCR-defective CS-A (GM01856, CS3BE) fibroblasts, following exposure to 10 J/m^2 UV-C (254 nm) radiation. The incubation times are indicated. Differential regulation of expression is represented in colour and red represents upregulation, while green, downregulation. *Abbreviations*: hrs, hours.

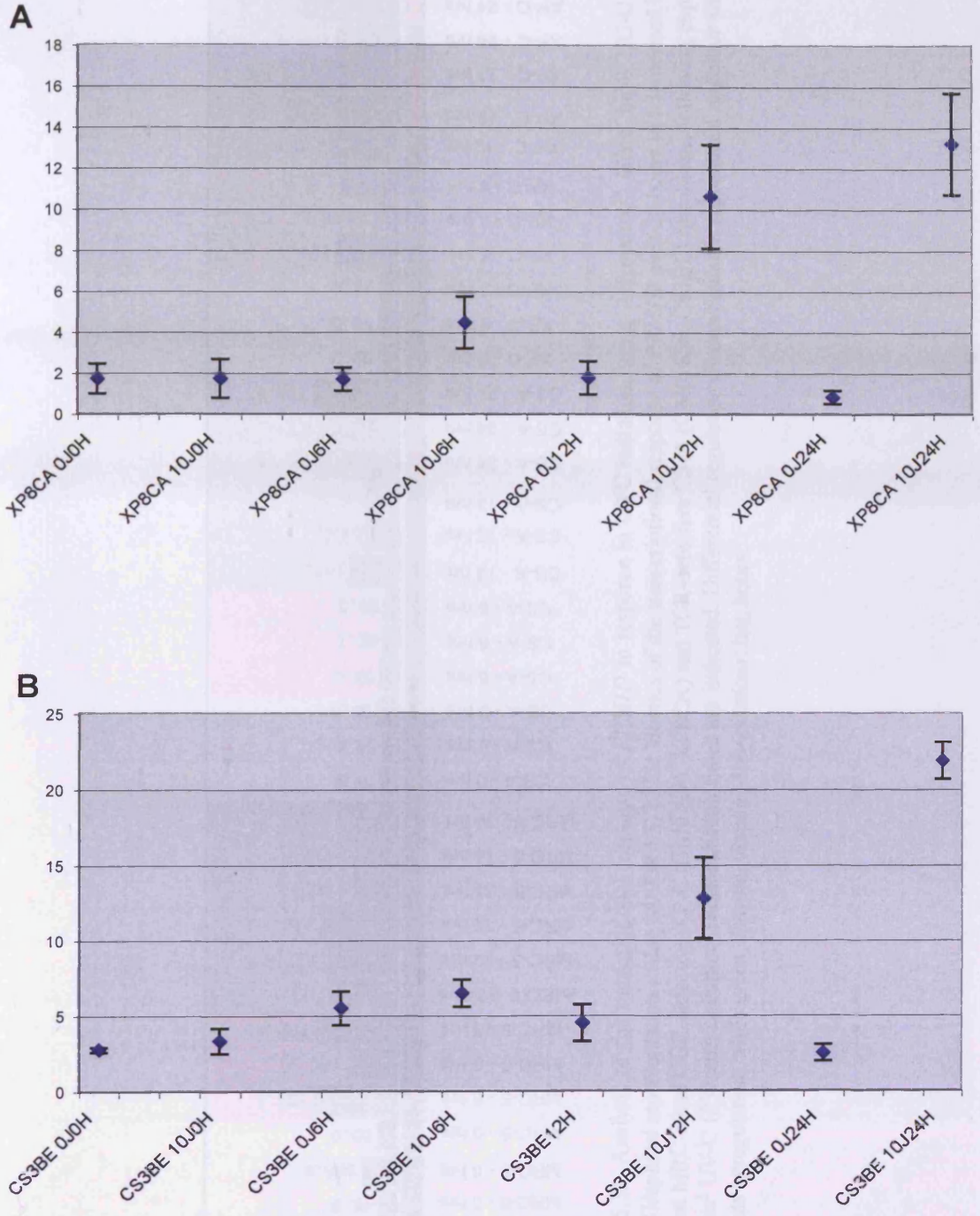

Figure 5.31. Verification of *SAT* mRNA by quantitative RT-PCR. RT-PCR of *SAT* in hTERT-immortalised (A) XP-C (GM02996, XP8CA) and (B) CS-A (GM01856, CS3BE) dermal fibroblasts at the indicated time points following UVC-irradiation (10 J/m^2) or mock-irradiation (0 J/m^2). The amplification of *GAPDH* was performed to normalise *SAT* expressison levels (data not shown).

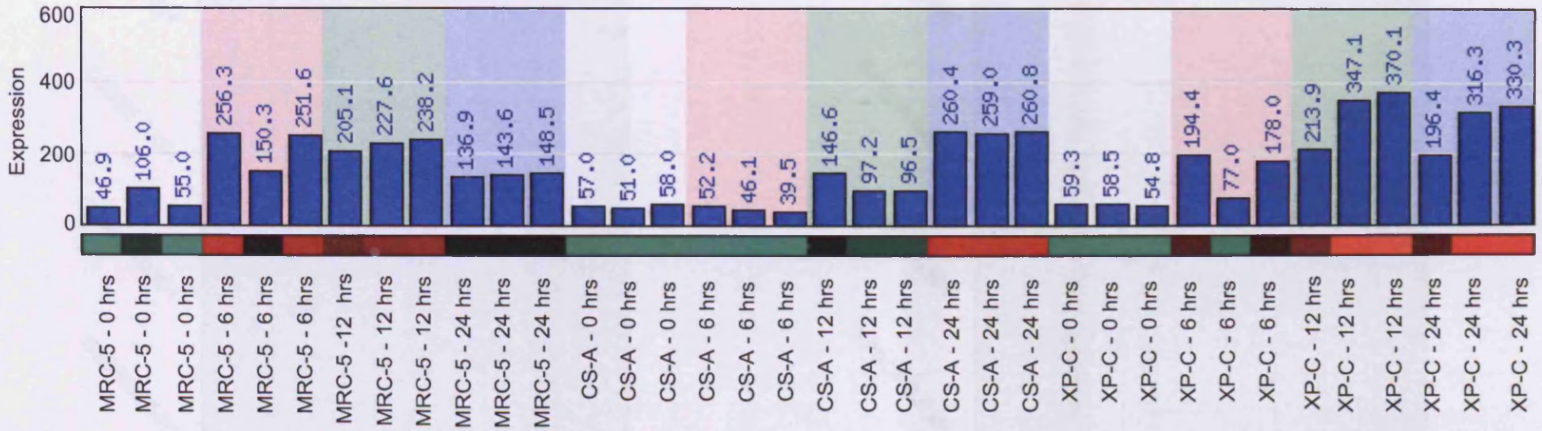

Figure 5.32. Analysis of the transcriptional response of *PPM1D* in response to UVC radiation, using Affymetrix™ GeneChip® HG-U133A arrays. Graphical representation (using MADRAS) of the kinetics of the transcriptional response of *PPM1D* over 24 hours in telomerised NER-proficient MRC-5 and GGR-defective XP-C (GM02996, XP8CA) and TCR-defective CS-A (GM01856, CS3BE) fibroblasts, following exposure to 10 J/m^2 UV-C (254 nm) radiation. The incubation times are indicated. Differential regulation of expression is represented in colour and red represents upregulation, while green, downregulation. *Abbreviations*: hrs, hours.

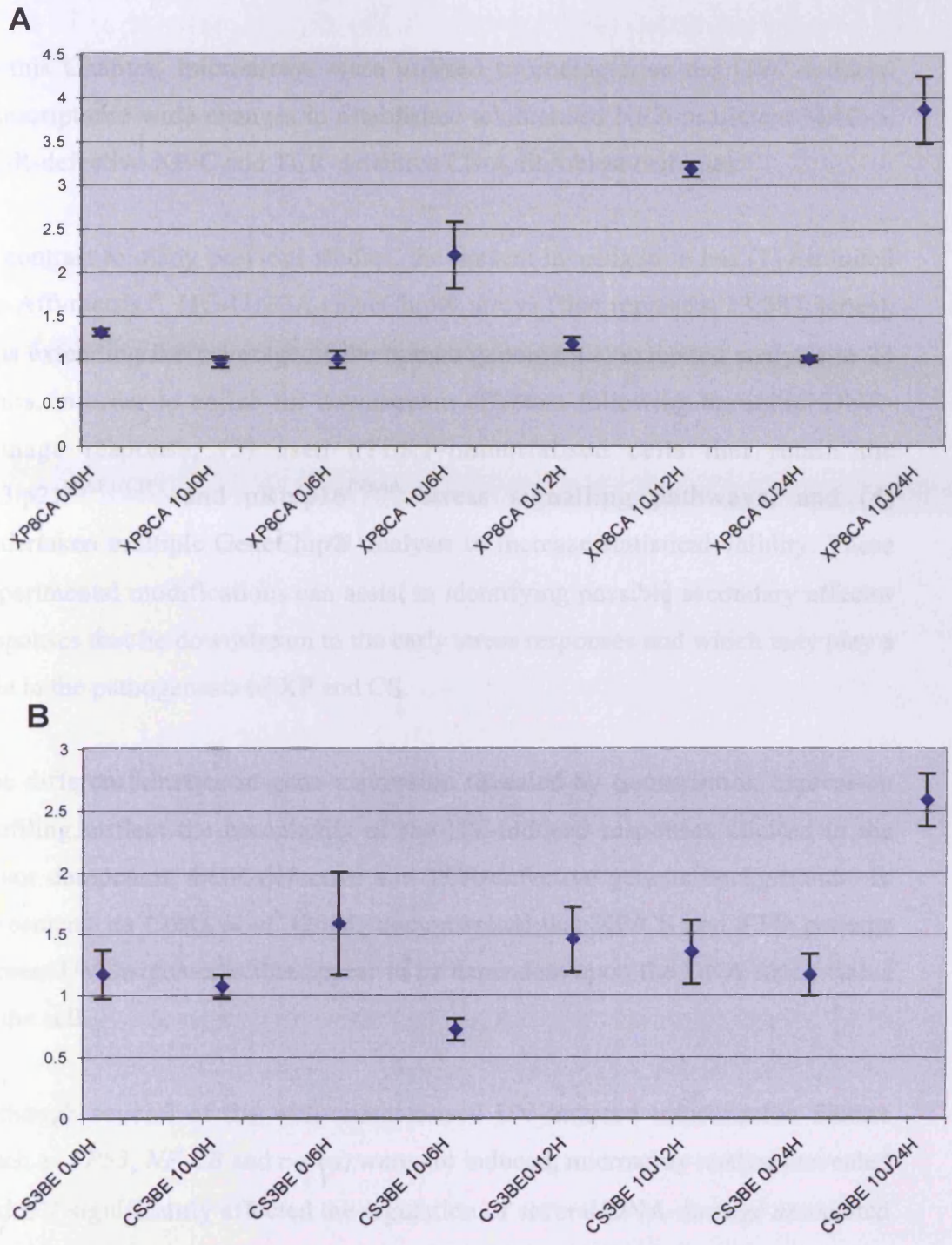

Figure 5.33. Verification of *PPM1D* mRNA by quantitative RT-PCR. RT-PCR of *PPM1D* in hTERT-immortalised (A) XP-C (GM02996, XP8CA) and (B) CS-A (GM01856, CS3BE) dermal fibroblasts at the indicated time points following UVC-irradiation (10 J/m^2) or mock-irradiation (0 J/m^2). The amplification of *GAPDH* was performed to normalise *PPM1D* expression levels (data not shown).

5.5 Discussion

In this Chapter, microarrays were utilised to characterise the UVC-induced transcriptome-wide changes in established telomerised NER-proficient MRC-5, GGR-defective XP-C and TCR-defective CS-A fibroblast cell lines.

In contrast to many previous studies, the present investigation has (1) exploited the Affymetrix™ HG-U133A GeneChip® arrays (that represent 13,387 genes), thus extending the coverage of the human genome, (2) extended analysis to 24 hours, in order to enrich for downstream effectors following the initial DNA-damage response, (3) used hTERT-immortalised cells that retain the p53/p21$^{WAF1/CIP1}$ and pRb/p16^{INK4A} stress signalling pathways, and (4) undertaken multiple GeneChip® analysis to increase statistical validity. These experimental modifications can assist in identifying possible secondary effector responses that lie downstream to the early stress responses and which may play a role in the pathogenesis of XP and CS.

The different kinetics in gene expression revealed by transcription expression profiling, reflect the complexity of the UV-induced responses elicited in the repair competent, GGR-defective and TCR-defective genetic backgrounds. In agreement, da Costa *et al.* (2005) demonstrated that XP/CS and TTD patients present UVC signatures that appear to be dependent upon the DNA repair status of the cell.

Although several of the well-characterised UV-induced transcription factors (such as *TP53*, *NF-κB* and *c-Fos*) were not induced, microarray analysis revealed that UV significantly affected the regulation of several DNA-damage associated transcription factors. For example, members of the AP-1 family of transcription factors (such as the Jun, Maf and ATF subfamilies) were differentially regulated. Among the transcription factors identified in this study, ATF3, a member of the ATF/CREB family of transcription factors, was found differentially regulated at both the mRNA and protein levels. Notably, although *ATF3* was upregulated in a UV-dependent manner in telomerised MRC-5, XP-C and CS-A cells, the kinetics

of induction differed considerably among the cell lines. A rapid induction of *ATF3* occurred in MRC-5 cells, while a sustained upregulation was observed in XP-C and CS-A cells. In agreement with these data, numerous studies have reported the induction of *ATF3* in response to UV-A (Abe *et al.*, 2003; Andley *et al.*, 2004), UV-B (Yang *et al.*, 2006) and UV-C (da Costa *et al.*, 2005; Gentile *et al.*, 2003; Rieger & Chu, 2004). Although the precise function of ATF3 remains unclear, several lines of evidence have suggested that ATF3 plays a role in the negative regulation of cell cycle progression, wound healing, cell adhesion, apoptosis and cell signalling (Fan *et al.*, 2002; Chen *et al.*, 1996; Hai & Hartman, 2001; Mashima *et al.*, 2001; Wolfgang *et al.*, 2000). Recently, Yan *et al.* (2005) suggested that ATF3 interacts with p53 in response to a broad spectrum of genotoxic stresses, and augments the stabilisation of p53 by preventing its ubiquitylation and subsequent MDM2-mediated degradation. Recently, Hamdi *et al.* (2005) identified ATF3 as an important sensor of persistent DNA damage in the transcribed strand of active genes. They found that ATF3 was selectively activated in total NER defective (XP-A and XP-D) cells after irradiation with 3 or 5 J/m^2 of UV-C, while ATF3 was activated in TCR-deficient CS cells following doses of 5 to 10 J/m^2 of UV-C. Interestingly, the TCR-deficient (CS-A) cell line used in this study, namely CS3BE, was also investigated in their study, and induction of ATF3 was also observed following 10 J/m^2 of UV. They also reported that ATF3 induction was only observed in NER-proficient and GGR-deficient (XP-C; XP8CA) cells after a high dose of 20 J/m^2 of UV-C. In contrast, the data presented here showed that ATF3 activation occurred in NER-proficient MRC-5 and GGR-defective XP-C (XP8CA) cells after 10 J/m^2 of UV-C at both the mRNA and protein levels.

Other transcription factors revealed by microarray analysis to be differentially regulated in MRC-5, XP-C and CS-A cells included *XBP-1*, *HRY* and *TAFII30*. Several sequence-specific transcription factor families were also identified. The ID-family of transcriptional repressors are dominant negative inhibitors of helix-loop-helix transcription factors that negatively regulate cell cycle inhibitory effects by repressing transcription of p16^{INK4A} (*Id1*) and overriding pRb (*Id2*). Both *Id1* and *Id2* were upregulated in XP-C and CS-A cells. Similarly, *Id4*, a

regulator of RNA Pol II transcription was found upregulated in XP-C and CS-A cells.

In agreement with previous findings (Gentile *et al.*, 2003; Li *et al.*, 2001; Yang *et al.*, 2006), the microarray data presented here showed that the actual level of *TP53* mRNA was not significantly altered in a UV-dependent manner in telomerised MRC-5, XP-C or CS-A cells during the course of the experiment, and remained at basal levels. These findings can be explained by data obtained by other investigators (Bean & Stark, 2001; Prives, 1998; Shieh *et al.*, 1997; Webley *et al.*, 2000) and data presented earlier in this thesis (Chapter 4). These suggest the UV-dependent modulation of p53 occurs through translational and post-translational protein modifications rather than a direct effect on *TP53* transcript levels. For example, in this thesis (Chapter 4), it was shown that p53 stabilisation was mediated via phosphorylation at Ser15, which occurred in an UVC- and time-dependent manner. Although an extensive investigation into the UVC-mediated translational modification of p53 was beyond the scope of this study, the importance of such modifications were clearly evident. A subset of UV-induced p53 regulated downstream target genes, which orchestrate the immediate DNA-damage signalling cascades and cellular responses (such as cell cycle arrest, DNA repair and apoptosis), were identified as differentially regulated genes in this study (such as *CDKN1A*, *GADD45α*, *DDB2*, *PMAIP*1 and *DTR*). Accordingly, the array data clearly demonstrated the importance of selecting telomerised cell lines as appropriate *in vitro* models when investigating the DNA-damage response at the transcriptome level, as the transcriptional activation of these downstream p53 targets is dependent on intact p53 function and its posttranslational modification. In agreement, Cleaver *et al.* (in press) suggested that the use of SV40-transformed XP or CS cells may conceal important differences associated with these syndromes. Altogether the data demonstrated that, although the temporal kinetics of gene expression differed significantly between the normal (MRC-5), GGR-defective (XP-C) and TCR-defective (CS-A) cell lines, expression of p53-responsive genes (such as *CDKN1A*, *GADD45α* and *PMAIP1*) was observed in the TCR- and transcription-defective CS-A cell line. In concordance with the CS-A data obtained in this

thesis, Proietti-De-Santis *et al.* (2006) showed that CSB was not required for the transcription of p53-responsive genes (such as *GADD45* and *MDM2*) following genotoxic attack.

CDKN1A, the gene that encodes the CDK inhibitor $p21^{WAF1/CIP1}$, was upregulated at both mRNA and protein levels, with the highest levels observed in CS-A cells after UV. It has been shown that following a transient p53-dependent increase the degradation of $p21^{WAF1/CIP1}$ is required to facilitate NER (Bendjennat *et al.*, 2003). However, in conflict with Bendjennat *et al.* (2003), degradation of $p21^{WAF1/CIP1}$ was not observed at the mRNA or protein levels in this study. In concordance with the data here, Cleaver *et al.* (in press) also showed a marked increase in $p21^{WAF1/CIP1}$ protein levels in CS cells after UV. Cleaver *et al.* (in press) also showed that the half-life of $p21^{WAF1/CIP1}$ following UV was 1.5 hours in normal cells compared to 3 hours in CS-B cells, thus indicating a slower rate of degradation. From these data, they speculated that the lack of correlation between the severity of CS phenotypes and the biochemical and genetic defects is attributed to the dysregulation of downstream targets of CS-dependent regulation, independent of the TCR defect. They further suggested that the accumulation of $p21^{WAF1/CIP1}$ occurred due to insufficient ubiquitylation by CS-dependent E3 ligase activity. The abnormal accumulation of $p21^{WAF1/CIP1}$ in CS cells, resulting from dysregulation in protein processing, may have significant consequence for the CS phenotype, as increases in $p21^{WAF/CIP1}$ may not only explain the growth defects displayed by CS patients, but also the absence of malignancy, which is a primary hallmark of XP.

GADD45α, a p53- and BRCA1-regulated stress-inducible gene, has been characterised as an instrumental player in orchestrating the cellular response to a multiplicity of DNA damage agents (reviewed by Zhan, 2005). Here, the data showed that, although the induction of *GADD45α* was observed in NER-proficient MRC-5, GGR-deficient XP-C and TCR-deficient CS-A cell lines, there was a marked variation in the kinetics of induction over the time course between the cell lines. In disagreement with these data, Chang *et al.* (2003) found that *GADD45α* was significantly upregulated within 30 minutes after

UVC-irradiation in SV40-transformed *XPC* (XP4PA) mutant cells, but was not upregulated in NER-proficient HeLa cells. The data presented in this thesis also showed that the highest level of induction was observed in the CS-A cell line. In conflict with these data, Chang *et al.* (2003) showed that *GADD45α* was induced in NER mutant XP-A and XP-D cells; however a similar induction in CS-B TCR-deficient cells was not observed. This led Chang *et al.* (2003) to speculate that GADD45α up-regulation is dependent on a GGR defect and may even facilitate the restoration of NER, thus providing a compensatory mechanism for the defect in GGR.

PPM1D (or *Wip1*), the gene that encodes a member of the serine/threonine specific protein phosphatase type 2C (PP2C) family, was found upregulated in MRC-5, XP-C and CS-A cells. Although *PPM1D* is a known downstream target of p53 (Takekawa *et al.*, 2000), the precise role of PPM1D in response to UV-induced damage remains unclear. It has been suggested that PPM1D participates in a negative feedback regulatory loop of p38 MAPK-p53 signalling in response to UV, by suppressing the ATM/ATR-mediated DNA damage response, via dephosphorylation of p53 at Ser15 and Chk1 at Ser 345 (Lu *et al.*, 2005; Takekawa *et al.*, 2000). From these findings it has been speculated that PPM1D functions as a 'master switch' for the removal of the DNA-damage response (Lu *et al.*, 2005). Additionally, the overexpression of *PPM1D* has been implicated in tumorigenesis. Notably, *PPM1D* mRNA was overexpressed in telomerised XP-C cells following UV exposure. PPM1D is also thought to suppress the BER enzyme, uracil DNA glycosylase (or UNG2) through dephosphorylation of threonine 6. This suggested a homeostatic regulatory mechanism for DNA repair and demonstrates a further direct link between p53 signalling and DNA repair (Lu *et al.*, 2004). However, a direct link between PPM1D and NER repair remains unreported.

As previously discussed (Chapter 1), chromatin remodelling is required to facilitate access of DNA repair factors to damaged regions of DNA. Notably, microarray analysis revealed the upregulation of histones *HIST1H1C*, *HIST1H2BE*, *HIST2H2AA*, *HIST1H2BK* and *HIST2H2BE* in DNA repair

defective XP-C and CS-A cells. These histones are involved in chromatin assembly and disassembly.

Although several genes directly associated with DNA repair were differentially expressed following UVC-irradiation, few genes directly associated with NER were found differentially regulated in a UV-dependent manner. These findings were consistent with several previous studies (Reiger & Chu, 2004; Gentile *et al.*, 2003), which showed that the core components of the NER apparatus (such as *XPA*, *XPB*, *XPD*, *XPF*, *XPG*, *CSA* and *CSB*) are not differentially regulated at the mRNA level following UV. It has been speculated that the repair proteins directly involved in NER are not regulated transcriptionally, but are present in sufficient amounts under 'normal' physiological conditions and are functionally activated through posttranslational modification or translocation to the site of damage. In conflict with the data presented here and elsewhere, da Costa *et al.* (2005) reported the UV-induced upregulation of *XPG*.

In agreement with previous studies (Hwang *et al.*, 1999; Adimoolam & Ford, 2002), the GGR-specific genes, *DDB2* and *XPC*, were identified as UV-inducible. Although a multiplicity of microarray studies have been undertaken, few have reported *DDB2* and *XPC* as being UV-inducible (Enk *et al.*, 2006; Gentile *et al.*, 2003; Koch-Paiz *et al.*, 2004; Rieger & Chu, 2004). This may be explained by the fact that many investigators have used SV40-transformed cell lines that are compromised in the p53/p21$^{WAF1/CIP1}$ pathway, as both *XPC* and *DDB2* expression is regulated in a UV- and p53-dependent manner (Adimoolam & Ford, 2002; Hwang *et al.*, 1999). Data presented elsewhere in this thesis (Chapter 3; Ridley *et al.*, 2005), also showed that the basal level of XPC protein can vary among cell lines due to its inducible nature (Adimoolam & Ford, 2002). Notably, although only a slight induction of *DDB2* was observed in normal MRC-5 and TCR-defective CS-A cells, a marked upregulation of *DDB2* occurred in GGR-defective XP-C cells. It is possible that in the absence of XPC, *DDB2* is dramatically upregulated to compensate for the GGR defect in the XP-C cell line. Alternatively, it has been speculated that for XPC modification to occur, the ubiquitylation and subsequent degradation of DDB2 is required (Ford, 2005). This suggests a possible negative regulatory role of XPC on *DDB2*

expression. The data presented here supports this function, as *DDB2* mRNA appears to accumulate in the absence of XPC. *PCNA*, the gene that encodes a homotrimeric protein that is involved in repair synthesis following the core NER reaction, was found upregulated in MRC-5, XP-C and CS-A cells following UV.

The TCR-specific genes, *CSA* (*CKN1*) and *CSB*, were not induced by UV. In disagreement with these data, Rieger & Chu (2004) showed that although *CSA* and *CSB* were not within the top 200 responsive genes, CSA was repressed 1.5-fold and CSB was induced 2.3-fold. From these findings, Reiger & Chu (2004) speculated that CSB might play a role in processing UV damage after the completion of TCR.

The signalling cascades regulating cell proliferation and apoptosis appeared complex. Among the UV-responsive genes that regulates cell proliferation, included *TOB1*, a member of the tob/btg1 family of anti-proliferative proteins. Interestingly, *TOB1* was rapidly induced in MRC-5 and XP-C cells, which was followed by rapid repression. In contrast, CS-A displayed a temporal pattern of delayed expression. Moreover, unlike MRC-5 and XP-C, *TOB1* induction continued to increase throughout the time course and failed to return to pre-irradiation mRNA levels. This suggested that the CS-A cells failed to recover from the DNA damage induced by UV and where maintained in an anti-proliferative state. Notably, both anti- and pro-apoptotic genes were highly expressed. For example, the anti-apoptotic gene *IER3* (immediate early response 3) gene that functions to protect cells from Fas- or TNF∝-induced apoptosis was upregulated in CS-A cells. In contrast, several proapoptotic-associated genes were also found upregulated in CS-A cells. For example, the p53 downstream target, *PMAIP1* (*NOXA*), was found upregulated in MRC-5, XP-C and CS-A cells. Interestingly, both higher levels of *PMAIP1* mRNA and PMAIP1 protein were observed in CS-A cells. In concordance with other studies (Gentile *et al.*, 2003), these data indicate that UV-induced DNA damage elicits apoptosis via PMAIP1. The p53-regulated pro-apoptotic gene, *FDXR*, which encodes a mitochondrial flavoprotein, was found upregulated in XP-C and CS-A cells in response to UV. Similarly, DTR, a heparin-binding growth factor was induced in CS-A and XP-C cells in response to UV and is involved in the pro-apoptotic

response. SAT, a rate-limiting enzyme is involved in the catabolic pathway of polyamine metabolism. Polyamines are involved in either inducing or repressing apoptosis in a genotype-specific manner. Interestingly, *SAT* was found upregulated in CS-A cells in a UV-dependent manner. *PPP1R15A* (protein phosphatase 1, regulatory (inhibitor) subunit 15A) is a member of a group of genes whose transcript levels are known to increase following treatment with DNA-damaging agents. *PPP1R15A* was upregulated in CS-A cells following UV exposure. As expected, the anti-apoptotic gene, *BCL2L1*, which regulates outer mitochondrial membrane channel opening, release of ROS and cytochrome C was repressed in CS-A cells following UV, while an upregulation was observed in MRC-5 cells. Additionally, the pro-apoptotic *MOAP1* (modulator of apoptosis 1) was induced in CS-A cells in response to UV. Surprisingly, the pro-apoptotic BID (BH3 interaction domain) gene that triggers cytochrome c release via caspase 8 (CASP8) was repressed in CS-A cells after UV exposure. Similarly, several capsases (such as *CASP1*, *CSAP4*, *CASP6*, *CASP8*) were also repressed in CS-A cells, whereas *CASP3* was induced in CS-A cells after UV exposure. Interestingly, McKay *et al.* (2004) showed that the expression of large anti-apoptotic genes was suppressed following UV, whereas the expression of small pro-apoptotic genes (such as *PMAIP1* and *FDXR*) was induced. McKay *et al.* (2004) speculated that gene size is an important determinant of UV-induced gene expression, as UV-induced genes enriched for compact genes with fewer and small introns, such as those involved in the mitochondrial apoptotic cascade were found upregulated. From the data, McKay *et al.* (2004) have suggested that UV-responsive genes, caused by passive effects of UV lesions on transcription act as a molecular dosimeter, ensuring the removal of cells sustaining irreparable transcription-blocking DNA damage.

Although the experimental design and statistical approaches adopted in this investigation were comparatively comprehensive compared to previous studies, it is important to note the caveats associated with the present study. As previously reported, transcriptional responses can differ considerably in different cell types, and in response to different wavelengths (and/or doses) and at different time points. The selection of cell type is of particular importance when undertaking transcription expression profiling studies, as cells such as keratinocytes are

habitually exposed to UV radiation, and are therefore more resistant to UV compared to fibroblasts due to the development of specialised cell-type-specific responses (Otto *et al.*, 1999). In this study, many of these issues were addressed by characterising the transcriptional portraits of telomerised XP-C and CS-A fibroblasts in three independent biological replicates at several time points over a 24 hour time course. Although NER-proficient telomerised MRC-5 fibroblasts were used as a control for comparative analysis with the telomerised GGR-defective XP-C and TCR-defective CS-A cell lines, the control cell line used during this investigation was derived from foetal lung. Hierarchical clustering of the microarray data highlighted this major caveat of using telomerised MRC-5 fibroblasts as a control cell line. The pattern of high or low transcript levels observed here, suggested that regulation occurred in a UV-independent manner, as the level of expression observed at ~6, ~12 and ~24 hours was similar to that observed immediately (0 hours) following UV. Moreover, the differential expression observed in cluster 1 was also independent of time (Fig. 5.4). Therefore, it is possible that the transcriptional responses observed in the wild-type MRC-5 fibroblasts compared to the DNA repair defective XP-C and CS-A dermal fibroblasts, was attributed to cell-type-specific variability, rather than the state of the NER repair pathway. In retrospect, a telomerised wild-type dermal fibroblast cell line would have provided a more statistically robust *in vitro* model for comparative analysis with the telomerised XP-C and CS-A dermal fibroblast cell lines.

The transcription expression profiles of telomerised XP-C and CS-A cells appeared similar in clusters 1 and 4 of the genotype-specific changes compared to the MRC-5 cells (Fig 5.4). Notably, genotype-specific signatures were also observed between telomerised XP-C and CS-A cell lines. Moreover, the marked level of low and high expression observed in the CS-A cells (cluster 2 & 3, respectively; Fig. 5.4), compared to XP-C appeared independent of UV. However, it was difficult to substantiate whether these transcriptional signatures were attributed to the XP and CS phenotypes, or merely due to variations between the dermal fibroblasts, as a single telomerised XP-C and CS-A clone was used for analysis. Furthermore, a single XP-C (GM02996, XP8CA) and CS-A (GM01856, CS3BE) donor was used. To eliminate this variation from the

present study, further investigation would require the establishment of several telomerised XP-C and CS-A cell lines derived from donors that exhibit an *XPC* or *CSA* null phenotype, respectively. Alternatively, the establishment of a *XPC* or *CSA* null phenotype could have been achieved experimentally, by knocking out *XPC* or *CSA* in a NER-proficient telomerised cell line that was used as a wild-type control. This would facilitate the establishment of NER-proficient and deficient cell lines, whose phenotype would be isogenic and any differences would be exclusively attributed to the different NER status. However, homologous recombination technology was beyond the scope of this investigation. Alternatively, to minimise differences in genetic backgrounds, investigators have used isogenic cell lines transfected with a mammalian vector expressing the wild type gene. For example, Kyang *et al.* (2003) used CS-B SV40-transformed fibroblasts transfected with a plasmid expressing the *CSB* wt gene, thus resulting in the generation of an isogenic TCR-proficient control. However, it is possible that the corrected cell line remained compromised, irrespective of the restoration of its CSB function, and it is difficult to substantiate whether the plasmid is expressing physiologically relevant levels of CSB protein. Furthermore, although the exploitation of RNAi technologies has resulted in the establishment of XPA^{KD}, XPC^{KD} and CSB^{KD} phenotypes in NER-proficient cell lines (Biard *et al.*, 2005; Feng *et al.*, 2006), data presented in this thesis (Chapter 6), suggested that phenotypes generated by RNAi are complex and can result in a partial biological effect. This results in the generation of a cell line that does not fully recapitulate the desired null phenotype.

Transcriptional portraits obtained in this study were obtained for a single cell type derived from a single donor for each genetic background following a single UV dose. As previously mentioned, the data presented here clearly demonstrated cell-type- and genotype-specific signatures between the MRC-5, XP-C and CS-A fibroblasts that were both independent and dependent of UV-irradiation. Moreover, although many of the differentially regulated genes and patterns of expression that were identified in this study were observed in both the NER-proficient, GGR-deficient and TCR-deficient cells, the kinetics of differential regulation differed between cell types. For example, the response of many of the genes identified in the CS-A cell line exhibited delayed kinetics of transcript

induction. However, the transcriptional responses in the current study were limited to a 24 hour time course. Therefore, to further delineate the kinetics of differential transcript regulation in the cell lines, further investigation would necessitate the inclusion of longer time points.

In addition to inter-individual variability, an unavoidable caveat encountered during this investigation was possible clonal variation among isogenic monoclonal cell populations, as a single XP-C (clone 19) and CS-A (clone 3) clone was used throughout this investigation. Additionally, the selection of an appropriate wavelength when undertaking transcriptome analysis in response to UV is particularly controversial. Although the vast majority of studies have used UV-C, it has been suggested that these studies lack physiological relevance (Sesto *et al.*, 2004), as UV-C is absorbed by atmospheric ozone (Kock-Paiz *et al.*, 2004). Therefore, many investigators believe that the transcriptional response to UV-C does not recapitulate the response following exposure to biologically pertinent wavelengths such as UV-A or UV-B. However, my study was exclusively interested in the molecular phenotypes exhibited by NER defective cells in response to the UV-induced photolesions, CPDs and 6-4PPs. For this reason, the use of alternative UV wavelengths was deemed inappropriate, as both UV-A and UV-B introduce further variability into the *in vitro* model. For example, both UV wavelengths target cellular constituents other than DNA such as proteins and lipids, and a diverse range of lesions are introduced into DNA, which elicits the activation of additional DNA repair systems such as BER.

In this thesis, cells were immediately refed with fresh medium after UV treatment. It has been reported that fibroblasts present patterns of differential gene expression in response to serum (Iyer *et al.*, 1999). Therefore, investigators have either used serum-starved cultures, or reused culture medium in order to minimise these responses. It is possible that responses observed during this investigation were attributed serum. However, RT-PCR and Western blotting (which included time-matched non-irradiated controls) showed no evidence of a serum response. Furthermore, the most appropriate culture conditions remain controversial, as serum starvation can elicit stress signalling pathways.

Although the issue of statistical validity was addressed in the present study by undertaking several independent biological replicates at each time point, the issue of inter individual variability was, as previously stated a further caveat in this investigation. To eliminate inter clonal variability; the analysis of several independently isolated telomerised XP-C and CS-A clones would have been required. To address all the experimental caveats identified in this study, further investigation would have required a much larger number of HG-U133A arrays, which was financially beyond the scope of the current study. Despite this issue, the transcriptional portraits obtained for telomerised XP-C and CS-A, for the first time, provides detailed information on the molecular signatures of cells defective in the GGR and TCR subpathways of NER, without the possibility of compromised DNA-damage signalling pathways.

Genes associated with the removal of oxidative damage were upregulated in telomerised CS-A fibroblasts. For example, the antioxidant enzymes *GPX1*, *GPX7* (glutathione peroxidase 1 and 7) and *HO-1* (heme oxygenase 1) were induced; *HO-1* induction is known to occur in most oxidative stressed mammalian cells (Keyse & Tyrrel, 1987). da Costa *et al.* (2005) also reported an increase in *HO-1* expression, with higher levels observed in TTD cells compared to XP/CS. They speculated that the high level of *HO-1* in TTD cells is an indicator of cellular stress during proliferation. *SOD2*, the gene that encodes superoxide dismutase 2, was also induced in telomerised CS-A cells. COLEC12, a scavenger receptor, was highly induced in CS-A cells, whereas it was repressed in MRC-5 and XP-C cells. COLEC12 plays a role in recognising oxidised phospholipids and removes oxidatively damaged or apoptotic cells. *FTH1*, an essential mediator of the antioxidant and protective activities of NFκB was also upregulated in CS-A cells. The upregulation of ferratin by FTH1 inhibits TNFα-induced apoptosis via NFκB, by suppressing ROS. The induction of this subset of genes that protect the cell from oxidative damage is particularly interesting, as the growth and neurological defects in CS have been attributed to the accumulation of oxidative-induced damage generated endogenously by cellular metabolism.

The generation of ROS can occur as a result of high $p21^{WAF1/CIP1}$ levels, which is thought to occur through its interaction with mitochondrial apoptosis activating factors (Macip *et al.*, 2002). As previously mentioned, a high level of $p21^{WAF1/CIP1}$ was observed in telomerised CS-A cells. Cleaver *et al.* (in press) recently showed that under normal *in vitro* growth conditions (high level of oxygenation), a greater level of DNA damage was detected using the double strand break marker γH2AX, and was observed in both CS-A and CS-B cells compared to XP-A and XP-C cells. They speculated that since XP-C cells are defective in GGR and XP-A cells are devoid of both GGR and TCR, the increased level of spontaneous DNA damage in CS cells was attributed to more than simply the repair defect. Cleaver *et al.* (in press) suggested that the increase level of $p21^{WAF1/CIP1}$ in CS-B might be a cause of increased level of ROS generation, resulting in further *in vivo* change such as apoptosis in neuronal cells.

To examine the validity of the microarray data, quantitative RT-PCR was performed. RT-PCR validation of all the UV-responsive genes was beyond the scope of this investigation; so several differentially regulated genes that represented a diverse range of biologically functional groups (such as transcription, cell cycle regulation, growth, DNA repair, apoptosis and metabolism) were assayed. The data suggested that the mRNA levels detected by microarrays generally reflected those obtained by RT-PCR. Notably, however, the inclusion of time-matched, non-irradiated controls in the RT-PCR assays reiterated the limitations associated with the interpretation of large datasets derived from treated samples in the absence of time-matched, non-irradiated controls. For example, the level *of DDB2* in CS-A cells was similar at 0, ~6 and ~12 hours in both UV-irradiated and non-irradiated samples. Similarly, the level of *PPM1D* mRNA in irradiated CS-A cells was similar to untreated CS-A fibroblasts at 0 and ~12 hours, while a marked increase in *PPM1D* was observed at ~6 hours in the non-irradiated control, compared to its time-matched irradiated counterpart. Notably, although the genes validated in this study represented a diverse range of functional groups, all transcripts (except *Ccng2*) were found in cluster 2 of the time-dependent changes.

Although microarray technologies facilitate the measurement of changes in mRNA level across the entire transcriptome, it is modulation of protein expression, function or location that ultimately mediates changes in biological function. For this reason, validation of microarray data was performed at the protein level by Western blotting. The data suggested that, changes at the protein level recapitulate the changes observed at the mRNA level. For example, the accumulation of $p21^{WAF1/CIP1}$ protein observed in telomerised MRC-5, XP-C and CS-A reflected the kinetics of *CDKN1A* induction following UVC-irradiation. Additionally, the upregulation of ATF3 and PMAIP1 protein corresponded to the induction of *AFT3* and *PMAIP1* at the transcript level. Although Western blot analysis revealed fluctuations in GADD45α protein levels, compared to the levels of *GADD45α* mRNA, a similar pattern of upregulation was observed following UV. In contrast, the level of FDXR protein displayed marked differences compared to the *FDXR* mRNA levels. Although the majority of differentially regulated genes that were analysed at the protein level were concordant with the mRNA levels, these data suggested that significant caution should be applied when extrapolating biological function based on the modulation of transcriptional responses.

There has been significant debate over whether the intricate clinical phenotype presented by CS patients occurs as a result of the primary defect in DNA repair or transcription, as CS cells fail to resume basal transcription following UV-irradiation (Balajee *et al.*, 1997; Van den Boom *et al.*, 2004). This has remained controversial, as the CS defect in the TCR of photolesions fails to explain the growth and neurological manifestations displayed by CS. In addition to the DNA repair and transcription defect, emerging evidence has implicated that defects in protein processing contribute to the complex phenotype observed in CS (Cleaver et al., in press). The data presented here suggested that the temporal kinetics of transcription modulation, in response to genotoxic stress such as UV, could contribute significantly to the pathogenesis of syndromes defective in NER such as XP and CS. This was particularly evident in CS-A, where the UVC-induced signatures differed considerably compared to the MRC-5 and XP-C cell lines. The CS-A cell line displayed kinetics of (1) delayed induction or repression over

the time course, (2) a failure to return to pre-damage mRNA levels within the time course, (3) a sustained transcriptional response throughout the time course. In concordance with these data, Kyang *et al.* (2003) showed that the overall induction of expression following oxidative stress was impaired in CS-B cells. Moreover, da Costa *et al.* (2005) showed that the transcriptional response to UV was delayed in XPB/CS cells. Therefore, the data presented here provides further evidence supporting the idea that the phenotype presented by CS is in part attributed to a dysregulation of the transcriptional response to genotoxic stress. Recently, Newman *et al.* (2006) provided evidence that CS may be an inflammatory disease, as they found that; (1) a large number of inflammatory pathways were upregulated such as the TGFβ and TNFα/JNK pathways, (2) transcription factor binding site (TFBS) analysis in the promoters of CSB-regulated genes were enriched for NF-κB-related sites, (3) CSB upregulates many genes that are also upregulated by anti-inflammatory drugs, (4) the hypoxia-response is upregulated in the absence of *CSB*. Newman *et al.* (2006) concluded that the inflammatory phenotype displayed by CS might explain the neurodegenerative and wasting symptoms presented by the syndrome. In concordance with Newman *et al.* (2006), several proinflammatory members of the TNFα pathway (such as *TNFAIP2* and *TNFSF9*) were upregulated in CS-A cells in my study. The TNFα pathway is also known to initiate the apoptotic pathway.

Annotation of the resultant lists of differentially regulated genes was undertaken using the frequently adopted approach of trying to manually link single gene transcripts to yield some form of biological significance. However, the requirement to correct for multiple correction and select a significance level during statistical analysis can prove problematic, as other genes in a differentially activated functional pathway may fall outside this cut off, and hence an interesting line of interpretation and explanation may be missed. To overcome these challenges, several methods have been established to enable a more comprehensive and less biased functional interpretation of gene lists.

Hosack *et al.* (2003) developed the Expression Analysis Systematic Explorer (EASE), which can assist in identifying biological themes in a gene list by looking for over-representation of a biological theme within the list under test when compared with the global background. The hypothesis for an analysis takes the form of "are there more genes involved in apoptosis within my list than I would expect by chance if I was to randomly sample an equivalent sized gene list from my array?" EASE can look for over-represented "terms" against a number of annotation resources including Gene Ontology and the public pathway databases (GenMapp, KEGG).

Breitling *et al.* (2004) developed a method termed Iterative Group Analysis (iGA). iGA extends the functional annotation analysis beyond just the probe sets contained within a significant gene list to the whole dataset. The method interrogates the results of statistical testing for changes in transcription levels for all the genes identified as belonging to a functional class (e.g. apoptosis), which can be derived from many different origins (Gene Ontology, BLAST results, key words, literature extracts). As a result, iGA can detect changes in transcription level which may be missed by selecting genes at a pre-defined cut-off, so if all or many genes within a pathway show moderate changes in transcription this can be identified and flagged as significant.

Building on the idea of looking at the full dataset rather than a subset, Gene Set Enrichment Analysis (GSEA) (Subramanian *et al.*, 2005) is a knowledge-based approach for interpreting genome-wide expression profiles that evaluate microarrays at the level of gene sets rather than a single transcript approach. GSEA can help identify functional linkage between groups of genes that share common biological functions, chromosomal location, or regulation and will weight its results according to the predefined significance level (from statistical testing) for the members of a functional class. This method has been successfully implemented to identify a p53-like, cisplatin-induced transcriptional response in mouse embryonic stem cells (Kruse *et al.*, in press).

Recent advances in bioinformatics methods for the analysis of sequences regulating transcription have identified potential factors involved in key

regulatory networks underlying a transcriptional response (Ho Sui *et al.*, 2005). Ho Sui *et al.* (2005) have developed a novel method, oPOSSUM, which allows for the analysis of statistically over-represented TFBSs in the promoters of sets of co-expressed genes. oPOSSUM is based on the assumption that some subset of the co-expressed genes is co-regulated by one or more common TFs, therefore the observed number of binding sites for those TFs should be greater than would be expected by chance. Newman *et al.* (2006) applied oPOSSUM to their dataset generated from CS-B cells and found that NF-κB TFBSs were significantly over-represented in differentially regulated genes identified in CSB null cells. Similarly, oPOSSUM may assist in the identification of site over-representation in genes differentially expressed in XP-C and CS-A cells, and may assist in unravelling potential defects in transcriptional regulation of gene expression that may contribute to the pathophysiological manifestations observed in XP and CS patients.

Alternatively, systems biology and pathway analysis applications have become commercially available, which are designed to assist in the functional annotation of microarray data and extend the annotation corpus available by interrogating manually curated databases of human protein-protein and protein-DNA interactions, transcription factors, signalling or metabolic pathways. Examples of such tools include packages such as Metacore (GeneGo, Inc.), Ingenuity Pathway Analysis 5.0 (IPA; Ingenuity® systems) or Explain (BioBase).

These packages also claim to provide intuitive tools for data visualisation, analysis and exchange along with the functionality to concurrently visualise multiple types of experimental data including gene expression, proteomic, metabolic, genetic and screening data. The interpretation of data across multiple platforms would be particularly useful for future investigation at the global proteome level in the different NER-defective backgrounds investigated in this study (Chapter 7).

The application of these annotation analysis methods to the Affymetrix™ data generated as part of this study may have assisting in the identification and

prioritisation of functional classes that are important to the molecular pathogenesis of XP and/or CS.

In summary, a transcriptome-wide approach was adopted to dissect the molecular pathways involved in the UV-induced DNA-damage-response and to identify potential genes that are involved in molecular pathogenesis of XP and CS. The UV-induced transcription expression profiles obtained for MRC-5 and XP-C was highly diverse, while CS-A cells displayed a UV signature that appeared to be of an oxidative-damage-induced, proinflammatory and proapoptotic nature. Many of the genes identified in this study represent pathways (such as transcription, cell cycle regulation, DNA repair and apoptosis) that have been well characterised, as part of the normal UV-induced transcriptional programme. However, the role of many UV-responsive genes revealed in this investigation remains poorly understood. For example, *ATF3*, *CDKN1A*, *GDF15*, *DDB2* and *FDXR* have all been implicated in oncogenesis (Yang *et al.*, 2006), yet their precise role remains unclear. The temporal regulation of gene expression in XP and CS is complex. The comprehensive characterisation of the transcription expression portraits in established telomerised XP-C and CS-A *in vitro* cell culture models may assist in unravelling how NER status can influence cell metabolism in response to damage. Additionally, these UV signatures may also facilitate the elucidation of the molecular mechanisms underlying cutaneous tumorigenesis and progeria observed in XP and CS, respectively. This is particularly important for CS, as mechanisms that lie downstream to CSA and CSB regulation (such as transcription regulation and ubiquitin ligase-mediated protein degradation) have been implicated in the molecular pathogenesis of CS. Therefore, the generation of expression profiles for CS, such as that presented here, could assist in identifying subtle differences at the molecular level that are attributed to these causative mechanisms. The data may also assist in our understanding of the early UV-radiation responses in both NER syndromes and the normal population and might facilitate the elucidation of molecular biomarkers to identify radiation susceptible individuals.

Chapter 6

Utility of RNAi in the Transient or Stable Modulation of the XPC or CSA Repair Protein

6.1 Introduction

Many technologies have been previously adopted to experimentally modulate or abolish gene expression in *in vitro* culture or in *in vivo* transgenic models, including; over expression of cDNA constructs, activation or inactivation by homologous recombination, activation by random insertion of strong promoters, creation of dominant-negative mutants, antisense oligonucleotides, engineered transcription factors and minor groove binders (reviewed by Case, 2003). More recently, however, functional genomic research has been revolutionised by the advent of RNA interference (RNAi) technologies. RNAi has facilitated the rapid and stable manipulation of gene expression in a cell-type- or pathway-specific manner with increased efficacy.

RNAi is utilised by eukaryotic organisms to modify gene expression at the pre- and post-transcriptional level. In lower eukaryotes (such as nematodes) and plants, the RNAi machinery has evolved to facilitate transposon silencing, viral processing and maintenance of chromosome integrity, thereby maintaining genome stability (Williams, 1997). RNAi is characterised by a series of cellular mechanisms that co-ordinate the silencing of specific genes, via the expression of small double-stranded RNAs (dsRNAs). RNAi was first described by Fire *et al.* (1998), who showed that injecting dsRNAs could elicit RNAi-mediated gene silencing in *C. elagans*. This resulted in the suppression of genes whose mRNA transcripts were complementary to the dsRNAs.

It was initially believed that analogous RNAi gene silencing mechanisms were not utilised by mammalian cells. Moreover, initial attempts to exploit RNAi technology as an experimental application in genetic manipulation studies, proved problematic due to the caveats associated with using long dsRNA molecules (≥50 bp). The delivery of exogenous dsRNA (≥50 bp) evokes a series of complex cellular responses to the foreign dsRNA molecules, which is part of the cell's antiviral mechanism (Williams *et al.*, 1997). Moreover, long dsRNAs cause the abolition of translation, mRNA degradation and interferon secretion (Stark *et al.*, 1998; reviewed by Sen, 2001; Bridge *et al.*, 2003; Sledze *et al.*, 2003). The initiation of the interferon (IFN) response is particularly problematic due to the activation of the interferon-induced dsRNA-dependent protein kinase (PKR), which occurs following its interaction with dsRNA and subsequent sequence-independent destruction of RNAs. This results in the abolition of protein synthesis (Williams, 1997).

It was previously shown that long dsRNA molecules could silence gene expression during early mouse development (Svoboda *et al.*, 2000; Wianny & Zernicka-Goetz, 2000). This led to the finding that transfection of short 21mer dsRNA duplexes, mediate gene-specific silencing in cultured mammalian cells, without inducing the IFN pathway (Elbashir *et al.*, 2001). Since these findings, the RNAi mechanism has been identified in several eukaryotic organisms (Hannon, 2002).

The delivery of targeted siRNA duplexes in *in vitro* mammalian cell culture models is accomplished via two principal modes. Firstly, transient post-transcriptional gene silencing is achieved through the transfection of short (~19-mer nucleotide) dsRNA targeted siRNA duplexes with symmetric 2-3 nt 3' overhangs and 5'-phosphate and 3' hydroxyl groups, which contain one strand complementary to the target mRNA. The delivery of siRNA duplexes in mammalian cells is achieved using lipid-based transfection reagents. Although siRNA-transfected methodologies facilitate immediate and efficient gene silencing, the applicability of this technology is limited due to its transient nature. Conversely, stable and permanent post-transcriptional gene silencing is

achieved through the retroviral infection of target cells with siRNA-based plasmid-borne virus systems (retrovirus, lentivirus, or adenovirus), encoding a short hairpin (sh) RNA stem-loop structure, driven by a polymerase III promoter. Two principle types of retroviral vectors have been adopted as vehicles for the delivery of shRNA into mammalian cells. These include the oncoretrovirus vectors based on the murine stem cell virus (MSCV) or the Moloney murine leukaemia virus (MoMuLV; Brummelkamp *et al.*, 2002; Paddison *et al.*, 2002) and lentivirus vectors derived from human immunodeficiency virus-1 (HIV-1; Stewart *et al.*, 2003; Rubinson *et al.*, 2003; Qin *et al.*, 2003). The shRNA is subsequently processed into a 21mer siRNA duplex by the enzymatic activity of Dicer. Although shRNA methodologies rely upon *de novo* siRNA synthesis within the cell, the integration of a selectable marker within the retroviral construct, such as puromycin drug resistance, facilitates the stable knockdown of protein expression. This permits the establishment of permanent genetically manipulated mammalian *in vitro* cell culture models, derived from single-cell clones that confer resistance to the selectable drug marker. This facilitates the isolation, sub-cloning and screening of cells displaying high levels of knockdown, from a polyclonal cell population that displays heterogeneous levels of gene expression. Furthermore, the utilisation of retroviral-based vectors, expressing shRNAs, permits the expression of siRNA and the efficient posttranscriptional gene silencing in slow-growing and post-mitotic cells. shRNAs therefore provide an alternative and more advantageous method for the delivery of siRNAs in cells resistant to transfection. However, the applicability of plasmid-based systems as a vehicle for the delivery of siRNAs is limited in cells that can only be maintained in culture for a limited time, such as primary cultures that display a protracted proliferative capacity.

The exploitation of RNAi technology, in modulating DNA repair and tumour suppressor gene expression, has resulted in the successful elucidation of the mechanistic functioning of DNA repair enzymes and the explication of complex stress signalling/DNA damage checkpoint pathways (reviewed by Miller & Grollman, 2003). Cortez *et al.* (2001) first reported the modulation of ATR. Further reports have demonstrated the successful abrogation of the DNA glycosylase, Neil 1 (Rosenquist *et al.* 2003), in murine embryonic stem cells and

the knockdown of 53BP1 (Wang *et al.*, 2002). Semizarov *et al.* (2004) adopted a global genome approach to dissect mammalian intracellular signalling pathways, by exploiting a combination of siRNA mediated gene silencing and Affymetrix™ GeneChip® expression profiling technologies, followed by systematic pathways analysis.

The applicability of RNAi in the experimental modulation of the NER pathway was first demonstrated by Lee *et al.* (2002), who showed that the repression of the *C. elegans* CSB homologue hypersensitised *C. elegans* to UV radiation, enhanced cell proliferation arrest and apoptosis, and increased embryonic lethality. More recently, however, transient siRNA technology has been utilised to dissect the NER pathway in mammalian cells, through the modulation of genes involved in NER, such as p53 (Porter *et al.*, 2006), ATR (Wu *et al.*, 2006), Ubc9 (Wang *et al.*, 2005c), XPV (Liu & Chen, 2006), XPA (Reynolds *et al.*, 2004) and hHR23B (Glockzin *et al.*, 2003).

Interestingly, numerous studies have adopted plasmid-based expression systems to ablate NER gene function. For example, Biard *et al.* (2005) successfully established stable and permanent XPA^{KD} and XPC^{KD} phenotypes in HeLa cells, using Epstein bar virus- (EBV) based shRNA vectors, targeting the *XPA* or *XPC* gene, respectively. Moreover, Biard *et al.* (2005) reported the isolation of several clones, which displayed undetectable levels of XPA or XPC protein, whilst maintained in culture for >300 days. More recently, Feng *et al.* (2006) demonstrated the utility of RNAi technologies in the modulation of the NER repair protein, CSB, by constructing vectors expressing *CSB*-specific siRNAs. Feng *et al.* (2006) found that the siRNA-mediated silencing of *CSB* caused cells to proliferate more slowly, increase the sensitivity to genotoxicants, modify UV radiation-induced cell cycle changes and potentate radiation-induced apoptosis and anti-proliferative effect. In another study, Proietti-De-Santis *et al.* (2006) used *CSB*-targeted siRNAs to show that the transcription of p53-responsive genes does not require CSB.

To date, the utilisation of conventional methodologies such as HR to ablate gene function, has resulted in the establishment >200 different strains of mice, in which the expression of one/more DNA repair and/or DNA damage-signaling proteins have been abolished (Friedberg & Meira, 2006). Moreover, 35 of these mouse strains carry various combinations of targeted mutations in the NER repair pathway (Friedberg & Meira, 2006). This has resulted in the creation of transgenic models of rare human hereditary DNA repair syndromes, such as XP, CS, TTD and more recently XP/CS (Andressoo *et al.*, 2006). However, the establishment of transgenic models of disease, through the utility of methodologies such as HR, are technically problematic and largely time-consuming. Furthermore, the abolition of gene function may not modify the phenotype, which is indicative of redundancy within the pathway of interest. Although transgenic mouse models have permitted further investigation into areas that remain poorly delineated, such as the paradoxical absence of cancer development in TTD and CS phenotypes notwithstanding their NER deficiencies, transgenic models possess a multitude of caveats, as they may not fully recapitulate the clinical manifestations exhibited by the human disease of interest. In addition, the abrogation of certain DNA repair genes results in the generation of a phenotype that exhibits severe lethality and is not compatible with life. Furthermore, the applicability of murine models of NER syndromes such as XP, CS and TTD are particularly controversial, as rodent cells display reduced GGR due to the absence of a p53 response element that facilitates p53-dependent transactivation of the *DDB2* gene (Tan & Chu, 2002; Tang *et al.*, 2000). Many of the phenotypic characteristics observed in XP-A and CS patients such as neuopathological features and severe accelerated ageing respectively, are absent in $Xpa^{-/-}$ and $Csa^{-/-}$ mice (de Vries *et al.*, 1995; Nakane *et al.*, 1995; van der Horst *et al.*, 2002). It has been proposed that the lack of these clinical features in murine models is attributed to their protracted lifespan (~2-3 years), as these pathological processes may require more time. The absence of clinical features suggests that murine models may also differ at the cellular level.

6.2 Aims

The current availability of permanent human cell lines defective in NER are limited to characterised rare human genetic diseases, such as XP, CS and TTD, which are defective in a subset of DNA repair genes. Therefore, the aim of this chapter was to use RNAi technology for the transient knockdown of *XPC* or *CSA* gene expression in NER-proficient, hTERT-immortalised MRC-5 fibroblasts.

A CS-A (GM01856, CS3BE) fibroblast cell line was previously characterised (Chapter 3) and immortalised by the ectopic expression of hTERT (Chapter 4). The second aim of this chapter was to create a permanent and stable double XPC^{KD}/CS-A double knockdown phenotype, through the retroviral transduction of the hTERT-immortalised CS-A fibroblast cell line, with a vector co-expressing an *XPC*-specific targeted shRNA and the gene encoding puromycin resistance. From the current literature it can be speculated that the DNA damage response of a double XPC^{KD}/CS-*A* phenotype will recapitulate the DNA damage response of an *XPA* null phenotype. Interestingly, Köberle *et al.* (2006) recently supported the targeted knockdown of XPC protein, using RNAi technology.

6.3 Materials & Methods

Normal telomerised MRC-5 fibroblast (previously prepared in the laboratory and made available as a general reagent) were transfected with three individual 21mer oligonucleotide siRNA duplexes, targeting the *XPC* or *CSA* DNA repair genes. In addition, telomerised MRC-5 fibroblasts were transfected with a non-targeted scramble, which provided a control for the detection of off-target effects (Section 2.3).

The SUPER RNAi™ library, based on the pSUPER RNAi system (Brummelkamp *et al.*, 2002) and the human SUPER RNAi™ library (Berns *et al.*, 2004), provided by CRUK, was used to create a permanent and stable hTERT-immortalised double XPC^{KD}/*CS-A* knockdown phenotype (Sections

2.4.0-2.4.3). The pRETROSUPER mammalian expression vector, harbouring the 59mer shRNA expression cassette, that regulated the expression of a 21mer *XPC*-specific siRNA duplex, was isolated from the DH5α bacterial stock that was stored in a 96-well format (Section 2.4.4). The *XPC*-specific sequence was confirmed by sequencing. Two of the possible three *XPC*-specific shRNA constructs were recovered from the DH5α bacterial stock. The isolated plasmids, containing the two *XPC*-specific shRNA expression cassettes, was independently expanded and confirmed by sequencing.

For retroviral supernatant production, the isolated plasmid DNA expressing the *XPC*-specific shRNA constructs was transfected into subconfluent FLY A13 human epithelial cells, using a standard calcium phosphate transfection protocol (Section 2.4.8). As controls, retroviral supernatants were generated from plasmid DNA expressing an *XPA*-specific shRNA (previously isolated and validated in the laboratory by Rebecca Capper (technician)), or an empty pBABE-puro vector. The control transfections were performed in parallel. Retroviral supernatants were harvested 24 hours and 48 hours post feeding.

Subconfluent hTERT-immortalised CS-A fibroblasts were transduced with retroviral supernatants expressing the *XPC* (construct 1 or 2)/*XPA* shRNA constructs, the empty pBABE-puro vector or mock infected (Section 2.4.9). As an infection control, a retroviral supernatant, expressing the empty pBABE-puro vector, that was previously prepared and validated in our lab, was transduced into hTERT-immortalised CS-A fibroblasts.

The transient or permanent knockdown of XPC, CSA or XPA at the protein level was confirmed by immunoblotting. Briefly, WCEs were prepared (Sections 2.9.1-2.9.2), proteins were separated on SDS-PAGE gels (Section 2.9.3), transferred to PVDF membranes (Section 2.9.3) and exposed to an anti-XPC mouse monoclonal antibody (1:500), an anti-CSA goat polyclonal antibody (1:100) or an anti-XPA mouse monoclonal antibody (1:100; Section 2.9.4). Blots were visualised using an appropriate HRP-coupled secondary antibody and an

ECL system using Hyperfilm (Section 2.9.4). Equal protein loading was confirmed by staining the PVDF membrane with India ink (Section 2.9.5).

The establishment of a permanent XPC^{KD}/CS-A or a XPA^{KD}/CS-A double knockdown phenotype was further confirmed by the immunocytochemical detection of XPC or XPA, using the VECTRASTAIN® ABC system (Vector Laboratories, Peterborough, UK) as previously described (Section 2.10). The primary anti-XPC and anti-XPA mouse monoclonal antibodies used to verify the knockdown phenotypes by immunocytochemical analysis, were identical to those used for immunoblotting.

The global repair of CPDs and 6-4PPs was measured using a standard immuno-slot-blot assay. Briefly, subconfluent hTERT-immortalised CS-A fibroblasts, transduced with the *XPC*-specific shRNA (sequence 2) were irradiated with UVC (10 J/m^2). Dishes were maintained under routine culture conditions for an indicated period of time (hours). Genomic DNA was isolated and purified, using RNase A treatment and overnight proteinase K digestion, followed by phenol/chloroform extraction (Section 2.11.1). The immuno-slot-blot assay was undertaken using the Bio-Dot SF Microfiltration apparatus. The detection of CPDs or 6-4PPs was performed using the H3 CPD- or 6-4PP-specific monoclonal mouse antibody.

6.4 Results

6.4.1 Transient knockdown of XPC or CSA utilising XPC- and CSA-targeted 21mer siRNA duplexes

hTERT-immortalised MRC-5 fibroblasts were transfected (treatments) separately with three individual *XPC*- or *CSA*-specific 21mer oligonucleotide siRNA duplexes, which targeted the *XPC* or *CSA* genes, respectively. The MRC-5 cells received three individual treatments during the course of a nine-day treatment

cycle (Table 2.1). As a control, MRC-5 fibroblasts were transfected in parallel with a non-targeting siRNA scramble control.

Western blot analysis revealed that both XPC and CSA protein levels were reduced in MRC-5 cells transfected with *XPC*- or *CSA*-specific siRNA duplexes, respectively, compared to the scramble control (Figs. 6.1A & C, 6.2A & C). The expected ~125 kDa XPC band was visualised in the WCE derived from non-transfected normal hTERT-immortalised MRC-5 fibroblasts (positive control), but was absent from the non-transfected, telomerised XP-C WCE (negative control) derived from subject XP8CA (Fig. 6.1A).

Both *XPC* siRNA #1 and #2 produced a reduction in XPC levels, although multiple rounds of treatment were required for the maximal effect. Reductions in XPC expression were not observed following transfection of the non-targeting siRNA control scramble (Fig. 6.1C).

As expected, Western blot analysis, using the anti-CSA goat polyclonal antibody, resulted in the detection of a lower non-specific cross-reacting band (as described in Chapter 3; Ridley *et al.*, 2005). However, an upper band (~44 kDa) indicative of CSA was detected in the non-transfected MRC-5 WCE (Figs. 6.2A & C). In contrast, an upper corresponding band, indicative of CSA was not detected in the non-transfected telomerised CS-A WCE derived from subject CS3BE (Figs. 6.2A & C). Both *CSA* siRNA #1 and #2 produced a reduction in CSA protein levels, although multiple rounds of treatment were required for the maximal effect (Fig. 6.2A). In contrast, an upper band indicative of CSA was observed in MRC-5 WCEs, transfected with *CSA* siRNA(#3) following each treatment (Fig. 6.2C). The level of expression was comparable to the levels of CSA protein observed in non-transfected MRC-5 cells (Fig. 6.2C). This suggested that CSA expression was not attenuated by the transfection of *CSA* siRNA(#3). Like XPC protein expression, CSA expression was not attenuated in MRC-5 cells by the non-targeting siRNA scramble (Fig. 6.2C).

Significant apoptosis was observed in MRC-5 fibroblasts transfected with either *XPC*- or *CSA*-specific siRNA duplexes. Because MRC-5 cells transfected with the non-targeting siRNA scramble control also exhibited an equally high level of cell death, this indicated that the progressive increase in apoptosis was attributed to the cytotoxic effect of the oligofectamine transfection reagent, or the elicitation of protective mechanisms by the MRC-5 cells, in response to the transfection of siRNA molecules *per se*, irrespective of sequence specificity.

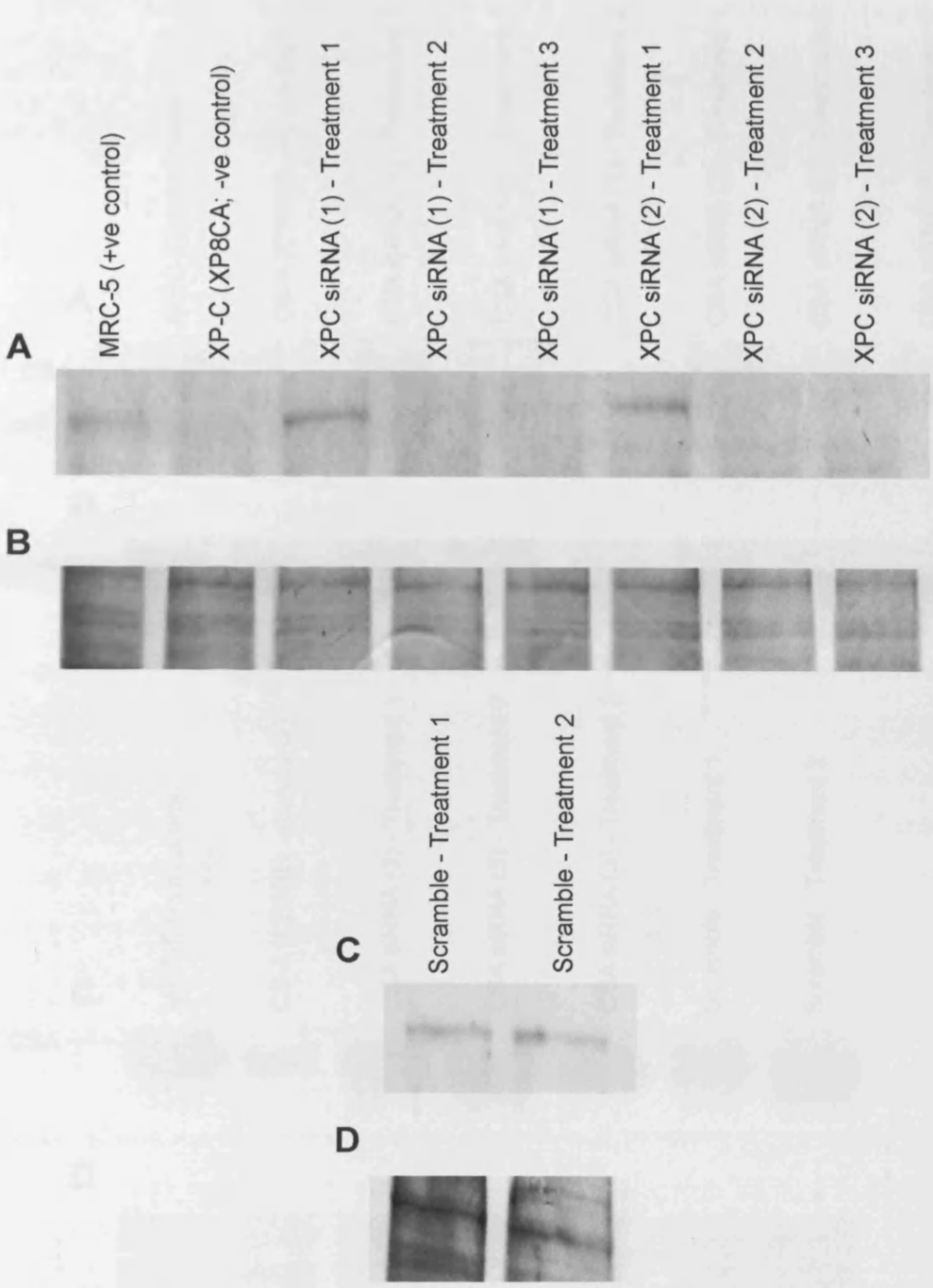

Figure 6.1. Transient knockdown of XPC in hTERT-immortalised MRC-5 fibroblasts, transfected with *XPC*-specific 21mer siRNA duplexes. (A) XPC protein expression detected by Western blot analysis, using an anti-XPC mouse monoclonal antibody (1:500), in a normal MRC-5 WCE, XP-C (XP8CA) WCE and in MRC-5 fibroblasts following transfection (treatments) with *XPC* siRNA duplexes (sequences 1 and 2). (B) Equal protein loading was confirmed by staining the PVDF membrane with India ink. (C) Detection of XPC protein following transfection (treatments) with the non-targeting siRNA control scramble. (D) The level of protein loading was determined by India ink staining. A band of approximately 125 kDa was indicative of XPC. 20 μg of each WCE was loaded into each lane.

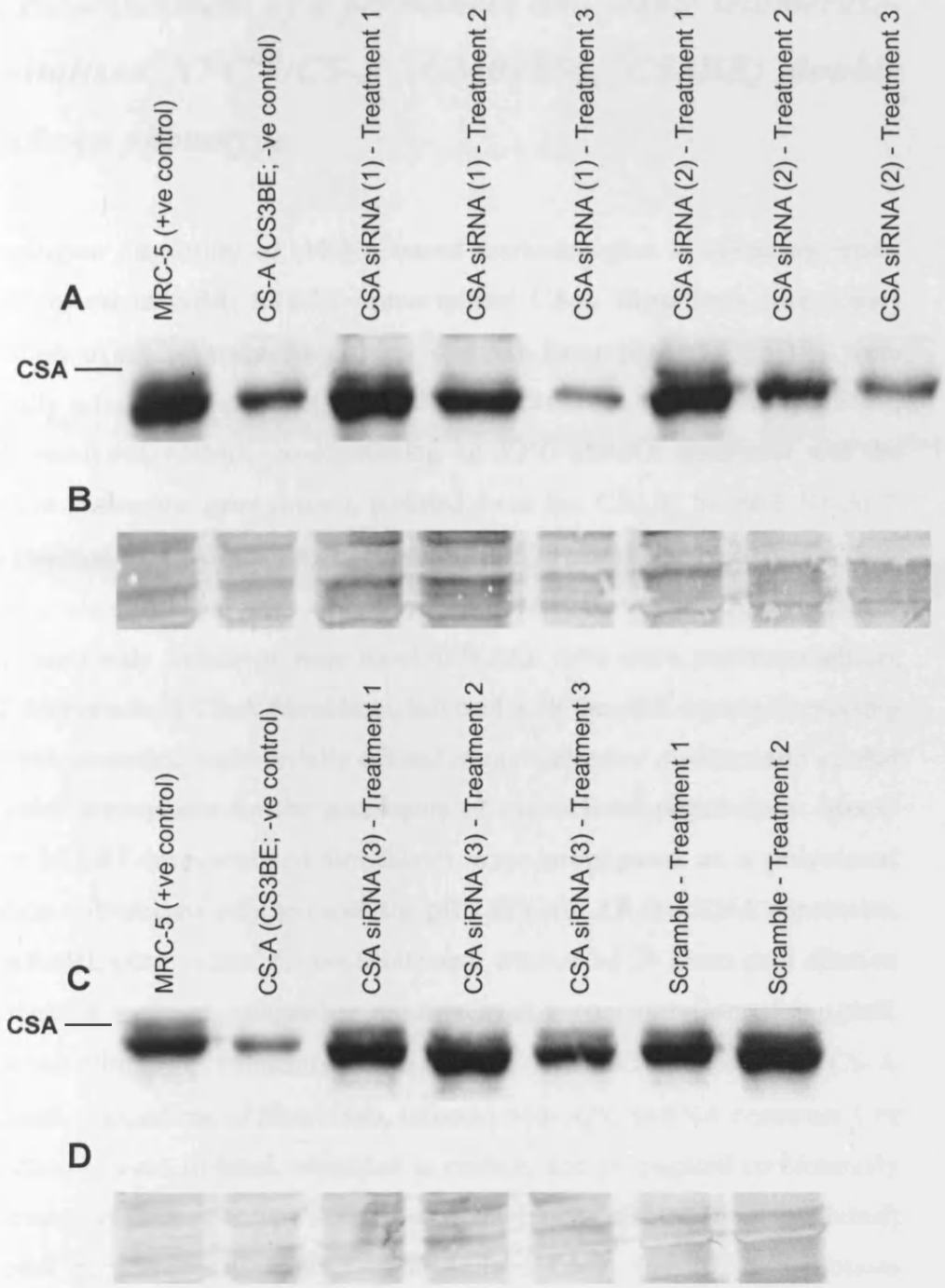

Figure 6.2. Transient knockdown of CSA protein in hTERT-immortalised MRC-5 fibroblasts transfected with *CSA*-specific 21mer siRNA duplexes. (A) CSA protein expression detected by Western blot analysis, using an anti-CSA goat polyclonal antibody (1:100), in a normal MRC-5 WCE, CS-A (CS3BE) WCE and in MRC-5 fibroblasts following transfection (treatments) with *CSA* siRNA duplexes (sequences 1 and 2). (B) Equal protein loading was confirmed by staining the PVDF membrane with India ink. (C) Detection of CSA protein following transfection with *CSA* siRNA duplex (sequence 3) and the non-targeting control scramble. (D) The level of protein loading was determined by India ink staining. A band of approximately 44 kDa (*upper band*) was indicative of CSA. 20 μg of each WCE was loaded into each lane.

6.4.2 Establishment of a permanent and stable telomerase-immortalised XPC^{KD}/CS-A (GM01856, CS3BE) double knockdown phenotype

To investigate the utility of shRNA-based methodologies in silencing repair genes involved in NER, hTERT-immortalised CS-A fibroblasts (previously established using primary fibroblasts derived from patient CS3BE) were retrovirally infected independently with two replication-defective pRS (pMSCV) shRNA retroviral vectors, co-expressing an *XPC* shRNA construct and the puromycin resistance gene (*puro*), isolated from the CRUK SUPER RNAi™ library (Sections 2.4.0-2.4.9). As controls, hTERT-immortalised CS-A (CS3BE) fibroblasts were infected with a previously validated *XPA* shRNA construct, a pBABE-puro only vector or were mock-infected. Two days posttransduction, hTERT-immortalised CS-A fibroblasts, infected with the pRS vectors expressing the shRNA cassettes, were serially diluted in non-selective medium and seeded at densities appropriate for the generation of monoclonal populations. Mock-infected hTERT-immortalised fibroblasts were propagated as a polyclonal population. Fibroblasts infected with the pRS *XPC* (or *XPA*) shRNA constructs, empty pBABE-puro vector, or mock-infected, were refed 24 hours post dilution with selective medium, containing puromycin at a concentration of 1 μg/ml. After serial dilution of transduced cells, 16 and 7 hTERT-immortalised CS-A monoclonal populations of fibroblasts, infected with *XPC* shRNA construct 1 or 2 respectively, were isolated, expanded in culture, and propagated continuously with puromycin drug selection. As expected, the mock-infected (nontransduced) polyclonal population of hTERT-immortalised CS-A (CS3BE) fibroblasts exhibited significant cell death ~2 days after puromycin drug selection.

Western blot analysis revealed that the retroviral infection of hTERT-immortalised CS-A fibroblast with the *XPC* shRNA (sequence 1 or 2) constructs resulted in the heterogeneous silencing of XPC protein in isolated monoclonal populations (Figs. 6.3A & C, 6.4A and 6.5A). Although several hTERT-immortalised CS-A (CS3BE) monoclonal populations (clones 4, 20 and 21),

infected with *XPC* shRNA sequence 1, displayed a significant reduction in XPC protein levels, no clones were isolated that displayed undetectable levels of XPC protein by Western blot analysis (Figs. 6.3A, 6.3C and 6.4A). Like the isolation of monoclonal populations of CS-A cells infected with *XPC* shRNA sequence 1, the retroviral infection of hTERT-immortalised CS-A cells with *XPC* shRNA sequence 2, resulted in the isolation of clones expressing heterogeneous levels of XPC protein (Fig. 6.4A & 6.5A). However, transduction of telomerised CS-A cells with *XPC* shRNA sequence 2 appeared to have a greater affect on XPC expression, as several clones (3, 6 & 15) were isolated displaying a significant reduction in XPC protein expression (Fig. 6.4A). Moreover, transduction of the XPC shRNA sequence 2 construct, resulted in the isolation of clones 10 and 13, which no longer showed detectable XPC expression (Figs. 6.4A & 6.5A, respectively). This suggested the complete knockdown of XPC at the translational level. It is possible, however, that these two hTERT-immortalised double XPC^{KD}/CS-A fibroblast clones expressed residual levels of XPC protein, which remain undetected by Western blot analysis. Equal protein loading was determined by India ink staining (Figs. 6.3B, 6.3D, 6.4B & 6.5B).

The Western blot and immunocytochemical analysis suggested that the hTERT-immortalised CS-A (CS3BE) clones 10 and 13, infected with *XPC* shRNA sequence 2, were the only isolated clones that failed to express detectable XPC protein. From these data, clone 10 was therefore selected for further investigation.

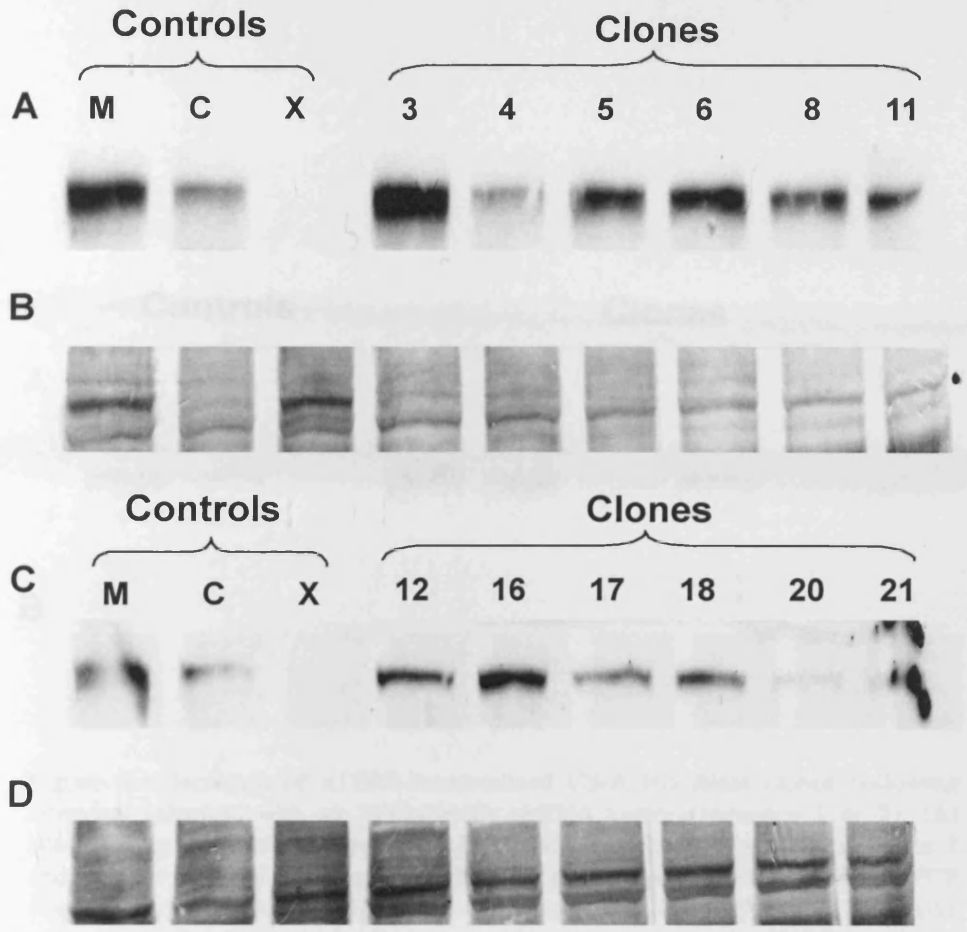

Figure 6.3. Isolation of hTERT-immortalised CS-A fibroblast clones following retroviral infection with an *XPC*-specific shRNA vector (sequence 1). (A) Western blot analysis of 6 clones; M, MRC-5 WCE (+ve control); C, CS-A (CS3BE) WCE (+ve control); X, XP-C (XP8CA) WCE (-ve control). (B) Equal protein loading was confirmed by staining the PVDF membrane with India ink. (C) Western blot analysis of 6 clones; M, MRC-5 WCE (+ve control); C, CS-A (CS3BE) WCE (+ve control); X, XP-C (XP8CA) WCE (-ve control). (D) The level of protein loading was determined by India ink staining. 20 μg of each WCE was loaded into each lane.

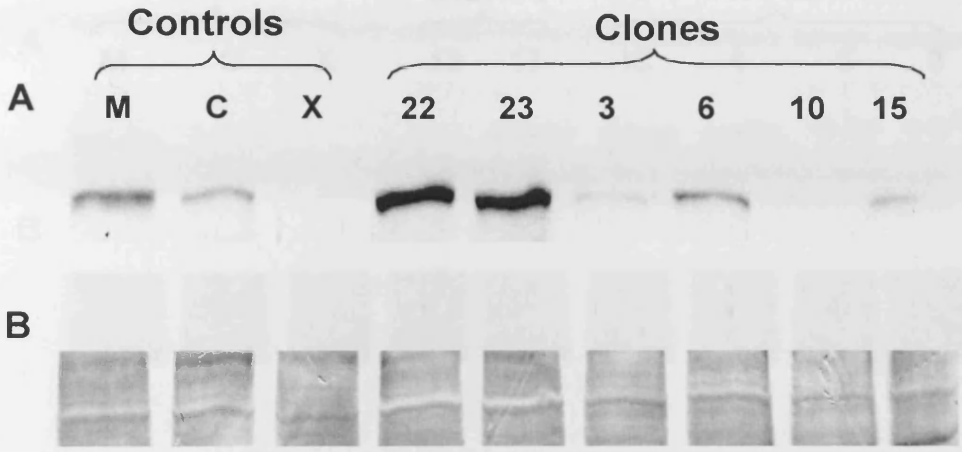

Figure 6.4. Isolation of hTERT-immortalised CS-A fibroblast clones following retroviral infection with an *XPC*-specific shRNA vector (sequence 1 or 2). (A) Western blot analysis of 2 clones (22 & 23) infected with *XPC* shRNA sequence 1 and 4 clones (3, 6, 10 & 15) infected with *XPC* shRNA sequence 2; M, MRC-5 WCE (+ve control); C, CS-A (CS3BE) WCE (+ve control); X, XP-C (XP8CA) WCE (-ve control). (B) Equal protein loading was confirmed by staining the PVDF membrane with India ink. 20 μg of each WCE was loaded into each lane.

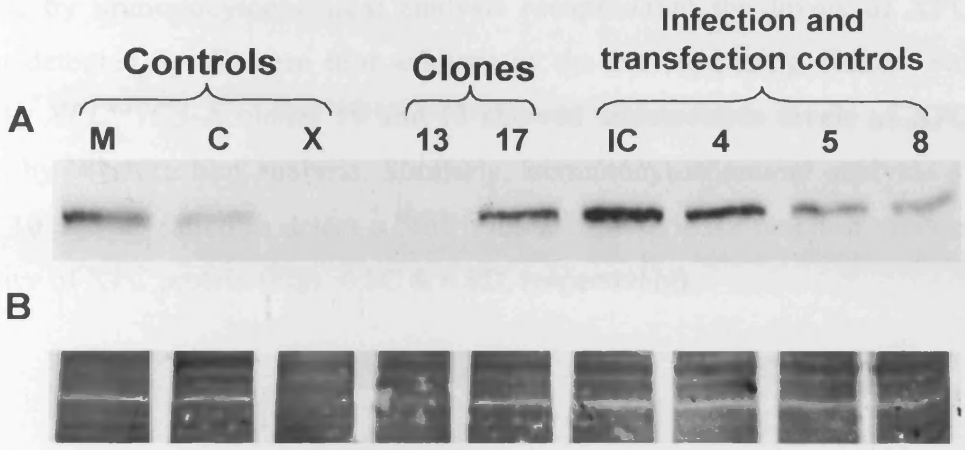

Figure 6.5. Isolation of hTERT-immortalised CS-A fibroblast clones following retroviral infection with an *XPC*-specific shRNA vector (sequence 2). (A) Western blot analysis of 2 clones (13 & 17) infected with *XPC* shRNA sequence 2; M, MRC-5 WCE (+ve control); C, CS-A (CS3BE) WCE (+ve control); X, XP-C (XP8CA) WCE (-ve control); IC (infection control), polyclonal population of hTERT-immortalised CS-A fibroblasts infected with (previously prepared) pBABE-puro retroviral supernatant; transfecction controls, monoclonal populations of hTERT-immortalised CS-A fibroblasts (clones 4, 5 and 8) infected with a retroviral supernatant expressing the empty pBABE-puro vector (pBABE-puro supernatant used for the transfectioin controls was prepared in parallel with the *XPC* and *XPA* shRNA cDNA plasmid transfections and infections). (B) Equal protein loading was confirmed by staining the PVDF membrane with India ink. 20 μg of each WCE was loaded into each lane.

Immunocytochemical analysis further confirmed the heterogeneous levels of XPC protein expression in telomerised CS-A fibroblast clones infected with either *XPC* shRNA constructs 1 or 2 (Figs. 6.6A-H, 6.7A-F & 6.8A-F). As expected, both the hTERT-immortalised normal MRC-5 and CS-A (CS3BE) fibroblasts were immunopositive for XPC (Figs 6.6A & 6.6C, respectively). In contrast, nuclear staining was not detected in the hTERT-immortalised XP-C (XP8CA) fibroblasts (Fig. 6.6B). In general, the levels of XPC expression detected by immunocytochemical analysis recapitulated the levels of XPC protein detected by Western blot analysis in the corresponding clones. For example, XPC^{KD}/CS-A clones 10 and 13 showed undetectable levels of XPC protein by Western blot analysis. Similarly, immunocytochemical analysis of clones 10 and 13 failed to detect a brown nuclear peroxidase reaction product indicative of XPC protein (Figs. 6.8C & 6.8D, respectively).

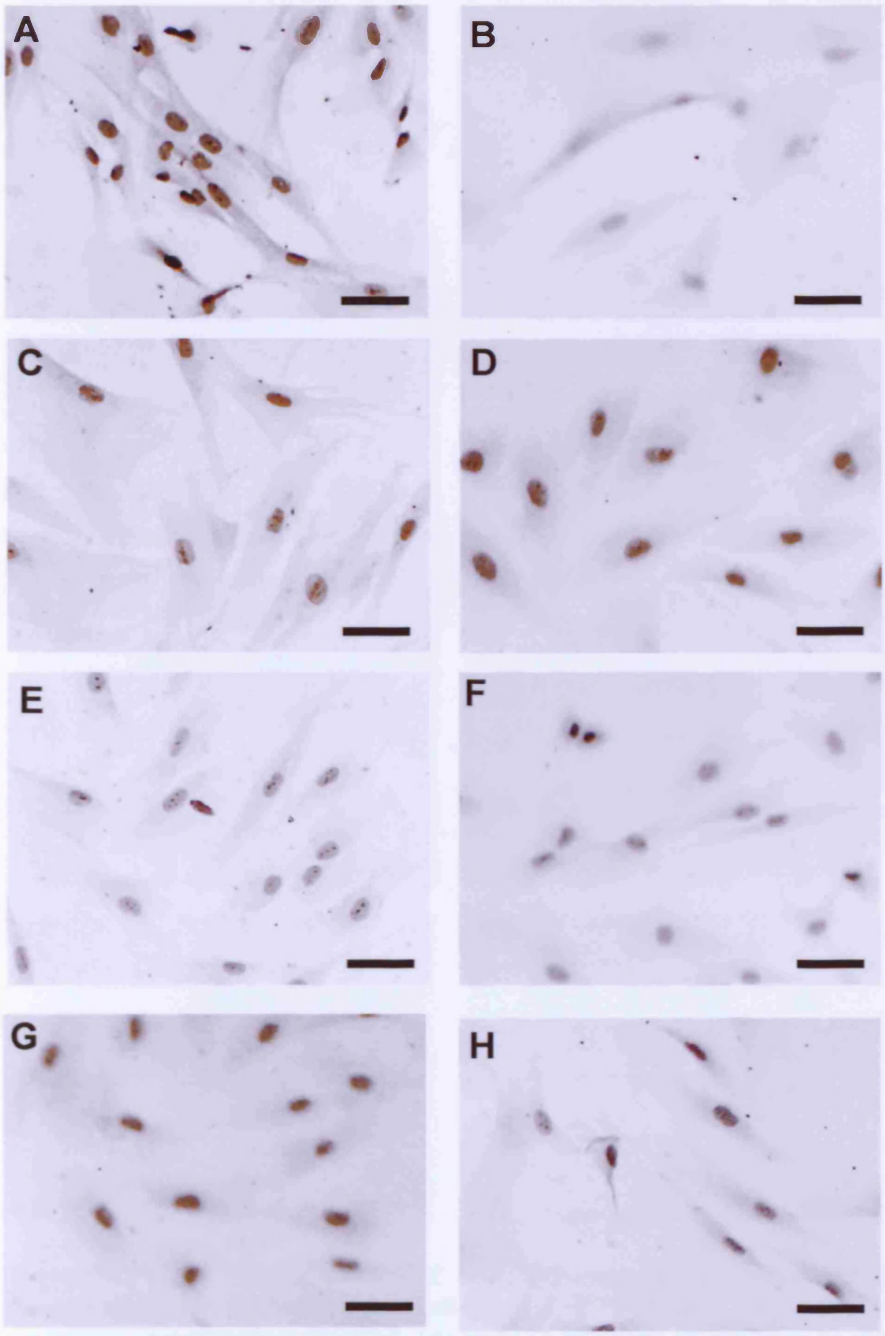

Figure 6.6. Immunocytochemical detection of XPC protein in hTERT-immortalised CS-A (CS3BE) fibroblast clones, following the retroviral infection of a pRETROSUPER vector expressing the XPC shRNA contruct 1. (A) hTERT-immortalised normal MRC-5 fibroblasts (positive control). (B) hTERT-immortalised XP-C (XP8CA; negative control) fibroblasts. (C) hTERT-immortalised CS-A (CS3BE; positive control) fibroblasts. (D) Polyclonal population of hTERT-immortalised CS-A fibroblasts infected with an empty pBABE-puro vector (infection control). Stable hTERT-immortalised CS-A (E) clone 3, (F) clone 4, (G) clone 5 and (H) clone 6 infected with a pRETROSUPER vector expressing the XPC-targeted shRNA construct 1. Positivity indicated by brown peroxidase reaction product. Nuclei were counterstained with haematoxylin to aid visualisation. Bar = 25 μm.

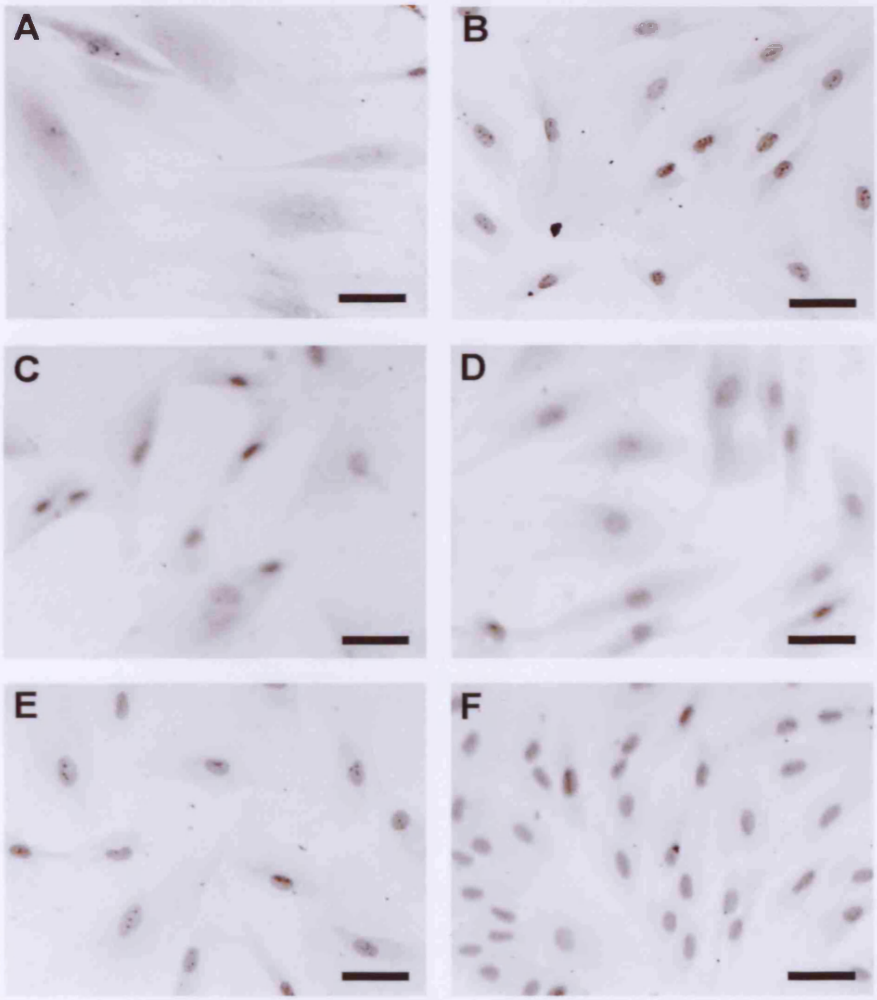

Figure 6.7. Stable knockdown of XPC in hTERT-immortalised CS-A (CS3BE) humanl fibroblasts. Immunocytochemical detection of XPC protein was performed on hTERT-immortalised stable CS-A (A) clone 11, (B) clone 12, (C) clone 14, (D) clone 16, (E) clone 17 and (F) clone 23 isolated as monoclonal populations of hTERT-immortalised CS-A fibroblasts infected with a pRETROSUPER vector expressing the XPC-targeted shRNA construct 1. Positivity indicated by brown peroxidase reaction product. Nuclei were counterstained with haematoxylin to aid visualisation. Bar = 25 μm.

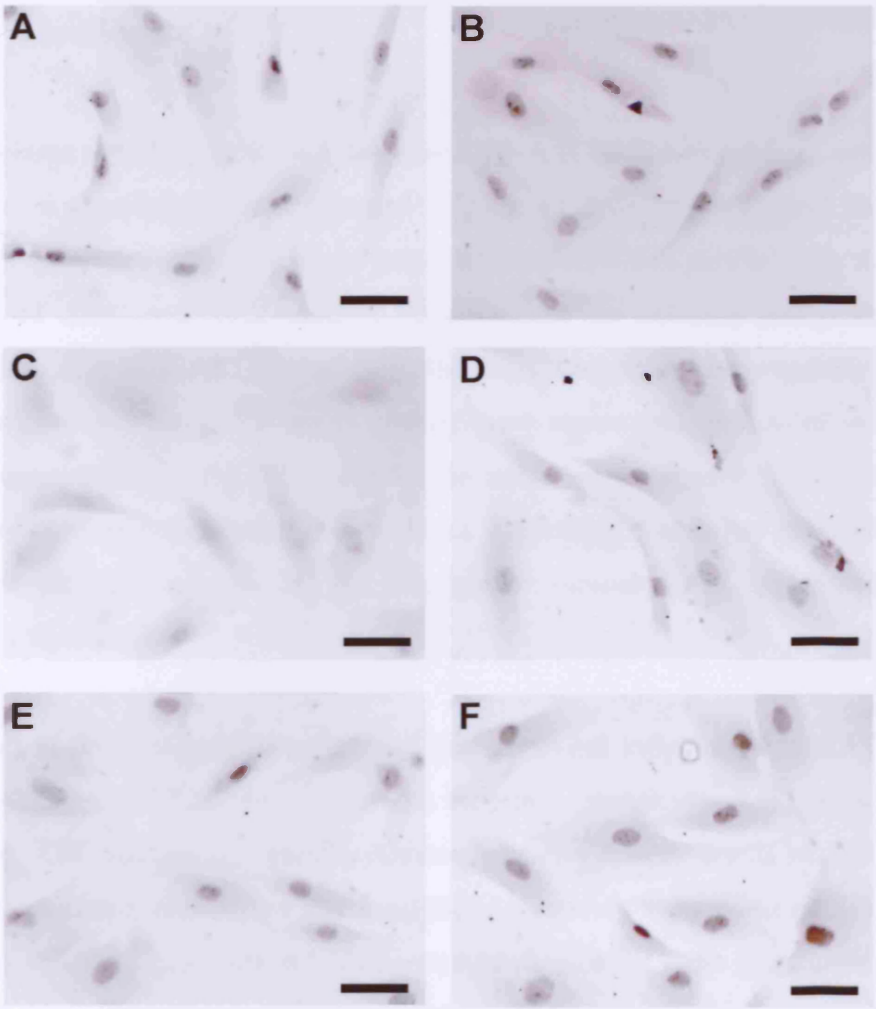

Figure 6.8. Immunocytochemical detection of XPC protein in hTERT-immortalised CS-A (CS3BE) fibroblasts, following the retroviral infection of a pRETROSUPER vector expressing the *XPC* shRNA construct 2. hTERT-immortalised CS-A (A) clone 1, (B) clone 6, (C) clone 10, (D) clone 13, (E) clone 15 and (F) clone 17 isolated as monoclonal populations of hTERT-immortalised CS-A fibroblasts infected with a pRETROSUPER vector expressing the *XPC*-targeted shRNA construct 2. Positivity indicated by brown peroxidase reaction product. Nuclei were counterstained with haematoxylin to aid visualisation. Bar = 25μm.

6.4.3 Retroviral infection of an empty pBABE-puro (control) vector had no detectable effects on XPC expression in hTERT-immortalised CS-A (GM01856, CS3BE) fibroblasts

As a transfection control, hTERT-immortalised CS-A (CS3BE) fibroblasts were infected with a supernatant that expressed an empty pBABE-puro vector. The pBABE-puro retroviral supernatant was prepared from cDNA in parallel with the generation of *XPC* and *XPA* shRNA supernatants, by calcium phosphate transfections, using FLY A13 human epithelial cells. Following the preparation of the retroviral supernatant, the empty pBABE-puro vector was transduced into hTERT-immmortalised CSA fibroblasts. The cells were serially diluted to produce monoclonal populations, and 5 clones expressing the empty pBABE-puro vector were isolated, expanded and propagated continuously in culture with puromycin drug selection.

Western blot analysis clearly demonstrated that retroviral infection of hTERT-immortalised CS-A (CS3BE) fibroblasts with the empty pBABE-puro vector had no effect on XPC protein expression. Although heterogeneous levels of XPC protein were detected, clones 4, 5 and 8 exhibited relatively high levels of XPC protein (Fig. 6.5A). Equal protein loading was confirmed by India ink staining (Fig. 6.5B). In concordance with these data, immunocytochemical analysis resulted in the detection of a brown nuclear peroxidase reaction product (indicative of XPC) in the monoclonal populations of hTERT-immortalised CS-A (CS3BE) fibroblasts, infected with the empty pBABE-puro vector without either of the *XPC* shRNA sequences (Figs. 6.9 A-D).

As an infection control, hTERT-immortalised CS-A fibroblasts were transduced with retroviral supernatant, expressing the empty pBABE-puro vector that was previously prepared and validated in our laboratory from a plasmid containing *puro* cDNA. Following retroviral infection of the pBABE-puro vector, the CS-A fibroblasts were maintained in culture as a polyclonal population with puromycin

drug selection. Both Western blot and immunocytochemical analysis of the polyclonal population of CS-A fibroblasts, infected with the pBABE-puro supernatant, displayed high levels of XPC protein (Figs. 6.5A & 6.6D, respectively). This suggested that the retroviral infection of an empty pBABE-puro vector, expressing the gene for puromycin drug resistance alone, had no effect on XPC expression.

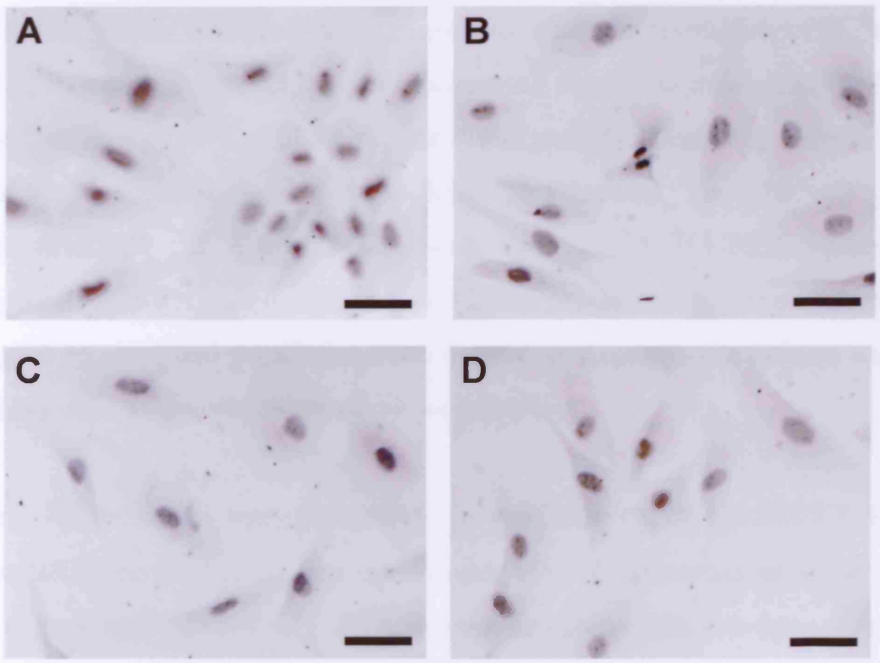

Figure 6.9. Detection of XPC in hTERT-immortalised CS-A (CS3BE) human fibroblasts. Immunocytochemical detection of XPC protein in hTERT-immortalised CS-A (A) clone 1, (B) clone 5, (C) clone 8 and (D) clone 14 isolated as monoclonal populations, following retroviral infection of an empty pBABE-puro vector. Positivity indicated by brown peroxidase reaction product. Nuclei were counterstained with haematoxylin to aid visualisation. Bar = 25 μm.

6.4.4 Establishment of a permanent and stable double XPA^{KD}/CS-A (GM01856, CS3BE) double knockdown phenotype

As a transfection control, hTERT-immortalised CS-A (CS3BE) fibroblasts were transduced with a previously validated *XPA* shRNA vector, isolated from the CRUK SUPER RNAi™ library. The retroviral infection of the CS-A cells with the *XPA* shRNA vector was performed in parallel with the transduction of the *XPC* shRNA (sequences 1 or 2) vectors. Following retroviral infection, CS-A cell infected with the *XPA* shRNA vector were serially diluted at densities appropriate for the production of monoclonal populations. Transduction of hTERT-immortalised CS-A fibroblasts with the pRETROSUPER vector, expressing the *XPA* shRNA construct, resulted in the production of fewer clones. However, nine monoclonal populations were isolated, expanded in culture and propagated continuously with puromycin drug selection.

As expected, Western blot analysis resulted in the detection of a doublet (~46 kDa) in the WCE derived from non-transduced hTERT-immortalised MRC-5 fibroblasts (Fig. 6.10). Interestingly, XPA was not detected in the non-transduced hTERT-immortalised CS-A fibroblast WCE derived from patient CS3BE (Fig. 6.10). This was attributed to the degradation of the CS-A WCE, as the expression of XPA was clearly evident in hTERT-immortalised CS-A fibroblasts infected with an empty pBABE-puro vector, following immunocytochemical detection (Fig. 6.11C). As expected, Western blot analysis failed to detect XPA protein in the non-transduced hTERT-immortalised XP-A WCE derived from patient XP12BE. Interestingly, Western blot analysis revealed that the retroviral infection of hTERT-immortalised CS-A fibroblasts with the *XPA* shRNA vector resulted in the isolation of clones expressing heterogeneous levels of XPA protein (Fig. 6.10). However, none of the 8 isolated hTERT-immortalised CS-A clones, infected with the *XPA* shRNA vector, exhibited complete cessation of XPA protein expression. As expected, immunocytochemical analysis, using the same anti-XPA antibody, resulted in the detection of a brown peroxidase reaction

product in hTERT-immortalised normal MRC-5 fibroblasts, which was indicative of XPA expression (Fig. 6.11A). Conversely, hTERT-immortalised XP-A fibroblasts, derived from patient XP12BE were immunonegative for XPA (Fig. 6.11B). Moreover, in agreement with the Western blot data, immunocytochemical analysis resulted in the detection of heterogeneous levels of XPA protein expression among the isolated monoclonal populations of hTERT-immortalised CS-A (CS3BE) fibroblasts infected with the *XPA* shRNA vector (Figs. 6.11D-H & 6.12A-B).

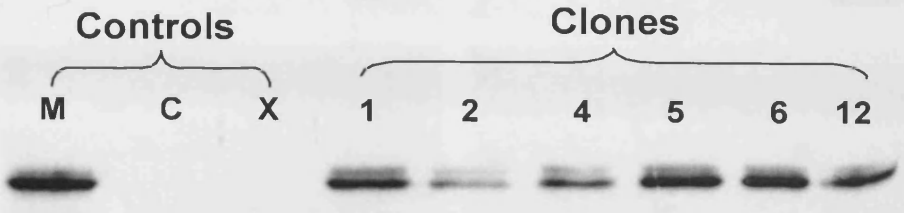

Figure 6.10. Isolation of hTERT-immortalised CS-A fibroblast clones following retroviral infection with an *XPA*-specific shRNA. Western blot analysis of 6 clones, using an anti-XPA mouse monoclonal antibody (1:100); M, MRC-5 WCE (+ve control); C, CS-A (CS3BE) WCE (+ve control); X, XP-A (XP12BE) WCE (-ve control). 20 μg of each WCE was loaded into each lane.

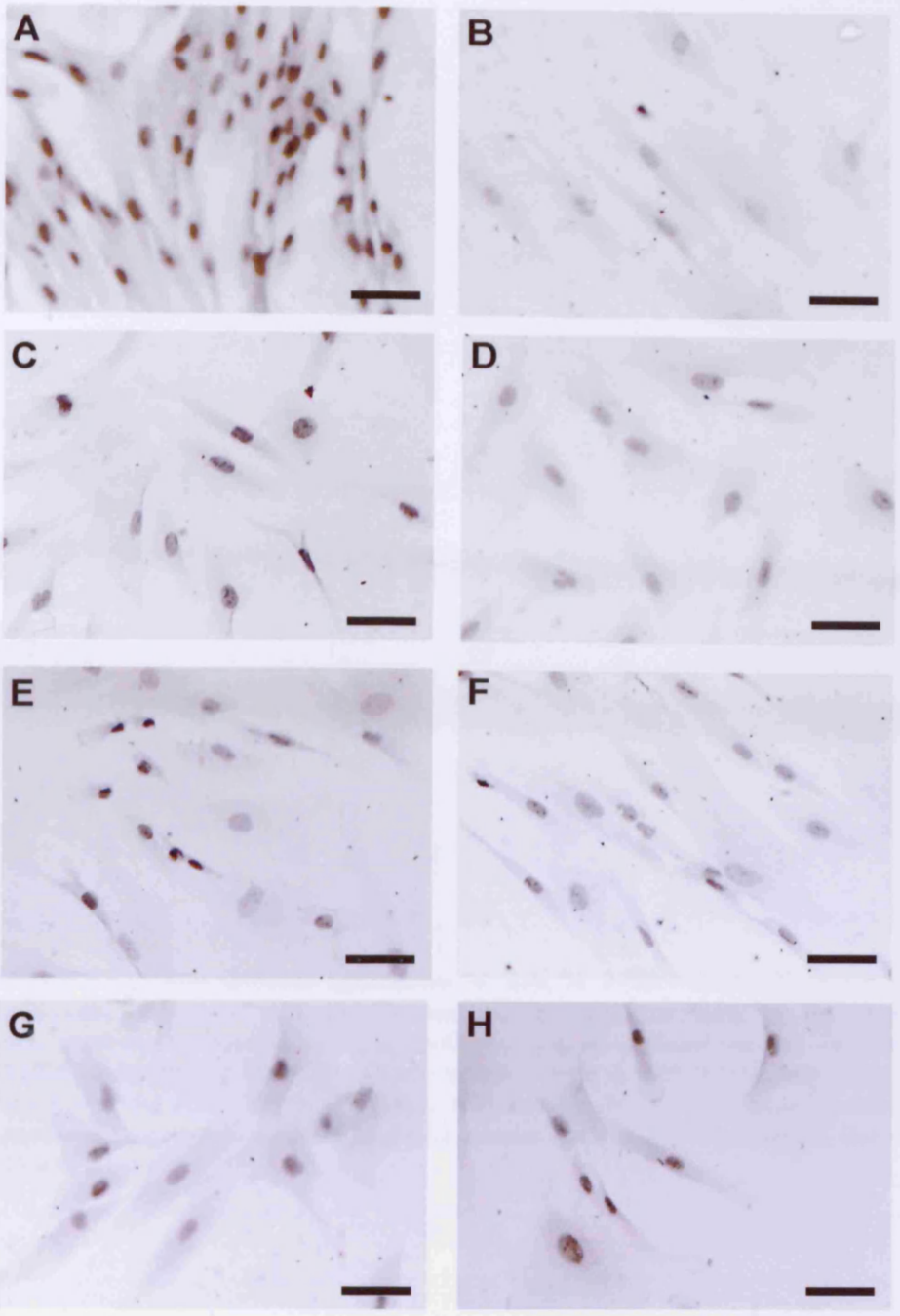

Figure 6.11. Heterogeneous knockdown of XPA protein in hTERT-immortalised CS-A (CS3BE) human fibroblasts, following retroviral infection of an *XPA* shRNA vector. Immunocytochemical detection of XPA protein was performed on hTERT-immortalised (A) normal MRC-5 (positive control) fibroblasts; (B) XP-A (XP12BE; negative control) fibroblasts; (C) hTERT-immortalised CS-A (CS3BE) fibroblasts infected with an empty pBABE-puro vector (infection control); hTERT-immortalised CS-A (D) clone 1, (E) clone 2, (F) clone 4, (G) clone 5 and (H) clone 6 isolated as monoclonal populations, following retroviral infection with the pRETROSUPER vector expressing the *XPA*-targeted shRNA. Positivity indicated by brown peroxidase reaction product. Nuclei were counterstained with haematoxylin to aid visualisation. Bar = 25 μm.

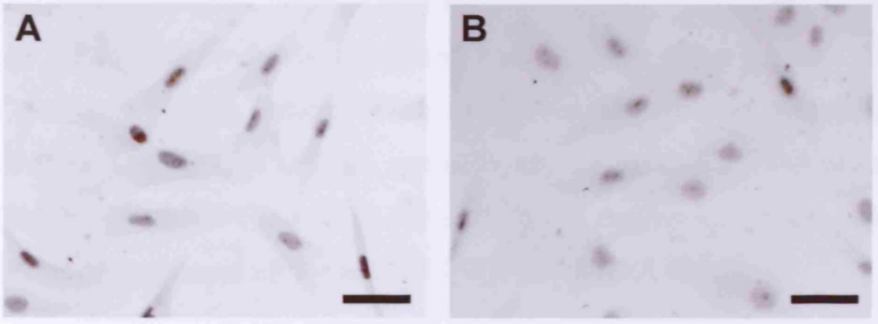

Figure 6.12. Heterogeneous knockdown of XPA in hTERT-immortalised CS-A (CS3BE) fibroblasts. Immunocytochemical detection of XPA protein was performed on (A) clone 7 and (B) clone 8 isolated as monoclonal populations from hTERT-immortalised CS-A fibroblasts infected with a pRETROSUPER vector expressing the *XPA* shRNA. Positivity indicated by brown peroxidase reaction product. Nuclei were counterstained with haematoxylin to aid visualisation. Bar = 25 μm.

6.4.5 Retroviral infection of an empty pBABE-puro control vector in hTERT-immortalised CS-A (GM01856, CS3BE) dermal fibroblasts had no detectable effects on XPA protein expression

As with protein expression, the levels of XPA appeared unaltered in hTERT-immortalised CS-A fibroblasts infected with an empty pBABE-puro vector (Fig. 6.13). Immunocytochemical analysis resulted in the detection of a brown nuclear peroxidase reaction product in the monoclonal populations of hTERT-immortalised CS-A fibroblasts, infected with the pBABE-puro vector, which was indicative of XPA. The evidence presented here, clearly suggests that the isolation of clones displaying reduced levels of XPC or XPA protein, following transduction of an *XPC* or *XPA* shRNA, respectively, occurred as a result of the targeted affect of the shRNA construct rather than the expression of the *puro* gene, which was co-expressed by the pRETROSUPER shRNA vector.

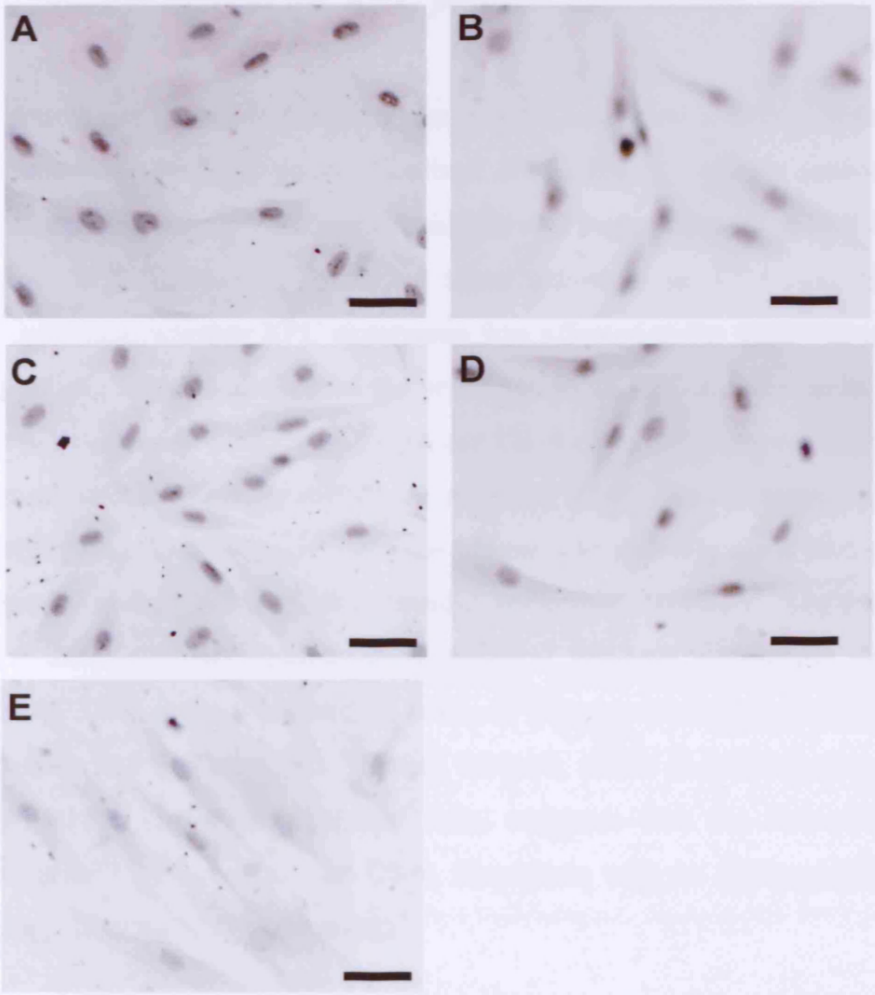

Figure 6.13. No detectable effect on XPA expression in hTERT-immortalised CS-A (CS3BE) fibroblasts. Immunocytochemical detection of XPA protein was performed on hTERT-immortalised CS-A (A) clone 4, (B) clone 5, (C) clone 8, (D) clone 14 isolated as monoclonal populations from hTERT-immortalised CS-A fibroblasts infected with an empty pBABE-puro vector (transfection control). (E) hTERT-immortalised XP-A (XP12BE) fibroblasts (negative control). Positivity indicated by brown peroxidase reaction product. Nuclei were counterstained with haematoxylin to aid visualisation. Bar = 25 μm.

6.4.6 Retroviral infection of a pRETROSUPER vector expressing an XPA shRNA construct in hTERT-immortalised CS-A (GM01856, CS3BE) dermal fibroblasts had no off-target effects on XPC protein expression

It has been previously shown that siRNAs can elicit a non-specific effect on the protein levels of non-targeted genes (Scacheri *et al.*, 2004). For this reason, Western blot and immunocytochemical analysis was undertaken on hTERT-immortalised CS-A fibroblasts, following transduction of an *XPA*-specific shRNA, to determine whether XPC expression was affected at the translational level. Western blot analysis confirmed the preservation of XPC expression in 6 monoclonal populations of hTERT-immortalised CS-A cells following retroviral transduction of the *XPA*-specific shRNA vector (Fig. 6.14). The heterogeneous levels of XPC expression observed between clones was possibly attributed to clonal variation and/or the well-documented inducible nature of XPC. In agreement with these data, immunocytochemical analysis confirmed the maintenance of XPC at the translational level, as a brown nuclear peroxidase reaction product was detected in all clones assayed, albeit at heterogeneous levels (Fig. 6.15). The data presented here, suggests that the retroviral transduction of hTERT-immortalised CS-A fibroblasts with an *XPA*-specific shRNA had no affect on XPC expression.

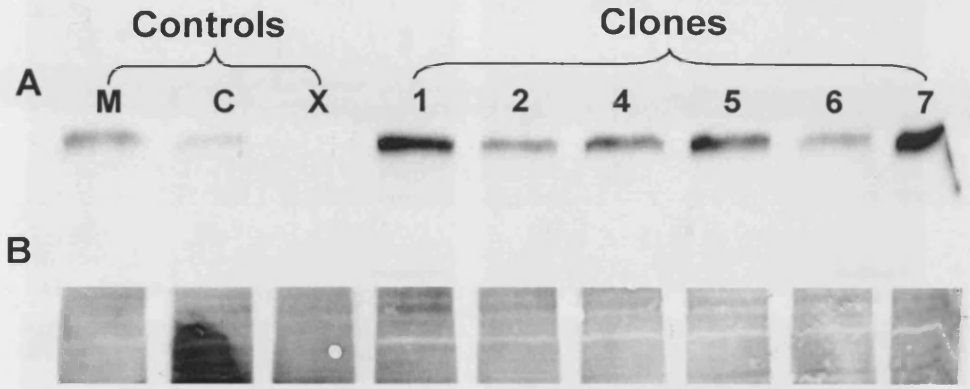

Figure 6.14. Retroviral infection of hTERT-immortalised CS-A fibroblasts with an *XPA*-specific shRNA vector had no off-target effects on XPC expression. (A) Western blot analysis of 6 XPA shRNA infected clones, using an anti-XPC mouse monoclonal antibody (1:500). M, MRC-5 WCE (+ve control); C, CS-A (CS3BE) WCE (+ve control); X, XP-C (XP8CA) WCE (-ve control). (B) Equal protein loading was confirmed by staining the PVDF membrane with India ink. 20 μg of each WCE was loaded into each lane.

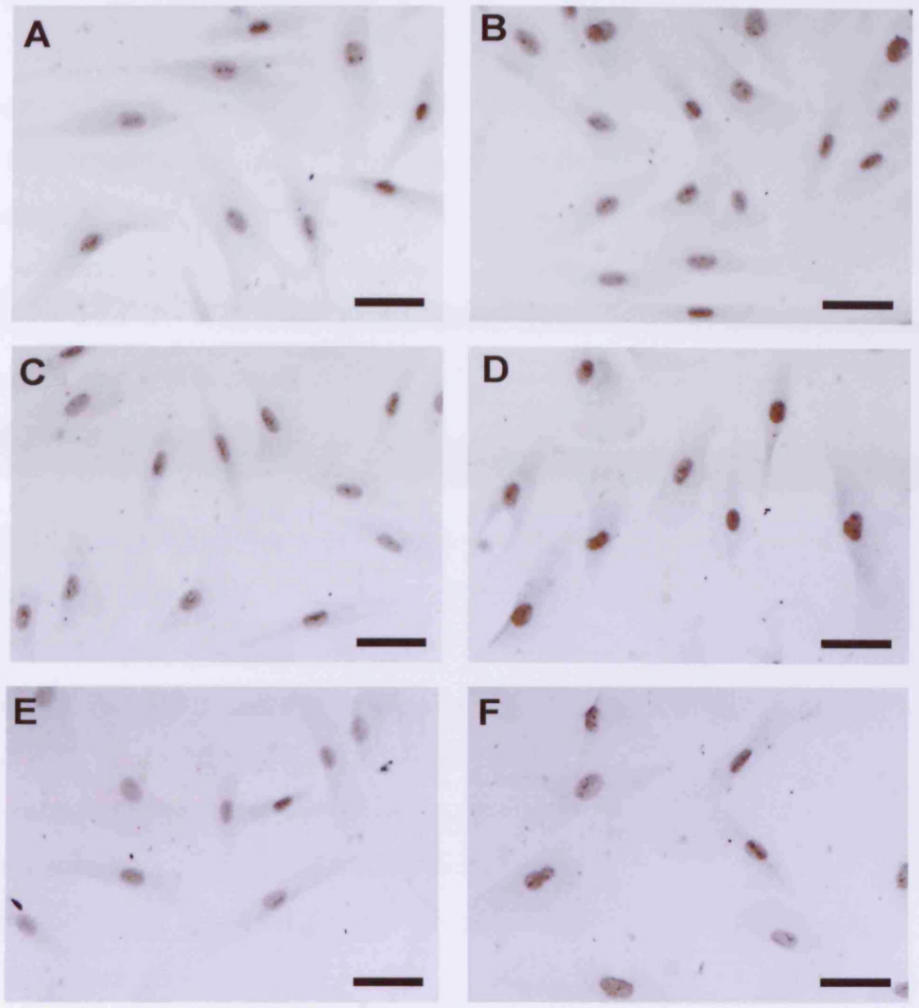

Figure 6.15. No off-target effects on XPC protein expression in hTERT-immortalised CS-A (CS3BE) fibroblasts. Immunocytochemical detection of XPC protein was performed on hTERT-immortalised stable CS-A (A) clone 2, (B) clone 4, (C) clone 5, (D) clone 6, (E) clone 7 and (F) clone 8 isolated as monoclonal populations of hTERT-immortalised CS-A fibroblasts infected with an *XPA*-targeted shRNA construct. Positivity indicated by brown peroxidase reaction product. Nuclei were counterstained with haematoxylin to aid visualisation. Bar = 25 μm.

6.4.7 Measurement of global CPD and 6-4PP repair in hTERT-immortalised XPC^{KD}/CS-A (GM01856, CS3BE) double knockdown

To investigate whether the retroviral transduction of an *XPC*-targeted shRNA in CS-A hTERT-immortalised (*XPC*^{KD}/CS-A) fibroblasts affected the removal of UV-C radiation-induced lesions from the global genome, an immunological slot-blot assay was undertaken by Dr. Shirong Yu on DNA extracts (as previously described in Chapter 4). This assay measures the global removal of CPDs and 6-4PPs from genomic DNA, using specific monoclonal antibodies raised against these photolesions (Mori *et al.*, 1991).

Figure 4.19 (Chapter 4) shows representative slot-blots of the kinetics of the removal of 6-4PPs (Fig. 4.19A) and CPDs (Fig. 4.19B) from the global genome in hTERT-immortalised CS-A fibroblasts (clone 10), following retroviral transduction of the *XPC* shRNA (sequence 2) construct. Interestingly, the silencing of XPC in the hTERT-immortalised *XPC*^{KD}/CS-A cell line, resulted in a marked reduction in the removal of CPDs from the global genome, compared to the nontransduced isogenic hTERT-immortalised CS-A cell line (Fig. 6.16). At ~6 hours following UV, the hTERT-immortalised *XPC*^{KD}/CS-A (clone 10) cell line removed only 21.1% of CPDs, while nontransduced hTERT-immortalised CS-A cells removed 55.6% of CPDs. Similarly, the hTERT-immortalised *XPC*^{KD}/CS-A cell line removed only 28.4% and 46.3% of CPDs from the genome at ~12 and ~24 hours after UV, respectively. In contrast, the nontransduced hTERT-immortalised CS-A cell line displayed repair rates of 58.5% and 74.1% at ~12 and ~24 hours, respectively. These observations provide further evidence that suggested that the retroviral infection of hTERT-immortalised CS-A fibroblasts with an *XPC*-specific shRNA vector impaired the removal of CPDs from the global genome, thus suggesting that the *XPC* shRNA had a biological effect on the hTERT-immortalised CS-A cell line. Moreover, the telomerised *XPC*^{KD}/CS-A cell line displayed similar repair capacity for the removal of CPDs as the nontransduced telomerised XP-C (GM02996, XP8CA)

cell line (Fig. 6.16). This provided further supporting evidence for the biological effect of knocking down XPC in the telomerised CS-A cell line.

Surprisingly, however, immuno-slot-blot analysis revealed that the transduction of the hTERT-immortalised CS-A (GM01856, CS3BE) cell line, with the *XPC* shRNA (sequence 2) construct, had minimal affect on the global repair of 6-4PPs from the genome. The level of 6-4PP repair observed in the XPC^{KD}/CS-A cell line was similar to that observed in both the hTERT-immortalised normal MRC-5 and nontransduced isogenic CS-A (GM01856, CS3BE) cell lines (Fig. 6.16). At ~6 hours after UV-irradiation, the hTERT-immortalised XPC^{KD}/CS-A cell line removed 91.5% of 6-4PPs from the genome, while the hTERT-immortalised MRC-5 and CS-A cell lines removed 95.7% and 95.9% of 6-4PPs from the genome, respectively. Moreover, the hTERT-immortalised XPC^{KD}/CS-A cell line removed 93.6% and 95.7% of 6-4PPs from the genome at ~12 and ~24 hours after UV, respectively. As expected, the hTERT-immortalised XP-C (GM02996, XP8CA) cell line removed only 46% of 6-4PPs from the genome ~24 hours after UV-C treatment. Accordingly, although retroviral transduction of the *XPC* shRNA in hTERT-immortalised CS-A fibroblasts had a biological effect on global CPD repair, a similar effect on the removal of 6-4PPs from the global genome was not observed.

From these data, it can be speculated that the greater repair capacity observed in the XPC^{KD}/CS-A cell line was attributed to a failure to completely knockdown the expression of XPC at the translational level. Therefore, it was possible that the hTERT-immortalised XPC^{KD}/CS-A cell line expressed residual levels of XPC protein, which remained undetected by Western blotting or ICC and were sufficient to retain proficient GGR of 6-4PPs, but not CPDs.

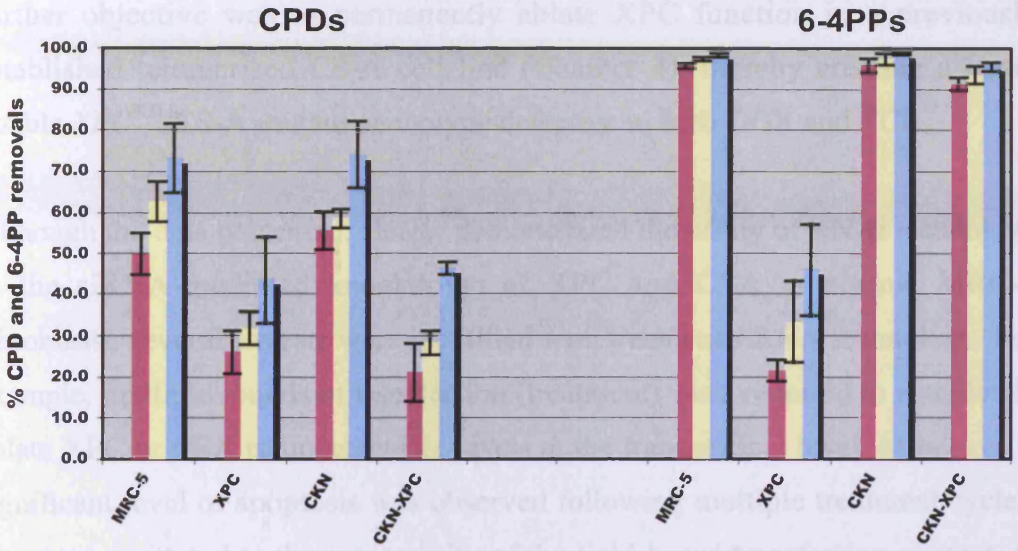

Figure 6.16. Time-course of the removal of CPDs or 6-4PPs from the overall genome in hTERT-immortalised MRC-5, XP-C (GM02996, XP8CA), CS-A (CKN; GM01856, CS3BE) cell lines and CS-A infected with a pRETROSUPER retroviral vector expressing an *XPC*-specific shRNA construct (*XPC*^{KD}/CS-A; clone 10) cell lines irradiated with UV-C (254 nm; 10 J/m^2). Removal of CPDs or 6-4PPs was measured at 6 hrs (purple), 12 hrs (yellow) and 24 hrs (blue) following UV-C treatment, using monoclonal CPD- or 6-4PP-specific antibodies, respectively. Immuno-slot-blot assays were undertaken using 1000 ng of genomic DNA isolated at each time point. Each point represents the mean of three independent biological replicates.

6.5 Discussion

The advent of RNAi-mediated gene silencing technologies has facilitated the establishment of permanent cell lines with loss-of-function phenotypes that recapitulate cells derived from specific genetic backgrounds. The aim of this investigation was to extend the utility of RNAi technologies by transiently ablating XPC or CSA in normal telomerised MRC-5 fibroblasts. Moreover, a further objective was to permanently ablate XPC function in a previously established telomerised CS-A cell line (Chapter 4), thereby creating a novel double XPC^{KD}/CS-A mutant phenotype defective in both GGR and TCR.

Although the data presented, clearly demonstrated the utility of RNAi technology in the siRNA-mediated knockdown of XPC and CSA in normal MRC-5 fibroblasts, several caveats were identified with transient siRNA technology. For example, multiple rounds of transfection (treatment) were required to completely ablate XPC or CSA to undetectable levels at the translational level. Moreover, a significant level of apoptosis was observed following multiple treatment cycles. This was attributed to the cytotoxicity of the lipid-based transfection reagent, as similar levels of apoptosis were observed in telomerised MRC-5 cells, transfected with the non-targeting siRNA scramble control. Therefore, the CRUK SUPER RNAi™ library based on the pSUPER RNAi system (Brummelkamp *et al.*, 2002) and the human SUPER RNAi™ library (Berns, *et al.*, 2004) was used to create a permanent and stable double XPC^{KD}/CS-A knockdown phenotype. This approach, based on an shRNA expression vector system, was adopted to circumvent the multiplicity of experimental caveats associated with siRNA technology, which have been observed here and elsewhere in the literature (reviewed by Dykxhoorn *et al.*, 2003).

To date, the manipulation of the NER pathway, using RNAi-mediated technologies, have been undertaken in NER-proficient cells (Biard *et al.*, 2005; Feng *et al.*, 2006). Evidence presented in this study suggested that the retroviral transduction of telomerised CS-A cells with a pRS vector, expressing an *XPC* shRNA construct, resulted in the creation of a double XPC^{KD}/CS-A mutant

phenotype. This was confirmed by Western blot analysis and ICC, which revealed the isolation of two monoclonal populations (clones 10 and 13) of telomerised CS-A cells with undetectable levels of XPC protein. In agreement, Biard *et al.* (2005) showed that HeLa cells, infected with EBV-based vectors expressing an *XPC* or *XPA* shRNA, displayed undetectable levels of XPC or XPA protein respectively, when maintained in culture for >300 days. However, although XPC protein was undetected in clone 10, the resultant XPC^{KD}/CS-A double mutant phenotype appeared extremely complex, as the loss of XPC protein expression appears to have only partially affected the repair phenotype of the double XPC^{KD}/CS-A mutant. Immuno-slot-blot analysis was undertaken on the XPC^{KD}/CS-A double mutant to determine whether the undetectable levels of XPC protein observed in the telomerised CS-A cell line, infected with the *XPC*-targeted shRNA, had a biological effect on the removal of CPDs and 6-4PPs. Interestingly, the data suggested that the loss of XPC protein expression observed in the XPC^{KD}/CS-A knockdown had a biological effect on the removal of CPDs from the overall genome, as the repair kinetics of CPDs in the XPC^{KD}/CS-A cell line appeared significantly reduced, compared to that observed in the nontransduced isogenic telomerised CS-A cell line. Additionally, the repair kinetics displayed by the XPC^{KD}/CS-A double knockdown was similar to the level of repair observed in the telomerised XP-C cell line. This suggested that the retroviral transduction of the *XPC*-targeted shRNA vector caused a reduction in the global repair of CPDs. In stark contrast, a similar reduction in the global repair of 6-4PPs was not observed, as the level of repair in the overall genome observed in the XPC^{KD}/CS-A double knockdown was similar to that observed in the nontransduced telomerised isogenic CS-A and NER-proficient MRC-5 cell lines. As previously mentioned (Chapter 4), the repair of 6-4PPs can occur at least five-fold faster than that of CPDs (Van Hoffen *et al.*, 1995), and is thought to occur within the first few hours after UV. However, the rate of repair was examined over a limited number of time points (0, 6, 12 and 24 hours) post UV. Accordingly, it is possible that assessing the repair kinetics at earlier time points (0.5-4 hours) would have allowed the detection of slower 6-4PP repair in the telomerised CS-A cell line transduced with an *XPC* shRNA (XPC^{KD}/CS-A) compared to the nontransduced isogenic telomerised CS-A cell line.

Although Western blotting and ICC analysis suggested that the retroviral transduction of the *XPC*-targeted shRNA vector, in a telomerised CS-A cell line, resulted in the complete ablation of XPC expression, the repair data suggested that the *XPC* shRNA had only a partial effect on GGR. The data presented here indicate that the pRS shRNA construct utilised in this investigation may be unable to target the entire *XPC* mRNA transcripts. It is possible that, the XPC^{KD}/CS-A cell line created, may have translated a small amount of XPC protein from residual *XPC* mRNA transcripts that remained untargeted by the *XPC* shRNA. If this is the case, the residual amount of XPC protein was undetectable by Western blotting and ICC. Hence, the residual amount of XPC protein translated by the XPC^{KD}/CS-A double knockdown from the small remaining pool of untargeted mRNA transcripts may have been used preferentially for the global repair of 6-4PPs. In contrast, it appears that low amounts of XPC were insufficient to retain the GGR capacity of CPDs that was observed in the nontransduced CS-A cell line, thus explaining the partial effect. In agreement, Hey *et al.* (2002) showed that the XPC-hHR23B complex preferentially binds 6-4PPs in high affinity. However, conflicting data published by Emmert *et al.* (2000) showed that XPC selectively repairs CPDs compared to 6-4PPs. The precise role(s) of XPC in the removal of different UV-induced lesions remains unclear.

Köberle *et al.* (2006) speculated that NER factors such as XPA, RPA, TFIIH, XPG and ERCC-1-XPF are present at approximately 100,000-200,000 protein molecules per un-irradiated HeLa cell, while XPC is present at about 25,000 protein molecules per cell (Araújo *et al.*, 2001). For this reason, Köberle *et al.* (2006) suggested that XPC provided the obvious target for abolishing GGR by RNAi technology. However, Khan *et al.* (2002) previously showed that low levels of XPC expression (~10 XPC mRNA molecules per cell) were sufficient to maintain normal levels of repair activity in normal cells. This supports the possibility that in the XPC^{KD}/CS-A double knockdown cell line, created in my study, low levels of XPC were sufficient to retain some GGR of 6-4PPs. In contrast, Biard *et al.* (2005) suggested that shRNA-mediated knockdown of XPA and XPC in NER-proficient cells, facilitated the establishment of cell lines that mimic the characteristics of XP cells, namely impaired unscheduled DNA

synthesis. However, they showed that *XPC*^{KD} HeLa cells are more sensitive to UV than *XPA*^{KD} cells.

During this investigation, the XPC^{KD}/CS-A (clone 10) cell line was maintained in culture with puromycin drug selection. The effect of the withdrawal of puromycin on the phenotype of the XPC^{KD}/CS-A cell line was not investigated. Interestingly, Biard *et al.* (2005) showed that the removal of hygromycin B drug selection lead to the loss of the EBV shRNA expressing vectors. This resulted in the restoration of either XPA or XPC protein. Notably, they observed the reversion of the XP phenotype to a wild-type phenotype in HeLa *XPA*^{KD} cells, but not in HeLa *XPC*^{KD} cells, which remained sensitive to UV. Moreover, they showed that hygromycin B withdrawal restored a normal cell cycle arrest in *XPA*^{KD} cells, whereas reverted *XPC*^{KD} cells accumulated at the G_1-early/S transition, thus maintaining the XP phenotype. Biard *et al.* (2005) concluded that a deficiency in XPC triggers irreversible genetic defects. They also speculated that XPC is not only important in DNA repair and mutagenesis, but also in damage signalling and cell cycle progression.

As previously discussed (Chapter 5), many of the core components of the NER machinery (such as XPA, XPB, XPD, XPF, XPG) are not regulated at the transcriptional level. However, it has been shown that *XPC* is a DNA damage-inducible p53-regulated gene that mediates a role in the p53-dependent NER pathway (Adimoolam & Ford, 2002). In agreement, the transcription expression profiling data presented in this thesis (Chapter 5), identified XPC as UV-inducible at the mRNA level in the telomerised nontransduced CS-A cell line. Therefore, it is possible that *XPC* mRNA was transcriptionally upregulated in the XPC^{KD}/CS-A double knockdown in a p53-dependent manner following UV, thus resulting in a higher *XPC* mRNA transcript to *XPC* shRNA ratio, as the expression of the *XPC* shRNA relies upon *de novo* synthesis.

It was previously speculated in this thesis (Section 1.14, Chapter 1) that an *XPC/CSA* null would exhibit the repair kinetics of an *XPA* null cell. However, immuno-slot-blot analysis undertaken on a telomerised XP-A (XP12BE) cell line established in our laboratory revealed that this is not the case (data not shown),

as the repair kinetics observed in the *XPC*^{KD}/CS-A cell line does not reflect the level of repair observed in XP-A cells. In agreement with the data presented here, Verhage *et al.* (1996) showed that although yeast double mutants of *RAD26* (*CSB*) with the GGR determinants *RAD7* (*rad7* and *rad26*) and *RAD16* (*rad16* and *rad26*) appeared more UV sensitive that the single *rad7* or *rad16* mutant strains alone, they were not as sensitive as the completely NER-deficient *rad14* (*XPA*) strain. Verhage *et al.* (1996) speculated that TCR and GGR are partially overlapping. Although the relevance of the yeast data is questionable, as orthologs of the *RAD7* and *RAD16* have yet-to-be identified in humans, the concept that separately removing a TCR gene's and GGR gene's function may not reflect the phenotype of a cell totally defective in NER, remains a possibility. This concept might have been testable via a double knock out, but homozygous *Csa*$^{-/-}$/Xpc$^{-/-}$ double transgenic mice were severely runted and died within a month of birth (van der Horst *et al.*, 2002).

Although Biard *et al.* (2005) recently demonstrated the applicability of RNAi technology, through the establishment of stable and permanent XPA^{KD} and XPC^{KD} null phenotypes, using NER-proficient HeLa cell lines, investigators have shown that NER is severely compromised in transformed cells, due to the abolition of p53 function (Bowman *et al.*, 2000; El-Mahdy *et al.*, 2000; Ferguson & Oh, 2005; Ford *et al.*, 1998; Therrien *et al.*, 1999). In particular, HeLa cells express the viral E6 oncoprotein, which not only abolishes GGR activity, but also inhibits p53-dependent apoptosis in the TCR pathway (Ljungman & Zhang, 1996), thereby potentially reducing the expected death rate observed after UV (Biard *et al.*, 2005). This may explain why they observed a higher sensitivity in the GGR-defective *XPC*^{KD} cells compared to the GGR- and TCR-defective *XPA*^{KD} cells.

It is noteworthy that several telomerised CS-A clones were isolated and propagated, following transduction of the *XPA*-targeted shRNA vector, but none of the clones displayed undetectable XPA protein levels. Hence, a double *XPA*^{KD}/CS-A double total knockdown may create a lethal phenotype.

Recently, Feng *et al.* (2006) demonstrated the potential applicability of RNAi technology in ameliorating the efficacy of tailored cancer therapy by targeting the TCR pathway. They targeted the *CSB* gene, using vector-mediated siRNAs, and found that the inactivation of the *CSB* gene caused HeLa cells to proliferate more slowly and sensitised cells to genotoxicants such as UV and cisplatin (via apoptosis). Additionally, inactivation of *CSB* resulted in spontaneous apoptosis and altered UV-induced cell cycle responses. From these findings, they suggested that CSB provides a potential target, which can be exploited in combination with radiotherapy or chemotherapy.

In summary, the utility of RNAi to investigate DNA repair has been demonstrated. The data presented suggest that, the transfection of *XPC*- or *CSA*-specific 21mer siRNA duplexes in telomerised MRC-5 fibroblasts resulted in the transient suppression of XPC or CSA at the translational level. Several caveats were identified, including the requirement of multiple rounds of treatments to reduce XPC or CSA protein to undetectable levels by western blotting. Moreover, the cytotoxic effect of the lipid-based transfection reagent resulted in extensive apoptosis. This prevented long-term *in vitro* analysis of siRNA generated NER-deficient phenotypes for several reasons. Firstly, the transient nature of the siRNA duplexes suggested that the transfected cells would rapidly lose the NER-defective phenotype and revert back to a wild-type background. Furthermore, as previously mentioned, any long-term *in vitro* investigation of the NER-defective phenotypes would require multiple treatment cycles. Therefore, it would be particularly problematic to determine whether the levels of apoptosis observed in the siRNA transfected cells was attributed to the NER defect exhibited by the cells as a result of knocking down the gene of interest, thereby creating the desired NER defective phenotype, or an artifactual consequence of the cytotoxicity of the transfection reagent. Furthermore, although the utilisation of shRNA technology resulted in the stable knockdown of XPC in the telomerised CS-A dermal fibroblast cell line, the repair data suggested that the ablation of XPC protein resulted only in a partial biological effect. Therefore, although the applicability of RNAi technology has been demonstrated as a possible tool for unravelling the molecular cause of cancer susceptibility (Biard *et al.*, 2005), the data presented here suggests that significant caution should be

applied when using RNAi as a tool to manipulate gene expression for the creation of specific genetic backgrounds. These data also highlight the need for rigorous characterisation at both the biochemical and functional level.

Chapter 7

General Discussion and Future Investigation

In the present study, the characterisation (Ridley *et al.*, 2005) and establishment of hTERT-immortalised XP-C (GM02996, XP8CA) and CS-A (GM01856, CS3BE) dermal fibroblast cell lines was described (Chapters 3 & 4, respectively). From the data presented here, and in concordance with other investigators (Newman *et al.*, 2006; Oullette *et al.*, 2000), it can be concluded that telomerase-mediated immortalisation extends the proliferative capacity of fibroblast cultures irrespective of defects in NER. However, unlike previous investigations (Newman *et al.*, 2006; Oullette *et al.*, 2000), this thesis has extended the investigation to the characterisation of p53/p21$^{WAF1/CIP1}$ and pRb/p16^{INK4A} function in telomerised NER-defective cell lines (Chapter 4). The data suggest that both p53/p21$^{WAF1/CIP1}$ and pRb/p16^{INK4A} activity is retained in *XPC* and *CSA* null cell lines, following the ectopic expression of hTERT. Furthermore, these data confirm the preservation of p53 stabilisation and functionality through phosphorylation at Ser15 and the transcriptional activation of the downstream CDK inhibitor, p21$^{WAF1/CIP1}$. In disagreement with a previous study (Naka *et al.*, 2004), the data presented here also suggests that telomerase-mediated immortalisation is sufficient to maintain cells derived from genome instability and progeroid syndromes in long-term culture without the induction of SIPS.

The characterisation and establishment of hTERT-immortalised XP-C and CS-A cell lines described here, has extended the repertoire of currently available telomerised GGR- and TCR-defective cells that appear to retain the original NER defect displayed by their primary isogenic counterpart. Therefore, the establishment of telomerised XP-C and CS-A cell lines provide an alternative genomically stable *in vitro* cell system to investigate the DNA damage responses

and molecular mechanisms underlying the cellular phenotypes exhibited by XP-C and CS-A.

The microarray experiments undertaken during this investigation exclusively focused on transcription expression profiling the UVC-induced damage responses elicited by telomerised XP-C and CS-A dermal fibroblasts defective in the GGR and TCR subpathways of NER (Chapter 5). However, other investigators have shown that in addition to the general DNA damage responses (such as cell cycle arrest, DNA repair and apoptosis) cells elicit a series of transcriptional responses in a cell-types-specific manner. Therefore, a detailed investigation into the cell-type-specific responses mediated by other skin cell types such as kerationcytes and melanocytes is required (previous investigators have not addressed the differences between cell-type-specific transcription profiles observed in normal compared to NER-defective cell lines). This will facilitate the identification of any cell-type-specific responses in NER-defective cells lines and provide a possible avenue for the elucidation of molecular mechanisms involved in the early initiation, development and progression of cutaneous malignancy in XP patients compared to the normal population. Extending expression profiling to several different cell-types may facilitate the elucidation of the underlying cell-type-specific changes that contribute to the progeroid phenotype observed in CS patients.

Although beyond the scope of the current investigation, the establishment of telomerised cell lines derived from patients representing all XP, CS and TTD complementation groups, would facilitate the generation of comprehensive transcription expression profiles for these syndromes. This would permit the establishment of a molecular taxonomy for the different syndromes (XP, CS and TTD) and complementation groups (XP-A to XP-G, CS-A and CS-B) both in the response to the presence and absence of exogenous and/or endogenous stress (such as UV and oxidative DNA damage). In support of this, Newman *et al.* (2006) recently demonstrated the applicability of expression microarrays in unravelling the role of CSB in chromatin maintenance and remodelling under normal physiological conditions in the absence of external stress. Moreover, comprehensive analysis of the entire transcriptome of the different genetic

backgrounds will facilitate the establishment of transcriptional portraits to give a detailed picture of the complex transcriptional programme presented by these complex NER syndromes. This will potentially facilitate the establishment of sub-classifications of the existing XP and CS complementation groups at the molecular level, in addition to the current complementation groups that are based on classification according to gene defect. As previously discussed (Chapter 3), this is particularly important in CS, as there appears to be no obvious clinical or cellular differences between patients assigned to the CS-A and CS-B complementation groups. Moreover, there also appears to be no correlation between the location or type of mutation and the clinical phenotype. Therefore, the lack of genotype-phenotype relationships in CS, suggests that pathophysiological manifestations presented by CS patients are determined by unknown mechanisms.

In addition to unravelling the precise phenotype-genotype relationships between the NER syndromes (such as XP, CS, TTD, XP-CS, XP-TTD, COFS and $UV^{S}S$), the establishment of a molecular taxonomy may further facilitate the identification of prognostic markers or therapeutic targets for the development of tailored therapies. Moreover, a molecular taxonomy of XP and CS may further assist in elucidating the precise molecular events that promote cutaneous malignancy and progeria in the normal population.

The transcription expression profiling experiments described in Chapter 5, using Affymetrix™ HG-U133A GeneChip® arrays, resulted in the identification of genes differentially regulated in response to UV exposure. Among these genes, were transcription factors, which are requisites to the initiation of many well-characterised responses to DNA damage such as cell cycle arrest, DNA repair and apoptosis. In concordance with previous studies, the ATF/CREB transcription factor, ATF-3, was found significantly upregulated in all cell lines transcription expression profiled in this study. Despite many transcription factors (such as ATF3) being identified as UV-inducible, the precise molecular mechanisms underlying the UV-mediated induction of these genes remains unknown.

Gene expression in eukaryotic organisms is controlled by regulatory elements that recruit transcription factors with specific DNA binding properties (Wei *et al.*, 2006). Although many of the genes (particularly transcription factors and DNA binding proteins) identified in this study and previous investigations are known to define the programmed set of responses of the cell cycle, DNA repair and apoptotic pathways, the precise relationship and interactions between these genes remains poorly delineated. To date, investigators that have characterised the cellular transcriptional response to UV have not attempted to elucidate the functional elements such as TFBS, or the transcriptional gene targets that lie downstream to these transcription factors on a global scale. This in part has been attributed to the lack of experimental tools that facilitate the global mapping of sites of DNA/protein interaction. Until recently, individual ChIP assays were used extensively to characterise DNA/protein interactions and to validate direct targets of transcription factors, such as p53-target genes (Mirza *et al.*, 2003). More recently, Jiang & Sancar (2006) demonstrated the applicability of ChIP in the investigation of DNA repair. They developed a ChIP assay for analysing the binding of repair and checkpoint proteins to DNA base lesions in any given region of the genome. However, this method is highly inefficient and time consuming for identifying transcriptional targets on a global scale. The recent development of ChIP-on-CHIP, which encompasses both ChIP technology and whole-genome tiling arrays, has permitted the global characterisation of DNA/protein interactions and the identification of novel transcriptional targets. This method has been successfully used for whole-genome localisation analysis in yeast (Ren *et al.*, 2000). Until recently, the exploitation of this technology has been limited in humans due to the large size and complexity of the genome. However, the recent development of high-resolution tiling arrays, such as the Affymetrix™ GeneChip® Human Tiling 1.0R or 2.0R Arrays has facilitated the accurate mapping of DNA/protein interactions, novel transcript discovery and the identification of global epigenomic changes such as methylation and acetylation across the entire human genome. Therefore, adopting a ChIP-on-CHIP approach will not only facilitate the identification of novel downstream transcriptional targets to those transcription factors identified in the present expression profiling study (such as ATF3 and p53), but also it will assist in the delineation of the

sequential and temporal response of genes involved in the UVC-induced transcriptional response. For example, inherited polymorphisms in the *TP53* gene has been reported to dictate melanoma risk. Therefore, the variation in the capacity of p53, ATF3 or other transcription factors to induce downstream targets may, in part explain these findings and facilitate the identification of the underlying molecular defects contributing to the XP or CS phenotype. In addition, ChIP-on-CHIP analysis of the telomerised XP-C and CS-A cell lines will permit the identification of molecular defects in the regulation of gene expression such as dysfunctional transcription factor binding, between cell lines defective in GGR, TCR or both. ChIP-on-CHIP analysis over a time course will further facilitate the identification of changes in transcription kinetics, thus permitting the elucidation of subtle differences in transcription initiation and repression between normal and NER-defective phenotypes in response to UV. This is particularly important with regards to CS, as defects in TCR are known to abolish the resumption of basal transcription following UV-irradiation, which may in part explain the delayed and prolonged kinetics of differential gene expression observed in this investigation.

ChIP-on-CHIP will further assist in elucidating possible cross talk between transcription and DNA repair. For example, the multiprotein TFIIH complex has been implicated in orchestrating a multiplicity of functions such as basal transcription, activated transcription, NER and TC-NER. Furthermore, CSA and CSB have been implicated in regulating the phosphorylation state of the RNA Pol II CTD domain, which regulates the initiation of RNA Pol II-dependent transcription.

It is important to note that the UV-responsive genes identified in this investigation represented changes in mRNA transcript levels. However, these changes in expression are not necessarily indicative of rates of transcription, as it is possible that the transcript levels revealed by microarrays is attributed to changes in the rate of transcript degradation. For example, exposure to UV promotes the stabilisation of *c-Fos* mRNA and other short lived mRNAs (Blattner *et al.*, 2000). Therefore, future microarray studies should incorporate the use of transcription inhibitors (such as actinomycin D), to determine whether

the differential regulation of transcription is due a change in transcription rates or degradation.

As previously discussed (Chapter 5), transcription expression profiling operates under the pretense that changes in transcript levels ultimately reflect subsequent changes at the protein level. However, this assumption is not necessarily true with all genes. Furthermore, gene expression profiling provides no information regarding posttranslational modification. Although several genes were investigated at the protein level in the present study (Chapters 4 & 5), proteome wide analysis was beyond the scope of this investigation. Therefore, the utilisation of protein arrays would not only facilitate the global characterisation of protein expression in response to UV exposure, but would further assist in the characterisation of novel protein-protein interactions and posttranslational modifications, such as phosphorylation, ubiquitylation and sumolation. This would be particularly advantageous in understanding how these proteins interact and assist in the regulation of NER, especially as recent evidence implicates the ubiquitin-proteasome pathway in the regulation of NER. A preliminary investigation, undertaken by Cleaver *et al.* (in press) used a protein array (composed of 500 monoclonal antibodies) to screen normal and CS-B cells to identify possible targets for CSB-dependent over-expression at the proteome level.

As previously discussed (Chapters 1 & 3), although the mechanistic function of the p53/p21$^{WAF1/CIP1}$ and pRb/p16^{INK4A} pathways has been rigorously investigated, the precise role(s) of these pathways in NER remain poorly delineated and controversial. Therefore, a combination of ChIP-on-CHIP and proteome wide applications should assist in elucidating the precise role(s) of p53/p21$^{WAF1/CIP1}$ and pRb/p16^{INK4A} in NER and the DNA damage response following UV. In particular, both technologies will help unravel the transcriptional regulation of NER factors (such as *DDB2* and *XPC*) by p53. Moreover, p53 has been implicated in regulating NER through direct interaction with numerous NER factors (such as XPB and XPD), which is independent of transcriptional modifications. Therefore, protein arrays will facilitate the precise characterisation of these interactions and permit the identification of novel

protein-protein interactions between proteins, so revealing physical and functional links between NER and the DNA damage response. For example, Wu *et al.* (2006) recently demonstrated that phosphorylation of XPA at Ser196 by ATR, positively regulated NER activity. From these data, Wu *et al.* (2006) speculated that an ATR DNA damage response facilitated cells to recover from NER-related DNA damage, thus providing evidence for the existence of links between NER and the DNA damage signalling pathways. The implementation of ChIP-on-CHIP and protein array technologies will validate these findings on a global scale.

Although the kinetics of CPD repair has been extensively investigated in defined genomic regions, using the well-established strand-specific DNA repair assay (Bohr *et al.*, 1985), which is based on Southern blot technology and the functional properties of T4 endonuclease V, the repair kinetics of CPDs at the genome wide level remains unknown. Previous investigations have shown a strand bias for the repair of CPDs on the transcribed strand of a limited number of active genes, compared to the nontranscribed strand and transcriptionally silent regions of the genome. In addition to preferential TCR repair, the heterogeneity of CPD repair in mammalian genomic sequences has been observed at many other levels. For example, in addition to the slower repair of CPDs in upstream promoter sequences, a 10-fold faster repair rate has been reported at the transcription initiation site in *Jun* (Tu *et al.*, 1996). Furthermore, the fast repair close to the transcription start site was also observed in the non-transcribed strand (Tu *et al.*, 1996). The complexity of repair kinetics is particularly evident in the transcribed strand, as a gradient of DNA repair has been reported, with the rate decreasing nearer the 3'-end of the gene (Tu *et al.*, 1996). Although TCR was discovered more than 19 years ago (Mellon *et al.*, 1987), no genome wide survey of differential repair has been undertaken. Therefore, it would be of significant interest to extend the utility of the Southern-blot based methodology on a global scale. For example, the strand-specific repair assays could be exploited to measure the repair kinetics of UV-responsive genes identified in this investigation by the transcription expression profiling studies (Chapter 5). This will provide a global picture of repair that will complement the existing expression data obtained from the transcription expression profile

studies. This will also provide further information regarding the association between the kinetics of the DNA damage response elicited following UV and the kinetics of GGR and TCR repair of those genes. It would be particularly interesting to compare the DNA damage response kinetics of differential gene expression observed between the wild-type (MRC-5), GGR-defective (XP-C) and TCR-defective (CS-A) cell lines with their global repair kinetics obtained from Southern blot analysis. A working hypothesis is that those genes activated as part of the cell's initial response to stress are likely to be repaired first by TCR. Therefore, it is possible that, in addition to the rapid repair of the transcribed strand, preferential repair may occur in genes (such as ATF3, p53 and $p21^{WAF1/CIP1}$) that orchestrate the initial DNA damage response.

The microarray data presented here, for the first time, has generated entire genome wide transcriptome profiles for telomerised GGR-defective (XP-C) and TCR-defective (CS-A) cells following UV. However, further investigation is required to delineate the precise cause of the different transcription kinetics observed between the cell lines. It is possible that the delayed and prolonged UV-induced transcriptional responses displayed by the telomerised CS-A cell line is simply attributed to the failure to resume mRNA synthesis following UV damage. Alternatively, the responses may have been attributed to a defect at the molecular level that remains uncharacterised.

Although the transient and stable utility of RNAi was demonstrated in this investigation (Chapter 6), the precise effect of knocking down XPC in the telomerised CS-A cell line on NER remains unclear, as immuno-slot-blot analysis revealed only a partial effect on NER. These findings may have been simply attributed to the presence of undetectable levels of XPC protein that facilitate the preservation of the GGR subpathway, albeit at a reduced activity. Alternatively, these data may provide evidence supporting the suggestion that there is a complex role for XPC in the recognition and repair of different UV-induced photolesions. To further investigate the precise effect of the *XPC*-targeted shRNA vector on the telomerised CS-A cell line, qRT-PCR will facilitate the detection of any residual *XPC* mRNA molecules that have the potential to translate into functional XPC protein. Furthermore, the utilisation of

strand-specific DNA repair assays (as previously discussed) to measure repair along the transcribed and non-transcribed strand should further assist in clarifying the repair phenotypes of the cell line.

Extending the present investigation by exploiting ChIP-on-CHIP and proteomic technologies will further assist in answering many of the remaining questions. However, this will rely on ChIP grade antibodies, specific proteins or tagged varieties of them. For example, the precise mechanistic steps involved in lesion recognition remains poorly understood. Although the formation of a pre-assembled repairosome complex has been largely dismissed, the sequential assembly and dynamics of protein trafficking of the NER apparatus remains to be fully delineated.

A further area of significant controversy includes the cancer-ageing dichotomy in XP and CS. Currently, it is believed that cancer predisposition observed in XP is attributed to the low levels of UV-induced apoptosis, while the neurological dysregulation, progeroid phenotype and lack of cancer susceptibility in CS has been attributed to high levels of DNA-damage-induced apoptosis. Further causes have also been suggested as possible explanations for the lack of cutaneous malignancy in CS such as differences in the immune response, transcriptional efficiency and oxidative metabolism. However, the precise underlying molecular defect(s) that contribute to the CS phenotype remain uncharacterised.

In conclusion, the characterisation and establishment of telomerised GGR-defective (XP-C) and TCR-defective (CS-A) cell lines extends the number of cell lines (to XP-C, CS-A, XP-E, XP-V and CS-B) generated by the ectopic expression of hTERT. These cell lines provide investigators with alternative *in vitro* models of defective NER, to those cell lines traditionally established through oncogenic transformation. The GGR and TCR subpathways of NER are highly complex, and defects in genes encoding protein products that regulate these pathways results in an intricate and a highly pleotrophic set of syndromes. Therefore, the generation of transcription expression portraits will assist in understanding the molecular defects exhibited by cells derived from NER syndromes. Additionally, the transcriptome data will help unravel the

heterogeneous nature of the pathophysiological manifestations displayed by XP and CS patients. Although the mechanistic function of the NER pathway has been well characterised at the level of naked DNA, the intricate network of events that is triggered in cells by DNA damage remains poorly understood. The data presented here contributes to furthering the understanding of these molecular events.

Appendix 1. Gene Ontology Classification of genotype-specific differentially regulated genes (Cluster 1).

Membrane	ALDH3A2, APLP2, ATP6AP2, ATP6V0C, BACE2, BZRP, C16orf30, C20orf35, C20orf59, CLIC3, CMKOR1, COPZ2, COX7A1, CYB561, CYB5R3, CYBA, CYP1B1, DPP4, EFEMP2, FAM26B, FAM38A, FAP, GHR, GOLPH2, GPC4, GPM6B, GPNMB, GPR30, HEPH, HERPUD1, ITGBL1, KCNJ8, KCNK1, KCNK2, LRP10, LRP3, LRRC15, LY6E, MFAP3L, NOTCH3, NRP1, OLFML2B, PGRMC1, PODXL, PSG1, PSG4, PSG9, PTGER3, RAB40B, RHOD, RNF130, SDC1, SLC1A4, SLC22A17, SLC39A4, SLC7A5, SLC7A8, SRPRB, THBD, TMED3, TNFSF9, TSPAN13, UNC5B, VKORC1
Integral to membrane	ADAM12, ALDH3A2, APLP2, ATP6AP2, BACE2, BZRP, C16orf30, C20orf35, C20orf59, CMKOR1, COX7A1, DPP4, FAM26B, FAM38A, FAP, FLJ23191, GABRE, GPM6B, GPNMB, GPR30, HEPH, HERPUD1, ITGBL1, KCNJ8, KCNK1, KCNK2, LRP10, LRP3, LRRC15, MALL, MFAP3L, NOTCH3, NRP1, PLXNC1, PSG1, PSG4, PSG9, PTGER3, RNF130, SGCD, SGCG, SLC22A17, SLC39A4, SLC7A5, SLC7A8, SRPRB, TMED3, UNC5B, VKORC1
Protein binding	ACTA2, ADAM12, AKAP12, APLP2, ASS, BAG1, C20orf35, CCND1, CD99, CDKN2A, CHFR, CLIC3, COL18A1, COL6A1, COMP, DNM1, DPT, EFEMP2, EFS, EMX2, FASN, FKBP1A, FTH1, GHR, HOXA9, HSPB2, ISLR, LDOC1, LMNA, MALL, NBL1, PARVB, PML, PYCARD, RCN3, RNF130, RNF144, SH3BP5, SH3GL1, SLIT3, SPP1, THBS2, THY1, TNC, UNC5B, WISP2
Nucleus	AHNAK, APLP2, C20orf11, CCND1, CDKN2A, CHFR, CLIC3, CMPK, EMX2, EN1, FOXL2, GATA2, HIST2H2AA, HIST2H2BE, HOXA10, HOXA11, HOXA9, HOXC10, HOXC11, HOXC6, ID1, ID2, ID4, IRX5, LDOC1, LMNA, MAFB, MGMT, MSX1, NET1, PML, PRRX1, RNF144, RUNX3, TFAP2C
Integral to plasma membrane	ADRA2A, ANPEP, CCRL1, CD99, CYB561, ENPP2, GABBR2, GABRE, GHR, GOLPH2, GPC4, GPR30, LY6E, NOTCH3, PGRMC1, PODXL, PPAP2A, PTGER3, SDC1, SLC1A4, SLC7A8, THBD, THY1, TNFSF9, TSPAN13
Cytoplasm	AEBP1, AKAP12, ASS, BAG1, C20orf35, CD99, CKB, CLIC3, CMPK, COL18A1, COL1A1, COL1A2, COL5A1, COL5A3, COL6A1, COL6A2, COL8A2, CRIP1, EFS, ELN, EVL, PYCARD, SH3GL1, UPP1
Cell adhesion	ADAM12, AEBP1, CD99, COL18A1, COL5A1, COL5A3, COL6A1, COMP, CXCL12, DPT, EFS, FN1, HSPG2, ISLR, ITGBL1, NRP1, PARVB, PLXNC1, PODXL, SPOCK1, SPP1, THBS2, TNC, WISP2
Metal ion binding	ADAM12, ADAMTS2, ANPEP, ATP6V0C, C9orf3, CHFR, COL18A1, CRIP1, CYB561, CYBA, CYP1B1, FTH1, GATA2, HEPH, HMOX1, IGFBP3, LOX, LOXL1, MT1M, NQO2, PML, RASA4, RNF130, RNF144
Receptor activity	ADRA2A, ANPEP, ATP6AP2, BZRP, CCRL1, CMKOR1, EPS8L2, FKBP1A, GABBR2, GHR, GPR30, LRP10, LRP3, MRC2, NOTCH3, NRP1, PGRMC1, PLXNC1, PTGER3, SRPRB, UNC5B
Signal transduction	ADRA2A, AKAP12, BZRP, CCRL1, CLIC3, CMKOR1, CXCL12, GABBR2, GPR30, GRP, IGFBP6, NET1, NMB, NMU, NRP1, PENK, PTGER3, PYCARD, TNFSF9, UNC5B, WISP2
Extracellular matrix (Sensu Metazoa)	ADAMTS2, BGN, COMP, DCN, DPT, ELN, FBLN2, FBN1, FN1, GPC4, LOX, LTBP2, LUM, MFAP2, MFAP5, SPOCK1, SPP1, THBS2, TIMP3, TNC
Oxidoreductase activity	AKR7A2, ALDH1A3, ALDH3A2, CBR3, CDO1, COX7A1, CYB5R3, CYBA, FASN, FN1, FTH1, GPX7, HEPH, HMOX1, HSD17B12, IDH2, LOX, LOXL1, NQO2, VKORC1
Extracellular space	CXCL12, FBN1, GRP, HSPG2, HTRA1, IGFBP6, LTBP2, MFAP5, PSG1, PSG4, PSG5, PSG6, PSG7, SLIT3, SPOCK1, SPP1, SULF1, TNFAIP2, TNFSF9
Extracellular matrix structural constituent	BGN, COL18A1, COL1A1, COL1A2, COL5A1, COL5A3, COL6A1, COL6A2, COL8A2, COMP, EFEMP2, ELN, FBLN2, FBN1, FN1, LUM, MFAP2, MFAP5, WNT2
Transcription factor activity	AEBP1, EMX2, EN1, FOXL2, GAS7, GATA2, HOXA10, HOXA11, HOXA9, HOXC10, HOXC11, HOXC6, IRX5, MSX1, PML, PRRX1, PRRX2, RUNX3, TFAP2C
Regulation of transcription, DNA-dependent	CDKN2A, EMX2, EN1, FOXL2, GATA2, HOXA10, HOXA11, HOXA9, HOXC10, HOXC11, HOXC6, IRX5, MAFB, MSX1, NOTCH3, PML, PRRX1, PRRX2, RUNX3
Extracellular region	CGB, CLEC11A, CLEC3B, COMP, CTSL, CXCL12, FN1, IGFBP3, INHBB, LOXL1, PSG3, PSG9, SERPINE1, SERPINE2, SERPING1, THBS2, WISP2, WNT2
Development	BST1, CREG1, EMX2, FBN1, HOXA10, HOXA9, HOXC11, HOXC6, ID1, ID2, MSX1, NGFB, PLXNC1, PRRX1, PRRX2, SPOCK1, UNC5B, WNT2
Molecular function unknown	ARMET, AUTS2, BZRP, C10orf116, C21orf2, C9orf16, COL6A1, FN5, GPM6B, HERPUD1, HOXA9, MN1, PSG3, PSG9, RNF130, THY1, TIMP3
Cellular component unknown	ARMET, AUTS2, BZRP, C10orf116, C21orf2, C9orf16, CCND1, CHFR, DSCR1L1, EGFL3, FN5, MN1, NET1, PSG3, RNASE4, THY1
Calcium ion binding	COMP, EFEMP2, EGFL3, FBLN2, FBN1, FKBP9, LTBP2, NOTCH3, PML, RCN3, S100A4, SLIT3, SPARC, SPOCK1, THBD, THBS2
Zinc ion binding	ADAM12, ADAMTS2, ANPEP, C9orf3, CHFR, COL18A1, CRIP1, DKFZP686A01247, GATA2, MT1M, NQO2, PML, RASA4, RNF130, RNF144, SLC39A4
Nucleotide binding	ACTA2, ASS, CMPK, DMPK, DNM1, DSCR1L1, GUK1, MYO1D, NME4, RAB40B, RHOD, RP6-213H19.1, SPHK1, SRP46, SRPRB
Proteolysis and peptidolysis	ADAM12, ADAMTS2, AEBP1, ANPEP, C9orf3, CTSB, CTSF, CTSK, CTSL, DPP4, FAP, HTRA1, LGMN, QPCT, RNF130

Appendix 1. *Continued (cluster 1)*

Biological process unknown	ARMET, AUTS2, BGN, BZRP, C10orf116, C21orf2, C9orf16, CMKOR1, COL1A2, EGFL3, FN5, HOXA9, MN1, PTGER3, THY1
Plasma membrane	ADAM12, ADRA2A, ARFIP2, CCRL1, CD99, ENPP2, FTH1, PLXNC1, PPAP2A, PTGER3, SGCD, SGCG, SLC7A5, SLC7A8
Transferase activity	ABAT, CMPK, DMPK, FASN, GUK1, MGMT, NME4, PRPS1, QPCT, RP6-213H19.1, SAT, SPHK1
Endoplasmic reticulum	ALDH3A2, CYB5R3, CYP1B1, FKBP9, HMOX1, PDIA5, PGRMC1, RCN3, SRPRB, SULF1, TXNDC5, VKORC1
ATP binding	ACTA2, ASS, CMPK, DMPK, GUK1, MXRA5, MYO1D, NME4, RP6-213H19.1, RUNX3, SPHK1
G-protein coupled receptor protein signaling pathway	ADRA2A, AKAP12, APLP2, CCRL1, CMKOR1, CXCL12, ENPP2, GABBR2, GPR30, PTGER3, SPHK1
Protein folding	BAG1, CKAP1, FKBP11, FKBP1A, FKBP9, HSPB2, HSPB3, HSPB7, PDIA5, SGNE1
Metabolism	ALDH1A3, ALDH3A2, ASNS, CBR3, FN1, HSD17B12, IDH2, LHPP, MTHFS, SULF1
Cell differentiation	ANPEP, GAS7, GPM6B, INHBB, NOTCH3, NRP1, SERPINE2, SFRP4, SLIT3, TNFAIP2
Membrane fraction	BACE2, HMOX1, KCNJ8, KCNK1, NRP1, PPAP2A, PSG9, SLC1A4, SPHK1, TSPAN13
Hydrolase activity	ATP6V0C, BST1, DNM1, ENPP2, FAP, LHPP, PPAP2A, PPP1R3C, RNASE4, SULF1
Skeletal development	AEBP1, CLEC3B, COL1A1, COL1A2, COMP, EN1, FBN1, GHR, MSX1
Electron transporter activity	AKR7A2, CDO1, COX7A1, CYBA, CYP1B1, LOXL1, NQO2, PDIA5, TXNDC5
Cell-cell signaling	CXCL12, NGFB, NMB, NRP1, PENK, SPP1, TFAP2C, TNFSF9, WISP2
Ion transport	ATP6V0C, CLIC3, GABRE, HEPH, KCNJ8, KCNK1, KCNK2, SLC22A17, SLC39A4
Negative regulation of cell proliferation	CDKN2A, COL18A1, FTH1, GPNMB, IGFBP6, LDOC1, PPAP2A, TP53I11
cell proliferation	CREG1, CRIP1, ELN, FTH1, GPC4, RUNX3, SPOCK1, TNFSF9
Electron transport	COX7A1, CYB561, CYB5R3, CYBA, CYP1B1, NQO2, PDIA5, TXNDC5
Organogenesis	COL18A1, COL5A3, COMP, DCN, ELN, EVL, MSX1, NRP1
Phosphate transport	COL18A1, COL1A1, COL1A2, COL5A1, COL5A3, COL6A1, COL6A2, COL8A2
Transcription	CDKN2A, FOXL2, GATA2, MAFB, NOTCH3, PML, RUNX3, TFAP2C
Apoptosis	BAG1, CDKN2A, MAGEH1, PML, RNF130, SULF1, TNFSF9, UNC5B
Structural molecule activity	COL18A1, COL5A1, EGFL3, HSPG2, LMNA, SLIT3, THBS2
Mitochondrion	ABAT, BZRP, COX7A1, CYBA, IDH2, NME4, SH3BP5
GTP binding	ARFIP2, DNM1, ELN, RAB40B, RHOD, SGNE1, SRPRB
Golgi stack	AKR7A2, C20orf35, COPZ2, GOLPH2, RP6-213H19.1, SULF1, TMED3
Collagen	COL18A1, COL1A1, COL1A2, COL5A1, COL5A3, COL6A1, COL6A2
Neurogenesis	AHNAK, EVL, GAS7, GPM6B, NRP1, SERPINE2, SPOCK1
Pregnancy	PSG1, PSG3, PSG4, PSG5, PSG6, PSG7, PSG9
Cytoskeleton	ACTA2, DSP, PARVB, SGCD, SGCG, TNS1
Regulation of cell growth	CREG1, HTRA1, IGFBP3, IGFBP6, NET1, WISP2
Cell cycle	CCND1, CDKN2A, CHFR, MN1, NBL1, PYCARD
Iron ion binding	CDO1, CYB561, CYBA, CYP1B1, HEPH, HMOX1
DNA binding	APLP2, CDKN2A, HIST2H2AA, HIST2H2BE, MGMT, SPHK1
Magnesium ion binding	DMPK, MTHFS, NME4, PRPS1, RP6-213H19.1, SPHK1
Protein modification	BACE2, BAG1, HERPUD1, LOX, LOXL1, QPCT
Growth factor activity	CLEC11A, CXCL12, GRP, INHBB, NGFB, SPP1
Soluble fraction	ASNS, GRP, NMB, PENK, SPHK1, WISP2
Kinase activity	CMPK, GUK1, MRC2, NME4, PRPS1
Lysosome	CTSB, CTSF, CTSK, CTSL, LGMN
Transmembrane receptor protein	COL1A2, FN1, LOX, SPARC, TIMP3

Appendix 1. *Continued (cluster 1)*

Tyrosine kinase signaling pathway	
Visual perception	COL18A1, CYP1B1, FBN1, LUM, TIMP3
Transport	C20orf59, SGNE1, SLC1A4, SLC7A5, SLC7A8
Regulation of transcription from RNA polymerase II promoter	CREG1, HOXC6, ID1, ID4, TFAP2C
Catalytic activity	FASN, KCNK2, LHPP, PML, PODXL
Muscle development	AEBP1, COL5A3, LMNA, SGCD, SGCG
Intracellular signaling cascade	EFS, RASA4, SH3BP5, SPHK1, TNS1
Defence response	INHBB, LY6E, PSG3, PSG4, PSG9
Heparin binding	COL5A1, FN1, PCOLCE2, SERPINE2, THBS2
Morphogenesis	EN1, GPC4, HOXA11, HOXC10, NOTCH3
Cytosol	CBR3, HSPB2, MTHFS, SPHK1, THY1
Copper ion binding	HEPH, LOX, LOXL1, MT1M, SPARC
Immune response	CCRL1, CXCL12, DPP4, FTH1, TNFSF9
Isomerase activity	FKBP11, FKBP1A, FKBP9, PDIA5, TXNDC5
Neuropeptide signaling pathway	GRP, NMB, NMU, PENK, SGNE1
Actin binding	DKFZP686A01247, MYO1D, PARVB, PDE4DIP, TNS1
Nucleic acid binding	CLEC11A, ENPP2, PML, RNASE4, SRP46
Rhodopsin-like receptor activity	ADRA2A, CCRL1, CMKOR1, GPR30, PTGER3
Serine-type endopeptidase inhibitor activity	APLP2, SERPINE1, SERPINE2, SERPING1
Blood coagulation	EFEMP2, SERPINE1, SERPING1, THBD
Circulation	CXCL12, CYB5R3, ELN, SERPING1
Microsome	ALDH3A2, CYP1B1, HMOX1, PGRMC1
Insulin-like growth factor binding	HTRA1, IGFBP3, IGFBP6, WISP2
Peptidase activity	BACE2, HTRA1, QPCT, RNF130
Negative regulation of progression through cell cycle	CDKN2A, MN1, NBL1, PYCARD
Basement membrane	COL8A2, EFEMP2, HSPG2, SPARC
Unfolded protein binding	BAG1, CKAP1, HSPB7, SGNE1
Cell motility	ADRA2A, ARFIP2, ENPP2, SPOCK1
Actin cytoskeleton organization and biogenesis	ADRA2A, ARFIP2, ARHGAP8, PDE4DIP
Angiogenesis	ANPEP, NRP1, THY1, TNFAIP2
Aminopeptidase activity	ANPEP, C9orf3, DPP4, FAP
Ligase activity	ASNS, ASS, CHFR, MTHFS
Sugar binding	CLEC11A, CLEC3B, MRC2, THBD
Synaptic transmission	ABAT, DNM1, GABBR2, QPRT
Potassium ion transport	EN1, KCNJ8, KCNK1, KCNK2
Response to unfolded protein	HERPUD1, HSPB2, HSPB3, HSPB7
Cytoskeleton organization and biogenesis	PDE4DIP, SGCD, SGCG, THY1
Positive regulation of cell proliferation	ADRA2A, CLEC11A, HOXC10, NRP1

Appendix 1. *Continued (cluster 1)*

Anti-apoptosis	BAG1, SPHK1, SPP1, TXNDC5
Epidermis development	ALDH3A2, COL1A1, DSP
Intracellular	CTSB, PDE4DIP, PML
Regulation of apoptosis	CTSB, PYCARD, RP6-213H19.1
Neutral amino acid transporter activity	SLC1A4, SLC7A5, SLC7A8
RNA polymerase II transcription factor activity	CREG1, HOXC10, HOXC11
Transcription corepressor activity	CREG1, HOXC6, ID4
Coated pit	DNM1, LRP10, LRP3
Transcription regulator activity	ID1, ID2, ID4
Regulation of transcription	ID1, ID2, ID4
Collagen binding	FN1, LUM, SPARC
Iron ion transport	CYB5R3, FTH1, HEPH
Central nervous system development	ALDH3A2, DSCR1L1, SLIT3
Cell surface receptor linked signal Transduction	BAG1, EVL, LY6E
Nucleoside metabolism	NME4, PRPS1, UPP1
Signal transducer activity	HMOX1, NGFB, WNT2
Chemotaxis	CCRL1, CXCL12, ENPP2
Ubiquitin cycle	CHFR, FBXL8, RNF144
Ion channel activity	GABRE, KCNK1, KCNK2
Protein transport	C20orf35, RAB40B, TMED3
Voltage-gated ion channel activity	KCNJ8, KCNK1, KCNK2
Potassium channel activity	KCNJ8, KCNK1, KCNK2
Voltage-gated potassium channel complex	EN1, KCNJ8, KCNK1
Potassium Ion binding	KCNJ8, KCNK1, KCNK2
DNA repair	ELN, MGMT, PML
Hormone activity	CGB, INHBB, NMB
Cell cycle arrest	CDKN2A, GAS7, PML
Cell-cell adhesion	COL6A2, COL8A2, THY1
Endonuclease activity	ELN, ENPP2, RNASE4
Protein amino acid phosphorylation	DMPK, MXRA5, RP6-213H19.1
Rho protein signal transduction	ADRA2A, ARHGEF3, RHOD
Peptidyl-prolyl cis-trans isomerase activity	FKBP11, FKBP1A, FKBP9
GTP biosynthesis	GUK1, NME4
Structural constituent of cytoskeleton	ACTA2, DSP
Intermediate filament	DSP, LMNA
Cell surface	PGRMC1, SULF1
Enzyme inhibitor activity	SGNE1, TIMP3
Sensory perception	CXCL12, TIMP3

Appendix 1. *Continued (cluster 1)*

Amino acid metabolism	SLC7A5, SLC7A8
Amino acid transport	SLC7A5, SLC7A8
Amino acid permease activity	SLC7A5, SLC7A8
Endocytosis	GHR, LRP10
Microtubule	CKAP1, DNM1
Sh3 domain binding	EVL, SH3BP5
Guanyl-nucleotide exchange factor activity	FLJ10357, NET1
Cytochrome-B5 reductase activity	CYB561, CYB5R3
Aldehyde dehydrogenase [Nad(P)+] activity	ALDH1A3, ALDH3A2
Aldehyde metabolism	AKR7A2, ALDH3A2
Lipid metabolism	ALDH1A3, ALDH3A2
Small GTPase mediated signal transduction	ARFIP2, RAB40B
Carbohydrate metabolism	AKR7A2, IDH2
Collagen type I	COL1A1, COL1A2
Perception of sound	COL1A1, COL1A2
Structural constituent of bone	COL1A1, COL1A2
Heme binding	CYBA, CYP1B1
Nucleosome	HIST2H2AA, HIST2H2BE
Chromosome	HIST2H2AA, HIST2H2BE
Nucleosome assembly	HIST2H2AA, HIST2H2BE
Chromosome organization and biogenesis (Sensu Eukaryota)	HIST2H2AA, HIST2H2BE
Protein complex assembly	PML, SLC7A8
Membrane alanyl aminopeptidase Activity	ANPEP, C9orf3
ER-golgi intermediate compartment	ANPEP, FN1
Metallopeptidase activity	ANPEP, C9orf3
Metalloendopeptidase activity	ADAM12, FAP
Integrin-mediated signaling pathway	ADAM12, ITGBL1
Transferase activity, transferring glycosyl groups	QPRT, UPP1
Collagen type V	COL5A1, COL5A3
Microfibril	MFAP2, MFAP5
Response to stress	PDIA5, TP53I11
Calcium-mediated signaling	DSCR1L1, SPHK1
Protein-lysine 6-oxidase activity	LOX, LOXL1
Positive regulation of I-kappa B kinase/Nf-Kappa B cascade	FKBP1A, HMOX1
Transmembrane receptor activity	EFEMP2, THBD
Intracellular protein transport	COPZ2, SGNE1
Enzyme activator activity	HSPB2, SGNE1

Appendix 1. *Continued (cluster 1)*

Peptide hormone processing	BACE2, SGNE1
Transcription from RNA polymerase II promoter	GATA2, RUNX3
Receptor mediated endocytosis	DNM1, LRP3
Chloride transport	CLIC3, GABRE
Postsynaptic membrane	GABBR2, GABRE
Regulation of progression through cell cycle	CCND1, LTBP2
Protein targeting	AKAP12, LTBP2
Protein secretion	BACE2, LTBP2
Amino acid biosynthesis	ASNS, ASS
Acyltransferase activity	QPCT, SAT
Cytokine activity	INHBB, SPP1
Growth	GHR, INHBB
Protein homodimerization activity	FAP, INHBB
Cell-matrix adhesion	ITGBL1, SPP1
Transcription coactivator activity	PML, PRRX1
Receptor binding	NMU, PLXNC1
Neuropeptide hormone activity	GRP, PENK
Sarcoglycan complex	SGCD, SGCG
Binding	APLP2, FTH1
GTPase activator activity	ARHGAP8, RASA4
G1/S transition of mitotic cell cycle	CCND1, PML
Cell division	CCND1, CHFR
Protein kinase C activation	PPAP2A, SPHK1
Extracellular matrix organization and biogenesis	COL6A2, COL8A2
Protein binding, bridging	COL6A2, COL8A2
Lipid raft	MALL, THY1
Nucleotide metabolism	ENPP2, NME4
Vascular endothelial growth factor receptor activity	MXRA5, NRP1
Negative regulation of adenylate cyclase activity	ADRA2A, GABBR2
Ossification	SPARC, SPP1
Integrin binding	SPP1, THY1
Gtpase activity	DNM1, RHOD
Dipeptidyl-peptidase IV activity	DPP4, FAP
Prolyl oligopeptidase activity	DPP4, FAP
Lamellipodium	EVL, FAP
Induction of apoptosis	PML, PYCARD
Axon guidance	EVL, NRP1
Motor activity	DNM1, MYO1D
Calmodulin binding	MYO1D, SPHK1

Appendix 1. *Continued (cluster 1)*

Protein serine/threonine kinase activity	DMPK, RP6-213H19.1
Protein self binding	DMPK, RP6-213H19.1
Transporter activity	C20orf59, SLC22A17
Regulation of heart contraction rate	DMPK, HSPB7
Positive regulation of cell migration	ARHGAP8, SPHK1

Appendix 1. *Continued (cluster 2)*

Membrane	ABCB1, AMFR, ATP9A, CDH13, ChGn, CLGN, CSF1, GPR56, GPRC5B, IL13RA2, ITGB5, LGALS3BP, NT5E, OSTM1, PDGFRL, PTGS1, SLC1A1, SLC6A15, SRPX, STOM, TRPV2, TSPAN12
Protein binding	AMFR, CDH13, ChGn, COL15A1, GPR56, ICAM2, INHBA, ITGB5, LGALS3BP, SNCA, SPON2, SRPX
Integral to membrane	ABCB1, AMFR, ATP9A, ChGn, CLGN, CSF1, GPRC5B, IL13RA2, ITGB5, OSTM1, TSPAN12
Integral to plasma membrane	EDNRB, GPR56, ICAM2, MME, SEMA4F, SLC1A1, SLC6A15, STOM, TRPV2
Metal ion binding	AMFR, ChGn, LPXN, ME1, MME, NT5E, PIR, PTGS1, SOD2
Cell adhesion	CDH13, COL15A1, GPR56, ITGB5, LGALS3BP, LPXN, SPON2, SRPX
Receptor activity	AMFR, EDNRB, GPR56, GPRC5B, IL13RA2, ITGB5, PDGFRL, SEMA4F
Nucleus	HOXB5, HOXB6, HOXB7, PHLDA1, PIR, PTGS1, SVIL, TCF21
Extracellular space	AKR1B1, BMP2, CSF1, IL13RA2, LGALS3BP, SPON2
Nucleotide binding	ABCB1, ATP9A, CUGBP2, MYO6, NT5E, TUBA3
Cell-cell signaling	BMP2, GPR56, INHBA, MME, SEMA4F, STC1
Signal transduction	AMFR, GPR56, GPRC5B, LGALS3BP, LPXN
Cytoplasm	COL15A1, LPXN, PTGS1, SNCA, SVIL
Plasma membrane	EDNRB, ICAM2, MME, SEMA4F, SVIL
Membrane fraction	ABCB1, NT5E, SEMA4F, SLC1A1, TSPAN12
Development	HOXB6, HOXB7, ITGB5, SPON2
Oxidoreductase activity	AKR1B1, ME1, PTGS1, SOD2
Zinc ion binding	AMFR, LPXN, MME, NT5E
Calcium ion binding	CDH13, CLGN, SVIL, TRPV2
Cell differentiation	COL15A1, CSF1, INHBA, SEMA4F
Neurogenesis	ChGn, EDNRB, INHBA, SEMA4F
Regulation of transcription, DNA-Dependent	HOXB5, HOXB6, HOXB7, TCF21
Extracellular matrix (Sensu Metazoa)	COL15A1, LGALS3BP, SPON2
Carbohydrate metabolism	AKR1B1, GLB1, ME1
Hydrolase activity	ATP9A, BCHE, DUSP3
Perception of sound	COCH, EDNRB, MYO6
Extracellular region	BCHE, INHBA, STC1
Transcription factor activity	HOXB5, HOXB6, HOXB7
ATP binding	ABCB1, ATP9A, MYO6
Electron transporter activity	AKR1B1, ME1
Lysosome	CTSC, GLB1
Proteolysis and peptidolysis	CTSC, MME
Immune response	CTSC, SPON2
Endoplasmic reticulum	AMFR, CLGN
Structural molecule activity	COL15A1, TUBA3
Hormone activity	INHBA, STC1
Cell surface receptor Linked signal Transduction	INHBA, STC1

Appendix 1. *Continued (cluster 2)*

Mesoderm development	INHBA, TCF21
Cell surface	ABCB1, SRPX
Iron ion binding	PIR, PTGS1
Cytokine activity	BMP2, INHBA
Growth factor activity	BMP2, INHBA
Growth	BMP2, INHBA
Morphogenesis	ChGn, HOXB5
Soluble fraction	ChGn, IL13RA2
Symporter activity	SLC1A1, SLC6A15
Biological process unknown	MYO6, SLC35F2
Molecular function unknown	MYO6, SLC35F2
Cell proliferation	ChGn, CSF1
Transport	ABCB1, SLC1A1
Atpase activity	ABCB1, ATP9A
Axon guidance	SEMA4F, SPON2
Cation transport	ATP9A, TRPV2

Appendix 1. *Continued (cluster 3)*

Nucleus	ABL1, ARID5B, BACH1, CREBBP, CUGBP1, DUSP10, HMGA2, HSA9761, IRS1, MEIS2, MSX2, NCOR1, NUP153, RBPSUH, SMURF2, SYNCRIP, TEAD4, TFAP2A, ZFHX1B
Protein binding	ABL1, CREBBP, CSNK2A1, IRS1, MARCH7, MSX2, NCOR1, NUP153, PPP2R2A, PSEN1, RBPSUH, SMURF2, TFAP2A
Regulation of transcription, DNA-dependent	ABL1, BACH1, CREBBP, HMGA2, MEIS2, MSX2, NCOR1, TEAD4, TFAP2A, ZFHX1B
Signal transduction	ARHGEF7, CREBBP, IRS1, PPP2R2A, PPP4R1, PRKAR2A, STAM, STK24, TFAP2A
Nucleotide binding	ABL1, CSNK2A1, CUGBP1, MAP4K3, PRKAR2A, STK24, SYNCRIP, TRIB2
Transcription factor activity	BACH1, CREBBP, MEIS2, MSX2, RBPSUH, TEAD4, TFAP2A, ZFHX1B
Protein amino acid phosphorylation	ABL1, CSNK2A1, MAP4K3, PRKAR2A, STK24, TRIB2
Transferase activity	ABL1, CREBBP, CSNK2A1, HSA9761, MAP4K3, STK24
Transcription	ARID5B, BACH1, HMGA2, RBPSUH, TEAD4, TFAP2A
DNA binding	ABL1, ARID5B, HMGA2, NCOR1, NUP153
Zinc ion binding	CREBBP, MARCH7, NUP153, USP3, ZFHX1B
Metal ion binding	CREBBP, MARCH7, NUP153, USP3, ZFHX1B
ATP binding	ABL1, CSNK2A1, MAP4K3, STK24, TRIB2
Cytoplasm	CREBBP, DUSP10, IRS1, PRKAR2A, TRIB2
Membrane	ITGB1BP1, NETO2, PSEN1, SPTAN1
Integral to membrane	NETO2, NUP153, PSEN1
Intracellular signaling cascade	ABL1, PRKAR2A, PSEN1
Membrane fraction	PRKAR2A, PSEN1, SPTAN1
Ubiquitin-dependent protein catabolism	SMURF2, USP3, USP47
Ubiquitin cycle	SMURF2, USP3, USP47
Protein serine/threonine kinase activity	CSNK2A1, MAP4K3, STK24
Transcription corepressor activity	MEIS2, NCOR1
Transcription from RNA polymerase II promoter	NCOR1, RBPSUH
RNA binding	PUM2, SYNCRIP
Binding	PPP4R1, PUM2
Structural constituent of cytoskeleton	KRT18, SPTAN1
Regulation of progression through cell cycle	ABL1, G0S2
Protein-tyrosine kinase activity	ABL1, STK24
Molecular function unknown	ABL1, G0S2
Cellular component unknown	ABL1, G0S2
Transcription coactivator activity	CREBBP, TFAP2A
Signal transducer activity	CREBBP, IRS1
Protein amino acid dephosphorylation	DUSP10, PPP2R2A
Plasma membrane	PRKAR2A, SSFA2
Protein kinase cascade	ITGB1BP1, MAP4K3
Endoplasmic reticulum	PSEN1, SYNCRIP
Chromosome organization and biogenesis (Sensu Eukaryota)	HMGA2, PSEN1

Appendix 1. *Continued (cluster 3)*

Negative regulation of transcription	SMURF2, ZFHX1B
Transcriptional repressor activity	ARID5B, ZFHX1B
Regulation of transcription from RNA polymerase II promoter	TEAD4, TFAP2A
Skeletal development	MSX2, TEAD4
Development	HMGA2, MSX2
Kinase activity	PRKAR2A, STK24
Rna polymerase II transcription factor activity	RBPSUH, TEAD4
Negative regulation of transcription, DNA-dependent	ARID5B, RBPSUH
Ribonucleoprotein complex	CUGBP1, SYNCRIP
Response to stress	DUSP10, MAP4K3
JNK Cascade	DUSP10, MAP4K3
Cysteine-type endopeptidase activity	USP3, USP47
Ubiquitin thiolesterase activity	USP3, USP47

Appendix 1. *Continued (cluster 4)*

Membrane	ABCB1, ABCG2, ADFP, ADORA2B, C9orf125, EDG2, EGFL5, EREG, F3, FZD6, GBP1, GPR37, GPRC5A, HRASLS3, HRH1, HSD17B2, LAMA5, MAN1C1, NID2, OGFRL1, OPN3, PPP2R1B, PTGER2, PTGER4, PTPRK, RAPGEF2, RTN1, SCN9A, SLC16A6, SLC7A11, SLITRK5, STAMBP, STOM, SV2A, SYNGR3, SYT11, TBC1D8, TEK, TJP2, TM4SF1, TRHDE, TRPA1, UCP2
Protein binding	ACTG2, ADRB2, APBA2, ARTS-1, BID, CASP1, CASP4, COL4A6, DMN, EREG, FOXF1, FST, GNAI1, IKBKAP, LAMA5, MCAM, NEO1, PDLIM1, PPARG, PPP2R1B, RAPGEF2, RBMX, RBPMS, RELN, RHOBTB3, RPP30, SAV1, STAMBP, TACC1, TJP2
Nucleus	AFF1, CDC14B, CREB1, ETS2, FOXF1, FOXF2, GATA3, HHEX, HNRPL, HOXA2, HOXA5, MEIS1, NR2F1, NR2F2, PARP4, PITX1, PLAGL2, POLB, PPARG, PPP2R1B, RPP30, STAMBP, TACC1, TBX2, TJP2
Integral to plasma membrane	ADORA2B, ADRB2, BDKRB1, BDKRB2, EDG2, EREG, F2R, FZD6, GPR37, GPRC5A, HRH1, MCAM, NEO1, OPN3, PTGER2, PTPRK, RAPGEF2, SLC16A6, STOM, SYNGR3, TEK, TJP2, TM4SF1, TRHDE, TRPA1
Integral to membrane	ABCB1, ABCC4, ABCG2, ARTS-1, C9orf125, EDG2, EGFL5, F3, HRASLS3, HSD17B2, LAMA5, MAN1C1, MCTP2, NEO1, OPN3, PTGER4, RTN1, SLC16A6, SLC7A11, SLITRK5, SV2A, SYT11, TMEM35, UCP2
Signal transduction	ADORA2B, BDKRB1, CASP1, CREB1, EDG2, F2R, GNAI1, GPR37, GPRC5A, HRH1, IGFBP5, NR2F1, NR2F2, NRGN, OPN3, PLAU, PPARG, PTGER2, PTGER4, RTN1, SAV1, TEK, TRHDE
Transcription factor activity	AFF1, CREB1, ETS2, FOXF1, FOXF2, GATA3, HHEX, HOXA2, HOXA5, MEIS1, NR2F1, NR2F2, PITX1, PLAGL2, PPARG, TBX2
Receptor activity	ADORA2B, ADRB2, BDKRB1, BDKRB2, EDG2, F2R, FZD6, GPR37, GPRC5A, HRH1, OGFRL1, OPN3, PTGER2, PTGER4, PTPRK, TEK
Nucleotide binding	ABCB1, ABCC4, ABCG2, ACTG2, GBP1, GNAI1, HNRPL, IGF2BP3, MAP3K5, MYLK, RBMX, RBPMS, TEK
G-protein coupled receptor protein signaling pathway	ADORA2B, ADRB2, BDKRB1, BDKRB2, EDG2, F2R, FZD6, GNAI1, GPR37, GPRC5A, OPN3, PTGER2, PTGER4
Cytoplasm	BID, CASP4, COL4A1, COL4A2, COL4A5, COL4A6, DUSP6, IGF2BP3, JUP, KYNU, POLB, TPP2
Regulation of transcription, DNA-dependent	CREB1, ETS2, FOXF2, GATA3, HHEX, HOXA2, HOXA5, MEIS1, NR2F1, PITX1, PLAGL2, TBX2
Calcium ion binding	EGFL5, HGF, LTBP1, MAN1C1, MCTP2, MYLK, NID2, NPTX1, RAPGEF2, SCN9A, SYT11
ATP binding	ABCB1, ABCC4, ABCG2, ACTG2, FRY, MAP3K5, MYLK, NEO1, PALLD, TEK
Extracellular region	ADFP, ARTS-1, FST, IGFBP5, IGFBP7, NOV, PLAT, SEMA3A, STC1, TFPI
Zinc ion binding	ARTS-1, C14orf130, GATA3, NR2F1, NR2F2, PDLIM1, PLAGL2, PPARG, STAMBP, TRHDE
Metal ion binding	ARTS-1, C14orf130, GATA3, NR2F1, NR2F2, PDLIM1, PLAGL2, PPARG, STAMBP, TRHDE
Development	FST, FZD6, HHEX, HOXA2, HOXA5, MEIS1, NEO1, RELN, SEMA3F, TBX2
Rhodopsin-like receptor activity	ADORA2B, ADRB2, BDKRB1, BDKRB2, F2R, GPR37, HRH1, OPN3, PTGER2, PTGER4
Membrane fraction	ABCB1, ABCC4, BID, JUP, MCTP2, SCN9A, SLC16A6, TRPA1, UCP2
Transport	ABCB1, ABCG2, NPTX1, PARP4, SLC16A6, SLC7A11, SV2A, SYT11, UCP2
Plasma membrane	ABCC4, ADRB2, BDKRB1, BDKRB2, EDG2, F2R, F3, MCAM, NEO1
Cell adhesion	COL4A6, JUP, LAMA5, MCAM, NEO1, NID2, RELN, VCL
Hydrolase activity	CDC14B, DUSP6, KYNU, MTMR1, NT5C2, PPT1, PTPRK, RPP30
Proteolysis and peptidolysis	CASP1, CASP4, HGF, PGA5, PLAT, PLAU, TPP2, TRHDE
Biological process unknown	ABCC4, DOC1, EGFL5, HRASLS3, LTBP1, RBMX, RHOBTB3, TM4SF1
Transcription	FOXF1, FOXF2, GATA3, NR2F1, NR2F2, PLAGL2, PPARG, TBX2
Protein amino acid phosphorylation	IKBKAP, MAP3K5, MYLK, NEO1, PALLD, TEK
Blood coagulation	F2R, F3, HGF, PLAT, PLAU, TFPI
Transferase activity	GYG2, MAP3K5, MYLK, POLB, SMS, TEK
Signal transducer activity	CASP1, GNAI1, IKBKAP, MYLK, RAPGEF2, RTN1

Appendix 1. *Continued (cluster 4)*

Protein amino acid dephosphorylation	CDC14B, DUSP6, MTMR1, PPP2R1B, PTPRK, TNS3
Transporter activity	ABCB1, ABCG2, SLC16A6, SV2A, SYT11, UCP2
Extracellular space	EREG, PLAU, PTN, RELN, SEMA3F, WFDC1
Neurogenesis	APBA2, NRGN, PPT1, PTN, SEMA3A
Cytoskeleton	ACTG2, JUP, PDLIM1, STOM, TMOD1
Peptidase activity	KYNU, PLAT, PLAU, RELN, TPP2
Regulation of progression through cell cycle	DUSP6, EREG, F2R, PPP2R1B, PTN
Cytosol	ALDH1A1, ARTS-1, BID, NT5C2, PPP2R1B
Cellular component unknown	ABCC4, EGFL5, HGF, HRASLS3, MTMR1
Molecular function unknown	DOC1, HRASLS3, RTN1, TM4SF1, WFDC1
Morphogenesis	F2R, GATA3, IGF2BP3, MCAM, PITX1
Cell-cell signaling	EREG, NEO1, STC1, TEK, TRHDE
Structural molecule activity	EGFL5, JUP, LAMA5, VCL
Oxidoreductase activity	ALDH1A1, ALDH2, HSD17B2, VCL
Sensory perception	BDKRB2, OPN3, PPT1, TRPA1
Soluble fraction	DUSP6, GYG2, JUP, PPP2R1B
Mitochondrion	ALDH2, BID, PPP2R1B, UCP2
Metabolism	ALDH1A1, ALDH2, HSD17B2, ISOC1
Inflammatory response	BDKRB1, BDKRB2, HRH1, PARP4
Immune response	F3, GBP1, IKBKAP, PTGER4
Kinase activity	IKBKAP, MYLK, PLAU, TEK
Ubiquitin cycle	C14orf130, NEDD4, STAMBP, USP46
Protein tyrosine phosphatase activity	CDC14B, DUSP6, MTMR1, PTPRK
RNA binding	HNRPL, IGF2BP3, RBMX, RBPMS
Growth factor activity	EREG, HGF, NOV, PTN
Extracellular matrix structural constituent	COL4A1, COL4A2, COL4A5, COL4A6
Collagen	COL4A1, COL4A2, COL4A5, COL4A6
Collagen type IV	COL4A1, COL4A2, COL4A5, COL4A6
Phosphate transport	COL4A1, COL4A2, COL4A5, COL4A6
Cell cycle	HRASLS3, LOH11CR2A, TACC1
Cell motility	F2R, NEO1, VCL
Regulation of cell growth	IGFBP5, IGFBP7, NOV
Insulin-like growth factor binding	IGFBP5, IGFBP7, NOV
Catalytic activity	DOC1, ISOC1, MEST
Response to drug	ABCB1, ABCG2, PARP4
Protein complex assembly	IKBKAP, PPP2R1B, SLC7A11
Magnesium ion binding	MAP3K5, MYLK, POLB
Extracellular matrix (Sensu Metazoa)	LAMA5, LTBP1, RELN
Positive regulation of cell proliferation	PTN, STAMBP, TBC1D8
ATPase activity	ABCB1, ABCC4, ABCG2
Endoplasmic reticulum	ADFP, BDKRB1, RTN1
Positive Regulation Of I-Kappa B	CASP1, EDG2, F2R

Appendix 1. *Continued (cluster 4)*

Elevation of cytoplasmic calcium ion concentration	BDKRB1, BDKRB2, EDG2
Serine-type endopeptidase activity	HGF, PLAU, RELN
Transcription coactivator activity	FOXF1, FOXF2, NR2F1
Regulation of transcription from RNA polymerase II promoter	FOXF1, NR2F2, PPARG
Steroid hormone receptor activity	NR2F1, NR2F2, PPARG
Protein serine/threonine phosphatase activity	CDC14B, DUSP6, MTMR1
Intracellular	CASP1, CASP4, NEDD4
Vascular endothelial growth factor receptor activity	NEO1, PALLD
Actin binding	TMOD1, VCL
Lysosome	ADRB2, PPT1
Protein modification	PLAT, PPT1
Visual perception	OPN3, PPT1
Negative regulation of cell proliferation	EREG, IGFBP7
Skeletal development	ETS2, PITX1
Aldehyde dehydrogenase (NAD) activity	ALDH1A1, ALDH2
Electron transporter activity	ALDH1A1, ALDH2
Carbohydrate metabolism	ALDH2, MAN1C1
Plasminogen activator activity	PLAT, PLAU
Cell differentiation	SEMA3A, SFRP1
DNA repair	PARP4, POLB
GTPase activity	GBP1, RHOBTB3
GTP binding	GBP1, GNAI1
Protein serine/threonine kinase activity	MAP3K5, MYLK
Calmodulin binding	MYLK, NRGN
Ubiquitin thiolesterase activity	STAMBP, USP46
Metallopeptidase activity	ARTS-1, STAMBP
Inactivation of MAPK activity	DUSP6, PPP2R1B
Binding	PPP2R1B, UCP2
Induction of apoptosis	CASP4, PPP2R1B
Regulation of cell adhesion	LAMA5, PPP2R1B
Negative regulation of cell growth	PPP2R1B, WFDC1
Protein heterodimerization activity	EREG, PPP2R1B
MAPKKK cascade	MAP3K5, RAPGEF2
ATPase activity, coupled to transmembrane movement of substances	ABCB1, ABCC4
Aminopeptidase activity	TPP2, TRHDE
Golgi stack	AP3M2, MAN1C1
Sodium ion binding	POLB, SCN9A
RNA processing	IGF2BP3, RBPMS

Appendix 1. *Continued (cluster 4)*

Apoptosis	F2R, MAP3K5
Caspase activator activity	CASP1, MAP3K5
Receptor binding	F2R, LAMA5
RNA polymerase II transcription factor activity	FOXF2, MEIS1
Circulation	BDKRB2, TBC1D8
Response to nutrients	PPARG, STC1
Prostaglandin E receptor activity	PTGER2, PTGER4
G-protein signaling, coupled to camp nucleotide second messenger	ADRB2, PTGER4
Negative regulation of progression through cell cycle	HRASLS3, LOH11CR2A
Angiogenesis	ARTS-1, EREG
Cell proliferation	EREG, PTN
Bradykinin receptor activity	BDKRB1, BDKRB2
Transmembrane receptor protein tyrosine kinase signaling pathway	BDKRB2, TEK
Activation of MAPK activity	ADORA2B, ADRB2
Adenylate cyclase activation	ADORA2B, ADRB2
Transcription factor complex	FOXF1, FOXF2
Transcription from RNA polymerase II promoter	FOXF2, GATA3
Cation channel activity	SCN9A, TRPA1
Cation transport	SCN9A, TRPA1
Lipid metabolism	NR2F2, PPARG
Ligand-regulated transcription factor activity	NR2F1, NR2F2
Cysteine-type peptidase activity	CASP1, CASP4
Caspase activity	CASP1, CASP4
Regulation of apoptosis	CASP1, CASP4
Serine-type endopeptidase inhibitor activity	TFPI, WFDC1
Extracellular matrix organisation and biogenesis	COL4A2, COL4A6
Ubiquitin-protein ligase activity	C14orf130, NEDD4
Heterogeneous nuclear ribonucleoprotein complex	HNRPL, RBMX
Membrane alanyl aminopeptidase activity	ARTS-1, TRHDE

Appendix 1. *Continued (cluster 5)*

Nucleus	DIP13B, DUSP2, EHD3, LHX2, NAP1L3, SHOX, TFAP2A, ZIC1
Protein binding	ANK1, BAIAP2, COL8A1, DIP13B, DSG2, POSTN, TFAP2A
Membrane	DIP13B, DSG2, GALNT14, PEX6, PRSS12, PTGIS
Signal transduction	ANK1, CRABP2, DIP13B, IRS2, TFAP2A
Regulation of transcription, DNA-dependent	CRABP2, LHX2, SHOX, TFAP2A
Transcription factor activity	LHX2, SHOX, TFAP2A, ZIC1
Cell adhesion	COL8A1, DSG2, HAPLN1, POSTN
Integral to membrane	DSG2, GALNT14, PTGIS, SEZ6L2
Structural molecule activity	ANK1, COL8A1, KRT19
Cytoplasm	COL8A1, DIP13B, PEX6
Cytoskeleton	ANK1, DSG2, GAS2L1
Extracellular matrix (Sensu Metazoa)	COL8A1, HAPLN1, POSTN
Metal ion binding	LHX2, PTGIS, ZIC1
Calcium ion binding	DSG2, EHD3, GALNT14
Structural constituent of cytoskeleton	ANK1, KRT19
Nucleotide binding	EHD3, PEX6
ATP binding	EHD3, PEX6
Cell proliferation	DIP13B, PSPHL
Plasma membrane	ANK1, OXTR
Zinc ion binding	LHX2, ZIC1
Receptor activity	OXTR, SEZ6L2
Skeletal development	POSTN, SHOX

Appendix 2. Gene Ontology Classification Time-dependent differentially regulated genes (Cluster 1).

Nucleus	ABI1, AFF1, AHR, APPBP2, ATF2, C14orf11, CAPN7, CDC73, CDK7, CDYL, CHD1, CITED2, CNOT2, CNOT4, CREBBP, CTBP2, CTCF, CTDSP2, CUGBP1, DIDO1, DUSP10, DYRK1A, EDD1, EIF4ENIF1, ELF4, EP300, EVI1, FOXJ3, FOXK2, GTF2E1, GTF2IRD1, HIVEP2, HMGA2, HRB, HSF2, HSPA4L, IFI16, IRF2, LDB1, LPIN2, MAPK14, MAX, MEIS1, MEIS2, MGA, MKL1, MKL2, MYST3, MYST4, N4BP1, NCOA2, NCOA3, NCOA6, NCOR1, NFATC3, NIPBL, NPAT, NR2C1, NRIP1, NUP153, OGT, ORC5L, PARP2, PHF20, PHTF1, PML, POLB, POLR3E, PPP2R1B, PPP2R5C, PRDM10, RAD17, RAI17, RBMS1, RBPSUH, REV3L, RNPC2, RNUT1, RPP30, RREB1, SAP30, SATB2, SFRS4, SFRS8, SH3BP4, SKIV2L2, SLC4A1AP, SMURF2, STAMBP, SYNCRIP, TACC2, TAF4, TCF4, TCF7L2, TEAD4, THRAP2, TLE1, TLE4, TLK1, TOB2, TRIM24, TRIM33, TRIP4, TULP3, UPF3A, UTX, WDR50, WHSC2, ZBTB20, ZFPM2, ZFYVE26, ZHX2, ZNF143, ZNF161, ZRANB1, ZZZ3
Protein binding	AHR, APAF1, BTBD3, CAB39, CASP7, CDC5L, CITED2, CKAP5, CNOT4, CREBBP, CSNK2A1, CUL1, DIDO1, DYRK1A, EDD1, EIF4ENIF1, ELF4, EPS15, GGA2, GNAI1, GTF2IRD1, HRB, IFI16, ITSN2, JMJD2B, KIAA0182, KLHL22, LRRC8D, MAP2K4, MAPK14, MARCH7, MARK3, MAST4, MID1, MKL1, MPP5, MYST3, MYST4, NCOA3, NCOA6, NCOR1, NMI, NRIP1, NUP153, OGT, PDHX, PEX14, PHF15, PHF20, PHF21A, PHF3, PHIP, PIK3R3, PKP4, PML, PPFIA1, PPP2R1B, PPP2R2A, PRKCBP1, PTEN, RAB11FIP5, RAPGEF2, RBPSUH, RGL1, RNF38, RPP30, SAP30, SAV1, SEC24B, SKIV2L2, SMURF2, SNX2, SNX4, SOCS5, SOS1, SOS2, SPRED2, STAM2, STAMBP, STARD13, TACC2, TAF4, TCF4, TNC, TP53BP2, TRIM33, VPS54, ZBTB20, ZHX2, ZRANB1
Regulation of transcription, DNA-dependent	AHR, ATF2, CDC5L, CDK8, CNOT2, CNOT4, CREBBP, DIDO1, ELF4, EP300, FOXJ3, FOXK2, GTF2E1, GTF2IRD1, HIVEP2, HMGA2, HSF2, IFI16, IRF2, JMJD2B, JUN, MAX, MEIS1, MEIS2, MGA, MKL1, MKL2, MYST3, MYST4, NCOA2, NCOA6, NCOR1, NFATC3, NR2C1, PHF15, PHF20, PHF21A, PHF3, PHTF1, PML, PRDM10, PRKCBP1, RAI17, RNPC2, RREB1, SAP30, SATB2, SFRS8, TAF4, TCF7L2, TEAD4, THRAP2, TLE1, TLE4, TRIM24, TRIM33, TRIP4, TULP3, WHSC2, ZBTB20
Transcription	ATF2, CDC73, CDK7, CDK8, CNOT4, CTCF, DIDO1, ELF4, FOXJ3, FOXK2, GTF2E1, GTF2IRD1, HIVEP2, HMGA2, HSF2, IFI16, IRF2, JUN, MKL1, MKL2, MYST3, MYST4, NCOA6, NR2C1, NRIP1, PCM1, PHF20, PHF3, PHTF1, PML, POLR3E, PRDM10, RAI17, RBPSUH, RNPC2, RREB1, SAP30, SFRS8, TAF4, TCF7L2, TEAD4, THRAP2, TRIM24, TRIM33, TRIP4, WHSC2, ZBTB20, ZFPM2, ZNF143, ZNF161
Zinc ion binding	ATF2, CNOT4, CREBBP, CTCF, DDEF2, DIDO1, EDD1, EP300, EVI1, FBXO11, GTF2E1, HIVEP2, HRB, IBRDC3, JMJD2B, KIAA0182, KIAA0853, MARCH7, MID1, MTMR3, MYST3, MYST4, NR2C1, NUP153, PHF15, PHF20, PHF21A, PHF3, PML, PRDM10, PRKCBP1, PRKD2, RAI17, REV3L, RNF38, RREB1, STAMBP, TRIM24, TRIM33, TRIP4, USP3, ZBTB20, ZFPM2, ZFYVE26, ZHX2, ZNF143, ZNF161, ZRANB1, ZZZ3
Nucleotide binding	ACVR1B, APAF1, BMPR1A, CDC2L5, CDK7, CDK8, CHD1, CNOT4, CSNK1D, CSNK2A1, CUGBP1, DDX10, DYRK1A, EIF2AK3, EPHB4, GNAI1, GRK5, HSPA4L, KIF2, LARP5, MAP2K4, MAP4K3, MAPK14, MARK3, MAST4, MKNK2, ORC5L, PIK3R4, PRKD2, PRKX, RAD17, RBMS1, REV3L, RNPC2, RPS6KC1, SART3, SFRS4, SKIV2L2, SLC22A5, STK24, SYNCRIP, TAOK3, TAP1, TBK1, TIAL1, TLK1, TRIO, UPF3A
Metal ion binding	ATF2, ATP6V1B2, B4GALT5, CNOT4, CREBBP, CTCF, DDEF2, DIDO1, EDD1, EP300, EVI1, FBXO11, GTF2E1, HIVEP2, HRB, IBRDC3, JMJD2B, KIAA0182, KIAA0853, MARCH7, MID1, MTMR3, MYST3, MYST4, NR2C1, NUP153, PHF15, PHF20, PHF3, PML, PRDM10, PRKCBP1, PRKD2, RAI17, REV3L, RNF38, RREB1, STAMBP, TRIM24, TRIM33, TRIP4, USP3, ZBTB20, ZFPM2, ZHX2, ZNF143, ZNF161, ZRANB1
ATP binding	ACVR1B, APAF1, ATP6V1B2, BMPR1A, CDC2L5, CDK7, CDK8, CHD1, CSNK1D, CSNK2A1, DDX10, DHX32, DYRK1A, EIF2AK3, EPHB4, GRK5, HSPA4L, KIF2, MAP2K4, MAP4K3, MAPK14, MARK3, MAST4, MKNK2, ORC5L, PIK3R4, PRKD2, PRKX, RAD17, RPS6KC1, SKIV2L2, SLC22A5, STK24, TAOK3, TAP1, TBK1, TLK1, TRIO
DNA binding	CDC5L, CHD1, EVI1, HIVEP2, HMGA2, HRB, IFI16, MAX, MKL1, MKL2, MYST3, MYST4, NCOR1, NUP153, PARP2, PCM1, PHF20, PRDM10, RAD17, RBMS1, REV3L, RREB1, SATB2, SOS1, SOS2, TCF4, TCF7L2, TIAL1, TRIM24, TRIM33, ZBTB20, ZFPM2, ZNF143, ZNF161, ZZZ3
Transferase activity	ACVR1B, BMPR1A, CDC2L5, CDK7, CDK8, CREBBP, CSNK1D, CSNK2A1, DYRK1A, EIF2AK3, EP300, EPHB4, GRK5, MAP2K4, MAP4K3, MAPK14, MARK3, MAST4, MKNK2, MYST3, MYST4, NCOA3, PIK3R4, POLB, POLR3E, PRKD2, PRKX, REV3L, RPS6KC1, STK24, TAOK3, TBK1, TLK1, TMEM23, TRIO

Appendix 2. *Continued (cluster 1)*

Membrane	ACVR1B, AP1GBP1, APPBP2, B4GALT5, BMPR1A, BTN2A2, CHD9, EGFL5, EIF2AK3, EPHB4, GGA2, GPRC5A, IBRDC3, KIAA0247, LRRC8D, MPP5, NUMB, OGFRL1, PAQR3, PEX14, PPP2R1B, RAPGEF2, SEC24B, SLC31A2, SPRED2, STAM2, STAMBP, STOM, STX3A, STX7, TAP1, TMEM23
Signal transduction	AHR, ARHGEF7, CREBBP, CSNK1D, EP300, GNAI1, GPRC5A, GRK5, IL15, INPP1, MAP2K4, NCOA2, NCOA3, OGT, PAFAH1B1, PBEF1, PPFIA1, PPP2R2A, PPP2R5C, PPP2R5E, PPP4R1, RPS6KC1, SAV1, STAM, STK24, TCF7L2, TLE1, TP53BP2
Transcription factor activity	AFF1, AHR, CITED2, CREBBP, CTCF, ELF4, EP300, FOXJ3, FOXK2, HSF2, IRF2, JUN, MAX, MEIS1, MEIS2, MGA, NFATC3, NR2C1, PHTF1, PML, RBPSUH, SATB2, TAF4, TCF7L2, TEAD4, ZHX2
Cytoplasm	APPBP2, ATG5, ATP6V1B2, CASP7, CREBBP, DUSP10, EIF4ENIF1, GRK5, HSPA4L, MAPK14, MTMR3, NCK1, NMI, PCM1, POLB, PPFIA1, PPP2R5E, PTEN, RREB1, SCHIP1, SOCS5, TP53BP2, TRIP4, UPF3A, ZRANB1
Protein amino acid phosphorylation	ACVR1B, BMPR1A, CDC2L5, CDK7, CDK8, CSNK1D, CSNK2A1, EIF2AK3, EPHB4, GRK5, MAP2K4, MAP4K3, MAPK14, MARK3, MAST4, MKNK2, PIK3R4, PRKD2, PRKX, RPS6KC1, STK24, TBK1, TLK1, TRIO
Protein serine/threonine kinase activity	ACVR1B, CDC2L5, CDK8, CSNK1D, CSNK2A1, DYRK1A, EIF2AK3, MAP2K4, MAP4K3, MAPK14, MARK3, MAST4, MKNK2, PIK3R4, PRKD2, PRKX, RPS6KC1, STK24, TAOK3, TBK1, TLK1, TRIO
Cellular component unknown	AMMECR1, CKAP5, CTDSP2, EGFL5, HDHD1A, HECA, KIAA0247, KIAA0553, PHF3, PHIP, PIK3R4, PLEKHA5, RALGDS, RBMS1, RGL1, SCHIP1, SLC35D2, SOS2, STXBP3, TIAL1, TLK1
Nucleic acid binding	ANKHD1, C10orf56, CTCF, EVI1, GCLC, GPATC2, IFI16, JMJD2B, KIAA0853, OBFC2A, PHF20, PML, PRDM10, RNPC2, RREB1, SART3, SKIV2L2, USP6, ZFYVE26
Integral to membrane	AKAP1, B4GALT5, BMPR1A, BTN2A2, CHD9, EGFL5, EIF2AK3, EPHB4, IBRDC3, KIAA0247, LRRC8D, NUP153, PAQR3, PPP2R5C, SLC22A5, SLC31A2, STX3A, TAP1, TMEM23
Cell cycle	AHR, CDC5L, CDC73, CDK7, CDK8, CLASP1, CTCF, CUL1, EP300, NIPBL, PAFAH1B1, PTEN, RAD17, SASH1, SH3BP4, TLK1, TP53BP2
Molecular function unknown	AMMECR1, CHMP7, CKAP5, CTDSP2, EVI1, FBXO34, HDHD1A, HECA, KIAA0174, KIAA0247, KIAA0553, MRPL39, ORC5L, PHF3, SCHIP1, STXBP3, TLE4
Binding	APPBP2, ARFGEF1, C15orf29, C1orf73, CAPN7, CKAP5, CLASP1, NIPBL, OGT, OSRF, PKP4, PPP2R1B, PPP4R1, PUM1, PUM2, UTX, ZUBR1
Biological process unknown	AMMECR1, CKAP5, CTDSP2, EGFL5, EVI1, HDHD1A, KIAA0247, KIAA0553, MRPL39, PLEKHA5, RAB11FIP5, SCHIP1, SLC35D2, STXBP3, TIAL1, TLE4
Ubiquitin cycle	CNOT4, CUL1, EDD1, FBXO34, FBXO42, MID1, RNF38, SENP6, SMURF2, STAMBP, UBE2G1, USP15, USP3, USP6, ZUBR1
Transcription coactivator activity	ATF2, CDK7, CREBBP, EP300, HSF2, MKL2, NCOA2, NCOA3, NFATC3, NRIP1, PML, TAF4, TRIM24, TRIP4
RNA binding	AKAP1, CDC5L, CNOT4, DDX10, HRB, PUM1, PUM2, RBMS1, RNPC2, SFRS8, SYNCRIP, TIAL1, UPF3A
Development	CDC2L5, EVI1, GTF2IRD1, HECA, HMGA2, LDB1, MEIS1, NUMB, PHF3, RREB1, SPRED2, TLE1, WHSC2
RNA polymerase II transcription factor activity	ATF2, CTCF, FOXK2, IRF2, JUN, MEIS1, RBPSUH, TCF4, TCF7L2, TEAD4, TIAL1, ZFPM2
Signal transducer activity	CASP8, CREBBP, GNAI1, GRK5, IL15, NCOA2, NCOA3, PPFIA1, PPP1R12A, RAPGEF2, SH3BP4, TBK1
Hydrolase activity	ATP6V1B2, CHD1, CTDSP2, DDX10, DUSP10, GNPDA1, INPP1, MTMR3, PTEN, RPP30, SKIV2L2
Regulation of transcription from RNA polymerase II promoter	CHD1, CITED2, FOXK2, NFATC3, TCF4, TCF7L2, TEAD4, TIAL1, ZFPM2, ZNF143, ZNF161
Intracellular protein transport	AP1GBP1, APPBP2, GGA2, SEC24B, SNX2, STAM, STAM2, STX3A, STX7, TLK1
Intracellular	APAF1, GGA2, GPATC2, KIAA0182, MID1, PAXIP1, PML, PRKD2, TRIM24, TRIM33
Integral to plasma membrane	ACVR1B, EPHB4, GPRC5A, IL15, NUMB, RAPGEF2, SLC31A2, STOM, STX7
Intracellular signaling cascade	ARHGAP29, NCK1, PIK3R3, PRKD2, SNX2, SNX4, SOCS5, SPSB1, TLK1
Transcription from RNA Pol II promoter	AHR, HSF2, NCOR1, NMI, RBPSUH, RREB1, TRIM24, TRIP4
Receptor activity	ACVR1B, BMPR1A, EPHB4, EPS15, GPRC5A, OGFRL1, PAQR3, THRAP2

Appendix 2. *Continued (cluster 1)*

DNA repair	CDK7, CSNK1D, NCOA6, PARP2, PML, POLB, RAD17, REV3L
Cytoskeleton	ABI1, CASP8, CLASP1, KIF2, PAFAH1B1, PKP4, STOM
Soluble fraction	ABI1, CTDSP2, EDD1, GRK5, PPP2R1B, PPP4R1, UNC119
Transport	HRB, NUP153, PRDM10, RNUT1, SLC22A5, TAP1, UPF3A
Apoptosis	AHR, ATG5, DIDO1, EP300, PML, TIAL1, TP53BP2
Cell proliferation	CDK7, EDD1, EPHB4, EPS15, IFI16, IRF2, PTEN
Calcium ion binding	AP1GBP1, EGFL5, EPS15, ITSN2, PML, RAPGEF2, SWAP70
Ubiquitin-dependent protein catabolism	EDD1, FBXO11, LOC220594, SMURF2, USP15, USP3, USP6
Neurogenesis	APAF1, CTCF, DYRK1A, EP300, PAFAH1B1, PHF20
Transcription corepressor activity	CTCF, MEIS2, NCOR1, NRIP1, SAP30, ZFPM2
Regulation of translation	EIF2AK3, MKNK2, PPP2R1B, PUM1, PUM2, RBMS1
Metabolism	C12orf5, CDYL, CTBP2, DHRS7, HDHD1A, PDHX
Nuclear mRNA splicing, via spliceosome	CDC40, CDC5L, RNPC2, SFRS4, SFRS8, SYNCRIP
Protein amino acid dephosphorylation	DNAJC6, DUSP10, MTMR3, PPP2R1B, PPP2R2A, PTEN
Protein transport	EIF4ENIF1, PEX14, SNX4, STXBP3, TAP1, VPS54
Guanyl-nucleotide exchange factor activity	ARFGEF1, ARHGEF7, BCAR3, RALGDS, SOS2, TRIO
Golgi stack	AP1GBP1, B4GALT5, DDEF2, GGA2, SEC24B, TMEM23
Regulation of progression through cell cycle	BCAR3, CDK8, HECA, PPP2R1B, TCF7L2, TOB2
Ligase activity	CNOT4, EDD1, GCLC, MID1, SMURF2, UBE2G1
Ubiquitin-protein ligase activity	EDD1, FBXO11, FBXW11, SMURF2, UBE2G1, ZUBR1
Microtubule	APPBP2, CLASP1, KIF2, MID1, PAFAH1B1
Cell division	CDC40, CDK7, CDK8, CLASP1, PAFAH1B1
Negative regulation of cell proliferation	ABI1, CTBP2, CUL1, PTEN, TOB2
Mitochondrion	AKAP1, CASP8, MRPL39, PDHX, PPP2R1B
Peptidase activity	CASP7, CDYL, PPP2R5C, USP15, USP6
Endocytosis	AP1GBP1, ITSN2, SH3BP4, SNX2, SNX4
Endoplasmic reticulum	ABI1, EIF2AK3, SEC24B, SYNCRIP, TAP1
Induction of apoptosis	PML, PPP2R1B, PTEN, TIAL1, TP53BP2
Negative regulation of progression through cell cycle	CDC73, CTCF, PTEN, SASH1, TP53BP2
Ubiquitin thiolesterase activity	LOC220594, STAMBP, USP15, USP3, USP6
Cytosol	ABI1, APAF1, OGT, PPP2R1B, UNC119
Small GTPase mediated signal transduction	BCAR3, RALGDS, RAPGEF2, RGL1, SOS2
DNA replication	NCOA6, ORC5L, RAD17, RBMS1, REV3L
Microtubule associated complex	APPBP2, KIF2, MID1, PAFAH1B1
Chromatin modification	MYST3, MYST4, NCOR1, TLK1
Regulation of transcription	MAX, NCOR1, PPP2R1B, ZZZ3
RNA splicing	CDC40, PPP2R1B, SFRS4, SYNCRIP
Protein phosphatase type 2a complex	PPP2R1B, PPP2R2A, PPP2R5C, PPP2R5E
Protein phosphatase type 2a regulator	PPP2R1B, PPP2R2A, PPP2R5C, PPP2R5E

Appendix 2. *Continued (cluster 1)*

Activity	
Transporter activity	NUP153, SEC24B, SLC22A5, TAP1
Protein transporter activity	EIF4ENIF1, SNX2, STX3A, STX7
Histone acetyltransferase activity	CREBBP, EP300, MYST4, NCOA3
Protein complex assembly	CREBBP, GGA2, PML, PPP2R1B
Specific RNA polymerase II transcription factor activity	MEIS2, TRIM24, ZNF143, ZNF161
Immune response	IFI16, IL15, IRF2, TAP1
Proteolysis and peptidolysis	CAPN7, CASP7, CASP8, SENP6
Cysteine-type peptidase activity	CAPN7, CASP7, CASP8, SENP6
Acyltransferase activity	MYST3, MYST4, NCOA3, PDHX
Negative regulation of transcription from RNA polymerase II promoter	CTCF, IRF2, MEIS2, NRIP1
Response to stress	AHR, DUSP10, MAP4K3, MAPK14
Positive regulation of transcription from RNA polymerase II promoter	ELF4, MKL2, NCOA6, NRIP1
Kinase activity	PIK3R3, PRKCBP1, STK24, TMEM23
Magnesium ion Binding	ACVR1B, BMPR1A, INPP1, POLB
Positive regulation of cell proliferation	CDC2L5, IL15, PBEF1, STAMBP
Protein-tyrosine kinase activity	EPHB4, MAP2K4, PRKX, STK24
Catalytic activity	C10orf6, CDYL, HDHD1A, PML
Transcriptional repressor activity	IFI16, LDB1, MYST4, PML
Cysteine-type endopeptidase activity	LOC220594, USP15, USP3, USP6
Transcription regulator activity	CNOT2, MAX, NCOA2, NCOA3
Transferase activity, transferring glycosyl groups	B4GALT5, OGT, PARP2, PBEF1
Ion transport	ATP6V1B2, SLC22A5, SLC31A2
Structural molecule activity	EGFL5, PKP4, WDR59
Nuclear pore	HRB, NUP153, RNUT1
Protein heterodimerization activity	PML, PPP2R1B, TAP1
Plasma membrane	SLC22A5, SSFA2, TULP3
Positive regulation of transcription, DNA-dependent	CDK7, CTCF, NCOA3
Protein kinase cascade	MAP4K3, MAPK14, MKNK2
Androgen receptor signaling pathway	CDK7, NCOA3, NRIP1
Androgen receptor binding	CDK7, NCOA3, NRIP1
JAK-STAT cascade	NMI, SOCS5, STAMBP
Chromatin	CDYL, CHD1, HMGA2
Chromatin binding	CDYL, CHD1, NCOA6
Sh3/Sh2 adaptor activity	ITSN2, STAM, TP53BP2

Appendix 2. *Continued (cluster 1)*

JNK cascade	DUSP10, MAP2K4, MAP4K3
Negative regulation of transcription, DNA-dependent	LDB1, RBPSUH, ZHX2
Transcriptional activator activity	ELF4, MYST4, RREB1
Protein self binding	CASP8, MKL2, ORC5L
ATP-dependent helicase activity	DDX10, DHX32, SKIV2L2
Protein folding	HSF2, HSPA4L, KIAA0674
Response to unfolded protein	EIF2AK3, HSF2, HSPA4L
Ubiquitin ligase complex	FBXO11, FBXW11, SMURF2
Negative regulation of transcription	MYST4, SMURF2, TRIM33
Transcription initiation from RNA polymerase II promoter	CDK7, GTF2E1, NCOA6
nucleoplasm	IFI16, PML, RNPC2
GTPase activator activity	ARHGAP12, DDEF2, STARD13
mRNA processing	CUGBP1, RNPC2, UPF3A
Wnt receptor signaling pathway	CSNK1D, CSNK2A1, FBXW11
Ribonucleoprotein complex	CUGBP1, MRPL39, SYNCRIP
G-protein coupled receptor protein signaling pathway	GNAI1, GPRC5A, TULP3
Manganese ion binding	ACVR1B, B4GALT5, BMPR1A
Lipid metabolism	PAFAH1B1, TMEM23
Cell motility	MAPK14, PAFAH1B1
Mitosis	CLASP1, PAFAH1B1
Cell differentiation	MKL2, PAFAH1B1
Oxidoreductase activity	CTBP2, DHRS7
Protein dimerization activity	ATF2, JUN
Outer membrane	AKAP1, NUP153
Cell adhesion	PKP4, TNC
Phosphoinositide binding	SNX2, SNX4
Response to hypoxia	CREBBP, EP300
Homeostasis	CREBBP, EP300
DNA-directed RNA polymerase activity	PCM1, POLR3E
Electron transport	MRPL39, PCM1
Inositol or phosphatidylinositol phosphatase activity	INPP1, MTMR3
Protein serine/threonine phosphatase activity	MTMR3, PTEN
Protein tyrosine phosphatase activity	MTMR3, PTEN
Membrane fraction	IL15, MTMR3
Protein phosphatase type 2a activity	PPP2R1B, PPP2R2A
Carbohydrate metabolism	B4GALT5, GNPDA1

Appendix 2. *Continued (cluster 1)*

Lysosome	TIAL1, USP6
Nucleosome	MYST3, MYST4
Nucleosome assembly	MYST3, MYST4
Cell surface receptor linked signal transduction	MAPK14, MKNK2
Estrogen receptor binding	NCOA6, NRIP1
Response to DNA damage stimulus	EDD1, TLK1
Microtubule motor activity	APPBP2, KIF2
Insulin receptor signaling pathway	PHIP, PIK3R3
mRNA splice site selection	CUGBP1, SFRS8
Vesicle-mediated transport	SEC24B, STXBP3
Inactivation of MAPK activity	PPP2R1B, SPRED2
Regulation of Wnt receptor signaling pathway	PPP2R1B, TCF7L2
Negative regulation of cell growth	PML, PPP2R1B
Transmembrane receptor protein tyrosine kinase signaling pathway	ABI1, EPHB4
Organogenesis	EPHB4, TLE1
Electron transporter activity	MRPL39, PDHX
MAPKKK cascade	RAPGEF2, TAOK3
Diacylglycerol binding	PRKD2, RAPGEF2
Chromatin assembly or disassembly	CDYL, CHD1
Frizzled signaling pathway	TLE1, TLE4
Spliceosome complex	CDC40, CDC5L
Transcription cofactor activity	LDB1, NMI
DNA-dependent DNA replication	POLB, REV3L
Sodium ion binding	POLB, SLC22A5
Ras protein signal transduction	RREB1, SOS1
Double-stranded DNA binding	IFI16, RBMS1
Rho GTPase activator activity	ARHGAP29, SOS1
Inflammatory response	NFATC3, NMI
Regulation of cyclin dependent protein kinase activity	CDK7, PTEN
Heart development	NCOA6, PTEN
Helicase activity	CHD1, DHX32
Chromosome organization and biogenesis (Sensu Eukaryota)	CHD1, HMGA2
Phosphoprotein phosphatase activity	CTDSP2, DNAJC6
Receptor binding	NCK1, TRIM24
Protein kinase activity	CDK8, MAST4
Regulation of apoptosis	APAF1, CASP8

Appendix 2. *Continued (Cluster 1)*

General RNA Pol II transcription factor activity	GTF2E1, TAF4
Endosome	IL15, STX7
Cell-cell signaling	IL15, PBEF1
Nucleolus	IFI16, RBPSUH
Response to virus	IFI16, TBK1
DNA damage response, signal transduction by p53 class mediator resulting in induction of apoptosis	IFI16, PML
Regulation of GTPase activity	DDEF2, HRB
mRNA nucleus export	HRB, UPF3A
Apoptotic programme	CASP7, CASP8
Caspase activity	CASP7, CASP8
G1/S transition of mitotic cell cycle	CUL1, PML
Cell cycle arrest	CUL1, PML
Establishment and/or maintenance of chromatin architecture	HMGA2, TCF7L2
DNA recombination	NCOA6, RBPSUH
Thyroid hormone receptor binding	NCOA3, NCOA6
Protein ubiquitination	FBXO11, FBXW11
PML body	ELF4, PML
Isomerase activity	C12orf5, KIAA0674
Transforming growth factor beta receptor activity	ACVR1B, BMPR1A
Positive regulation of I-Kappa B kinase/Nf-kappa B cascade	CASP8, TBK1
Translation initiation factor activity	EIF4ENIF1, WDR44

Appendix 2. *Continued (cluster 2)*

Nucleus	ATF3, C20orf11, CDKN1A, CEBPZ, DDB2, E2F6, EZH2, GADD45A, HEAB, HEXIM1, HIST1H1C, HIST2H2AA, HIST2H2BE, KCTD13, MAD2L1BP, MAFB, MBD4, NET1, NKRF, NOL1, NOL5A, NOLC1, NR4A2, NXF1, PNMA1, PNN, POLE3, POLR1C, PPM1D, RBM13, RBM4, RRS1, RSL1D1, SAS10, SESN1, SFPQ, SFRS7, SNIP1, SPEN, TAF7, TAF9, TCF8, TSC22D1, UBQLN2, ZBTB5, ZNF211, ZNF330, ZNF574
Protein binding	BYSL, CD3EAP, CDKN1A, EIF5, HEXIM1, ITSN1, KCTD13, KLHL21, MAD2L1BP, MBD4, MYD88, NOL1, NXF1, PLK2, PMAIP1, PNMA1, RNF139, RNF44, SFPQ, SFRS7, TAF7, TNFRSF10B, TOB1, TOPORS, ZBTB5, ZNF330
Nucleotide binding	ARS2, DYRK3, EIF5, EPHA2, GEM, HEAB, NOLC1, NXF1, PEO1, PLK2, RBM4, RFK, RRAD, SFPQ, SFRS7, SPEN, TAF9, TAOK1, TOR1B
Membrane	ARL6IP, C5orf15, CD44, EPHA2, FAS, GEM, HBEGF, IFNGR1, KCNJ8, KCTD13, MYD88, RNF139, SDF2, SLC10A3, SLC30A1, SLC35A2, STOM, TNFRSF10B
Regulation of transcription, DNA-dependent	ATF3, BTG2, CEBPZ, E2F6, EZH2, MAFB, NKRF, NR4A2, PNN, SFPQ, SPEN, TAF7, TAF9, TCF8, TSC22D1, ZBTB5, ZNF211
Transcription	ATF3, BTG2, CEBPZ, E2F6, EZH2, MAFB, NKRF, NR4A2, PNN, POLR1C, SFPQ, TAF9, TFAM, TSC22D1, ZBTB5, ZNF211
Zinc ion binding	CDKN1A, DNAJA1, NR4A2, RBM4, RFK, RNF139, RNF44, SFRS7, SLC30A1, TCF8, TOPORS, ZBTB5, ZNF211, ZNF330, ZNF574
DNA binding	ATF3, CEBPZ, EZH2, HIST1H1C, HIST2H2AA, HIST2H2BE, MBD4, NKRF, PNN, POLG2, POLR1C, SFPQ, SPEN, TAF9, ZBTB5
Metal ion binding	CDKN1A, DNAJA1, HCCS, NR4A2, RBM4, RNF139, RNF44, SFRS7, TCF8, TOPORS, ZBTB5, ZNF211, ZNF330, ZNF574
Transferase activity	AASDHPPT, DYRK3, EPHA2, ETNK1, HSPB8, NOL1, PLK2, POLE3, POLG2, POLR1C, RFK, SAT, TAF9, TAOK1
ATP binding	DYRK3, EPHA2, HEAB, NOLC1, PEO1, PLK2, POLG2, RFK, TAF9, TAOK1, TOR1B
Transcription factor activity	ATF3, BTG2, E2F6, NR4A2, TAF7, TCF8, TFAM, TSC22D1, ZNF211
Integral to membrane	ARL6IP, C5orf15, FAS, KCNJ8, RNF139, SLC10A3, SLC30A1, SLC35A2, TNFRSF10B
Cellular component unknown	ARS2, HSPB8, ITSN1, MRPL49, NET1, ODC1, RP5-1104E15.5, TRIAP1
Signal transduction	EPHA2, FAS, GDF15, HBEGF, IFNGR1, NET1, NR4A2, TNFRSF10B
RNA binding	EIF1AX, NOL5A, NXF1, RBM4, SFPQ, SFRS7, SPEN
Protein biosynthesis	ARL6IP, EIF1AX, EIF5, MRPL49, MRPS6, POLG2, RSL1D1
Mitochondrion	FDXR, HCCS, MRPL49, MRPS6, PEO1, POLG2, TFAM
Cytoplasm	BYSL, ETNK1, HEXIM1, MAD2L1BP, NOLC1, PNMA1, RFK
Cell cycle	CDKN1A, E2F6, GADD45A, NOLC1, PNN, PPM1D
Receptor activity	CD44, EPHA2, HBEGF, IFNGR1, RNF139, TNFRSF10B
Nucleolus	NOL1, NOL5A, NOLC1, PNMA1, ZNF330
Integral to plasma membrane	CD44, EPHA2, HBEGF, IFNGR1, STOM
DNA repair	BTG2, GADD45A, KCTD13, POLG2, SFPQ
Negative regulation of cell proliferation	BTG2, CDKN1A, PPM1D, SESN1, TOB1
Molecular function unknown	ARS2, MRPL49, RP5-1104E15.5, SAS10, TRIAP1
GtTP binding	EIF5, GEM, HEAB, NOLC1, RRAD
Structural constituent of ribosome	ARL6IP, MRPL49, MRPS6, RSL1D1
Protein serine/threonine kinase activity	DYRK3, HSPB8, PLK2, TAOK1

Appendix 2. *Continued (cluster 2)*

Protein amino acid phosphorylation	DYRK3, EPHA2, PLK2, TAOK1
Endoplasmic reticulum	CES2, EPM2AIP1, RNF139, TOR1B
Extracellular space	GDF15, HBEGF, IL11, SDF2
Immune response	CD3EAP, FAS, GEM, TCF8
Hydrolase activity	CES2, MBD4, PEO1, PPM1D
Biological process unknown	HSPB8, RP5-1104E15.5, TRIAP1, ZNF330
Calmodulin binding	GEM, MARCKSL1, RRAD
Protein folding	DNAJA1, HSPB8, TOR1B
Response to unfolded protein	DNAJA1, HSPB8, TOR1B
Unfolded protein binding	DNAJA1, HSPB8, TOR1B
Nuclear mRNA splicing, via spliceosome	RBM4, SFPQ, SFRS7
Translation initiation factor activity	EIF1AX, EIF5, MRPL49
Transcription coactivator activity	TAF7, TAF9, TCF8
Intracellular	ARL6IP, GMFB, MRPL49
Ribosome	ARL6IP, MRPL49, RSL1D1
Positive regulation of I-kappa B kinase/NF-kappa B cascade	MYD88, PLK2, TNFRSF10B
Nucleic acid binding	SPEN, ZNF211, ZNF574
Transcription from RNA Pol II promoter	CEBPZ, TAF9, TSC22D1
Magnesium ion binding	AASDHPPT, PPM1D, RFK
Cell cycle arrest	CDKN1A, GADD45A, SESN1
Kinase activity	CDKN1A, ETNK1, HSPB8
Growth factor activity	GDF15, GMFB, HBEGF
Transcription corepressor activity	ATF3, E2F6, TCF8
Protein dimerization activity	ATF3, MAFB, POLR1C
Nucleosome	HIST1H1C, HIST2H2AA, HIST2H2BE
Chromosome	HIST1H1C, HIST2H2AA, HIST2H2BE
Nucleosome assembly	HIST1H1C, HIST2H2AA, HIST2H2BE
Chromosome organization and biogenesis (Sensu Eukaryota)	HIST1H1C, HIST2H2AA, HIST2H2BE
Negative regulation of transcription From RNA Pol II promoter	E2F6, HEXIM1, TCF8
Ubiquitin cycle	FBXL14, RNF139, RNF44
Regulation of progression through cell cycle	E2F6, NOL1, PPM1D
Cell surface receptor linked signal transduction	GEM, MYD88, TNFRSF10B
DNA replication	KCTD13, PEO1, POLE3

Appendix 2. *Continued (cluster 2)*

Lyase activity	HCCS, ODC1
rRNA processing	NOL5A, NOLC1
Translational initiation	EIF1AX, MRPL49
Transcription factor TFIID complex	TAF7, TAF9
General RNA Pol II transcription factor activity	TAF7, TAF9
Guanyl-nucleotide exchange factor activity	ITSN1, NET1
signal transducer activity	MYD88, PLK2
Regulation of cyclin dependent protein kinase activity	CDKN1A, GADD45A
Protein kinase activity	CDKN1A, DYRK3
Cyclin-dependent protein kinase inhibitor activity	CDKN1A, HEXIM1
DNA-dependent DNA replication	POLG2, TFAM
Transmembrane receptor protein tyrosine kinase signaling pathway	CD3EAP, EPHA2
Development	EPHA2, SAS10
Cell adhesion	BYSL, CD44
Apoptosis	FAS, GADD45A
Electron transport	FDXR, HCCS
mRNA processing	HEAB, NXF1
Small GTPase mediated signal transduction	GEM, RRAD
Transmembrane receptor activity	FAS, MYD88
Cytosol	EIF5, FAS
Protein self binding	FAS, HSPB8
Regulation of apoptosis	FAS, TNFRSF10B
GTPase activity	EIF5, RRAD
Transport	NXF1, SLC10A3
Membrane fraction	GOLGA4, KCNJ8
Potassium ion transport	KCNJ8, KCTD13
Voltage-gated potassium channel complex	KCNJ8, KCTD13
Cytokine activity	GDF15, IL11
Cell-cell signaling	GDF15, IL11
Positive regulation of cell proliferation	IL11, NOL1
Oxidoreductase activity	FDXR, UBQLN2
Transcription From RNA Pol I	POLR1C, RRN3

Appendix 2. *Continued (cluster 2)*

Golgi stack	GOLGA4, SLC35A2
RNA Splicing	SFPQ, SFRS7

Appendix 2. *Continued (Cluster 3)*

Protein binding	AKT3, ANXA11, CBLB, CDH4, CHCHD3, CRSP8, DDEF1, FYN, GRB10, GSK3B, ITSN1, JMJD2C, KCNS3, MNAT1, MPDZ, MYH10, NCK2, NCOR1, NEK1, PARD3, PARN, PBX1, PBX3, PDZRN3, PPP2R3A, PRKCA, PRKD1, PTK2, RBPMS, SIPA1L1, SMARCA2, SMARCC1
Nucleus	APBB2, ATXN1, CBLB, CDC14B, CRSP8, DIP2C, EGR1, FAF1, JARID2, LDB2, MAD1L1, MLLT3, MNAT1, NCOA1, NCOR1, NEK1, PARN, PBX1, PBX3, PFTK1, POLR3B, PPP3CA, RNGTT, SMARCA2, SMARCC1, SSBP2, STK3, TBC1D1, TBL1X, ZNF291
Membrane	APBB2, CDC42BPA, CDH4, COVA1, COX10, DDEF1, EDG2, EXT1, FUT8, INPP5A, KCNS3, MPDZ, PARD3, PPAP2B, PTPRK, RHBDL2, SLC25A12, SLC25A13, TMCC1, TPST1, UST, ZDHHC14
Nucleotide binding	AKT3, ASCC3, CDC42BPA, COVA1, FYN, GNAQ, GSK3B, LARS2, MAP2K5, MYH10, MYO10, NEK1, NME7, PARN, PFTK1, PRKCA, PRKD1, PTK2, RBPMS, SMARCA2, STK3
Transferase activity	AKT3, CDC42BPA, COX10, FYN, GSK3B, MAP2K5, NCOA1, NEK1, NME7, PFTK1, PIP5K2A, POLR3B, PRKCA, PRKD1, PTK2, RNGTT, STK3, TPST1, UST, ZDHHC14
ATP binding	AKT3, ASCC3, CDC42BPA, FYN, GSK3B, LARS2, MAP2K5, MYH10, MYO10, NEK1, NME7, PFTK1, PRKCA, PRKD1, PTK2, SMARCA2, STK3, TMEM131
Zinc ion binding	CBLB, CDC42BPA, DDEF1, EGR1, JMJD2C, MIPEP, MNAT1, PDZRN3, POLR3B, PPP3CA, PRKCA, PRKD1, ZDHHC14, ZFAND3, ZNF291
Mitochondrion	AUH, CHCHD3, COX10, ETFA, LARS2, MIPEP, MRPS27, MRPS28, PCCB, SLC25A12, SLC25A13, SQRDL, SUCLG2
Integral to membrane	CDH4, COX10, EDG2, EXT1, FUT8, PPAP2B, RHBDL2, SLC25A12, STXBP6, TMCC1, TPST1, UST, ZDHHC14
Calcium ion binding	ANXA11, CBARA1, CBLB, CDH4, ITSN1, LTBP1, MIPEP, PPP2R3A, PPP3CA, PRKCA, SLC25A12, SLC25A13, ZZEF1
Cytoplasm	ANXA11, ATXN1, DERA, GNAQ, GRB10, NCK2, NEK1, PACSIN2, PARN, PFTK1, PMM2, STK3
Hydrolase activity	ASCC3, CDC14B, INPP5A, PARN, PDE6D, PPAP2B, PPP3CA, PRNPIP, PTPRK, RNGTT, SMARCA2
Protein amino acid phosphorylation	AKT3, CDC42BPA, FYN, GSK3B, MAP2K5, NEK1, PFTK1, PRKCA, PRKD1, PTK2, STK3
Regulation of transcription, DNA-dependent	ASCC3, CRSP8, EGR1, JARID2, JMJD2C, MLLT3, NCOR1, PBX1, PBX3, TBL1X
Metal ion binding	CDC42BPA, DDEF1, EGR1, JMJD2C, MNAT1, PDZRN3, POLR3B, PRKD1, ZDHHC14, ZNF291
Signal transduction	ADM, AKT3, EDG2, EXT1, GNAQ, MAP2K5, MYO10, NCOA1, STK3, TBL1X
Transcription	ASCC3, CRSP8, EGR1, JARID2, MLLT3, MNAT1, POLR3B, SMARCA2, TBL1X
Intracellular signaling cascade	APBB2, CDC42BPA, FYN, GRB10, NCK2, PRKCA, PRKD1, RIN3, TNS3
DNA binding	JARID2, NCOR1, POLR3B, SMARCA2, SMARCC1, SSBP2, ZFAND3
Biological process unknown	FN5, JMJD2C, LTBP1, MAPKAP1, MRPS28, MYH10, SIPA1L1
Molecular function unknown	AP2A2, FN5, JMJD2C, MAD1L1, MRPS28, SIPA1L1, ZFAND3
Cellular component unknown	FN5, FYN, ITSN1, JMJD2C, MAPKAP1, RIN3, SIPA1L1
Nucleic acid binding	ASCC3, COVA1, JMJD2C, MRPS28, R3HDM1, RNGTT, ZNF291
Protein serine/threonine kinase activity	AKT3, CDC42BPA, MAP2K5, NEK1, PFTK1, PRKD1, STK3
Protein amino acid dephosphorylation	CDC14B, PPP2R3A, PPP3CA, PTPRK, RNGTT, TNS3
Magnesium ion binding	CDC42BPA, MIPEP, NEK1, NME7, PARN, STK3
Regulation of transcription	APBB2, NCOA1, NCOR1, SMARCC1, SSBP2
Cell cycle	EXT1, MAD1L1, MNAT1, NEK1, PARD3
GTPase activator activity	DDEF1, RIN3, SIPA1L1, TBC1D1, TBC1D22A
Plasma membrane	CDH4, EDG2, GNAQ, GRB10, PRKD1

Appendix 2. *Continued (cluster 3)*

Integral to plasma membrane	EDG2, PRKD1, PTPRK, SLC25A12, SLC25A13
RNA binding	ATXN1, AUH, KIAA0427, PARN, RBPMS
binding	AP2A2, PTK2, RP3-477H23.1, SLC25A12, SLC25A13
Endocytosis	AP2A2, AP4S1, PACSIN2, RIN3
Golgi stack	AP2A2, EXT1, FUT8, UST
Metabolism	AUH, DIP2C, PMM2, SUCLG2
Protein-tyrosine kinase activity	FYN, MAP2K5, NEK1, PTK2
Catalytic activity	C20orf19, DIP2C, NCOA1, SUCLG2
Transcription coactivator activity	NCOA1, SMARCA2, SMARCC1
Nucleoplasm	ANXA11, SMARCA2, SMARCC1
Regulation of transcription from RNA Pol II promoter	MNAT1, SMARCA2, SMARCC1
Transporter activity	AP4S1, PACSIN2, SLC25A12
Intracellular protein transport	AP2A2, AP4S1, PACSIN2
Transcription factor activity	EGR1, PBX1, PBX3
Ligase activity	LARS2, PCCB, SUCLG2
Signal transducer activity	CBLB, GNAQ, NCOA1
Transport	AP4S1, SLC25A12, SLC25A13
Protein complex assembly	AP2A2, MNAT1, PARD3
Diacylglycerol binding	CDC42BPA, PRKCA, PRKD1
Membrane fraction	KCNS3, PRKCA, TPST1
Cytosol	COVA1, FAF1, PRKD1
Kinase activity	MAPKAP1, NME7, PIP5K2A
Transcription from RNA Pol II promoter	NCOR1, PBX1
Positive regulation of transcription, DNA-dependent	NCOA1, SMARCC1
Electron transport	COVA1, ETFA
Motor activity	MYH10, MYO10
Actin binding	MYH10, MYO10
Cytoskeleton	MYO10, PTK2
Myosin	MYH10, MYO10
Transferase activity, transferring glycosyl groups	EXT1, FUT8
Protein serine/threonine phosphatase activity	CDC14B, PPP3CA
Iron ion binding	MIPEP, PPP3CA
Calmodulin binding	MYH10, PPP3CA
G-protein coupled receptor protein signaling pathway	EDG2, GNAQ
Phospholipase C activation	EDG2, GNAQ

Appendix 2. *Continued (cluster 3)*

Cell-cell signaling	ADM, GRB10
Protein tyrosine phosphatase activity	CDC14B, PTPRK
Receptor activity	EDG2, PTPRK
Development	JARID2, LDB2
Mitochondrial inner membrane	SLC25A12, SLC25A13
Guanyl-nucleotide exchange factor activity	ITSN1, PSD3
Cell proliferation	MNAT1, PRKD1
Transcription regulator activity	NCOA1, SSBP2
Protein self binding	CDC42BPA, FYN
mRNA 3'-UTR binding	AUH, PARN
Exonuclease activity	PARN, PRNPIP
Apoptosis	FAF1, STK3
Protein kinase cascade	FYN, STK3
Positive regulation of apoptosis	FAF1, STK3
Embryonic development	PBX1, PBX3
Hindbrain development	PBX1, PBX3
Regulation of transcriptional pre-initiation complex formation	PBX1, PBX3
Visual perception	PDE6D, TBL1X
Golgi apparatus	PRKD1, TPST1
Protein tyrosine/serine/threonine phosphatase activity	CDC14B, RNGTT
Oxidoreductase activity	COVA1, SQRDL
Centrosome	CEP63, MAD1L1
Cell division	MAD1L1, NEK1
Lyase activity	AUH, DERA
Intracellular	CBARA1, PRNPIP
Acyltransferase activity	NCOA1, ZDHHC14
Cell surface receptor linked signal transduction	CBLB, PRKCA
NF-Kappa B binding	FAF1, GSK3B
Coated pit	AP2A2, AP4S1
Ribonucleoprotein complex	MRPS27, MRPS28
Phosphoprotein phosphatase activity	PPAP2B, TNS3
Transcription factor binding	APBB2, DIP2C
Ubiquitin cycle	FBXL7, TBL1X
Tight junction	MPDZ, PARD3
Ras GTPase binding	MAPKAP1, RIN3
Heat shock protein binding	DNAJC15, FAF1
Regulation of GTPase activity	DDEF1, SMAP1

Appendix 2. *Continued (cluster 3)*

Axonogenesis	APBB2, PARD3

Appendix 2. *Continued (Cluster 4)*

Membrane	ANK2, COG5, DIAPH2, DKFZP779L1558, DNAJC1, DOCK1, FARP1, LARGE, PTPRG, PTPRM, ROBO1, STX8, VPS13B
Protein binding	ADAM12, ANK2, CASK, COG5, CRADD, DOCK1, PRKCA, PTBP1, SMYD3
Nucleus	AHNAK, BCAS3, DNAJC1, EGR3, PLCB1, PTBP1, RPS6KA2, SMYD3, SUPT3H
Nucleotide binding	CASK, DSCR1L1, DYRK4, FARS2, NUBPL, PRKCA, PTBP1, RPS6KA2
Transferase activity	ADK, CASK, DYRK4, PDSS2, PRKCA, PRPS1, RPS6KA2, SMYD3
Zinc ion binding	ADAM12, C9orf3, EGR3, NQO2, PRKCA, PTPRG, SMYD3
Cytoplasm	DOCK1, EIF1, EVL, FARP1, GMDS, PLCB1
Signal transduction	ANK2, BRE, CRADD, DOCK1, GABBR2, RSU1
ATP binding	CASK, DYRK4, FARS2, NUBPL, PRKCA, RPS6KA2
Integral to membrane	ADAM12, DNAJC1, LARGE, SGCD, VPS13B
Metal ion binding	ADAM12, C9orf3, EGR3, NQO2, SMYD3
Integral to plasma membrane	GABBR2, PTPRG, PTPRM, ROBO1, STX8
Cellular component unknown	DSCR1L1, DYRK4, EIF1, LRBA, PTHB1
Cell adhesion	ADAM12, CASK, FARP1, ROBO1
Oxidoreductase activity	ANK2, BCKDHB, MSRA, NQO2
Calcium ion binding	C14orf143, FBN2, PLCB1, PRKCA
Hydrolase activity	ACYP2, PLCB1, PTPRG, PTPRM
Molecular function unknown	COG5, LRBA, NUBPL, PTHB1
Protein amino acid phosphorylation	CASK, DYRK4, PRKCA, RPS6KA2
Cytoskeleton	DOCK1, FARP1, SGCD
Plasma membrane	ADAM12, CASK, SGCD
Receptor activity	GABBR2, PTPRM, ROBO1
Golgi stack	COG5, DKFZP779L1558, LARGE
Protein transport	COG5, DKFZP779L1558, DNAJC1
Kinase activity	ADK, CASK, PRPS1
Regulation of progression through cell cycle	PLCB1, PRKCA, SUPT3H
Protein serine/threonine kinase activity	CASK, DYRK4, RPS6KA2
Neurogenesis	AHNAK, EVL, ROBO1
GTPase activator activity	DOCK1, TBC1D5
Guanyl-nucleotide exchange factor activity	DOCK1, FARP1
Actin cytoskeleton	ANK2, CASK
Proteolysis and peptidolysis	ADAM12, C9orf3
Integrin-mediated signaling pathway	ADAM12, DOCK1
Carbohydrate metabolism	GBE1, GMDS
Transmembrane receptor protein tyrosine phosphatase activity	PTPRG, PTPRM
Protein amino acid dephosphorylation	PTPRG, PTPRM
Magnesium ion binding	ADK, PRPS1

Appendix 2. *Continued (cluster 4)*

Ribonucleoside monophosphate biosynthesis	ADK, PRPS1
Mitochondrion	BCKDHB, FARS2
Protein biosynthesis	EIF1, FARS2
Cell differentiation	DIAPH2, ROBO1
Transcription	EGR3, SUPT3H
Muscle development	EGR3, SGCD
Synaptic transmission	GABBR2, LARGE
Biological process unknown	LRBA, PTHB1
Binding	KIAA1797, LRBA
Perception of sound	KIAA1199, LARGE
Cell surface receptor linked signal transduction	EVL, PRKCA
Intracellular signaling cascade	PLCB1, PRKCA
Protein modification	MSRA, TTLL5

Appendix 3. Gene Ontology Classification of differentially regulated genes following interaction analysis (Cluster 1).

Nucleus	ABI1, APBB2, BMP2K, CDC14B, CDC27, CDC73, CLOCK, CREBBP, CTBP2, CTDSPL, DIP2C, DUSP10, EDD1, ERBB2IP, FOXF1, G3BP, HIP2, HIVEP2, HMGA2, HNRPA3, HRB, IPO7, KPNA1, MBNL1, MEIS1, MNAT1, N4BP1, NPAT, NR3C1, NUP88, PARP4, PBX3, PDCD11, PHF20, PIK3C2A, PNN, PPARD, PPP2R5C, PPP3CA, PRPF4B, PWP1, RAI17, RANBP5, RB1, RBMS1, RBPSUH, RNUT1, SATB2, SFRS3, SH3BP4, SSX2IP, STK17A, STK39, STRN3, SYNCRIP, TARDBP, TCF12, TCF4, TCF8, TEX10, THRAP1, TJP2, TLE4, TLK1, TRIP4, UBE3A, USP7, WDR50, XRCC4, ZFPM2, ZMYM4
Protein binding	ACTR3, AKT3, ANXA11, APAF1, CAB39, CHCHD3, CREBBP, CSNK2A1, DDEF1, DICER1, DNMBP, EDD1, EPS8, ERBB2IP, EVI5, FGFR1, FOXF1, FYN, G3BP, GNA12, HRB, IL4R, JMJD2B, KIAA0182, KPNA1, LAMC1, MAP2K4, MNAT1, NR3C1, PBX3, PEX14, PHF20, PHIP, PIK3C2A, PKP4, PPP2R2A, PPP2R3A, PRPF4B, PTK2, RAPGEF2, RB1, RBPSUH, RRAS2, SEC24D, SIPA1L3, SNX13, SOCS5, SSX2IP, STAU1, TARDBP, TCF4, TJP2, UBE2D2, UBE2D3, UBE2E1, VPS54
Nucleotide binding	ACTR3, AKT3, APAF1, ASCC3, ATP2B1, BMP2K, CSNK2A1, DDX10, DICER1, FGFR1, FYN, G3BP, GNA12, GNAI3, GNAQ, HNRPA3, HNRPDL, HNRPH3, MAP2K4, MAP3K5, MAP4K4, MYO10, OPA1, PDGFRA, PRKAR2A, PRPF4B, PTK2, RAB2, RAP1B, RBMS1, ROCK1, RRAS2, SFRS3, STK17A, STK24, STK39, SYNCRIP, TARDBP, TLK1, TRIO
Membrane	APBB2, ARFGEF2, ATP2B1, C1orf22, CHD9, DDEF1, DKFZP779L1558, EDG2, EMP1, EXT1, FGFR1, GNA12, IL4R, INPP5A, LPGAT1, NRP1, NUMB, PDGFRA, PEX14, PPAP2B, PTPRK, RAP1B, RAPGEF2, SLC4A4, TEX10, TJP2, TPST1, VEGFC
Signal transduction	AKT3, ARHGEF7, CLOCK, CREBBP, EDG2, EPS8, EXT1, GNA12, GNAI3, GNAQ, IL4R, IPO7, MAP2K4, MYO10, NR3C1, NRP1, PAFAH1B1, PDE8A, PPP2R2A, PPP2R5C, PPP2R5E, PPP4R1, PRKAR2A, ROCK1, STAM, STK24, VEGFC
Zinc ion binding	ARFGAP3, CENTB2, CREBBP, DDEF1, DDEF2, EDD1, HIVEP2, HRB, JMJD2B, KIAA0182, LEREPO4, MBNL1, MIPEP, MNAT1, MORC2, NR3C1, PHF20, PPARD, PPP3CA, RAI17, ROCK1, TCF8, TRIM44, TRIP4, USP3, ZFPM2, ZMYM4
ATP binding	ACTR3, AKT3, APAF1, ASCC3, ATP2B1, BMP2K, CSNK2A1, DDX10, DICER1, FGFR1, FYN, G3BP, MAP2K4, MAP3K5, MAP4K4, MYO10, PDGFRA, PRPF4B, PTK2, ROCK1, STK17A, STK24, STK39, TLK1, TMEM131, TRIO
Transferase activity	AKT3, BMP2K, CREBBP, CSNK2A1, FGFR1, FYN, HMBS, LPGAT1, MAP2K4, MAP3K5, MAP4K4, PCMT1, PDGFRA, PIK3C2A, PIP5K2A, PRPF4B, PTK2, ROCK1, STK17A, STK24, STK39, TLK1, TPST1, TRIO
Metal ion binding	ARFGAP3, CENTB2, CREBBP, DDEF1, DDEF2, EDD1, HIVEP2, HRB, JMJD2B, KIAA0182, MBNL1, MNAT1, MORC2, NR3C1, PHF20, PPARD, RAI17, ROCK1, TCF8, TRIM44, TRIP4, USP3, ZFPM2
Regulation of transcription, DNA-dependent	ASCC3, CREBBP, HIP2, HIVEP2, HMGA2, JMJD2B, JUN, MEIS1, NR3C1, PBX3, PDCD11, PHF20, PNN, RAI17, RB1, SATB2, TARDBP, TCF8, THRAP1, TLE4, TRIP4
Cytoplasm	ANXA11, ATG5, CREBBP, DNMBP, DUSP10, DUSP6, ERBB2IP, G3BP, GNAQ, IPO7, KPNA1, MBNL1, NR3C1, PCM1, PPP2R5E, PREP, PRKAR2A, RANBP5, SOCS5, STK39, TRIP4
Transcription	ASCC3, CDC73, FOXF1, HIVEP2, HMGA2, JUN, MNAT1, PCM1, PHF20, PNN, PPARD, PWP1, RAI17, RB1, RBPSUH, TARDBP, THRAP1, TRIP4, ZFPM2
Protein amino acid phosphorylation	AKT3, BMP2K, CSNK2A1, FGFR1, FYN, MAP2K4, MAP3K5, MAP4K4, PDGFRA, PRKAR2A, PRPF4B, PTK2, ROCK1, STK17A, STK24, STK39, TLK1, TRIO
Binding	ARFGEF2, C15orf29, CDC27, CLASP1, IPO7, KIAA1012, PKP4, PPP4R1, PSME4, PTK2, PUM1, PUM2, RANBP5, RAP1GDS1, TEX10, TTC17
Transcription factor activity	CLOCK, CREBBP, FOXF1, HIP2, JUN, MEIS1, NR3C1, PBX3, PPARD, RB1, RBPSUH, SATB2, TARDBP, TCF8
RNA binding	DDX10, G3BP, HNRPA3, HNRPH3, HRB, MRPL3, PDCD11, PUM1, PUM2, RBMS1, SFRS3, SNRPA1, SYNCRIP, TARDBP
DNA binding	G3BP, HIVEP2, HMGA2, HRB, PARP4, PCM1, PHF20, PNN, RBMS1, SATB2, TCF12, TCF4, ZFPM2, ZMYM4
Hydrolase activity	ARSJ, ASCC3, ATP2B1, CDC14B, DDX10, DICER1, DUSP10, DUSP6, G3BP, INPP5A, PDE8A, PPAP2B, PPP3CA, PTPRK
Protein Ser/Thr kinase activity	AKT3, BMP2K, CSNK2A1, FGFR1, MAP2K4, MAP3K5, MAP4K4, PRPF4B, ROCK1, STK17A, STK24, TLK1, TRIO

Appendix 3. *Continued (cluster 1)*

Nucleic acid binding	ASCC3, G3BP, HNRPDL, JMJD2B, LEREPO4, MBNL1, OSBPL3, PHF20, QKI, R3HDM1, SFRS3, TARDBP
Signal transducer activity	CASP8, CLOCK, CREBBP, GNA12, GNAI3, GNAQ, PDE8A, PPP1R12A, RAPGEF2, SH3BP4, SNX13, WNT5B
Cell cycle	CDC73, CLASP1, ERBB2IP, EXT1, MNAT1, PAFAH1B1, PNN, SASH1, SH3BP4, STRN3, TLK1
Integral to membrane	CHD9, EDG2, EMP1, EXT1, LPGAT1, NRP1, PPAP2B, PPP2R5C, SLC4A4, TEX10, TPST1
Cellular component unknown	CTDSPL, FYN, KIAA0553, LRRFIP2, MAP4K4, PDE8A, PHIP, RAP1GDS1, RBMS1, SACS, TLK1
Ubiquitin cycle	EDD1, HIP2, NEDD4, UBE2D2, UBE2D3, UBE2E1, UBE3A, USP3, USP7, USP9X
Cytoskeleton	ABI1, CASP8, CLASP1, DNMBP, MYO10, PAFAH1B1, PKP4, PTK2, RAP1GDS1, ROCK1
Cell proliferation	CDC27, EDD1, EMP1, EPS8, EVI5, MNAT1, PDGFRA, PPARD, TCF8, VEGFC
Calcium ion binding	ANXA11, ARSJ, ATP2B1, C1orf22, MIPEP, PPP2R3A, PPP3CA, RAPGEF2, TBC1D9, ZZEF1
Intracellular signaling cascade	APBB2, ARFGEF2, DNMBP, FYN, PIK3C2A, PRKAR2A, ROCK1, SNX13, SOCS5, TLK1
Protein transport	DKFZP779L1558, IPO7, NUP88, PEX14, PRPF4B, RAB2, RANBP5, SNX13, VPS54
Cytosol	ABI1, APAF1, ARFGAP3, ARFGEF2, ARFIP1, PSMD14, PSMF1, STRN3, TNFSF5IP1
Ubiquitin-dependent protein catabolism	EDD1, PSMD14, PSMF1, UBE2E1, UBE3A, USP3, USP34, USP7, USP9X
Intracellular	APAF1, DICER1, G3BP, KIAA0182, NEDD4, ROCK1, STAU1, TRIM44, UBE3A
Integral to plasma membrane	ATP2B1, EDG2, FGFR1, IL4R, NUMB, PDGFRA, PTPRK, RAPGEF2, TJP2
Ubiquitin-protein ligase activity	EDD1, FBXW11, HIP2, NEDD4, UBE2D2, UBE2D3, UBE2E1, UBE3A
Ligase activity	EDD1, HIP2, NEDD4, PCCB, UBE2D2, UBE2D3, UBE2E1, UBE3A
Development	EMP1, EVI5, HMGA2, MEIS1, NUMB, TCF12, WNT5B, ZMYM4
Golgi stack	DDEF2, DKFZP779L1558, DNMBP, EXT1, GOLGA4, KIAA1012, RAB2, SEC24D
Molecular function unknown	ARFIP1, CTDSPL, KIAA0553, LPGAT1, RB1, SACS, SEC24D, TLE4
Mitochondrion	CASP8, CHCHD3, MIPEP, MRPL3, MRPS35, OPA1, PCCB, SQRDL
GTP binding	GNA12, GNAI3, GNAQ, OPA1, RAB2, RAP1B, RRAS2
Transport	G3BP, GNAI3, HRB, KIAA1012, PARP4, RNUT1, TEX10
Membrane fraction	EMP1, FGFR1, GOLGA4, NRP1, PRKAR2A, STRN3, TPST1
Biological process unknown	ARFIP1, CTDSPL, KIAA0553, LPGAT1, LRRFIP2, RAP1GDS1, TLE4
Receptor activity	EDG2, FGFR1, IL4R, NRP1, PDGFRA, PTPRK, THRAP1
Protein amino acid dephosphorylation	CDC14B, DUSP10, DUSP6, PPP2R2A, PPP2R3A, PPP3CA, PTPRK
Endoplasmic reticulum	ABI1, C1orf22, LPGAT1, PCMT1, RAB2, SEC24D, SYNCRIP
Apoptosis	ATG5, MAP3K5, PDCD10, PDCD11, PPARD, ROCK1, STK17A
Nuclear pore	HRB, IPO7, KPNA1, NUP88, RANBP5, RNUT1
RNA Pol II transcription factor activity	JUN, MEIS1, RBPSUH, TCF12, TCF4, ZFPM2
Intracellular protein transport	ARFGAP3, ARFIP1, KPNA1, SEC24D, STAM, TLK1
Regulation of GTPase activity	ARFGAP3, CENTB2, DDEF1, DDEF2, HRB, SMAP1
Regulation of transcription from RNA Pol II Promoter	CLOCK, FOXF1, MNAT1, TCF12, TCF4, ZFPM2
GTPase activator activity	ARHGAP12, CENTB2, DDEF1, DDEF2, RAP1GDS1, SIPA1L3
mRNA splicing, via spliceosome	HNRPH3, PRPF4B, SFRS3, SYNCRIP, TARDBP

Appendix 3. *Continued (Cluster 1)*

Cell adhesion	ERBB2IP, LAMC1, NRP1, PKP4, SSX2IP
Neurogenesis	APAF1, MBNL1, NRP1, PAFAH1B1, PHF20
Small GTPase mediated signal transduction	BCAR3, RAB2, RAP1B, RAPGEF2, RRAS2
Soluble fraction	ABI1, DUSP6, EDD1, IPO7, PPP4R1
Metabolism	ARSJ, ATP2B1, CTBP2, DIP2C, LPGAT1
Negative regulation of progression through cell cycle	CDC73, EXT1, PNN, RB1, SASH1
Transcription coactivator activity	CREBBP, FOXF1, RB1, TCF8, TRIP4
Guanyl-nucleotide exchange factor activity	ARFGEF2, ARHGEF7, BCAR3, DNMBP, TRIO
Protein-tyrosine kinase activity	FGFR1, FYN, MAP2K4, PTK2, STK24
Magnesium ion binding	ATP2B1, MAP3K5, MIPEP, OPA1, PDE8A
Proteolysis and peptidolysis	C1orf22, CASP8, MIPEP, PREP, UBE3A
Transcription from RNA pol II promoter	NR3C1, RBPSUH, TARDBP, TRIP4
Protein complex assembly	CREBBP, LAMC1, MNAT1, WASPIP
Protein transporter activity	ARFGAP3, IPO7, KPNA1, RANBP5
Cysteine-type endopeptidase activity	USP3, USP34, USP7, USP9X
Ubiquitin thiolesterase activity	USP3, USP34, USP7, USP9X
GTPase activity	GNA12, GNAI3, GNAQ, OPA1
G-protein coupled receptor protein signaling pathway	EDG2, GNA12, GNAI3, GNAQ
Transcription factor binding	APBB2, DIP2C, JUN, PDCD11
Protein phosphatase type 2a complex	PPP2R2A, PPP2R3A, PPP2R5C, PPP2R5E
Protein phosphatase type 2a regulator activity	PPP2R2A, PPP2R3A, PPP2R5C, PPP2R5E
RNA splicing	HNRPH3, PRPF4B, SNRPA1, SYNCRIP
ER to golgi transport	ARFGAP3, KIAA1012, RAB2, SEC24D
Plasma membrane	EDG2, GNAQ, PRKAR2A, SSFA2
Response to stress	DUSP10, MAP3K5, MAP4K4, STK39
Immune response	ANXA11, IL4R, TCF12, TCF8
Kinase activity	PIP5K2A, PRKAR2A, ROCK1, STK24
Mitosis	CLASP1, PAFAH1B1, TARDBP
Lipid Metabolism	PAFAH1B1, PPAP2B, PPARD
Cell Differentiation	NRP1, PAFAH1B1, VEGFC
Double-stranded RNA binding	DICER1, MBNL1, STAU1
Regulation of translation	PUM1, PUM2, RBMS1

Appendix 3. *Continued (cluster 1)*

Cell growth	EMP1, ERBB2IP, FGFR1
Peptidase activity	C1orf22, PPP2R5C, USP7
DNA repair	MNAT1, PARP4, XRCC4
Inflammatory response	NR3C1, PARP4, TPST1
Ribonucleoprotein complex	HNRPA3, PARP4, SYNCRIP
Protein serine/threonine phosphatase activity	CDC14B, DUSP6, PPP3CA
Calmodulin binding	ATP2B1, PPP3CA, STRN3
Protein kinase cascade	FYN, MAP4K4, STK17A
Protein tyrosine phosphatase activity	CDC14B, DUSP6, PTPRK
MAPKKK cascade	FGFR1, MAP3K5, RAPGEF2
Negative regulation of transcription From RNA Pol II Promoter	PPARD, RB1, TCF8
RNA processing	DICER1, HNRPDL, RBMS1
Protein self binding	CASP8, FYN, MAP3K5
Regulation of progression through cell cycle	BCAR3, DUSP6, VEGFC
Positive regulation of I-Kappa B kinase/NF-Kappa B cascade	CASP8, EDG2, PDCD11
ATP-dependent helicase activity	ASCC3, DDX10, DICER1
Ubiquitin conjugating enzyme activity	EDD1, UBE2E1, UBE3A
Nuclear membrane	ANXA11, PAFAH1B1
Microtubule	CLASP1, PAFAH1B1
Microtubule associated complex	PAFAH1B1, STAU1
Cell motility	ACTR3, PAFAH1B1
Cell division	CLASP1, PAFAH1B1
Protein-nucleus import, docking	IPO7, RANBP5
Small GTPase regulator activity	IPO7, MAP4K4
Ran GTPase binding	IPO7, RANBP5
Protein complex	PSMF1, TNFSF5IP1
Muscle development	MBNL1, TCF12
Negative regulation of cell proliferation	ABI1, CTBP2
Oxidoreductase activity	CTBP2, SQRDL
Cell death	EMP1, PARP4
Epidermis development	EMP1, PPARD
Endonuclease activity	DICER1, G3BP
Transporter activity	G3BP, NUP88

Appendix 3. *Continued (cluster 1)*

Vesicle-mediated transport	ARFGAP3, GOLGA4
Actin cytoskeleton	PPP1R12A, WASPIP
Structural molecule activity	ACTR3, PKP4
Motor activity	MYO10, OPA1
Actin binding	MYO10, WASPIP
Androgen receptor signaling pathway	RB1, THRAP1
Skeletal development	EXT1, FGFR1
Transferase activity, transferring glycosyl groups	EXT1, PARP4
Nls-bearing substrate-nucleus import	KPNA1, RANBP5
Nuclear localization sequence binding	KPNA1, RANBP5
Autophagy	ATG5, PRPF4B
Protein amino acid ADP-ribosylation	GNAQ, PARP4
Response to drug	BCAR3, PARP4
Fatty acid catabolism	PCCB, PPARD
Iron ion binding	MIPEP, PPP3CA
Response to DNA damage stimulus	EDD1, TLK1
Sh3/Sh2 adaptor activity	EPS8, STAM
Epidermal growth factor receptor signaling pathway	EPS8, ERBB2IP
Phospholipase C activation	EDG2, GNAQ
Blood coagulation	GNA12, GNAQ
Diacylglycerol binding	RAPGEF2, ROCK1
Vascular endothelial growth factor receptor activity	NRP1, PDGFRA
Transmembrane receptor protein tyrosine kinase signaling pathway	ABI1, PDGFRA
Chromatin	HMGA2, RB1
Negative regulation of cell growth	APBB2, RB1
JNK cascade	DUSP10, MAP2K4
Double-stranded DNA binding	HNRPDL, RBMS1
Single-stranded DNA binding	HNRPDL, RBMS1
Caspase activator activity	APAF1, MAP3K5
Regulation of apoptosis	APAF1, CASP8
DNA recombination	RBPSUH, XRCC4
Protein modification	PCMT1, SACS

Appendix 3. *Continued (cluster 1)*

Intracellular transporter activity	KIAA1012, STAU1
Negative regulation of signal transduction	SNX13, SOCS5
Integrin-mediated signaling pathway	ERBB2IP, PTK2
Map kinase phosphatase activity	DUSP10, DUSP6
Regulation of transcription	APBB2, TCF12
Heterogeneous nuclear ribonucleoprotein complex	HNRPDL, HNRPH3
Wnt receptor signaling pathway	CSNK2A1, FBXW11
Angiogenesis	NRP1, VEGFC
Positive regulation of cell proliferation	NRP1, VEGFC
Calcium ion transport	ATP2B1, FYN
Manganese ion binding	MIPEP, PDE8A
Transcription corepressor activity	TCF8, ZFPM2
Phosphoinositide binding	PIK3C2A, SNX13
Centrosome	CDC27, CEP63
Golgi membrane	ARFGEF2, ARFIP1

Appendix 3. *Continued (Cluster 2)*

Nucleus	ATF3, BRD1, C20orf11, C4orf9, CTDSP2, DIDO1, E2F6, EIF4ENIF1, ELF4, GADD45A, GTPBP4, HEAB, HEXIM1, HIST2H2BE, HSPC111, IHPK2, ING1, IPPK, KCTD13, MAD2L1BP, MAX, MBD4, MCL1, NFYA, NKRF, NXF1, PER2, PHLDA1, POLR1C, POLR2D, POLS, PPM1D, PPP2R1B, PTDSR, PUS1, RAE1, RARA, RBM14, RBM4, RBM4B, RNF4, RNPC2, RNPS1, SAS10, SFRS4, SNAPC4, SNAPC5, SNIP1, SPEN, SRRM1, STK17B, TAF7, TCF8, TOB2, TRIM32, UBE2B, UPF3A, ZBTB5, ZNF202, ZNF232, ZNF263, ZNF468, ZNF7
Protein binding	BRD1, DIDO1, EIF4ENIF1, EIF5, ELF4, HEXIM1, ING1, KCTD13, LRRC8D, MAD2L1BP, MBD4, MCL1, MYD88, NFYA, NXF1, PLK2, PMAIP1, PPP2R1B, RAB11FIP5, RFP2, RNF4, RNF44, SMNDC1, TAF7, TOB1, TRIM32, ZBTB5
Regulation of transcription, DNA-dependent	ATF3, BRD1, BTG2, DIDO1, E2F6, ELF4, ING1, MAX, NFYA, NKRF, PER2, RARA, RBM14, RNPC2, SNAPC4, SNAPC5, SPEN, TAF7, TCF8, ZBTB5, ZNF202, ZNF232, ZNF263, ZNF468, ZNF7
Nucleotide binding	ARS2, CSNK1D, DYRK2, EIF5, FLJ12529, GTPBP4, HEAB, IPPK, MKNK2, NXF1, PEO1, PLK2, PPRC1, RAB9A, RBM14, RBM4, RBM4B, RIT1, RNPC2, RNPS1, SFRS4, SPEN, STK17B, UPF3A
Transcription	ATF3, BTG2, DIDO1, E2F6, ELF4, NFYA, NKRF, PER2, POLR1C, POLR2D, RARA, RBM14, RNF4, RNPC2, RNPS1, SNAPC5, TFAM, ZBTB5, ZNF202, ZNF232, ZNF263, ZNF7
Zinc ion binding	ADAMTS1, BRD1, DIDO1, IBRDC3, ING1, RARA, RBM4, RBM4B, RFP2, RNF4, RNF44, TCF8, TRIM32, ZBTB5, ZNF202, ZNF232, ZNF263, ZNF468, ZNF7
Metal ion binding	ADAMTS1, BRD1, DIDO1, IBRDC3, ING1, RARA, RBM4, RBM4B, RFP2, RNF4, RNF44, TCF8, TRIM32, ZBTB5, ZNF202, ZNF232, ZNF263, ZNF468, ZNF7
Transcription factor activity	ATF3, BTG2, E2F6, ELF4, MAX, NFYA, RARA, RNF4, SNAPC5, SOLH, TAF7, TCF8, TFAM, ZNF202, ZNF232, ZNF263
Membrane	ADFP, CANT1, FAS, GPRC5A, IBRDC3, KCTD13, LRRC8D, MCL1, MYD88, PPP2R1B, RAB9A, RIT1, SLC25A28, SNN, UBE2B
RNA binding	CHERP, DKC1, NXF1, RAE1, RBM14, RBM4, RBM4B, RNASEH1, RNPC2, RNPS1, SPEN, SRRM1, UPF3A
DNA binding	ATF3, HIST2H2BE, MAX, MBD4, NKRF, POLR1C, POLS, SNAPC4, SPEN, SRRM1, ZBTB5, ZNF7
Molecular function unknown	ARS2, BRD1, CHMP7, CISH, CTDSP2, ING1, KIAA0174, MRPL49, RP5-1104E15.5, SAS10, TRIAP1
Transferase activity	CSNK1D, DYRK2, IHPK2, IPPK, MKNK2, PLK2, POLR1C, POLR2D, POLS, STK17B
Nucleic acid binding	FLJ12529, PPRC1, RBM14, RNPC2, SPEN, TRIM32, ZNF202, ZNF468, ZNF7
Signal transduction	CSNK1D, FAS, GDF15, GPRC5A, INPP1, NTF3, PER2, RARA, RIT1
Cytoplasm	CHERP, DYRK2, EIF4ENIF1, HEXIM1, MAD2L1BP, RAE1, SMNDC1, UPF3A
ATP binding	CSNK1D, DYRK2, HEAB, IPPK, MKNK2, PEO1, PLK2, STK17B
Hydrolase activity	CANT1, CTDSP2, INPP1, MBD4, MRPL44, PEO1, PPM1D, RNASEH1
Apoptosis	CROP, DIDO1, FAS, GADD45A, PHLDA1, SMNDC1, STK17B
Integral to membrane	CANT1, FAS, IBRDC3, LRRC8D, MCL1, SLC25A28, SNN
Cellular component unknown	AMD1, ARS2, CISH, CTDSP2, MRPL49, RP5-1104E15.5, TRIAP1
DNA repair	BTG2, CSNK1D, GADD45A, HUS1, KCTD13, RBM14, UBE2B
Negative regulation of cell proliferation	ADAMTS1, BTG2, CHERP, ING1, PPM1D, TOB1, TOB2
Nuclear mRNA splicing, via spliceosome	RBM4, RBM4B, RNPC2, RNPS1, SFRS4, SRRM1
Mitochondrion	MCL1, MRPL44, MRPL49, PEO1, PPP2R1B, TFAM
Intracellular	CARF, CHERP, MRPL49, RFP2, SOLH, ZNF7
Cell cycle	E2F6, GADD45A, ING1, POLS, PPM1D, RFP2

Appendix 3. *Continued (cluster 2)*

Transcription coactivator activity	RARA, RNF4, TAF7, TCF8, TRIM32
mRNA processing	HEAB, NXF1, RNPC2, SRRM1, UPF3A
Regulation of progression through cell cycle	DKC1, E2F6, PPM1D, PPP2R1B, TOB2
Protein serine/threonine kinase activity	CSNK1D, DYRK2, MKNK2, PLK2, STK17B
Signal transducer activity	CANT1, MYD88, PER2, PLK2, RFP2
Protein amino acid phosphorylation	CSNK1D, DYRK2, MKNK2, PLK2, STK17B
GTP binding	EIF5, GTPBP4, HEAB, RAB9A, RIT1
Biological process unknown	BRD1, CTDSP2, RAB11FIP5, RP5-1104E15.5, TRIAP1
RNA splicing	PPP2R1B, RNPS1, SFRS4, SMNDC1
Induction of apoptosis	FAS, PPP2R1B, SMNDC1, STK17B
Positive regulation of I-Kappa B kinase/NF-Kappa B cascade	CANT1, MYD88, PLK2, RFP2
DNA replication	KCTD13, PEO1, POLS, RBM14
Magnesium ion binding	DYRK2, INPP1, PPM1D, RNASEH1
Negative regulation of transcription from RNA Pol II promoter	E2F6, HEXIM1, TCF8, ZNF202
Anti-apoptosis	FAS, MCL1, NTF3
Cell differentiation	MCL1, PTDSR, TNFAIP2
Isomerase activity	C12orf5, DKC1, PUS1
Translation initiation factor activity	EIF4ENIF1, EIF5, MRPL49
Ubiquitin cycle	RNF44, TRIM32, UBE2B
Transcription corepressor activity	ATF3, E2F6, TCF8
Soluble fraction	CTDSP2, FAS, PPP2R1B
Cytosol	EIF5, FAS, PPP2R1B
Negative regulation of cell growth	IHPK2, ING1, PPP2R1B
Regulation of transcription	KCTD13, MAX, PPP2R1B
Transcription from RNA Pol II promoter	NFYA, POLR2D, SNAPC5
mRNA-nucleus export	NXF1, RAE1, UPF3A
Transport	NXF1, SLC25A28, UPF3A
Small GTPase mediated signal transduction	GTPBP4, RAB9A, RIT1
mRNA catabolism, nonsense-mediated decay	RNPS1, UPF3A
RNA splicing factor activity,	SFRS4, SMNDC1

Appendix 3. *Continued (cluster 2)*

transesterification mechanism	
Mitochondrial outer membrane	MCL1, RAB11FIP5
Regulation of apoptosis	FAS, MCL1
Protein heterodimerization activity	MCL1, PPP2R1B
Pseudouridylate synthase activity	DKC1, PUS1
Nucleoplasm	DKC1, RNPC2
rRNA processing	C4orf9, DKC1
Cell proliferation	DKC1, TCF8
Protein biosynthesis	EIF5, MRPL49
RNA processing	CHERP, MRPL44
Neurogenesis	CHERP, NTF3
Ligase activity	TRIM32, UBE2B
Extracellular space	GDF15, TNFAIP2
Protein dimerization activity	ATF3, POLR1C
Binding	PPP2R1B, SLC25A28
Regulation of translation	MKNK2, PPP2R1B
Protein complex assembly	FAS, PPP2R1B
Protein amino acid dephosphorylation	PPM1D, PPP2R1B
Manganese ion binding	DYRK2, PPM1D
Metabolism	C12orf5, SPR
Negative regulation of progression through cell cycle	ING1, RFP2
DNA-directed RNA Pol activity	POLR1C, POLR2D
Transcription factor complex	E2F6, RBM14
ribonucleoprotein complex	MRPL44, RBM14
Positive regulation of transcription From RNA Pol II promoter	ELF4, RBM14
Proteolysis and peptidolysis	ADAMTS1, SOLH
Transmembrane receptor activity	FAS, MYD88
Immune response	FAS, TCF8
Development	SAS10, ZNF7
Protein kinase cascade	MKNK2, STK17B
Cell-cell signaling	GDF15, NTF3
Growth factor activity	GDF15, NTF3
GTPase activity	EIF5, RAB9A
Endoplasmic reticulum	ADFP, CANT1
Cell surface receptor linked	MKNK2, MYD88

Appendix 3. *Continued (cluster 2)*

signal transduction	
Response to stress	CROP, SNN
Double-stranded RNA binding	CARF, MRPL44
Endonuclease activity	MRPL44, RNASEH1
Protein transport	EIF4ENIF1, RAB9A
Golgi stack	CANT1, RAB9A

Appendix 3. *Continued (cluster 3)*

Cytoplasm	COL1A2, GFPT1, RANBP5
Protein binding	ANK1, GORASP2, TNC
Biological process unknown	COL1A2, TBL2
Skeletal development	COL1A2, FBN1
Extracellular matrix structural constituent	COL1A2, FBN1
Golgi stack	AP3S1, GORASP2
Metabolism	GFPT1, MICAL2
Extracellular matrix (Sensu Metazoa)	FBN1, TNC
Cytoskeleton	ANK1, MICAL2
Signal transduction	ANK1, GABBR2
Nucleus	PHTF1, RANBP5
Integral to plasma membrane	GABBR2, HAS2
Membrane	GORASP2, HAS2
Zinc ion binding	C9orf3, MICAL2
Metal ion binding	C9orf3, MICAL2

References

ABE, T., OUE, N., YASUI, W. & RYOJI, M. (2003) Rapid and preferential induction of ATF3 transcription in response to low doses of UVA light. *Biochem Biophys Res Commun,* 310, 1168-74.

ABOUSSEKHRA, A., BIGGERSTAFF, M., SHIVJI, M. K., VILPO, J. A., MONCOLLIN, V., PODUST, V. N., PROTIC, M., HUBSCHER, U., EGLY, J. M. & WOOD, R. D. (1995) Mammalian DNA nucleotide excision repair reconstituted with purified protein components. *Cell,* 80, 859-68.

ADAMS, P. D. (2001) Regulation of the retinoblastoma tumor suppressor protein by cyclin/cdks. *Biochim Biophys Acta,* 1471, M123-33.

ADIMOOLAM, S. & FORD, J. M. (2002) p53 and DNA damage-inducible expression of the xeroderma pigmentosum group C gene. *Proc Natl Acad Sci U S A,* 99, 12985-90.

ADIMOOLAM, S. & FORD, J. M. (2003) p53 and regulation of DNA damage recognition during nucleotide excision repair. *DNA Repair (Amst),* 2, 947-54.

ADIMOOLAM, S., LIN, C. X. & FORD, J. M. (2001) The p53-regulated cyclin-dependent kinase inhibitor, p21 (cip1, waf1, sdi1), is not required for global genomic and transcription-coupled nucleotide excision repair of UV-induced DNA photoproducts. *J Biol Chem,* 276, 25813-22.

AFAQ, F., ADHAMI, V. M. & MUKHTAR, H. (2005) Photochemoprevention of ultraviolet B signaling and photocarcinogenesis. *Mutat Res,* 571, 153-73.

AGAR, N. S., HALLIDAY, G. M., BARNETSON, R. S., ANANTHASWAMY, H. N., WHEELER, M. & JONES, A. M. (2004) The basal layer in human squamous tumors harbors more UVA than UVB fingerprint mutations: a role for UVA in human skin carcinogenesis. *Proc Natl Acad Sci U S A,* 101, 4954-9.

AIKATA, H., TAKAISHI, H., KAWAKAMI, Y., TAKAHASHI, S., KITAMOTO, M., NAKANISHI, T., NAKAMURA, Y., SHIMAMOTO, F., KAJIYAMA, G. & IDE, T. (2000) Telomere reduction in human liver tissues with age and chronic inflammation. *Exp Cell Res,* 256, 578-82.

AL-BAKER, E. A., OSHIN, M., HUTCHISON, C. J. & KILL, I. R. (2005) Analysis of UV-induced damage and repair in young and senescent human dermal fibroblasts using the comet assay. *Mech Ageing Dev,* 126, 664-72.

ALCORTA, D. A., XIONG, Y., PHELPS, D., HANNON, G., BEACH, D. & BARRETT, J. C. (1996) Involvement of the cyclin-dependent kinase inhibitor p16 (INK4a) in replicative senescence of normal human fibroblasts. *Proc Natl Acad Sci U S A,* 93, 13742-7.

ALLAN, L. A. & FRIED, M. (1999) p53-dependent apoptosis or growth arrest induced by different forms of radiation in U2OS cells: p21WAF1/CIP1 repression in UV induced apoptosis. *Oncogene,* 18, 5403-12.

ALLSOPP, R. C., VAZIRI, H., PATTERSON, C., GOLDSTEIN, S., YOUNGLAI, E. V., FUTCHER, A. B., GREIDER, C. W. & HARLEY, C. B. (1992) Telomere length predicts replicative capacity of human fibroblasts. *Proc Natl Acad Sci U S A,* 89, 10114-8.

AMRANI, N., SACHS, M. S. & JACOBSON, A. (2006) Early nonsense: mRNA decay solves a translational problem. *Nat Rev Mol Cell Biol,* 7, 415-25.

AMUNDSON, S. A., LEE, R. A., KOCH-PAIZ, C. A., BITTNER, M. L., MELTZER, P., TRENT, J. M. & FORNACE, A. J., JR. (2003) Differential responses of stress genes to low dose-rate gamma irradiation. *Mol Cancer Res,* 1, 445-52.

AMUNDSON, S. A., PATTERSON, A., DO, K. T. & FORNACE, A. J., JR. (2002) A nucleotide excision repair master-switch: p53 regulated coordinate induction of global genomic repair genes. *Cancer Biol Ther,* 1, 145-9.

ANANTHASWAMY, H. N. & PIERCEALL, W. E. (1990) Molecular mechanisms of ultraviolet radiation carcinogenesis. *Photochem Photobiol,* 52, 1119-36.

ANDLEY, U. P., PATEL, H. C., XI, J. H. & BAI, F. (2004) Identification of genes responsive to UV-A radiation in human lens epithelial cells using complementary DNA microarrays. *Photochem Photobiol,* 80, 61-71.

ANDRESSOO, J. O. & HOEIJMAKERS, J. H. (2005) Transcription-coupled repair and premature ageing. *Mutat Res,* 577, 179-94.

ANDRESSOO, J. O., MITCHELL, J. R., DE WIT, J., HOOGSTRATEN, D., VOLKER, M., TOUSSAINT, W., SPEKSNIJDER, E., BEEMS, R. B., VAN STEEG, H., JANS, J., DE ZEEUW, C. I., JASPERS, N. G., RAAMS, A., LEHMANN, A. R., VERMEULEN, W., HOEIJMAKERS, J. H. & VAN DER HORST, G. T. (2006) An Xpd mouse model for the combined xeroderma pigmentosum/Cockayne syndrome exhibiting both cancer predisposition and segmental progeria. *Cancer Cell,* 10, 121-32.

ARAKI, M., MASUTANI, C., MAEKAWA, T., WATANABE, Y., YAMADA, A., KUSUMOTO, R., SAKAI, D., SUGASAWA, K., OHKUMA, Y. & HANAOKA, F. (2000) Reconstitution of damage DNA excision reaction from SV40 minichromosomes with purified nucleotide excision repair proteins. *Mutat Res,* 459, 147-60.

ARAKI, M., MASUTANI, C., TAKEMURA, M., UCHIDA, A., SUGASAWA, K., KONDOH, J., OHKUMA, Y. & HANAOKA, F. (2001) Centrosome protein centrin 2/caltractin 1 is part of the

xeroderma pigmentosum group C complex that initiates global genome nucleotide excision repair. *J Biol Chem,* 276, 18665-72.

ARAUJO, S. J., NIGG, E. A. & WOOD, R. D. (2001) Strong functional interactions of TFIIH with XPC and XPG in human DNA nucleotide excision repair, without a preassembled repairosome. *Mol Cell Biol,* 21, 2281-91.

ARAUJO, S. J., TIRODE, F., COIN, F., POSPIECH, H., SYVAOJA, J. E., STUCKI, M., HUBSCHER, U., EGLY, J. M. & WOOD, R. D. (2000) Nucleotide excision repair of DNA with recombinant human proteins: definition of the minimal set of factors, active forms of TFIIH, and modulation by CAK. *Genes Dev,* 14, 349-59.

ARIVAZHAGAN, P., MIZUTANI, E., FUJII, M. & AYUSAWA, D. (2004) Cardiolipin induces premature senescence in normal human fibroblasts. *Biochem Biophys Res Commun,* 323, 739-42.

AZZAM, E. I., NAGASAWA, H., YU, Y., LI, C. Y. & LITTLE, J. B. (2002) Cell cycle deregulation and xeroderma pigmentosum group C cell transformation. *J Invest Dermatol,* 119, 1350-4.

BAKALKIN, G., SELIVANOVA, G., YAKOVLEVA, T., KISELEVA, E., KASHUBA, E., MAGNUSSON, K. P., SZEKELY, L., KLEIN, G., TERENIUS, L. & WIMAN, K. G. (1995) p53 binds single-stranded DNA ends through the C-terminal domain and internal DNA segments via the middle domain. *Nucleic Acids Res,* 23, 362-9.

BALAJEE, A. S. & BOHR, V. A. (2000) Genomic heterogeneity of nucleotide excision repair. *Gene,* 250, 15-30.

BALAJEE, A. S., MAY, A. & BOHR, V. A. (1999) DNA repair of pyrimidine dimers and 6-4 photoproducts in the ribosomal DNA. *Nucleic Acids Res,* 27, 2511-20.

BALAJEE, A. S., MAY, A., DIANOV, G. L., FRIEDBERG, E. C. & BOHR, V. A. (1997) Reduced RNA polymerase II transcription in intact and permeabilized Cockayne syndrome group B cells. *Proc Natl Acad Sci U S A,* 94, 4306-11.

BALASUBRAMANIAN, D. (2000) Ultraviolet radiation and cataract. *J Ocul Pharmacol Ther,* 16, 285-97.

BARGONETTI, J., REYNISDOTTIR, I., FRIEDMAN, P. N. & PRIVES, C. (1992) Site-specific binding of wild-type p53 to cellular DNA is inhibited by SV40 T antigen and mutant p53. *Genes Dev,* 6, 1886-98.

BARLEY, R. D., ENNS, L., PATERSON, M. C. & MIRZAYANS, R. (1998) Aberrant p21WAF1-dependent growth arrest as the possible mechanism of abnormal resistance to ultraviolet light cytotoxicity in Li-Fraumeni syndrome fibroblast strains heterozygous for TP53 mutations. *Oncogene,* 17, 533-43.

BARNES, D. E., TOMKINSON, A. E., LEHMANN, A. R., WEBSTER, A. D. & LINDAHL, T. (1992) Mutations in the DNA ligase I gene of an individual with immunodeficiencies and cellular hypersensitivity to DNA-damaging agents. *Cell,* 69, 495-503.

BATES, S. E., ZHOU, N. Y., FEDERICO, L. E., XIA, L. & O'CONNOR, T. R. (2005) Repair of cyclobutane pyrimidine dimers or dimethylsulfate damage in DNA is identical in normal or telomerase-immortalized human skin fibroblasts. *Nucleic Acids Res,* 33, 2475-85.

BATTY, D., RAPIC'-OTRIN, V., LEVINE, A. S. & WOOD, R. D. (2000) Stable binding of human XPC complex to irradiated DNA confers strong discrimination for damaged sites. *J Mol Biol,* 300, 275-90.

BAUR, J. A., ZOU, Y., SHAY, J. W. & WRIGHT, W. E. (2001) Telomere position effect in human cells. *Science,* 292, 2075-7.

BAXTER, B. K. & SMERDON, M. J. (1998) Nucleosome unfolding during DNA repair in normal and xeroderma pigmentosum (group C) human cells. *J Biol Chem,* 273, 17517-24.

BEAN, L. J. & STARK, G. R. (2001) Phosphorylation of serines 15 and 37 is necessary for efficient accumulation of p53 following irradiation with UV. *Oncogene,* 20, 1076-84.

BECKER, B., VOGT, T., LANDTHALER, M. & STOLZ, W. (2001) Detection of differentially regulated genes in keratinocytes by cDNA array hybridization: Hsp27 and other novel players in response to artificial ultraviolet radiation. *J Invest Dermatol,* 116, 983-8.

BENDER, K., BLATTNER, C., KNEBEL, A., IORDANOV, M., HERRLICH, P. & RAHMSDORF, H. J. (1997) UV-induced signal transduction. *J Photochem Photobiol B,* 37, 1-17.

BENDJENNAT, M., BOULAIRE, J., JASCUR, T., BRICKNER, H., BARBIER, V., SARASIN, A., FOTEDAR, A. & FOTEDAR, R. (2003) UV irradiation triggers ubiquitin-dependent degradation of p21(WAF1) to promote DNA repair. *Cell,* 114, 599-610.

BENJAMINI, Y. & HOCHBERG, Y. (1995) Controlling the false discovery rate: a practical and powerful approach to multiple testing. *J R Stat Soc,*. 57, 289-300.

BERGMANN, E. & EGLY, J. M. (2001) Trichothiodystrophy, a transcription syndrome. *Trends Genet,* 17, 279-86.

BERNEBURG, M., LOWE, J. E., NARDO, T., ARAUJO, S., FOUSTERI, M. I., GREEN, M. H., KRUTMANN, J., WOOD, R. D., STEFANINI, M. & LEHMANN, A. R. (2000) UV damage causes uncontrolled DNA breakage in cells from patients with combined features of XP-D and Cockayne syndrome. *Embo J,* 19, 1157-66.

BERNS, K., HIJMANS, E. M., MULLENDERS, J., BRUMMELKAMP, T. R., VELDS, A.,

HEIMERIKX, M., KERKHOVEN, R. M., MADIREDJO, M., NIJKAMP, W., WEIGELT, B., AGAMI, R., GE, W., CAVET, G., LINSLEY, P. S., BEIJERSBERGEN, R. L. & BERNARDS, R. (2004) A large-scale RNAi screen in human cells identifies new components of the p53 pathway. *Nature,* 428, 431-7.

BERTOLA, D. R., CAO, H., ALBANO, L. M., OLIVEIRA, D. P., KOK, F., MARQUES-DIAS, M. J., KIM, C. A. & HEGELE, R. A. (2006) Cockayne syndrome type A: novel mutations in eight typical patients. *J Hum Genet,* 51, 701-5.

BIARD, D. S., DESPRAS, E., SARASIN, A. & ANGULO, J. F. (2005) Development of new EBV-based vectors for stable expression of small interfering RNA to mimick human syndromes: application to NER gene silencing. *Mol Cancer Res,* 3, 519-29.

BIERMAN, E. L. (1978) The effect of donor age on the in vitro life span of cultured human arterial smooth-muscle cells. *In Vitro,* 14, 951-5.

BIGGERSTAFF, M., SZYMKOWSKI, D. E. & WOOD, R. D. (1993) Co-correction of the ERCC1, ERCC4 and xeroderma pigmentosum group F DNA repair defects in vitro. *Embo J,* 12, 3685-92.

BIRRELL, G. W., GIAEVER, G., CHU, A. M., DAVIS, R. W. & BROWN, J. M. (2001) A genome-wide screen in Saccharomyces cerevisiae for genes affecting UV radiation sensitivity. *Proc Natl Acad Sci U S A,* 98, 12608-13.

BLACKBURN, E. H. (2000) Telomere states and cell fates. *Nature,* 408, 53-6.

BLASCO, M. A. (2003) Mammalian telomeres and telomerase: why they matter for cancer and aging. *Eur J Cell Biol,* 82, 441-6.

BLATTNER, C., KANNOUCHE, P., LITFIN, M., BENDER, K., RAHMSDORF, H. J., ANGULO, J. F. & HERRLICH, P. (2000) UV-Induced stabilization of c-fos and other short-lived mRNAs. *Mol Cell Biol,* 20, 3616-25.

BOCHKAREV, A., PFUETZNER, R. A., EDWARDS, A. M. & FRAPPIER, L. (1997) Structure of the single-stranded-DNA-binding domain of replication protein A bound to DNA. *Nature,* 385, 176-81.

BODNAR, A. G., OUELLETTE, M., FROLKIS, M., HOLT, S. E., CHIU, C. P., MORIN, G. B., HARLEY, C. B., SHAY, J. W., LICHTSTEINER, S. & WRIGHT, W. E. (1998) Extension of life-span by introduction of telomerase into normal human cells. *Science,* 279, 349-52.

BOERMA, M., VAN DER WEES, C. G., VRIELING, H., SVENSSON, J. P., WONDERGEM, J., VAN DER LAARSE, A., MULLENDERS, L. H. & VAN ZEELAND, A. A. (2005) Microarray analysis of gene expression profiles of cardiac myocytes and fibroblasts after mechanical stress, ionising or ultraviolet radiation. *BMC Genomics,* 6, 6.

BOHR, V. A., SANDER, M. & KRAEMER, K. H. (2005) Rare diseases provide rare insights into DNA repair pathways, TFIIH, aging and cancer center. *DNA Repair (Amst),* 4, 293-302.

BOHR, V. A., SMITH, C. A., OKUMOTO, D. S. & HANAWALT, P. C. (1985) DNA repair in an active gene: removal of pyrimidine dimers from the DHFR gene of CHO cells is much more efficient than in the genome overall. *Cell,* 40, 359-69.

BOND, J., HAUGHTON, M., BLAYDES, J., GIRE, V., WYNFORD-THOMAS, D. & WYLLIE, F. (1996) Evidence that transcriptional activation by p53 plays a direct role in the induction of cellular senescence. *Oncogene,* 13, 2097-104.

BOND, J. A., HAUGHTON, M. F., ROWSON, J. M., SMITH, P. J., GIRE, V., WYNFORD-THOMAS, D. & WYLLIE, F. S. (1999) Control of replicative life span in human cells: barriers to clonal expansion intermediate between M1 senescence and M2 crisis. *Mol Cell Biol,* 19, 3103-14.

BOOTSMA, D. (2001) The "Dutch DNA Repair Group", in retrospect. *Mutat Res,* 485, 37-41.

BOOTSMA, D. & HOEIJMAKERS, J. H. (1993) DNA repair. Engagement with transcription. *Nature,* 363, 114-5.

BOSCO, E. E. & KNUDSEN, E. S. (2005) Differential role of RB in response to UV and IR damage. *Nucleic Acids Res,* 33, 1581-92.

BOSCO, G., DU, W. & ORR-WEAVER, T. L. (2001) DNA replication control through interaction of E2F-RB and the origin recognition complex. *Nat Cell Biol,* 3, 289-95.

BOWMAN, K. K., SICARD, D. M., FORD, J. M. & HANAWALT, P. C. (2000) Reduced global genomic repair of ultraviolet light-induced cyclobutane pyrimidine dimers in simian virus 40-transformed human cells. *Mol Carcinog,* 29, 17-24.

BOYCE, R. P. & HOWARD-FLANDERS, P. (1964) Release Of Ultraviolet Light-Induced Thymine Dimers From Dna In E. Coli K-12. *Proc Natl Acad Sci U S A,* 51, 293-300.

BOYLE, J., KILL, I. R. & PARRIS, C. N. (2005) Heterogeneity of dimer excision in young and senescent human dermal fibroblasts. *Aging Cell,* 4, 247-55.

BRADSHER, J., AURIOL, J., PROIETTI DE SANTIS, L., IBEN, S., VONESCH, J. L., GRUMMT, I. & EGLY, J. M. (2002) CSB is a component of RNA pol I transcription. *Mol Cell,* 10, 819-29.

BRANDES, D., MURPHY, D. G., ANTON, E. B. & BARNARD, S. (1972) Ultrastructural and cytochemical changes in cultured human lung cells. *J Ultrastruct Res,* 39, 465-83.

BRASH, D. E., ZIEGLER, A., JONASON, A. S., SIMON, J. A., KUNALA, S. & LEFFELL, D. J. (1996) Sunlight and sunburn in human skin cancer: p53, apoptosis, and tumor promotion. *J Investig*

Dermatol Symp Proc, 1, 136-42.

BREGMAN, D. B., HALABAN, R., VAN GOOL, A. J., HENNING, K. A., FRIEDBERG, E. C. & WARREN, S. L. (1996) UV-induced ubiquitination of RNA polymerase II: a novel modification deficient in Cockayne syndrome cells. *Proc Natl Acad Sci U S A,* 93, 11586-90.

BREITLING, R., AMTMANN, A. & HERZYK, P. (2004) Iterative Group Analysis (iGA): A simple tool to enhance sensitivity and facilitate interpretation of microarray experiments. *Bioinformatics*, 5, 34-41.

BRENNER, A. J., STAMPFER, M. R. & ALDAZ, C. M. (1998) Increased p16 expression with first senescence arrest in human mammary epithelial cells and extended growth capacity with p16 inactivation. *Oncogene,* 17, 199-205.

BRIDGE, A. J., PEBERNARD, S., DUCRAUX, A., NICOULAZ, A. L. & IGGO, R. (2003) Induction of an interferon response by RNAi vectors in mammalian cells. *Nat Genet,* 34, 263-4.

BROOKMAN, K. W., LAMERDIN, J. E., THELEN, M. P., HWANG, M., REARDON, J. T., SANCAR, A., ZHOU, Z. Q., WALTER, C. A., PARRIS, C. N. & THOMPSON, L. H. (1996) ERCC4 (XPF) encodes a human nucleotide excision repair protein with eukaryotic recombination homologs. *Mol Cell Biol,* 16, 6553-62.

BROOKS, P. J. (2002) DNA repair in neural cells: basic science and clinical implications. *Mutat Res,* 509, 93-108.

BROUGHTON, B. C., LEHMANN, A. R., HARCOURT, S. A., ARLETT, C. F., SARASIN, A., KLEIJER, W. J., BEEMER, F. A., NAIRN, R. & MITCHELL, D. L. (1990) Relationship between pyrimidine dimers, 6-4 photoproducts, repair synthesis and cell survival: studies using cells from patients with trichothiodystrophy. *Mutat Res,* 235, 33-40.

BROUGHTON, B. C., STEINGRIMSDOTTIR, H. & LEHMANN, A. R. (1996) Five polymorphisms in the coding sequence of the xeroderma pigmentosum group D gene. *Mutat Res,* 362, 209-11.

BROWN, J. P., WEI, W. & SEDIVY, J. M. (1997) Bypass of senescence after disruption of p21CIP1/WAF1 gene in normal diploid human fibroblasts. *Science,* 277, 831-4.

BRUGAROLAS, J., MOBERG, K., BOYD, S. D., TAYA, Y., JACKS, T. & LEES, J. A. (1999) Inhibition of cyclin-dependent kinase 2 by p21 is necessary for retinoblastoma protein-mediated G1 arrest after gamma-irradiation. *Proc Natl Acad Sci U S A,* 96, 1002-7.

BRUMMELKAMP, T. R., BERNARDS, R. & AGAMI, R. (2002) A system for stable expression of short interfering RNAs in mammalian cells. *Science,* 296, 550-3.

BRYAN, T. M. & REDDEL, R. R. (1994) SV40-induced immortalization of human cells. *Crit Rev*

Oncog, 5, 331-57.

BUCHKOVICH, K., DUFFY, L. A. & HARLOW, E. (1989) The retinoblastoma protein is phosphorylated during specific phases of the cell cycle. *Cell,* 58, 1097-105.

BURK, P. G., LUTZNER, M. A., CLARKE, D. D. & ROBBINS, J. H. (1971) Ultraviolet-stimulated thymidine incorporation in xeroderma pigmentosum lymphocytes. *J Lab Clin Med,* 77, 759-67.

BURNS, J. L., GUZDER, S. N., SUNG, P., PRAKASH, S. & PRAKASH, L. (1996) An affinity of human replication protein A for ultraviolet-damaged DNA. *J Biol Chem,* 271, 11607-10.

BUSCH, D., GREINER, C., LEWIS, K., FORD, R., ADAIR, G. & THOMPSON, L. (1989) Summary of complementation groups of UV-sensitive CHO cell mutants isolated by large-scale screening. *Mutagenesis,* 4, 349-54.

BUSCHTA-HEDAYAT, N., BUTERIN, T., HESS, M. T., MISSURA, M. & NAEGELI, H. (1999) Recognition of nonhybridizing base pairs during nucleotide excision repair of DNA. *Proc Natl Acad Sci U S A,* 96, 6090-5.

BUTZ, K., GEISEN, C., ULLMANN, A., ZENTGRAF, H. & HOPPE-SEYLER, F. (1998) Uncoupling of p21WAF1/CIP1/SDI1 mRNA and protein expression upon genotoxic stress. *Oncogene,* 17, 781-7.

CADET, J., SAGE, E. & DOUKI, T. (2005) Ultraviolet radiation-mediated damage to cellular DNA. *Mutat Res,* 571, 3-17.

CAM, H., BALCIUNAITE, E., BLAIS, A., SPEKTOR, A., SCARPULLA, R. C., YOUNG, R., KLUGER, Y. & DYNLACHT, B. D. (2004) A common set of gene regulatory networks links metabolism and growth inhibition. *Mol Cell,* 16, 399-411.

CAMPISI, J. (1998) The role of cellular senescence in skin aging. *J Investig Dermatol Symp Proc,* 3, 1-5.

CAMPISI, J. (2000) Cancer, aging and cellular senescence. *In Vivo,* 14, 183-8.

CAMPISI, J. (2001) Cellular senescence as a tumor-suppressor mechanism. *Trends Cell Biol,* 11, S27-31.

CAMPISI, J. (2005) Senescent cells, tumor suppression, and organismal aging: good citizens, bad neighbors. *Cell,* 120, 513-22.

CAO, H., WILLIAMS, C., CARTER, M. & HEGELE, R. A. (2004) CKN1 (MIM 216400): mutations in Cockayne syndrome type A and a new common polymorphism. *J Hum Genet,* 49, 61-3.

CAO, L., LI, W., KIM, S., BRODIE, S. G. & DENG, C. X. (2003) Senescence, aging, and malignant transformation mediated by p53 in mice lacking the Brca1 full-length isoform. *Genes Dev,* 17, 201-13.

CARRIER, F., GEORGEL, P. T., POURQUIER, P., BLAKE, M., KONTNY, H. U., ANTINORE, M. J., GARIBOLDI, M., MYERS, T. G., WEINSTEIN, J. N., POMMIER, Y. & FORNACE, A. J., JR. (1999) Gadd45, a p53-responsive stress protein, modifies DNA accessibility on damaged chromatin. *Mol Cell Biol,* 19, 1673-85.

CARVALHO, H., DA COSTA, R. M., CHIGANCAS, V., WEINLICH, R., BRUMATTI, G., AMARANTE-MENDES, G. P., SARASIN, A. & MENCK, C. F. (2003) Effect of cell confluence on ultraviolet light apoptotic responses in DNA repair deficient cells. *Mutat Res,* 544, 159-66.

CASE, C. C. (2003) Transcriptional tools for aging research. *Mech Ageing Dev,* 124, 103-8.

CATANI, M. V., ROSSI, A., COSTANZO, A., SABATINI, S., LEVRERO, M., MELINO, G. & AVIGLIANO, L. (2001) Induction of gene expression via activator protein-1 in the ascorbate protection against UV-induced damage. *Biochem J,* 356, 77-85.

CHANG, H. C., TSAI, J., GUO, Y. L., HUANG, Y. H., TSAI, H. N., TSAI, P. C. & HUANG, W. (2003) Differential UVC-induced gadd45 gene expression in xeroderma pigmentosum cells. *Biochem Biophys Res Commun,* 305, 1109-15.

CHAO, C., SAITO, S., KANG, J., ANDERSON, C. W., APPELLA, E. & XU, Y. (2000) p53 transcriptional activity is essential for p53-dependent apoptosis following DNA damage. *Embo J,* 19, 4967-75.

CHAVANNE, F., BROUGHTON, B. C., PIETRA, D., NARDO, T., BROWITT, A., LEHMANN, A. R. & STEFANINI, M. (2000) Mutations in the XPC gene in families with xeroderma pigmentosum and consequences at the cell, protein, and transcript levels. *Cancer Res,* 60, 1974-82.

CHEN, B. P., WOLFGANG, C. D. & HAI, T. (1996) Analysis of ATF3, a transcription factor induced by physiological stresses and modulated by gadd153/Chop10. *Mol Cell Biol,* 16, 1157-68.

CHEN, D., TOONE, W. M., MATA, J., LYNE, R., BURNS, G., KIVINEN, K., BRAZMA, A., JONES, N. & BAHLER, J. (2003) Global transcriptional responses of fission yeast to environmental stress. *Mol Biol Cell,* 14, 214-29.

CHEN, J., MARECHAL, V. & LEVINE, A. J. (1993) Mapping of the p53 and mdm-2 interaction domains. *Mol Cell Biol,* 13, 4107-14.

CHEN, M., BROWN, P., BOTSTEIN, D. & FORD, JM. Global transcriptional responses in human cells following UV-irradiation induced DNA damage. *Proc. AM. Assoc. Cancer Res.* 43, 743.

CHOI, D., WHITTIER, P. S., OSHIMA, J. & FUNK, W. D. (2001) Telomerase expression prevents replicative senescence but does not fully reset mRNA expression patterns in Werner syndrome cell strains. *Faseb J,* 15, 1014-20.

CHRISTIANSEN, M., STEVNSNER, T., BOHR, V. A., CLARK, B. F. & RATTAN, S. I. (2000) Gene-specific DNA repair of pyrimidine dimers does not decline during cellular aging in vitro. *Exp Cell Res,* 256, 308-14.

CHRISTMANN, M., TOMICIC, M. T., ROOS, W. P. & KAINA, B. (2003) Mechanisms of human DNA repair: an update. *Toxicology,* 193, 3-34.

CHU, G. & CHANG, E. (1988) Xeroderma pigmentosum group E cells lack a nuclear factor that binds to damaged DNA. *Science,* 242, 564-7.

CITTERIO, E., RADEMAKERS, S., VAN DER HORST, G. T., VAN GOOL, A. J., HOEIJMAKERS, J. H. & VERMEULEN, W. (1998) Biochemical and biological characterization of wild-type and ATPase-deficient Cockayne syndrome B repair protein. *J Biol Chem,* 273, 11844-51.

CITTERIO, E., VAN DEN BOOM, V., SCHNITZLER, G., KANAAR, R., BONTE, E., KINGSTON, R. E., HOEIJMAKERS, J. H. & VERMEULEN, W. (2000) ATP-dependent chromatin remodeling by the Cockayne syndrome B DNA repair-transcription-coupling factor. *Mol Cell Biol,* 20, 7643-53.

CLARKSON, J. M. & PAINTER, R. B. (1974) Repair of x-ray damage in aging WI-38 cells. *Mutat Res,* 23, 107-12.

CLASSON, M. & HARLOW, E. (2002) The retinoblastoma tumour suppressor in development and cancer. *Nat Rev Cancer,* 2, 910-7.

CLEAVER, J. E. (1968) Defective repair replication of DNA in xeroderma pigmentosum. *Nature,* 218, 652-6.

CLEAVER, J. E. (1969) Xeroderma pigmentosum: a human disease in which an initial stage of DNA repair is defective. *Proc Natl Acad Sci U S A,* 63, 428-35.

CLEAVER, J. E., ARUTYUNYAN, R. M., SARKISIAN, T., KAUFMANN, W. K., GREENE, A. E. & CORIELL, L. (1980) Similar defects in DNA repair and replication in the pigmented xerodermoid and the xeroderma pigmentosum variants. *Carcinogenesis,* 1, 647-55.

CLEAVER, J.E., HEFNER, E., LAPOSA, R.R., KARENTZ, D. & MARTI, T. (2006) Cockayne syndrome exhibits dysregulation of p21 and other gene products that may be independent of transcription-coupled repair, *Neuroscience*, doi: 10.1016/j.neuroscience.2006.08.074.

CLEAVER, J. E. & THOMAS, G. H. (1993) Clinical syndromes associated with DNA repair deficiency and enhanced sun sensitivity. *Arch Dermatol,* 129, 348-50.

CLEAVER, J. E., THOMPSON, L. H., RICHARDSON, A. S. & STATES, J. C. (1999) A summary of mutations in the UV-sensitive disorders: xeroderma pigmentosum, Cockayne syndrome, and

trichothiodystrophy. *Hum Mutat,* 14, 9-22.

CLINE, S. D. & HANAWALT, P. C. (2003) Who's on first in the cellular response to DNA damage? *Nat Rev Mol Cell Biol,* 4, 361-72.

CLOUD, K. G., SHEN, B., STRNISTE, G. F. & PARK, M. S. (1995) XPG protein has a structure-specific endonuclease activity. *Mutat Res,* 347, 55-60.

COLELLA, S., NARDO, T., MALLERY, D., BORRONE, C., RICCI, R., RUFFA, G., LEHMANN, A. R. & STEFANINI, M. (1999) Alterations in the CSB gene in three Italian patients with the severe form of Cockayne syndrome (CS) but without clinical photosensitivity. *Hum Mol Genet,* 8, 935-41.

COMINGS, D. E. & OKADA, T. A. (1970) Electron microscopy of human fibroblasts in tissue culture during logarithmic and confluent stages of growth. *Exp Cell Res,* 61, 295-301.

COOPER, M. P., BALAJEE, A. S. & BOHR, V. A. (1999) The C-terminal domain of p21 inhibits nucleotide excision repair In vitro and In vivo. *Mol Biol Cell,* 10, 2119-29.

CORDEIRO-STONE, M., FRANK, A., BRYANT, M., OGUEJIOFOR, I., HATCH, S. B., MCDANIEL, L. D. & KAUFMANN, W. K. (2002) DNA damage responses protect xeroderma pigmentosum variant from UVC-induced clastogenesis. *Carcinogenesis,* 23, 959-65.

CORTEZ, D., GUNTUKU, S., QIN, J. & ELLEDGE, S. J. (2001) ATR and ATRIP: partners in checkpoint signaling. *Science,* 294, 1713-6.

COSSET, F. L., TAKEUCHI, Y., BATTINI, J. L., WEISS, R. A. & COLLINS, M. K. (1995) High-titer packaging cells producing recombinant retroviruses resistant to human serum. *J Virol,* 69, 7430-6.

COURCELLE, J., KHODURSKY, A., PETER, B., BROWN, P. O. & HANAWALT, P. C. (2001) Comparative gene expression profiles following UV exposure in wild-type and SOS-deficient Escherichia coli. *Genetics,* 158, 41-64.

COURDAVAULT, S., BAUDOUIN, C., CHARVERON, M., CANGUILHEM, B., FAVIER, A., CADET, J. & DOUKI, T. (2005) Repair of the three main types of bipyrimidine DNA photoproducts in human keratinocytes exposed to UVB and UVA radiations. *DNA Repair (Amst),* 4, 836-44.

COVERLEY, D., KENNY, M. K., LANE, D. P. & WOOD, R. D. (1992) A role for the human single-stranded DNA binding protein HSSB/RPA in an early stage of nucleotide excision repair. *Nucleic Acids Res,* 20, 3873-80.

COVERLEY, D., KENNY, M. K., MUNN, M., RUPP, W. D., LANE, D. P. & WOOD, R. D. (1991)

Requirement for the replication protein SSB in human DNA excision repair. *Nature,* 349, 538-41.

CRISTOFALO, V. J., ALLEN, R. G., PIGNOLO, R. J., MARTIN, B. G. & BECK, J. C. (1998a) Relationship between donor age and the replicative lifespan of human cells in culture: a reevaluation. *Proc Natl Acad Sci U S A,* 95, 10614-9.

CRISTOFALO, V. J. & KABAKJIAN, J. (1975) Lysosomal enzymes and aging in vitro: subcellular enzyme distribution and effect of hydrocortisone on cell life-span. *Mech Ageing Dev,* 4, 19-28.

CRISTOFALO, V. J. & KRITCHEVSKY, D. (1969) Cell size and nucleic acid content in the diploid human cell line WI-38 during aging. *Med Exp Int J Exp Med,* 19, 313-20.

CRISTOFALO, V. J., VOLKER, C., FRANCIS, M. K. & TRESINI, M. (1998b) Age-dependent modifications of gene expression in human fibroblasts. *Crit Rev Eukaryot Gene Expr,* 8, 43-80.

CROWLEY, D. J. & HANAWALT, P. C. (1998) Induction of the SOS response increases the efficiency of global nucleotide excision repair of cyclobutane pyrimidine dimers, but not 6-4 photoproducts, in UV-irradiated Escherichia coli. *J Bacteriol,* 180, 3345-52.

D'ADDA DI FAGAGNA, F., REAPER, P. M., CLAY-FARRACE, L., FIEGLER, H., CARR, P., VON ZGLINICKI, T., SARETZKI, G., CARTER, N. P. & JACKSON, S. P. (2003) A DNA damage checkpoint response in telomere-initiated senescence. *Nature,* 426, 194-8.

D'ERRICO, M., TESON, M., CALCAGNILE, A., NARDO, T., DE LUCA, N., LAZZARI, C., SODDU, S., ZAMBRUNO, G., STEFANINI, M. & DOGLIOTTI, E. (2005) Differential role of transcription-coupled repair in UVB-induced response of human fibroblasts and keratinocytes. *Cancer Res,* 65, 432-8.

DA COSTA, R. M., RIOU, L., PAQUOLA, A., MENCK, C. F. & SARASIN, A. (2005) Transcriptional profiles of unirradiated or UV-irradiated human cells expressing either the cancer-prone XPB/CS allele or the noncancer-prone XPB/TTD allele. *Oncogene,* 24, 1359-1374.

DANPURE, H. J. & TYRRELL, R. M. (1976) Oxygen-dependence of near UV (365 NM) lethality and the interaction of near UV and X-rays in two mammalian cell lines. *Photochem Photobiol,* 23, 171-7.

DATTA, A., BAGCHI, S., NAG, A., SHIYANOV, P., ADAMI, G. R., YOON, T. & RAYCHAUDHURI, P. (2001) The p48 subunit of the damaged-DNA binding protein DDB associates with the CBP/p300 family of histone acetyltransferase. *Mutat Res,* 486, 89-97.

DAVIS, T., HAUGHTON, M. F., JONES, C. J. & KIPLING, D. (2006) Prevention of accelerated cell aging in the Werner syndrome. *Ann N Y Acad Sci,* 1067, 243-7.

DAVIS, T. & KIPLING, D. (2005) Telomeres and telomerase biology in vertebrates: progress towards a non-human model for replicative senescence and ageing. *Biogerontology,* 6, 371-85.

DAYA-GROSJEAN, L. & SARASIN, A. (2005) The role of UV induced lesions in skin carcinogenesis: an overview of oncogene and tumor suppressor gene modifications in xeroderma pigmentosum skin tumors. *Mutat Res,* 571, 43-56.

DAZARD, J. E., GAL, H., AMARIGLIO, N., RECHAVI, G., DOMANY, E. & GIVOL, D. (2003) Genome-wide comparison of human keratinocyte and squamous cell carcinoma responses to UVB irradiation: implications for skin and epithelial cancer. *Oncogene,* 22, 2993-3006.

DE BOER, J., DONKER, I., DE WIT, J., HOEIJMAKERS, J. H. & WEEDA, G. (1998) Disruption of the mouse xeroderma pigmentosum group D DNA repair/basal transcription gene results in preimplantation lethality. *Cancer Res,* 58, 89-94.

DE BOER, J. & HOEIJMAKERS, J. H. (2000) Nucleotide excision repair and human syndromes. *Carcinogenesis,* 21, 453-60.

DE GRUIJL, F. R. (1999) Skin cancer and solar UV radiation. *Eur J Cancer,* 35, 2003-9.

DE GRUIJL, F. R. (2000) Photocarcinogenesis: UVA vs UVB. *Methods Enzymol,* 319, 359-66.

DE LAAT, A., VAN DER LEUN, J. C. & DE GRUIJL, F. R. (1997) Carcinogenesis induced by UVA (365-nm) radiation: the dose-time dependence of tumor formation in hairless mice. *Carcinogenesis,* 18, 1013-20.

DE LAAT, W. L., APPELDOORN, E., JASPERS, N. G. & HOEIJMAKERS, J. H. (1998a) DNA structural elements required for ERCC1-XPF endonuclease activity. *J Biol Chem,* 273, 7835-42.

DE LAAT, W. L., JASPERS, N. G. & HOEIJMAKERS, J. H. (1999) Molecular mechanism of nucleotide excision repair. *Genes Dev,* 13, 768-85.

DE LAAT, W. L., SIJBERS, A. M., ODIJK, H., JASPERS, N. G. & HOEIJMAKERS, J. H. (1998b) Mapping of interaction domains between human repair proteins ERCC1 and XPF. *Nucleic Acids Res,* 26, 4146-52.

DE SILVA, B. D., NAWROZ, I. & DOHERTY, V. R. (1999) Angiosarcoma of the head and neck associated with xeroderma pigmentosum variant. *Br J Dermatol,* 141, 166-7.

DE VRIES, A., VAN OOSTROM, C. T., HOFHUIS, F. M., DORTANT, P. M., BERG, R. J., DE GRUIJL, F. R., WESTER, P. W., VAN KREIJL, C. F., CAPEL, P. J., VAN STEEG, H. & ET AL. (1995) Increased susceptibility to ultraviolet-B and carcinogens of mice lacking the DNA excision repair gene XPA. *Nature,* 377, 169-73.

DE WEERD-KASTELEIN, E. A., KEIJZER, W. & BOOTSMA, D. (1972) Genetic heterogeneity of xeroderma pigmentosum demonstrated by somatic cell hybridization. *Nat New Biol,* 238, 80-3.

DECAPRIO, J. A., LUDLOW, J. W., FIGGE, J., SHEW, J. Y., HUANG, C. M., LEE, W. H., MARSILIO, E., PAUCHA, E. & LIVINGSTON, D. M. (1988) SV40 large tumor antigen forms a specific complex with the product of the retinoblastoma susceptibility gene. *Cell,* 54, 275-83.

DECAPRIO, J. A., LUDLOW, J. W., LYNCH, D., FURUKAWA, Y., GRIFFIN, J., PIWNICA-WORMS, H., HUANG, C. M. & LIVINGSTON, D. M. (1989) The product of the retinoblastoma susceptibility gene has properties of a cell cycle regulatory element. *Cell,* 58, 1085-95.

DENISSENKO, M. F., PAO, A., PFEIFER, G. P. & TANG, M. (1998) Slow repair of bulky DNA adducts along the nontranscribed strand of the human p53 gene may explain the strand bias of transversion mutations in cancers. *Oncogene,* 16, 1241-7.

DI DONNA, S., MAMCHAOUI, K., COOPER, R. N., SEIGNEURIN-VENIN, S., TREMBLAY, J., BUTLER-BROWNE, G. S. & MOULY, V. (2003) Telomerase can extend the proliferative capacity of human myoblasts, but does not lead to their immortalization. *Mol Cancer Res,* 1, 643-53.

DIANOV, G. L., THYBO, T., DIANOVA, II, LIPINSKI, L. J. & BOHR, V. A. (2000) Single nucleotide patch base excision repair is the major pathway for removal of thymine glycol from DNA in human cell extracts. *J Biol Chem,* 275, 11809-13.

DILLINGHAM, M. S., SPIES, M. & KOWALCZYKOWSKI, S. C. (2003) RecBCD enzyme is a bipolar DNA helicase. *Nature,* 423, 893-7.

DIMRI, G. P., LEE, X., BASILE, G., ACOSTA, M., SCOTT, G., ROSKELLEY, C., MEDRANO, E. E., LINSKENS, M., RUBELJ, I., PEREIRA-SMITH, O. & ET AL. (1995) A biomarker that identifies senescent human cells in culture and in aging skin in vivo. *Proc Natl Acad Sci U S A,* 92, 9363-7.

DIP, R., CAMENISCH, U. & NAEGELI, H. (2004) Mechanisms of DNA damage recognition and strand discrimination in human nucleotide excision repair. *DNA Repair (Amst),* 3, 1409-23.

DRAPKIN, R., REARDON, J. T., ANSARI, A., HUANG, J. C., ZAWEL, L., AHN, K., SANCAR, A. & REINBERG, D. (1994) Dual role of TFIIH in DNA excision repair and in transcription by RNA polymerase II. *Nature,* 368, 769-72.

DRESLER, S. L. (1985) Stimulation of deoxyribonucleic acid excision repair in human fibroblasts pretreated with sodium butyrate. *Biochemistry,* 24, 6861-9.

DUALAN, R., BRODY, T., KEENEY, S., NICHOLS, A. F., ADMON, A. & LINN, S. (1995) Chromosomal localization and cDNA cloning of the genes (DDB1 and DDB2) for the p127 and p48 subunits of a human damage-specific DNA binding protein. *Genomics,* 29, 62-9.

DUBAELE, S. & EGLY, J. M. (2002) Cockayne syndrome, between transcription and DNA repair

defects. *J Eur Acad Dermatol Venereol,* 16, 220-6.

DULIC, V., KAUFMANN, W. K., WILSON, S. J., TLSTY, T. D., LEES, E., HARPER, J. W., ELLEDGE, S. J. & REED, S. I. (1994) p53-dependent inhibition of cyclin-dependent kinase activities in human fibroblasts during radiation-induced G1 arrest. *Cell,* 76, 1013-23.

DUMAZ, N., DROUGARD, C., SARASIN, A. & DAYA-GROSJEAN, L. (1993) Specific UV-induced mutation spectrum in the p53 gene of skin tumors from DNA-repair-deficient xeroderma pigmentosum patients. *Proc Natl Acad Sci U S A,* 90, 10529-33.

DUMAZ, N., DUTHU, A., EHRHART, J. C., DROUGARD, C., APPELLA, E., ANDERSON, C. W., MAY, P., SARASIN, A. & DAYA-GROSJEAN, L. (1997) Prolonged p53 protein accumulation in trichothiodystrophy fibroblasts dependent on unrepaired pyrimidine dimers on the transcribed strands of cellular genes. *Mol Carcinog,* 20, 340-7.

DUMONT, P., BURTON, M., CHEN, Q. M., GONOS, E. S., FRIPPIAT, C., MAZARATI, J. B., ELIAERS, F., REMACLE, J. & TOUSSAINT, O. (2000) Induction of replicative senescence biomarkers by sublethal oxidative stresses in normal human fibroblast. *Free Radic Biol Med,* 28, 361-73.

DVIR, A., CONAWAY, J. W. & CONAWAY, R. C. (2001) Mechanism of transcription initiation and promoter escape by RNA polymerase II. *Curr Opin Genet Dev,* 11, 209-14.

DYKXHOORN, D. M., NOVINA, C. D. & SHARP, P. A. (2003) Killing the messenger: short RNAs that silence gene expression. *Nat Rev Mol Cell Biol,* 4, 457-67.

EGLY, J. M. (2001) The 14th Datta Lecture. TFIIH: from transcription to clinic. *FEBS Lett,* 498, 124-8.

EISEN, J. A. & HANAWALT, P. C. (1999) A phylogenomic study of DNA repair genes, proteins, and processes. *Mutat Res,* 435, 171-213.

EISEN, J. A., SWEDER, K. S. & HANAWALT, P. C. (1995) Evolution of the SNF2 family of proteins: subfamilies with distinct sequences and functions. *Nucleic Acids Res,* 23, 2715-23.

EL-DEIRY, W. S., KERN, S. E., PIETENPOL, J. A., KINZLER, K. W. & VOGELSTEIN, B. (1992) Definition of a consensus binding site for p53. *Nat Genet,* 1, 45-9.

EL-DEIRY, W. S., TOKINO, T., VELCULESCU, V. E., LEVY, D. B., PARSONS, R., TRENT, J. M., LIN, D., MERCER, W. E., KINZLER, K. W. & VOGELSTEIN, B. (1993) WAF1, a potential mediator of p53 tumor suppression. *Cell,* 75, 817-25.

EL-MAHDY, M. A., HAMADA, F. M., WANI, M. A., ZHU, Q. & WANI, A. A. (2000) p53-degradation by HPV-16 E6 preferentially affects the removal of cyclobutane pyrimidine dimers from non-transcribed strand and sensitizes mammary epithelial cells to UV-irradiation. *Mutat Res,* 459,

135-45.

ELBASHIR, S. M., HARBORTH, J., LENDECKEL, W., YALCIN, A., WEBER, K. & TUSCHL, T. (2001) Duplexes of 21-nucleotide RNAs mediate RNA interference in cultured mammalian cells. *Nature,* 411, 494-8.

ELLISON, A. R., NOUSPIKEL, T., JASPERS, N. G., CLARKSON, S. G. & GRUENERT, D. C. (1998) Complementation of transformed fibroblasts from patients with combined xeroderma pigmentosum-Cockayne syndrome. *Exp Cell Res,* 243, 22-8.

EMMERT, S., KOBAYASHI, N., KHAN, S. G. & KRAEMER, K. H. (2000) The xeroderma pigmentosum group C gene leads to selective repair of cyclobutane pyrimidine dimers rather than 6-4 photoproducts. *Proc Natl Acad Sci U S A,* 97, 2151-6.

EMMERT, S., SCHNEIDER, T. D., KHAN, S. G. & KRAEMER, K. H. (2001) The human XPG gene: gene architecture, alternative splicing and single nucleotide polymorphisms. *Nucleic Acids Res,* 29, 1443-52.

ENGLISH, J. S. & SWERDLOW, A. J. (1987) The risk of malignant melanoma, internal malignancy and mortality in xeroderma pigmentosum patients. *Br J Dermatol,* 117, 457-61.

ENK, C. D., JACOB-HIRSCH, J., GAL, H., VERBOVETSKI, I., AMARIGLIO, N., MEVORACH, D., INGBER, A., GIVOL, D., RECHAVI, G. & HOCHBERG, M. (2006) The UVB-induced gene expression profile of human epidermis in vivo is different from that of cultured keratinocytes. *Oncogene,* 25, 2601-14.

ENK, C. D., SHAHAR, I., AMARIGLIO, N., RECHAVI, G., KAMINSKI, N. & HOCHBERG, M. (2004) Gene expression profiling of in vivo UVB-irradiated human epidermis. *Photodermatol Photoimmunol Photomed,* 20, 129-37.

EVANS, E., FELLOWS, J., COFFER, A. & WOOD, R. D. (1997a) Open complex formation around a lesion during nucleotide excision repair provides a structure for cleavage by human XPG protein. *Embo J,* 16, 625-38.

EVANS, E., MOGGS, J. G., HWANG, J. R., EGLY, J. M. & WOOD, R. D. (1997b) Mechanism of open complex and dual incision formation by human nucleotide excision repair factors. *Embo J,* 16, 6559-73.

EVENO, E., QUILLIET, X., CHEVALLIER-LAGENTE, O., DAYA-GROSJEAN, L., STARY, A., ZENG, L., BENOIT, A., SAVINI, E., CIARROCCHI, G., KANNOUCHE, P. & ET AL. (1995) Stable SV40-transformation and characterisation of some DNA repair properties of fibroblasts from a trichothiodystrophy patient. *Biochimie,* 77, 906-12.

FAN, F., JIN, S., AMUNDSON, S. A., TONG, T., FAN, W., ZHAO, H., ZHU, X., MAZZACURATI, L.,

LI, X., PETRIK, K. L., FORNACE, A. J., JR., RAJASEKARAN, B. & ZHAN, Q. (2002) ATF3 induction following DNA damage is regulated by distinct signaling pathways and over-expression of ATF3 protein suppresses cells growth. *Oncogene,* 21, 7488-96.

FARAGHER, R. G. & KIPLING, D. (1998) How might replicative senescence contribute to human ageing? *Bioessays,* 20, 985-91.

FARWELL, D. G., SHERA, K. A., KOOP, J. I., BONNET, G. A., MATTHEWS, C. P., REUTHER, G. W., COLTRERA, M. D., MCDOUGALL, J. K. & KLINGELHUTZ, A. J. (2000) Genetic and epigenetic changes in human epithelial cells immortalized by telomerase. *Am J Pathol,* 156, 1537-47.

FENG, L., ZI-JIAN, Y., JIAN-LI, S., BEI, B. & PING-KUN, Z. (2006) siRNA-mediated silencing of Cockayne syndrome group B gene potentiates radiation-induced apoptosis and antiproliferative effect in HeLa cells. *Chinese Medical Journal,* 119, 731-739.

FENTON, M., BARKER, S., KURZ, D. J. & ERUSALIMSKY, J. D. (2001) Cellular senescence after single and repeated balloon catheter denudations of rabbit carotid arteries. *Arterioscler Thromb Vasc Biol,* 21, 220-6.

FERGUSON, B. E. & OH, D. H. (2005) Proficient global nucleotide excision repair in human keratinocytes but not in fibroblasts deficient in p53. *Cancer Res,* 65, 8723-9.

FINLAY, C. A., HINDS, P. W. & LEVINE, A. J. (1989) The p53 proto-oncogene can act as a suppressor of transformation. *Cell,* 57, 1083-93.

FIRE, A., XU, S., MONTGOMERY, M. K., KOSTAS, S. A., DRIVER, S. E. & MELLO, C. C. (1998) Potent and specific genetic interference by double-stranded RNA in Caenorhabditis elegans. *Nature,* 391, 806-11.

FISCHER, E., JUNG, E. G. & CLEAVER, J. E. (1980) Pigmented xerodermoid and XP-variants. *Arch Dermatol Res,* 269, 329-30.

FITCH, M. E., CROSS, I. V., TURNER, S. J., ADIMOOLAM, S., LIN, C. X., WILLIAMS, K. G. & FORD, J. M. (2003a) The DDB2 nucleotide excision repair gene product p48 enhances global genomic repair in p53 deficient human fibroblasts. *DNA Repair (Amst),* 2, 819-26.

FITCH, M. E., NAKAJIMA, S., YASUI, A. & FORD, J. M. (2003b) In vivo recruitment of XPC to UV-induced cyclobutane pyrimidine dimers by the DDB2 gene product. *J Biol Chem,* 278, 46906-10.

FONG, H. K., HURLEY, J. B., HOPKINS, R. S., MIAKE-LYE, R., JOHNSON, M. S., DOOLITTLE, R. F. & SIMON, M. I. (1986) Repetitive segmental structure of the transducin beta subunit: homology with the CDC4 gene and identification of related mRNAs. *Proc Natl Acad Sci U S A,* 83, 2162-6.

FORD, J. M. (2005) Regulation of DNA damage recognition and nucleotide excision repair: another role for p53. *Mutat Res,* 577, 195-202.

FORD, J. M., BARON, E. L. & HANAWALT, P. C. (1998) Human fibroblasts expressing the human papillomavirus E6 gene are deficient in global genomic nucleotide excision repair and sensitive to ultraviolet irradiation. *Cancer Res,* 58, 599-603.

FORD, J. M. & HANAWALT, P. C. (1995) Li-Fraumeni syndrome fibroblasts homozygous for p53 mutations are deficient in global DNA repair but exhibit normal transcription-coupled repair and enhanced UV resistance. *Proc Natl Acad Sci U S A,* 92, 8876-80.

FORD, J. M. & HANAWALT, P. C. (1997) Expression of wild-type p53 is required for efficient global genomic nucleotide excision repair in UV-irradiated human fibroblasts. *J Biol Chem,* 272, 28073-80.

FORNACE, A. J., JR., ALAMO, I., JR. & HOLLANDER, M. C. (1988) DNA damage-inducible transcripts in mammalian cells. *Proc Natl Acad Sci U S A,* 85, 8800-4.

FORSYTH, N. R., EVANS, A. P., SHAY, J. W. & WRIGHT, W. E. (2003) Developmental differences in the immortalization of lung fibroblasts by telomerase. *Aging Cell,* 2, 235-43.

FOUSTERI, M., VERMEULEN, W., VAN ZEELAND, A. A. & MULLENDERS, L. H. (2006) Cockayne Syndrome A and B Proteins Differentially Regulate Recruitment of Chromatin Remodeling and Repair Factors to Stalled RNA Polymerase II In Vivo. *Mol Cell,* 23, 471-82.

FRANCO, S., MACKENZIE, K. L., DIAS, S., ALVAREZ, S., RAFII, S. & MOORE, M. A. (2001) Clonal variation in phenotype and life span of human embryonic fibroblasts (MRC-5) transduced with the catalytic component of telomerase (hTERT). *Exp Cell Res,* 268, 14-25.

FREEDMAN, D. A. & LEVINE, A. J. (1998) Nuclear export is required for degradation of endogenous p53 by MDM2 and human papillomavirus E6. *Mol Cell Biol,* 18, 7288-93.

FRENCK, R. W., JR., BLACKBURN, E. H. & SHANNON, K. M. (1998) The rate of telomere sequence loss in human leukocytes varies with age. *Proc Natl Acad Sci U S A,* 95, 5607-10.

FRIEDBERG, E. C. (1996) Relationships between DNA repair and transcription. *Annu Rev Biochem,* 65, 15-42.

FRIEDBERG, E. C. (2001) How nucleotide excision repair protects against cancer. *Nat Rev Cancer,* 1, 22-33.

FRIEDBERG, E. C. (2003) DNA damage and repair. *Nature,* 421, 436-40.

FRIEDBERG, E. C. & MEIRA, L. B. (2006) Database of mouse strains carrying targeted mutations in

genes affecting biological responses to DNA damage Version 7. *DNA Repair (Amst),* 5, 189-209.

FRIEDBERG, E.C., WALKER, G.C., SIEDE, W., WOOD, R.D., WOOD, R.D., SCHULTZ, R.A. & ELLENBERGER, T. (2006) DNA Repair and Mutagenesis, 2nd Edn (ASM Press, Washington).

FRIEDMAN, P. N., CHEN, X., BARGONETTI, J. & PRIVES, C. (1993) The p53 protein is an unusually shaped tetramer that binds directly to DNA. *Proc Natl Acad Sci U S A,* 90, 3319-23.

FU, D., WAKASUGI, M., ISHIGAKI, Y., NIKAIDO, O. & MATSUNAGA, T. (2003) cDNA cloning of the chicken DDB1 gene encoding the p127 subunit of damaged DNA-binding protein. *Genes Genet Syst,* 78, 169-77.

FUJIWARA, Y., MASUTANI, C., MIZUKOSHI, T., KONDO, J., HANAOKA, F. & IWAI, S. (1999) Characterization of DNA recognition by the human UV-damaged DNA-binding protein. *J Biol Chem,* 274, 20027-33.

FURTH, J. J. (1991) The steady-state levels of type I collagen mRNA are reduced in senescent fibroblasts. *J Gerontol,* 46, B122-4.

GAILLARD, P. H., MARTINI, E. M., KAUFMAN, P. D., STILLMAN, B., MOUSTACCHI, E. & ALMOUZNI, G. (1996) Chromatin assembly coupled to DNA repair: a new role for chromatin assembly factor I. *Cell,* 86, 887-96.

GAILLARD, P. H., MOGGS, J. G., ROCHE, D. M., QUIVY, J. P., BECKER, P. B., WOOD, R. D. & ALMOUZNI, G. (1997) Initiation and bidirectional propagation of chromatin assembly from a target site for nucleotide excision repair. *Embo J,* 16, 6281-9.

GALE, J. M., NISSEN, K. A. & SMERDON, M. J. (1987) UV-induced formation of pyrimidine dimers in nucleosome core DNA is strongly modulated with a period of 10.3 bases. *Proc Natl Acad Sci U S A,* 84, 6644-8.

GALE, J. M. & SMERDON, M. J. (1990) UV induced (6-4) photoproducts are distributed differently than cyclobutane dimers in nucleosomes. *Photochem Photobiol,* 51, 411-7.

GALLOWAY, S. M. & BUCKTON, K. E. (1978) Aneuploidy and ageing: chromosome studies on a random sample of the population using G-banding. *Cytogenet Cell Genet,* 20, 78-95.

GARINIS, G. A., MITCHELL, J. R., MOORHOUSE, M. J., HANADA, K., DE WAARD, H., VANDEPUTTE, D., JANS, J., BRAND, K., SMID, M., VAN DER SPEK, P. J., HOEIJMAKERS, J. H., KANAAR, R. & VAN DER HORST, G. T. (2005) Transcriptome analysis reveals cyclobutane pyrimidine dimers as a major source of UV-induced DNA breaks. *Embo J,* 24, 3952-62.

GASCH, A. P., SPELLMAN, P. T., KAO, C. M., CARMEL-HAREL, O., EISEN, M. B., STORZ, G.,

BOTSTEIN, D. & BROWN, P. O. (2000) Genomic expression programs in the response of yeast cells to environmental changes. *Mol Biol Cell,* 11, 4241-57.

GASSER, S. M. (2000) A sense of the end. *Science,* 288, 1377-9.

GENTILE, M., LATONEN, L. & LAIHO, M. (2003) Cell cycle arrest and apoptosis provoked by UV radiation-induced DNA damage are transcriptionally highly divergent responses. *Nucleic Acids Res,* 31, 4779-90.

GIACCIA, A. J. & KASTAN, M. B. (1998) The complexity of p53 modulation: emerging patterns from divergent signals. *Genes Dev,* 12, 2973-83.

GIANNELLI, F., PAWSEY, S. A. & AVERY, J. A. (1982) Differences in patterns of complementation of the more common groups of xeroderma pigmentosum: possible implications. *Cell,* 29, 451-8.

GIBBS, S., BOELSMA, E., KEMPENAAR, J. & PONEC, M. (1998) Temperature-sensitive regulation of epidermal morphogenesis and the expression of cornified envelope precursors by EGF and TGF alpha. *Cell Tissue Res,* 292, 107-14.

GIGLIA-MARI, G., COIN, F., RANISH, J. A., HOOGSTRATEN, D., THEIL, A., WIJGERS, N., JASPERS, N. G., RAAMS, A., ARGENTINI, M., VAN DER SPEK, P. J., BOTTA, E., STEFANINI, M., EGLY, J. M., AEBERSOLD, R., HOEIJMAKERS, J. H. & VERMEULEN, W. (2004) A new, tenth subunit of TFIIH is responsible for the DNA repair syndrome trichothiodystrophy group A. *Nat Genet,* 36, 714-9.

GIGLIA-MARI, G. & SARASIN, A. (2003) TP53 mutations in human skin cancers. *Hum Mutat,* 21, 217-28.

GILLET, L. C. & SCHARER, O. D. (2006) Molecular mechanisms of mammalian global genome nucleotide excision repair. *Chem Rev,* 106, 253-76.

GILLETTE, T. G., YU, S., ZHOU, Z., WATERS, R., JOHNSTON, S. A. & REED, S. H. (2006) Distinct functions of the ubiquitin-proteasome pathway influence nucleotide excision repair. *Embo J,* 25, 2529-38.

GIRE, V., ROUX, P., WYNFORD-THOMAS, D., BRONDELLO, J. M. & DULIC, V. (2004) DNA damage checkpoint kinase Chk2 triggers replicative senescence. *Embo J,* 23, 2554-63.

GLOCKZIN, S., OGI, F. X., HENGSTERMANN, A., SCHEFFNER, M. & BLATTNER, C. (2003) Involvement of the DNA repair protein hHR23 in p53 degradation. *Mol Cell Biol,* 23, 8960-9.

GOLDSTEIN, S., MOERMAN, E. J., SOELDNER, J. S., GLEASON, R. E. & BARNETT, D. M. (1978) Chronologic and physiologic age affect replicative life-span of fibroblasts from diabetic, prediabetic, and normal donors. *Science,* 199, 781-2.

GOMES, X. V. & BURGERS, P. M. (2001) ATP utilization by yeast replication factor C. I. ATP-mediated interaction with DNA and with proliferating cell nuclear antigen. *J Biol Chem,* 276, 34768-75.

GONTIJO, A. M., GREEN, C. M. & ALMOUZNI, G. (2003) Repairing DNA damage in chromatin. *Biochimie,* 85, 1133-47.

GORBUNOVA, V. & SELUANOV, A. (2003) Telomerase as a growth-promoting factor. *Cell Cycle,* 2, 534-7.

GORBUNOVA, V., SELUANOV, A. & PEREIRA-SMITH, O. M. (2002) Expression of human telomerase (hTERT) does not prevent stress-induced senescence in normal human fibroblasts but protects the cells from stress-induced apoptosis and necrosis. *J Biol Chem,* 277, 38540-9.

GORBUNOVA, V., SELUANOV, A. & PEREIRA-SMITH, O. M. (2003) Evidence that high telomerase activity may induce a senescent-like growth arrest in human fibroblasts. *J Biol Chem,* 278, 7692-8.

GOROSPE, M., WANG, X. & HOLBROOK, N. J. (1998) p53-dependent elevation of p21Waf1 expression by UV light is mediated through mRNA stabilization and involves a vanadate-sensitive regulatory system. *Mol Cell Biol,* 18, 1400-7.

GOUKASSIAN, D., GAD, F., YAAR, M., ELLER, M. S., NEHAL, U. S. & GILCHREST, B. A. (2000) Mechanisms and implications of the age-associated decrease in DNA repair capacity. *Faseb J,* 14, 1325-34.

GOYAL, J. L., RAO, V. A., SRINIVASAN, R. & AGRAWAL, K. (1994) Oculocutaneous manifestations in xeroderma pigmentosa. *Br J Ophthalmol,* 78, 295-7.

GOZUKARA, E. M., KHAN, S. G., METIN, A., EMMERT, S., BUSCH, D. B., SHAHLAVI, T., COLEMAN, D. M., MILLER, M., CHINSOMBOON, N., STEFANINI, M. & KRAEMER, K. H. (2001) A stop codon in xeroderma pigmentosum group C families in Turkey and Italy: molecular genetic evidence for a common ancestor. *J Invest Dermatol,* 117, 197-204.

GRAHAM, F. L., SMILEY, J., RUSSELL, W. C. & NAIRN, R. (1977) Characteristics of a human cell line transformed by DNA from human adenovirus type 5. *J Gen Virol,* 36, 59-74.

GRAHAM, J. M., JR., ANYANE-YEBOA, K., RAAMS, A., APPELDOORN, E., KLEIJER, W. J., GARRITSEN, V. H., BUSCH, D., EDERSHEIM, T. G. & JASPERS, N. G. (2001) Cerebro-oculo-facio-skeletal syndrome with a nucleotide excision-repair defect and a mutated XPD gene, with prenatal diagnosis in a triplet pregnancy. *Am J Hum Genet,* 69, 291-300.

GRATCHEV, A., STREIN, P., UTIKAL, J. & SERGIJ, G. (2003) Molecular genetics of Xeroderma pigmentosum variant. *Exp Dermatol,* 12, 529-36.

GREEN, C. M. & ALMOUZNI, G. (2003) Local action of the chromatin assembly factor CAF-1 at sites of nucleotide excision repair in vivo. *Embo J,* 22, 5163-74.

GREENBERG, S. B., GROVE, G. L. & CRISTOFALO, V. J. (1977) Cell size in aging monolayer cultures. *In Vitro,* 13, 297-300.

GROISMAN, R., KURAOKA, I., CHEVALLIER, O., GAYE, N., MAGNALDO, T., TANAKA, K., KISSELEV, A. F., HAREL-BELLAN, A. & NAKATANI, Y. (2006) CSA-dependent degradation of CSB by the ubiquitin-proteasome pathway establishes a link between complementation factors of the Cockayne syndrome. *Genes Dev,* 20, 1429-34.

GROISMAN, R., POLANOWSKA, J., KURAOKA, I., SAWADA, J., SAIJO, M., DRAPKIN, R., KISSELEV, A. F., TANAKA, K. & NAKATANI, Y. (2003) The ubiquitin ligase activity in the DDB2 and CSA complexes is differentially regulated by the COP9 signalosome in response to DNA damage. *Cell,* 113, 357-67.

GROSSMAN, D. & LEFFELL, D. J. (1997) The molecular basis of nonmelanoma skin cancer: new understanding. *Arch Dermatol,* 133, 1263-70.

GROSSMAN, S. R., DEATO, M. E., BRIGNONE, C., CHAN, H. M., KUNG, A. L., TAGAMI, H., NAKATANI, Y. & LIVINGSTON, D. M. (2003) Polyubiquitination of p53 by a ubiquitin ligase activity of p300. *Science,* 300, 342-4.

GROSSMAN, S. R., PEREZ, M., KUNG, A. L., JOSEPH, M., MANSUR, C., XIAO, Z. X., KUMAR, S., HOWLEY, P. M. & LIVINGSTON, D. M. (1998) p300/MDM2 complexes participate in MDM2-mediated p53 degradation. *Mol Cell,* 2, 405-15.

GRUBER, S. B., ELLIS, N. A., SCOTT, K. K., ALMOG, R., KOLACHANA, P., BONNER, J. D., KIRCHHOFF, T., TOMSHO, L. P., NAFA, K., PIERCE, H., LOW, M., SATAGOPAN, J., RENNERT, H., HUANG, H., GREENSON, J. K., GRODEN, J., RAPAPORT, B., SHIA, J., JOHNSON, S., GREGERSEN, P. K., HARRIS, C. C., BOYD, J., RENNERT, G. & OFFIT, K. (2002) BLM heterozygosity and the risk of colorectal cancer. *Science,* 297, 2013.

GU, Y., TURCK, C. W. & MORGAN, D. O. (1993) Inhibition of CDK2 activity in vivo by an associated 20K regulatory subunit. *Nature,* 366, 707-10.

GULBIS, J. M., KELMAN, Z., HURWITZ, J., O'DONNELL, M. & KURIYAN, J. (1996) Structure of the C-terminal region of p21(WAF1/CIP1) complexed with human PCNA. *Cell,* 87, 297-306.

GUNZ, D., HESS, M. T. & NAEGELI, H. (1996) Recognition of DNA adducts by human nucleotide excision repair. Evidence for a thermodynamic probing mechanism. *J Biol Chem,* 271, 25089-98.

GUO, Y. L., CHANG, H. C., TSAI, J. H., HUANG, J. C., LI, C., YOUNG, K. C., WU, L. W., LAI, M. D., LIU, H. S. & HUANG, W. (2002) Two UVC-induced stress response pathways in HeLa cells

identified by cDNA microarray. *Environ Mol Mutagen,* 40, 122-8.

GUZDER, S. N., HABRAKEN, Y., SUNG, P., PRAKASH, L. & PRAKASH, S. (1995) Reconstitution of yeast nucleotide excision repair with purified Rad proteins, replication protein A, and transcription factor TFIIH. *J Biol Chem,* 270, 12973-6.

HAI, T. & HARTMAN, M. G. (2001) The molecular biology and nomenclature of the activating transcription factor/cAMP responsive element binding family of transcription factors: activating transcription factor proteins and homeostasis. *Gene,* 273, 1-11.

HALL, P. A., MCKEE, P. H., MENAGE, H. D., DOVER, R. & LANE, D. P. (1993) High levels of p53 protein in UV-irradiated normal human skin. *Oncogene,* 8, 203-7.

HALLIDAY, G. M. (2005) Inflammation, gene mutation and photoimmunosuppression in response to UVR-induced oxidative damage contributes to photocarcinogenesis. *Mutat Res,* 571, 107-20.

HAMDI, M., KOOL, J., CORNELISSEN-STEIJGER, P., CARLOTTI, F., POPEIJUS, H. E., VAN DER BURGT, C., JANSSEN, J. M., YASUI, A., HOEBEN, R. C., TERLETH, C., MULLENDERS, L. H. & VAN DAM, H. (2005) DNA damage in transcribed genes induces apoptosis via the JNK pathway and the JNK-phosphatase MKP-1. *Oncogene,* 24, 7135-44.

HANAWALT, P. C. (2002) Subpathways of nucleotide excision repair and their regulation. *Oncogene,* 21, 8949-56.

HANAWALT, P. C., FORD, J. M. & LLOYD, D. R. (2003) Functional characterization of global genomic DNA repair and its implications for cancer. *Mutat Res,* 544, 107-14.

HANNON, G. J. (2002) RNA interference. *Nature,* 418, 244-51.

HARA, E., SMITH, R., PARRY, D., TAHARA, H., STONE, S. & PETERS, G. (1996) Regulation of p16CDKN2 expression and its implications for cell immortalization and senescence. *Mol Cell Biol,* 16, 859-67.

HARA, R., MO, J. & SANCAR, A. (2000) DNA damage in the nucleosome core is refractory to repair by human excision nuclease. *Mol Cell Biol,* 20, 9173-81.

HARACSKA, L., JOHNSON, R. E., UNK, I., PHILLIPS, B., HURWITZ, J., PRAKASH, L. & PRAKASH, S. (2001) Physical and functional interactions of human DNA polymerase eta with PCNA. *Mol Cell Biol,* 21, 7199-206.

HARDIMAN, G. (2004) Microarray platforms--comparisons and contrasts. *Pharmacogenomics,* 5, 487-502.

HARLEY, C. B., FUTCHER, A. B. & GREIDER, C. W. (1990) Telomeres shorten during ageing of

human fibroblasts. *Nature,* 345, 458-60.

HARPER, J. W., ADAMI, G. R., WEI, N., KEYOMARSI, K. & ELLEDGE, S. J. (1993) The p21 Cdk-interacting protein Cip1 is a potent inhibitor of G1 cyclin-dependent kinases. *Cell,* 75, 805-16.

HARRINGTON, E. A., BRUCE, J. L., HARLOW, E. & DYSON, N. (1998) pRB plays an essential role in cell cycle arrest induced by DNA damage. *Proc Natl Acad Sci U S A,* 95, 11945-50.

HARRINGTON, L., ZHOU, W., MCPHAIL, T., OULTON, R., YEUNG, D. S., MAR, V., BASS, M. B. & ROBINSON, M. O. (1997) Human telomerase contains evolutionarily conserved catalytic and structural subunits. *Genes Dev,* 11, 3109-15.

HARRIS, C. C. & HOLLSTEIN, M. (1993) Clinical implications of the p53 tumor-suppressor gene. *N Engl J Med,* 329, 1318-27.

HARTMAN, A. R. & FORD, J. M. (2002) BRCA1 induces DNA damage recognition factors and enhances nucleotide excision repair. *Nat Genet,* 32, 180-4.

HASHEM, N., BOOTSMA, D., KEIJZER, W., GREENE, A., CORIELL, L., THOMAS, G. & CLEAVER, J. E. (1980) Clinical characteristics, DNA repair, and complementation groups in xeroderma pigmentosum patients from Egypt. *Cancer Res,* 40, 13-8.

HASTIE, N. D., DEMPSTER, M., DUNLOP, M. G., THOMPSON, A. M., GREEN, D. K. & ALLSHIRE, R. C. (1990) Telomere reduction in human colorectal carcinoma and with ageing. *Nature,* 346, 866-8.

HAUPT, Y., MAYA, R., KAZAZ, A. & OREN, M. (1997) Mdm2 promotes the rapid degradation of p53. *Nature,* 387, 296-9.

HAYFLICK, L. (1965) The Limited In Vitro Lifetime Of Human Diploid Cell Strains. *Exp Cell Res,* 37, 614-36.

HAYFLICK, L. & MOORHEAD, P. S. (1961) The serial cultivation of human diploid cell strains. *Exp Cell Res,* 25, 585-621.

HE, Y. Y., HUANG, J. L., SIK, R. H., LIU, J., WAALKES, M. P. & CHIGNELL, C. F. (2004) Expression profiling of human keratinocyte response to ultraviolet A: implications in apoptosis. *J Invest Dermatol,* 122, 533-43.

HE, Z., HENRICKSEN, L. A., WOLD, M. S. & INGLES, C. J. (1995) RPA involvement in the damage-recognition and incision steps of nucleotide excision repair. *Nature,* 374, 566-9.

HEESSEN, S., MASUCCI, M. G. & DANTUMA, N. P. (2005) The UBA2 domain functions as an intrinsic stabilization signal that protects Rad23 from proteasomal degradation. *Mol Cell,* 18,

225-35.

HEINLOTH, A. N., SHACKELFORD, R. E., INNES, C. L., BENNETT, L., LI, L., AMIN, R. P., SIEBER, S. O., FLORES, K. G., BUSHEL, P. R. & PAULES, R. S. (2003) ATM-dependent and -independent gene expression changes in response to oxidative stress, gamma irradiation, and UV irradiation. *Radiat Res,* 160, 273-90.

HENNING, K. A., LI, L., IYER, N., MCDANIEL, L. D., REAGAN, M. S., LEGERSKI, R., SCHULTZ, R. A., STEFANINI, M., LEHMANN, A. R. & MAYNE, L. V. (1995) The Cockayne syndrome group A gene encodes a WD repeat protein that interacts with CSB protein and a subunit of RNA polymerase II TFIIH. *Cell,* 82, 555-64.

HERBIG, U., JOBLING, W. A., CHEN, B. P., CHEN, D. J. & SEDIVY, J. M. (2004) Telomere shortening triggers senescence of human cells through a pathway involving ATM, p53, and p21(CIP1), but not p16(INK4a). *Mol Cell,* 14, 501-13.

HERMANSON-MILLER, I. L. & TURCHI, J. J. (2002) Strand-specific binding of RPA and XPA to damaged duplex DNA. *Biochemistry,* 41, 2402-8.

HERRERA, R. E., SAH, V. P., WILLIAMS, B. O., MAKELA, T. P., WEINBERG, R. A. & JACKS, T. (1996) Altered cell cycle kinetics, gene expression, and G1 restriction point regulation in Rb-deficient fibroblasts. *Mol Cell Biol,* 16, 2402-7.

HESS, M. T., SCHWITTER, U., PETRETTA, M., GIESE, B. & NAEGELI, H. (1997) Bipartite substrate discrimination by human nucleotide excision repair. *Proc Natl Acad Sci U S A,* 94, 6664-9.

HEY, T., LIPPS, G., SUGASAWA, K., IWAI, S., HANAOKA, F. & KRAUSS, G. (2002) The XPC-HR23B complex displays high affinity and specificity for damaged DNA in a true-equilibrium fluorescence assay. *Biochemistry,* 41, 6583-7.

HILDESHEIM, J. & FORNACE, A. J., JR. (2004) The dark side of light: the damaging effects of UV rays and the protective efforts of MAP kinase signaling in the epidermis. *DNA Repair (Amst),* 3, 567-80.

HOEIJMAKERS, J. H., EGLY, J. M. & VERMEULEN, W. (1996) TFIIH: a key component in multiple DNA transactions. *Curr Opin Genet Dev,* 6, 26-33.

HOLSTEGE, F. C., VAN DER VLIET, P. C. & TIMMERS, H. T. (1996) Opening of an RNA polymerase II promoter occurs in two distinct steps and requires the basal transcription factors IIE and IIH. *Embo J,* 15, 1666-77.

HONDA, R., TANAKA, H. & YASUDA, H. (1997) Oncoprotein MDM2 is a ubiquitin ligase E3 for tumor suppressor p53. *FEBS Lett,* 420, 25-7.

HONDA, T., SADAMORI, N., OSHIMURA, M., HORIKAWA, I., OMURA, H., KOMATSU, K. & WATANABE, M. (1996) Spontaneous immortalization of cultured skin fibroblasts obtained from a high-dose atomic bomb survivor. *Mutat Res,* 354, 15-26.

HOOGERVORST, E. M., VAN STEEG, H. & DE VRIES, A. (2005) Nucleotide excision repair- and p53-deficient mouse models in cancer research. *Mutat Res,* 574, 3-21.

HOOGSTRATEN, D., NIGG, A. L., HEATH, H., MULLENDERS, L. H., VAN DRIEL, R., HOEIJMAKERS, J. H., VERMEULEN, W. & HOUTSMULLER, A. B. (2002) Rapid switching of TFIIH between RNA polymerase I and II transcription and DNA repair in vivo. *Mol Cell,* 10, 1163-74.

HOSACK, D.A., DENNIS., G., Jr., SHERMAN, B.T., LANE, H.C. & LEMPICKI, R.A. (2003) Identifying biological themes within lists of genes with EASE. *Genome Biol,* 4, R7.

HO SUI, S.J., MORTIMER, J.R., ARENILLAS, D.J., BRUMM, J., WALSH, C.J., KENNEDY, B.P. & WASSERMAN, W.W. (2005) oPOSSUM: identification of over-represented transcription factor binding sites in co-expressed genes. *Nucleic Acids Res.*, 33, 3154-64.

HOUGHTON, A. N. & POLSKY, D. (2002) Focus on melanoma. *Cancer Cell,* 2, 275-8.

HOWELL, B. G., WANG, B., FREED, I., MAMELAK, A. J., WATANABE, H. & SAUDER, D. N. (2004) Microarray analysis of UVB-regulated genes in keratinocytes: downregulation of angiogenesis inhibitor thrombospondin-1. *J Dermatol Sci,* 34, 185-94.

HRUZA, L. L. & PENTLAND, A. P. (1993) Mechanisms of UV-induced inflammation. *J Invest Dermatol,* 100, 35S-41S.

HUANG, T. T. & D'ANDREA, A. D. (2006) Regulation of DNA repair by ubiquitylation. *Nat Rev Mol Cell Biol,* 7, 323-34.

HUMBERT, S., VAN VUUREN, H., LUTZ, Y., HOEIJMAKERS, J. H., EGLY, J. M. & MONCOLLIN, V. (1994) p44 and p34 subunits of the BTF2/TFIIH transcription factor have homologies with SSL1, a yeast protein involved in DNA repair. *Embo J,* 13, 2393-8.

HWANG, B. J., FORD, J. M., HANAWALT, P. C. & CHU, G. (1999) Expression of the p48 xeroderma pigmentosum gene is p53-dependent and is involved in global genomic repair. *Proc Natl Acad Sci U S A,* 96, 424-8.

HWANG, B. J., TOERING, S., FRANCKE, U. & CHU, G. (1998) p48 Activates a UV-damaged-DNA binding factor and is defective in xeroderma pigmentosum group E cells that lack binding activity. *Mol Cell Biol,* 18, 4391-9.

IBEN, S., TSCHOCHNER, H., BIER, M., HOOGSTRATEN, D., HOZAK, P., EGLY, J. M. &

GRUMMT, I. (2002) TFIIH plays an essential role in RNA polymerase I transcription. *Cell,* 109, 297-306.

ICHIHASHI, M., UEDA, M., BUDIYANTO, A., BITO, T., OKA, M., FUKUNAGA, M., TSURU, K. & HORIKAWA, T. (2003) UV-induced skin damage. *Toxicology,* 189, 21-39.

ISHIDA, S., HUANG, E., ZUZAN, H., SPANG, R., LEONE, G., WEST, M. & NEVINS, J. R. (2001) Role for E2F in control of both DNA replication and mitotic functions as revealed from DNA microarray analysis. *Mol Cell Biol,* 21, 4684-99.

ITOH, M., HAYASHI, M., SHIODA, K., MINAGAWA, M., ISA, F., TAMAGAWA, K., MORIMATSU, Y. & ODA, M. (1999) Neurodegeneration in hereditary nucleotide repair disorders. *Brain Dev,* 21, 326-33.

ITOH, T., CADO, D., KAMIDE, R. & LINN, S. (2004) DDB2 gene disruption leads to skin tumors and resistance to apoptosis after exposure to ultraviolet light but not a chemical carcinogen. *Proc Natl Acad Sci U S A,* 101, 2052-7.

ITOH, T., FUJIWARA, Y., ONO, T. & YAMAIZUMI, M. (1995) UVs syndrome, a new general category of photosensitive disorder with defective DNA repair, is distinct from xeroderma pigmentosum variant and rodent complementation group I. *Am J Hum Genet,* 56, 1267-76.

ITOH, T. & LINN, S. (2005) The fate of p21CDKN1A in cells surviving UV-irradiation. *DNA Repair (Amst),* 4, 1457-62.

ITOH, T., LINN, S., ONO, T. & YAMAIZUMI, M. (2000) Reinvestigation of the classification of five cell strains of xeroderma pigmentosum group E with reclassification of three of them. *J Invest Dermatol,* 114, 1022-9.

ITOH, T., O'SHEA, C. & LINN, S. (2003) Impaired regulation of tumor suppressor p53 caused by mutations in the xeroderma pigmentosum DDB2 gene: mutual regulatory interactions between p48(DDB2) and p53. *Mol Cell Biol,* 23, 7540-53.

ITOH, T., SHIOMI, T., SHIOMI, N., HARADA, Y., WAKASUGI, M., MATSUNAGA, T., NIKAIDO, O., FRIEDBERG, E. C. & YAMAIZUMI, M. (1996) Rodent complementation group 8 (ERCC8) corresponds to Cockayne syndrome complementation group A. *Mutat Res,* 362, 167-74.

ITOH, T. & YAMAIZUMI, M. (2000) UVs syndrome: establishment and characterization of fibroblastic cell lines transformed with simian virus 40 DNA. *J Invest Dermatol,* 114, 101-6.

IYER, N., REAGAN, M. S., WU, K. J., CANAGARAJAH, B. & FRIEDBERG, E. C. (1996) Interactions involving the human RNA polymerase II transcription/nucleotide excision repair complex TFIIH, the nucleotide excision repair protein XPG, and Cockayne syndrome group B (CSB) protein. *Biochemistry,* 35, 2157-67.

IYER, V. R., EISEN, M. B., ROSS, D. T., SCHULER, G., MOORE, T., LEE, J. C., TRENT, J. M., STAUDT, L. M., HUDSON, J., JR., BOGUSKI, M. S., LASHKARI, D., SHALON, D., BOTSTEIN, D. & BROWN, P. O. (1999) The transcriptional program in the response of human fibroblasts to serum. *Science,* 283, 83-7.

JACKSON, D. A., HASSAN, A. B., ERRINGTON, R. J. & COOK, P. R. (1994) Sites in human nuclei where damage induced by ultraviolet light is repaired: localization relative to transcription sites and concentrations of proliferating cell nuclear antigen and the tumour suppressor protein, p53. *J Cell Sci,* 107 (Pt 7), 1753-60.

JANS, J., SCHUL, W., SERT, Y. G., RIJKSEN, Y., REBEL, H., EKER, A. P., NAKAJIMA, S., VAN STEEG, H., DE GRUIJL, F. R., YASUI, A., HOEIJMAKERS, J. H. & VAN DER HORST, G. T. (2005) Powerful skin cancer protection by a CPD-photolyase transgene. *Curr Biol,* 15, 105-15.

JANUS, F., ALBRECHTSEN, N., KNIPPSCHILD, U., WIESMULLER, L., GROSSE, F. & DEPPERT, W. (1999) Different regulation of the p53 core domain activities 3'-to-5' exonuclease and sequence-specific DNA binding. *Mol Cell Biol,* 19, 2155-68.

JAYARAMAN, J. & PRIVES, C. (1995) Activation of p53 sequence-specific DNA binding by short single strands of DNA requires the p53 C-terminus. *Cell,* 81, 1021-9.

JEAN, S., BIDEAU, C., BELLON, L., HALIMI, G., DE MEO, M., ORSIERE, T., DUMENIL, G., BERGE-LEFRANC, J. L. & BOTTA, A. (2001) The expression of genes induced in melanocytes by exposure to 365-nm UVA: study by cDNA arrays and real-time quantitative RT-PCR. *Biochim Biophys Acta,* 1522, 89-96.

JENTSCH, S., MCGRATH, J. P. & VARSHAVSKY, A. (1987) The yeast DNA repair gene RAD6 encodes a ubiquitin-conjugating enzyme. *Nature,* 329, 131-4.

JHAPPAN, C., NOONAN, F. P. & MERLINO, G. (2003) Ultraviolet radiation and cutaneous malignant melanoma. *Oncogene,* 22, 3099-112.

JIANG, G. & SANCAR, A. (2006) Recruitment of DNA damage checkpoint proteins to damage in transcribed and nontranscribed sequences. *Mol Cell Biol,* 26, 39-49.

JIANG, W., ANANTHASWAMY, H. N., MULLER, H. K. & KRIPKE, M. L. (1999a) p53 protects against skin cancer induction by UV-B radiation. *Oncogene,* 18, 4247-53.

JIANG, X. R., JIMENEZ, G., CHANG, E., FROLKIS, M., KUSLER, B., SAGE, M., BEECHE, M., BODNAR, A. G., WAHL, G. M., TLSTY, T. D. & CHIU, C. P. (1999b) Telomerase expression in human somatic cells does not induce changes associated with a transformed phenotype. *Nat Genet,* 21, 111-4.

JIMENEZ, G. S., NISTER, M., STOMMEL, J. M., BEECHE, M., BARCARSE, E. A., ZHANG, X. Q.,

O'GORMAN, S. & WAHL, G. M. (2000) A transactivation-deficient mouse model provides insights into Trp53 regulation and function. *Nat Genet,* 26, 37-43.

JIN, S., TONG, T., FAN, W., FAN, F., ANTINORE, M. J., ZHU, X., MAZZACURATI, L., LI, X., PETRIK, K. L., RAJASEKARAN, B., WU, M. & ZHAN, Q. (2002) GADD45-induced cell cycle G2-M arrest associates with altered subcellular distribution of cyclin B1 and is independent of p38 kinase activity. *Oncogene,* 21, 8696-704.

JOHNSON, R. E., PRAKASH, S. & PRAKASH, L. (1999) Efficient bypass of a thymine-thymine dimer by yeast DNA polymerase, Poleta. *Science,* 283, 1001-4.

JONES, C. J. & WOOD, R. D. (1993) Preferential binding of the xeroderma pigmentosum group A complementing protein to damaged DNA. *Biochemistry,* 32, 12096-104.

JUNG, E. G. (1970) New form of molecular defect in xeroderma pigmentosum. *Nature,* 228, 361-2.

KAMB, A., SHATTUCK-EIDENS, D., EELES, R., LIU, Q., GRUIS, N. A., DING, W., HUSSEY, C., TRAN, T., MIKI, Y., WEAVER-FELDHAUS, J. & ET AL. (1994) Analysis of the p16 gene (CDKN2) as a candidate for the chromosome 9p melanoma susceptibility locus. *Nat Genet,* 8, 23-6.

KAMIUCHI, S., SAIJO, M., CITTERIO, E., DE JAGER, M., HOEIJMAKERS, J. H. & TANAKA, K. (2002) Translocation of Cockayne syndrome group A protein to the nuclear matrix: possible relevance to transcription-coupled DNA repair. *Proc Natl Acad Sci U S A,* 99, 201-6.

KAMPINGA, H. H., VAN WAARDE-VERHAGEN, M. A., VAN ASSEN-BOLT, A. J., NIEUWENHUIS, B., RODEMANN, H. P., PROWSE, K. R. & LINSKENS, M. H. (2004) Reconstitution of active telomerase in primary human foreskin fibroblasts: effects on proliferative characteristics and response to ionizing radiation. *Int J Radiat Biol,* 80, 377-88.

KANG, M. K., KAMETA, A., BALUDA, M. A. & PARK, N. H. (2003) Telomere shortening does not occur during postmaturational aging in situ in normal human oral fibroblasts. *Mech Ageing Dev,* 124, 873-6.

KANNAN, K., SHARPLESS, N. E., XU, J., O'HAGAN, R. C., BOSENBERG, M. & CHIN, L. (2003) Components of the Rb pathway are critical targets of UV mutagenesis in a murine melanoma model. *Proc Natl Acad Sci U S A,* 100, 1221-5.

KANTOR, G. J., BARSALOU, L. S. & HANAWALT, P. C. (1990) Selective repair of specific chromatin domains in UV-irradiated cells from xeroderma pigmentosum complementation group C. *Mutat Res,* 235, 171-80.

KAPETANAKI, M. G., GUERRERO-SANTORO, J., BISI, D. C., HSIEH, C. L., RAPIC-OTRIN, V. & LEVINE, A. S. (2006) The DDB1-CUL4ADDB2 ubiquitin ligase is deficient in xeroderma

pigmentosum group E and targets histone H2A at UV-damaged DNA sites. *Proc Natl Acad Sci U S A,* 103, 2588-93.

KASTAN, M. B. & BARTEK, J. (2004) Cell-cycle checkpoints and cancer. *Nature,* 432, 316-23.

KASTAN, M. B. & KUERBITZ, S. J. (1993) Control of G1 arrest after DNA damage. *Environ Health Perspect,* 101 Suppl 5, 55-8.

KEENEY, S., CHANG, G. J. & LINN, S. (1993) Characterization of a human DNA damage binding protein implicated in xeroderma pigmentosum E. *J Biol Chem,* 268, 21293-300.

KEENEY, S., EKER, A. P., BRODY, T., VERMEULEN, W., BOOTSMA, D., HOEIJMAKERS, J. H. & LINN, S. (1994) Correction of the DNA repair defect in xeroderma pigmentosum group E by injection of a DNA damage-binding protein. *Proc Natl Acad Sci U S A,* 91, 4053-6.

KEIJZER, W., VERKERK, A. & BOOTSMA, D. (1982) Phenotypic correction of the defect in xeroderma pigmentosum cells after fusion with isolated cytoplasts. *Exp Cell Res,* 140, 119-25.

KENNEDY, B. K., BARBIE, D. A., CLASSON, M., DYSON, N. & HARLOW, E. (2000) Nuclear organization of DNA replication in primary mammalian cells. *Genes Dev,* 14, 2855-68.

KERIEL, A., STARY, A., SARASIN, A., ROCHETTE-EGLY, C. & EGLY, J. M. (2002) XPD mutations prevent TFIIH-dependent transactivation by nuclear receptors and phosphorylation of RARalpha. *Cell,* 109, 125-35.

KEYSE, S. M. & TYRRELL, R. M. (1987) Both near ultraviolet radiation and the oxidizing agent hydrogen peroxide induce a 32-kDa stress protein in normal human skin fibroblasts. *J Biol Chem,* 262, 14821-5.

KHAN, S. G., LEVY, H. L., LEGERSKI, R., QUACKENBUSH, E., REARDON, J. T., EMMERT, S., SANCAR, A., LI, L., SCHNEIDER, T. D., CLEAVER, J. E. & KRAEMER, K. H. (1998) Xeroderma pigmentosum group C splice mutation associated with autism and hypoglycinemia. *J Invest Dermatol,* 111, 791-6.

KHAN, S. G., METIN, A., GOZUKARA, E., INUI, H., SHAHLAVI, T., MUNIZ-MEDINA, V., BAKER, C. C., UEDA, T., AIKEN, J. R., SCHNEIDER, T. D. & KRAEMER, K. H. (2004) Two essential splice lariat branchpoint sequences in one intron in a xeroderma pigmentosum DNA repair gene: mutations result in reduced XPC mRNA levels that correlate with cancer risk. *Hum Mol Genet,* 13, 343-52.

KHAN, S. G., METTER, E. J., TARONE, R. E., BOHR, V. A., GROSSMAN, L., HEDAYATI, M., BALE, S. J., EMMERT, S. & KRAEMER, K. H. (2000) A new xeroderma pigmentosum group C poly(AT) insertion/deletion polymorphism. *Carcinogenesis,* 21, 1821-5.

KHAN, S. G., MUNIZ-MEDINA, V., SHAHLAVI, T., BAKER, C. C., INUI, H., UEDA, T., EMMERT, S., SCHNEIDER, T. D. & KRAEMER, K. H. (2002) The human XPC DNA repair gene: arrangement, splice site information content and influence of a single nucleotide polymorphism in a splice acceptor site on alternative splicing and function. *Nucleic Acids Res,* 30, 3624-31.

KHAN, S. G., OH, K. S., SHAHLAVI, T., UEDA, T., BUSCH, D. B., INUI, H., EMMERT, S., IMOTO, K., MUNIZ-MEDINA, V., BAKER, C. C., DIGIOVANNA, J. J., SCHMIDT, D., KHADAVI, A., METIN, A., GOZUKARA, E., SLOR, H., SARASIN, A. & KRAEMER, K. H. (2006) Reduced XPC DNA repair gene mRNA levels in clinically normal parents of xeroderma pigmentosum patients. *Carcinogenesis,* 27, 84-94.

KILIAN, A., BOWTELL, D. D., ABUD, H. E., HIME, G. R., VENTER, D. J., KEESE, P. K., DUNCAN, E. L., REDDEL, R. R. & JEFFERSON, R. A. (1997) Isolation of a candidate human telomerase catalytic subunit gene, which reveals complex splicing patterns in different cell types. *Hum Mol Genet,* 6, 2011-9.

KIM, J. K., PATEL, D. & CHOI, B. S. (1995) Contrasting structural impacts induced by cis-syn cyclobutane dimer and (6-4) adduct in DNA duplex decamers: implication in mutagenesis and repair activity. *Photochem Photobiol,* 62, 44-50.

KIM, N. W., PIATYSZEK, M. A., PROWSE, K. R., HARLEY, C. B., WEST, M. D., HO, P. L., COVIELLO, G. M., WRIGHT, W. E., WEINRICH, S. L. & SHAY, J. W. (1994) Specific association of human telomerase activity with immortal cells and cancer. *Science,* 266, 2011-5.

KIM SH, S. H., KAMINKER, P. & CAMPISI, J. (2002) Telomeres, aging and cancer: in search of a happy ending. *Oncogene,* 21, 503-11.

KIPLING, D., DAVIS, T., OSTLER, E. L. & FARAGHER, R. G. (2004) What can progeroid syndromes tell us about human aging? *Science,* 305, 1426-31.

KIYONO, T., FOSTER, S. A., KOOP, J. I., MCDOUGALL, J. K., GALLOWAY, D. A. & KLINGELHUTZ, A. J. (1998) Both Rb/p16INK4a inactivation and telomerase activity are required to immortalize human epithelial cells. *Nature,* 396, 84-8.

KLEIMAN, F. E., WU-BAER, F., FONSECA, D., KANEKO, S., BAER, R. & MANLEY, J. L. (2005) BRCA1/BARD1 inhibition of mRNA 3' processing involves targeted degradation of RNA polymerase II. *Genes Dev,* 19, 1227-37.

KNUDSEN, E. S., BUCKMASTER, C., CHEN, T. T., FERAMISCO, J. R. & WANG, J. Y. (1998) Inhibition of DNA synthesis by RB: effects on G1/S transition and S-phase progression. *Genes Dev,* 12, 2278-92.

KOBERLE, B., ROGINSKAYA, V. & WOOD, R. D. (2006) XPA protein as a limiting factor for

nucleotide excision repair and UV sensitivity in human cells. *DNA Repair (Amst),* 5, 641-8.

KOCH-PAIZ, C. A., AMUNDSON, S. A., BITTNER, M. L., MELTZER, P. S. & FORNACE, A. J., JR. (2004) Functional genomics of UV radiation responses in human cells. *Mutat Res,* 549, 65-78.

KOERING, C. E., POLLICE, A., ZIBELLA, M. P., BAUWENS, S., PUISIEUX, A., BRUNORI, M., BRUN, C., MARTINS, L., SABATIER, L., PULITZER, J. F. & GILSON, E. (2002) Human telomeric position effect is determined by chromosomal context and telomeric chromatin integrity. *EMBO Rep,* 3, 1055-61.

KOMATSU, A., SUZUKI, S., INAGAKI, T., YAMASHITA, K. & HASHIZUME, K. (2004) A kindred with Cockayne syndrome caused by multiple splicing variants of the CSA gene. *Am J Med Genet A,* 128, 67-71.

KRAEMER, K. H. (1997) Sunlight and skin cancer: another link revealed. *Proc Natl Acad Sci U S A,* 94, 11-4.

KRAEMER, K. H., LEE, M. M., ANDREWS, A. D. & LAMBERT, W. C. (1994) The role of sunlight and DNA repair in melanoma and nonmelanoma skin cancer. The xeroderma pigmentosum paradigm. *Arch Dermatol,* 130, 1018-21.

KRAEMER, K. H., LEE, M. M. & SCOTTO, J. (1987) Xeroderma pigmentosum. Cutaneous, ocular, and neurologic abnormalities in 830 published cases. *Arch Dermatol,* 123, 241-50.

KRTOLICA, A., PARRINELLO, S., LOCKETT, S., DESPREZ, P. Y. & CAMPISI, J. (2001) Senescent fibroblasts promote epithelial cell growth and tumorigenesis: a link between cancer and aging. *Proc Natl Acad Sci U S A,* 98, 12072-7.

KRUSE, J.J.C.M., SVENSSON, J.P., HUIGSLOOT, M., GIPHART-GASSLER, M., SCHOONEN, W.G.E.J, POLMAN, J.E.M., HORBACH, G.J., WATER, B. & VRIELING, H. (in press) A portrait of cisplatin-induced transcriptional changes in mouse embryonic stem cells reveals a dominant p53-like response. Mutat.: Fundam. Mol. Mech. Mutagen.

KRUTMANN, J. (2000) Ultraviolet A radiation-induced biological effects in human skin: relevance for photoaging and photodermatosis. *J Dermatol Sci,* 23 Suppl 1, S22-6.

KULAKSIZ, G., REARDON, J. T. & SANCAR, A. (2005) Xeroderma pigmentosum complementation group E protein (XPE/DDB2): purification of various complexes of XPE and analyses of their damaged DNA binding and putative DNA repair properties. *Mol Cell Biol,* 25, 9784-92.

KUMAZAKI, T., HIYAMA, K., TAKAHASHI, T., OMATSU, H., TANIMOTO, K., NOGUCHI, T., HIYAMA, E., MITSUI, Y. & NISHIYAMA, M. (2004) Differential gene expressions during immortalization of normal human fibroblasts and endothelial cells transfected with human telomerase reverse transcriptase gene. *Int J Oncol,* 24, 1435-42.

KURAOKA, I., MORITA, E. H., SAIJO, M., MATSUDA, T., MORIKAWA, K., SHIRAKAWA, M. & TANAKA, K. (1996) Identification of a damaged-DNA binding domain of the XPA protein. *Mutat Res,* 362, 87-95.

KUSUMOTO, R., MASUTANI, C., SUGASAWA, K., IWAI, S., ARAKI, M., UCHIDA, A., MIZUKOSHI, T. & HANAOKA, F. (2001) Diversity of the damage recognition step in the global genomic nucleotide excision repair in vitro. *Mutat Res,* 485, 219-27.

KVAM, E., HEJMADI, V., RYTER, S., POURZAND, C. & TYRRELL, R. M. (2000) Heme oxygenase activity causes transient hypersensitivity to oxidative ultraviolet A radiation that depends on release of iron from heme. *Free Radic Biol Med,* 28, 1191-6.

KVEIBORG, M., KASSEM, M., LANGDAHL, B., ERIKSEN, E. F., CLARK, B. F. & RATTAN, S. I. (1999) Telomere shortening during aging of human osteoblasts in vitro and leukocytes in vivo: lack of excessive telomere loss in osteoporotic patients. *Mech Ageing Dev,* 106, 261-71.

KYNG, K. J., MAY, A., BROSH, R. M., JR., CHENG, W. H., CHEN, C., BECKER, K. G. & BOHR, V. A. (2003) The transcriptional response after oxidative stress is defective in Cockayne syndrome group B cells. *Oncogene,* 22, 1135-49.

LAI, Z., FERRY, K. V., DIAMOND, M. A., WEE, K. E., KIM, Y. B., MA, J., YANG, T., BENFIELD, P. A., COPELAND, R. A. & AUGER, K. R. (2001) Human mdm2 mediates multiple mono-ubiquitination of p53 by a mechanism requiring enzyme isomerization. *J Biol Chem,* 276, 31357-67.

LANDER, E. S., LINTON, L. M., BIRREN, B., NUSBAUM, C., ZODY, M. C., BALDWIN, J., DEVON, K., DEWAR, K., DOYLE, M., FITZHUGH, W., FUNKE, R., GAGE, D., HARRIS, K., HEAFORD, A., HOWLAND, J., KANN, L., LEHOCZKY, J., LEVINE, R., MCEWAN, P., MCKERNAN, K., MELDRIM, J., MESIROV, J. P., MIRANDA, C., MORRIS, W., NAYLOR, J., RAYMOND, C., ROSETTI, M., SANTOS, R., SHERIDAN, A., SOUGNEZ, C., STANGE-THOMANN, N., STOJANOVIC, N., SUBRAMANIAN, A., WYMAN, D., ROGERS, J., SULSTON, J., AINSCOUGH, R., BECK, S., BENTLEY, D., BURTON, J., CLEE, C., CARTER, N., COULSON, A., DEADMAN, R., DELOUKAS, P., DUNHAM, A., DUNHAM, I., DURBIN, R., FRENCH, L., GRAFHAM, D., GREGORY, S., HUBBARD, T., HUMPHRAY, S., HUNT, A., JONES, M., LLOYD, C., MCMURRAY, A., MATTHEWS, L., MERCER, S., MILNE, S., MULLIKIN, J. C., MUNGALL, A., PLUMB, R., ROSS, M., SHOWNKEEN, R., SIMS, S., WATERSTON, R. H., WILSON, R. K., HILLIER, L. W., MCPHERSON, J. D., MARRA, M. A., MARDIS, E. R., FULTON, L. A., CHINWALLA, A. T., PEPIN, K. H., GISH, W. R., CHISSOE, S. L., WENDL, M. C., DELEHAUNTY, K. D., MINER, T. L., DELEHAUNTY, A., KRAMER, J. B., COOK, L. L., FULTON, R. S., JOHNSON, D. L., MINX, P. J., CLIFTON, S. W., HAWKINS, T., BRANSCOMB, E., PREDKI, P., RICHARDSON, P., WENNING, S., SLEZAK, T., DOGGETT, N., CHENG, J. F., OLSEN, A., LUCAS, S., ELKIN,

C., UBERBACHER, E., FRAZIER, M., et al. (2001) Initial sequencing and analysis of the human genome. *Nature,* 409, 860-921.

LANE, D. P. & BENCHIMOL, S. (1990) p53: oncogene or anti-oncogene? *Genes Dev,* 4, 1-8.

LANE, D. P. & CRAWFORD, L. V. (1979) T antigen is bound to a host protein in SV40-transformed cells. *Nature,* 278, 261-3.

LATONEN, L. & LAIHO, M. (2005) Cellular UV damage responses--functions of tumor suppressor p53. *Biochim Biophys Acta,* 1755, 71-89.

LEE, D. H. & PFEIFER, G. P. (2003) Deamination of 5-methylcytosines within cyclobutane pyrimidine dimers is an important component of UVB mutagenesis. *J Biol Chem,* 278, 10314-21.

LEE, J. H., PARK, C. J., ARUNKUMAR, A. I., CHAZIN, W. J. & CHOI, B. S. (2003) NMR study on the interaction between RPA and DNA decamer containing cis-syn cyclobutane pyrimidine dimer in the presence of XPA: implication for damage verification and strand-specific dual incision in nucleotide excision repair. *Nucleic Acids Res,* 31, 4747-54.

LEE, K. M., LEE, J. G., SEO, E. Y., LEE, W. H., NAM, Y. H., YANG, J. M., KEE, S. H., SEO, Y. J., PARK, J. K., KIM, C. D. & LEE, J. H. (2005) Analysis of genes responding to ultraviolet B irradiation of HaCaT keratinocytes using a cDNA microarray. *Br J Dermatol,* 152, 52-9.

LEE, M. H., AHN, B., CHOI, I. S. & KOO, H. S. (2002a) The gene expression and deficiency phenotypes of Cockayne syndrome B protein in Caenorhabditis elegans. *FEBS Lett,* 522, 47-51.

LEE, S., CAVALLO, L. & GRIFFITH, J. (1997) Human p53 binds Holliday junctions strongly and facilitates their cleavage. *J Biol Chem,* 272, 7532-9.

LEE, S. K., YU, S. L., PRAKASH, L. & PRAKASH, S. (2002b) Requirement of yeast RAD2, a homolog of human XPG gene, for efficient RNA polymerase II transcription. implications for Cockayne syndrome. *Cell,* 109, 823-34.

LEE, W. H., BOOKSTEIN, R., HONG, F., YOUNG, L. J., SHEW, J. Y. & LEE, E. Y. (1987) Human retinoblastoma susceptibility gene: cloning, identification, and sequence. *Science,* 235, 1394-9.

LEFFELL, D. J. & BRASH, D. E. (1996) Sunlight and skin cancer. *Sci Am,* 275, 52-3, 56-9.

LEGERSKI, R. & PETERSON, C. (1992) Expression cloning of a human DNA repair gene involved in xeroderma pigmentosum group C. *Nature,* 359, 70-3.

LEHMANN, A. R. (2001) The xeroderma pigmentosum group D (XPD) gene: one gene, two functions, three diseases. *Genes Dev,* 15, 15-23.

LEHMANN, A. R. (2003) DNA repair-deficient diseases, xeroderma pigmentosum, Cockayne syndrome

and trichothiodystrophy. *Biochimie,* 85, 1101-11.

LEHMANN, A. R., KIRK-BELL, S., ARLETT, C. F., HARCOURT, S. A., DE WEERD-KASTELEIN, E. A., KEIJZER, W. & HALL-SMITH, P. (1977) Repair of ultraviolet light damage in a variety of human fibroblast cell strains. *Cancer Res,* 37, 904-10.

LEVEILLARD, T., ANDERA, L., BISSONNETTE, N., SCHAEFFER, L., BRACCO, L., EGLY, J. M. & WASYLYK, B. (1996) Functional interactions between p53 and the TFIIH complex are affected by tumour-associated mutations. *Embo J,* 15, 1615-24.

LEVINE, A. J. (1997) p53, the cellular gatekeeper for growth and division. *Cell,* 88, 323-31.

LI, D. & ROBERTS, R. (2001) WD-repeat proteins: structure characteristics, biological function, and their involvement in human diseases. *Cell Mol Life Sci,* 58, 2085-97.

LI, D., TURI, T. G., SCHUCK, A., FREEDBERG, I. M., KHITROV, G. & BLUMENBERG, M. (2001) Rays and arrays: the transcriptional program in the response of human epidermal keratinocytes to UVB illumination. *Faseb J,* 15, 2533-5.

LI, L., BALES, E. S., PETERSON, C. A. & LEGERSKI, R. J. (1993) Characterization of molecular defects in xeroderma pigmentosum group C. *Nat Genet,* 5, 413-7.

LI, L., ELLEDGE, S. J., PETERSON, C. A., BALES, E. S. & LEGERSKI, R. J. (1994) Specific association between the human DNA repair proteins XPA and ERCC1. *Proc Natl Acad Sci U S A,* 91, 5012-6.

LI, L., LU, X., PETERSON, C. & LEGERSKI, R. (1997) XPC interacts with both HHR23B and HHR23A in vivo. *Mutat Res,* 383, 197-203.

LI, L., LU, X., PETERSON, C. A. & LEGERSKI, R. J. (1995a) An interaction between the DNA repair factor XPA and replication protein A appears essential for nucleotide excision repair. *Mol Cell Biol,* 15, 5396-402.

LI, L., PETERSON, C. A., LU, X. & LEGERSKI, R. J. (1995b) Mutations in XPA that prevent association with ERCC1 are defective in nucleotide excision repair. *Mol Cell Biol,* 15, 1993-8.

LI, R., HANNON, G. J., BEACH, D. & STILLMAN, B. (1996) Subcellular distribution of p21 and PCNA in normal and repair-deficient cells following DNA damage. *Curr Biol,* 6, 189-99.

LIANG, C., KRAEMER, K. H., MORRIS, A., SCHIFFMANN, R., PRICE, V. H., MENEFEE, E. & DIGIOVANNA, J. J. (2005) Characterization of tiger-tail banding and hair shaft abnormalities in trichothiodystrophy. *J Am Acad Dermatol,* 52, 224-32.

LICHT, C. L., STEVNSNER, T. & BOHR, V. A. (2003) Cockayne syndrome group B cellular and

biochemical functions. *Am J Hum Genet,* 73, 1217-39.

LILL, N. L., TEVETHIA, M. J., ECKNER, R., LIVINGSTON, D. M. & MODJTAHEDI, N. (1997) p300 family members associate with the carboxyl terminus of simian virus 40 large tumor antigen. *J Virol,* 71, 129-37.

LIMOLI, C. L., GIEDZINSKI, E., BONNER, W. M. & CLEAVER, J. E. (2002) UV-induced replication arrest in the xeroderma pigmentosum variant leads to DNA double-strand breaks, gamma -H2AX formation, and Mre11 relocalization. *Proc Natl Acad Sci U S A,* 99, 233-8.

LIMOLI, C. L., GIEDZINSKI, E., MORGAN, W. F. & CLEAVER, J. E. (2000) Inaugural article: polymerase eta deficiency in the xeroderma pigmentosum variant uncovers an overlap between the S phase checkpoint and double-strand break repair. *Proc Natl Acad Sci U S A,* 97, 7939-46.

LIN, J. Y. & SIMMONS, D. T. (1991) The ability of large T antigen to complex with p53 is necessary for the increased life span and partial transformation of human cells by simian virus 40. *J Virol,* 65, 6447-53.

LINDAHL, T. (1993) Instability and decay of the primary structure of DNA. *Nature,* 362, 709-15.

LINDENBAUM, Y., DICKSON, D., ROSENBAUM, P., KRAEMER, K., ROBBINS, I. & RAPIN, I. (2001) Xeroderma pigmentosum/cockayne syndrome complex: first neuropathological study and review of eight other cases. *Eur J Paediatr Neurol,* 5, 225-42.

LINDVALL, C., HOU, M., KOMURASAKI, T., ZHENG, C., HENRIKSSON, M., SEDIVY, J. M., BJORKHOLM, M., TEH, B. T., NORDENSKJOLD, M. & XU, D. (2003) Molecular characterization of human telomerase reverse transcriptase-immortalized human fibroblasts by gene expression profiling: activation of the epiregulin gene. *Cancer Res,* 63, 1743-7.

LING, H., BOUDSOCQ, F., WOODGATE, R. & YANG, W. (2001) Crystal structure of a Y-family DNA polymerase in action: a mechanism for error-prone and lesion-bypass replication. *Cell,* 107, 91-102.

LINSKENS, M. H., FENG, J., ANDREWS, W. H., ENLOW, B. E., SAATI, S. M., TONKIN, L. A., FUNK, W. D. & VILLEPONTEAU, B. (1995) Cataloging altered gene expression in young and senescent cells using enhanced differential display. *Nucleic Acids Res,* 23, 3244-51.

LINZER, D. I. & LEVINE, A. J. (1979) Characterization of a 54K dalton cellular SV40 tumor antigen present in SV40-transformed cells and uninfected embryonal carcinoma cells. *Cell,* 17, 43-52.

LIPETZ, J. & CRISTOFALO, V. J. (1972) Ultrastructural changes accompanying the aging of human diploid cells in culture. *J Ultrastruct Res,* 39, 43-56.

LIU, G. & CHEN, X. (2006) DNA polymerase eta, the product of the xeroderma pigmentosum variant

gene and a target of p53, modulates the DNA damage checkpoint and p53 activation. *Mol Cell Biol,* 26, 1398-413.

LJUNGMAN, M., O'HAGAN, H. M. & PAULSEN, M. T. (2001) Induction of ser15 and lys382 modifications of p53 by blockage of transcription elongation. *Oncogene,* 20, 5964-71.

LJUNGMAN, M. & ZHANG, F. (1996) Blockage of RNA polymerase as a possible trigger for u.v. light-induced apoptosis. *Oncogene,* 13, 823-31.

LLOYD, D. R. & HANAWALT, P. C. (2000) p53-dependent global genomic repair of benzo[a]pyrene-7,8-diol-9,10-epoxide adducts in human cells. *Cancer Res,* 60, 517-21.

LLOYD, D. R. & HANAWALT, P. C. (2002) p53 controls global nucleotide excision repair of low levels of structurally diverse benzo(g)chrysene-DNA adducts in human fibroblasts. *Cancer Res,* 62, 5288-94.

LOIGNON, M., FETNI, R., GORDON, A. J. & DROBETSKY, E. A. (1997) A p53-independent pathway for induction of p21waf1cip1 and concomitant G1 arrest in UV-irradiated human skin fibroblasts. *Cancer Res,* 57, 3390-4.

LOMBARD, D. B., CHUA, K. F., MOSTOSLAVSKY, R., FRANCO, S., GOSTISSA, M. & ALT, F. W. (2005) DNA repair, genome stability, and aging. *Cell,* 120, 497-512.

LOMMEL, L., ORTOLAN, T., CHEN, L., MADURA, K. & SWEDER, K. S. (2002) Proteolysis of a nucleotide excision repair protein by the 26 S proteasome. *Curr Genet,* 42, 9-20.

LOU, Z. & CHEN, J. (2006) Cellular senescence and DNA repair. *Exp Cell Res,* 312, 2641-6.

LOU, Z., MINTER-DYKHOUSE, K., FRANCO, S., GOSTISSA, M., RIVERA, M. A., CELESTE, A., MANIS, J. P., VAN DEURSEN, J., NUSSENZWEIG, A., PAULL, T. T., ALT, F. W. & CHEN, J. (2006) MDC1 maintains genomic stability by participating in the amplification of ATM-dependent DNA damage signals. *Mol Cell,* 21, 187-200.

LOWRY, R. B., MACLEAN, R., MCLEAN, D. M. & TISCHLER, B. (1971) Cataracts, microcephaly, kyphosis, and limited joint movement in two siblings: a new syndrome. *J Pediatr,* 79, 282-4.

LU, H. & LEVINE, A. J. (1995) Human TAFII31 protein is a transcriptional coactivator of the p53 protein. *Proc Natl Acad Sci U S A,* 92, 5154-8.

LU, X., BOCANGEL, D., NANNENGA, B., YAMAGUCHI, H., APPELLA, E. & DONEHOWER, L. A. (2004) The p53-induced oncogenic phosphatase PPM1D interacts with uracil DNA glycosylase and suppresses base excision repair. *Mol Cell,* 15, 621-34.

LU, X., NANNENGA, B. & DONEHOWER, L. A. (2005) PPM1D dephosphorylates Chk1 and p53 and

abrogates cell cycle checkpoints. *Genes Dev,* 19, 1162-74.

MA, L., SIEMSSEN, E. D., NOTEBORN, H. M. & VAN DER EB, A. J. (1994) The xeroderma pigmentosum group B protein ERCC3 produced in the baculovirus system exhibits DNA helicase activity. *Nucleic Acids Res,* 22, 4095-102.

MACIERA-COELHO, A., GARCIA-GIRALT, E. & ADRIAN, M. (1971) Changes in lysosomal associated structures in human fibroblasts kept in resting phase. *Proc Soc Exp Biol Med,* 138, 712-8.

MACINNES, M. A., BINGHAM, J. M., THOMPSON, L. H. & STRNISTE, G. F. (1984) DNA-mediated cotransfer of excision repair capacity and drug resistance into chinese hamster ovary mutant cell line UV-135. *Mol Cell Biol,* 4, 1152-8.

MACINNES, M. A., DICKSON, J. A., HERNANDEZ, R. R., LEARMONTH, D., LIN, G. Y., MUDGETT, J. S., PARK, M. S., SCHAUER, S., REYNOLDS, R. J., STRNISTE, G. F. & ET AL. (1993) Human ERCC5 cDNA-cosmid complementation for excision repair and bipartite amino acid domains conserved with RAD proteins of Saccharomyces cerevisiae and Schizosaccharomyces pombe. *Mol Cell Biol,* 13, 6393-402.

MACIP, S., IGARASHI, M., FANG, L., CHEN, A., PAN, Z. Q., LEE, S. W. & AARONSON, S. A. (2002) Inhibition of p21-mediated ROS accumulation can rescue p21-induced senescence. *Embo J,* 21, 2180-8.

MACKENZIE, K. L., FRANCO, S., MAY, C., SADELAIN, M. & MOORE, M. A. (2000) Mass cultured human fibroblasts overexpressing hTERT encounter a growth crisis following an extended period of proliferation. *Exp Cell Res,* 259, 336-50.

MAKI, C. G. & HOWLEY, P. M. (1997) Ubiquitination of p53 and p21 is differentially affected by ionizing and UV radiation. *Mol Cell Biol,* 17, 355-63.

MALDONADO, E., SHIEKHATTAR, R., SHELDON, M., CHO, H., DRAPKIN, R., RICKERT, P., LEES, E., ANDERSON, C. W., LINN, S. & REINBERG, D. (1996) A human RNA polymerase II complex associated with SRB and DNA-repair proteins. *Nature,* 381, 86-9.

MALLERY, D. L., TANGANELLI, B., COLELLA, S., STEINGRIMSDOTTIR, H., VAN GOOL, A. J., TROELSTRA, C., STEFANINI, M. & LEHMANN, A. R. (1998) Molecular analysis of mutations in the CSB (ERCC6) gene in patients with Cockayne syndrome. *Am J Hum Genet,* 62, 77-85.

MALTZMAN, W. & CZYZYK, L. (1984) UV irradiation stimulates levels of p53 cellular tumor antigen in nontransformed mouse cells. *Mol Cell Biol,* 4, 1689-94.

MARIN, M. S., LOPEZ-CIMA, M. F., GARCIA-CASTRO, L., PASCUAL, T., MARRON, M. G. &

TARDON, A. (2004) Poly (AT) polymorphism in intron 11 of the XPC DNA repair gene enhances the risk of lung cancer. *Cancer Epidemiol Biomarkers Prev,* 13, 1788-93.

MARKEY, M. P., ANGUS, S. P., STROBECK, M. W., WILLIAMS, S. L., GUNAWARDENA, R. W., ARONOW, B. J. & KNUDSEN, E. S. (2002) Unbiased analysis of RB-mediated transcriptional repression identifies novel targets and distinctions from E2F action. *Cancer Res,* 62, 6587-97.

MASHIMA, T., UDAGAWA, S. & TSURUO, T. (2001) Involvement of transcriptional repressor ATF3 in acceleration of caspase protease activation during DNA damaging agent-induced apoptosis. *J Cell Physiol,* 188, 352-8.

MASUTANI, C., ARAKI, M., SUGASAWA, K., VAN DER SPEK, P. J., YAMADA, A., UCHIDA, A., MAEKAWA, T., BOOTSMA, D., HOEIJMAKERS, J. H. & HANAOKA, F. (1997) Identification and characterization of XPG-binding domain of hHR23B. *Mol Cell Biol,* 17, 6915-23.

MASUTANI, C., ARAKI, M., YAMADA, A., KUSUMOTO, R., NOGIMORI, T., MAEKAWA, T., IWAI, S. & HANAOKA, F. (1999) Xeroderma pigmentosum variant (XP-V) correcting protein from HeLa cells has a thymine dimer bypass DNA polymerase activity. *Embo J,* 18, 3491-501.

MASUTANI, C., SUGASAWA, K., YANAGISAWA, J., SONOYAMA, T., UI, M., ENOMOTO, T., TAKIO, K., TANAKA, K., VAN DER SPEK, P. J., BOOTSMA, D. & ET AL. (1994) Purification and cloning of a nucleotide excision repair complex involving the xeroderma pigmentosum group C protein and a human homologue of yeast RAD23. *Embo J,* 13, 1831-43.

MATHONNET, G., LEGER, C., DESNOYERS, J., DROUIN, R., THERRIEN, J. P. & DROBETSKY, E. A. (2003) UV wavelength-dependent regulation of transcription-coupled nucleotide excision repair in p53-deficient human cells. *Proc Natl Acad Sci U S A,* 100, 7219-24.

MATSUDA, N., AZUMA, K., SAIJO, M., IEMURA, S., HIOKI, Y., NATSUME, T., CHIBA, T., TANAKA, K. & TANAKA, K. (2005) DDB2, the xeroderma pigmentosum group E gene product, is directly ubiquitylated by Cullin 4A-based ubiquitin ligase complex. *DNA Repair (Amst),* 4, 537-45.

MATSUI, M. S. & DELEO, V. A. (1991) Longwave ultraviolet radiation and promotion of skin cancer. *Cancer Cells,* 3, 8-12.

MATSUMURA, T. (1980) Multinucleation and polyploidization of aging human cells in culture. *Adv Exp Med Biol,* 129, 31-8.

MATSUMURA, T., PFENDT, E. A. & HAYFLICK, L. (1979) DNA synthesis in the human diploid cell strain WI-38 during in vitro aging: an autoradiography study. *J Gerontol,* 34, 323-7.

MAYNE, L. V. & LEHMANN, A. R. (1982) Failure of RNA synthesis to recover after UV irradiation: an

early defect in cells from individuals with Cockayne's syndrome and xeroderma pigmentosum. *Cancer Res,* 42, 1473-8.

MAYNE, L. V., PRIESTLEY, A., JAMES, M. R. & BURKE, J. F. (1986) Efficient immortalization and morphological transformation of human fibroblasts by transfection with SV40 DNA linked to a dominant marker. *Exp Cell Res,* 162, 530-8.

MCCLINTOCK, B. (1939) The Behavior in Successive Nuclear Divisions of a Chromosome Broken at Meiosis. *Proc Natl Acad Sci U S A,* 25, 405-16.

MCKAY, B. C., BECERRIL, C. & LJUNGMAN, M. (2001) P53 plays a protective role against UV- and cisplatin-induced apoptosis in transcription-coupled repair proficient fibroblasts. *Oncogene,* 20, 6805-8.

MCKAY, B. C., BECERRIL, C., SPRONCK, J. C. & LJUNGMAN, M. (2002) Ultraviolet light-induced apoptosis is associated with S-phase in primary human fibroblasts. *DNA Repair (Amst),* 1, 811-20.

MCKAY, B. C., CHEN, F., PERUMALSWAMI, C. R., ZHANG, F. & LJUNGMAN, M. (2000) The tumor suppressor p53 can both stimulate and inhibit ultraviolet light-induced apoptosis. *Mol Biol Cell,* 11, 2543-51.

MCKAY, B. C. & LJUNGMAN, M. (1999) Role for p53 in the recovery of transcription and protection against apoptosis induced by ultraviolet light. *Neoplasia,* 1, 276-84.

MCKAY, B. C., LJUNGMAN, M. & RAINBOW, A. J. (1998) Persistent DNA damage induced by ultraviolet light inhibits p21wafl and bax expression: implications for DNA repair, UV sensitivity and the induction of apoptosis. *Oncogene,* 17, 545-55.

MCKAY, B. C., LJUNGMAN, M. & RAINBOW, A. J. (1999) Potential roles for p53 in nucleotide excision repair. *Carcinogenesis,* 20, 1389-96.

MCKAY, B. C., STUBBERT, L. J., FOWLER, C. C., SMITH, J. M., CARDAMORE, R. A. & SPRONCK, J. C. (2004) Regulation of ultraviolet light-induced gene expression by gene size. *Proc Natl Acad Sci U S A,* 101, 6582-6.

MEIRA, L. B., GRAHAM, J. M., JR., GREENBERG, C. R., BUSCH, D. B., DOUGHTY, A. T., ZIFFER, D. W., COLEMAN, D. M., SAVRE-TRAIN, I. & FRIEDBERG, E. C. (2000) Manitoba aboriginal kindred with original cerebro-oculo- facio-skeletal syndrome has a mutation in the Cockayne syndrome group B (CSB) gene. *Am J Hum Genet,* 66, 1221-8.

MEKEEL, K. L., TANG, W., KACHNIC, L. A., LUO, C. M., DEFRANK, J. S. & POWELL, S. N. (1997) Inactivation of p53 results in high rates of homologous recombination. *Oncogene,* 14, 1847-57.

MELLON, I., BOHR, V. A., SMITH, C. A. & HANAWALT, P. C. (1986) Preferential DNA repair of an active gene in human cells. *Proc Natl Acad Sci U S A,* 83, 8878-82.

MELLON, I. & HANAWALT, P. C. (1989) Induction of the Escherichia coli lactose operon selectively increases repair of its transcribed DNA strand. *Nature,* 342, 95-8.

MELLON, I., HOCK, T., REID, R., PORTER, P. C. & STATES, J. C. (2002) Polymorphisms in the human xeroderma pigmentosum group A gene and their impact on cell survival and nucleotide excision repair. *DNA Repair (Amst),* 1, 531-46.

MELLON, I., RAJPAL, D. K., KOI, M., BOLAND, C. R. & CHAMPE, G. N. (1996) Transcription-coupled repair deficiency and mutations in human mismatch repair genes. *Science,* 272, 557-60.

MELLON, I., SPIVAK, G. & HANAWALT, P. C. (1987) Selective removal of transcription-blocking DNA damage from the transcribed strand of the mammalian DHFR gene. *Cell,* 51, 241-9.

MELNIKOVA, V. O. & ANANTHASWAMY, H. N. (2005) Cellular and molecular events leading to the development of skin cancer. *Mutat Res,* 571, 91-106.

MERCIER, G., DENIS, Y., MARC, P., PICARD, L. & DUTREIX, M. (2001) Transcriptional induction of repair genes during slowing of replication in irradiated Saccharomyces cerevisiae. *Mutat Res,* 487, 157-72.

MERK, O. & SPEIT, G. (1997) Characterization of SV40-transformed xeroderma pigmentosum cell lines for their usability in HPRT mutation studies. *Mutagenesis,* 12, 391-5.

MERKLE, T. J., O'BRIEN, K., BROOKS, P. J., TARONE, R. E. & ROBBINS, J. H. (2004) DNA repair in human fibroblasts, as reflected by host-cell reactivation of a transfected UV-irradiated luciferase gene, is not related to donor age. *Mutat Res,* 554, 9-17.

MEYERSON, M., COUNTER, C. M., EATON, E. N., ELLISEN, L. W., STEINER, P., CADDLE, S. D., ZIAUGRA, L., BEIJERSBERGEN, R. L., DAVIDOFF, M. J., LIU, Q., BACCHETTI, S., HABER, D. A. & WEINBERG, R. A. (1997) hEST2, the putative human telomerase catalytic subunit gene, is up-regulated in tumor cells and during immortalization. *Cell,* 90, 785-95.

MIETZ, J. A., UNGER, T., HUIBREGTSE, J. M. & HOWLEY, P. M. (1992) The transcriptional transactivation function of wild-type p53 is inhibited by SV40 large T-antigen and by HPV-16 E6 oncoprotein. *Embo J,* 11, 5013-20.

MILLER, H. & GROLLMAN, A. P. (2003) DNA repair investigations using siRNA. *DNA Repair (Amst),* 2, 759-63.

MILLIGAN, A., GABRIELLI, B. G., CLARK, J. M., HAYWARD, N. K. & ELLEM, K. A. (1998) Involvement of p16CDKN2A in cell cycle delays after low dose UV irradiation. *Mutat Res,* 422,

43-53.

MILLIKAN, R. C., HUMMER, A., BEGG, C., PLAYER, J., DE COTRET, A. R., WINKEL, S., MOHRENWEISER, H., THOMAS, N., ARMSTRONG, B., KRICKER, A., MARRETT, L. D., GRUBER, S. B., CULVER, H. A., ZANETTI, R., GALLAGHER, R. P., DWYER, T., REBBECK, T. R., BUSAM, K., FROM, L., MUJUMDAR, U. & BERWICK, M. (2006) Polymorphisms in nucleotide excision repair genes and risk of multiple primary melanoma: the Genes Environment and Melanoma Study. *Carcinogenesis,* 27, 610-8.

MILLIS, A. J., HOYLE, M., MCCUE, H. M. & MARTINI, H. (1992a) Differential expression of metalloproteinase and tissue inhibitor of metalloproteinase genes in aged human fibroblasts. *Exp Cell Res,* 201, 373-9.

MILLIS, A. J., MCCUE, H. M., KUMAR, S. & BAGLIONI, C. (1992b) Metalloproteinase and TIMP-1 gene expression during replicative senescence. *Exp Gerontol,* 27, 425-8.

MILNER, J. & MEDCALF, E. A. (1991) Cotranslation of activated mutant p53 with wild type drives the wild-type p53 protein into the mutant conformation. *Cell,* 65, 765-74.

MILYAVSKY, M., SHATS, I., EREZ, N., TANG, X., SENDEROVICH, S., MEERSON, A., TABACH, Y., GOLDFINGER, N., GINSBERG, D., HARRIS, C. C. & ROTTER, V. (2003) Prolonged culture of telomerase-immortalized human fibroblasts leads to a premalignant phenotype. *Cancer Res,* 63, 7147-57.

MINAMINO, T., MIYAUCHI, H., YOSHIDA, T., ISHIDA, Y., YOSHIDA, H. & KOMURO, I. (2002) Endothelial cell senescence in human atherosclerosis: role of telomere in endothelial dysfunction. *Circulation,* 105, 1541-4.

MIRZA, A., WU, Q., WANG, L., MCCLANAHAN, T., BISHOP, W. R., GHEYAS, F., DING, W., HUTCHINS, B., HOCKENBERRY, T., KIRSCHMEIER, P., GREENE, J. R. & LIU, S. (2003) Global transcriptional program of p53 target genes during the process of apoptosis and cell cycle progression. *Oncogene,* 22, 3645-54.

MIRZAYANS, R., ENNS, L., DIETRICH, K., BARLEY, R. D. & PATERSON, M. C. (1996) Faulty DNA polymerase delta/epsilon-mediated excision repair in response to gamma radiation or ultraviolet light in p53-deficient fibroblast strains from affected members of a cancer-prone family with Li-Fraumeni syndrome. *Carcinogenesis,* 17, 691-8.

MISSURA, M., BUTERIN, T., HINDGES, R., HUBSCHER, U., KASPARKOVA, J., BRABEC, V. & NAEGELI, H. (2001) Double-check probing of DNA bending and unwinding by XPA-RPA: an architectural function in DNA repair. *Embo J,* 20, 3554-64.

MITCHELL, D. L. (1988) The relative cytotoxicity of (6-4) photoproducts and cyclobutane dimers in

mammalian cells. *Photochem Photobiol,* 48, 51-7.

MITCHELL, D. L., JEN, J. & CLEAVER, J. E. (1992) Sequence specificity of cyclobutane pyrimidine dimers in DNA treated with solar (ultraviolet B) radiation. *Nucleic Acids Res,* 20, 225-9.

MITCHELL, D. L. & NAIRN, R. S. (1989) The biology of the (6-4) photoproduct. *Photochem Photobiol,* 49, 805-19.

MITCHELL, D. L., NGUYEN, T. D. & CLEAVER, J. E. (1990) Nonrandom induction of pyrimidine-pyrimidone (6-4) photoproducts in ultraviolet-irradiated human chromatin. *J Biol Chem,* 265, 5353-6.

MITCHELL, J. R., HOEIJMAKERS, J. H. & NIEDERNHOFER, L. J. (2003) Divide and conquer: nucleotide excision repair battles cancer and ageing. *Curr Opin Cell Biol,* 15, 232-40.

MITSUI, Y. & SCHNEIDER, E. L. (1976) Relationship between cell replication and volume in senescent human diploid fibroblasts. *Mech Ageing Dev,* 5, 45-56.

MIYAUCHI-HASHIMOTO, H., AKAEDA, T., MAIHARA, T., IKENAGA, M. & HORIO, T. (1998) Cockayne syndrome without typical clinical manifestations including neurologic abnormalities. *J Am Acad Dermatol,* 39, 565-70.

MIYAZAKI, T., TOMIYAMA, N., SHINJOH, M. & HOSHINO, T. (2002) Molecular cloning and functional expression of D-sorbitol dehydrogenase from Gluconobacter suboxydans IF03255, which requires pyrroloquinoline quinone and hydrophobic protein SldB for activity development in E. coli. *Biosci Biotechnol Biochem,* 66, 262-70.

MOAN, J., DAHLBACK, A. & SETLOW, R. B. (1999) Epidemiological support for an hypothesis for melanoma induction indicating a role for UVA radiation. *Photochem Photobiol,* 70, 243-7.

MOGGS, J. G. & ALMOUZNI, G. (1999) Chromatin rearrangements during nucleotide excision repair. *Biochimie,* 81, 45-52.

MOMAND, J., ZAMBETTI, G. P., OLSON, D. C., GEORGE, D. & LEVINE, A. J. (1992) The mdm-2 oncogene product forms a complex with the p53 protein and inhibits p53-mediated transactivation. *Cell,* 69, 1237-45.

MOORE, M., TERESKY, A. K., LEVINE, A. J. & SEIBERG, M. (1992) p53 mutations are not selected for in simian virus 40 T-antigen-induced tumors from transgenic mice. *J Virol,* 66, 641-9.

MORALES, C. P., GANDIA, K. G., RAMIREZ, R. D., WRIGHT, W. E., SHAY, J. W. & SPECHLER, S. J. (2003) Characterisation of telomerase immortalised normal human oesophageal squamous cells. *Gut,* 52, 327-33.

MORALES, C. P., HOLT, S. E., OUELLETTE, M., KAUR, K. J., YAN, Y., WILSON, K. S., WHITE, M. A., WRIGHT, W. E. & SHAY, J. W. (1999) Absence of cancer-associated changes in human fibroblasts immortalized with telomerase. *Nat Genet,* 21, 115-8.

MORI, T., NAKANE, M., HATTORI, T., MATSUNAGA, T., IHARA, M. & NIKAIDO, O. (1991) Simultaneous establishment of monoclonal antibodies specific for either cyclobutane pyrimidine dimer or (6-4)photoproduct from the same mouse immunized with ultraviolet-irradiated DNA. *Photochem Photobiol,* 54, 225-32.

MOSER, J., VOLKER, M., KOOL, H., ALEKSEEV, S., VRIELING, H., YASUI, A., VAN ZEELAND, A. A. & MULLENDERS, L. H. (2005) The UV-damaged DNA binding protein mediates efficient targeting of the nucleotide excision repair complex to UV-induced photo lesions. *DNA Repair (Amst),* 4, 571-82.

MOUTON, R. E. & VENABLE, M. E. (2000) Ceramide induces expression of the senescence histochemical marker, beta-galactosidase, in human fibroblasts. *Mech Ageing Dev,* 113, 169-81.

MOYSAN, A., MORLIERE, P., MARQUIS, I., RICHARD, A. & DUBERTRET, L. (1995) Effects of selenium on UVA-induced lipid peroxidation in cultured human skin fibroblasts. *Skin Pharmacol,* 8, 139-48.

MOYZIS, R. K., BUCKINGHAM, J. M., CRAM, L. S., DANI, M., DEAVEN, L. L., JONES, M. D., MEYNE, J., RATLIFF, R. L. & WU, J. R. (1988) A highly conserved repetitive DNA sequence, (TTAGGG)n, present at the telomeres of human chromosomes. *Proc Natl Acad Sci U S A,* 85, 6622-6.

MU, D., HSU, D. S. & SANCAR, A. (1996) Reaction mechanism of human DNA repair excision nuclease. *J Biol Chem,* 271, 8285-94.

MU, D., PARK, C. H., MATSUNAGA, T., HSU, D. S., REARDON, J. T. & SANCAR, A. (1995) Reconstitution of human DNA repair excision nuclease in a highly defined system. *J Biol Chem,* 270, 2415-8.

MU, D. & SANCAR, A. (1997) Model for XPC-independent transcription-coupled repair of pyrimidine dimers in humans. *J Biol Chem,* 272, 7570-3.

MUDGETT, J. S. & MACINNES, M. A. (1990) Isolation of the functional human excision repair gene ERCC5 by intercosmid recombination. *Genomics,* 8, 623-33.

MUELLER, S. N., ROSEN, E. M. & LEVINE, E. M. (1980) Cellular senescence in a cloned strain of bovine fetal aortic endothelial cells. *Science,* 207, 889-91.

MUGGLETON-HARRIS, A. L. & HAYFLICK, L. (1976) Cellular aging studied by the reconstruction of replicating cells from nuclei and cytoplasms isolated from normal human diploid cells. *Exp Cell*

Res, 103, 321-30.

MURAKAMI, T., FUJIMOTO, M., OHTSUKI, M. & NAKAGAWA, H. (2001) Expression profiling of cancer-related genes in human keratinocytes following non-lethal ultraviolet B irradiation. *J Dermatol Sci,* 27, 121-9.

NAG, A., BONDAR, T., SHIV, S. & RAYCHAUDHURI, P. (2001) The xeroderma pigmentosum group E gene product DDB2 is a specific target of cullin 4A in mammalian cells. *Mol Cell Biol,* 21, 6738-47.

NAKA, K., TACHIBANA, A., IKEDA, K. & MOTOYAMA, N. (2004) Stress-induced premature senescence in hTERT-expressing ataxia telangiectasia fibroblasts. *J Biol Chem,* 279, 2030-7.

NAKAJIMA, S., LAN, L., KANNO, S., TAKAO, M., YAMAMOTO, K., EKER, A. P. & YASUI, A. (2004) UV light-induced DNA damage and tolerance for the survival of nucleotide excision repair-deficient human cells. *J Biol Chem,* 279, 46674-7.

NAKAMURA, H., FUKAMI, H., HAYASHI, Y., KIYONO, T., NAKATSUGAWA, S., HAMAGUCHI, M. & ISHIZAKI, K. (2002) Establishment of immortal normal and ataxia telangiectasia fibroblast cell lines by introduction of the hTERT gene. *J Radiat Res (Tokyo),* 43, 167-74.

NAKAMURA, T., ONO, T., YOSHIMURA, K., ARAO, T., KONDO, S., ICHIHASHI, M., MATSUMOTO, A. & FUJIWARA, Y. (1991) Malignant schwannoma associated with xeroderma pigmentosum in a patient belonging to complementation group D. *J Am Acad Dermatol,* 25, 349-53.

NAKAMURA, T. M., MORIN, G. B., CHAPMAN, K. B., WEINRICH, S. L., ANDREWS, W. H., LINGNER, J., HARLEY, C. B. & CECH, T. R. (1997) Telomerase catalytic subunit homologs from fission yeast and human. *Science,* 277, 955-9.

NAKANE, H., TAKEUCHI, S., YUBA, S., SAIJO, M., NAKATSU, Y., MURAI, H., NAKATSURU, Y., ISHIKAWA, T., HIROTA, S., KITAMURA, Y. & ET AL. (1995) High incidence of ultraviolet-B-or chemical-carcinogen-induced skin tumours in mice lacking the xeroderma pigmentosum group A gene. *Nature,* 377, 165-8.

NAKANISHI, M., ADAMI, G. R., ROBETORYE, R. S., NODA, A., VENABLE, S. F., DIMITROV, D., PEREIRA-SMITH, O. M. & SMITH, J. R. (1995) Exit from G0 and entry into the cell cycle of cells expressing p21Sdi1 antisense RNA. *Proc Natl Acad Sci U S A,* 92, 4352-6.

NAKATSU, Y., ASAHINA, H., CITTERIO, E., RADEMAKERS, S., VERMEULEN, W., KAMIUCHI, S., YEO, J. P., KHAW, M. C., SAIJO, M., KODO, N., MATSUDA, T., HOEIJMAKERS, J. H. & TANAKA, K. (2000) XAB2, a novel tetratricopeptide repeat protein involved in transcription-coupled DNA repair and transcription. *J Biol Chem,* 275, 34931-7.

NAKAYAMA, J., TAHARA, H., TAHARA, E., SAITO, M., ITO, K., NAKAMURA, H., NAKANISHI, T., IDE, T. & ISHIKAWA, F. (1998) Telomerase activation by hTRT in human normal fibroblasts and hepatocellular carcinomas. *Nat Genet,* 18, 65-8.

NANCE, M. A. & BERRY, S. A. (1992) Cockayne syndrome: review of 140 cases. *Am J Med Genet,* 42, 68-84.

NARITA, M., NUNEZ, S., HEARD, E., LIN, A. W., HEARN, S. A., SPECTOR, D. L., HANNON, G. J. & LOWE, S. W. (2003) Rb-mediated heterochromatin formation and silencing of E2F target genes during cellular senescence. *Cell,* 113, 703-16.

NEER, E. J., SCHMIDT, C. J., NAMBUDRIPAD, R. & SMITH, T. F. (1994) The ancient regulatory-protein family of WD-repeat proteins. *Nature,* 371, 297-300.

NEWMAN, J. C., BAILEY, A. D. & WEINER, A. M. (2006) Cockayne syndrome group B protein (CSB) plays a general role in chromatin maintenance and remodeling. *Proc Natl Acad Sci U S A,* 103, 9613-8.

NG, J. M., VERMEULEN, W., VAN DER HORST, G. T., BERGINK, S., SUGASAWA, K., VRIELING, H. & HOEIJMAKERS, J. H. (2003) A novel regulation mechanism of DNA repair by damage-induced and RAD23-dependent stabilization of xeroderma pigmentosum group C protein. *Genes Dev,* 17, 1630-45.

NIEDERNHOFER, L. J., ESSERS, J., WEEDA, G., BEVERLOO, B., DE WIT, J., MUIJTJENS, M., ODIJK, H., HOEIJMAKERS, J. H. & KANAAR, R. (2001) The structure-specific endonuclease Ercc1-Xpf is required for targeted gene replacement in embryonic stem cells. *Embo J,* 20, 6540-9.

NISHI, R., OKUDA, Y., WATANABE, E., MORI, T., IWAI, S., MASUTANI, C., SUGASAWA, K. & HANAOKA, F. (2005) Centrin 2 stimulates nucleotide excision repair by interacting with xeroderma pigmentosum group C protein. *Mol Cell Biol,* 25, 5664-74.

NITTA, M., SAIJO, M., KODO, N., MATSUDA, T., NAKATSU, Y., TAMAI, H. & TANAKA, K. (2000) A novel cytoplasmic GTPase XAB1 interacts with DNA repair protein XPA. *Nucleic Acids Res,* 28, 4212-8.

NOBLE, J. R., ZHONG, Z. H., NEUMANN, A. A., MELKI, J. R., CLARK, S. J. & REDDEL, R. R. (2004) Alterations in the p16(INK4a) and p53 tumor suppressor genes of hTERT-immortalized human fibroblasts. *Oncogene,* 23, 3116-21.

NOUSPIKEL, T. & HANAWALT, P. C. (2002) DNA repair in terminally differentiated cells. *DNA Repair (Amst),* 1, 59-75.

O'DONOVAN, A., DAVIES, A. A., MOGGS, J. G., WEST, S. C. & WOOD, R. D. (1994) XPG

endonuclease makes the 3' incision in human DNA nucleotide excision repair. *Nature,* 371, 432-5.

O'DONOVAN, A. & WOOD, R. D. (1993) Identical defects in DNA repair in xeroderma pigmentosum group G and rodent ERCC group 5. *Nature,* 363, 185-8.

O'HARE, M. J., BOND, J., CLARKE, C., TAKEUCHI, Y., ATHERTON, A. J., BERRY, C., MOODY, J., SILVER, A. R., DAVIES, D. C., ALSOP, A. E., NEVILLE, A. M. & JAT, P. S. (2001) Conditional immortalization of freshly isolated human mammary fibroblasts and endothelial cells. *Proc Natl Acad Sci U S A,* 98, 646-51.

ODA, K., ARAKAWA, H., TANAKA, T., MATSUDA, K., TANIKAWA, C., MORI, T., NISHIMORI, H., TAMAI, K., TOKINO, T., NAKAMURA, Y. & TAYA, Y. (2000) p53AIP1, a potential mediator of p53-dependent apoptosis, and its regulation by Ser-46-phosphorylated p53. *Cell,* 102, 849-62.

OH, D. H. & YEH, K. (2005) Differentiating human keratinocytes are deficient in p53 but retain global nucleotide excision repair following ultraviolet radiation. *DNA Repair (Amst),* 4, 1149-59.

OHTA, M., NITTA, M. & YAMAIZUMI, M. (1999) High sensitivity of the ultraviolet-induced p53 response in ultraviolet-sensitive syndrome, a photosensitive disorder with a putative defect in deoxyribonucleic acid repair of actively transcribed genes. *Mutat Res,* 433, 23-32.

OKUDA, Y., NISHI, R., NG, J. M., VERMEULEN, W., VAN DER HORST, G. T., MORI, T., HOEIJMAKERS, J. H., HANAOKA, F. & SUGASAWA, K. (2004) Relative levels of the two mammalian Rad23 homologs determine composition and stability of the xeroderma pigmentosum group C protein complex. *DNA Repair (Amst),* 3, 1285-95.

OLIVIER, M., EELES, R., HOLLSTEIN, M., KHAN, M. A., HARRIS, C. C. & HAINAUT, P. (2002) The IARC TP53 database: new online mutation analysis and recommendations to users. *Hum Mutat,* 19, 607-14.

OLOVNIKOV, A. M. (1971) [Principle of marginotomy in template synthesis of polynucleotides]. *Dokl Akad Nauk SSSR,* 201, 1496-9.

OLOVNIKOV, A. M. (1973) A theory of marginotomy. The incomplete copying of template margin in enzymic synthesis of polynucleotides and biological significance of the phenomenon. *J Theor Biol,* 41, 181-90.

OLSEN, J. H., HAHNEMANN, J. M., BORRESEN-DALE, A. L., BRONDUM-NIELSEN, K., HAMMARSTROM, L., KLEINERMAN, R., KAARIAINEN, H., LONNQVIST, T., SANKILA, R., SEERSHOLM, N., TRETLI, S., YUEN, J., BOICE, J. D., JR. & TUCKER, M. (2001) Cancer in patients with ataxia-telangiectasia and in their relatives in the nordic countries. *J Natl Cancer*

Inst, 93, 121-7.

ORREN, D. K., DIANOV, G. L. & BOHR, V. A. (1996) The human CSB (ERCC6) gene corrects the transcription-coupled repair defect in the CHO cell mutant UV61. *Nucleic Acids Res,* 24, 3317-22.

ORTOLAN, T. G., CHEN, L., TONGAONKAR, P. & MADURA, K. (2004) Rad23 stabilizes Rad4 from degradation by the Ub/proteasome pathway. *Nucleic Acids Res,* 32, 6490-500.

OTRIN, V. R., MCLENIGAN, M., TAKAO, M., LEVINE, A. S. & PROTIC, M. (1997) Translocation of a UV-damaged DNA binding protein into a tight association with chromatin after treatment of mammalian cells with UV light. *J Cell Sci,* 110 (Pt 10), 1159-68.

OTTO, A. I., RIOU, L., MARIONNET, C., MORI, T., SARASIN, A. & MAGNALDO, T. (1999) Differential behaviors toward ultraviolet A and B radiation of fibroblasts and keratinocytes from normal and DNA-repair-deficient patients. *Cancer Res,* 59, 1212-8.

OUELLETTE, M. M., MCDANIEL, L. D., WRIGHT, W. E., SHAY, J. W. & SCHULTZ, R. A. (2000) The establishment of telomerase-immortalized cell lines representing human chromosome instability syndromes. *Hum Mol Genet,* 9, 403-11.

PADDISON, P. J. & HANNON, G. J. (2002) RNA interference: the new somatic cell genetics? *Cancer Cell,* 2, 17-23.

PAINTER, R. B., CLARKSON, J. M. & YOUNG, B. R. (1973) Letter: Ultraviolet-induced repair replication in aging diploid human cells (WI-38). *Radiat Res,* 56, 560-4.

PAN, Z. Q., REARDON, J. T., LI, L., FLORES-ROZAS, H., LEGERSKI, R., SANCAR, A. & HURWITZ, J. (1995) Inhibition of nucleotide excision repair by the cyclin-dependent kinase inhibitor p21. *J Biol Chem,* 270, 22008-16.

PARK, C. H., MU, D., REARDON, J. T. & SANCAR, A. (1995) The general transcription-repair factor TFIIH is recruited to the excision repair complex by the XPA protein independent of the TFIIE transcription factor. *J Biol Chem,* 270, 4896-902.

PARK, C. H. & SANCAR, A. (1994) Formation of a ternary complex by human XPA, ERCC1, and ERCC4(XPF) excision repair proteins. *Proc Natl Acad Sci U S A,* 91, 5017-21.

PARK, M. T. & LEE, S. J. (2003) Cell cycle and cancer. *J Biochem Mol Biol,* 36, 60-5.

PARK, W. Y., HWANG, C. I., KANG, M. J., SEO, J. Y., CHUNG, J. H., KIM, Y. S., LEE, J. H., KIM, H., KIM, K. A., YOO, H. J. & SEO, J. S. (2001) Gene profile of replicative senescence is different from progeria or elderly donor. *Biochem Biophys Res Commun,* 282, 934-9.

PARRINELLO, S., SAMPER, E., KRTOLICA, A., GOLDSTEIN, J., MELOV, S. & CAMPISI, J. (2003) Oxygen sensitivity severely limits the replicative lifespan of murine fibroblasts. *Nat Cell Biol,* 5, 741-7.

PEHRSON, J. R. (1995) Probing the conformation of nucleosome linker DNA in situ with pyrimidine dimer formation. *J Biol Chem,* 270, 22440-4.

PENA, S. D. & SHOKEIR, M. H. (1974) Autosomal recessive cerebro-oculo-facio-skeletal (COFS) syndrome. *Clin Genet,* 5, 285-93.

PETIT, C. & SANCAR, A. (1999) Nucleotide excision repair: from E. coli to man. *Biochimie,* 81, 15-25.

PFEIFER, G. P. (1997) Formation and processing of UV photoproducts: effects of DNA sequence and chromatin environment. *Photochem Photobiol,* 65, 270-83.

PFEIFER, G. P., YOU, Y. H. & BESARATINIA, A. (2005) Mutations induced by ultraviolet light. *Mutat Res,* 571, 19-31.

PHAM, C. G., BUBICI, C., ZAZZERONI, F., PAPA, S., JONES, J., ALVAREZ, K., JAYAWARDENA, S., DE SMAELE, E., CONG, R., BEAUMONT, C., TORTI, F. M., TORTI, S. V. & FRANZOSO, G. (2004) Ferritin heavy chain upregulation by NF-kappaB inhibits TNFalpha-induced apoptosis by suppressing reactive oxygen species. *Cell,* 119, 529-42.

PIPAS, J. M. & LEVINE, A. J. (2001) Role of T antigen interactions with p53 in tumorigenesis. *Semin Cancer Biol,* 11, 23-30.

PIRZIO, L. M., FREULET-MARRIERE, M. A., BAI, Y., FOULADI, B., MURNANE, J. P., SABATIER, L. & DESMAZE, C. (2004) Human fibroblasts expressing hTERT show remarkable karyotype stability even after exposure to ionizing radiation. *Cytogenet Genome Res,* 104, 87-94.

PISARCHIK, A., WORTSMAN, J. & SLOMINSKI, A. (2004) A novel microarray to evaluate stress-related genes in skin: effect of ultraviolet light radiation. *Gene,* 341, 199-207.

PODDA, M., TRABER, M. G., WEBER, C., YAN, L. J. & PACKER, L. (1998) UV-irradiation depletes antioxidants and causes oxidative damage in a model of human skin. *Free Radic Biol Med,* 24, 55-65.

POLAGER, S., KALMA, Y., BERKOVICH, E. & GINSBERG, D. (2002) E2Fs up-regulate expression of genes involved in DNA replication, DNA repair and mitosis. *Oncogene,* 21, 437-46.

POLLOCK, P. M., PEARSON, J. V. & HAYWARD, N. K. (1996) Compilation of somatic mutations of the CDKN2 gene in human cancers: non-random distribution of base substitutions. *Genes Chromosomes Cancer,* 15, 77-88.

POON, R. Y., JIANG, W., TOYOSHIMA, H. & HUNTER, T. (1996) Cyclin-dependent kinases are inactivated by a combination of p21 and Thr-14/Tyr-15 phosphorylation after UV-induced DNA damage. *J Biol Chem,* 271, 13283-91.

PORTER, P. C., CLARK, D. R., MCDANIEL, L. D., MCGREGOR, W. G. & STATES, J. C. (2006) Telomerase-immortalized human fibroblasts retain UV-induced mutagenesis and p53-mediated DNA damage responses. *DNA Repair (Amst),* 5, 61-70.

PRICE, V. H., ODOM, R. B., WARD, W. H. & JONES, F. T. (1980) Trichothiodystrophy: sulfur-deficient brittle hair as a marker for a neuroectodermal symptom complex. *Arch Dermatol,* 116, 1375-84.

PRIVES, C. (1998) Signaling to p53: breaking the MDM2-p53 circuit. *Cell,* 95, 5-8.

PROIETTI DE SANTIS, L., GARCIA, C. L., BALAJEE, A. S., LATINI, P., PICHIERRI, P., NIKAIDO, O., STEFANINI, M. & PALITTI, F. (2002) Transcription coupled repair efficiency determines the cell cycle progression and apoptosis after UV exposure in hamster cells. *DNA Repair (Amst),* 1, 209-23.

PROIETTI-DE-SANTIS, L., DRANE, P. & EGLY, J. M. (2006) Cockayne syndrome B protein regulates the transcriptional program after UV irradiation. *Embo J,* 25, 1915-23.

QIN, X. F., AN, D. S., CHEN, I. S. & BALTIMORE, D. (2003) Inhibiting HIV-1 infection in human T cells by lentiviral-mediated delivery of small interfering RNA against CCR5. *Proc Natl Acad Sci U S A,* 100, 183-8.

QIN, X. Q., LIVINGSTON, D. M., KAELIN, W. G., JR. & ADAMS, P. D. (1994) Deregulated transcription factor E2F-1 expression leads to S-phase entry and p53-mediated apoptosis. *Proc Natl Acad Sci U S A,* 91, 10918-22.

QUEILLE, S., DROUGARD, C., SARASIN, A. & DAYA-GROSJEAN, L. (2001) Effects of XPD mutations on ultraviolet-induced apoptosis in relation to skin cancer-proneness in repair-deficient syndromes. *J Invest Dermatol,* 117, 1162-70.

RADEMAKERS, S., VOLKER, M., HOOGSTRATEN, D., NIGG, A. L., MONE, M. J., VAN ZEELAND, A. A., HOEIJMAKERS, J. H., HOUTSMULLER, A. B. & VERMEULEN, W. (2003) Xeroderma pigmentosum group A protein loads as a separate factor onto DNA lesions. *Mol Cell Biol,* 23, 5755-67.

RAMANATHAN, B. & SMERDON, M. J. (1986) Changes in nuclear protein acetylation in u.v.-damaged human cells. *Carcinogenesis,* 7, 1087-94.

RAMANATHAN, B. & SMERDON, M. J. (1989) Enhanced DNA repair synthesis in hyperacetylated nucleosomes. *J Biol Chem,* 264, 11026-34.

RAMIREZ, R. D., MORALES, C. P., HERBERT, B. S., ROHDE, J. M., PASSONS, C., SHAY, J. W. & WRIGHT, W. E. (2001) Putative telomere-independent mechanisms of replicative aging reflect inadequate growth conditions. *Genes Dev,* 15, 398-403.

RAMSEY, K. L., SMITH, J. J., DASGUPTA, A., MAQANI, N., GRANT, P. & AUBLE, D. T. (2004) The NEF4 complex regulates Rad4 levels and utilizes Snf2/Swi2-related ATPase activity for nucleotide excision repair. *Mol Cell Biol,* 24, 6362-78.

RANGANATHAN, V., HEINE, W. F., CICCONE, D. N., RUDOLPH, K. L., WU, X., CHANG, S., HAI, H., AHEARN, I. M., LIVINGSTON, D. M., RESNICK, I., ROSEN, F., SEEMANOVA, E., JAROLIM, P., DEPINHO, R. A. & WEAVER, D. T. (2001) Rescue of a telomere length defect of Nijmegen breakage syndrome cells requires NBS and telomerase catalytic subunit. *Curr Biol,* 11, 962-6.

RANISH, J. A., HAHN, S., LU, Y., YI, E. C., LI, X. J., ENG, J. & AEBERSOLD, R. (2004) Identification of TFB5, a new component of general transcription and DNA repair factor IIH. *Nat Genet,* 36, 707-13.

RAPIC OTRIN, V., KURAOKA, I., NARDO, T., MCLENIGAN, M., EKER, A. P., STEFANINI, M., LEVINE, A. S. & WOOD, R. D. (1998) Relationship of the xeroderma pigmentosum group E DNA repair defect to the chromatin and DNA binding proteins UV-DDB and replication protein A. *Mol Cell Biol,* 18, 3182-90.

RAPIC-OTRIN, V., MCLENIGAN, M. P., BISI, D. C., GONZALEZ, M. & LEVINE, A. S. (2002) Sequential binding of UV DNA damage binding factor and degradation of the p48 subunit as early events after UV irradiation. *Nucleic Acids Res,* 30, 2588-98.

RAPIN, I., LINDENBAUM, Y., DICKSON, D. W., KRAEMER, K. H. & ROBBINS, J. H. (2000) Cockayne syndrome and xeroderma pigmentosum. *Neurology,* 55, 1442-9.

RAVANAT, J. L., DOUKI, T. & CADET, J. (2001) Direct and indirect effects of UV radiation on DNA and its components. *J Photochem Photobiol B,* 63, 88-102.

REARDON, J. T., BESSHO, T., KUNG, H. C., BOLTON, P. H. & SANCAR, A. (1997) In vitro repair of oxidative DNA damage by human nucleotide excision repair system: possible explanation for neurodegeneration in xeroderma pigmentosum patients. *Proc Natl Acad Sci U S A,* 94, 9463-8.

REARDON, J. T., MU, D. & SANCAR, A. (1996) Overproduction, purification, and characterization of the XPC subunit of the human DNA repair excision nuclease. *J Biol Chem,* 271, 19451-6.

REARDON, J. T., NICHOLS, A. F., KEENEY, S., SMITH, C. A., TAYLOR, J. S., LINN, S. & SANCAR, A. (1993a) Comparative analysis of binding of human damaged DNA-binding protein (XPE) and Escherichia coli damage recognition protein (UvrA) to the major ultraviolet

photoproducts: T[c,s]T, T[t,s]T, T[6-4]T, and T[Dewar]T. *J Biol Chem,* 268, 21301-8.

REARDON, J. T. & SANCAR, A. (2003) Recognition and repair of the cyclobutane thymine dimer, a major cause of skin cancers, by the human excision nuclease. *Genes Dev,* 17, 2539-51.

REARDON, J. T., THOMPSON, L. H. & SANCAR, A. (1993b) Excision repair in man and the molecular basis of xeroderma pigmentosum syndrome. *Cold Spring Harb Symp Quant Biol,* 58, 605-17.

REDDEL, R. R. (2000) The role of senescence and immortalization in carcinogenesis. *Carcinogenesis,* 21, 477-84.

REED, S. H. (2005) Nucleotide excision repair in chromatin: the shape of things to come. *DNA Repair (Amst),* 4, 909-18.

REN, B., ROBERT, F., WYRICK, J. J., APARICIO, O., JENNINGS, E. G., SIMON, I., ZEITLINGER, J., SCHREIBER, J., HANNETT, N., KANIN, E., VOLKERT, T. L., WILSON, C. J., BELL, S. P. & YOUNG, R. A. (2000) Genome-wide location and function of DNA binding proteins. *Science,* 290, 2306-9.

REN, Y., SAIJO, M., NAKATSU, Y., NAKAI, H., YAMAIZUMI, M. & TANAKA, K. (2003) Three novel mutations responsible for Cockayne syndrome group A. *Genes Genet Syst,* 78, 93-102.

REYNOLDS, M., PETERSON, E., QUIEVRYN, G. & ZHITKOVICH, A. (2004) Human nucleotide excision repair efficiently removes chromium-DNA phosphate adducts and protects cells against chromate toxicity. *J Biol Chem,* 279, 30419-24.

RHEINWALD, J. G. & GREEN, H. (1975) Serial cultivation of strains of human epidermal keratinocytes: the formation of keratinizing colonies from single cells. *Cell,* 6, 331-43.

RIDLEY, A. J., COLLEY, J., WYNFORD-THOMAS, D. & JONES, C. J. (2005) Characterisation of novel mutations in Cockayne syndrome type A and xeroderma pigmentosum group C subjects. *J Hum Genet,* 50, 151-4.

RIEBER, M. & STRASBERG RIEBER, M. (2000) Apoptosis-inducing levels of UV radiation and proteasome inhibitors produce opposite effects on p21(WAF1) in human melanoma cells. *Int J Cancer,* 86, 462-7.

RIEDL, T., HANAOKA, F. & EGLY, J. M. (2003) The comings and goings of nucleotide excision repair factors on damaged DNA. *Embo J,* 22, 5293-303.

RIEGER, K. E. & CHU, G. (2004) Portrait of transcriptional responses to ultraviolet and ionizing radiation in human cells. *Nucleic Acids Res,* 32, 4786-803.

RIVA, F., ZUCO, V., VINK, A. A., SUPINO, R. & PROSPERI, E. (2001) UV-induced DNA incision and

proliferating cell nuclear antigen recruitment to repair sites occur independently of p53-replication protein A interaction in p53 wild type and mutant ovarian carcinoma cells. *Carcinogenesis,* 22, 1971-8.

ROCKX, D. A., MASON, R., VAN HOFFEN, A., BARTON, M. C., CITTERIO, E., BREGMAN, D. B., VAN ZEELAND, A. A., VRIELING, H. & MULLENDERS, L. H. (2000) UV-induced inhibition of transcription involves repression of transcription initiation and phosphorylation of RNA polymerase II. *Proc Natl Acad Sci U S A,* 97, 10503-8.

RODRIGUEZ, M. S., DESTERRO, J. M., LAIN, S., LANE, D. P. & HAY, R. T. (2000) Multiple C-terminal lysine residues target p53 for ubiquitin-proteasome-mediated degradation. *Mol Cell Biol,* 20, 8458-67.

ROGAKOU, E. P., BOON, C., REDON, C. & BONNER, W. M. (1999) Megabase chromatin domains involved in DNA double-strand breaks in vivo. *J Cell Biol,* 146, 905-16.

RONEN, A. & GLICKMAN, B. W. (2001) Human DNA repair genes. *Environ Mol Mutagen,* 37, 241-83.

ROSENQUIST, T. A., ZAIKA, E., FERNANDES, A. S., ZHARKOV, D. O., MILLER, H. & GROLLMAN, A. P. (2003) The novel DNA glycosylase, NEIL1, protects mammalian cells from radiation-mediated cell death. *DNA Repair (Amst),* 2, 581-91.

ROSENSTEIN, B. S. & MITCHELL, D. L. (1987) Action spectra for the induction of pyrimidine(6-4)pyrimidone photoproducts and cyclobutane pyrimidine dimers in normal human skin fibroblasts. *Photochem Photobiol,* 45, 775-80.

ROTMAN, G. & SHILOH, Y. (1998) ATM: from gene to function. *Hum Mol Genet,* 7, 1555-63.

RUBBI, C. P. & MILNER, J. (2003) p53 is a chromatin accessibility factor for nucleotide excision repair of DNA damage. *Embo J,* 22, 975-86.

RUBINSON, D. A., DILLON, C. P., KWIATKOWSKI, A. V., SIEVERS, C., YANG, L., KOPINJA, J., ROONEY, D. L., IHRIG, M. M., MCMANUS, M. T., GERTLER, F. B., SCOTT, M. L. & VAN PARIJS, L. (2003) A lentivirus-based system to functionally silence genes in primary mammalian cells, stem cells and transgenic mice by RNA interference. *Nat Genet,* 33, 401-6.

RUSSELL, S. J., REED, S. H., HUANG, W., FRIEDBERG, E. C. & JOHNSTON, S. A. (1999) The 19S regulatory complex of the proteasome functions independently of proteolysis in nucleotide excision repair. *Mol Cell,* 3, 687-95.

SAKAMURO, D., SABBATINI, P., WHITE, E. & PRENDERGAST, G. C. (1997) The polyproline region of p53 is required to activate apoptosis but not growth arrest. *Oncogene,* 15, 887-98.

SAMEC, S., JONES, T. A., CORLET, J., SCHERLY, D., SHEER, D., WOOD, R. D. & CLARKSON, S.

G. (1994) The human gene for xeroderma pigmentosum complementation group G (XPG) maps to 13q33 by fluorescence in situ hybridization. *Genomics,* 21, 283-5.

SANCAR, A. (1996) DNA excision repair. *Annu Rev Biochem,* 65, 43-81.

SATO, M., NISHIGORI, C., YAGI, T. & TAKEBE, H. (1996) Aberrant splicing and truncated-protein expression due to a newly identified XPA gene mutation. *Mutat Res,* 362, 199-208.

SAXOWSKY, T. T. & DOETSCH, P. W. (2006) RNA polymerase encounters with DNA damage: transcription-coupled repair or transcriptional mutagenesis? *Chem Rev,* 106, 474-88.

SCHAEFFER, L., MONCOLLIN, V., ROY, R., STAUB, A., MEZZINA, M., SARASIN, A., WEEDA, G., HOEIJMAKERS, J. H. & EGLY, J. M. (1994) The ERCC2/DNA repair protein is associated with the class II BTF2/TFIIH transcription factor. *Embo J,* 13, 2388-92.

SCHAEFFER, L., ROY, R., HUMBERT, S., MONCOLLIN, V., VERMEULEN, W., HOEIJMAKERS, J. H., CHAMBON, P. & EGLY, J. M. (1993) DNA repair helicase: a component of BTF2 (TFIIH) basic transcription factor. *Science,* 260, 58-63.

SCHENA, M., SHALON, D., DAVIS, R. W. & BROWN, P. O. (1995) Quantitative monitoring of gene expression patterns with a complementary DNA microarray. *Science,* 270, 467-70.

SCHERLY, D., NOUSPIKEL, T., CORLET, J., UCLA, C., BAIROCH, A. & CLARKSON, S. G. (1993) Complementation of the DNA repair defect in xeroderma pigmentosum group G cells by a human cDNA related to yeast RAD2. *Nature,* 363, 182-5.

SCHMITT, C. A., FRIDMAN, J. S., YANG, M., LEE, S., BARANOV, E., HOFFMAN, R. M. & LOWE, S. W. (2002) A senescence program controlled by p53 and p16INK4a contributes to the outcome of cancer therapy. *Cell,* 109, 335-46.

SCHOENFELD, A. R., PARRIS, T., EISENBERGER, A., DAVIDOWITZ, E. J., DE LEON, M., TALASAZAN, F., DEVARAJAN, P. & BURK, R. D. (2000) The von Hippel-Lindau tumor suppressor gene protects cells from UV-mediated apoptosis. *Oncogene,* 19, 5851-7.

SCHULTZ, P., FRIBOURG, S., POTERSZMAN, A., MALLOUH, V., MORAS, D. & EGLY, J. M. (2000) Molecular structure of human TFIIH. *Cell,* 102, 599-607.

SCHWEIZER, U., HEY, T., LIPPS, G. & KRAUSS, G. (1999) Photocrosslinking locates a binding site for the large subunit of human replication protein A to the damaged strand of cisplatin-modified DNA. *Nucleic Acids Res,* 27, 3183-9.

SEDELNIKOVA, O. A., HORIKAWA, I., ZIMONJIC, D. B., POPESCU, N. C., BONNER, W. M. & BARRETT, J. C. (2004) Senescing human cells and ageing mice accumulate DNA lesions with unrepairable double-strand breaks. *Nat Cell Biol,* 6, 168-70.

SEGAWA, K., MINOWA, A., SUGASAWA, K., TAKANO, T. & HANAOKA, F. (1993) Abrogation of p53-mediated transactivation by SV40 large T antigen. *Oncogene,* 8, 543-8.

SELBY, C. P. & SANCAR, A. (1993) Molecular mechanism of transcription-repair coupling. *Science,* 260, 53-8.

SELBY, C. P. & SANCAR, A. (1997a) Cockayne syndrome group B protein enhances elongation by RNA polymerase II. *Proc Natl Acad Sci U S A,* 94, 11205-9.

SELBY, C. P. & SANCAR, A. (1997b) Human transcription-repair coupling factor CSB/ERCC6 is a DNA-stimulated ATPase but is not a helicase and does not disrupt the ternary transcription complex of stalled RNA polymerase II. *J Biol Chem,* 272, 1885-90.

SELZER, R. R., NYAGA, S., TUO, J., MAY, A., MUFTUOGLU, M., CHRISTIANSEN, M., CITTERIO, E., BROSH, R. M., JR. & BOHR, V. A. (2002) Differential requirement for the ATPase domain of the Cockayne syndrome group B gene in the processing of UV-induced DNA damage and 8-oxoguanine lesions in human cells. *Nucleic Acids Res,* 30, 782-93.

SEMIZAROV, D., KROEGER, P. & FESIK, S. (2004) siRNA-mediated gene silencing: a global genome view. *Nucleic Acids Res,* 32, 3836-45.

SEN, G. C. (2001) Viruses and interferons. *Annu Rev Microbiol,* 55, 255-81.

SEO, Y. R. & JUNG, H. J. (2004) The potential roles of p53 tumor suppressor in nucleotide excision repair (NER) and base excision repair (BER). *Exp Mol Med,* 36, 505-9.

SERRANO, M., LIN, A. W., MCCURRACH, M. E., BEACH, D. & LOWE, S. W. (1997) Oncogenic ras provokes premature cell senescence associated with accumulation of p53 and p16INK4a. *Cell,* 88, 593-602.

SESHADRI, T. & CAMPISI, J. (1990) Repression of c-fos transcription and an altered genetic program in senescent human fibroblasts. *Science,* 247, 205-9.

SESTO, A., NAVARRO, M., BURSLEM, F. & JORCANO, J. L. (2002) Analysis of the ultraviolet B response in primary human keratinocytes using oligonucleotide microarrays. *Proc Natl Acad Sci U S A,* 99, 2965-70.

SETLOW, R. B. (2001) Human cancer: etiologic agents/dose responses/DNA repair/cellular and animal models. *Mutat Res,* 477, 1-6.

SETLOW, R. B. & CARRIER, W. L. (1964) The Disappearance Of Thymine Dimers From Dna: An Error-Correcting Mechanism. *Proc Natl Acad Sci U S A,* 51, 226-31.

SETLOW, R. B., REGAN, J. D., GERMAN, J. & CARRIER, W. L. (1969) Evidence that xeroderma

pigmentosum cells do not perform the first step in the repair of ultraviolet damage to their DNA. *Proc Natl Acad Sci U S A,* 64, 1035-41.

SETO, E., USHEVA, A., ZAMBETTI, G. P., MOMAND, J., HORIKOSHI, N., WEINMANN, R., LEVINE, A. J. & SHENK, T. (1992) Wild-type p53 binds to the TATA-binding protein and represses transcription. *Proc Natl Acad Sci U S A,* 89, 12028-32.

SEVERINO, J., ALLEN, R. G., BALIN, S., BALIN, A. & CRISTOFALO, V. J. (2000) Is beta-galactosidase staining a marker of senescence in vitro and in vivo? *Exp Cell Res,* 257, 162-71.

SHAN, B. & LEE, W. H. (1994) Deregulated expression of E2F-1 induces S-phase entry and leads to apoptosis. *Mol Cell Biol,* 14, 8166-73.

SHARMA, G. G., GUPTA, A., WANG, H., SCHERTHAN, H., DHAR, S., GANDHI, V., ILIAKIS, G., SHAY, J. W., YOUNG, C. S. & PANDITA, T. K. (2003) hTERT associates with human telomeres and enhances genomic stability and DNA repair. *Oncogene,* 22, 131-46.

SHAY, J. W., PEREIRA-SMITH, O. M. & WRIGHT, W. E. (1991) A role for both RB and p53 in the regulation of human cellular senescence. *Exp Cell Res,* 196, 33-9.

SHAY, J. W. & WRIGHT, W. E. (2000) Hayflick, his limit, and cellular ageing. *Nat Rev Mol Cell Biol,* 1, 72-6.

SHAY, J. W. & WRIGHT, W. E. (2005) Senescence and immortalization: role of telomeres and telomerase. *Carcinogenesis,* 26, 867-74.

SHEIKH, M. S., CHEN, Y. Q., SMITH, M. L. & FORNACE, A. J., JR. (1997) Role of p21Waf1/Cip1/Sdi1 in cell death and DNA repair as studied using a tetracycline-inducible system in p53-deficient cells. *Oncogene,* 14, 1875-82.

SHELTON, D. N., CHANG, E., WHITTIER, P. S., CHOI, D. & FUNK, W. D. (1999) Microarray analysis of replicative senescence. *Curr Biol,* 9, 939-45.

SHEN, H., STURGIS, E. M., KHAN, S. G., QIAO, Y., SHAHLAVI, T., EICHER, S. A., XU, Y., WANG, X., STROM, S. S., SPITZ, M. R., KRAEMER, K. H. & WEI, Q. (2001) An intronic poly (AT) polymorphism of the DNA repair gene XPC and risk of squamous cell carcinoma of the head and neck: a case-control study. *Cancer Res,* 61, 3321-5.

SHERR, C. J. (1996) Cancer cell cycles. *Science,* 274, 1672-7.

SHERR, C. J. & ROBERTS, J. M. (1995) Inhibitors of mammalian G1 cyclin-dependent kinases. *Genes Dev,* 9, 1149-63.

SHERR, C. J. & ROBERTS, J. M. (1999) CDK inhibitors: positive and negative regulators of G1-phase

progression. *Genes Dev,* 13, 1501-12.

SHERR, C. J. & WEBER, J. D. (2000) The ARF/p53 pathway. *Curr Opin Genet Dev,* 10, 94-9.

SHIEH, S. Y., IKEDA, M., TAYA, Y. & PRIVES, C. (1997) DNA damage-induced phosphorylation of p53 alleviates inhibition by MDM2. *Cell,* 91, 325-34.

SHIEH, S. Y., TAYA, Y. & PRIVES, C. (1999) DNA damage-inducible phosphorylation of p53 at N-terminal sites including a novel site, Ser20, requires tetramerization. *Embo J,* 18, 1815-23.

SHIN, K. H., KANG, M. K., DICTEROW, E., KAMETA, A., BALUDA, M. A. & PARK, N. H. (2004) Introduction of human telomerase reverse transcriptase to normal human fibroblasts enhances DNA repair capacity. *Clin Cancer Res,* 10, 2551-60.

SHIOMI, T., HARADA, Y., SAITO, T., SHIOMI, N., OKUNO, Y. & YAMAIZUMI, M. (1994) An ERCC5 gene with homology to yeast RAD2 is involved in group G xeroderma pigmentosum. *Mutat Res,* 314, 167-75.

SHIVJI, M. K., GREY, S. J., STRAUSFELD, U. P., WOOD, R. D. & BLOW, J. J. (1994) Cip1 inhibits DNA replication but not PCNA-dependent nucleotide excision-repair. *Curr Biol,* 4, 1062-8.

SHIVJI, M. K., PODUST, V. N., HUBSCHER, U. & WOOD, R. D. (1995) Nucleotide excision repair DNA synthesis by DNA polymerase epsilon in the presence of PCNA, RFC, and RPA. *Biochemistry,* 34, 5011-7.

SHIYANOV, P., NAG, A. & RAYCHAUDHURI, P. (1999) Cullin 4A associates with the UV-damaged DNA-binding protein DDB. *J Biol Chem,* 274, 35309-12.

SHORE, D. (1997) Telomerase and telomere-binding proteins: controlling the endgame. *Trends Biochem Sci,* 22, 233-5.

SIBGHATULLAH, HUSAIN, I., CARLTON, W. & SANCAR, A. (1989) Human nucleotide excision repair in vitro: repair of pyrimidine dimers, psoralen and cisplatin adducts by HeLa cell-free extract. *Nucleic Acids Res,* 17, 4471-84.

SIJBERS, A. M., DE LAAT, W. L., ARIZA, R. R., BIGGERSTAFF, M., WEI, Y. F., MOGGS, J. G., CARTER, K. C., SHELL, B. K., EVANS, E., DE JONG, M. C., RADEMAKERS, S., DE ROOIJ, J., JASPERS, N. G., HOEIJMAKERS, J. H. & WOOD, R. D. (1996) Xeroderma pigmentosum group F caused by a defect in a structure-specific DNA repair endonuclease. *Cell,* 86, 811-22.

SLEDZ, C. A., HOLKO, M., DE VEER, M. J., SILVERMAN, R. H. & WILLIAMS, B. R. (2003) Activation of the interferon system by short-interfering RNAs. *Nat Cell Biol,* 5, 834-9.

SLOMINSKI, A. & PAWELEK, J. (1998) Animals under the sun: effects of ultraviolet radiation on mammalian skin. *Clin Dermatol,* 16, 503-15.

SLOMINSKI, A. & WORTSMAN, J. (2000) Neuroendocrinology of the skin. *Endocr Rev,* 21, 457-87.

SLOR, H., BATKO, S., KHAN, S. G., SOBE, T., EMMERT, S., KHADAVI, A., FRUMKIN, A., BUSCH, D. B., ALBERT, R. B. & KRAEMER, K. H. (2000) Clinical, cellular, and molecular features of an Israeli xeroderma pigmentosum family with a frameshift mutation in the XPC gene: sun protection prolongs life. *J Invest Dermatol,* 115, 974-80.

SMERDON, M. J. (1991) DNA repair and the role of chromatin structure. *Curr Opin Cell Biol,* 3, 422-8.

SMERDON, M. J. & CONCONI, A. (1999) Modulation of DNA damage and DNA repair in chromatin. *Prog Nucleic Acid Res Mol Biol,* 62, 227-55.

SMERDON, M. J., LAN, S. Y., CALZA, R. E. & REEVES, R. (1982) Sodium butyrate stimulates DNA repair in UV-irradiated normal and xeroderma pigmentosum human fibroblasts. *J Biol Chem,* 257, 13441-7.

SMERDON, M. J. & LIEBERMAN, M. W. (1978) Nucleosome rearrangement in human chromatin during UV-induced DNA- reapir synthesis. *Proc Natl Acad Sci U S A,* 75, 4238-41.

SMITH, C. A., BAETEN, J. & TAYLOR, J. S. (1998) The ability of a variety of polymerases to synthesize past site-specific cis-syn, trans-syn-II, (6-4), and Dewar photoproducts of thymidylyl-(3'-->5')-thymidine. *J Biol Chem,* 273, 21933-40.

SMITH, J. R., VENABLE, S., ROBERTS, T. W., METTER, E. J., MONTICONE, R. & SCHNEIDER, E. L. (2002) Relationship between in vivo age and in vitro aging: assessment of 669 cell cultures derived from members of the Baltimore Longitudinal Study of Aging. *J Gerontol A Biol Sci Med Sci,* 57, B239-46.

SMITH, M. L., CHEN, I. T., ZHAN, Q., BAE, I., CHEN, C. Y., GILMER, T. M., KASTAN, M. B., O'CONNOR, P. M. & FORNACE, A. J., JR. (1994) Interaction of the p53-regulated protein Gadd45 with proliferating cell nuclear antigen. *Science,* 266, 1376-80.

SMITH, M. L., CHEN, I. T., ZHAN, Q., O'CONNOR, P. M. & FORNACE, A. J., JR. (1995) Involvement of the p53 tumor suppressor in repair of u.v.-type DNA damage. *Oncogene,* 10, 1053-9.

SMITH, M. L., FORD, J. M., HOLLANDER, M. C., BORTNICK, R. A., AMUNDSON, S. A., SEO, Y. R., DENG, C. X., HANAWALT, P. C. & FORNACE, A. J., JR. (2000) p53-mediated DNA repair responses to UV radiation: studies of mouse cells lacking p53, p21, and/or gadd45 genes. *Mol Cell Biol,* 20, 3705-14.

SMITH, M. L. & FORNACE, A. J., JR. (1997) p53-mediated protective responses to UV irradiation. *Proc*

Natl Acad Sci U S A, 94, 12255-7.

SMITH, T. F., GAITATZES, C., SAXENA, K. & NEER, E. J. (1999) The WD repeat: a common architecture for diverse functions. *Trends Biochem Sci,* 24, 181-5.

SOUSSI, T., CARON DE FROMENTEL, C. & MAY, P. (1990) Structural aspects of the p53 protein in relation to gene evolution. *Oncogene,* 5, 945-52.

SOUSSI, T., CARON DE FROMENTEL, C., MECHALI, M., MAY, P. & KRESS, M. (1987) Cloning and characterization of a cDNA from Xenopus laevis coding for a protein homologous to human and murine p53. *Oncogene,* 1, 71-8.

SOUSSI, T. & LOZANO, G. (2005) p53 mutation heterogeneity in cancer. *Biochem Biophys Res Commun,* 331, 834-42.

SOUTHERN, E. M. (1975) Detection of specific sequences among DNA fragments separated by gel electrophoresis. *J Mol Biol,* 98, 503-17.

SPIVAK, G. (2004) The many faces of Cockayne syndrome. *Proc Natl Acad Sci U S A,* 101, 15273-4.

SPIVAK, G. (2005) UV-sensitive syndrome. *Mutat Res,* 577, 162-9.

SPIVAK, G. & HANAWALT, P. C. (2006) Host cell reactivation of plasmids containing oxidative DNA lesions is defective in Cockayne syndrome but normal in UV-sensitive syndrome fibroblasts. *DNA Repair (Amst),* 5, 13-22.

SPIVAK, G., ITOH, T., MATSUNAGA, T., NIKAIDO, O., HANAWALT, P. & YAMAIZUMI, M. (2002) Ultraviolet-sensitive syndrome cells are defective in transcription-coupled repair of cyclobutane pyrimidine dimers. *DNA Repair (Amst),* 1, 629-43.

STARK, G. R., KERR, I. M., WILLIAMS, B. R., SILVERMAN, R. H. & SCHREIBER, R. D. (1998) How cells respond to interferons. *Annu Rev Biochem,* 67, 227-64.

STARY, A. & SARASIN, A. (2002) The genetics of the hereditary xeroderma pigmentosum syndrome. *Biochimie,* 84, 49-60.

STATES, J. C., MCDUFFIE, E. R., MYRAND, S. P., MCDOWELL, M. & CLEAVER, J. E. (1998) Distribution of mutations in the human xeroderma pigmentosum group A gene and their relationships to the functional regions of the DNA damage recognition protein. *Hum Mutat,* 12, 103-13.

STEFANINI, M., FAWCETT, H., BOTTA, E., NARDO, T. & LEHMANN, A. R. (1996) Genetic analysis of twenty-two patients with Cockayne syndrome. *Hum Genet,* 97, 418-23.

STEFANINI, M., GILIANI, S., NARDO, T., MARINONI, S., NAZZARO, V., RIZZO, R. &

TREVISAN, G. (1992) DNA repair investigations in nine Italian patients affected by trichothiodystrophy. *Mutat Res,* 273, 119-25.

STEFANINI, M., LAGOMARSINI, P., ARLETT, C. F., MARINONI, S., BORRONE, C., CROVATO, F., TREVISAN, G., CORDONE, G. & NUZZO, F. (1986) Xeroderma pigmentosum (complementation group D) mutation is present in patients affected by trichothiodystrophy with photosensitivity. *Hum Genet,* 74, 107-12.

STEINERT, S., SHAY, J. W. & WRIGHT, W. E. (2000) Transient expression of human telomerase extends the life span of normal human fibroblasts. *Biochem Biophys Res Commun,* 273, 1095-8.

STEWART, S. A., BEN-PORATH, I., CAREY, V. J., O'CONNOR, B. F., HAHN, W. C. & WEINBERG, R. A. (2003a) Erosion of the telomeric single-strand overhang at replicative senescence. *Nat Genet,* 33, 492-6.

STEWART, S. A., DYKXHOORN, D. M., PALLISER, D., MIZUNO, H., YU, E. Y., AN, D. S., SABATINI, D. M., CHEN, I. S., HAHN, W. C., SHARP, P. A., WEINBERG, R. A. & NOVINA, C. D. (2003b) Lentivirus-delivered stable gene silencing by RNAi in primary cells. *Rna,* 9, 493-501.

STIVALA, L. A., RIVA, F., CAZZALINI, O., SAVIO, M. & PROSPERI, E. (2001) p21(waf1/cip1)-null human fibroblasts are deficient in nucleotide excision repair downstream the recruitment of PCNA to DNA repair sites. *Oncogene,* 20, 563-70.

STUCKI, M., CLAPPERTON, J. A., MOHAMMAD, D., YAFFE, M. B., SMERDON, S. J. & JACKSON, S. P. (2005) MDC1 directly binds phosphorylated histone H2AX to regulate cellular responses to DNA double-strand breaks. *Cell,* 123, 1213-26.

SUBRAMANIAN, A., TAMAYO, P., MOOTHA, V.K., MUKHERJEE, S., EBERT., B.L., GILLETTE, M.A., PAULOVICH, A., POMEROY, S.L., GOLUB, T.R., LANDER, E.S. &MESIROV, J.P. (2005) Gene set enrichment analysis: A knowledge-based approach for interpreting genome-wide expression profiles. *Proc Natl Acad Sci U S A,* 102, 15545-50.

SUGASAWA, K., MASUTANI, C. & HANAOKA, F. (1993) Cell-free repair of UV-damaged simian virus 40 chromosomes in human cell extracts. I. Development of a cell-free system detecting excision repair of UV-irradiated SV40 chromosomes. *J Biol Chem,* 268, 9098-104.

SUGASAWA, K., MASUTANI, C., UCHIDA, A., MAEKAWA, T., VAN DER SPEK, P. J., BOOTSMA, D., HOEIJMAKERS, J. H. & HANAOKA, F. (1996) HHR23B, a human Rad23 homolog, stimulates XPC protein in nucleotide excision repair in vitro. *Mol Cell Biol,* 16, 4852-61.

SUGASAWA, K., NG, J. M., MASUTANI, C., IWAI, S., VAN DER SPEK, P. J., EKER, A. P.,

HANAOKA, F., BOOTSMA, D. & HOEIJMAKERS, J. H. (1998) Xeroderma pigmentosum group C protein complex is the initiator of global genome nucleotide excision repair. *Mol Cell,* 2, 223-32.

SUGASAWA, K., NG, J. M., MASUTANI, C., MAEKAWA, T., UCHIDA, A., VAN DER SPEK, P. J., EKER, A. P., RADEMAKERS, S., VISSER, C., ABOUSSEKHRA, A., WOOD, R. D., HANAOKA, F., BOOTSMA, D. & HOEIJMAKERS, J. H. (1997) Two human homologs of Rad23 are functionally interchangeable in complex formation and stimulation of XPC repair activity. *Mol Cell Biol,* 17, 6924-31.

SUGASAWA, K., OKAMOTO, T., SHIMIZU, Y., MASUTANI, C., IWAI, S. & HANAOKA, F. (2001) A multistep damage recognition mechanism for global genomic nucleotide excision repair. *Genes Dev,* 15, 507-21.

SUGASAWA, K., OKUDA, Y., SAIJO, M., NISHI, R., MATSUDA, N., CHU, G., MORI, T., IWAI, S., TANAKA, K. & HANAOKA, F. (2005) UV-induced ubiquitylation of XPC protein mediated by UV-DDB-ubiquitin ligase complex. *Cell,* 121, 387-400.

SUNG, P., BAILLY, V., WEBER, C., THOMPSON, L. H., PRAKASH, L. & PRAKASH, S. (1993) Human xeroderma pigmentosum group D gene encodes a DNA helicase. *Nature,* 365, 852-5.

SVEJSTRUP, J. Q. (2002) Mechanisms of transcription-coupled DNA repair. *Nat Rev Mol Cell Biol,* 3, 21-9.

SVEJSTRUP, J. Q. (2003) Rescue of arrested RNA polymerase II complexes. *J Cell Sci,* 116, 447-51.

SVEJSTRUP, J. Q., WANG, Z., FEAVER, W. J., WU, X., BUSHNELL, D. A., DONAHUE, T. F., FRIEDBERG, E. C. & KORNBERG, R. D. (1995) Different forms of TFIIH for transcription and DNA repair: holo-TFIIH and a nucleotide excision repairosome. *Cell,* 80, 21-8.

SVOBODA, P., STEIN, P., HAYASHI, H. & SCHULTZ, R. M. (2000) Selective reduction of dormant maternal mRNAs in mouse oocytes by RNA interference. *Development,* 127, 4147-56.

SWEDER, K. & MADURA, K. (2002) Regulation of repair by the 26S proteasome. *J Biomed Biotechnol,* 2, 94-105.

TAKAHASHI, E., SHIOMI, N. & SHIOMI, T. (1992) Precise localization of the excision repair gene, ERCC5, to human chromosome 13q32.3-q33.1 by direct R-banding fluorescence in situ hybridization. *Jpn J Cancer Res,* 83, 1117-9.

TAKAI, H., SMOGORZEWSKA, A. & DE LANGE, T. (2003) DNA damage foci at dysfunctional telomeres. *Curr Biol,* 13, 1549-56.

TAKAO, J., ARIIZUMI, K., DOUGHERTY, II & CRUZ, P. D., JR. (2002) Genomic scale analysis of the

human keratinocyte response to broad-band ultraviolet-B irradiation. *Photodermatol Photoimmunol Photomed,* 18, 5-13.

TAKAO, M., ABRAMIC, M., MOOS, M., JR., OTRIN, V. R., WOOTTON, J. C., MCLENIGAN, M., LEVINE, A. S. & PROTIC, M. (1993) A 127 kDa component of a UV-damaged DNA-binding complex, which is defective in some xeroderma pigmentosum group E patients, is homologous to a slime mold protein. *Nucleic Acids Res,* 21, 4111-8.

TAKEBE, H., NISHIGORI, C. & TATSUMI, K. (1989) Melanoma and other skin cancers in xeroderma pigmentosum patients and mutation in their cells. *J Invest Dermatol,* 92, 236S-238S.

TAKEKAWA, M., ADACHI, M., NAKAHATA, A., NAKAYAMA, I., ITOH, F., TSUKUDA, H., TAYA, Y. & IMAI, K. (2000) p53-inducible wip1 phosphatase mediates a negative feedback regulation of p38 MAPK-p53 signaling in response to UV radiation. *Embo J,* 19, 6517-26.

TAN, T. & CHU, G. (2002) p53 Binds and activates the xeroderma pigmentosum DDB2 gene in humans but not mice. *Mol Cell Biol,* 22, 3247-54.

TANAKA, K., KAWAI, K., KUMAHARA, Y., IKENAGA, M. & OKADA, Y. (1981) Genetic complementation groups in cockayne syndrome. *Somatic Cell Genet,* 7, 445-55.

TANAKA, K., KAWAI, K., KUMAHARA, Y., UCHIDA, T. & OKADA, Y. (1985) Establishment of Cockayne syndrome fibroblast cell line belonging to complementation group B by SV40 transformation. *Jinrui Idengaku Zasshi,* 30, 21-9.

TANAKA, K., MIURA, N., SATOKATA, I., MIYAMOTO, I., YOSHIDA, M. C., SATOH, Y., KONDO, S., YASUI, A., OKAYAMA, H. & OKADA, Y. (1990) Analysis of a human DNA excision repair gene involved in group A xeroderma pigmentosum and containing a zinc-finger domain. *Nature,* 348, 73-6.

TANAKA, K., SATOKATA, I., OGITA, Z., UCHIDA, T. & OKADA, Y. (1989) Molecular cloning of a mouse DNA repair gene that complements the defect of group-A xeroderma pigmentosum. *Proc Natl Acad Sci U S A,* 86, 5512-6.

TANG, J. Y., HWANG, B. J., FORD, J. M., HANAWALT, P. C. & CHU, G. (2000) Xeroderma pigmentosum p48 gene enhances global genomic repair and suppresses UV-induced mutagenesis. *Mol Cell,* 5, 737-44.

TANTIN, D. (1998) RNA polymerase II elongation complexes containing the Cockayne syndrome group B protein interact with a molecular complex containing the transcription factor IIH components xeroderma pigmentosum B and p62. *J Biol Chem,* 273, 27794-9.

TANTIN, D., KANSAL, A. & CAREY, M. (1997) Recruitment of the putative transcription-repair coupling factor CSB/ERCC6 to RNA polymerase II elongation complexes. *Mol Cell Biol,* 17,

6803-14.

TAPIAS, A., AURIOL, J., FORGET, D., ENZLIN, J. H., SCHARER, O. D., COIN, F., COULOMBE, B. & EGLY, J. M. (2004) Ordered conformational changes in damaged DNA induced by nucleotide excision repair factors. *J Biol Chem,* 279, 19074-83.

TASSIN, J., MALAISE, E. & COURTOIS, Y. (1979) Human lens cells have an in vitro proliferative capacity inversely proportional to the donor age. *Exp Cell Res,* 123, 388-92.

THERRIEN, J. P., DROUIN, R., BARIL, C. & DROBETSKY, E. A. (1999) Human cells compromised for p53 function exhibit defective global and transcription-coupled nucleotide excision repair, whereas cells compromised for pRb function are defective only in global repair. *Proc Natl Acad Sci U S A,* 96, 15038-43.

THERRIEN, J. P., LOIGNON, M., DROUIN, R. & DROBETSKY, E. A. (2001) Ablation of p21waf1cip1 expression enhances the capacity of p53-deficient human tumor cells to repair UVB-induced DNA damage. *Cancer Res,* 61, 3781-6.

THOGERSEN, V. B., SORENSEN, B. S., POULSEN, S. S., ORNTOFT, T. F., WOLF, H. & NEXO, E. (2001) A subclass of HER1 ligands are prognostic markers for survival in bladder cancer patients. *Cancer Res,* 61, 6227-33.

THOMA, B. S. & VASQUEZ, K. M. (2003) Critical DNA damage recognition functions of XPC-hHR23B and XPA-RPA in nucleotide excision repair. *Mol Carcinog,* 38, 1-13.

THOMPSON, L. H. (1998) Chinese hamster cells meet DNA repair: an entirely acceptable affair. *Bioessays,* 20, 589-97.

THOMPSON, L. H., BROOKMAN, K. W., WEBER, C. A., SALAZAR, E. P., REARDON, J. T., SANCAR, A., DENG, Z. & SICILIANO, M. J. (1994) Molecular cloning of the human nucleotide-excision-repair gene ERCC4. *Proc Natl Acad Sci U S A,* 91, 6855-9.

THOMPSON, L. H., CARRANO, A. V., SATO, K., SALAZAR, E. P., WHITE, B. F., STEWART, S. A., MINKLER, J. L. & SICILIANO, M. J. (1987) Identification of nucleotide-excision-repair genes on human chromosomes 2 and 13 by functional complementation in hamster-human hybrids. *Somat Cell Mol Genet,* 13, 539-51.

THUT, C. J., CHEN, J. L., KLEMM, R. & TJIAN, R. (1995) p53 transcriptional activation mediated by coactivators TAFII40 and TAFII60. *Science,* 267, 100-4.

TIBBETTS, R. S., BRUMBAUGH, K. M., WILLIAMS, J. M., SARKARIA, J. N., CLIBY, W. A., SHIEH, S. Y., TAYA, Y., PRIVES, C. & ABRAHAM, R. T. (1999) A role for ATR in the DNA damage-induced phosphorylation of p53. *Genes Dev,* 13, 152-7.

TICE, R. R., SCHNEIDER, E. L., KRAM, D. & THORNE, P. (1979) Cytokinetic analysis of the impaired proliferative response of peripheral lymphocytes from aged humans to phytohemagglutinin. *J Exp Med,* 149, 1029-41.

TIRODE, F., BUSSO, D., COIN, F. & EGLY, J. M. (1999) Reconstitution of the transcription factor TFIIH: assignment of functions for the three enzymatic subunits, XPB, XPD, and cdk7. *Mol Cell,* 3, 87-95.

TOKINO, T., THIAGALINGAM, S., EL-DEIRY, W. S., WALDMAN, T., KINZLER, K. W. & VOGELSTEIN, B. (1994) p53 tagged sites from human genomic DNA. *Hum Mol Genet,* 3, 1537-42.

TOMKINSON, A. E. & LEVIN, D. S. (1997) Mammalian DNA ligases. *Bioessays,* 19, 893-901.

TOMMASI, S., DENISSENKO, M. F. & PFEIFER, G. P. (1997) Sunlight induces pyrimidine dimers preferentially at 5-methylcytosine bases. *Cancer Res,* 57, 4727-30.

TORNALETTI, S. & HANAWALT, P. C. (1999) Effect of DNA lesions on transcription elongation. *Biochimie,* 81, 139-46.

TORNALETTI, S. & PFEIFER, G. P. (1994) Slow repair of pyrimidine dimers at p53 mutation hotspots in skin cancer. *Science,* 263, 1436-8.

TORNALETTI, S., ROZEK, D. & PFEIFER, G. P. (1993) The distribution of UV photoproducts along the human p53 gene and its relation to mutations in skin cancer. *Oncogene,* 8, 2051-7.

TOYODA, H., KOMURASAKI, T., UCHIDA, D. & MORIMOTO, S. (1997) Distribution of mRNA for human epiregulin, a differentially expressed member of the epidermal growth factor family. *Biochem J,* 326 (Pt 1), 69-75.

TREMEAU-BRAVARD, A., PEREZ, C. & EGLY, J. M. (2001) A role of the C-terminal part of p44 in the promoter escape activity of transcription factor IIH. *J Biol Chem,* 276, 27693-7.

TROELSTRA, C., ODIJK, H., DE WIT, J., WESTERVELD, A., THOMPSON, L. H., BOOTSMA, D. & HOEIJMAKERS, J. H. (1990) Molecular cloning of the human DNA excision repair gene ERCC-6. *Mol Cell Biol,* 10, 5806-13.

TROELSTRA, C., VAN GOOL, A., DE WIT, J., VERMEULEN, W., BOOTSMA, D. & HOEIJMAKERS, J. H. (1992) ERCC6, a member of a subfamily of putative helicases, is involved in Cockayne's syndrome and preferential repair of active genes. *Cell,* 71, 939-53.

TSUTSUI, T., KUMAKURA, S., YAMAMOTO, A., KANAI, H., TAMURA, Y., KATO, T., ANPO, M., TAHARA, H. & BARRETT, J. C. (2002) Association of p16(INK4a) and pRb inactivation with immortalization of human cells. *Carcinogenesis,* 23, 2111-7.

TU, Y., BATES, S. & PFEIFER, G. P. (1997) Sequence-specific and domain-specific DNA repair in xeroderma pigmentosum and Cockayne syndrome cells. *J Biol Chem,* 272, 20747-55.

TU, Y., DAMMANN, R. & PFEIFER, G. P. (1998) Sequence and time-dependent deamination of cytosine bases in UVB-induced cyclobutane pyrimidine dimers in vivo. *J Mol Biol,* 284, 297-311.

TU, Y., TORNALETTI, S. & PFEIFER, G. P. (1996) DNA repair domains within a human gene: selective repair of sequences near the transcription initiation site. *Embo J,* 15, 675-83.

TUO, J., JARUGA, P., RODRIGUEZ, H., DIZDAROGLU, M. & BOHR, V. A. (2002) The cockayne syndrome group B gene product is involved in cellular repair of 8-hydroxyadenine in DNA. *J Biol Chem,* 277, 30832-7.

TUSHER, V. G., TIBSHIRANI, R. & CHU, G. (2001) Significance analysis of microarrays applied to the ionizing radiation response. *Proc Natl Acad Sci U S A,* 98, 5116-21.

TYRRELL, R. M. & KEYSE, S. M. (1990) New trends in photobiology. The interaction of UVA radiation with cultured cells. *J Photochem Photobiol B,* 4, 349-61.

UCHIDA, A., SUGASAWA, K., MASUTANI, C., DOHMAE, N., ARAKI, M., YOKOI, M., OHKUMA, Y. & HANAOKA, F. (2002) The carboxy-terminal domain of the XPC protein plays a crucial role in nucleotide excision repair through interactions with transcription factor IIH. *DNA Repair (Amst),* 1, 449-61.

ULLRICH, S. E., ALCALAY, J., APPLEGATE, L. A. & KRIPKE, M. L. (1989) Immunosuppression in phototherapy. *Ciba Found Symp,* 146, 131-9; discussion 139-47.

URA, K., ARAKI, M., SAEKI, H., MASUTANI, C., ITO, T., IWAI, S., MIZUKOSHI, T., KANEDA, Y. & HANAOKA, F. (2001) ATP-dependent chromatin remodeling facilitates nucleotide excision repair of UV-induced DNA lesions in synthetic dinucleosomes. *Embo J,* 20, 2004-14.

URA, K. & HAYES, J. J. (2002) Nucleotide excision repair and chromatin remodeling. *Eur J Biochem,* 269, 2288-93.

VALERY, C., GROB, J. J. & VERRANDO, P. (2001) Identification by cDNA microarray technology of genes modulated by artificial ultraviolet radiation in normal human melanocytes: relation to melanocarcinogenesis. *J Invest Dermatol,* 117, 1471-82.

VAN DEN BOOM, V., CITTERIO, E., HOOGSTRATEN, D., ZOTTER, A., EGLY, J. M., VAN CAPPELLEN, W. A., HOEIJMAKERS, J. H., HOUTSMULLER, A. B. & VERMEULEN, W. (2004) DNA damage stabilizes interaction of CSB with the transcription elongation machinery. *J Cell Biol,* 166, 27-36.

VAN DER HORST, G. T., MEIRA, L., GORGELS, T. G., DE WIT, J., VELASCO-MIGUEL, S., RICHARDSON, J. A., KAMP, Y., VREESWIJK, M. P., SMIT, B., BOOTSMA, D., HOEIJMAKERS, J. H. & FRIEDBERG, E. C. (2002) UVB radiation-induced cancer predisposition in Cockayne syndrome group A (Csa) mutant mice. *DNA Repair (Amst),* 1, 143-57.

VAN DER SPEK, P. J., EKER, A., RADEMAKERS, S., VISSER, C., SUGASAWA, K., MASUTANI, C., HANAOKA, F., BOOTSMA, D. & HOEIJMAKERS, J. H. (1996) XPC and human homologs of RAD23: intracellular localization and relationship to other nucleotide excision repair complexes. *Nucleic Acids Res,* 24, 2551-9.

VAN DUIN, M., DE WIT, J., ODIJK, H., WESTERVELD, A., YASUI, A., KOKEN, H. M., HOEIJMAKERS, J. H. & BOOTSMA, D. (1986) Molecular characterization of the human excision repair gene ERCC-1: cDNA cloning and amino acid homology with the yeast DNA repair gene RAD10. *Cell,* 44, 913-23.

VAN DUIN, M., VREDEVELDT, G., MAYNE, L. V., ODIJK, H., VERMEULEN, W., KLEIN, B., WEEDA, G., HOEIJMAKERS, J. H., BOOTSMA, D. & WESTERVELD, A. (1989) The cloned human DNA excision repair gene ERCC-1 fails to correct xeroderma pigmentosum complementation groups A through I. *Mutat Res,* 217, 83-92.

VAN GOOL, A. J., CITTERIO, E., RADEMAKERS, S., VAN OS, R., VERMEULEN, W., CONSTANTINOU, A., EGLY, J. M., BOOTSMA, D. & HOEIJMAKERS, J. H. (1997) The Cockayne syndrome B protein, involved in transcription-coupled DNA repair, resides in an RNA polymerase II-containing complex. *Embo J,* 16, 5955-65.

VAN HOFFEN, A., NATARAJAN, A. T., MAYNE, L. V., VAN ZEELAND, A. A., MULLENDERS, L. H. & VENEMA, J. (1993) Deficient repair of the transcribed strand of active genes in Cockayne's syndrome cells. *Nucleic Acids Res,* 21, 5890-5.

VAN HOFFEN, A., VENEMA, J., MESCHINI, R., VAN ZEELAND, A. A. & MULLENDERS, L. H. (1995) Transcription-coupled repair removes both cyclobutane pyrimidine dimers and 6-4 photoproducts with equal efficiency and in a sequential way from transcribed DNA in xeroderma pigmentosum group C fibroblasts. *Embo J,* 14, 360-7.

VAN OOSTERWIJK, M. F., VERSTEEG, A., FILON, R., VAN ZEELAND, A. A. & MULLENDERS, L. H. (1996) The sensitivity of Cockayne's syndrome cells to DNA-damaging agents is not due to defective transcription-coupled repair of active genes. *Mol Cell Biol,* 16, 4436-44.

VAN VUUREN, A. J., APPELDOORN, E., ODIJK, H., YASUI, A., JASPERS, N. G., BOOTSMA, D. & HOEIJMAKERS, J. H. (1993) Evidence for a repair enzyme complex involving ERCC1 and complementing activities of ERCC4, ERCC11 and xeroderma pigmentosum group F. *Embo J,* 12, 3693-701.

VAN WAARDE-VERHAGEN, M. A., KAMPINGA, H. H. & LINSKENS, M. H. (2006) Continuous growth of telomerase-immortalised fibroblasts: How long do cells remain normal? *Mech Ageing Dev,* 127, 85-7.

VARGAS, D. A., TAKAHASHI, S. & RONAI, Z. (2003) Mdm2: A regulator of cell growth and death. *Adv Cancer Res,* 89, 1-34.

VAZIRI, H. & BENCHIMOL, S. (1998) Reconstitution of telomerase activity in normal human cells leads to elongation of telomeres and extended replicative life span. *Curr Biol,* 8, 279-82.

VAZIRI, H., SQUIRE, J. A., PANDITA, T. K., BRADLEY, G., KUBA, R. M., ZHANG, H., GULYAS, S., HILL, R. P., NOLAN, G. P. & BENCHIMOL, S. (1999) Analysis of genomic integrity and p53-dependent G1 checkpoint in telomerase-induced extended-life-span human fibroblasts. *Mol Cell Biol,* 19, 2373-9.

VENEMA, J., MULLENDERS, L. H., NATARAJAN, A. T., VAN ZEELAND, A. A. & MAYNE, L. V. (1990) The genetic defect in Cockayne syndrome is associated with a defect in repair of UV-induced DNA damage in transcriptionally active DNA. *Proc Natl Acad Sci U S A,* 87, 4707-11.

VENEMA, J., VAN HOFFEN, A., KARCAGI, V., NATARAJAN, A. T., VAN ZEELAND, A. A. & MULLENDERS, L. H. (1991) Xeroderma pigmentosum complementation group C cells remove pyrimidine dimers selectively from the transcribed strand of active genes. *Mol Cell Biol,* 11, 4128-34.

VENOT, C., MARATRAT, M., DUREUIL, C., CONSEILLER, E., BRACCO, L. & DEBUSSCHE, L. (1998) The requirement for the p53 proline-rich functional domain for mediation of apoptosis is correlated with specific PIG3 gene transactivation and with transcriptional repression. *Embo J,* 17, 4668-79.

VENTER, J. C., ADAMS, M. D., MYERS, E. W., LI, P. W., MURAL, R. J., SUTTON, G. G., SMITH, H. O., YANDELL, M., EVANS, C. A., HOLT, R. A., GOCAYNE, J. D., AMANATIDES, P., BALLEW, R. M., HUSON, D. H., WORTMAN, J. R., ZHANG, Q., KODIRA, C. D., ZHENG, X. H., CHEN, L., SKUPSKI, M., SUBRAMANIAN, G., THOMAS, P. D., ZHANG, J., GABOR MIKLOS, G. L., NELSON, C., BRODER, S., CLARK, A. G., NADEAU, J., MCKUSICK, V. A., ZINDER, N., LEVINE, A. J., ROBERTS, R. J., SIMON, M., SLAYMAN, C., HUNKAPILLER, M., BOLANOS, R., DELCHER, A., DEW, I., FASULO, D., FLANIGAN, M., FLOREA, L., HALPERN, A., HANNENHALLI, S., KRAVITZ, S., LEVY, S., MOBARRY, C., REINERT, K., REMINGTON, K., ABU-THREIDEH, J., BEASLEY, E., BIDDICK, K., BONAZZI, V., BRANDON, R., CARGILL, M., CHANDRAMOULISWARAN, I., CHARLAB, R., CHATURVEDI, K., DENG, Z., DI FRANCESCO, V., DUNN, P., EILBECK, K., EVANGELISTA, C., GABRIELIAN, A. E., GAN, W., GE, W., GONG, F., GU, Z., GUAN, P., HEIMAN, T. J., HIGGINS, M. E., JI, R. R., KE, Z., KETCHUM, K. A., LAI, Z., LEI, Y., LI, Z.,

LI, J., LIANG, Y., LIN, X., LU, F., MERKULOV, G. V., MILSHINA, N., MOORE, H. M., NAIK, A. K., NARAYAN, V. A., NEELAM, B., NUSSKERN, D., RUSCH, D. B., SALZBERG, S., SHAO, W., SHUE, B., SUN, J., WANG, Z., WANG, A., WANG, X., WANG, J., WEI, M., WIDES, R., XIAO, C., YAN, C., et al. (2001) The sequence of the human genome. *Science,* 291, 1304-51.

VERHAGE, R. A., VAN GOOL, A. J., DE GROOT, N., HOEIJMAKERS, J. H., VAN DE PUTTE, P. & BROUWER, J. (1996) Double mutants of Saccharomyces cerevisiae with alterations in global genome and transcription-coupled repair. *Mol Cell Biol,* 16, 496-502.

VERMEULEN, W., SCOTT, R. J., RODGERS, S., MULLER, H. J., COLE, J., ARLETT, C. F., KLEIJER, W. J., BOOTSMA, D., HOEIJMAKERS, J. H. & WEEDA, G. (1994) Clinical heterogeneity within xeroderma pigmentosum associated with mutations in the DNA repair and transcription gene ERCC3. *Am J Hum Genet,* 54, 191-200.

VICHI, P., COIN, F., RENAUD, J. P., VERMEULEN, W., HOEIJMAKERS, J. H., MORAS, D. & EGLY, J. M. (1997) Cisplatin- and UV-damaged DNA lure the basal transcription factor TFIID/TBP. *Embo J,* 16, 7444-56.

VILE, G. F., BASU-MODAK, S., WALTNER, C. & TYRRELL, R. M. (1994) Heme oxygenase 1 mediates an adaptive response to oxidative stress in human skin fibroblasts. *Proc Natl Acad Sci U S A,* 91, 2607-10.

VOLKER, M., MONE, M. J., KARMAKAR, P., VAN HOFFEN, A., SCHUL, W., VERMEULEN, W., HOEIJMAKERS, J. H., VAN DRIEL, R., VAN ZEELAND, A. A. & MULLENDERS, L. H. (2001) Sequential assembly of the nucleotide excision repair factors in vivo. *Mol Cell,* 8, 213-24.

VON ZGLINICKI, T., SARETZKI, G., DOCKE, W. & LOTZE, C. (1995) Mild hyperoxia shortens telomeres and inhibits proliferation of fibroblasts: a model for senescence? *Exp Cell Res,* 220, 186-93.

VON ZGLINICKI, T., SARETZKI, G., LADHOFF, J., D'ADDA DI FAGAGNA, F. & JACKSON, S. P. (2005) Human cell senescence as a DNA damage response. *Mech Ageing Dev,* 126, 111-7.

VREESWIJK, M. P., VAN HOFFEN, A., WESTLAND, B. E., VRIELING, H., VAN ZEELAND, A. A. & MULLENDERS, L. H. (1994) Analysis of repair of cyclobutane pyrimidine dimers and pyrimidine 6-4 pyrimidone photoproducts in transcriptionally active and inactive genes in Chinese hamster cells. *J Biol Chem,* 269, 31858-63.

WAGA, S., HANNON, G. J., BEACH, D. & STILLMAN, B. (1994) The p21 inhibitor of cyclin-dependent kinases controls DNA replication by interaction with PCNA. *Nature,* 369, 574-8.

WAKASUGI, M., KAWASHIMA, A., MORIOKA, H., LINN, S., SANCAR, A., MORI, T., NIKAIDO,

O. & MATSUNAGA, T. (2002) DDB accumulates at DNA damage sites immediately after UV irradiation and directly stimulates nucleotide excision repair. *J Biol Chem,* 277, 1637-40.

WAKASUGI, M. & SANCAR, A. (1998) Assembly, subunit composition, and footprint of human DNA repair excision nuclease. *Proc Natl Acad Sci U S A,* 95, 6669-74.

WAKASUGI, M. & SANCAR, A. (1999) Order of assembly of human DNA repair excision nuclease. *J Biol Chem,* 274, 18759-68.

WAKASUGI, M., SHIMIZU, M., MORIOKA, H., LINN, S., NIKAIDO, O. & MATSUNAGA, T. (2001) Damaged DNA-binding protein DDB stimulates the excision of cyclobutane pyrimidine dimers in vitro in concert with XPA and replication protein A. *J Biol Chem,* 276, 15434-40.

WALKER, K. K. & LEVINE, A. J. (1996) Identification of a novel p53 functional domain that is necessary for efficient growth suppression. *Proc Natl Acad Sci U S A,* 93, 15335-40.

WALL, M. A., COLEMAN, D. E., LEE, E., INIGUEZ-LLUHI, J. A., POSNER, B. A., GILMAN, A. G. & SPRANG, S. R. (1995) The structure of the G protein heterotrimer Gi alpha 1 beta 1 gamma 2. *Cell,* 83, 1047-58.

WANG, B., MATSUOKA, S., CARPENTER, P. B. & ELLEDGE, S. J. (2002) 53BP1, a mediator of the DNA damage checkpoint. *Science,* 298, 1435-8.

WANG, C. I. & TAYLOR, J. S. (1991) Site-specific effect of thymine dimer formation on dAn.dTn tract bending and its biological implications. *Proc Natl Acad Sci U S A,* 88, 9072-6.

WANG, J., HANNON, G. J. & BEACH, D. H. (2000) Risky immortalization by telomerase. *Nature,* 405, 755-6.

WANG, J., XIE, L. Y., ALLAN, S., BEACH, D. & HANNON, G. J. (1998) Myc activates telomerase. *Genes Dev,* 12, 1769-74.

WANG, J. A., FAN, S., YUAN, R. Q., MA, Y. X., MENG, Q., GOLDBERG, I. D. & ROSEN, E. M. (1999) Ultraviolet radiation down-regulates expression of the cell-cycle inhibitor p21WAF1/CIP1 in human cancer cells independently of p53. *Int J Radiat Biol,* 75, 301-16.

WANG, Q. E., WANI, M. A., CHEN, J., ZHU, Q., WANI, G., EL-MAHDY, M. A. & WANI, A. A. (2005a) Cellular ubiquitination and proteasomal functions positively modulate mammalian nucleotide excision repair. *Mol Carcinog,* 42, 53-64.

WANG, Q. E., ZHU, Q., WANI, G., EL-MAHDY, M. A., LI, J. & WANI, A. A. (2005b) DNA repair factor XPC is modified by SUMO-1 and ubiquitin following UV irradiation. *Nucleic Acids Res,* 33, 4023-34.

WANG, S. Q., SETLOW, R., BERWICK, M., POLSKY, D., MARGHOOB, A. A., KOPF, A. W. & BART, R. S. (2001) Ultraviolet A and melanoma: a review. *J Am Acad Dermatol,* 44, 837-46.

WANG, X. Q., GABRIELLI, B. G., MILLIGAN, A., DICKINSON, J. L., ANTALIS, T. M. & ELLEM, K. A. (1996) Accumulation of p16CDKN2A in response to ultraviolet irradiation correlates with late S-G(2)-phase cell cycle delay. *Cancer Res,* 56, 2510-4.

WANG, X. W., YEH, H., SCHAEFFER, L., ROY, R., MONCOLLIN, V., EGLY, J. M., WANG, Z., FREIDBERG, E. C., EVANS, M. K., TAFFE, B. G. & ET AL. (1995) p53 modulation of TFIIH-associated nucleotide excision repair activity. *Nat Genet,* 10, 188-95.

WANG, Y., REED, M., WANG, P., STENGER, J. E., MAYR, G., ANDERSON, M. E., SCHWEDES, J. F. & TEGTMEYER, P. (1993) p53 domains: identification and characterization of two autonomous DNA-binding regions. *Genes Dev,* 7, 2575-86.

WANI, M. A., EL-MAHDY, M. A., HAMADA, F. M., WANI, G., ZHU, Q., WANG, Q. E. & WANI, A. A. (2002a) Efficient repair of bulky anti-BPDE DNA adducts from non-transcribed DNA strand requires functional p53 but not p21(waf1/cip1) and pRb. *Mutat Res,* 505, 13-25.

WANI, M. A., WANI, G., YAO, J., ZHU, Q. & WANI, A. A. (2002b) Human cells deficient in p53 regulated p21(waf1/cip1) expression exhibit normal nucleotide excision repair of UV-induced DNA damage. *Carcinogenesis,* 23, 403-10.

WANI, M. A., ZHU, Q. Z., EL-MAHDY, M. & WANI, A. A. (1999) Influence of p53 tumor suppressor protein on bias of DNA repair and apoptotic response in human cells. *Carcinogenesis,* 20, 765-72.

WANO, C., KITA, K., TAKAHASHI, S., SUGAYA, S., HINO, M., HOSOYA, H. & SUZUKI, N. (2004) Protective role of HSP27 against UVC-induced cell death in human cells. *Exp Cell Res,* 298, 584-92.

WATANABE, M. & HORIKAWA, M. (1974) Analysis of differential sensitivities of synchronized HeLa S3 cells to radiations and chemical carcinogen during the cell cycle. II. Ultraviolet light. *Biochem Biophys Res Commun,* 58, 185-91.

WATSON, J. D. (1972) Origin of concatemeric T7 DNA. *Nat New Biol,* 239, 197-201.

WATSON, J. D. & CRICK, F. H. (1953) Molecular structure of nucleic acids; a structure for deoxyribose nucleic acid. *Nature,* 171, 737-8.

WEBER, C. A., SALAZAR, E. P., STEWART, S. A. & THOMPSON, L. H. (1988) Molecular cloning and biological characterization of a human gene, ERCC2, that corrects the nucleotide excision repair defect in CHO UV5 cells. *Mol Cell Biol,* 8, 1137-46.

WEBER, C. A., SALAZAR, E. P., STEWART, S. A. & THOMPSON, L. H. (1990) ERCC2: cDNA cloning and molecular characterization of a human nucleotide excision repair gene with high homology to yeast RAD3. *Embo J,* 9, 1437-47.

WEBLEY, K., BOND, J. A., JONES, C. J., BLAYDES, J. P., CRAIG, A., HUPP, T. & WYNFORD-THOMAS, D. (2000) Posttranslational modifications of p53 in replicative senescence overlapping but distinct from those induced by DNA damage. *Mol Cell Biol,* 20, 2803-8.

WEEDA, G., VAN HAM, R. C., MASUREL, R., WESTERVELD, A., ODIJK, H., DE WIT, J., BOOTSMA, D., VAN DER EB, A. J. & HOEIJMAKERS, J. H. (1990a) Molecular cloning and biological characterization of the human excision repair gene ERCC-3. *Mol Cell Biol,* 10, 2570-81.

WEEDA, G., VAN HAM, R. C., VERMEULEN, W., BOOTSMA, D., VAN DER EB, A. J. & HOEIJMAKERS, J. H. (1990b) A presumed DNA helicase encoded by ERCC-3 is involved in the human repair disorders xeroderma pigmentosum and Cockayne's syndrome. *Cell,* 62, 777-91.

WEI, C. L., WU, Q., VEGA, V. B., CHIU, K. P., NG, P., ZHANG, T., SHAHAB, A., YONG, H. C., FU, Y., WENG, Z., LIU, J., ZHAO, X. D., CHEW, J. L., LEE, Y. L., KUZNETSOV, V. A., SUNG, W. K., MILLER, L. D., LIM, B., LIU, E. T., YU, Q., NG, H. H. & RUAN, Y. (2006) A global map of p53 transcription-factor binding sites in the human genome. *Cell,* 124, 207-19.

WEI, W., HEMMER, R. M. & SEDIVY, J. M. (2001) Role of p14(ARF) in replicative and induced senescence of human fibroblasts. *Mol Cell Biol,* 21, 6748-57.

WEINBERG, R. A. (1995) The retinoblastoma protein and cell cycle control. *Cell,* 81, 323-30.

WEINRICH, S. L., PRUZAN, R., MA, L., OUELLETTE, M., TESMER, V. M., HOLT, S. E., BODNAR, A. G., LICHTSTEINER, S., KIM, N. W., TRAGER, J. B., TAYLOR, R. D., CARLOS, R., ANDREWS, W. H., WRIGHT, W. E., SHAY, J. W., HARLEY, C. B. & MORIN, G. B. (1997) Reconstitution of human telomerase with the template RNA component hTR and the catalytic protein subunit hTRT. *Nat Genet,* 17, 498-502.

WEINTRAUB, S. J., CHOW, K. N., LUO, R. X., ZHANG, S. H., HE, S. & DEAN, D. C. (1995) Mechanism of active transcriptional repression by the retinoblastoma protein. *Nature,* 375, 812-5.

WEST, M. D., PEREIRA-SMITH, O. M. & SMITH, J. R. (1989) Replicative senescence of human skin fibroblasts correlates with a loss of regulation and overexpression of collagenase activity. *Exp Cell Res,* 184, 138-47.

WEST, M. D., SHAY, J. W., WRIGHT, W. E. & LINSKENS, M. H. (1996) Altered expression of plasminogen activator and plasminogen activator inhibitor during cellular senescence. *Exp Gerontol,* 31, 175-93.

WESTERVELD, A., HOEIJMAKERS, J. H., VAN DUIN, M., DE WIT, J., ODIJK, H., PASTINK, A., WOOD, R. D. & BOOTSMA, D. (1984) Molecular cloning of a human DNA repair gene. *Nature,* 310, 425-9.

WHYTE, P., BUCHKOVICH, K. J., HOROWITZ, J. M., FRIEND, S. H., RAYBUCK, M., WEINBERG, R. A. & HARLOW, E. (1988) Association between an oncogene and an anti-oncogene: the adenovirus E1A proteins bind to the retinoblastoma gene product. *Nature,* 334, 124-9.

WIANNY, F. & ZERNICKA-GOETZ, M. (2000) Specific interference with gene function by double-stranded RNA in early mouse development. *Nat Cell Biol,* 2, 70-5.

WICK, M., BURGER, C., BRUSSELBACH, S., LUCIBELLO, F. C. & MULLER, R. (1994) A novel member of human tissue inhibitor of metalloproteinases (TIMP) gene family is regulated during G1 progression, mitogenic stimulation, differentiation, and senescence. *J Biol Chem,* 269, 18953-60.

WILLIAMS, B. R. (1997) Role of the double-stranded RNA-activated protein kinase (PKR) in cell regulation. *Biochem Soc Trans,* 25, 509-13.

WILSON, C. L. & MILLER, C. J. (2005) Simpleaffy: a BioConductor package for Affymetrix Quality Control and data analysis. *Bioinformatics,* 21, 3683-5.

WINKLER, G. S., SUGASAWA, K., EKER, A. P., DE LAAT, W. L. & HOEIJMAKERS, J. H. (2001) Novel functional interactions between nucleotide excision DNA repair proteins influencing the enzymatic activities of TFIIH, XPG, and ERCC1-XPF. *Biochemistry,* 40, 160-5.

WINSEY, S. L., HALDAR, N. A., MARSH, H. P., BUNCE, M., MARSHALL, S. E., HARRIS, A. L., WOJNAROWSKA, F. & WELSH, K. I. (2000) A variant within the DNA repair gene XRCC3 is associated with the development of melanoma skin cancer. *Cancer Res,* 60, 5612-6.

WOLFGANG, C. D., LIANG, G., OKAMOTO, Y., ALLEN, A. E. & HAI, T. (2000) Transcriptional autorepression of the stress-inducible gene ATF3. *J Biol Chem,* 275, 16865-70.

WOOD, L. D., HALVORSEN, T. L., DHAR, S., BAUR, J. A., PANDITA, R. K., WRIGHT, W. E., HANDE, M. P., CALAF, G., HEI, T. K., LEVINE, F., SHAY, J. W., WANG, J. J. & PANDITA, T. K. (2001a) Characterization of ataxia telangiectasia fibroblasts with extended life-span through telomerase expression. *Oncogene,* 20, 278-88.

WOOD, R. D., MITCHELL, M., SGOUROS, J. & LINDAHL, T. (2001b) Human DNA repair genes. *Science,* 291, 1284-9.

WOOD, R. D., ROBINS, P. & LINDAHL, T. (1988) Complementation of the xeroderma pigmentosum DNA repair defect in cell-free extracts. *Cell,* 53, 97-106.

WOODHEAD, A. D., SETLOW, R. B. & TANAKA, M. (1999) Environmental factors in nonmelanoma and melanoma skin cancer. *J Epidemiol,* 9, S102-14.

WOUDSTRA, E. C., GILBERT, C., FELLOWS, J., JANSEN, L., BROUWER, J., ERDJUMENT-BROMAGE, H., TEMPST, P. & SVEJSTRUP, J. Q. (2002) A Rad26-Def1 complex coordinates repair and RNA pol II proteolysis in response to DNA damage. *Nature,* 415, 929-33.

WRIGHT, W. E. & HAYFLICK, L. (1975) Nuclear control of cellular aging demonstrated by hybridization of anucleate and whole cultured normal human fibroblasts. *Exp Cell Res,* 96, 113-21.

WRIGHT, W. E., PEREIRA-SMITH, O. M. & SHAY, J. W. (1989) Reversible cellular senescence: implications for immortalization of normal human diploid fibroblasts. *Mol Cell Biol,* 9, 3088-92.

WRIGHT, W. E., PIATYSZEK, M. A., RAINEY, W. E., BYRD, W. & SHAY, J. W. (1996) Telomerase activity in human germline and embryonic tissues and cells. *Dev Genet,* 18, 173-9.

WRIGHT, W. E. & SHAY, J. W. (1992) The two-stage mechanism controlling cellular senescence and immortalization. *Exp Gerontol,* 27, 383-9.

WU, X., BAYLE, J. H., OLSON, D. & LEVINE, A. J. (1993) The p53-mdm-2 autoregulatory feedback loop. *Genes Dev,* 7, 1126-32.

WU, X. & LEVINE, A. J. (1994) p53 and E2F-1 cooperate to mediate apoptosis. *Proc Natl Acad Sci U S A,* 91, 3602-6.

WU, X., SHELL, S. M., YANG, Z. & ZOU, Y. (2006) Phosphorylation of nucleotide excision repair factor xeroderma pigmentosum group A by ataxia telangiectasia mutated and Rad3-related-dependent checkpoint pathway promotes cell survival in response to UV irradiation. *Cancer Res,* 66, 2997-3005.

WYLLIE, F. S., JONES, C. J., SKINNER, J. W., HAUGHTON, M. F., WALLIS, C., WYNFORD-THOMAS, D., FARAGHER, R. G. & KIPLING, D. (2000) Telomerase prevents the accelerated cell ageing of Werner syndrome fibroblasts. *Nat Genet,* 24, 16-7.

XIAO, H., PEARSON, A., COULOMBE, B., TRUANT, R., ZHANG, S., REGIER, J. L., TRIEZENBERG, S. J., REINBERG, D., FLORES, O., INGLES, C. J. & ET AL. (1994) Binding of basal transcription factor TFIIH to the acidic activation domains of VP16 and p53. *Mol Cell Biol,* 14, 7013-24.

XIONG, Y., HANNON, G. J., ZHANG, H., CASSO, D., KOBAYASHI, R. & BEACH, D. (1993) p21 is a universal inhibitor of cyclin kinases. *Nature,* 366, 701-4.

XU, G., SNELLMAN, E., BYKOV, V. J., JANSEN, C. T. & HEMMINKI, K. (2000) Effect of age on the

formation and repair of UV photoproducts in human skin in situ. *Mutat Res,* 459, 195-202.

YAGI, T. & TAKEBE, H. (1983) Establishment by SV40 transformation and characteristics of a cell line of xeroderma pigmentosum belonging to complementation group F. *Mutat Res,* 112, 59-66.

YAN, C., LU, D., HAI, T. & BOYD, D. D. (2005) Activating transcription factor 3, a stress sensor, activates p53 by blocking its ubiquitination. *Embo J,* 24, 2425-35.

YANG, G., ZHANG, G., PITTELKOW, M. R., RAMONI, M. & TSAO, H. (2006) Expression Profiling of UVB Response in Melanocytes Identifies a Set of p53-Target Genes. *J Invest Dermatol,* 126, 2490-506.

YANG, J., YU, Y., HAMRICK, H. E. & DUERKSEN-HUGHES, P. J. (2003) ATM, ATR and DNA-PK: initiators of the cellular genotoxic stress responses. *Carcinogenesis,* 24, 1571-80.

YANG, M., KANG, M. J., CHOI, Y., KIM, C. S., LEE, S. M., PARK, C. W., LEE, H. S. & TAE, K. (2005) Associations between XPC expression, genotype, and the risk of head and neck cancer. *Environ Mol Mutagen,* 45, 374-9.

YANG, N. C. & HU, M. L. (2005) The limitations and validities of senescence associated-beta-galactosidase activity as an aging marker for human foreskin fibroblast Hs68 cells. *Exp Gerontol,* 40, 813-9.

YANG, Y., LI, C. C. & WEISSMAN, A. M. (2004) Regulating the p53 system through ubiquitination. *Oncogene,* 23, 2096-106.

YANISHEVSKY, R. & CARRANO, A. V. (1975) Prematurely condensed chromosomes of dividing and non-dividing cells in aging human cell cultures. *Exp Cell Res,* 90, 169-74.

YEGOROV, Y. E., AKIMOV, S. S., HASS, R., ZELENIN, A. V. & PRUDOVSKY, I. A. (1998) Endogenous beta-galactosidase activity in continuously nonproliferating cells. *Exp Cell Res,* 243, 207-11.

YOKOI, M., MASUTANI, C., MAEKAWA, T., SUGASAWA, K., OHKUMA, Y. & HANAOKA, F. (2000) The xeroderma pigmentosum group C protein complex XPC-HR23B plays an important role in the recruitment of transcription factor IIH to damaged DNA. *J Biol Chem,* 275, 9870-5.

YOU, J. S., WANG, M. & LEE, S. H. (2003) Biochemical analysis of the damage recognition process in nucleotide excision repair. *J Biol Chem,* 278, 7476-85.

YOU, Y. H., LEE, D. H., YOON, J. H., NAKAJIMA, S., YASUI, A. & PFEIFER, G. P. (2001) Cyclobutane pyrimidine dimers are responsible for the vast majority of mutations induced by UVB irradiation in mammalian cells. *J Biol Chem,* 276, 44688-94.

YU, A., FAN, H. Y., LIAO, D., BAILEY, A. D. & WEINER, A. M. (2000a) Activation of p53 or loss of the Cockayne syndrome group B repair protein causes metaphase fragility of human U1, U2, and 5S genes. *Mol Cell,* 5, 801-10.

YU, J. J., LEE, K. B., MU, C., LI, Q., ABERNATHY, T. V., BOSTICK-BRUTON, F. & REED, E. (2000b) Comparison of two human ovarian carcinoma cell lines (A2780/CP70 and MCAS) that are equally resistant to platinum, but differ at codon 118 of the ERCC1 gene. *Int J Oncol,* 16, 555-60.

YU, J. J., MU, C., LEE, K. B., OKAMOTO, A., REED, E. L., BOSTICK-BRUTON, F., MITCHELL, K. C. & REED, E. (1997) A nucleotide polymorphism in ERCC1 in human ovarian cancer cell lines and tumor tissues. *Mutat Res,* 382, 13-20.

YUZHAKOV, A., KELMAN, Z., HURWITZ, J. & O'DONNELL, M. (1999) Multiple competition reactions for RPA order the assembly of the DNA polymerase delta holoenzyme. *Embo J,* 18, 6189-99.

ZENG, G. & MILLIS, A. J. (1994) Expression of 72-kDa gelatinase and TIMP-2 in early and late passage human fibroblasts. *Exp Cell Res,* 213, 148-55.

ZHAN, Q. (2005) Gadd45a, a p53- and BRCA1-regulated stress protein, in cellular response to DNA damage. *Mutat Res,* 569, 133-43.

ZHANG, Y., YUAN, F., WU, X., RECHKOBLIT, O., TAYLOR, J. S., GEACINTOV, N. E. & WANG, Z. (2000) Error-prone lesion bypass by human DNA polymerase eta. *Nucleic Acids Res,* 28, 4717-24.

ZHAO, R., GISH, K., MURPHY, M., YIN, Y., NOTTERMAN, D., HOFFMAN, W. H., TOM, E., MACK, D. H. & LEVINE, A. J. (2000) Analysis of p53-regulated gene expression patterns using oligonucleotide arrays. *Genes Dev,* 14, 981-93.

ZHOU, B. B. & ELLEDGE, S. J. (2000) The DNA damage response: putting checkpoints in perspective. *Nature,* 408, 433-9.

ZHU, Q., WANI, M. A., EL-MAHDY, M. & WANI, A. A. (2000) Decreased DNA repair efficiency by loss or disruption of p53 function preferentially affects removal of cyclobutane pyrimidine dimers from non-transcribed strand and slow repair sites in transcribed strand. *J Biol Chem,* 275, 11492-7.

ZHU, Q., YAO, J., WANI, G., WANI, M. A. & WANI, A. A. (2001) Mdm2 mutant defective in binding p300 promotes ubiquitination but not degradation of p53: evidence for the role of p300 in integrating ubiquitination and proteolysis. *J Biol Chem,* 276, 29695-701.

ZIEGLER, A., JONASON, A. S., LEFFELL, D. J., SIMON, J. A., SHARMA, H. W., KIMMELMAN, J.,

REMINGTON, L., JACKS, T. & BRASH, D. E. (1994) Sunburn and p53 in the onset of skin cancer. *Nature,* 372, 773-6.

ZIEGLER, A., LEFFELL, D. J., KUNALA, S., SHARMA, H. W., GAILANI, M., SIMON, J. A., HALPERIN, A. J., BADEN, H. P., SHAPIRO, P. E., BALE, A. E. & ET AL. (1993) Mutation hotspots due to sunlight in the p53 gene of nonmelanoma skin cancers. *Proc Natl Acad Sci U S A,* 90, 4216-20.

ZOLAN, M. E., CORTOPASSI, G. A., SMITH, C. A. & HANAWALT, P. C. (1982) Deficient repair of chemical adducts in alpha DNA of monkey cells. *Cell,* 28, 613-9.

ZOU, Y., SFEIR, A., GRYAZNOV, S. M., SHAY, J. W. & WRIGHT, W. E. (2004) Does a sentinel or a subset of short telomeres determine replicative senescence? *Mol Biol Cell,* 15, 3709-18.

ZOU, Y. & VAN HOUTEN, B. (1999) Strand opening by the UvrA(2)B complex allows dynamic recognition of DNA damage. *Embo J,* 18, 4889-901.